Tailoring Intra- and Intermolecular Properties: from Cyclophanes to Daisy Chains

Inauguraldissertation

zur Erlangung der Würde eines Doktors der Philosophie

vorgelegt der

Philosophisch-Naturwissenschaftlichen Fakultät der Universität Basel

von

Jürgen Stefan Rotzler

aus Lörrach, Deutschland

Basel 2012

Genehmigt von der Philosophisch-Naturwissenschaftlichen Fakultät der Universität Basel auf Antrag von

Prof. Dr. Marcel Mayor

Prof. Dr. Karl Gademann

Prof. Dr. Jean-Pierre Sauvage

Basel, den 24.04.2012

Prof. Dr. Martin Spiess

für Bernadette und meine Eltern

Ein Gelehrter in seinem Laboratorium ist nicht nur ein Techniker;

er steht auch vor den Naturgesetzen wie ein Kind vor der Märchenwelt.

Marie Curie

Acknowledgments

I wish to express my gratitude to my supervisor Professor Dr. Marcel Mayor. Marcel, it was an honor and pleasure to work in your group. I thank you for giving me the opportunity to work on these interesting and challenging projects, your constant support, not only in chemical aspects, but also in the difficult times of my PhD. I further thank you for your confidence, the useful discussions and the freedom given to me in my research.

I would like to thank Professor Dr. Jean-Pierre Sauvage for the co-examination of this thesis.

I thank Professor Dr. Karl Gademann for his support in finding a PostDoc grant, for the useful and interesting discussions about organic chemistry and for the co-examination of my thesis.

Moreover, Prof. Dr. Catherine Housecroft is acknowledged for chairing the exam.

Successful research in nanotechnology is only possible when experts in all areas of science work together. Therefore I am very thankful for all the fruitful collaborations I had during my work. Especially I want to thank Dr. Daniel Häussinger and Heiko Gsellinger for their fantastic contribution in all my projects by measuring and analyzing a variety of NMR experiments. Furthermore I thank Dr. Alex Boeglin, Dr. Alberto Barsella and Prof. Dr. Alain Fort for measuring and interpreting EFISH experiments. I thank Prof. Dr. Willem Klopper and Angela Bihlmeier for quantum mechanical calculations and the fruitful discussions about racemization dynamics of biphenyls. I thank Dr. Emanuele Orgiu, Dr. Nuria Crivillers and Prof. Dr. Paolo Samori for involving me in their research on OTFT. I want to thank Dr. Oliver Hampe for measuring high resolution MS of the daisy chains. I thank Prof. Dr. Thomas Wandlowski and Dr. Artem Mishchenko for performing single molecule conductance measurements. Finally I thank Prof. Dr. Oliver Trapp for providing his software tools, which allowed to analyze the atropisomerization of biphenyls with HPLC.

Moreover, I like to thank Dr. David Vonlanthen and Markus Gantenbein for providing a variety of biphenyl compounds.

I am very thankful to Lukas Jundt, Markus Gantenbein and Michel Rickhaus for their enthusiastic work during their Master theses which I was allowed to supervise.

I thank Lukas Jundt, Nicola Polimene, Heiko Gsellinger, Gino Günzburger, Gregor Meier, David Bossert, Lukas Felix and Silas Götz for their contribution to my work during lab courses.

A big thank you goes to Michel Rickhaus, Dr. Christian Ebner and Sylvie Drayss who spent their time proof-reading the manuscript.

Especially I want to thank Michel Rickhaus for providing wonderful artwork for numerous publications and presentations, as well as Sandra Jensen for designing the cover picture.

I want to thank all former and present members of Lab OC04 for the nice working atmosphere we had in our second home.

I thank the former and present members of the Mayor-group for their intellectual input to my projects.

Moreover, I like to acknowledge all chemists I was allowed to learn from in lab courses, especially Dr. Axel Franzke, Dr. Björn Gschwend, Dr. Sergio Grunder and Dr. Marcel Müri.

I would like to thank Dr. Heinz Nadig for FAB and EI mass spectrometry measurements and Werner Kirsch for elemental analyses. I thank Dr. Stefan Schürch and co-workers for recording high resolution mass spectra. I am grateful to Dr. Markus Neuburger and Dr. Silvia Schaffner for measuring solid state structures. Then I would like to thank Markus Hauri, Roy Lips, the workshop team and the secretaries Beatrice Erismann, Brigitte Howald and Marina Mambelli-Johnson.

I thank all past and present colleagues in the department who made the time at the University of Basel that enjoyable.

I thank Chris, Denise and Jörg for all the learning sessions during our studies and for being such good friends.

Furthermore I would like to thank my good friends Alex, Laura, Sophie, my godchildren Jonas and Niklas, Uli, Dani, Tommy and the Hammers for their constant support in difficult times and all the fun we had so far.

I thank my family, especially my parents and grandparents who made it possible to achieve my goals with their support and love throughout my life.

Especially I thank the most important person in my life, Bernadette, for her constant support, her patience and her love.

Finally the Swiss National Science Foundation is acknowledged for financial support.

This cumulative PhD-Thesis is based on the following publications and manuscripts:

Part A:

"*Molecular Daisy Chains*", Jürgen Rotzler, Marcel Mayor*, prepared for submission to *Chem. Soc. Rev.*

"*Synthesis and Aggregation Studies of an Amphiphilic Molecular Rod*", Jürgen Rotzler, Marcel Mayor*, prepared for submission to *Chem. Eur. J.*

Part B:

"*Synthesis and Aggregation Studies of a Molecular "Daisy Chain" formed by Amphiphilic Molecular Rods for Electron Transport Investigations in a Bimolecular Junction*", Jürgen Rotzler, Daniel Häussinger*, Marcel Mayor*, prepared for submission.

Part C:

"*Variation of the Backbone Conjugation in NLO Model Compounds: Torsion-Angle-Restricted, Biphenyl-Based Push-Pull-Systems*", Jürgen Rotzler, David Vonlanthen, Alberto Barsella, Alex Boeglin*, Alain Fort, and Marcel Mayor*, *Eur. J. Org. Chem*. **2010**, *6*, 1096 – 1110.

"*Synthesis of Rotationally Restricted and Modular Biphenyl Building Blocks*", David Vonlanthen, Jürgen Rotzler, Markus Neuburger, Marcel Mayor*, *Eur. J. Org. Chem.* **2010**, *1*, 120 – 133.

"*Conformationally Controlled Electron Delocalization in n-Type Rods: Synthesis, Structure, and Optical, Electrochemical, and Spectroelectrochemical Properties of Dicyanocyclophanes*", David Vonlanthen, Alexander Rudnev, Artem Mishchenko, Alexander Käslin, Jürgen Rotzler, Markus Neuburger, Thomas Wandlowski*, Marcel Mayor*, *Chem. Eur. J.* **2011**, *17*, 7236 – 7250.

"*Racemisation dynamics of torsion angle restricted biphenyl push-pull cyclophanes*", Jürgen Rotzler, Heiko Gsellinger, Markus Neuburger, David Vonlanthen, Daniel Häussinger* and Marcel Mayor*, *Org. Biomol. Chem.* **2011**, *9*, 86 – 91.

"Electronic responses of donor acceptor substituted twisted biphenyls" A. Boeglin, A. Barsella, H. Chaumeil, E. Ay, J. Rotzler, M. Mayor, A. Fort, *Proceedings of SPIE* **2010**, 7774 (Linear and Nonlinear Optics of Organic Materials X).

Part D:

"*Thermodynamic Studies of 4 and 4' Substituted Torsion Angle Restricted 2,2' Propyl-Bridged Biphenyl Cyclophanes*", Jürgen Rotzler, Heiko Gsellinger, Angela Bihlmeier, Markus Gantenbein, David Vonlanthen, Daniel Häussinger*, Wim Klopper*, Marcel Mayor*, prepared for submission to *J. Phys. Chem. A*.

Part E:

"*Tuning the charge injection of P3HT-based organic thin-film transistors through electrode functionalization with oligophenylene SAMs*", Emanuele Orgiu, Nuria Crivillers, Jürgen Rotzler, Marcel Mayor* and Paolo Samori*, *J. Mater. Chem.* **2010**, *20*, 10798 – 10800.

Abstract

Todays high-tech society is striving for faster, cheaper and higher performing devices in all circumstances. Traditional materials have long since reached their limits making the search for new materials with altered properties inevitable. Easy processable, long-term stable polymeric materials with improved handling or switchable properties for use in plastics, conducting single molecular wires, switches, rectifiers in computer industry, nonlinear optic materials for data transmission at the speed of light, devices for flexible displays and luminescent materials operating with less energy are needed in the nearby future. Hence fundamental research in material science and nanotechnology is urgently necessary to provide the base for potential future applications.

This PhD-Thesis is divided in five different parts addressing the above mentioned topics:

Part A: The synthesis and aggregation studies of a hermaphroditic molecular rod comprising a terminal water soluble loop are presented. A mono-functionalized Diederich-type cylophane, acting as the loop subunit, containing a hydrophobic cavity was synthesized in 10 or 7 steps, respectively. Functional group transformations of this hydrophilic macrocycle and final coupling of an oligophenylene-ethynylene hydrophobic molecular rod provided the envisaged target compound in 21 or 17 synthetic steps. By dissolving this amphiphile in polar solvents the hydrophobic rod threads into the cavity of the macrocycle driven by a strong hydrophobic effect. Aggregation studies by ^{1}H-NMR titrations, fluorescence titrations and mass spectrometry confirmed the formation of dimers at low concentrations and longer oligomers at higher concentrations. Such molecular daisy chains are potential candidates towards new polymers with altered macroscopic properties

Part B: The functionalization of the molecular rod of the amphiphilic daisy chain monomer at the terminus with thiol anchoring groups for investigations in molecular electronics is shown. Aggregation studies revealed a similar self-complexation behavior as the unfunctionalized version. Below concentrations of 0.37 mM the formation of [c2]daisy chains was observed. Such thiol-functionalized pseudorotaxanes are potential candidates for investigations of bimolecular bridges in mechanically controlled break junctions (MCBJ) potentially resulting in new design possibilities in single molecular electronics. Furthermore the mechanically adjustable stacking surface of the molecular rods allows for mimicking a macroscopic potentiometer by mechanical minute opening and closing the gap between two electrodes.

Part C: Terminal piperidinyl and nitro functionalized biphenyls, bridged between 2 and 2' position by a variable number of methylene groups, were synthesized and fully characterized. These push-pull systems with defined and restricted torsion angles between their phenyl rings are ideal model compounds to investigate the influence of the chromophore's conjugation in nonlinear optic (NLO) responses. A general implementable synthetic route towards these model compounds is reported, starting from dibromo or ditriflate biphenyls. *Hartwig-Buchwald* cross-coupling, a selective azacycloalkylation of diaminobiphenyls and a mild oxidation of primary amines to nitro groups in presence of a tertiary amine summarizes the synthetic pathway. NLO properties of the series of torsionally constrained push-pull biphenyls were collected by electric field induced second harmonic generation (EFISH) experiments. The results agree qualitatively with semi-empirical simulations based on the AM1 Hamiltonian. A linear dependence of the quadratic response on the $\cos^2\Phi$ of the inter-aryl dihedral angle is observed, which points to oscillator strength loss as the dominant effect of increasing backbone twist.

Towards potential applications of organic nonlinear optic materials the molecular noncentrosymmetry has to be transformed to the macroscopic scale. One possibility is to grow noncentrosymmetric crystals out of enantiomerically pure nonlinear optic active compounds. The 2,2' alkyl-bridged push-pull biphenyls exhibit axial chirality and are therefore ideal candidates to obtain nonlinear optic active compounds which crystallize in a noncentrosymmetric point group. To get insight into the conformational stability, the thermodynamics of the atropisomerization of these torsion angle restricted, axial chiral biphenyl based push-pull cyclophanes were studied. Using ^{1}H-NMR coalescence measurements the rotation barrier around the central C-C bond was determined to be 50 kJ/mol for the propyl-bridged biphenyl derivative, displaying only a negligible solvent dependence. By protonation of the piperidinyl nitrogen as electron donor the free energy $\Delta G^{\ddagger}(T)$ of the rotation barrier increased, indicating that the tendency of the push-pull system to planarize may be considered as a driving force for the atropisomerization. For the more restricted butyl-bridged cyclophane a rotation barrier of $\Delta G^{\ddagger}(T)$ = 90 kJ/mol was measured using dynamic chromatography.

Part D: Encouraged by the promising results of the push-pull cyclophanes, the influence of 2,2' propyl-bridged and 4,4' electron donor or electron acceptor substituted axial chiral biphenyl cyclophanes on their atropisomerization process was studied. Estimated free energies $\Delta G^{\ddagger}$(T) of the rotation around the central biphenyl bond, which were obtained from ^{1}H-NMR coalescence measurements, were correlated to the Hammett-parameters σ_p as a

measure for electron donor and acceptor strength. It is demonstrated that the resulting linear correlation is mainly based on the influence of the different substituents on the π-system of the biphenyl cyclophanes. By line shape analysis the rate constants were calculated and the enthalpic and entropic contributions were evaluated using the Eyring equation. Density functional theory calculations show a planar transition state of these isomerization processes and the calculated energy barriers based on these mechanistic studies are in good agreement with the experimentally obtained free energies. Additionally it was shown that the acidity of the solvent used for ^{1}H-NMR coalescence measurements alters the enthalpic and entropic contribution to the free energy $\Delta G^{\ddagger}$(T). In addition the butyl-bridged derivatives were studied by dynamic HPLC. The same trends than for the propyl-bridged cyclophanes were observed. By quantum chemical calculations the reaction mechanism was computed, showing a planar transition state.

Part E: A series of mono-thiolated torsion angle restricted biphenyl based cyclophanes were synthesized. These model compounds allowed for modulation of the field-effect mobility and threshold voltage of organic thin film transistors (OTFT). By functionalizing gold electrodes with chemisorbed SAMs of aromatic thiols having an increasing number of phenylenes, the contact resistance in poly(3-hexylthiophene)-based OTFTs was found to be ruled by the joint effect of the energetic alignment between metal and semiconductor, the interfacial morphology and tunneling resistance of the SAMs.

Table of Contents

Material Science

"Observe, comprehend, execute" has always been the key principle for any scientist to use natural phenomena for his own purpose. To recognize and understand the specific properties of materials that allows creation of helping tools is the fundament not only of material science but also for the comfort we are used to in our daily life. To fulfill the continuous needs in todays technologies it is not sufficient any more to just make use of a certain property of a natural material: enhancing or designing properties of materials from scratch have moved into the focus throughout all topics in contemporary research.[1,2] Researchers have basically moved from the investigation of chemical compositions to the understanding of the interplay of additives. The knowledge of the influence of each ingredient to the whole system allows to predict what happens if one is exchanged or altered.[3] Understanding such material-property-relationships is the key to design systems with a well defined property. One excellent example is the development of concrete – a product obtained by manipulation of lime-stone. Adding various additives whose influence to the basic material was well investigated allowed to make concrete much more resistant and easier to handle.[4] An additional dimension of design possibility is generated when the materials are assembled such that the property is not changed but combined like in self-cleaning paint where pigments are mixed with hydrophobic crystals to avoid adsorption of dirt.[5] Moreover functional materials with defined properties can be arranged in an order that the user can decide which property is dominant.[6] Potentiometers are examples for such devices where the insulating property of a material is used to reduce conductivity.[7] By designing different resistors and make them individually addressable the user can regulate the electric current reaching the next device. The knowledge of the function of each individual component opens up the possibility to manipulate materials by changing their composition and therefore to generate a tailored property.[8,9] This is one of the most fascinating findings of mankind and the key of the successful story of material science.

The property of a material can be defined as the response to an applied external input (light, gravitation, mechanical stress, chemical, electromagnetic, etc.). In principle each material has a distinct property. It is possible to divide materials according to their response on external influences into two categories – one including materials whose properties are resistant against external stimuli and one where the interaction of an external input with the material results in either a changed or enhanced output.[1,8] The response of material to external inputs is caused by processes on the molecular level of the material. In simple terms, if a blacksmith hits his

hammer on a piece of iron both deformation and sound are caused because the molecular structure of the metal is distorted to compensate the applied force. The sound is generated due to vibrations of the metal framework meaning mechanical stress is converted into an acoustic wave. Understanding of the fundamental process that can be conformational changes, chemical reactions, absorption of light by a chromophore, emission of light, generation of charges or even prevention of an interaction allows the directed redesign of matter at the molecular level. Therefore particular parts of material science are focused on the alteration and tailorability of material properties by designing the molecular or even atomic structure.[10] The designed molecules can provide new matter which can lead to new applications (figure 1).[11] The transformation of molecular properties to the macroscopic dimension requires correct and defined assembly of the molecules. Variation of this intermolecular arrangement of molecules on the other hand gives access to a new dimension of design flexibility since a different spatial arrangement of molecules can result in altered macroscopic properties (figure 1).

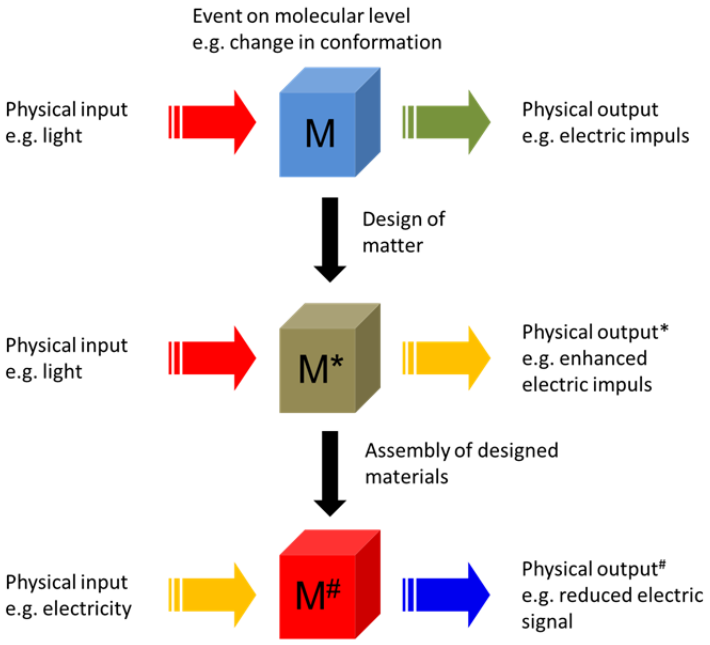

Figure 1. Conceptual sketch how physical properties can be altered by manipulation of matter.

The concept of altering properties of materials by changing the molecular composition led as a representative example to the incorporation of nanoparticles into materials which provided more resistant ceramics[12], transparent sunblockers[13] or new catalysts for fuel production[14]. Furthermore nano-crystalline semiconductors, quantum dots which fluoresce in UV light depending on the size in different colors, were coupled on proteins which allowed tracing of them in human bodies and thus found their way into medicinal research.[15]

Part A. An Amphiphilic Molecular Rod Comprising a Terminal Loop: Synthesis and Applications of Mechanically Interlocked Macromolecules

Polymer Science

One of the most amazing examples where the investigations of structure-property relationships are used to design matter with distinct properties is the production of polymers. As depicted above the properties of materials are directly linked to their molecular composition. The nature of the monomeric structural units and the correct position within the macromolecule define the macroscopic properties and the function.[16] All life on earth is based on natural polymers. With about 4 different nucleobases and 20 amino acids a variety of polymers (DNA and Proteins) with very distinct functions are accessible. The wrong placement of just one important monomer can lead to mismatch and therefore to dysfunction of the whole interplay.[17] By realizing that organic materials comprise a higher diversity of different structures it is no wonder why traditional materials in daily life are more and more replaced by synthetic organic polymers.[18,19]

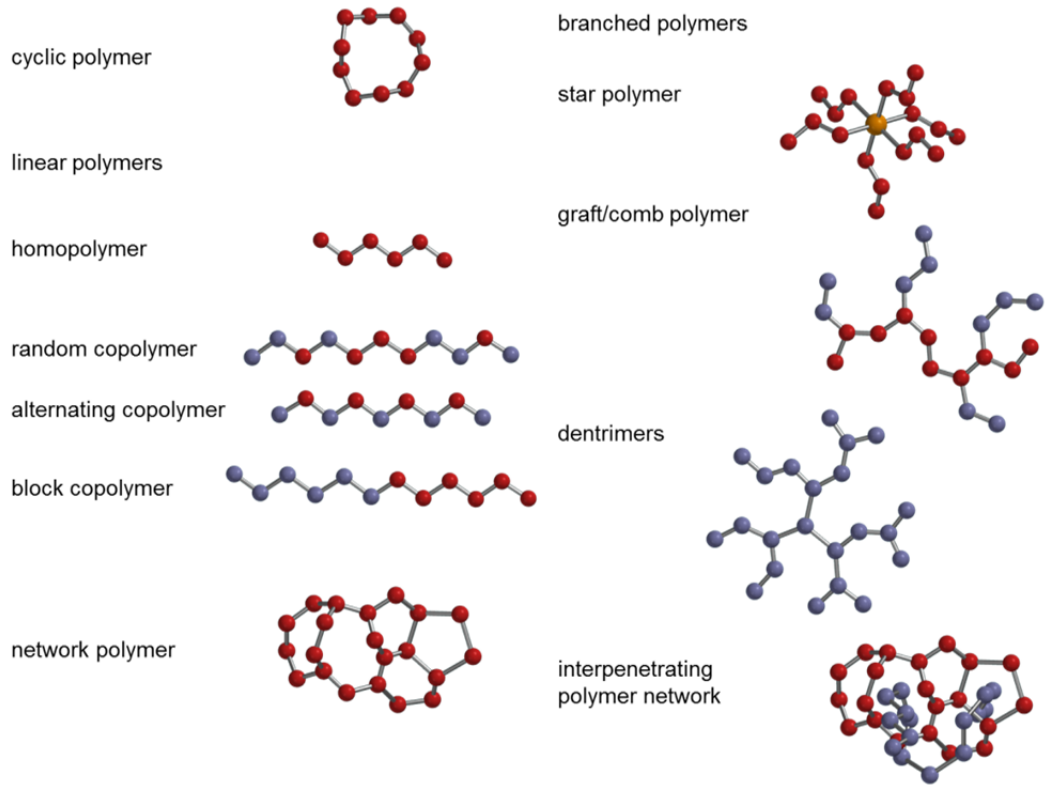

Figure 2. Schematic representation of different polymer topologies.[18]

The production of more versatile polymeric structures covering a wider range of properties is directly linked to the availability of synthetic methods in organic chemistry where it is possible to precisely synthesize designed molecules by a bunch of well established reactions. To design macromolecules with distinct properties, chemical and architectural aspects have to be considered.[20] The chemical aspects include the knowledge of the properties of individual structural units (monomers), three-dimensional aggregates (solid state structure, physical properties), solubility and bulk properties like crystallinity, melting temperature, glass transition etc.[18] Depending on the composition of the polymer different topologies can be achieved which can vary considerably the macroscopic properties (figure 2).

Mechanically Bonded Macromolecules

A special case of polymers which attracted considerable attention in the last decades are mechanically bonded macromolecules/polymers. Polyrotaxanes, polycatenanes, daisy chains and mechanically interlocked dentrimers are members of this family of non-covalently linked polymers or oligomers (figure 3).[21–24] Despite the fact that such constitutionally and topologically divers targets are of synthetic nature, proteins and DNA fragments are known to contain mechanical bonds as well.[25]

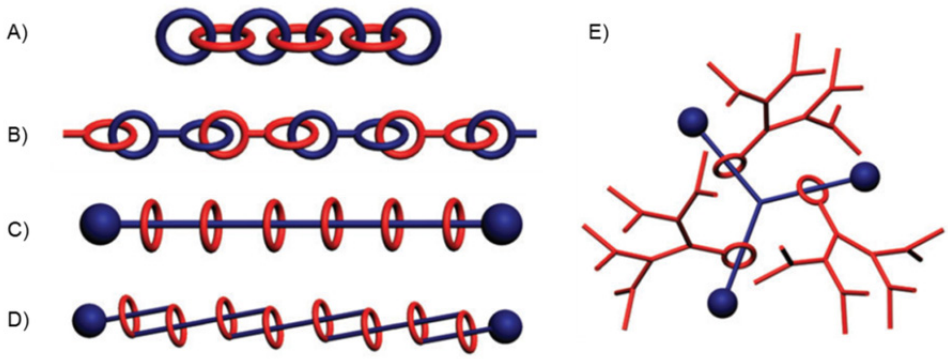

Figure 3. Non-covalently interlocked macromolecules; A), B) poly[n]catenane, C) poly[n]rotaxane, D) poly[n]daisy chain, E) mechanically interlocked dentrimer. Reprinted from Fang *et al*.[25]

In mechanically interlocked polymers the covalent bonds of traditional polymers are replaced by mechanical bonds often supported by non-covalent interactions of the subunits like for example hydrogen bonds, charge transfer and hydrophobic interactions. In some cases dramatic changes in their macroscopic properties are triggered by these non-covalent interactions.[23] Therefore they are an ideal example of how changes on the molecular level of materials can sophistically change their macroscopic properties. For example polyrotaxanes formed by encircling a linear polymer with cyclodextrins, which have a hydrophilic exterior

and a hydrophobic cavity, make them water soluble in contrast to the parent hydrophobic polymer.[26] Furthermore an improved shielding of the parent polymer caused by cyclic molecules can result in an increased stability against bleaching or oxidation or even in enhanced conductivities.[21] Maybe the most important changes in macroscopic properties of mechanically interlocked macromolecules are the alteration of viscosity[27,28], phase behavior[29] and exterior functionality[21] which lead to materials which are easier processable compared to most of the parent polymers.

Mechanically interlocked polymers are defined as molecules and not supramolecular complexes since at least one covalent bond has to be broken to separate the two parts.[23] It has to be mentioned that this definition is valid at standard conditions, because for example Vögtle could show a reversible, thermally activated threading of macrocycles with previously attached stoppers on the thread. While in polycatenanes the rings are interlocked, bulky stoppers or strong attractive intermolecular forces prevent polyrotaxanes and daisy chains from dethreading.[24] In principle the synthesis of the monomers is based on the threading of a linear molecule (thread) into a macrocycle. Subsequent cyclization results in catenanes (figure 4, right pathway) and coupling of bulky stopper units by chemical means to the linear axis to rotaxanes.[30] In daisy chain monomers the thread is covalently coupled to the macrocycle.

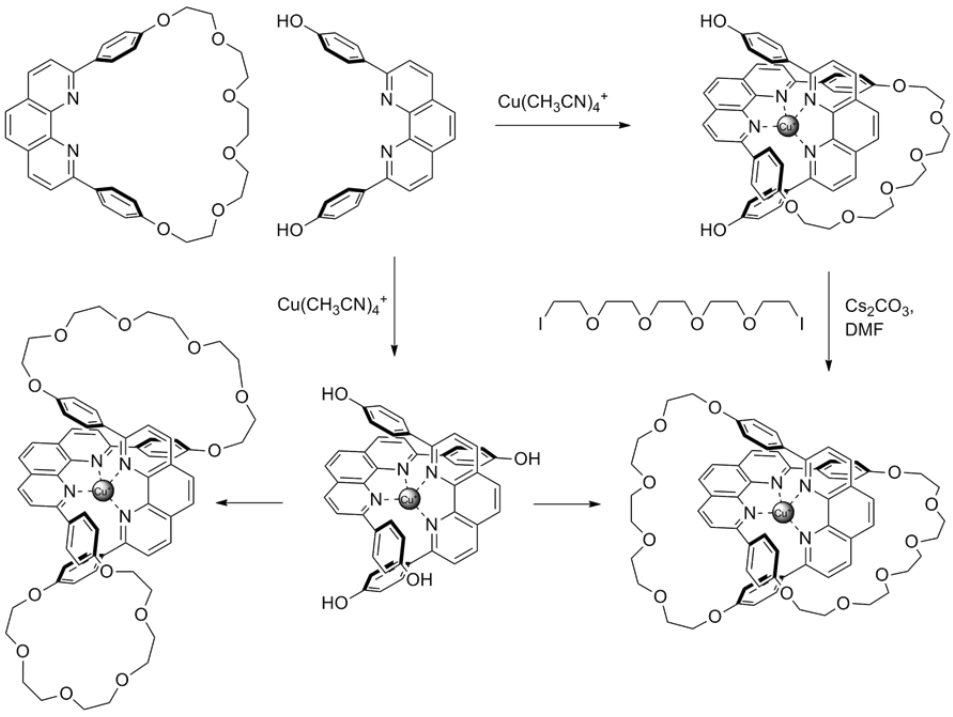

Figure 4. Representative example of the two synthetic strategies towards synthesis of catenanes. In this particular case the formation of well defined metal-complexes was used to preorganize the individual catenane parts.[31] The pathway shown at the bottom can also lead to undesired macrocycles (*bottom left*).

A second synthetic approach used to synthesize mechanically interlocked molecules is the formation of strong complexes (either metal or supramolecular complexes) of two linear precursors of the two different structural parts and final ring closure by complementary half circles (figure 4, left pathway).[18]

Emanating from the outstanding findings in host-guest chemistry more and more hosts for complexing neutral guest were developed which were more or less all used to synthesize catenanes or rotaxanes. The most prominent examples among them are cyclodextrins[32–34], crown ethers[35–37], cyclophanes[38–40], calixarenes[41] and curcurbiturils[42]. Some examples are shown in figure 5.

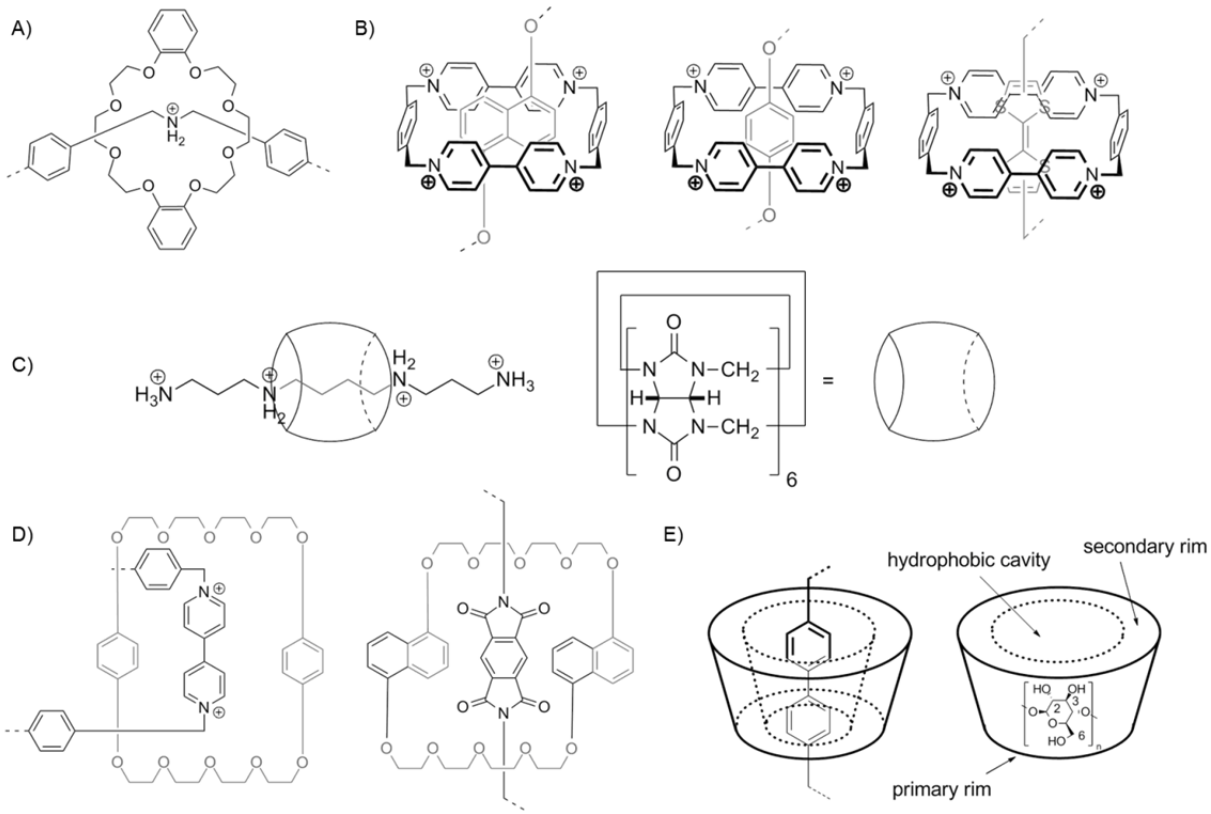

Figure 5. Examples of host-guest binding motifs used to synthesize rotaxanes and catenanes. A) crown ether/dibenzylammonium; B) cyclobis(paraquat-*p*-phenylene)/electron-rich guests; C) curcurbituril/dialkylammonium; D) crown ether/electron-deficient guests; E) cyclodextrin/aromatic guests.[22]

The use of supramolecular interactions enabled the assembly of molecular machines, rotors and shuttles.[43–45] By an external input the recognition sites are influenced which affects the binding affinity of the inclusion complex and therefore causes an internal motion of the cyclic host resulting in altered physical output. The delicate balance of the system is set off by the external stimulus and the system relaxes into a new thermodynamic equilibrium.

The challenge in preparation of oligo- or poly- mechanically interlocked molecules (MIM) mainly relies on the difficulty to prepare the MIM themselves which is not possible in gram scale up to date. Towards polycatenanes three synthetic concepts were followed: i) the spontaneous formation of mechanical bonds while building up the macromolecule; ii) covalent polymerization of already preformed MIM; iii) incorporation of mechanical bonds onto an already existing polymeric scaffold.[25] For the synthesis of oligo[n]main-chain catenanes only synthetic strategy i) is practical.[46] For the assembly of polyrotaxanes a higher diversity of synthetic routes were reported in literature.[47–50] Maybe the most straight forward assembly is the encircling of a linear polymer by either clipping the macrocycles after formation of supramolecular complexes of half circles or by threading-and-stoppering in analogy to the preparation of rotaxanes (figure 6).[25] The clipping procedure enables the use of dynamic covalent bonds which make the process reversible and therefore introduces error checking and proof reading. This approach is under thermodynamic control and thus the product distribution only depends on the stability of the final product.

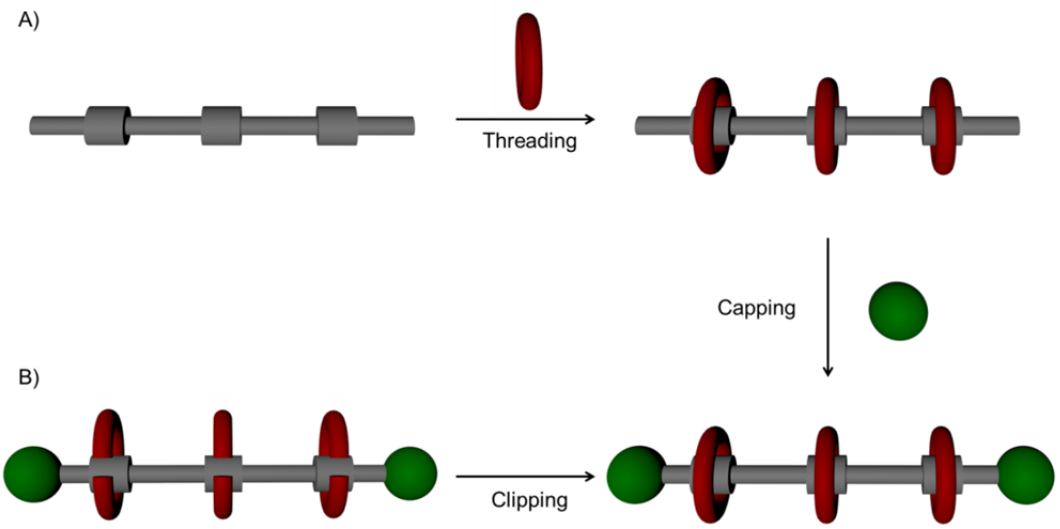

Figure 6. Conceptual approaches to the template-directed synthesis of polyrotaxanes. Method A: "threading-followed-by-stoppering" approach. Method B: thermodynamically controlled clipping approach.[51]

Also conventional polymerization of the thread of preformed rotaxanes as well as embedding the macrocycle in a polymer was used to successfully assemble main-chain polyrotaxanes. The same holds true for side-chain polyrotaxanes.[22] The same binding motifs as in the parent monomer rotaxanes were used to assemble polyrotaxanes including the combinations of cyclodextrin/polyethylene glycol[52–55], crown ether/electron-deficient binding sites[56–58], electron-deficient cyclophanes/electron-rich benzenes or naphthyls[59,60] to name just a few.

Polycatenanes and daisy chains are completely new macromolecules whose properties strongly depend on the composition and thus allow the alteration of the macroscopic properties by external physical inputs including switching and intrinsic motion.[22] Polyrotaxanes on the other hand are macromolecules where already known polymers are encircled by supramolecular hosts. Rotaxanation of polymers (thread) causes a change in hydrophilicity, better shielding, improved rigidity, better processability and polyfunctionality.[22,23]

The synthesis of defined mechanically bonded macromolecules is key towards new applications in all areas of research. The unique properties of such systems not only resulted in improvement of already existing processing techniques in polymer science but also in advances in molecular electronics[47], drug delivery[61], sensing[62] and tissue engineering[63] to name just a few. For example polyconjugated polymers which are able to conduct electric current are normally insoluble and not meltable and therefore difficult to process. Additionally they are sensitive against moisture, light and oxygen and tend to cross link. By insulation with cyclodextrins the molecular wires became water soluble and thus processable as well as more stable. Furthermore the stiffness of the system was increased which resulted in enhanced fluorescence.[47] The introduction of further functionalities on the macrocycles allowed for covalent drug binding. Cutting off the stoppers by enzymes allows drug release at a defined destination in human bodies and is therefore a promising approach towards more efficient therapies.[61] Furthermore the functionalities allow hydrogel and network formation which is a property that can lead to tissue engineering where long-term stable but hydrolyzable hydrogels are needed.[63] However, low overall yields and laborious, multi-step synthetic routes towards mechanically interlocked molecules, as well as the lack of control over the polymerization process are issues which have to be addressed before mechanically interlocked macromolecules will find their way towards applications.

A special case of mechanically interlocked macromolecules are daisy chains which potentially allow alteration of macroscopic properties by switching mechanisms on a molecular scale. An integral part of this thesis is the synthesis and aggregation investigation of a molecular rod comprising a water soluble macrocycle which is able to form daisy chains in aqueous solutions by making use of a strong hydrophobic effect. To gain detailed insight into the structure-property relationships of such supermolecules the following review was prepared.

Molecular Daisy Chains

Jürgen Rotzler and Marcel Mayor

In its original sense a daisy chain is a daisy (flower) garland where the stems are interlinked to form a chain or a chaplet (figure 7). The term daisy chaining is widely used in computer technology for the serial connection of hardware components leading to bus-systems. A molecular daisy chain is an array of identical molecules that consist of both a linear thread (guest) and a threadable macrocycle (host) which are covalently bound together – in principle nothing else than coupling of a rotaxane thread to the encircling macrocycle. Such monomeric units are called plerotopic, hermaphroditic, heteroditopic or self-complementary. Threading of the macrocycle by a linear section of another component mediated by intermolecular recognition – rather than intramolecular recognition (preventing "head-tail-biting) – leads to the formation of either cyclic or acyclic molecular arrays, so called daisy chains.

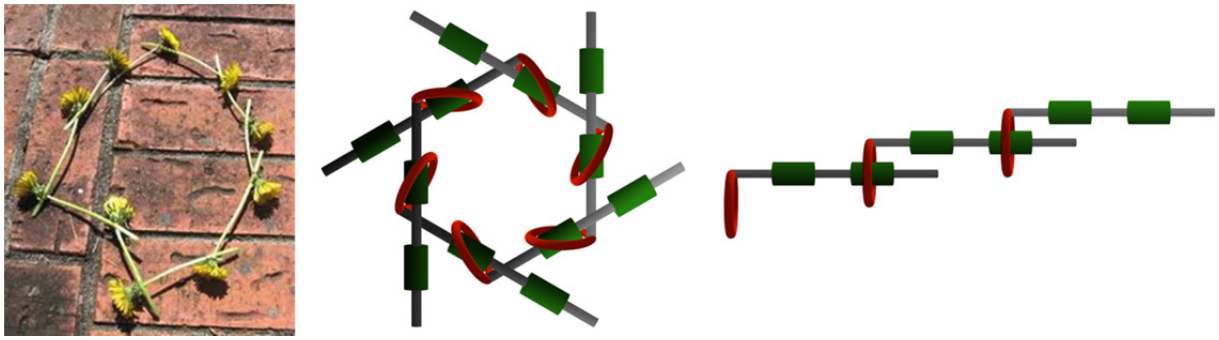

Figure 7. *left*: original daisy chain composed of flowers; *middle*: schematic representation of a molecular cyclic daisy chain; *right*: acyclic daisy chain.

In polyrotaxanes an already existing polymer is encircled with macrocycles to alter the macroscopic properties of the parent polymer. In contrast to this approach in systems like polycatenanes or daisy chains the mechanical bond is an integral part of the polymer chain.[22,25] Furthermore polyrotaxanes are composed of interlocked macrocycles which exhibit only a motional freedom of the cycle, whereas daisy chains and polycatenanes can alter the length of the polymer providing something like "elongation adaptability" (figure 8).[64] In principle self-complementary, plerotopic daisy chain monomers allow the formation of long mechanically bonded polymeric structures which exhibit a linear longitudinal mobility.[25] These integrated mechanical bonds can potentially lead to new polymers with entirely modified properties.

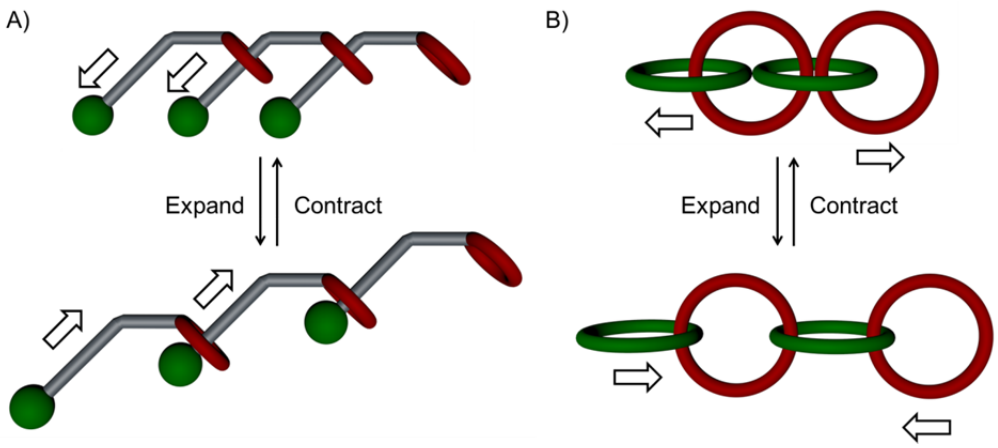

Figure 8. Possible internal elongation mobility of A) daisy chains and B) polycatenanes.[64]

This can result in unusual viscoelastic properties like a very large modulus loss, a low activation energy for the viscous flow and rapid stress relaxation. By careful design of the recognition sites and incorporation of different guests in one tail of the plerotopic molecules a by external input triggered intramolecular motion in daisy chains can be achieved which results in a controlled elongation mobility by switching mechanisms and therefore to potential formation of molecular actuators or even molecular muscles.[25] The fundamental question in preparation of daisy chains is whether the covalently interlinked hosts and guests form acyclic long oligomers or cyclic structures (figure 7).[65] By analysis of the stability of these two options the cyclized systems seem to be thermodynamically more stable than acyclic systems. Since for example in the smallest cyclic version consisting of two monomers where the guest of one monomer is complexed by the host of the second monomer and vice versa ([c2]daisy chain) in one supermolecule two stabilizing host-guest interactions are present in contradiction to the acyclic version where for two stabilizing interactions three monomers are needed (figure 9). Furthermore the formation of long acyclic daisy chains is an entropically unfavored process which can only be overcome if a high monomer concentration is used together with strong binding affinities.

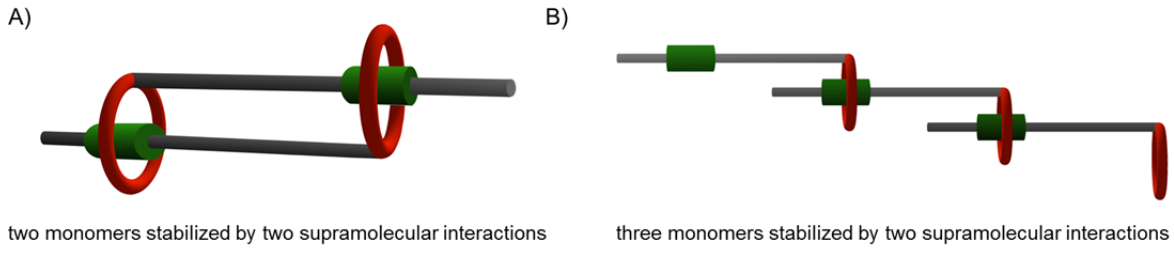

Figure 9. Host-Guest interactions in daisy chains. A) smallest possible cyclic daisy chain ([c2]daisy chain); B) acyclic trimeric daisy chain ([a3]daisy chain).

Despite two examples where once anion-templating[66] and once metal-templating[67] was used to construct daisy chains the synthetics efforts towards polymeric mechanically interlinked daisy chains were mainly focused on host-guest supramolecular interactions. Two binding motifs are reported in various publications which are the formation of inclusion complexes by hydrophobic guests into the hydrophobic cavity of cyclodextrins and complexation of dialkylammonium centers by crown ethers. The hydrophobic effect in polar solvents in the cyclodextrin motifs causes strong association in contrast to the crown ether-cation motif leaving more space for synthetic manipulations and therefore to more design possibilities.

Cyclodextrin Based Systems

Hirotsu, Fujita and Tabushi were the first who studied the formation of daisy chains in 1982 although indirect evidences were reported before.[68] They substituted *β*-cyclodextrins with a *tert*-butyl protected benzylic sulfide. Solid state structures of these plerotopic molecules confirmed that at higher aqueous concentrations the hydrophobic *tert*-butyl group was located inside the hydrophobic cavity of another *β*-cyclodextrin and superstructures like dimers, trimers and also polymers were present (figure 10). In solution it was shown that dimer was present up to a concentration of $2 \cdot 10^{-4}$ M, which already confirms the strong hydrophobic effect.

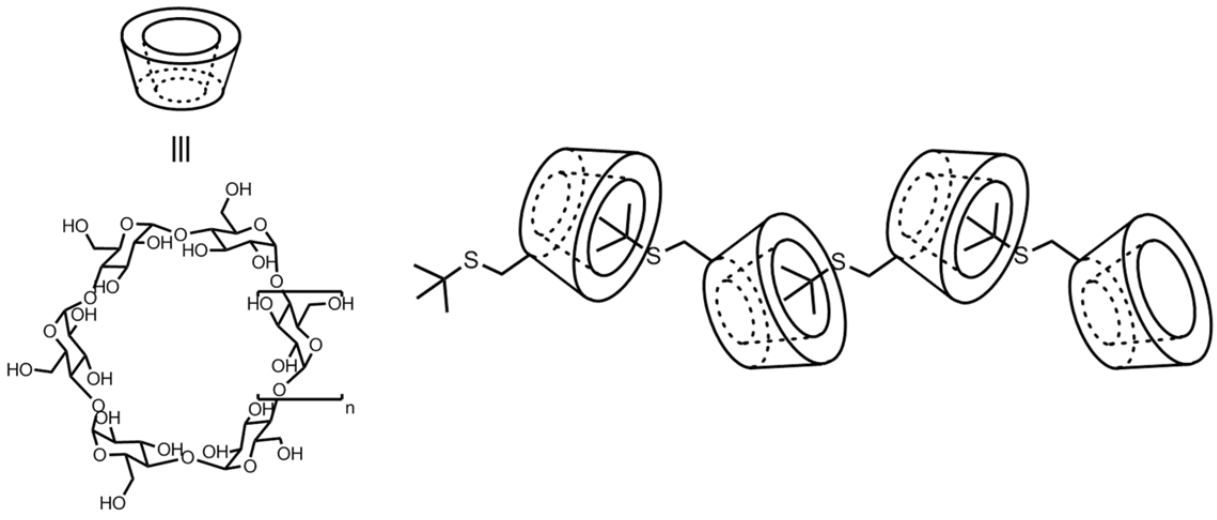

Figure 10. Linear acyclic daisy chain array of in 6 position *tert*-butyl sulfane functionalized *β*-cyclodextrins (n = 2). The *t*BuS groups are intermolecularly included in the hydrophobic cavity of the macrocycle.[68]

This study was further confirmed by crystal structures of other, for the use in modeling enzymes synthesized, modified cyclodextrins.[69] It was demonstrated that the hydrophobic linkers attached to cyclodextrins are incorporated into the cavity. The strong hydrophobic

binding of aromatic guests to cyclodextrins was used to assemble a variety of daisy chains based on this binding motif. Therefore Kaneda *et al*. coupled 4'-hydroxyazobenzenes to an in 6 position tosylated permethylated *α*-cyclodextrin (**R1a** – **c,** table 1).[70–72] The self-aggregation of the resulting plerotopic monomer was studied by ^{1}H-NMR-titration experiments and an aggregation number of $n = 2$ was found in water-methanol mixtures. 2D-NOESY-NMR confirmed the formation of a cyclic dimeric daisy chain ([c2]daisy chain) in a fixed structure. Fixation of the dimer was achieved by attaching 2-naphtol-3,6-disulfonic acid to the remaining free amines (figure 11).

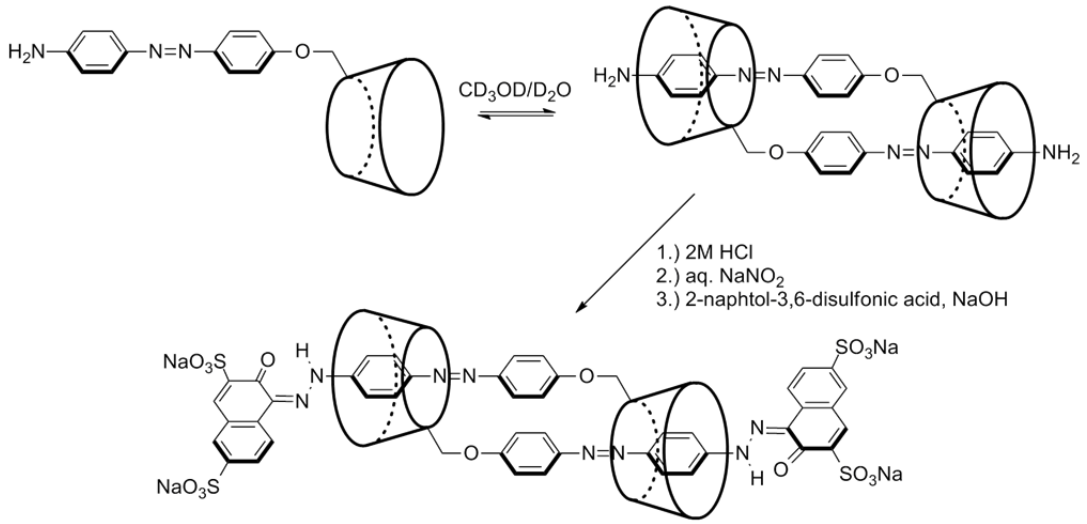

Figure 11. Self-aggregation of azobenzene substituted *α*-cyclodextrin. Attachment of 2-naphtol-3,6-disulfonic acid to the remaining free amines prevented deaggregation.[72]

The effect of *E*/*Z* isomerization in compounds **R1b** and **R1c** on the aggregation behavior was studied revealing that photoisomerization of the central azo-bond from the thermodynamic stable *E*-isomer to the *Z*-isomer caused a dissociation of the pseudorotaxane.[73] After thermal back-reaction the [c2]daisy chain was restored. The self-aggregation behavior was therefore dynamically controlled by an external physical input which resulted in a dramatic change in aggregate formation. Elongation of the rod (compounds **R2** and **R3**, table 1) provided mainly [c2]daisy chains, whereas for compound **R3** traces of a tetrameric complex were found by NMR.[70,71] Also 4,4'-diaminostilbene was coupled to an *α*-cyclodextrin (**R4**) which formed [c2]daisy chains in aqueous solution in a monomer:dimer ratio of 1:50 and a 65% yield after capping with 2,4,6-trinitrobenzenesulfonate.[74] By several analytic methods only the presence of dimer was observed providing further evidence that the cyclic dimer is the thermodynamically most stable oligomer. Additionally cinnamoyl amines and alcohols were used as tails for plerotopic cyclodextrin based monomers (**R5a** – **d**).[75–78] Interestingly the

different substitution pattern used where the tail was linked to the 3 position of α-cyclodextrin caused formation of supramolecular oligomers with up to 15 repeat units in aqueous solution (compound **R5c** and **R5d**) (figure 12).[77,78] The mean averaged molecular weight and the hydrodynamic radius of self-aggregated higher oligomers was determined by vapor-pressure-osmometry (VPO), mass spectroscopy and by determination of the self-diffusion coefficient with PFG-NMR.

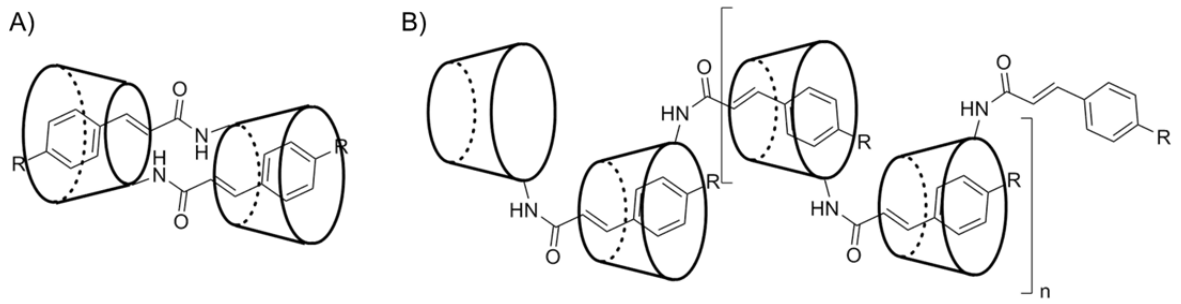

Figure 12. Formation of A) [c2]daisy chains by 6-cinnamoyl α-cyclodextrins and B) oligomers with n = 15 by 3-cinnamoyl α-cyclodextrins.[77]

The importance of the linking position on the cyclodextrin was demonstrated by studies on photoisomerizable stilbenes (**R8**).[79] Linking of *trans*-stilbene to the hydroxyl group in 2 position afforded double threaded dimers at high concentrations, whereas *cis*-stilbene obtained after photoisomerization gave acyclic oligomers. In contrast, linkage of *trans*-stilbene to the hydroxyl group in 3 position lead to formation of acyclic oligomers at high aqueous concentrations and *cis*-stilbene to [c2]daisy chains (figure 13).

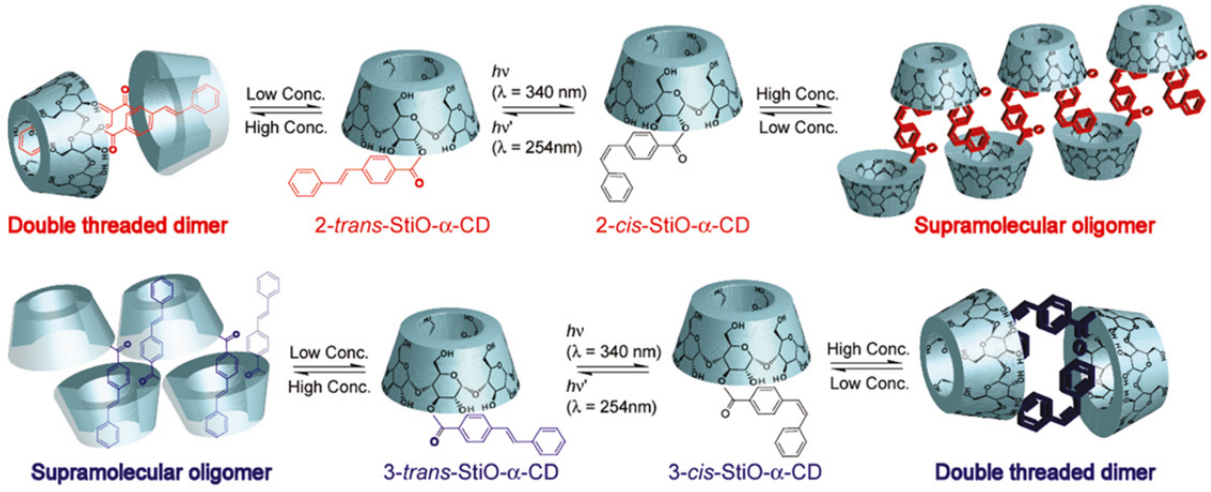

Figure 13. Aggregation behavior of in 2 or 3 position photoisomerizable stilbene functionalized α-cyclodextrins. Depending of the substitution position either the *trans*- or *cis*-isomers form supramolecular oligomers. Reprinted from Kanaya *et al.*[79]

Table 1. Studied *α*-cyclodextrins containing molecular threads.

Compound		Binding position	Aggregation number *n*
R1	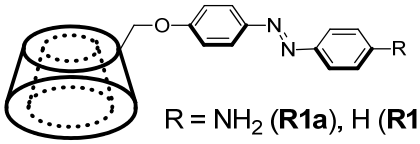 R = NH_2 (**R1a**), H (**R1b**), OH (**R1c**)	6	*trans* $n = 2$ *cis* $n = 1$
R2	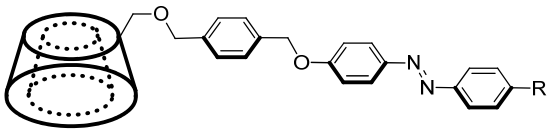 R = H (**R2a**), OH (**R2b**)	6	2
R3	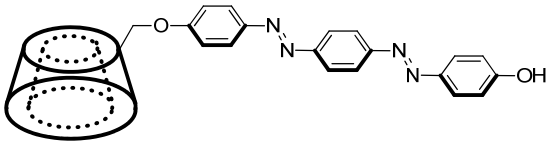	6	2, 4
R4	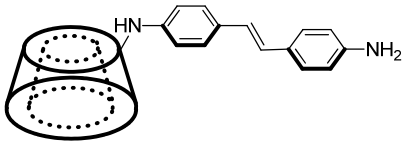	6	2
R5	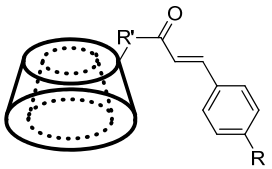 R' = CH_2O, R = H (**R5a**) R' = CH_2O, R = NH_2 (**R5b**) R' = NH, R = H (**R5c**) R' = NH, R = ^{t}Boc (**R5d**)	**5a,b** 6 **5c** 6 **5c** 3 **5d** 3	3 2 12 >15
R6	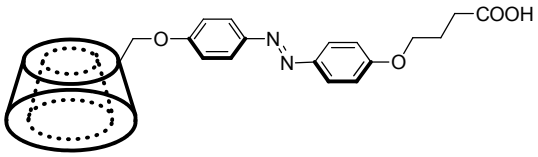	6	2
R7	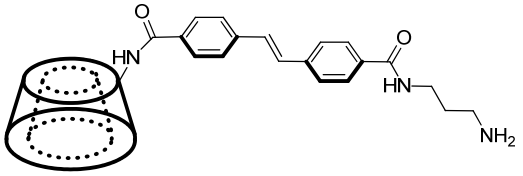	6	2

Table 1. continued

Compound	Binding position	Aggregation number *n*
R8 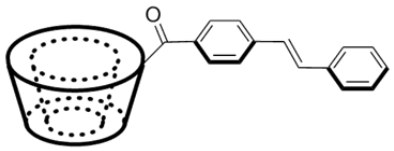	2	*trans* $n = 2$
	2	*cis* oligomer
	3	*trans* oligomer
	3	*cis* $n = 2$

Calixarene Based Daisy Chains

In contrast Floriani *et al*. modified calix[4]arenes with tungsten which was bound by the oxomatrix of this bowl-shaped molecular hosts.[80] This functionalization allowed not only the alteration of the calixarene shape but also further complexation of phenoxy groups which act as aromatic guest molecules (figure 14). By X-ray analysis the self-assembly in columnar structures of these compounds was shown. Since the tungsten complex blocked the oxo-side of the calixarene cavity no formation of cyclic dimeric species was possible. Engbersen and Reinhoudt demonstrated by merging the cyclodextrin binding motif with calix[4]arenes – functionalized with polyethylene glycols – to which a chromophore was attached in the opposed side to the oxomatrix that two possible superstructures are formed (figure 14).[81] One where the chromophore is incorporated into the cavity of the cyclodextrin intramolecularly which forms vesicles and a second one where poly[n]daisy chains are formed by intermolecular recognition leading to fibers.

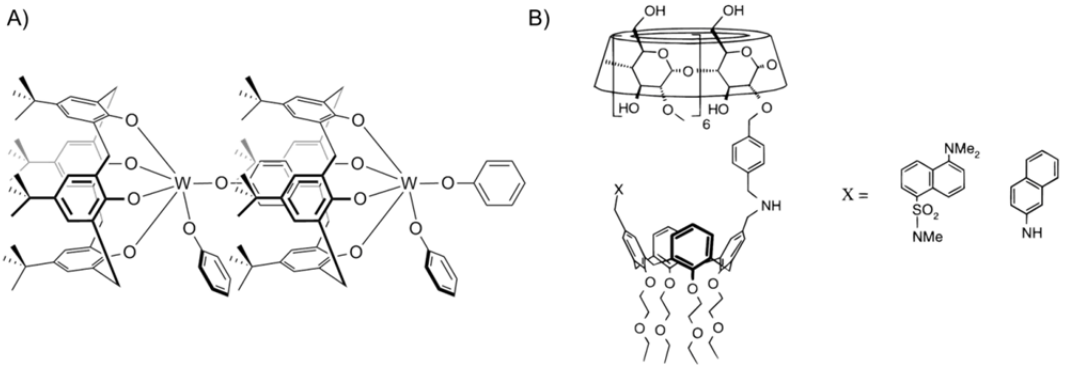

Figure 14. A) Tungsten functionalized calix[4]arene which forms columnar stacks in the solid state; B) merged cyclodextrin and calixarene motifs. Substituent X can either be included in the cyclodextrin intra- or intermolecularly.

Crown Ether Based Daisy Chains

The from molecular shuttles well known crown ether/dialkylammonium recognition motif was first utilized by Stoddart and Williams in 1998 to form daisy chains.[65] A 2-formyl mono-functionalized dibenzo[24]crown-8 ether was synthesized which was coupled with benzyl amine by reductive amination (**R9**, table 2). The heteroditopicity was established by final protonation of the free amine. In this study the methodology of daisy chains was introduced and the question came up whether such self-complementary molecules will form cyclic or acyclic chains. By solid state structures and mass spectroscopy the formation of cyclic [c2]daisy chains was confirmed in the solid state as well as in the gas phase (figure 15). The recognition in such binding motifs is based on cooperative stabilizing π-π interactions of the catechol units and by hydrogen bonds between $R_2NH_2^+$ and the polyether oxygens.

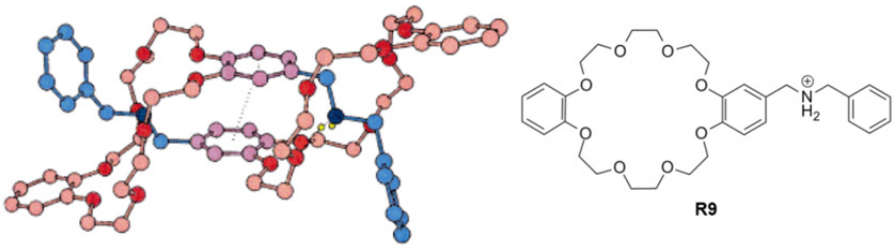

Figure 15. Crystal structure of a [c2]daisy chain formed by a plerotopic crown ether/dialkylammonium monomer (**R9**).[65]

The formation of [c2]daisy chains demonstrated the difficulty in generating infinite supramolecular arrays in non-covalent synthesis under thermodynamic control and therefore posed the question how to overcome enthalpic and entropic costs. Based on this study demonstrating the possibility of daisy chain formation using the mentioned recognition motif, several chemical modifications on the dibenzo[24]crown ether moiety as well as on the guest molecule were made to overcome the aggregation to the thermodynamically more stable [c2]daisy chain (also called Janus[2]rotaxane) (table 2; compound **R10** and **R11**).[82–84] Since a π-π stacking between the host catechol units was observed in solid state structures of the parent test molecule (figure 15) which potentially favored dimer formation, these units were replaced by phthalimides and the "tail" was exchanged to viologens (paraquat) (**R12** – **R14**).[82] By preventing the stabilizing interaction between two parts of the hosts, acyclic pentamers to dimers were detected by mass spectroscopy in solution. This finding was further confirmed by concentration dependent ^{1}H-NMR-shifts where a peak broadening was observed at high concentrations and UV/Vis spectroscopy which showed a nonlinear correlation of

absorbance with changing concentration and therefore gives evidence for aggregation. In contrast [c2]daisy chains were observed in the solid state structures. Additionally it was shown by Gibson *et al*. that expanding of the crown ethers cavity to dibenzo[32]crown-10 and using a rigid viologen-tail (compound **R15**) to avoid self complexation causes the formation of oligomers with up to 50 repeat units in a 2 M acetone solution (figure 16).[83] The observed signal broadening in ^{1}H-NMR at high concentration was related to the increased viscosity of the solution when polymers are present.

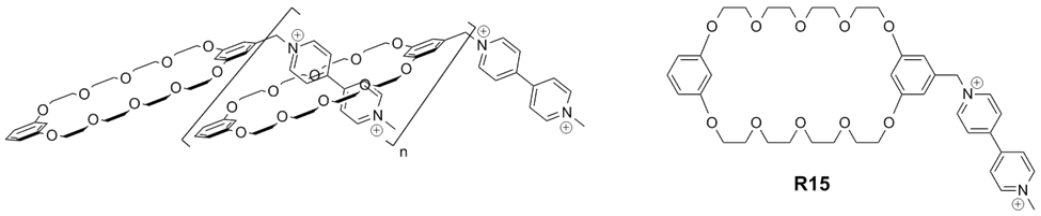

Figure 16. Formation of linear acyclic daisy chains with up to 50 repeat units by use of a crown ether/viologen binding motif.[83]

The inclusion of the viologen in the crown ether cavity was demonstrated by monitoring nuclear-overhauser-effects (NOE) of the viologen protons with protons inside the cavity. The presence of small cyclic aggregates was excluded by viscosity measurements and the higher viscosity compared to the unsubstituted crown ether. Because of their smaller hydrodynamic radius small aggregates should have a decreased viscosity compared to the linear aggregates. By differential scanning calorimetry (DSC) two glass transitions were observed which were higher than the reference system further supporting the formation of daisy chains with a higher extend of self-organization. Another important finding by using such binding motifs was the observation of diastereoselective dimer formation in the parent catechol-based crown ether host (figure 17) (compound **R9**).[84]

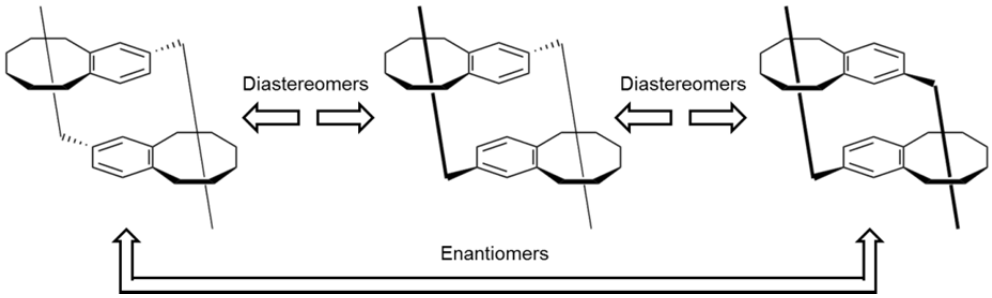

Figure 17. Schematic representation of the three stereoisomers which can form upon dimerization of compound **R9**.[84]

The stereoisomers arise from the prochirality of the interacting cations. The absence of *meso*-forms in the solid state arising from maintenance of opposed prochiralities was explained by the diastereoselective crystallization process.

Table 2. Studied hermaphroditic crown ethers.

Compound		Aggregation number *n*
R9	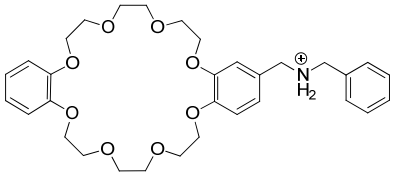	2
R10	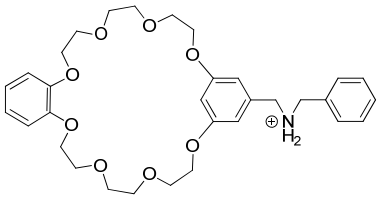	2, 3
R11	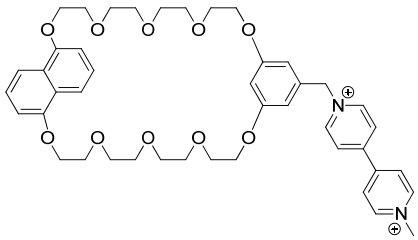	5 - 1
R12	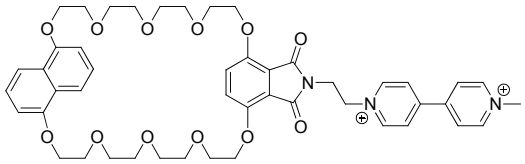	5 - 1
R13	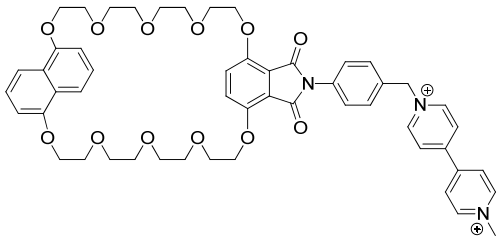	4 - 1

Table 2. continued

Compound		Aggregation number *n*
R14	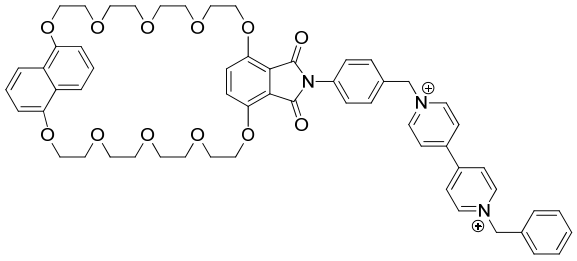	4 - 1
R15	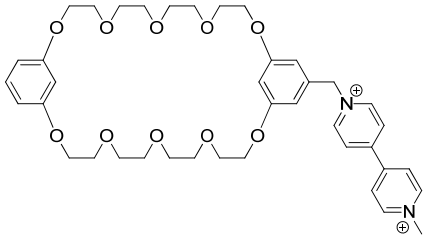	50
R16	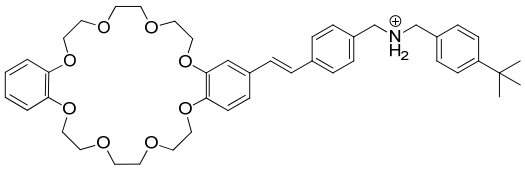	5
R17	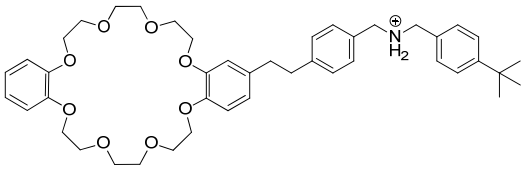	2
R18	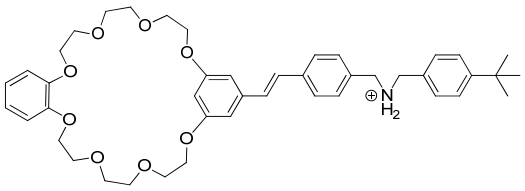	2, 3
R19	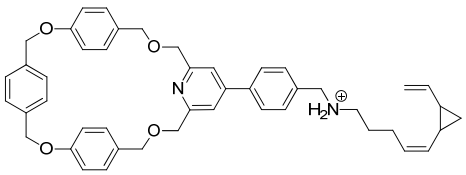	2
R20	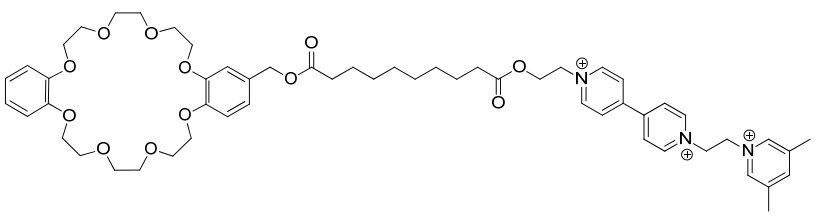	45

To overcome the aggregation of self-complementary head-tail monomers to the thermodynamically favored cyclic dimer several attempts were reported. Rowan and Stoddart used so called surrogate-stoppered rotaxanes to construct linear polymeric acyclic daisy chains.[64,85,86] This attempt makes use of the conventional covalent polymerization. Based on the dibenzo[24]crown-8 ether/dialkylammonium motif a crown ether mono-functionalized with an aldehyde on the catechol was threaded with a dibenzylammonium ion which was stoppered at one end with *tert*-butyl groups. After threading, the pseudorotaxane was capped with triphenylphosphine. By treatment with sodium hydride the phosphonium was converted into an ylid which was able to undergo a Wittig reaction with the aldehyde moiety attached to the host molecule (compound **R16**, **R17**, **R18**). After regenerating the binding site by addition of acid, aggregates from [c2]daisy chains to acyclic pentamers were obtained in dichloromethane depending on the concentration. At lower concentrations mainly [c2]daisy chains were observed because the macrocyclization was favored over the chain propagation (figure 18). At higher concentrations oligomers were obtained including 5 monomers (compound **R16**). Interestingly only cyclic species were detected when the reaction was performed in dimethylformamide, maybe because of the insolubility of the deprotonated intermediate.

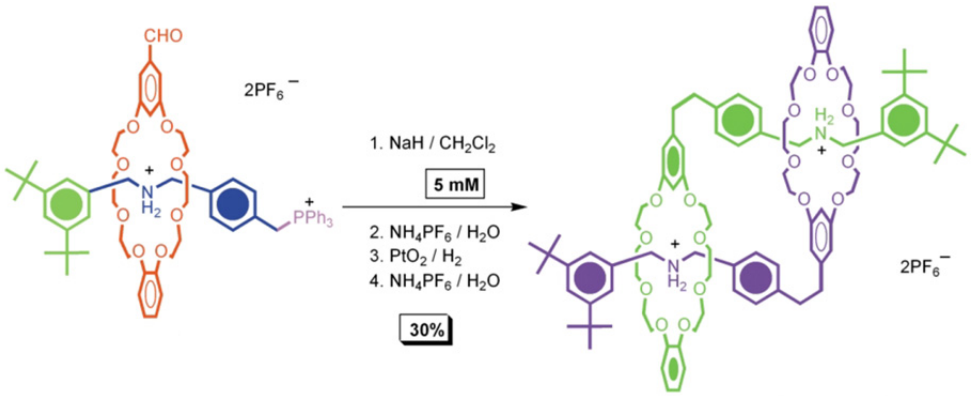

Figure 18. [c2]Daisy chain synthesized with the "surrogate-stoppered" approach. The preformed crown ether/dialkylammonium complex was capped with triphenylphospine and then cyclized by an intermolecular Wittig-reaction. Hydrogenation followed by restoring the binding site yielded [c2]daisy chains. Using similar conditions also yielded longer acyclic daisy chains with up to five repeat units. Reprinted from Chiu *et al*.[85]

The preformation of rotaxanes prior to interlinking them was also performed by using cyclobis(paraquat-*p*-phenylene) cyclophanes encircling a polyethylene glycol based thread containing two hydroquinone recognition sites.[87] Coupling of the functionalized cyclophane to one of the rotaxane stoppers afforded dimers. Repetition of this protocol has a high potential towards longer main-chain polymers. This assembling methodology was also used in

a method called threading-followed-by-polymerization. With an acid chloride mono substituted dibenzo[24]crown-8 ether was threaded with a 1,2-bis(pyridinium)ethane unit substituted with a hydroxyl group, followed by esterification (compound **R20**).[88] The temperature in the reaction was kept low to slow down the esterification and maximize the threading. Afterwards the temperature was raised to obtain full conversion (figure 19). By this acyclic oligomers including 45 monomer units were synthesized which was observed in UV/Vis, NMR and viscosity measurements.

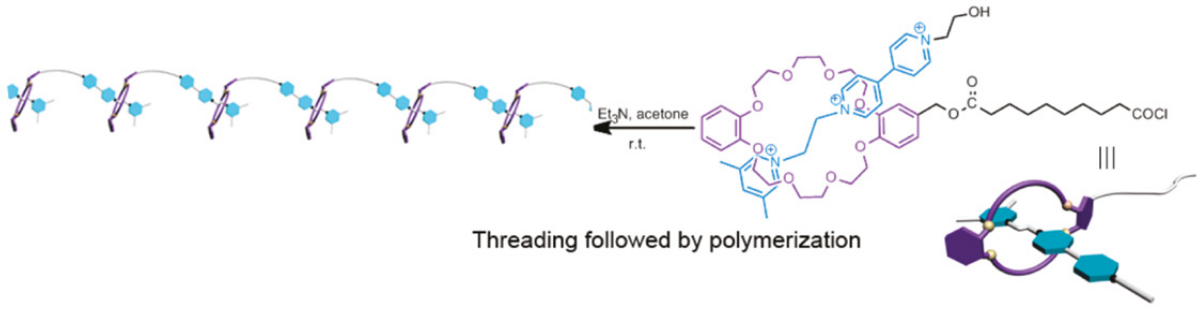

Figure 19. Schematic representation of the preparation of a long acyclic daisy chain with up to 45 repeat units. This threading-followed-by-polymerization approach is based on the polycondensation of a dynamic bifunctional pseudorotaxane. Reprinted from Zhang *et al*.[88]

In other studies it was proposed that making the host and the guest more rigid can avoid homo dimer formation. Even though this approach was unsuccessful and only [c2]daisy chains were obtained an interesting stoppering method was used, the so called threading-followed-by-swelling. For this the rigid tails were functionalized with dialkenylcyclopropanes and after aggregation heated to form a cycloheptadiene by a [3,3]-sigmatropic rearrangement (compound **R19**) (figure 20).[89]

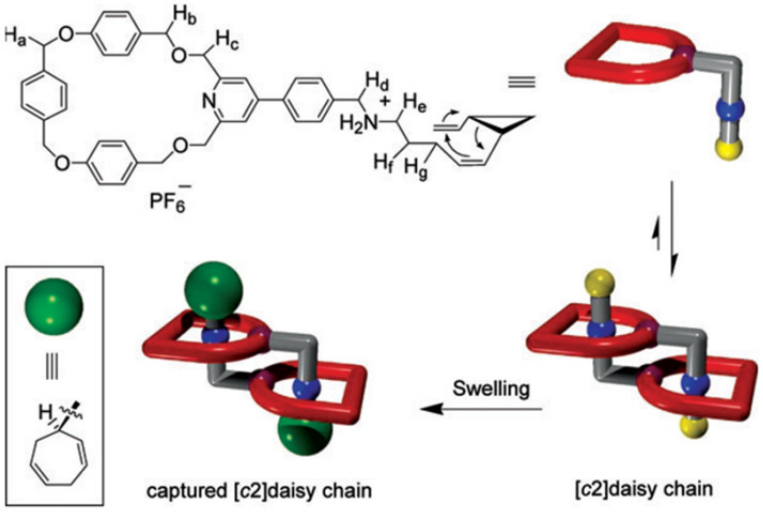

Figure 20. Fixing a preformed [c2]daisy chain by using a swelling approach. Reprinted from Ueng *et al*.[89]

The clipping methodology used for synthesis of poly[n]rotaxanes was also applied to assemble [c2]daisy chains.[66] To an isophthalamide based half cycle functionalized at the two ends with alkenes which can undergo ring-closing metathesis a hydrocarbon rod containing a 3,5-dicarbamoyl-1-methylpyridinium chloride was attached. The isophthalamide is then able to complex the chloride in apolar solvents. By ring-closing metathesis the macrocycle was "clipped" around the complexed thread which resulted in a product mixture of [c2]daisy chains and "self-biting" monomers (figure 21). Even though the yields of dimer formation were low, this approach represents a novel potential route towards mechanically interlocked molecules.

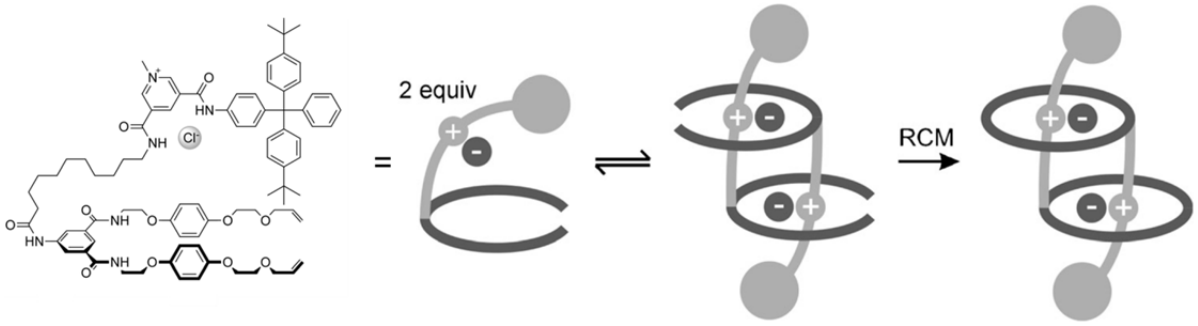

Figure 21. Schematic illustration of the synthesis of a pyridinium/isophthalamide [c2]daisy chain using an anion-templating approach. Reprinted from Evans *et al*.[66]

Molecular Muscles

A further dimension of material manipulation can be obtained by the inclusion of two binding motifs on the molecular thread. It is then not only possible to generate macromolecules where the mechanical bond is an integral part of the main-chain polymer but also to alter the properties by an external stimulus. In analogy to molecular shuttles, where two binding sites for a macrocycle are present in the thread of a rotaxane, the external stimulus can disturb the thermodynamical equilibrium leading to the movement of the macrocycle to the new global energy minimum. Therefore chemical, electrochemical or photochemical inputs can be converted to mechanical linear motion in [c2]daisy chains what leads to artificial muscular behavior due to the reversible contraction and extension (figure 22). [c2]Daisy chains are ideal candidates to investigate such processes because of their compactness, their kinetic and thermodynamic stability and the linear arrangement of the two threads with respect to each other. The dibenzo[24]crown-8 ether/dibenzylammonium binding motif was used to generate pseudo[c2]daisy chain rotaxanes.[90] The end standing benzyl was further functionalized with a benzylic bromide which enabled to cap the supermolecule with a 3,5-di-*tert*-butylbenzyl substituted paraquat to generate a kinetically stable [c2]daisy chain. In the favored co-

conformation the two hosts complexed the ammonium centers by [NH^+-O] hydrogen bonds. By deprotonation of the recognition site a migration to the paraquat station was obtained which caused a contraction of the [c2]daisy chain (figure 22). The process was monitored by ^{1}H-NMR where a downfield shift due to association of the two electron-poor paraquat units was observed. Reprotonation of the amine reversed the whole process.

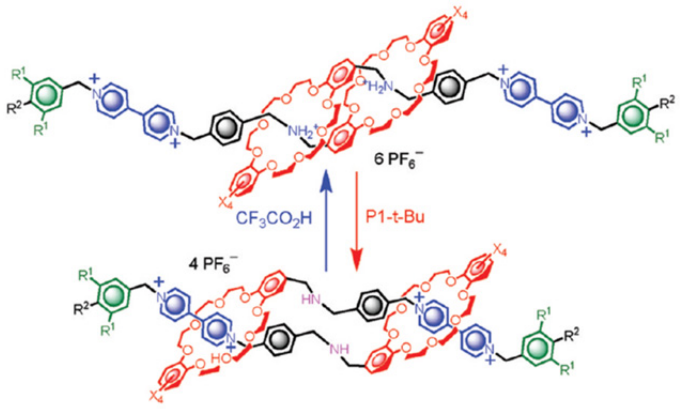

Figure 22. Acid/base switchable [c2]daisy chain. Reprinted from Fang *et al*.[91]

Up to 11 repeat units were obtained by an [AA+BB]-type conventional polymerization when the stoppers in this system were further functionalized with acetylenes.[92] For polymerization a copper mediated 1,3-dipolar cycloaddition between attached alkenyls and diazides was used. The averaged molecular weight and the polydispersity of the polymers obtained were estimated by Zimm-plot analysis from size exclusion chromatography. The switching mechanism was monitored by ^{1}H-NMR, UV/Vis and cyclic voltammetry. Quantitative, efficient and reversible switching in solution was observed of the oligomer where the contraction/extension was even faster compared to the "monomeric" [c2]daisy chain. The contraction and extension were identified as the rate limiting steps which are slower than the acid/base reaction. This approach is a perfect example that correlated molecular motion in oligomers is possible and therefore can be regarded as a first step towards conversion of molecular properties to the macroscopic scale.

Based on the observation that heteroditopic cyclodextrins can form [c2]daisy chains with azobenzenes and that photochemical *E*/*Z* isomerization leads to dissociation of the pseudorotaxanes, the described systems were capped with bulky anilines and then polymerized with *para*-bis(bromomethyl)benzene to obtain oligomers including up to five [c2]daisy chains.[93] The stoppers and the *N*,*N*-linkage prevented dethreading of the *Z*-isomer when photochemically switched. The *Z*-form is significantly shorter than the *E*-form which

results in contraction of the oligomer by irradiation and can therefore be regarded as the first light-driven molecular muscle (figure 23).

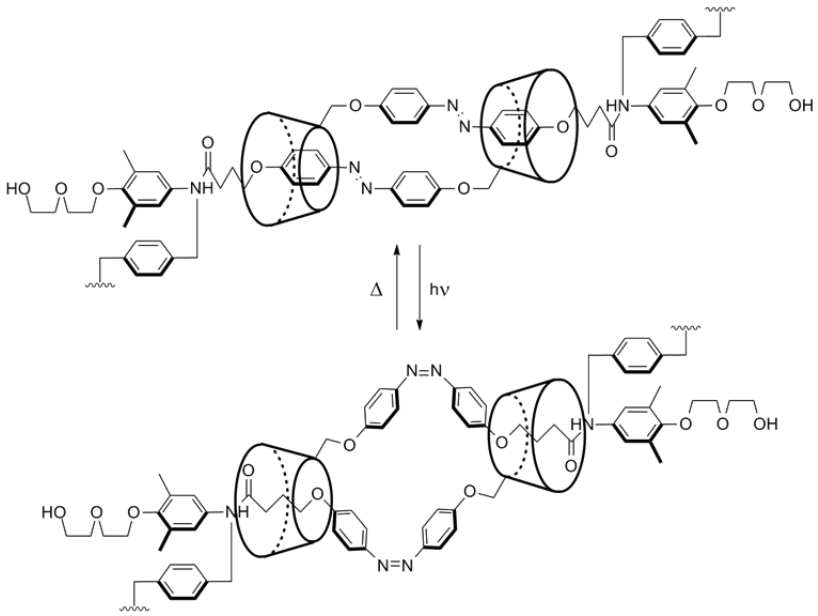

Figure 23. Light-driven molecular muscle based on azobenzene functionalized *α*-cyclodextrins.[93].

The same was possible by photoisomerization of stilbene based cyclodextrin [c2]daisy chains.[94] By photoisomerization the *trans*-stilbene was converted into the *cis*-form which caused a slipping of the cyclodextrin towards the alkyl chains attached to the stilbenes.

The very first example of artificial molecular muscles was based on a metal-templating approach and represents until today the [c2]daisy chain system with the highest contraction efficiency.[67] Sauvage and co-workers coupled a linear, bidentate phenanthroline moiety to a macrocycle containing a second phenanthroline binding site. The monomers were templated by addition of Cu^{I} to form a [c2]daisy chain where the bidentate ligands form a tetrahedral metal complex. The linear rods where then capped by a terpyridine substituted 4-(*tris*(4-(*tert*-butyl)phenyl)methyl)phenol to install the second – in this case tridentate – binding site. Metal exchange promoted by potassium cyanide, and subsequent addition of Zn^{II} resulted in a penta-coordinated metal complex between the bidentate ligands of the macrocycles and the terpyridine stations (figure 24). By this the whole system was contracted by an amazing 27% which is in the dimension of natural muscle contraction.

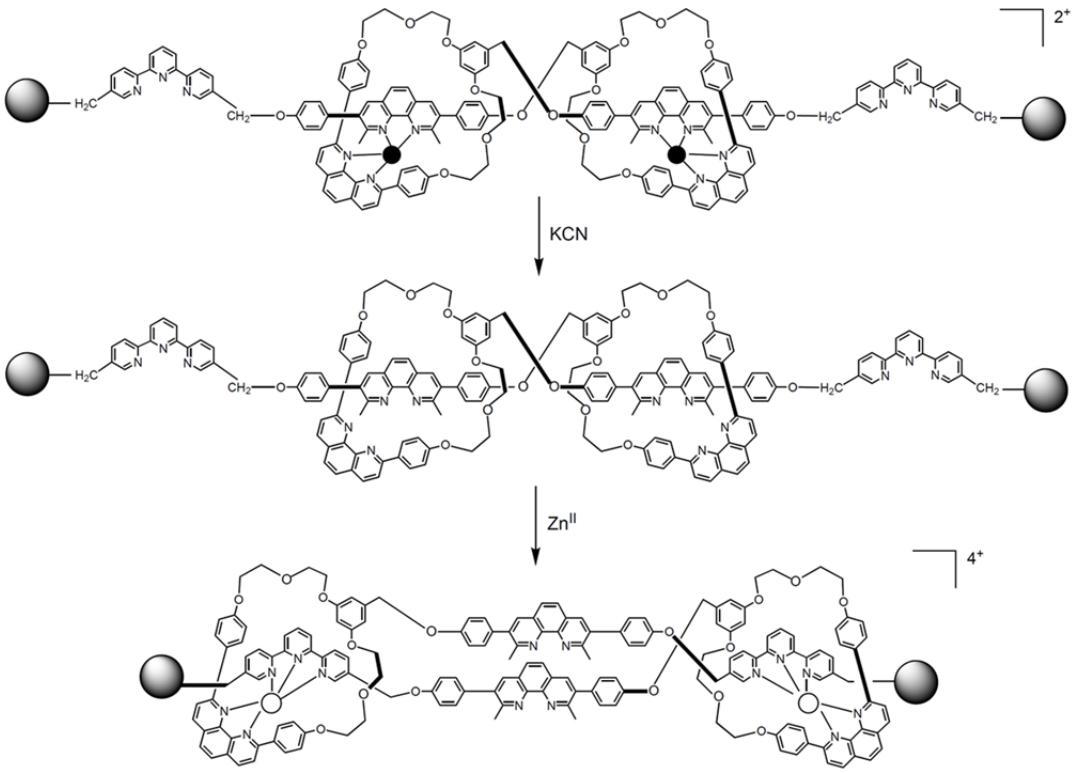

Figure 24. First reported unimolecular muscle by Sauvage *et al*.[67]

Molecular Design Analysis

By careful analysis of the systems used to prepare poly[n]daisy chains it is possible to gain evidence which structural features are necessary to obtain oligomerization (table 1 and 2). Functionalization of the cylindrical cyclodextrin structures in 6 position – the smaller side of the cavity – results almost exclusively in formation of [c2]daisy chains (table 1). In contrast to this, functionalization with a rigid rod in 3 position on the secondary hydroxyl side leads to oligomer formation as found by Harada *et al*.[77] Furthermore in all modified cyclodextrins the molecular tail enters the hydrophobic cavity from the primary hydroxyl side which can be explained by the formation of a stronger supramolecular inclusion complex. As a result the rods coupled in 6 position enter the cyclodextrin cavity from the primary hydroxyl side which places the second rod in ideal position to form stable [c2]daisy chains and therefore to find its thermodynamic global minimum. If the rod is included from the secondary hydroxyl side the reversibility of the system prevents formation of long acyclic species (figure 25). The same situation occurs if the molecular tail is placed in 3 position, but in contradiction the formation of cyclic dimers is now thermodynamically not the most favored situation which causes again deaggregation because of the reversibility of the system (figure 25). Inclusion from the

primary hydroxyl side of the cyclodextrin can be therefore seen as the first propagation step towards oligomers. The dynamic behavior thus leads to self-healing oligomers.

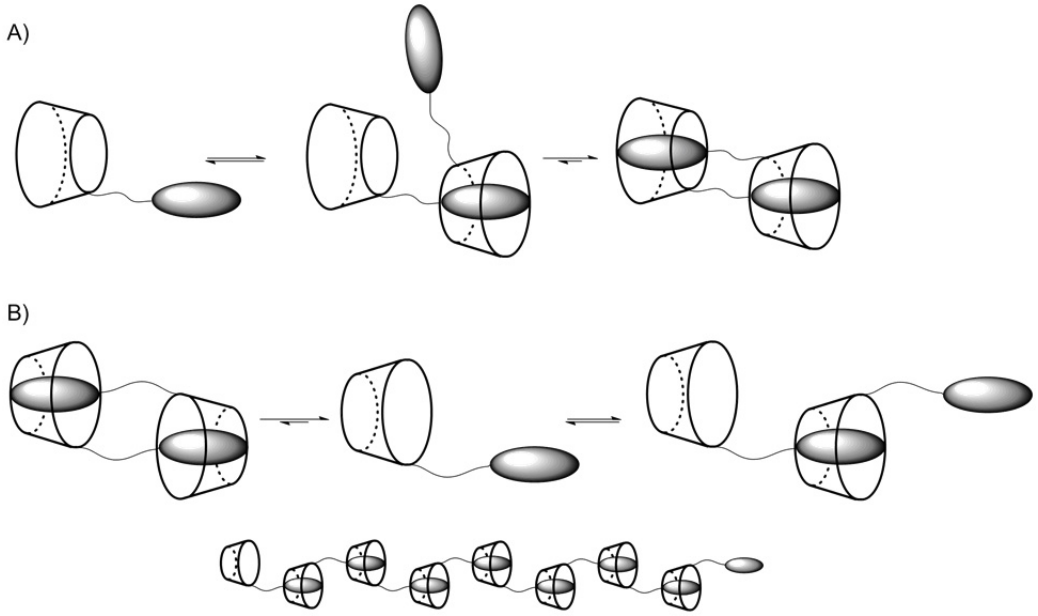

Figure 25. Schematic illustration of the aggregation behavior of hermaphroditic cyclodextrins with: A) thread attached in 6 position; B) thread attached in 3 position.

Also the rigidity of the rod seems to play a major role since the attachment of stilbenes, azobenzenes and cinnamoyls on the primary alcohol in 6 position leads to cyclic dimer formation. Unfortunately no example is known were a rigid molecular rod is attached on the secondary alcohol in a benzylic position. Therefore no conclusion can be drawn about the influence of such a flexible part in the molecular rod.

The situation in case of the crown ether based hermaphroditic molecules is somehow more complex since no discrimination of one side of the cavity can be expected. Comparison of the systems used as ditopic monomers (table 2) provides some indications about the structure-property relation of such compounds. While compound **R16** forms pentamers compound **R17**, being the dehydrogenated version of **R16**, only forms [c2]daisy chains. Therefore the presence of rigid rods as threads which somehow can prevent perfect inclusion seems to be crucial for the ability to form oligomeric superstructures (figure 26, A) and B)).

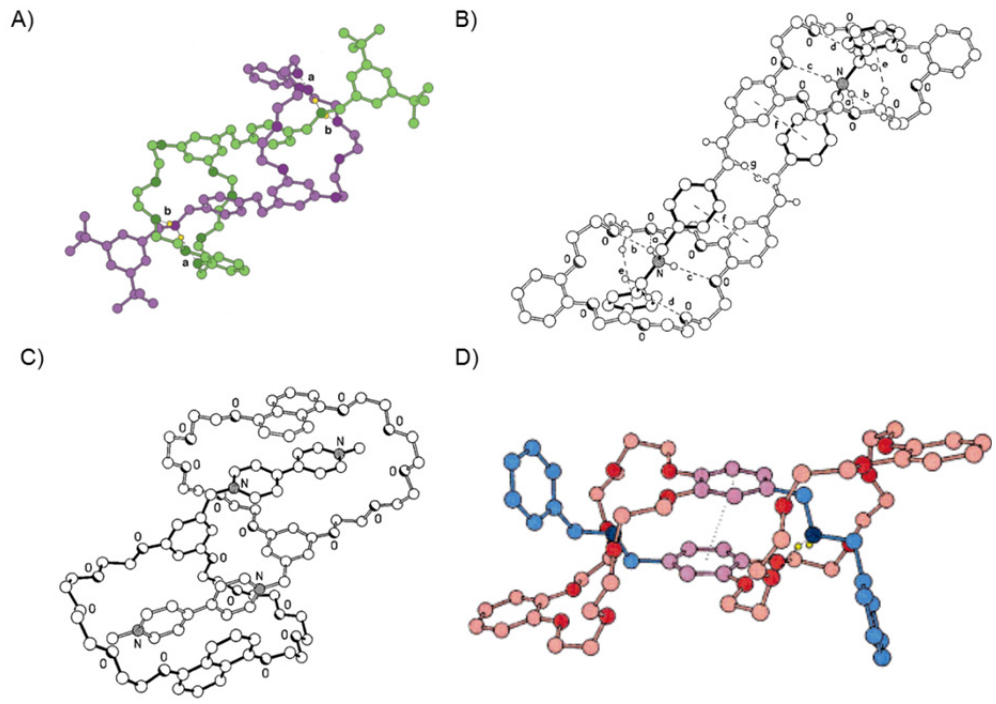

Figure 26. Solid state structures of compound **R17** (A),[85] **R16** (B),[95] **R11** (C)[82] and **R9** (D)[65] displaying the different stabilizing interactions between the host and the guest.

The exchange of catechols (compound **R9**) by 1,5-dihydroxynaphthyl units (compounds **R11** – **R14**) results in formation of pentamers. Solid state structures showed that the naphthyl moiety is able to complex the electron-poor paraquat tails by π-π stacking, and the resorcinol units stabilizes the tail by edge-to-face interaction (figure 26, C)).[82] No interaction in the solid state structure of compound **R11** between the two resorcinol moieties can be observed in contrast to compound **R9** where the two functionalized catechols stack with each other (figure 26, C) and D)).[65] Thus prevention of the host-host interaction seems to enhance the probability for formation of acyclic aggregates. The same holds true for compounds **R12** – **R14** where the phthalimide units prevent host-host stacking. The reason why hermaphroditic compound **R15** forms daisy chains with aggregation numbers up to 50 remains unclear. Unfortunately only in a few cases the association constants were determined and therefore no conclusions about the stability of these complexes can be drawn. The inclusion complex in **R15** seems to be stable enough to overcome the entropic costs of oligomer formation. Even for compound **R20**, which contains a long aliphatic part and hence not a rigid rod, long oligomers were observed, but in this case a different synthetic route was chosen making it impossible to compare the system with others (figure 19). Nevertheless, indications were gained that preventing host-host interactions and the rigidity of the tail considerably influence the ability to form higher daisy chain aggregates. Furthermore the size of the cavity and the

stability of the inclusion complexes seem to play an important role in the formation of oligomeric species. Thus a perfectly designed ditopic monomer should in principle consist of a well defined cavity which allows strong host-guest interactions to overcome the entropic costs of polymerization. In an ideal case the inclusion complex is formed by an induced complexation like change of solvent, structural change of the cavity by an external trigger or external stimulation of the thread. Furthermore the molecular rod should be rigid and only weak host-host interactions should prevent [c2]daisy chain formation. As in the case of cyclodextrin systems discrimination of complexation from the side of the cavity where the tail is attached should also lead to formation of higher oligomers (figure 27).

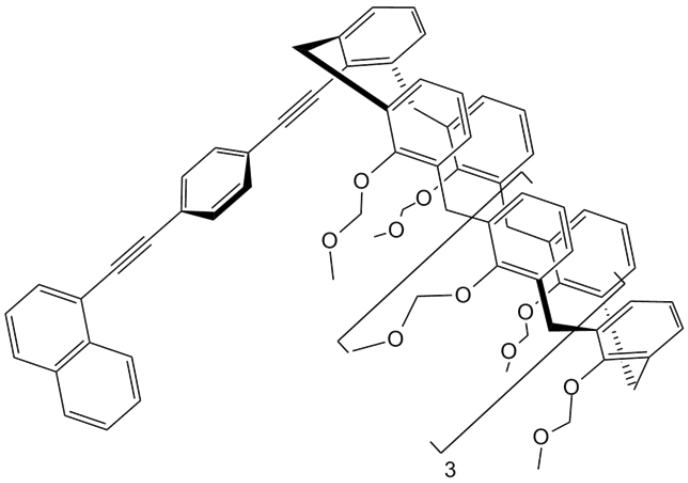

Figure 27. Proposed hermaphroditic molecule with a well defined cavity, a rigid thread and a cavity which potentially allows threading from the unfunctionalized side of the cavity. The driving force for complexation is the hydrophobic effect which occurs by dissolving in water.

Nevertheless, the assembly to [c2]daisy chains is thermodynamically favored and therefore more precise. Polymerization of such dimers using conventional covalent coupling allows the preparation of well defined oligomers and is thus maybe the most promising route towards novel functional materials.[92,93]

Arising from these structure-property relations we designed a host-guest system where the driving force for complexation is the hydrophobic effect like in the cyclodextrin systems. It largely contains a rigid molecular rod, a well defined size of the cavity and allows for alteration by introduction of substituents. The first results of these investigations are summarized in the following section.

Synthesis and Aggregation Studies of an Amphiphilic Molecular Rod

Jürgen Rotzler and Marcel Mayor

Introduction

One of the main targets of material science is the conversion of macroscopic physical phenomena into altered and tailored phenomena with a specific physical output. Therefore the macroscopic input has to induce a change on the microscopic level of the investigated material which then provides the desired physical output. Such changes in the molecular dimension can be of structural[96], conformational[97–102], electrochemical[103], photochemical[104,105] nature or in the intermolecular arrangement of molecules.[106–108] Current research in surface and polymer science is thus focused on the development of such new potential structures which are able to fulfill the desired needs of providing for example more scratch-resistant lacquer and plastics,[109] conducting plastics[110,111] or self-cleaning surfaces[112] to name just a few. One of the major drawbacks in polymer science is that for each different purpose a completely new macromolecule has to be synthesized starting from increasingly complex monomers. To overcome this time consuming and challenging problem secondary interactions (hydrogen bonding, hydrophobic effects, π-π-stacking or van der Waals interactions) were used to assemble oligomeric or polymeric structures by mechanical bonding.[113] Due to the reversibility of these dynamic aggregates these regimes are thermodynamically controlled. This in turn can lead to self-healing as incorrect chain extensions can be reversed since the system strives for energy minimization.[114] Furthermore the thermodynamic control of chain propagation allows precise chemical engineering on a supramolecular scale by changing the external conditions used for the propagation reaction.[113–115] As a positive side effect only monomers have to be synthesized. Studying and understanding the aggregation behavior allows for the development of suited reaction conditions to form diverse architectural devices.[116,117] Various recognition motifs were introduced to achieve such daisy chain polymers where in all cases a photo- or electrochemical input was used to generate internal motion. None of the examples in literature feature a structural motif that allows altering the physical output by internal motion. Therefore we report an inversed recognition motif where the complexation behavior of neutral aromatic compounds to water soluble Diederich-type cyclophanes was used.[118,119] In this case the driving force for assembly is the hydrophobic effect and allows complexation in polar solvents like water or alcohols. Investigations of Anderson *et al*. showed that such cyclophane

structures are able to form rather strong complexes in polar solvents with oligophenylene-ethynylene molecules (OPE) ($K_a = 2.7 \cdot 10^4$ M^{-1}).[120–122] In this project it is of interest how such OPE comprising a terminal loop aggregate in water and if daisy chains differing in length can be observed by just variation of concentration. If a defined assembly can be obtained, like in example [c2]daisy chains, it will then be of interest to functionalize the monomers such that by a simple reaction higher oligomers can be synthesized resulting in a higher control of molecular architecture. Moreover the inversed binding motif in principle allows alteration of physical outputs by applying mechanic stress in stark contrast to the systems known up to date where altering internal motion was the initial aim.

The synthesis and self-aggregation studies of the monomer **A1** (figure 28) is presented to provide a platform for future investigations on mechanically bonded oligomers or even polymers. The design of target compound **A1** profits to a large extend from the outstanding work of Diederich *et al.* (figure 28, B)).[118,119,123–125] Similarly to this proceeding work, two diphenylmethane units function as rigid spacers and cavity walls. The introduced quaternary amines provide the water solubility of the cyclophane; by varying the counterions the solubility can be fine-tuned. From solid state structures it is known that these quaternary amines are located remotely from the cavity and the oxygens are faced outwards, away from the cavity, making it hydrophobic – a necessity for the final supramolecular assembly. The size of the cavity is defined by the length of the interlinking alkyl chains between the two diphenylmethane units. According to studies of Diederich a propyl chain was chosen, which gives the cavity a size large enough to complex benzene cores.[118] Molecular complexation of neutral substituted benzene guests in aqueous solution is driven by a strong hydrophobic effect.[119] Therefore a hydrophobic oligophenylene-ethynylene rod is linked to the mono-functionalized cyclophane via a benzyl-group which gives the host system further additional flexibility and hence allows for a perfect thermodynamically driven binding of the guest (figure 28).

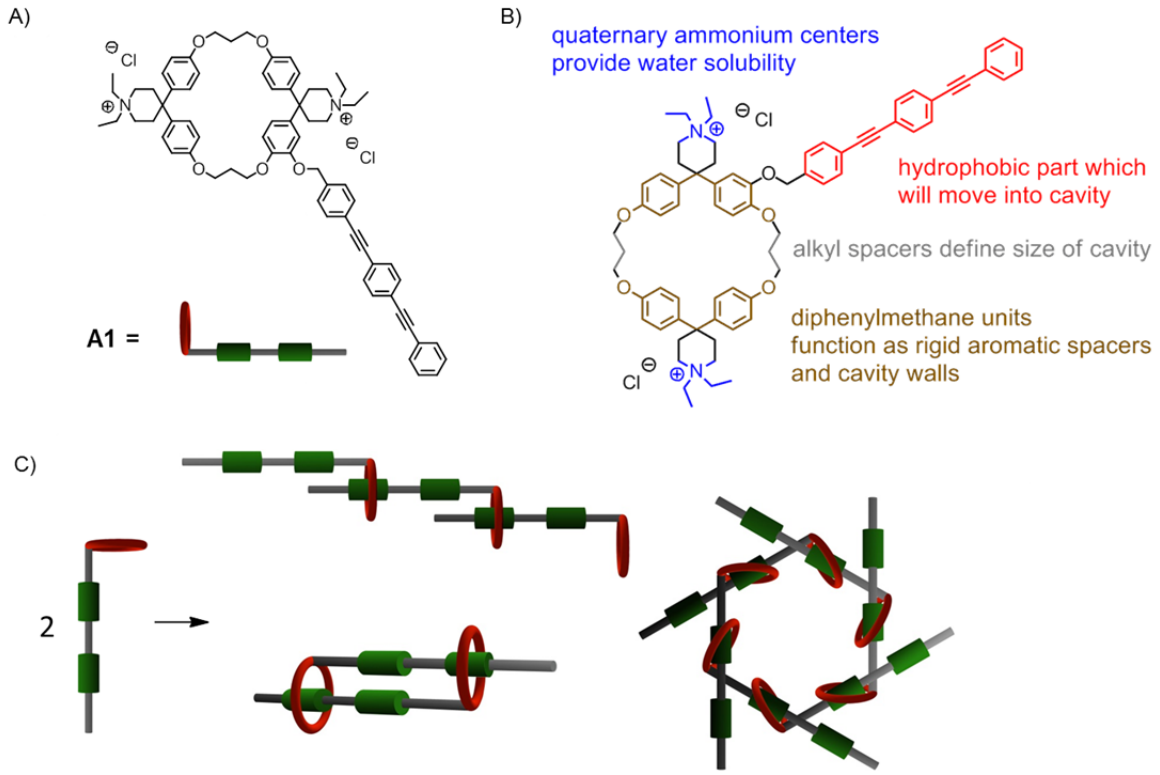

Figure 28. A) Hermaphroditic monomer **A1** with inversed recognition motif. B) structure-property relationship of the target amphiphile **A1**. C) Possible aggregates formed in polar solvents.

Retrosynthetic Analysis

The synthesis of such a complex target structure can be carried out in many different ways. In a retrosynthetic aspect the most straight forward disconnection is the division of target structure **A1** in the alkylated cyclophane unit **A3** and the oligophenylene-ethynylene (OPE) **A5** (**A**) (scheme 1). The introduction of the OPE **A5** at the last step of the synthesis opens up the possibility to alter the length or the functionalization of the OPE rod in rapid and simple fashion. However, the tetraethylated cyclophane **A3** has the tertiary amine **A4** as a precursor for which chemoselective ethylation (**B**) in presence of a free phenol is likely to be tedious. This then would make the introduction and cleavage of protection groups on the phenolic hydroxyl group necessary leading to manipulation steps at the late stage of the synthetic route. A coupling of the OPE subunit **A5** prior to the ethylation step (**C** and **D**) makes these protecting steps unnecessary.

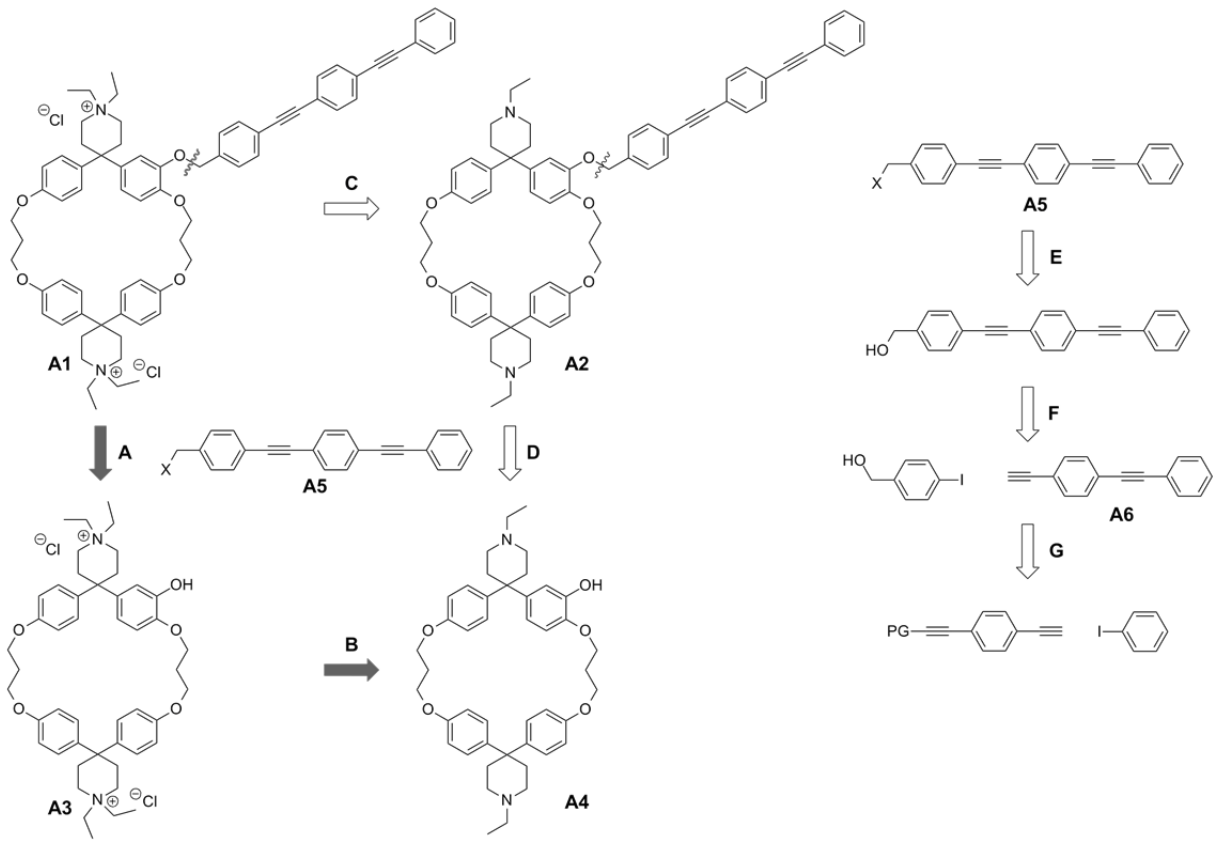

Scheme 1. Retrosynthetic analysis of the assembly of the loop subunit and the molecular rod (**A – B** and **C – D**) (*left*) and a possible assembly of the OPE **A5** (**E – G**) (*right*). PG = protecting group.

For the synthesis of the OPE rod **A5** a variety of different strategies based on classical Sonogashira cross-coupling reactions are literature known.[126] One of different possibilities is displayed in scheme 1, including an Appel-reaction to convert a benzylic alcohol to the benzylic bromide (**E**) necessary for etherification with the cyclophane **A3** or **A4**. The benzylic alcohol can be obtained from OPE **A6** and commercially available 4-iodobenzyl alcohol (**F**). For the synthesis of OPE **A6** a Sonogashira cross-coupling of mono-protected 1,4-diethynylbenzene and iodobenzene is envisaged.

Another possibility to interlink the OPE moiety with the cyclophane is the cross coupling of OPE **A6** with an already on the ethylated cyclophane **A7** attached 4-iodobenzyl linker (scheme 2, **H**). This retrosynthetic consideration makes an introduction of protecting groups on the free phenol unnecessary since the benzyl linker acts in this particular case as a valuable protection group to achieve chemoselective ethylation of the tertiary amines in cyclophane **A8**. Therefore introduction of the molecular rod at the last step of the synthesis is again possible without causing further steps. As a drawback of this final assembly (**H**) of the subunits **A6** and **A7** the potential difficulties in performing a Sonogashira cross-coupling with

an organic salt have to be mentioned. Therefore again a cross-coupling prior to ethylation (**J** – **K**) has to be considered as a resort of probable difficulties in pathway (**H** – **I**). However both considerations have cyclophane **A8** as a common precursor for which either an introduction of the benzyl linker prior to reduction of the protecting amides (**L** – **M**) or reduction prior to etherification (**N** – **O**) can be considered (scheme 2.).

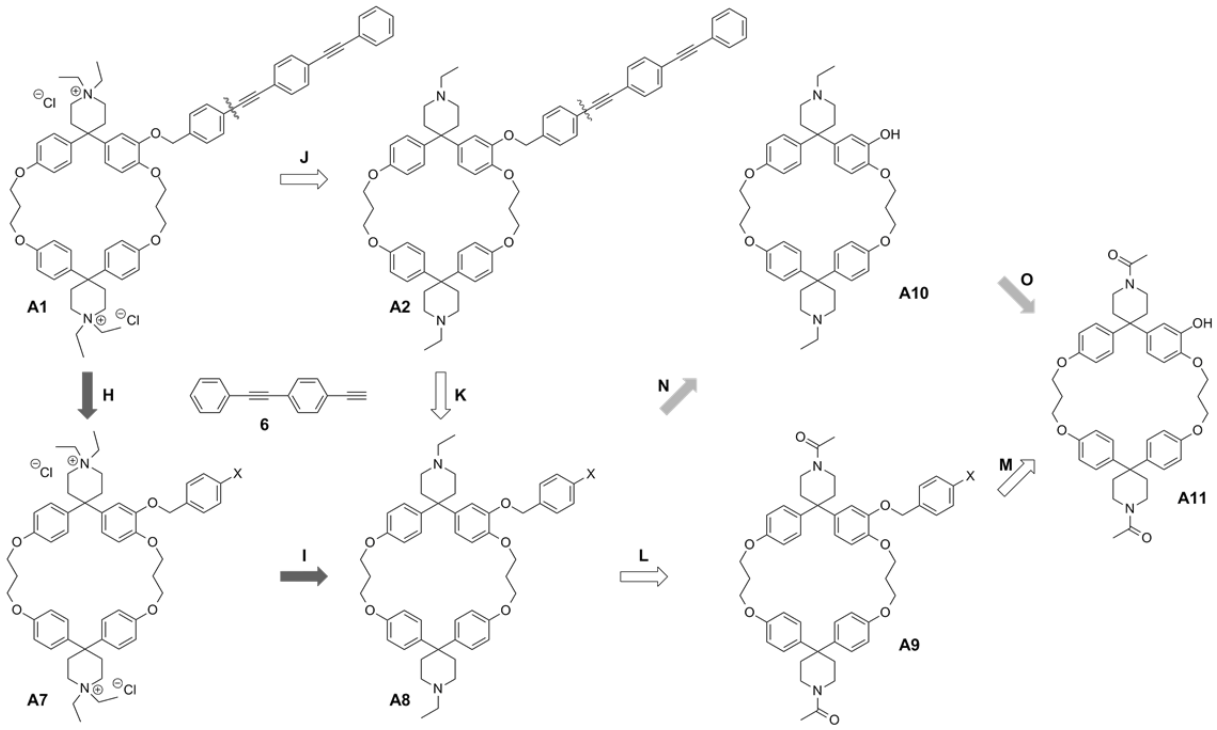

Scheme 2. Alternative synthetic routes towards target compound **A1** having cyclophane **A11**, OPE **A6** and commercially available 4-iodobenzyl bromide as precursors.

Towards mono-functionalized cyclophane **A11** several pathways have been demonstrated by Diederich *et al*.[118,119,123–125] In principle, a stepwise intramolecular or an intermolecular single step macrocyclization can be considered (scheme 3, **P** and **T**). In both possible synthetic routes the alcohol functionality of **A11** has to be protected by a suitable protection group. The stepwise macrocyclization approach requires assembly of the "symmetric" half circle **A13** and the "asymmetric" half circle **A14** (**Q**). Connection at every cavity wall forming phenol is possible which provides a set of different pathways. For simplification only one possibility is shown. To avoid homo-dimerization it was envisaged to attach the interlinking propyl chains, comprising leaving groups with divers leaving group abilities, on one part of the corresponding half circles (compound **A13**). One of the two phenolic groups of diphenol piperidine **A14** has to be protected orthogonally to the mono-functionality to prevent statistic coupling and oligomerization of **A13**. For the synthesis of asymmetric diphenol piperidine

A14 either an addition of mono-protected catechol to 5,6-dihydropyridine **A15** or an addition of phenol to di-protected 4-(3,4-dihydroxyphenyl)-5,6-dihydropyridine is feasible (**R**). The same type of reaction is possible to achieve **A13** from literature known compound **A16** (**S**).

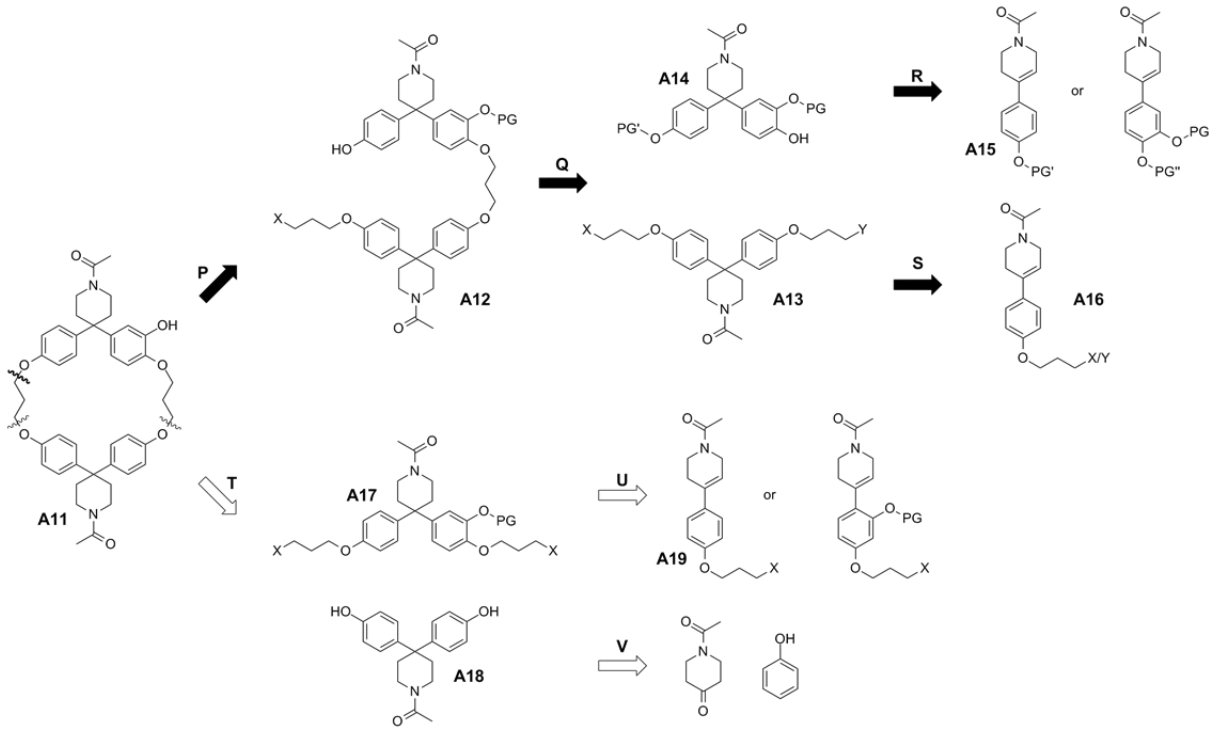

Scheme 3. Retrosynthetic strategies towards cyclophane **A11** either by a stepwise assembly (**P** – **S**) or by intermolecular macrocyclization (**T** – **V**).

Installation of two equal leaving groups to one part of the cyclophane (**A17**) allows for intermolecular macrocyclization (**T**). Despite of expected lower yields due to formation of higher oligomers or larger macrocycles, fewer steps are required. Furthermore the possibility to synthesize bisphenol **A18** in a single step starting from *N*-acetyl-4-piperidone and phenol allows for a rapid synthesis of cyclophane **A11**. For the synthesis of the asymmetric part **A17** the same strategy as described for pathway **P** – **S** can be considered.

Results and Discussion

Synthesis

The assembly of the loop subunit profits to a large extend from the cyclophane chemistry developed by Diederich[123–125] while the rigid molecular rod is based on classical Sonogashira coupling chemistry[126]. Due to potential handling disadvantages like solubility, reactivity and stability as well as the necessity of protection groups, the synthetic pathways **H**,**I**,**L**,**M** or **J** – **M** (scheme 2) were envisaged for the final assembly of the terminal loop and the molecular

rod. The oligophenylene-ethynylene **A6** is considered to be coupled to the cyclophane **A11** at a late stage of the synthesis which allows to alter the length and substitution pattern of the molecular rod and thus to optimize the extent of intermolecular stacking.

As already mentioned amphiphilic monomer **A1** was synthesized inspired by the numerous synthetic routes towards mono-functionalized Diederich-type water soluble cyclophanes reported in literature.[118,119,123–125] Molecules **A19** and **A20** were synthesized according to a literature known procedure[125] by a Grignard reaction of 4-bromoanisol and *N*-acetyl-piperidin-4-one followed by elimination of the resulting tertiary alcohol **A19** and deprotection of the methoxy group in one step using strong Lewis acidic boron tribromide (scheme 4). Since for the purification of the resulting phenol only washing of the crude with water and diethyl ether is required, the reaction protocol was applicable for synthesis in larger scales (25 g starting material) where a 63% overall yield was obtained. In the following step the free phenolic hydroxyl group was again protected with a photocleavable 2-nitrobenzyl group in 79% yield, a reaction that was necessary because a stepwise cyclization protocol was chosen for cyclophane assembly.[124] Afterwards the cavity wall, bearing the mono-functionalization, was introduced by addition of 2-methoxyphenol (guaiacol) to the styrene double-bond of **A15** in strong Lewis acidic media using large excess of boron trifluoride (scheme 4).[125]

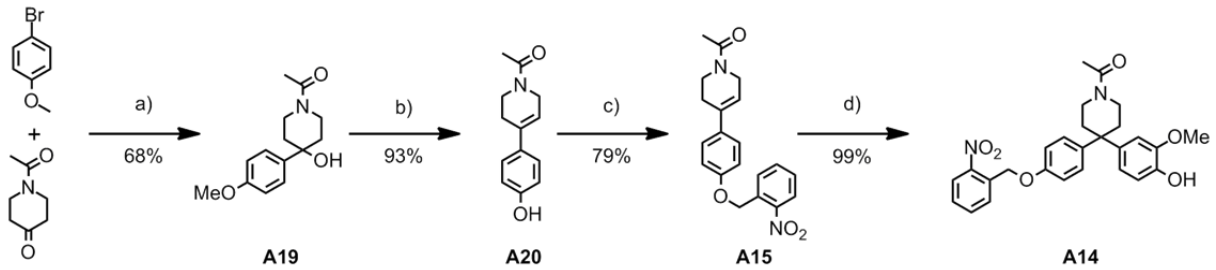

Scheme 4. Synthesis of the functionalized cyclophane part **A14**. a) Mg, THF, reflux, 1.5 h, then *N*-Acetyl-piperidin-4-one, THF, rt, 4 h; b) BBr_3, CH_2Cl_2, reflux, 3 h; c) 2-nitrobenzyl chloride, K_2CO_3, MeCN, reflux, 6.5 h; d) 2-methoxyphenol, $BF_3 \cdot OEt_2$, CH_2Cl_2, 9 d, rt.

The addition of guaiacol seems to be reversible leading to the electronically and thermodynamically favored *para* to the hydroxyl group coupled product after 9 d stirring at room temperature (99%). Shorter reaction times led to formation of regioisomers.

The symmetric part **A13** of the cyclophane was synthesized starting from phenol **A20** by introduction of 1,3-dichloropropane in a S_N2-reaction, followed by addition of phenol to the remaining alkene in a yield of 99% after column chromatography and recrystallization with acetonitrile. To avoid homo-coupling of the symmetrical diphenylpiperidine moiety **A21** the

second alkyl spacer of cyclophane **A11** was installed at the remaining free hydroxyl group of **A21**. Therefore phenol **A21** was reacted with 1,3-diiodopropane in the presence of radical inhibitor BHT and potassium carbonate as a base yielding the symmetric part **A13** equipped with two different leaving groups as a colorless oil in 67% yield (scheme 5).

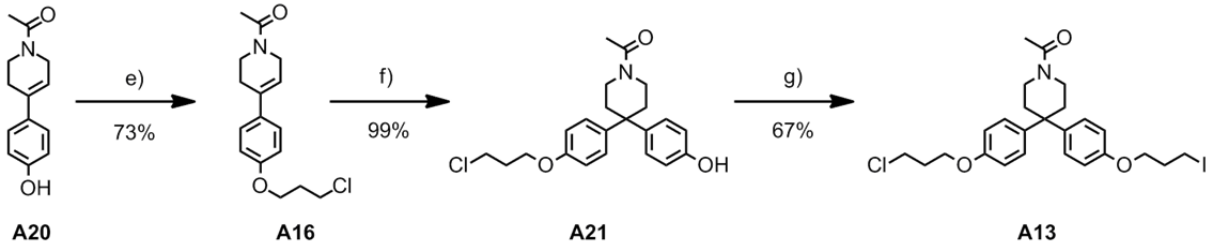

Scheme 5. Synthesis of the unfunctionalized cyclophane part **A13**. e) 1,3-dichloropropane, K_2CO_3, MeCN, reflux, 26 h; f) phenol, $BF_3 \cdot OEt_2$, CH_2Cl_2, 23 h, rt; g) 1,3-diiodopropane, BHT, K_2CO_3, acetone, reflux, 5 h.

Nucleophilic substitution of the two cyclophane parts **A13** and **A14** afforded dimer **A22** in moderate 48% yield (scheme 6). Since both alkyl spacers were coupled to only one part of the cyclophane homo-dimerization was excluded. By carefully adjusting the reaction conditions (Cs_2CO_3, acetone, 40°C, 16 h) only the iodide as the better leaving group in nucleophilic substitutions reacted. Prior to performing the intramolecular macrocyclization the protecting group was removed by photolytic debenzylation. Therefore the nitrobenzyl protected alcohol **A22** was irradiated for 5 h at room temperature with alternating 300 nm and 366 nm UV-lamps in a Rayonet® photochemical reactor (scheme 6). To suppress enrichment of various decomposition products of 2-nitrosobenzaldehyde, which is formed by photolytic cleavage of 2-nitrobenzyl groups, a radical inhibitor (BHT) was added to the reaction mixture as reported by Diederich *et al*.[124] After flash column chromatography alcohol **A12** was isolated in 97% yield (scheme 6). The chloroalkylated phenol **A12** underwent an intramolecular macrocyclization to afford methoxy-cyclophane **A23** in excellent 72% yield (scheme 6). To prevent oligomerization the concentration of **A12** in solution was kept low by adding the starting material slowly (30 h) to a refluxing suspension of cesium carbonate in acetonitrile.[124] Even though the synthesis of methoxy protected cyclophane **A23** was successfully accomplished the initial goal of this synthesis was the development of a protocol for synthesizing large quantities in an easy and modular approach. Furthermore the troublesome coupling of the two subunits **A13** and **A14** led to an overall yield of the cyclization procedure of moderate 34% which is in the range of reported intermolecular macrocyclizations but far from an optimal procedure.[123] Therefore it was decided to shorten the synthetic route mainly by using an intermolecular cyclization procedure.

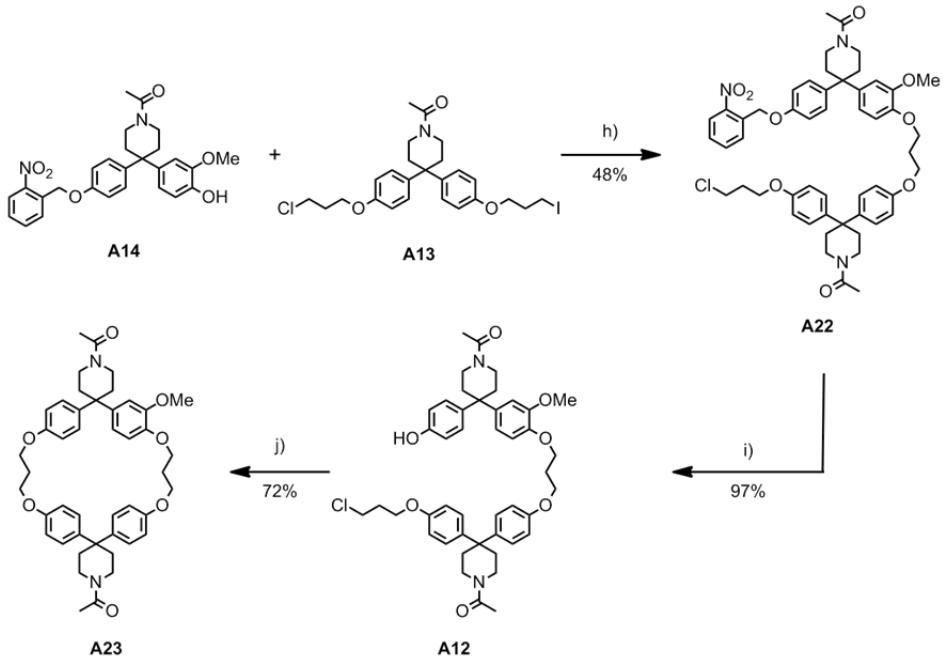

Scheme 6. Stepwise cyclization procedure towards mono-functionalized cyclophane **A23**. h) Cs_2CO_3, acetone, 40°C, 16 h; i) BHT, THF, *hv*, rt, 5 h; j) Cs_2CO_3, MeCN, reflux, 36 h.

Thus phenol **A20** was substituted with 1,3-dibromopropane in 71% yield to introduce one of the alkyl-linkers, followed by addition of guaiacol to the alkene moiety of **A24** in 94% yield after column chromatography. Final nucleophilic substitution of the remaining phenol with 1,3-dibromopropane in 91% yield gave the desired mono-functionalized part **A17** of cyclophane **A11** as a colorless oil (scheme 7).

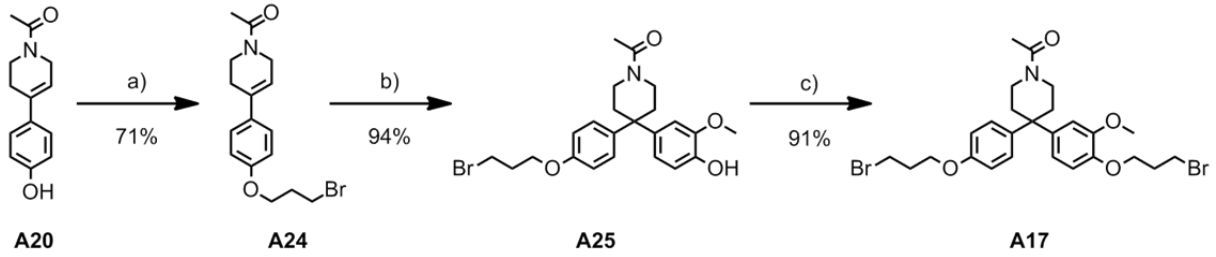

Scheme 7. Synthesis of the mono-functionalized cyclophane part **A17**. a) 1,3-dibromopropane, K_2CO_3, MeCN, reflux, 5 h; b) guaiacol, $BF_3 \cdot OEt_2$, CH_2Cl_2, rt, 9 d; c) 1,3-dibromopropane, K_2CO_3, acetone, reflux, 20 h.

For the intermolecular cyclization it turned out to be crucial having two leaving groups with the same reactivity present to avoid oligomerization. This mono-functionalized part **A17** of the cyclophane was coupled by nucleophilic substitution under high dilution reaction conditions with *bis*-hydroxydiphenylpiperidine **A18** which was synthesized following a literature known protocol in a single step from *N*-acetyl-piperidin-4-one and phenol in acidic media.[118] Cyclophane **A23** equipped with a methoxy group was then obtained after column

chromatography and precipitation with ethanol as a white powder in 31% yield (scheme 8) which is equal to the overall yield of the stepwise cyclization procedure. Analyses of side products by ESI-MS documented the formation of the tetrameric product in traces, as well as the formation of higher oligomers. Furthermore hints were obtained that over the long reaction time (24 h) the amide was cleaved to a certain extend. Nevertheless, the simple purification and the possibility to synthesize the cyclophane precursors **A17** and **A18** in bulk revealed this strategy towards mono-functionalized cyclophane **A11** as the method of choice.

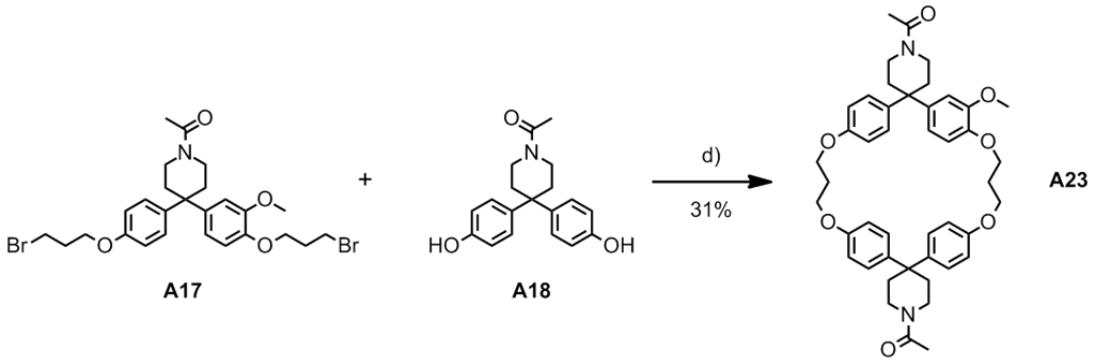

Scheme 8. Assembly of cyclophane **A23** using an intermolecular approach. f) Cs_2CO_3, acetonitrile, reflux, 20 h.

Having the desired mono-functionalized cyclophane **A23** in hand, it was now of interest to transform the masked functionality into a suitable reaction center for Sonogashira cross-coupling. Following synthetic pathways **H**,**I**,**L**,**M** or **J** – **M** (scheme 2) the methoxy group had to be cleaved without cleavage of the cyclophane alkoxy-groups. The use of nucleophilic demethylation conditions turned out to be the method of choice. Therefore the cyclophane was reacted with sodium thiomethoxide in dry DMF at 160°C for 6 h.[127] After quenching with 0.1 M aqueous HCl-solution and recrystallization with methanol the desired, in most common solvents insoluble, phenol **A11** was obtained in excellent yield of 98% (scheme 9). As rather harsh reaction conditions had to be used to ensure full conversion, in some cases nucleophilic aromatic substitution of thiomethoxide to one of the phenyls was observed. For demethylation using thiophenol or boron tribromide no conversion was obtained as indicated by TLC. In the next step it was decided to introduce a 4-iodobenzyl group mainly to assist dimer formation by increasing the flexibility. Directly linking the molecular rod to the cyclophane, which would require transformation of the free phenol **A11** to a triflate, would potentially lead to prevention of aggregation because of unfavorable spatial arrangement of the cyclophane with respect to the rigid rod. Furthermore our primary target was to synthesize [c2]daisy chains which – when further functionalized – can be polymerized by conventional methods. Therefore a further degree of flexibility in the otherwise rigid OPE rod seems to be

crucial. The benzyl linker was installed in a S_N2-reaction of the phenol **A11** with 4-iodobenzyl bromide in the presence of cesium carbonate in DMF at 85°C. According to these reaction conditions compound **A9** was isolated after column chromatography in 98% (scheme 9). The use of a weaker base like potassium carbonate did not lead to full conversion after 48 h. Before cross-coupling of the oligophenylene-ethynylene **A6** the acetyl-protecting groups of the piperidinyl moiety were reduced to the corresponding alkyls to avoid formation of possible side products. The reduction was performed by slowly adding DIBAL-*H* to a diluted solution of diamide **A9** in dichloromethane at 0°C. After addition of the reducing agent the reaction was allowed to warm to room temperature.

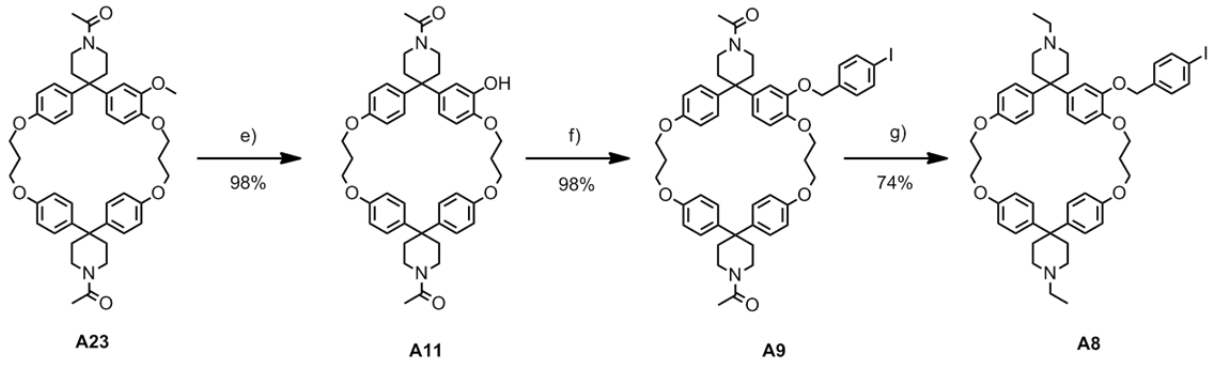

Scheme 9. Introduction of a benzyl linker bearing a suitable halide for Sonogashira cross-coupling reactions and activation of the piperidine-nitrogen for alkylation. e) sodium thiomethoxide, DMF, 160°C, 6 h; f) 4-iodobenzyl bromide, Cs_2CO_3, DMF, 85°C, 20 h; g) DIBAL-*H*, CH_2Cl_2, 0°C then rt, 4 h.

This reaction turned out to be one of the key steps in the synthesis of monomer **A1** because at room temperature not only the amides were reduced but also the iodobenzyl ether was cleaved to a certain extend (around 50%). Unfortunately the reaction did not show full conversion at 0°C and small amounts of inseparable mono-reduced byproduct were observed by ESI-MS. Therefore the chosen reaction conditions are a compromise to obtain amine **A8** in 74% yield (scheme 9). Other reducing reagents like $BH_3 \cdot THF$ led to partial defunctionalization of the iodide functionality and were therefore neglected.

The molecular wire **A6** was synthesized starting from 1,4-diiodobenzene where in a first step acetylenes with orthogonal protecting groups, namely trimethylsilyl and dimethylpropargyl alcohol (HOP) were statistically cross-coupled. The in 45% yield obtained product **A26** was then selectively deprotected on the HOP side with sodium hydroxide in refluxing toluene (scheme 10).[128]

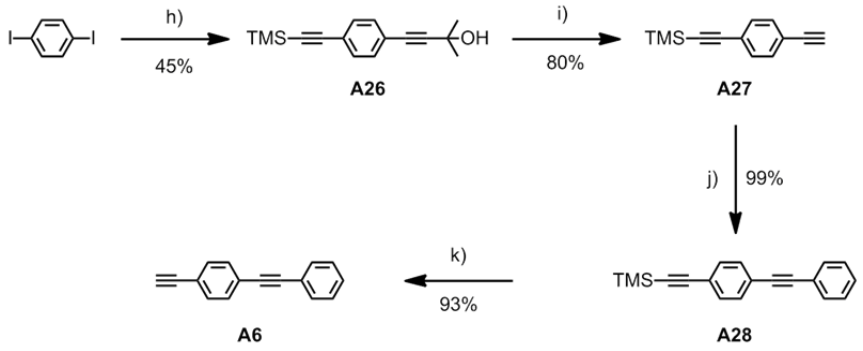

Scheme 10. Synthesis of the oligophenylene-ethynylene building block **A6**. h) $PdCl_2(PPh_3)_2$, CuI, DIPA, THF, 1.) TMS-acetylene, rt, 4 h, 2.) 2-methyl-3-butyn-2-ol, rt, 16 h; i) NaOH, toluene, 80°C, 1 h; j) iodobenzene, $PdCl_2(PPh_3)_2$, CuI, DIPA, THF, rt, 4 h; k) TBAF, Ac_2O, AcOH, THF, 0°C then rt, 2 h.

The free acetylene **A27** was cross-coupled using a Sonogashira protocol with iodobenzene (scheme 10). In a final step the TMS-protecting group was removed using TBAF to yield the desired OPE **A6** in a total yield of 33% over 4 steps including one statistical Sonogashira cross-coupling.

By having 4-iodobenzyl substituted cyclophane **A8** and OPE **A6** in hand, it was then of interest to assemble these two parts by either an ethylation-cross-coupling sequence (**H**, **I**) or vice versa (**K**, **L**). As depicted in the retrosynthetic analysis a Sonogashira cross-coupling at the last step of the synthesis would allow for the fast and easy preparation of altered amphiphiles. Hence cyclophane **A8** was ethylated using freshly distilled iodoethane. The product **A7** was isolated in 71% yield by column chromatography using a mixture of acetone:1 M aq. ammonium chloride:acetonitrile 14:2:1, followed by Soxhlet® extraction with dichloromethane. The subsequent Sonogashira cross-coupling of the chloride salt **A7** and the OPE **A6** in DMF was unfortunately not successful. Therefore the OPE-rod **A6** was, now following to synthetic strategy **K**, **L**, cross-coupled to the cyclophane **A8** using $Pd(dba)_2$, triphenylphosphine, CuI and diisopropylamine in THF at room temperature. These rather unusual conditions with a large excess of base were crucial for the successful assembly since in presence of catalysts like $Pd(PPh_3)_4$ or $PdCl_2(PPh_3)_2$ or without large excess of the base no conversion was observed. The crude was purified by extraction and column chromatography to yield the desired scaffold **A2** in 92% yield as a white solid (scheme 11). The tertiary amines were finally alkylated in dichloromethane using freshly distilled iodoethane. After stirring for 5 d at room temperature monomer **A1** was isolated by column chromatography using silica which was preconditioned with a 12% (w/v) methanolic sodium bromide solution.[129] The product was eluted with a dichloromethane, 5% methanol mixture. After

Soxhlet® extraction with dichloromethane and ion exchange chromatography (DOWEX 1X8, 200 – 400 mesh, Cl^-) the desired hydrophobic molecular rod comprising a terminal hydrophilic loop **A1** was obtained as a chloride salt in 59% yield as an off-white hygroscopic solid (scheme 11).

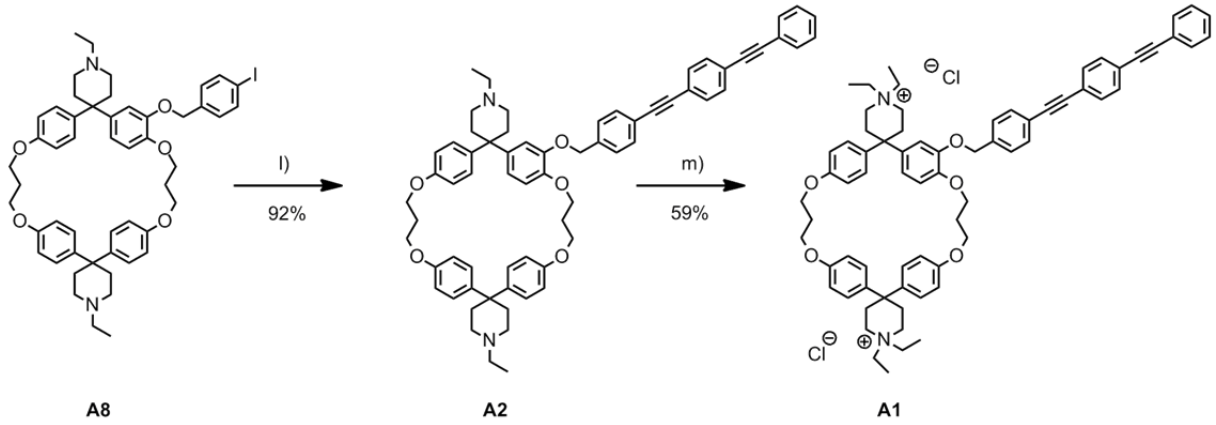

Scheme 11. Final assembly of the amphiphilic monomer **A1**. l) OPE **A6**, $Pd(dba)_2$, PPh_3, CuI, DIPA, THF, rt, 3 h; m) iodoethane, CH_2Cl_2, rt, 5 d, then ion exchange (DOWEX 1X8, 200-400 mesh, Cl^-).

According to the described procedure the hydrophobic oligophenylene-ethynylene rod comprising a terminal hydrophilic loop **A1** was synthesized in 21 steps via an intramolecular stepwise cyclophane assembly or in 17 steps by intermolecular macrocyclization. Thereby it was shown that cyclophane **A11** can be synthesized in large quantities (2 g) and interlinking of the hydrophobic and hydrophilic parts **A8** and **A2** is possible in good yields. The hermaphroditic monomer **A1** was analyzed by low resolution ESI-MS (figure 29) and by ^{1}H-NMR.

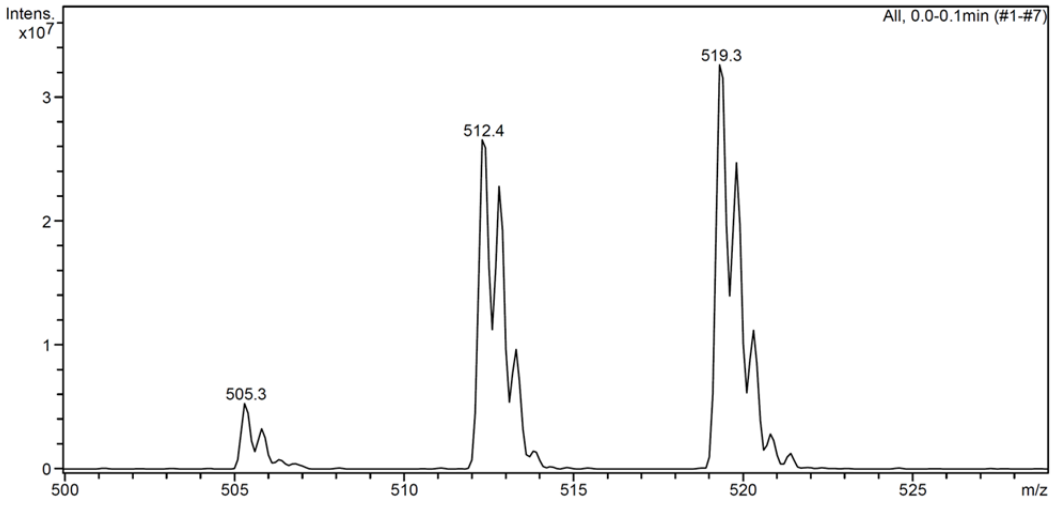

Figure 29. ESI-MS spectrum of the doubly charged amphiphile **A1** showing $[M^{2+}]$ (519 m/z), $[M^{2+}\text{-}CH_3]$ and $[M^{2+}\text{-}C_2H_5]$.

Aggregation Studies

Having the desired hermaphroditic monomer **A1** in hand it was then of interest to study its aggregation behavior in polar solvents. As outlined in the introduction such amphiphilic molecules can form various aggregates (figure 30).[114]

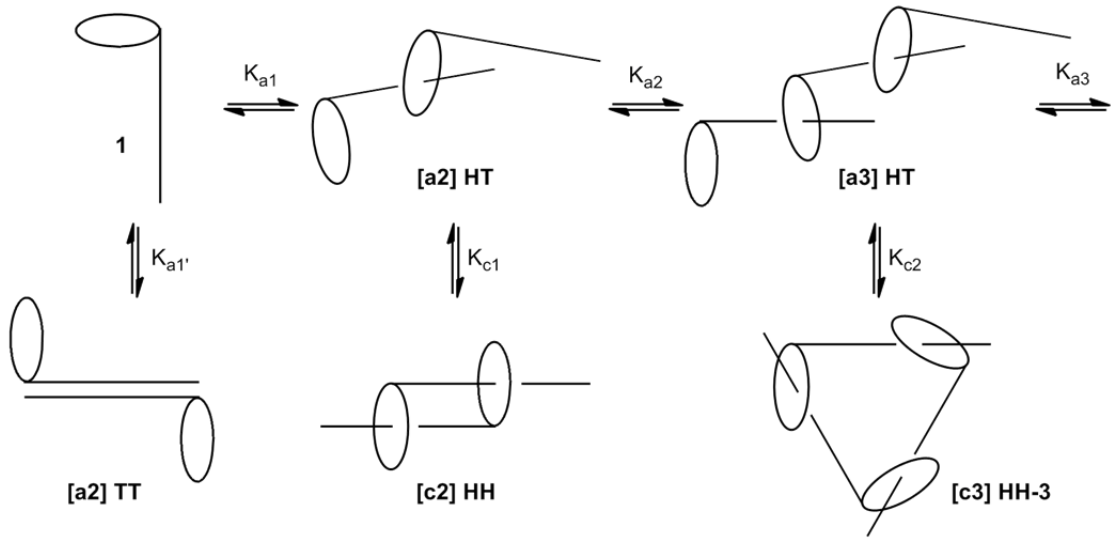

Figure 30. Possible aggregates formed by amphiphile **A1** in polar solvents.

Monomer **A1** can potentially form three different dimer structures excluding aggregation of the organic ions as well as assemblies where the OPE rod comes into close proximity to the spiro-piperidinyl moieties (figure 30). The formation of [c2]daisy chains (**[c2]HH**) is well known in literature and is often a thermodynamic stable aggregate preventing formation of longer oligomers.[113] Also the aggregation of two hydrophobic OPE rods (**[a2]TT**) is possible but it is expected that such a binding is weaker than the inclusion of the rod into the hosts cavity and therefore causes, because of the reversible aggregation, no interruption of oligomerization. Formation of an acyclic head-tail dimer (**[a2]HT**) can be seen as the first propagation step towards polymerization. Nevertheless each possible *n*-mer of the propagating chain has the possibility to form, because of the expected reversible binding, its cyclic analoga. The hypothetical formation of this variety of aggregates makes a detailed analysis difficult. ^{1}H-NMR spectroscopy and fluorescence measurements were performed for this purpose.

Previous publications have shown that concentration dependent ^{1}H-NMR spectroscopy can be used to determine the aggregation number *n* and the association constant K_a.[130–132] Thus ^{1}H-

NMR spectra were recorded at constant temperature at different concentrations of monomer **A1** in a 3:2 mixture of D_2O:methanol-d4 (figure 31).

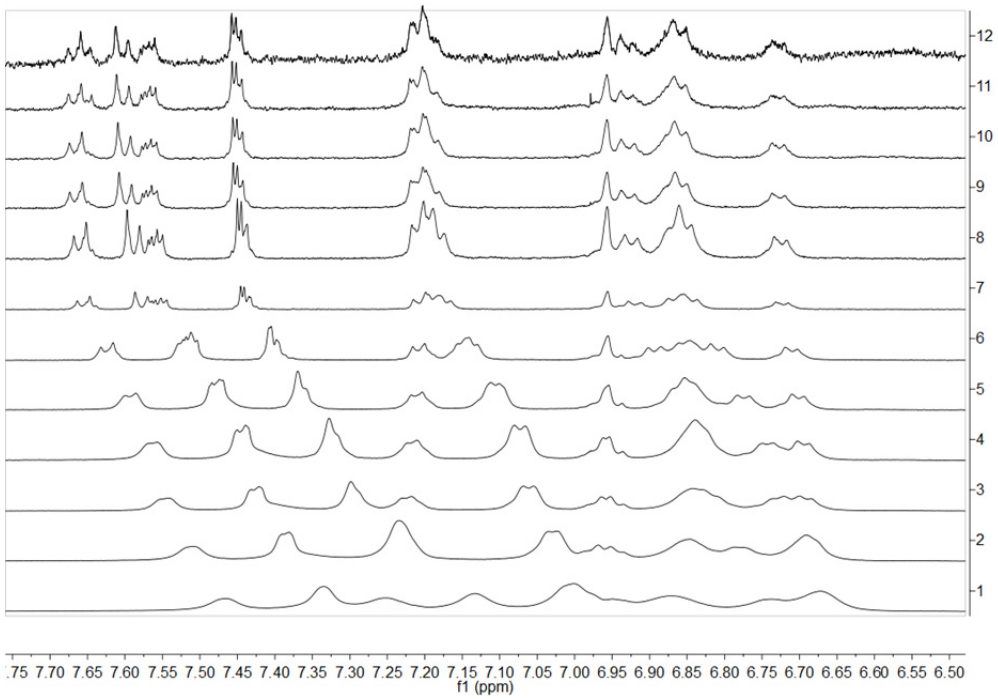

Figure 31. Stacked ^{1}H-NMR spectra of the aromatic region of monomer **A1** recorded in D_2O:MeOD 3:2 on a 500 MHz spectrometer. 12) 0.014 mM, 11) 0.026 mM, 10) 0.055 mM, 9) 0.091 mM, 8) 0.22 mM, 7) 0.32 mM, 6) 1.12 mM, 5) 1.49 mM, 4) 1.99 mM, 3) 2.99 mM, 2) 3.98 mM, 1) 7.96 mM.

The NMR-spectra show that the protons are under fast exchange on the NMR time scale. Therefore the observed chemical shift (δ_{obs}) can be expressed as the sum of the chemical shifts of the monomer (δ_{mon}) and those of the individual aggregates (δ_{agg}), each one averaged with its molar fraction (equation (1)).[133]

$$\delta_{obs} = \delta_{mon}(C_{mon}/C_{tot}) + \delta_{agg1}(C_{agg1}/C_{tot}) + \delta_{agg2}(C_{agg2}/C_{tot}) + \ldots \qquad (1)$$

When assuming that the concentration of an aggregate which is predominant in a certain concentration range remains constant above a certain concentration, a plot of δ_{obs} versus the inverse concentration should give a straight line after each individual change in aggregation. The intersection of these lines then gives directly the critical aggregation concentration (CAC) for each individual aggregate.[131] For simplification only one equilibrium was considered for each aggregate and concentration range and cooperative effects were excluded what means that for all equilibria the same association constant was assumed ($K_{a1} = K_{a2} = K_{a3}$ etc.). Thus equation (1) simplifies to a linear function.

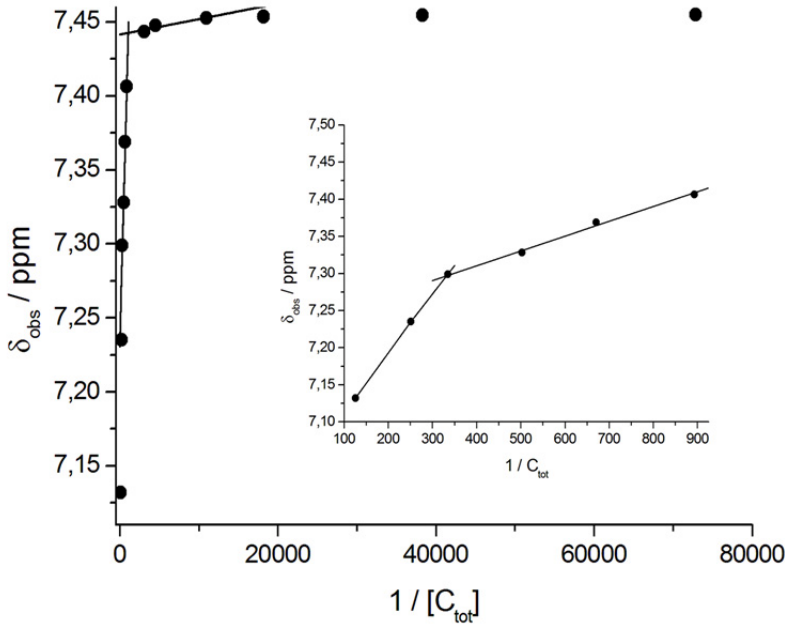

Figure 32. Plot of the observed chemical shift against the inverse of the concentration. From the intersection of the straight lines (linear regression) the critical aggregation concentration (CAC) was calculated. The inset represents the second CAC at higher concentrations.

In figure 32 a representative plot of δ_{obs} against the inverse total concentration C_{tot} for one proton of the amphiphile **A1** (assigned to the OPE part by 2D-NMR spectra) is illustrated which indicates two critical aggregation concentrations at 0.941 mM ($1/C_{tot}$ = 1062.7 M^{-1}) and 3.03 mM ($1/C_{tot}$ = 330.0 M^{-1}). Below 1 mM the observed chemical shift remains constant indicating that only one aggregate or monomer is dominant. Above 3 mM no further conclusion can be drawn since the ^{1}H-NMR signals broaden and therefore further assignment of individual protons is impossible (figure 31).

Large upfield shifts of the aromatic signals assigned to the OPE were obtained above the CAC of 1 mM in contrast to the proton shifts below 7.00 ppm where only weak shifts were observed (figure 31). By threading of the OPE into the cavity of the cyclophane the phenyl protons of the rod experience a ring current from the aromatic systems in the cavity wall leading to an induced chemical shift change. Thus the large upfield shift can be seen as a first evidence for the threading of the OPE into the cavity of the cyclophane. In addition the rims of the cavity, especially the protons of the aromatic systems, are non-equivalent in the case of a [c2] and an [a2]daisy chain (figure 33). Furthermore, in the acyclic version at least one cyclophane should be unthreaded and therefore show differing proton signals compared to the threaded macrocycles. Unfortunately the aromatic cyclophane protons are not well resolved in

the ^{1}H-NMR which allows no conclusion about the structure of the aggregates. Moreover, the protons at the interlinking alkyl chains of the cavity should get non-equivalent upon complexation if the fluctuations of the propyls are prevented by the guest. In solid state structures of inclusion complexes of such cyclophanes and benzene derivatives the carbon atoms of the interlinking alkyl chains and the cavity wall forming aryls are in the same plane.[119] Therefore the methylene protons at the individual carbon atoms of the alkyl linker should get diastereotopic and experience a chemical shift deviation (one set of four protons which point inside the cavity and one set of four protons pointing outside) compared to the monomer (figure 33).

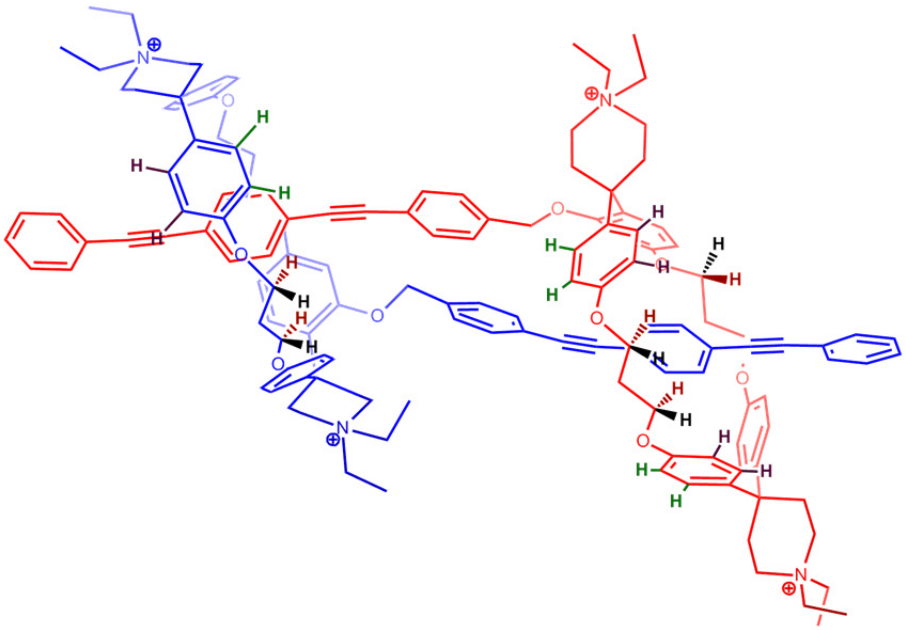

Figure 33. Aggregation of the amphiphile **A1** in polar solvent forming a [c2]daisy chain. Upon complexation the aromatic cyclophane protons gets non-equivalent (green and violet protons). The protons of the interlinking propyl chains pointing inside the cavity (brown) should experience the influence of the ring currents of the OPE benzenes, whereas the protons pointing outside the cavity (black) should not be influenced.

Indeed differences can be observed by comparing the NMR-signals of **A1** in MeOD and MeOD:D_2O 3:2 (figure 34). The eight alkoxy-protons show two distinct multiplets in MeOD which are integrated as two and six respectively, caused by the unsymmetric design of **A1**, displaying the expected situation in a monomer. In the aqueous solution again two multiplets are observed but which are both integrated to four protons. Such a situation can be seen as evidence that the protons pointing inside the cavity and the protons pointing away from the cavity have different chemical environments and therefore different chemical shifts. In addition the alkyl-protons show a larger chemical shift difference in aqueous solution than in deuterated methanol. Even though no direct conclusion about the structure of the aggregate

itself can be drawn, it is a strong indication that supramolecular complexes are formed in aqueous solution.

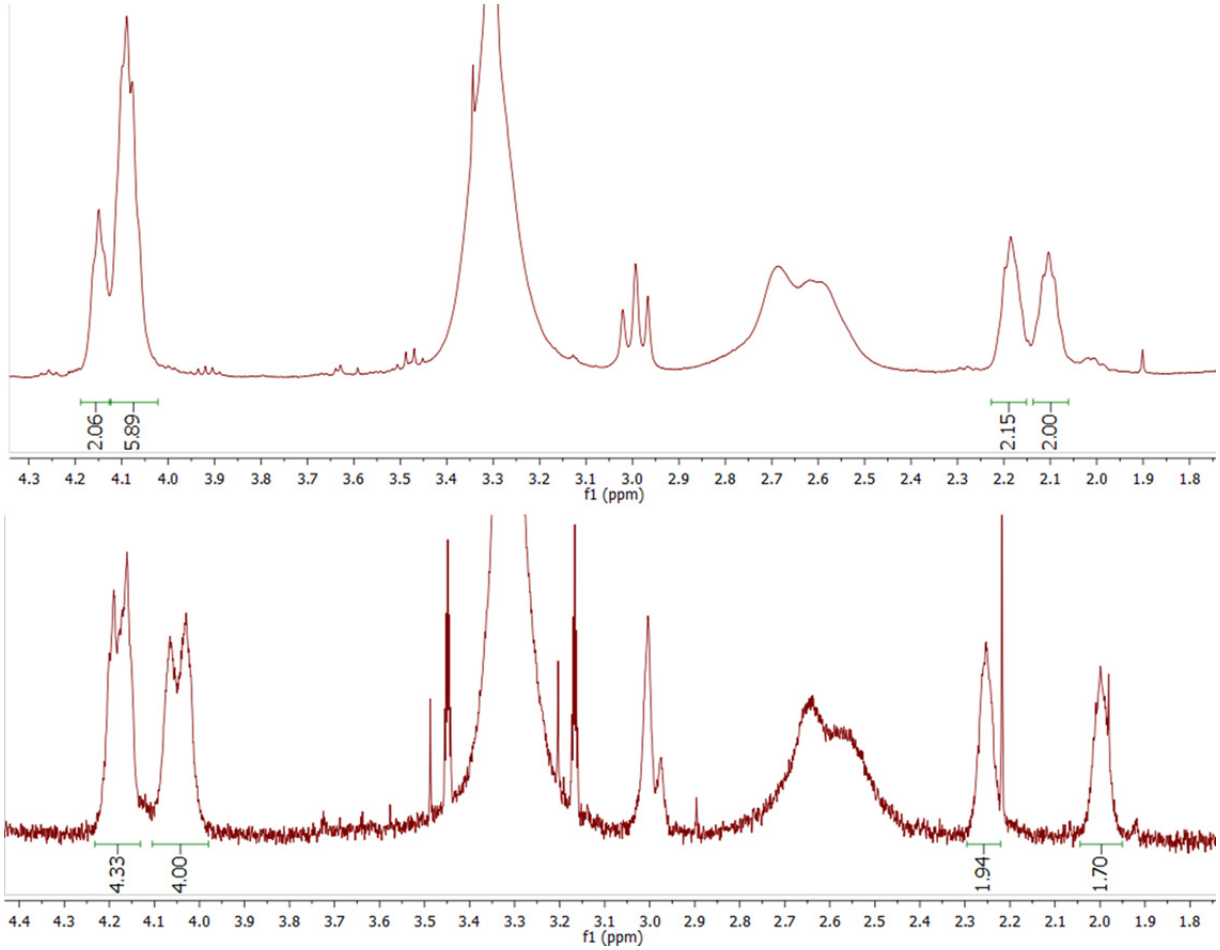

Figure 34. Aliphatic region of the ^{1}H-NMR of amphiphile **A1**. The integrated signals are the alkoxy (δ ≈ 4.2 – 4.0 ppm) and the alkyl (δ ≈ 2.3 – 2.0 ppm) methylene protons. *Top*: MeOD; *bottom*: MeOD:D_2O 3:2.

As already mentioned the ^{1}H-NMR data can also be employed to obtain the aggregation number *n* and the association constant K_a by the following expression describing an equilibrium where n monomers form a single aggregate (see appendix).[130–133]

$$\ln[C_{tot}(|\delta_{obs}-\delta_{mon}|)] = n \ln[C_{tot}(|\delta_{agg}-\delta_{obs}|)] + \ln K_a + \ln n - (n-1)\ln(|\delta_{agg}-\delta_{mon}|) \quad (2)$$

Plots of $\ln[C_{tot}(|\delta_{obs}-\delta_{mon}|)]$ vs. $\ln[C_{tot}(|\delta_{agg}-\delta_{obs}|)]$ (figure 36) give a straight line from which the slope and the intercept can be calculated yielding *n* and K_a, respectively. By plotting δ_{obs} against the total concentration and extrapolating to zero amphiphile the chemical shift of the monomer (δ_{mon}) was approximated.[128,132] Extrapolation of the concentration to infinity yielded the chemical shift of the aggregate (δ_{agg}) (figure 35).[132]

The variation of the slopes in the in figure 36 illustrated plots clearly demonstrate that the by

NMR-titration obtained data can be divided into three different concentration ranges as already indicated by plotting the observed chemical shifts against the inverse concentration. An aggregation number of $n = 2$ was obtained by analysis of the concentration range between 0.014 mM and 1 mM. Different aromatic signals as well as shifting signals in the aliphatic region gave relative narrow aggregation values in the range of 1.97 – 2.10, strongly suggesting the formation of dimeric structures.

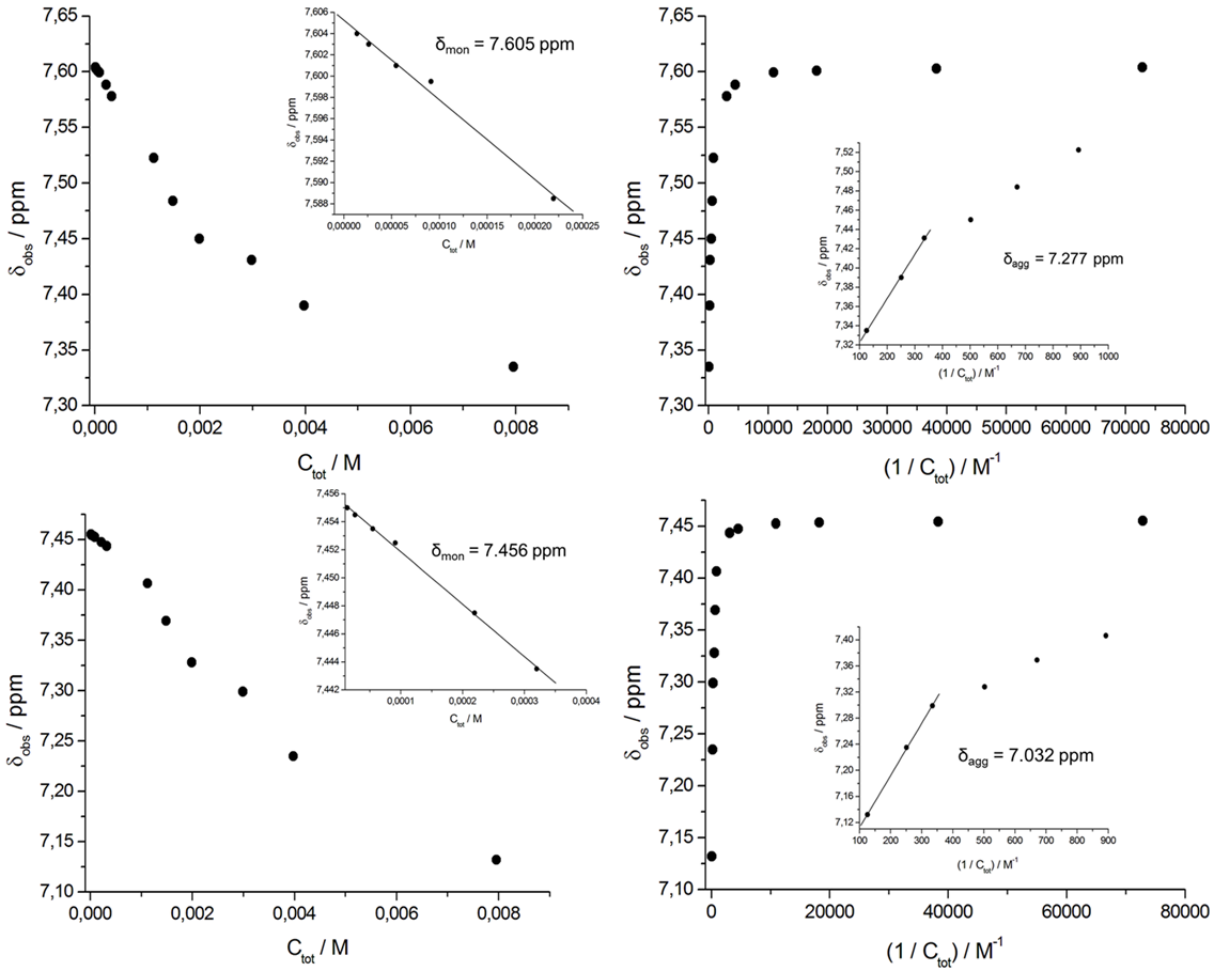

Figure 35. *left*: Titration curves of selected protons of **A1** in D_2O:MeOD 3:2. Inset shows the titration curve at low concentrations. The linear regression used to estimate graphically δ_{mon} is shown as the solid line. *right*: Plots of δ_{obs} against the inverse total concentration. Extrapolation to zero is equal to extrapolation of the concentration to infinity. Inset shows the titration curve at high concentrations. The linear regression used to estimate graphically δ_{agg} is shown as the solid line.

Furthermore, by analysis of just the concentration range where dimer formation is observed an association constant of $K_a = 9.8 \cdot 10^6$ M^{-1} was obtained when the chemical shift of the aggregate was replaced by the shift of the dimer. Interpretation of the association constant has to be taken with caution since the assumption was made that in each concentration range only one aggregate is dominant. The concentration range where the transition from monomer to

dimer can be observed was unfortunately not reached by this NMR-titration due to the instrumental limits. By closer inspection of the titration curve obtained by plotting δ_{obs} against the concentration it became clear that only the first part of the expected dimer plateau was reached what makes a precise prediction of the monomer chemical shift δ_{mon} impossible.

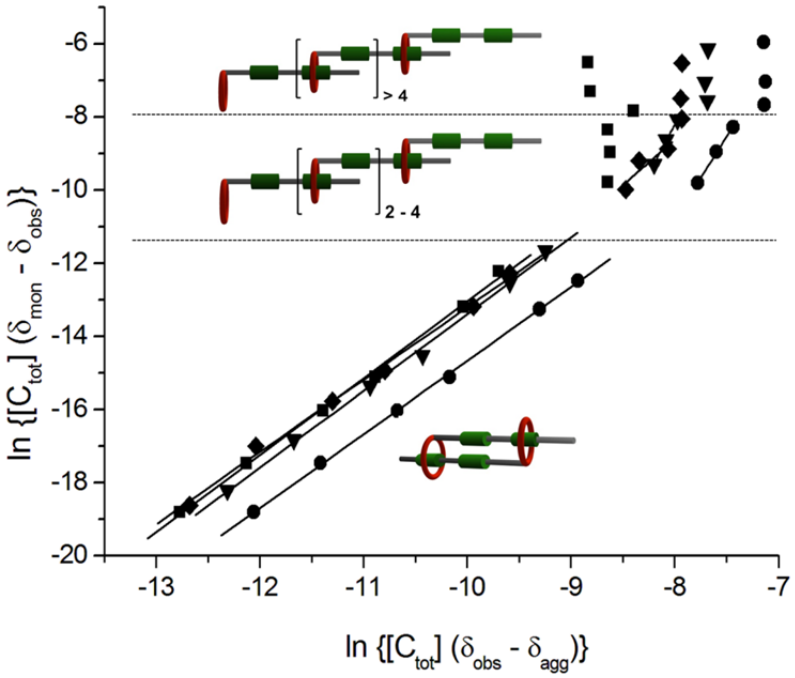

Figure 36. Plot of $\ln[C_{tot}(|\delta_{obs}-\delta_{mon}|)]$ against $\ln[C_{tot}(|\delta_{agg}-\delta_{obs}|)]$. Straight lines represent linear regression from which the aggregation number *n* and K_a were calculated.

In the concentration range between the two CACs aggregation numbers between 4.5 and 6 were obtained. Even though the protons are in fast exchange in the NMR time scale the wide concentration range in which dimerization can be observed gives evidence for a strong hydrophobic effect. It is however safe to conclude that higher oligomers at concentrations above 1 mM are formed as indicated by the plots in figure 36. Furthermore the strong broadening of the proton signals which is typical for polymer formation, due to an increased viscosity, strongly supports this finding. Nevertheless it was shown that the dimer is the predominant species in a broad concentration range what leaves space for the aim of further functionalization allowing for polymerization.

To gain further insight into the dimerization of the hermaphroditic compound **A1** fluorescence titration covering a concentration range between 0.028 mM and $6.6 \cdot 10^{-6}$ mM was performed. Compound **A1** in a mixture of water:methanol 3:2 was excited at the absorption wavelength of the π-π* transition of the hydrophobic oligophenylene-ethynylene part (321 nm). Emission

at 355 nm, 369 nm and a shoulder at around 380 nm was observed which decreases with decreasing concentration as illustrated in figure 37.

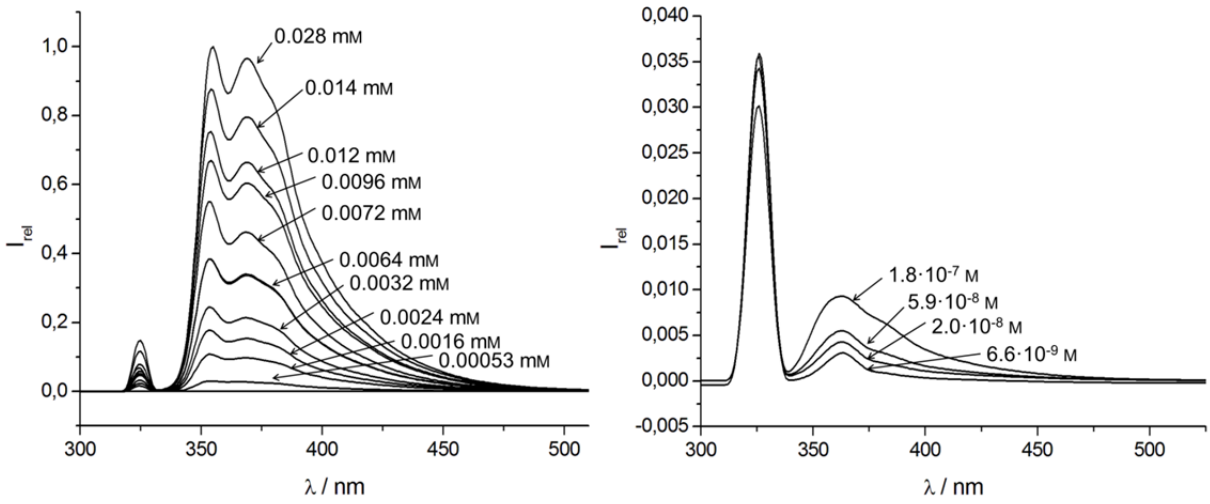

Figure 37. Emission spectra of compound **A1** in water:methanol 3:2 in a concentration range between 0.028 mM (highest rel. intensity) and $6.6 \cdot 10^{-6}$ mM (lowest rel. intensity). On the right hand side the emission of the lowest concentrations is displayed.

When these emission spectra were compared with the emission spectra of monomer **A1** recorded in dichloromethane, where dimer formation should be less pronounced (figure 38), emission at the same wavelengths was found.

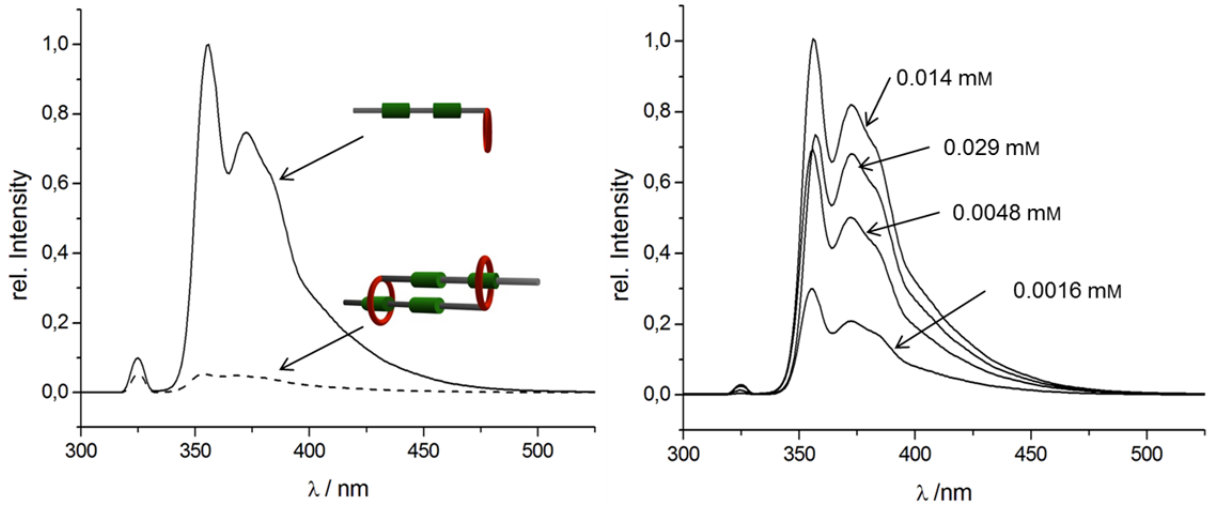

Figure 38. *left*: Fluorescence spectra of amphiphile **A1** in dichloromethane (solid line) and amphiphile **A1** in a water:methanol 3:2 (dotted line) at 1.6 10^{-6} M. *right*: Fluorescence spectra of amphiphile **A1** in dichloromethane at 0.029 mM, 0.014 mM, 0.0048 mM and 0.0016 mM. The lower intensity at 0.029 mM indicates a strong inner filter effect.

The observed relative intensities of **A1** are significantly lower in aqueous solution compared to dichloromethane at the same concentration. Even though a decrease in intensity is expected due to solvent effects, the dramatic decrease is indicative for the inclusion of the OPE rod into

the cavity as a result of the insulating nature of the macrocycles. Furthermore no excimer formation was observed which excludes possible dimeric structures where the hydrophobic rods aggregate outside the cavity (**[a2]TT**).[130] Since it is expected that a dimer like a [c2]daisy chain should potentially allow for excimer formation this finding suggest an unfavorable arrangement of the two hydrophobic rods in respect to each other in the cavity or a structure where only one rod is embedded in the cavity of another, like in a [a2]daisy chain.

A plot of the inner filter effect corrected relative intensities against the concentration shows dimer formation up to a CAC of 1.83 10^{-6} M. Below this CAC the intensities decrease linearly with a decreased slope (figure 39).

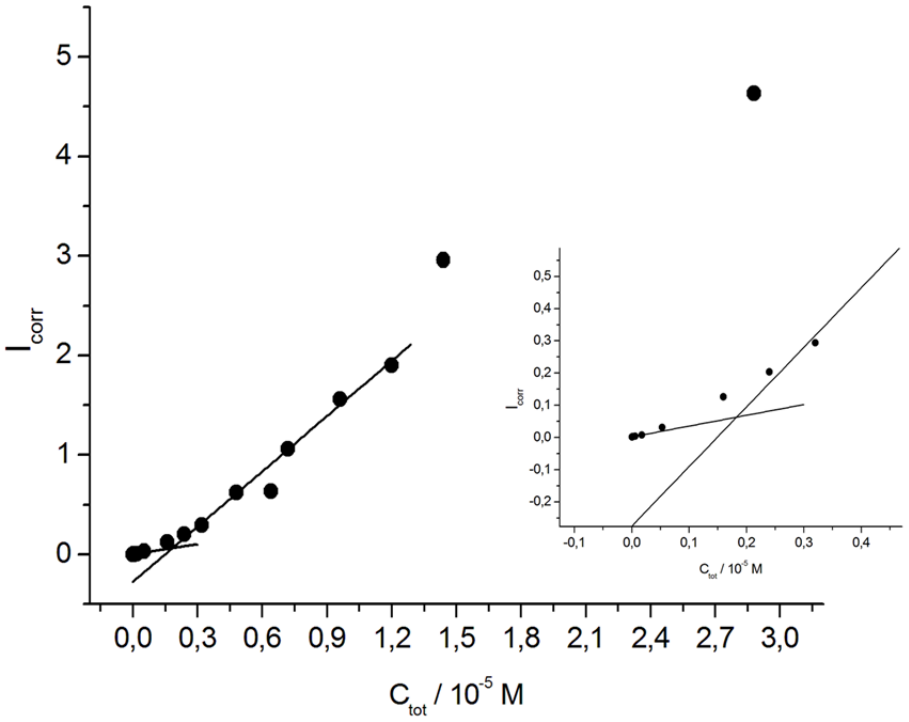

Figure 39. Plot of the relative intensities at 355 nm against the concentration. In the inset the graphical extrapolation to estimate the CAC is shown.

By the NMR-titrations it was demonstrated that at the concentrations used to record the fluorescence spectra the dimerization is the dominant process. The association constant K_a can be thus expressed as

$$K_a = [C_{dim}] / [C_{mon}]^2 \quad (3)$$

The total amphiphile concentration is therefore

$$[C_{tot}] = [C_{mon}] + 2[C_{dim}] \quad (4)$$

Substitution of the dimer concentration gives

$$[C_{tot}] = [C_{mon}] + 2\ K_a\ [C_{mon}]^2 \qquad (5)$$

Since it was shown that the fluorescence of the monomer is significantly higher than the fluorescence of the dimer, a good approximation to estimate K_a is to assume that the fluorescence of the monomer is directly proportional to its concentration. Hence eq. (5) can be written as demonstrated by Margalit *et al*.[134,135] as

$$[C_{tot}] / I_{corr} = k + 2k^2 K_a\ I_{corr} \qquad (6)$$

where k is an experimental coefficient. From the slope and the intercept of a plot of $[C_{tot}]/I_{corr}$ against I_{corr} the association constant was calculated to be $1.33 \cdot 10^6$ M^{-1} (figure 40).

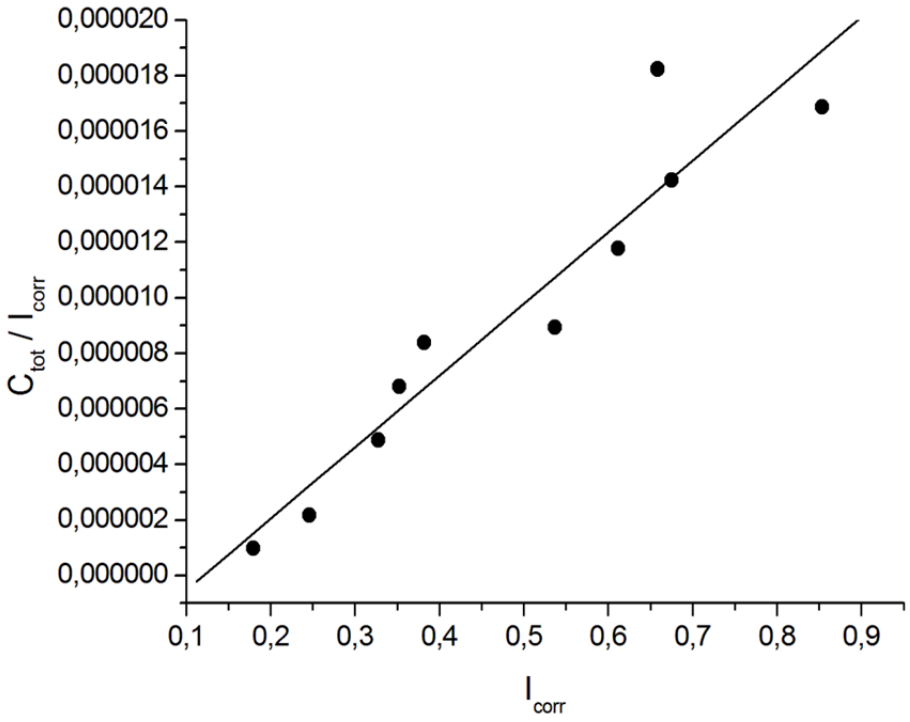

Figure 40. Plot of $[C_{tot}]/I_{corr}$ against I_{corr} for estimation of the association constant K_a.

The rather high association is in good agreement to the observation of a strong hydrophobic effect and in good agreement to association constants reported by Anderson *et al*. for threading Diederich-type cyclophanes with dicationic oligophenylene-ethynylenes.[121] Despite the fact that direct evidence for the formation of daisy chain aggregates in solution was not obtained – mainly due to the complicated ^{1}H-NMR spectra – the high association constant, the prominent upfield chemical shift with increasing concentration, the observation of dimers over a broad concentration range and at very low concentrations, as well as the strongly decreased emission in water:methanol mixtures are strong indicators that it was

possible to design and synthesize an amphiphilic monomer which can form daisy chains. Furthermore it was shown that the nature of these daisy chains can be varied just by changing the concentration.

A direct proof for the formation of aggregates was obtained in the gas phase by high resolution ESI-MS using a nanospray source (figure 41). By measuring a 10^{-5} M aqueous solution of **A1**, oligomers were detected with the composition M_xCl_y, where M is the monomer as a dication. Accordingly, these oligomers carry a positive charge of 2x-y. Masses corresponding to dimers, trimers, tetramers and up to pentamers were observed in this rather low concentration.

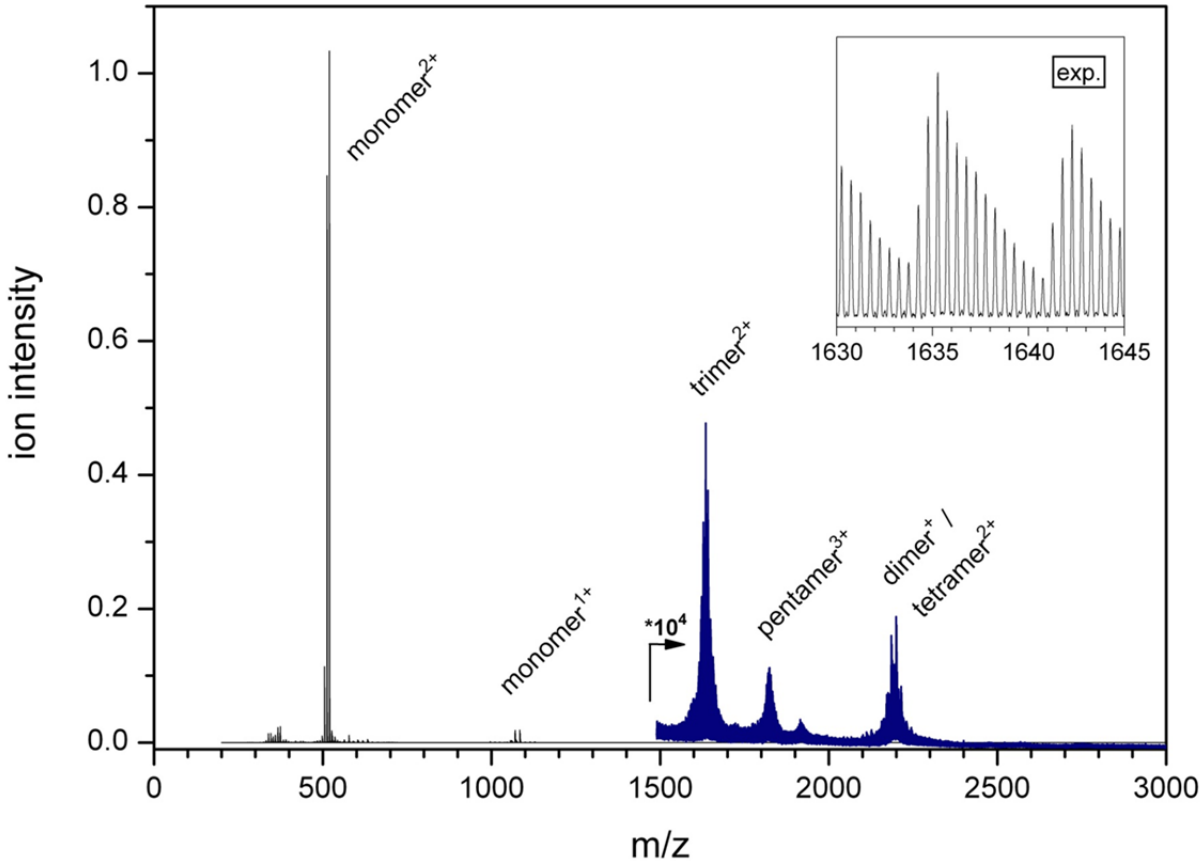

Figure 41. High resolution ESI-MS spectrum of compound **A1**. Displaying the formation of dimers to pentamers.

The peak with the highest intensity in this mass spectrum was the monomer peak which is not surprising since the ions get isolated from the solution in the ion trap and therefore the driving force for aggregation is missing. Due to ion exchange of the chloride anions with other ions in the aqueous solution peak broadening for the masses of the oligomers was observed. Despite the fact that the aggregation behavior of hermaphroditic daisy chain monomer **A1** in solution

and in the gas phase can not be directly compared – especially because of the missing hydrophobic effect – the observation of higher oligomers in the gas phase, together with the indications obtained by ^{1}H-NMR and emission spectroscopy in solution, demonstrates the high potential of this new binding concept towards long oligomeric daisy chains.

Conclusion

An OPE comprising a terminal loop **A1** was successfully synthesized in either 21 or 17 synthetic steps with excellent yields, including that the cyclophane **A11** can be synthesized in large scale. By inspiration of the pioneering work of Diederich it was possible to synthesize mono-functionalized cyclophane **A11** by two different pathways. The synthesis of the hydrophobic OPE **A6** profited from classical Sonogashira cross-coupling. Furthermore ^{1}H-NMR titration experiments showed the formation of dimers up to a concentration of 1 mM. Above this concentration, evidence for aggregation to higher oligomers was found by graphically determination of the aggregation number. Fluorescence studies indicate dimerization down to concentrations of 10^{-6} M. The drop of emission intensity compared to the amphiphile **A1** in dichloromethane suggests inclusion of both rods into the cavity forming a thermodynamically stable [c2]daisy chain which is further supported by a high association constant K_a. Direct evidence for the formation of aggregates was obtained in the gas phase by high resolution ESI-MS, where masses of dimers to pentamers were observed already at low concentrations (10^{-5} M). It was demonstrated that such aggregation behaviour, taking advantage of the hydrophobic effect, can play a major role in the controlled assembly of mechanically interlinked polymers. It was then of interest to study the effect of functionalizations on the hydrophobic rod to be able to generate well defined mechanically interlinked macromolecules.

Experimental Section

General Remarks: All chemicals were directly used for the syntheses without purification if not stated otherwise. Dry solvents were purchased from *Fluka*. The solvents for chromatography and extractions were distilled before use. When Schlenk-technique was used the solvents were degased with argon for several minutes. For column chromatography *silica gel 60* (40-63 μm) from *Fluka* or *SilicaFlash® P60* (40-63 μm) from *Silicycle* was used. TLC were carried out on *Silica gel 60 F_{254}* glass plates with a thickness of 0.25 mm from *Merck*. Characterizations were performed with the following instruments: ^{1}H-NMR and ^{13}C-NMR spectra were recorded on a *Bruker DPX-NMR* (400 MHz) or a *Bruker DRX-500* (500MHz),

the *J* values are given in Hz. Solvents were obtained from *Cambridge Isotope Laboratories*. All spectra were recorded at 298 K. Mass spectra were measured on a *finnigan MAT 95Q* for Electron Impact (EI) and an *esquire 3000 plus* (Bruker) for Electron Spray Ionisation (ESI); measured in *m/z* (%). Elementary analyses were obtained from a *varioMICROcube* from *Elementar*. High resolution mass spectra were recorded by the Schürch group at the University of Bern on a *LTQ Orbitrap XL* from *Thermo Fisher Scientific* using a nanoelectrospray ion source.

NMR-Titrations: A stock solution of 8.84 mg monomer **A1** in 1.0 mL D_2O:methanol-d4 3:2 was prepared. By dilution of this solution the other concentrations were obtained. NMR spectra of the corresponding samples were recorded on a *Bruker DRX-500* (500 MHz) spectrometer at 295 K. Solvents were obtained from *Cambridge Isotope Laboratories*. The samples were locked on methanol-d4. To assign the peaks in the individual spectra COESY spectra were recorded for each individual sample.

Fluorescence Measurements: A stock solution of 0.48 mg monomer **A1** in 3 mL MilliQ water:methanol 3:2 was prepared. By dilution of this solution the other concentrations were obtained. Emission spectra were recorded on a *Shimadzu RF-5301 PC* spectrofluorophotometer using 1 cm *115F-QS Hellma* cuvettes at room temperature in the presence of air. The excitation wavelength was 321 nm which was determined by UV/Vis spectroscopy. Following instrument parameters were used: excitation slit width 1.5 nm; emission slit width 3 nm; response time 2.0 s; sampling interval 1.0 nm.

1-(4-Hydroxy-4-(4-methoxyphenyl)piperidin-1-yl)ethanone (**A19**):[125] In an oven-dried

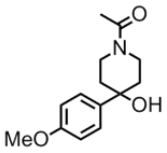

500 mL 2-neck-flask magnesium (1.91 g, 0.920 equiv., 78.8 mmol) was stirred *neat* for 10 min under argon atmosphere. Afterwards 15 mL THF (crown-cap) was added. To this mixture 4-bromoanisol (10.7 mL, 16.0 g, 1.00 equiv., 85.6 mmol) was added dropwise until the reaction started. Then the remaining 4-bromoanisole was diluted with 60 mL THF and the solution was added dropwise by keeping the reaction mixture under a continuous reflux. After stirring for 1.5 h at reflux the Grignard-solution was cooled to 0°C and while vigorously stirring a solution of *N*-acetyl-4-piperidone (9.04 mL, 10.3 g, 0.827 equiv., 70.8 mmol) in 65 mL THF (crown-cap) was added dropwise. After stirring the resulting milky suspension for 4 h at rt the reaction mixture was carefully quenched with sat. aq. ammonium chloride solution and the mixture was stirred for 17 h at rt. Then the solvents were removed and the residue was dissolved in a water/dichloromethane (200 mL each) mixture. The phases were separated and the aqueous one extracted twice with

dichloromethane (2x200 mL). The combined org. layers were dried with sodium sulfate, filtered and concentrated. The yellow solid was washed with diethyl ether to obtain the desired target compound **A19** as a white powder (68%).

R_f = 0.03 (SiO_2; hexanes:EtOAc 1:1, 5% NEt_3); **m.p.** 130°C; **^{1}H-NMR** (400 MHz, $CDCl_3$): δ = 7.37 (d, ^3J(H,H) = 8.9 Hz, 2H, H2(ar)), 6.88 (d, ^3J(H,H) = 8.8 Hz, 2H, H3(ar)), 4.55 – 4.52 (dm, 1H), 3.80 (s, 3H, -OCH_3), 3.72 – 3.64 (m, 1H), 3.63 – 3.53 (m, 1H), 3.13 – 3.04 (m, 1H), 2.11 (s, 3H, -(CO)-CH_3), 2.02 – 1.86 (m, 2H), 1.97 (s, 1H, -O*H*), 1.86 – 1.73 (m, 2H) ppm; **^{13}C-NMR** (101 MHz, $CDCl_3$): δ = 169.0 (C_q, 1C, *C*=O), 158.9 (C_q, 1C, *C*4(ar)-OCH_3), 140.0 (C_q, 1C, *C*1(ar)), 125.8 (C_t, 2C, *C*2(ar)), 113.9 (C_t, 2C, *C*3(ar)), 71.1 (C_q, 1C, *C*-OH), 55.4 (C_p, 1C, -O*C*H_3), 42.9 (C_s, 1C), 39.0 (C_s, 1C), 37.9 (C_s, 1C), 37.9 (C_s, 1C), 21.5 (C_p, 1C, -(CO)-*C*H_3) ppm; **MS** (EI +, 70 eV): m/z (%) = 249 (38), 231 (15), 206 (62), 188 (10), 163 (15), 162 (16), 135 (100), 114 (19), 86 (19), 72 (12), 57 (20), 56 (16), 44 (13), 43 (23).

1-(4-(4-Hydroxyphenyl)-5,6-dihydropyridin-1(*2H*)-yl)ethanone (**A20**):[125] Alcohol **A19**

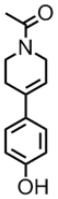

(10.4 g, 1.00 equiv., 41.7 mmol) was dissolved in 300 mL dichloromethane under argon atmosphere. BBr_3 (19.7 mL, 52.2 g, 5.00 equiv., 209 mmol) was added dropwise and the resulting brown reaction mixture was heated at reflux for 3 h. After cooling to 0°C the reaction mixture was carefully quenched with 100 mL methanol. The solvents were evaporated under reduced pressure and the resulting residue was taken up in demin. water. The white solid alkene **A20** was filtered off and washed with plenty of demin. water and Et_2O (93%).

R_f = 0.37 (SiO_2; CH_2Cl_2, 5% MeOH); **m.p.** 186°C; **^{1}H-NMR** (400 MHz, CD_3OD): δ = 7.26 (d, ^3J(H,H) = 7.2 Hz, 2H, H2(ar)), 6.74 (d, ^3J(H,H) = 8.4 Hz, 2H, H3(ar)), 5.96 (s, 1H, -C=C*H*-CH_2-), 4.20 – 4.13 (m, 2H), 3.77, 3.71 (2t, ^3J(H,H) = 5.8 Hz, 2H), 2.61 – 2.45 (2m, 2H), 2.17, 2.13 (2s, 3H, -(CO)-CH_3) ppm; **^{13}C-NMR** (101 MHz, $CDCl_3$): δ = 171.9, 171.8 (C_q, 1C, *C*=O), 158.2, 158.1 (C_q, 1C, *C*4(ar)), 137.1, 136.4 (C_q, 1C, *C*1(ar)), 133.0, 133.0 (C_q, 1C, -*C*=C-CH_2-), 127.1, 127.1 (C_t, 2C, *C*2(ar)), 118.8, 118.2 (C_t, 1C, -C=*C*-CH_2-), 116.1 (C_t, 2C, *C*3(ar)), 46.9, 44.7 (C_s, 1C), 43.2, 39.8 (C_s, 1C), 28.8, 28.1 (C_s, 1C), 21.6, 21.2 (C_p, 1C, -(CO)-*C*H_3), (2 conformers) ppm; **MS** (EI +, 70 eV): m/z (%) = 218 (14), 217 (100), 175 (27), 174 (57), 159 (12), 158 (16), 146 (24), 131 (10), 43 (11).

1-(4-(4-(2-Nitrobenzyloxy)phenyl)-5,6-dihydropyridin-1(*2H*)-yl)ethanone (A15): 1-(4-(4-hydroxyphenyl)-5,6-dihydropyridin-1(*2H*)-yl)ethanone (**A20**) (1.50 g, 1.00 equiv., 6.90 mmol) and 2-nitrobenzylchloride (1.54 g, 1.30 equiv., 8.97 mmol) were suspended in 22.5 mL MeCN under argon atmosphere and purged for 15 min with argon. Afterwards potassium carbonate (1.91 g, 2.00 equiv., 13.8 mmol) was added and the suspension was heated at reflux for 6.5 h. The precipitate was filtered and washed with MeCN. After evaporation the residue was dissolved in toluene and washed with 2.5 M aq. NaOH (twice) and once with sat. brine. The organic layer was dried with sodium sulfate, filtered and concentrated. The crude was purified by column chromatography (SiO_2; CH_2Cl_2, 5% MeOH) and then recrystallized with EtOH to afford product **A15** as a pale brown solid (79%).

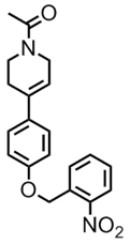

***R*f** = 0.55 (SiO_2; CH_2Cl_2, 2.5% MeOH); **m.p.** 130 – 131°C; **^{1}H-NMR** (400 MHz, $CDCl_3$): δ = 8.17 (d, ^3J(H,H) = 8.2 Hz, 1H, H3(*o*NO_2ar)), 7.88 (d, ^3J(H,H) = 7.8 Hz, 1H, H5(*o*NO_2ar)), 7.68 (t, ^3J(H,H) = 7.6 Hz, 1H), 7.49 (t, ^3J(H,H) = 7.8 Hz, 1H), 7.32 (m, 2H, H2(ar)), 6.95 (d, ^3J(H,H) = 8.6 Hz, 2H, H3(ar)), 6.02 – 5.91 (dm, 1H, -C=C*H*-CH_2-), 5.49 (s, 2H, CH_2(benzyl)), 4.22 (m, 1H), 4.11 (m, 1H), 3.80 (t, ^3J(H,H) = 5.7 Hz, 1H), 3.65 (t, ^3J(H,H) = 5.7 Hz, 1H), 2.59 – 2.47 (dm, 2H), 2.16, 2.13 (2s, 3H, -(CO)-C*H*$_3$) ppm; **^{13}C-NMR** (101 MHz, $CDCl_3$): δ = 169.4, 169.3 (C_q, 1C, *C*=O), 157.7, 157.2 (C_q, 1C, *C*4(ar)), 147.0 (C_q, 1C, C(ar)-NO_2), 136.1 (C_q, 1C), 134.2, 134.1 (C_t, 1C), 133.9, 133.9 (C_q, 1C), 133.8, 133.7 (C_q, 1C), 128.5, 128.4 (C_t, 1C), 126.3, 126.3 (C_t, 2C, *C*2(ar)), 125.1 (C_t, 1C), 119.9 (C_t, 1C), 118.2 (C_t, 1C, -C=*C*H-CH_2-), 114.7 (C_t, 2C, *C*3(ar)), 67.0 (C_s, 1C, -O-*C*H_2-ar), 45.9, 43.5 (C_s, 1C), 42.2 (C_s, 1C), 38.4 (C_s, 1C), 28.1 (C_s, 1C), 27.2 (C_s, 1C), 22.0, 21.6 (C_p, 1C, -(CO)-*C*H_3), (2 conformers) ppm; **MS** (EI +, 70 eV): m/z (%) = 353 (18), 352 (77), 217 (12), 216 (58), 175 (14), 174 (100), 146 (13), 136 (46), 78 (18), 43 (10); **elemental analysis** calcd (%) for $C_{20}H_{20}N_2O_4$: C 68.17, H 5.72, N 7.95; found: C 68.09, H 5.75, N 7.90.

1-(4-(4-Hydroxy-3-methoxyphenyl)-4-(4-(2-nitrobenzyloxy)phenyl)piperidin-1-yl)-ethanone (A14): Alkene **A15** (832 mg, 1.00 equiv., 2.36 mmol), 2-methoxyphenol (1.57 mL, 1.76 g, 6.00 equiv., 14.2 mmol) and $BF_3 \cdot OEt_2$ (2.04 mL, 2.35 g, 7.00 equiv., 16.5 mmol) were dissolved in 6.5 mL CH_2Cl_2 and stirred at rt for 9 d under exclusion of light. Then the mixture was quenched with 5 mL MeOH and diluted with dichloromethane. The organic layer was washed with water and brine, dried with sodium sulfate, filtered and concentrated. The crude red oil was purified by column chromatography (SiO_2; CH_2Cl_2, 5% MeOH). The

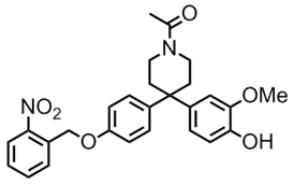

resulting colorless oil was washed with MeCN and the white solid precipitate **A14** was filtered off (99%).

R_f = 0.36 (SiO_2; CH_2Cl_2, 5% MeOH); **m.p.** 156°C; **^{1}H-NMR** (400 MHz, $CDCl_3$): δ = 8.16 (d, ^3J(H,H) = 8 Hz, 1H, H3(*o*NO_2Ar)), 7.86 (d, ^3J(H,H) = 8 Hz, 1H, H5(*o*NO_2Ar)), 7.68 (t, ^3J(H,H) = 8 Hz, 1H), 7.49 (t, ^3J(H,H) = 8 Hz, 1H), 7.16 (d, ^3J(H,H) = 8 Hz, 2H, Ar-H), 6.92 (d, ^3J(H,H) = 8 Hz, 2H, Ar-H), 6.84 (d, ^3J(H,H) = 8 Hz, 1H, Ar-H), 6.76 – 6.71 (m, 1H, Ar-H), 6.66 (d, ^3J(H,H) = 2.5 Hz, 1H, Ar-H), 5.59 (s, 1H, -OH), 5.45 (s, 2H, CH_2(benzyl)), 3.80 (s, 3H, -OCH_3), 3.71 – 3.59 (m, 2H), 3.53 – 3.44 (m, 2H), 2.41 – 2.26 (m, 4H), 2.09 (s, 3H, -(CO)-CH_3) ppm; **^{13}C-NMR** (101 MHz, $CDCl_3$): δ = 169.0 (C_q, 1C, *C*=O), 156.4 (C_q, 1C), 147.1 (C_q, 1C), 146.7 (C_q, 1C), 144.2 (C_q, 1C), 139.7 (C_q, 1C), 138.6 (C_q, 1C), 134.1 (C_t, 1C), 134.0 (C_q, 1C), 128.7 (C_t, 1C), 128.5 (C_t, 1C), 128.2 (C_t, 2C), 125.1 (C_t, 1C), 119.8 (C_t, 1C), 115.1 (C_t, 2C), 114.3 (C_t, 1C), 109.8 (C_t, 1C), 67.0 (C_s, 1C, *C*H_2(benzyl)), 56.0 (C_p, 1C, -O*C*H_3), 44.4 (C_s, 1C), 43.8 (C_s, 1C), 38.8 (C_s, 1C), 37.2 (C_q, 1C), 36.3 (C_s, 1C), 21.6 (C_p, 1C, -(CO)-*C*H_3) ppm; **MS** (ESI, positive ion mode): m/z (%) = 499 ([M+Na]$^+$); **elemental analysis** calcd (%) for $C_{27}H_{28}N_2O_6$: C 68.05, H 5.92, N 5.88; found: C 67.53, H 6.11, N 5.57.

1-(4-(4-(3-Chloropropoxy)phenyl)-5,6-dihydropyridin-1(2H)-yl)ethanone (A16):[125]

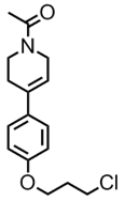

Alcohol **A20** (176 mg, 1.00 equiv., 0.810 mmol) was suspended in 4 mL MeCN. Afterwards potassium carbonate (560 mg, 5.00 equiv., 4.05 mmol) and 1,3-dichloropropane (0.770 mL, 915 mg, 10.0 equiv., 8.10 mmol) were added. The reaction mixture was heated at reflux for 26 h. After cooling to rt the solid was filtered off and washed with plenty of EtOH. The filtrate was concentrated *in vacuo* and the resulting solid was purified by column chromatography (SiO_2; CH_2Cl_2, 5% MeOH). The achieved yellow solid was recrystallized with EtOH to afford **A16** as a colorless solid (73%).

R_f = 0.29 (SiO_2; CH_2Cl_2, 2.5% MeOH); **m.p.** 116 - 117°C; **^{1}H-NMR** (400 MHz, $CDCl_3$): δ = 7.34 – 7.27 (m, 2H, H2(ar)), 6.87 (d, ^3J(H,H) = 8.7 Hz, 2H, H3(ar)), 6.01 – 5.90 (2m, 1H, -C=C*H*-CH_2-), 4.24 – 4.19 (m, 1H), 4.15 – 4.09 (m, 3H), 3.81 (t, ^3J(H,H) = 5.7 Hz, 1H), 3.74 (t, ^3J(H,H) = 6.3 Hz, 2H, -CH_2-CH_2-Cl), 3.65 (t, ^3J(H,H) = 5.7 Hz, 1H), 2.59 – 2.47 (2m, 2H), 2.23 (quint, ^3J(H,H) = 6.1 Hz, 2H, -CH_2-CH_2-CH_2-), 2.16, 2.13 (2s, 3H, -(CO)-CH_3) ppm; **^{13}C-NMR** (101 MHz, $CDCl_3$): δ = 169.5, 169.3 (C_q, 1C, -*C*=O), 158.4, 158.3 (C_q, 1C, *C*4(ar)), 136.2, 134.3 (C_q, 1C,), 133.2, 133.2 (C_q, 1C), 126.2, 126.2 (C_t, 2C, *C*2(ar)), 119.6, 117.9 (C_t, 1C, -C=*C*H-CH_2-), 114.5 (C_t, 2C, *C*3(ar)), 64.4 (C_s, 1C, -O-*C*H_2-CH_2-), 45.9, 43.5 (C_s, 1C), 42.3, 38.4 (C_s, 1C), 41.6 (C_s, 1C, -CH_2-*C*H_2-Cl), 32.4 (C_s, 1C, -CH_2-*C*H_2-CH_2-),

28.1, 27.3 (C_s, 1C), 22.0, 21.6 (C_p, 1C, -(CO)-*C*H_3), (2 conformers) ppm; **MS** (EI +, 70 eV): m/z (%) = 295 (34), 294 (23), 293 (100), 292 (14), 252 (17), 251 (22), 250 (49), 222 (11), 200 (17), 174 (34), 158 (28), 146 (16), 145 (14), 43 (17).

1-(4-(4-(3-Chloropropoxy)phenyl)-4-(4-hydroxyphenyl)piperidin-1-yl)ethanone (A21):

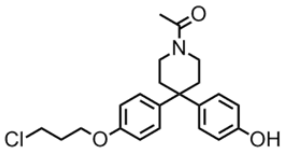

Alkene **A16** (700 mg, 1.00 equiv., 2.38 mmol) was dissolved in 7 mL CH_2Cl_2 (abs.) in an oven-dried Schlenk-tube. Then $BF_3 \cdot OEt_2$ (2.11 mL, 7.00 equiv., 16.7 mmol) was added as well as phenol (1.34 g, 6.00 equiv., 14.3 mmol). The dark-brown reaction mixture was stirred for 23 h at rt. After quenching with 3.5 mL MeOH the mixture was poured into water and extracted three times with EtOAc. The combined organic layers were dried with sodium sulfate, filtered and concentrated. The resulting red oil was purified by column chromatography (SiO_2; CH_2Cl_2, 5% MeOH). The achieved colorless oil was recrystallized from MeCN to isolate target molecule **A21** as a colorless solid.

R_f = 0.15 (SiO_2; CH_2Cl_2, 2.5% MeOH); **m.p.** 246°C; **^{1}H-NMR** (400 MHz, $CDCl_3$): δ = 7.32 (s, 1H, Ar-O*H*), 7.11 (d, ^3J(H,H) = 8 Hz, 2H), 7.03 (d, ^3J(H,H) = 8 Hz, 2H), 6.81 (d, ^3J(H,H) = 8 Hz, 2H), 6.78 (d, ^3J(H,H) = 8 Hz, 2H), 4.06 (t, ^3J(H,H) = 6 Hz, 2H, -O-CH_2-CH_2-), 3.72 (t, ^3J(H,H) = 6 Hz, 2H, -CH_2-CH_2-Cl), 3.68 – 3.61 (m, 2H), 3.50 – 3.45 (m, 2H), 2.34 – 2.26 (dm, 4H), 2.20 (quint, ^3J(H,H) = 6.1 Hz, 2H, -CH_2-CH_2-CH_2-), 2.10 (s, 3H, -(CO)-CH_3) ppm; **^{13}C-NMR** (101 MHz, $CDCl_3$): δ = 169.5 (C_q, 1C, *C*=O), 156.9 (C_q, 1C, *C*4(chloropropoxyphenyl), 154.8 (C_q, 1C, *C*4(phenol)), 139.1 (C_q, 1C), 137.7 (C_q, 1C), 128.0 (C_t, 4C), 115.6 (C_t, 2C), 114.5 (C_t, 2C), 64.3 (C_s, 1C, -O-*C*H_2-CH_2-), 43.8 (C_s, 1C), 41.6 (C_s, 1C), 39.0 (C_s, 1C), 37.0 (C_s, 1C), 36.2 (C_s, 1C), 32.4 (C_s, 1C), 21.5 (C_p, 1C, -(CO)-*C*H_3); **MS** (EI +, 70 eV): m/z (%) = 389 (35), 388 (26), 387 (100 [M^+]), 303 (19), 302 (33), 301 (48 [M^+-C_4H_8NO]), 300 (28), 293 (16 [M^+-C_6H_5O]), 277 (33), 276 (18), 275 (99 [M^+-$C_6H_{11}NO$]), 225 (14), 224 (11), 223 (12), 217 (53 [M^+-$C_9H_{10}ClO$]), 209 (25), 197 (19), 131 (11), 119 (14), 112 (23 [$C_6H_{11}NO$]), 107 (16), 99 (32), 57 (41), 56 (28), 43 (25 [C_2H_3O]), 42 (16); **elemental analysis** calcd (%) for $C_{22}H_{26}ClNO_3$: C 68.12, H 6.76, N 3.61; found: C 68.11, H 6.87, N 3.57.

1-(4-(4-(3-Chloropropoxy)phenyl)-4-(4-(3-iodopropoxy)phenyl)piperidin-1-yl)ethanone (A13):

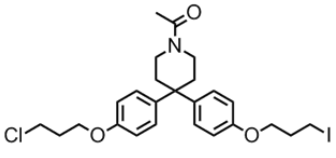

The alcohol **A21** (11.2 g, 1.00 equiv., 28.8 mmol) and BHT (635 mg, 0.100 equiv., 2.88 mmol) were dissolved in 240 mL acetone. To this suspension 1,3-diiodopropane (16.5 mL,

42.6 g, 5.00 equiv., 144 mmol) and K_2CO_3 (11.9 g, 3.00 equiv., 86.4 mmol) were added and the suspension was heated at reflux for 5 h. After cooling to rt the solid was filtered off and washed with plenty of acetone. The filtrate was concentrated and purified by flash column chromatography (SiO_2; CH_2Cl_2:MeOH 80:1) to obtain target molecule **A13** as a colorless oil.

R_f = 0.17 (SiO_2; CH_2Cl_2:MeOH 100:1); **^{1}H-NMR** (400 MHz, $CDCl_3$): δ = 7.13 (d, ^3J(H,H) = 8 Hz, 4H, H2(ar)), 6.83 (d, ^3J(H,H) = 8 Hz, 4H, H3(ar)), 4.07 (t, ^3J(H,H) = 6 Hz, 2H), 4.00 (t, ^3J(H,H) = 6 Hz, 2H), 3.73 (t, ^3J(H,H) = 6 Hz, 2H, -CH_2-CH_2-Cl), 3.68 – 3.61 (m, 2H), 3.51 – 3.45 (m, 2H), 3.35 (t, ^3J(H,H) = 7 Hz, 2H, -CH_2-CH_2-I), 2.38 – 2.27 (m, 4H), 2.25 (quint, ^3J(H,H) = 6 Hz, 2H), 2.21 (quint, ^3J(H,H) = 6 Hz, 2H), 2.08 (s, 3H, -(CO)-CH_3) ppm; **^{13}C-NMR** (101 MHz, $CDCl_3$): δ = 169.0 (C_q, 1C, *C*=O), 156.9 (C_q, 1C), 139.1 (C_q, 1C), 139.0 (C_q, 1C), 128.1 (C_t, 4C), 117.8 (C_q, 1C), 114.8 (C_q, 1C), 114.6 (C_t, 1C), 114.6 (C_t, 1C), 67.3 (C_s, 1C, -O-*C*H_2-CH_2-CH_2-I), 64.3 (C_s, 1C, -O-*C*H_2-CH_2-CH_2-Cl), 44.0 (C_s, 1C), 43.8 (C_q, 1C), 41.7 (C_s, 1C), 38.8 (C_s, 1C), 37.1 (C_s, 1C), 36.2 (C_s, 1C), 33.1 (C_s, 1C), 32.4 (C_s, 1C), 21.6 (C_p, 1C, -(CO)-*C*H_3), 2.74 (C_s, 1C, -CH_2-*C*H_2-I) ppm; **MS** (ESI, positive ion mode, MeCN): m/z = 578 ([M+Na]$^+$); **HRMS** (ESI): m/z calcd for [$C_{25}H_{31}ClINO_3$+H]$^+$: 556.1110; found: 556.1110.

1-(4-(4-(3-(4-(1-Acetyl-4-(4-((2-nitrobenzyl)oxy)phenyl)piperidin-4-yl)-3-methoxy-phenoxy)propoxy)phenyl)-4-(4-(3-chloropropoxy)phenyl)piperidin-1-yl)ethanone (A22):

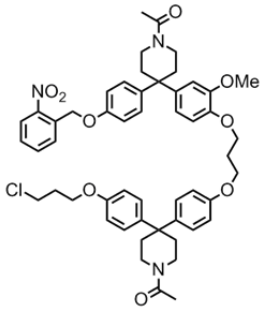

The unfunctionalized part of the cyclophane **A13** (6.06 g, 1.30 equiv., 10.9 mmol) and 1-(4-(4-hydroxy-2-methoxyphenyl)-4-(4-(2-nitro-benzyloxy)phenyl)piperidin-1-yl)ethanone (**A14**) (3.99 g, 1.00 equiv., 8.38 mmol) were dissolved in 360 mL acetone. Then cesium carbonate (5.52 g, 2.00 equiv., 16.8 mmol) was added and the reaction mixture was stirred at 40°C for 17 h. After cooling to rt the suspension was filtered and washed with acetone. The filtrate was concentrated and purified by flash column chromatography (SiO_2; CH_2Cl_2, 2.5% MeOH) to obtain the desired target compound **A22** as a colorless foam (48%).

R_f = 0.30 (SiO_2; CH_2Cl_2, 5% MeOH); **^{1}H-NMR** (500 MHz, $CDCl_3$): δ = 8.15 (d, ^3J(H,H) = 8 Hz, 1H, *nitrobenzyl*), 7.88 (d, ^3J(H,H) = 7.5 Hz, 1H, *nitrobenzyl*), 7.68 (t, ^3J(H,H) = 8 Hz, 1H, *nitrobenzyl*), 7.49 (t, ^3J(H,H) = 7.5 Hz, 1H, *nitrobenzyl*), 7.15 (d, ^3J(H,H) = 8.5 Hz, 2H, Ar-H)), 7.13 – 7.08 (m, 4H, Ar-H), 6.91 (d, ^3J(H,H) = 8.5 Hz, 2H, Ar-H), 6.86 – 6.77 (m, 6H, Ar-H), 6.77 – 6.73 (m, 1H, H6(3-methoxyphenol)), 6.70 – 6.67 (m, 1H, H2(3-

methoxyphenol), 5.45 (s, 2H, CH_2(*benzyl*)), 4.18 – 4.04 (3t, 6H, Ar-O-CH_2-), 3.75 (s, 3H, -OCH_3), 3.72 (t, ^3J(H,H) = 6 Hz, 2H), 3.67 – 3.60 (m, 4H), 3.51 – 3.44 (m, 4H), 2.37 – 2.28 (m, 8H), 2.26 (t, ^3J(H,H) = 6 Hz, 2H), 2.20 (t, ^3J(H,H) = 6 Hz, 2H), 2.09, 2.08 (2s, 6H, -(CO)-CH_3) ppm; **^{13}C-NMR** (126 MHz, $CDCl_3$): δ = 169.0 (C_q, 2C, *C*=O), 157.1 (C_q, 1C), 156.9 (C_q, 1C), 156.4 (C_q, 1C), 149.4 (C_q, 1C), 147.0 (C_q, 1C), 146.8 (C_q, 1C), 139.6 (C_q, 1C), 139.1 (C_q, 1C), 138.8 (C_q, 1C), 134.1 (C_t, 1C), 134.0 (C_q, 1C), 128.7 (C_t, 1C), 128.4 (C_t, 1C), 128.2 (C_t, 2C), 128.1 (C_t, 2C), 128.0 (C_t, 2C), 125.1 (C_t, 1C), 119.3 (C_t, 1C), 115.0 (C_t, 2C), 114.6 (C_t, 4C), 112.9 (C_t, 1C), 111.4 (C_t, 1C), 67.0 (C_s, 1C), 65.6 (C_s, 1C), 64.5 (C_s, 1C), 64.3 (C_s, 2C), 56.2 (C_p, 1C, -O*C*H_3), 44.3 (C_s, 1C), 44.0 (C_s, 1C), 43.7 (C_s, 1C), 41.7 (C_s, 1C), 38.7 (C_s, 2C), 37.1 (C_q, 1C), 37.1 (C_s, 1C), 36.2 (C_q, 1C), 36.1 (C_s, 1C), 32.4 (C_s, 1C), 29.4 (C_s, 1C), 21.6 (C_p, 2C, -(CO)-*C*H_3), ppm; **MS** (ESI, positive ion mode, MeCN): m/z = 926 ($[M+Na]^+$), 904 ($[M]^+$); **HRMS** (ESI): m/z calcd for $[C_{52}H_{58}ClN_3O_9+H]^+$: 904.3934; found: 904.3934.

1-(4-(4-(3-(4-(1-Acetyl-4-(4-(3-chloropropoxy)phenyl)piperidin-4-yl)phenoxy)propoxy)-2-methoxyphenyl)-4-(4-hydroxyphenyl)piperidin-1-yl)ethanone (A12): The nitrobenzyl protected alcohol **A22** (500 mg, 1.00 equiv., 0.553 mmol) was dissolved in 40 mL THF and then radical inhibitor BHT (123 mg, 1.01 equiv., 0.559 mmol) was added. The reaction mixture was irradiated in a Rayonet® spectrophotometer with alternating UV-lamps emitting at 300 nm and 366 nm for 7 h at rt. Afterwards the solvent was evaporated and the residue subjected to column chromatography (SiO_2; CH_2Cl_2:MeOH 20:1). After evaporation of the solvent alcohol **A12** was obtained as a colorless foam (97%).

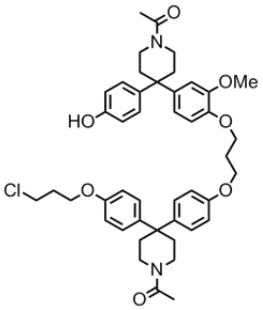

***R*$_f$** = 0.27 (SiO_2; CH_2Cl_2, 5% MeOH); **^{1}H-NMR** (400 MHz, $CDCl_3$): δ = 7.14 – 7.02 (m, 6H, Ar-H), 6.85 – 6.74 (m, 7H), 6.71 (d, ^3J(H,H) = 8.8 Hz, 2H), 6.72 (m, 1H, H6(3-methoxyphenol)), 6.68 (m, 1H, H2(3-methoxyphenol)), 6.48 (s (broad), 1H, -O*H*), 4.18 – 4.04 (m, 6H), 3.74 (s, 3H, -OCH_3), 3.75 – 3.70 (m, 2H), 3.68 – 3.58 (m, 4H), 3.51 – 3.44 (m, 4H), 2.37 – 2.17 (m, 12H), 2.09 (s, 6H, -(CO)-CH_3) ppm; **^{13}C-NMR** (101 MHz, $CDCl_3$): δ = 169.3 (C_q, 1C, *C*=O), 169.3 (C_q, 1C, *C*=O), 159.3 (C_q, 1C), 158.9 (C_q, 1C), 157.1 (C_q, 1C), 156.9 (C_q, 1C), 154.3 (C_q, 1C), 139.0 (C_q, 1C), 138.7 (C_q, 1C), 138.1 (C_q, 1C), 128.3 (C_t, 1C), 128.1 (C_t, 2C), 128.0 (C_t, 4C), 127.4 (C_q, 1C), 114.8 (C_t, 2C), 114.6 (C_t, 4C), 104.6 (C_t, 1C, *C*6(3-methoxyphenol)), 101.2 (C_t, 1C, *C*2(3-methoxyphenol)), 64.4 (C_s, 1C), 64.3 (C_s, 1C), 55.4 (C_p, 1C, -O*C*H_3), 44.0 (C_q, 1C), 43.9 (C_s, 1C), 43.8 (C_s, 1C), 43.3 (C_s, 1C), 41.7 (C_s, 1C),

39.1 (C_s, 1C), 38.9 (C_s, 1C), 37.0 (C_s, 1C), 36.1 (C_s, 1C), 35.9 (C_s, 1C), 35.5 (C_s, 1C), 32.4 (C_s, 1C), 29.5 (C_q, 1C), 29.4 (C_s, 1C), 21.5 (C_p, 1C, -(CO)-*C*H_3), 21.5 (C_p, 1C, -(CO)-*C*H_3) ppm; **MS** (ESI, positive ion mode, MeCN): m/z = 791 ([M+Na]$^+$); **elemental analysis** calcd (%) for $C_{45}H_{53}ClN_2O_7$: C 70.25, H 6.94, N 3.64; found: C 69.90, H 7.009, N 3.63.

1,1"-Diacteyl-5'-methoxy-dispiro[piperidine-4,2'-[7,11,21,25]-tetraoxacyclopenta-[24.2.2.2^{3,6}.2^{12,15}.2^{17,20}]hexatriaconta[3,5,12,14,17,19,26,28,29,31,33,35]dodecaene-16,4"-piperidine] (**A23**) (intramolecular): Cesium carbonate (1.54 g, 6.00 equiv., 4.68 mmol) was

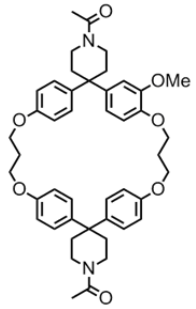

suspended in 25 mL MeCN and heated to reflux. To this suspension a solution of phenol **A12** (600 mg, 1.00 equiv., 0.780 mmol) in 60 mL MeCN was added dropwise over 30 h. After further heating for 14 h the solvent was evaporated and the crude purified by column chromatography (SiO_2; CH_2Cl_2, 5% MeOH). A yellow oil was obtained from which the product was precipitated with EtOH. The white solid was filtered off and washed once with EtOH and once with Et_2O (72%).

***R*$_f$** = 0.36 (SiO_2; CH_2Cl_2, 5% MeOH); **m.p.** 266°C; **^{1}H-NMR** (400 MHz, $CDCl_3$): δ = 7.16 – 7.07 (m, 6H, Ar-H), 6.76 – 6.67 (m, 8H, Ar-H), 6.63 – 6.59 (m, 1H, Ar-H), 4.08 – 3.98 (m, 8H), 3.85 – 3.74 (m, 1H), 3.68 – 3.58 (m, 5H, including s at 3.62 (-OC*H*$_3$)), 3.58 – 3.40 (m, 5H), 2.46 – 2.27 (m, 8H), 2.24 – 2.11 (m, 4H), 2.07, 2.07 (ds, 6H, -(CO)-C*H*$_3$) ppm; **^{13}C-NMR** (101 MHz, $CDCl_3$): δ = 168.9 (C_q, 2C, *C*=O), 157.3 (C_q, 1C), 157.2 (C_q, 1C), 157.2 (C_q, 1C), 149.4 (C_q, 1C), 147.0 (C_q, 1C), 140.0 (C_q, 1C), 138.9 (C_q, 1C), 138.6 (C_q, 1C), 138.0 (C_q, 1C), 127.2 (C_t, 2C), 126.9 (C_t, 4C), 118.0 (C_t, 1C), 114.8 (C_t, 2C), 114.8 (C_t, 2C), 114.7 (C_t, 2C), 113.1 (C_t, 1C), 110.4 (C_t, 1C), 64.7 (C_s, 1C), 63.6 (C_s, 1C), 63.4 (C_s, 1C), 63.3 (C_s, 1C), 55.9 (C_p, 1C, -O*C*H$_3$), 43.7 (C_q, 1C), 43.6 (C_s, 2C), 43.1 (C_q, 1C), 38.6 (C_s, 1C), 38.6 (C_s, 1C), 36.0 (C_s, 1C), 35.8 (C_s, 1C), 35.1 (C_s, 1C), 34.8 (C_s, 1C), 29.7 (C_s, 1C), 29.6 (C_s, 1C), 21.6 (C_p, 2C, -(CO)-*C*H$_3$) ppm; **MS** (ESI, positive ion mode, MeCN): m/z = 771 ([M+K]$^+$), 755 ([M+Na]$^+$), 733 ([M+H]$^+$); **elemental analysis** calcd (%) for $C_{45}H_{52}N_2O_7$: C 73.75, H 7.15, N 3.82; found: C 73.73, H 6.96, N 3.82.

1-(4-(4-(3-Bromopropoxy)phenyl)-5,6-dihydropyridin-1(2H)-yl)ethanone (A24):

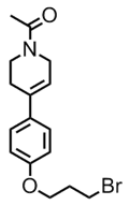

1-Acetyl-4-(4-hydroxyphenyl)-3,4-dehydropiperidine (**A20**) (10.5 g, 1.00 equiv., 48.1 mmol) was suspended in 250 mL MeCN (dry). To this suspension 1,3-dibromopropane (49.0 mL, 10.0 equiv., 481 mmol) and potassium carbonate (33.2 g, 5.00 equiv., 241 mmol) were added and the resulting reaction mixture

heated at reflux for 5 h. The precipitate was filtered off and washed with plenty of EtOH. The filtrate was concentrated and the residue purified by flash column chromatography (SiO_2; CH_2Cl_2, 5% MeOH). The resulting solid was recrystallized with EtOH to afford the alkylated phenol **A24** as a white solid (71%).

R_f = 0.34 (SiO_2; CH_2Cl_2, 2.5% MeOH); **m.p.** 120 - 121°C; **^{1}H-NMR** (400 MHz, $CDCl_3$): δ = 7.33 – 7.26 (m, 2H, H2(ar)), 6.90 – 6.84 (m, 2H, H3(ar)), 6.01 – 5.89 (2m, 1H, -C=C*H*-CH_2-), 4.24 – 4.19 (m, 1H), 4.14 – 4.08 (m, 3H), 3.83 – 3.77 (m, 1H), 3.67 – 3.63 (m, 1H), 3.60 (t, ^3J(H,H) = 6 Hz, 2H, -CH_2-C*H*$_2$-Br), 2.59 – 2.47 (2m, 2H), 2.31 (quint, ^3J(H,H) = 6 Hz, 2H, -CH_2-C*H*$_2$-CH_2-), 2.16, 2.13 (2s, 3H, -(CO)-C*H*$_3$) ppm; **^{13}C-NMR** (101 MHz, $CDCl_3$): δ = 169.4, 169.3 (C_q, 1C, -*C*=O), 158.3, 158.2 (C_q, 1C, *C*4(ar)), 136.2, 134.3 (C_q, 1C,), 133.3, 133.2 (C_q, 1C), 126.2, 126.1 (C_t, 2C, *C*2(ar)), 119.6, 117.9 (C_t, 1C, -C=*C*H-CH_2-), 114.6 (C_t, 2C, *C*3(ar)), 64.5 (C_s, 1C, -O-*C*H_2-CH_2-), 45.9, 43.5 (C_s, 1C), 42.2, 38.4 (C_s, 1C), 32.5 (C_s, 1C, -CH_2-*C*H_2-CH_2-), 30.1 (C_s, 1C, -CH_2-*C*H_2-Br), 28.1, 27.3 (C_s, 1C), 22.0, 21.6 (C_p, 1C, -(CO)-*C*H_3), (2 conformers) ppm; **MS** (EI +, 70 eV): m/z (%) = 340 (17), 339 (99), 338 (28), 337 (100), 336 (11), 297 (17), 296 (39), 295 (17), 294 (39), 280 (11), 216 (11), 200 (24), 174 (43), 159 (11), 158 (35), 146 (17), 145 (16), 43 (11); **elemental analysis** calcd (%) for $C_{16}H_{20}BrNO_2$: C 56.82, H 5.96, N 4.14; found C 56.99, H 5.87, N 4.17.

1-(4-(4-(3-Bromopropoxy)phenyl)-4-(4-hydroxy-3-methoxyphenyl)piperidin-1-yl)-ethanone (A25): To a solution of alkene **A24** (9.91 g, 1.00 equiv., 29.3 mmol) in 80 mL dichloromethane guaiacol (19.5 mL, 21.8 g, 6.00 equiv., 176 mmol) followed by boron trifluoride dietherate (25.3 mL, 29.1 g, 7.00 equiv, 205 mmol) were added under argon atmosphere. The reaction mixture was stirred for 9 d at rt under exclusion of light. Then the mixture was quenched with 60 mL MeOH and poured into demin. water. Afterwards the solution was extracted with EtOAc (3x160 mL), dried with sodium sulfate, filtered and concentrated. The red crude was suspended in a mixture of dichloromethane, 2.5% MeOH and the white solid was filtered off and washed with dichloromethane and diethyl ether. The filtrate was concentrated and the residue purified by column chromatography (SiO_2; CH_2Cl_2, 2.5% MeOH). The two product fractions were combined and dissolved in EtOAc. After evaporation of the solvent the desired product **A25** was obtained as a white solid (94%).

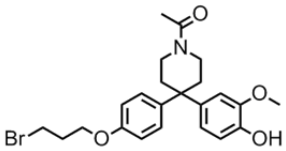

R_f = 0.29 (SiO_2; CH_2Cl_2, 2.5% MeOH); **m.p.** 164 - 165°C; **^{1}H-NMR** (400 MHz, $CDCl_3$): δ = 7.13 (d, ^3J(H,H) = 8 Hz, 2H), 6.87 – 6.80 (m, 3H), 6.73 (dd, ^3J(H,H) = 8 Hz, ^4J(H,H) = 2 Hz,

1H, H6(4-hydroxy-3-methoxyphenyl), 6.66 (d, ^4J(H,H) = 2 Hz, 1H, H2(4-hydroxy-3-methoxyphenyl)), 5.66 (s, 1H, Ar-O*H*), 4.07 (t, ^3J(H,H) = 6 Hz, 2H, -O-C*H*$_2$-CH$_2$-), 3.80 (s, 3H, -OC*H*$_3$), 3.73 – 3.55 (m, 4H), 3.55 – 3.42 (m, 2H), 2.40 – 2.23 (m, 6H), 2.09 (s, 3H, -(CO)-C*H*$_3$) ppm; **^{13}C-NMR** (101 MHz, $CDCl_3$): δ = 169.0 (C_q, 1C, *C*=O), 157.0 (C_q, 1C, *C*4(bromopropoxyphenyl), 146.7 (C_q, 1C), 144.0 (C_q, 1C), 138.9 (C_q, 1C), 138.7 (C_q, 1C), 128.1 (C_t, 2C), 119.8 (C_t, 1C), 114.6 (C_t, 2C), 114.4 (C_t, 1C), 109.8 (C_t, 1C), 65.3 (C_s, 1C, -O-*C*H$_2$-CH$_2$-), 56.0 (C_p, 1C), 44.3 (C_s, 1C), 43.8 (C_q, 1C), 38.8 (C_s, 1C), 37.2 (C_s, 1C), 36.3 (C_s, 1C), 32.5 (C_s, 1C), 30.2 (C_s, 1C), 21.6 (C_p, 1C, -(CO)-*C*H$_3$) ppm; **MS** (EI +, 70 eV): m/z (%) = 464 (23), 463 (100), 462 (24), 461 (98 [M$^+$]), 378 (15), 377 (36), 376 (38), 375 (37), 374 (22-[M$^+$-C$_4$H$_9$NO]), 352 (14), 351 (87), 350 (15), 349 (88), 347 (10), 345 (12), 339 (16), 337 (16 [M$^+$-C$_7$H$_8$O$_2$]), 253 (11), 247 (29-[M$^+$-C$_9$H$_{11}$BrO]), 239 (21), 229 (10), 137 (11), 112 (22), 99 (30), 56 (28), 57 (47), 56 (35), 43 (33), 42 (21), 41 (14); **elemental analysis** calcd (%) for $C_{23}H_{28}BrNO_4$: C 59.74, H 6.10, N 3.03; found C 59.61, H 6.19, N 3.10.

1-(4-(4-(3-Bromopropoxy)-3-methoxyphenyl)-4-(4-(3-bromopropoxy)phenyl)piperidin-1-yl)ethanone (A17): The phenol **A25** (12.7 g, 1.00 equiv., 27.5 mmol) was dissolved in

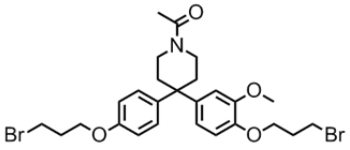

110 mL acetone under argon atmosphere in a preheated flask. Then 1,3-dibromopropane (14.0 mL, 27.8 g, 5.00 equiv., 138 mmol) and potassium carbonate (11.5 g, 3.00 equiv., 82.5 mmol) were added and the resulting reaction mixture was heated at reflux for 20 h. After cooling to rt the suspension was filtered and the solid washed several times with acetone. The filtrate was concentrated and the residue purified by column chromatography (SiO_2; CH_2Cl_2, 2.5% MeOH) (91%).

***R*$_f$** = 0.34 (SiO_2; CH_2Cl_2, 2.5% MeOH); **^{1}H-NMR** (400 MHz, $CDCl_3$): δ = 7.14 (d, ^3J(H,H) = 8 Hz, 2H), 6.86 – 6.80 (m, 3H), 6.78 – 6.73 (m, 1H, H6(4-hydroxy-3-methoxyphenyl), 6.71 (d, ^4J(H,H) = 2 Hz, 1H, H2(4-hydroxy-3-methoxyphenyl)), 4.15 – 4.04 (m, 4H, -O-C*H*$_2$-CH$_2$-), 3.77 (s, 3H, -OC*H*$_3$), 3.65 – 3.45 (m, 8H), 2.39 – 2.25 (m, 8H), 2.08, 2.04 (s, 3H, -(CO)-C*H*$_3$) ppm; **^{13}C-NMR** (101 MHz, $CDCl_3$): δ = 169.0 (C_q, 1C, *C*=O), 157.0 (C_q, 1C, *C*4(bromopropoxyphenyl), 149.6 (C_q, 1C), 146.6 (C_q, 1C), 140.1 (C_q, 1C), 138.7 (C_q, 1C), 128.1 (C_t, 2C), 119.3 (C_t, 1C), 114.6 (C_t, 2C), 113.4 (C_t, 1C), 111.5 (C_t, 1C), 66.7 (C_s, 1C, -O-*C*H$_2$-CH$_2$-), 65.3 (C_s, 1C, -O-*C*H$_2$-CH$_2$-), 56.3 (C_p, 1C), 44.3 (C_s, 1C), 43.8 (C_q, 1C), 38.8 (C_s, 1C), 37.2 (C_s, 1C), 36.2 (C_s, 1C), 32.5 (C_s, 1C), 31.2 (C_s, 1C), 30.3 (C_s, 1C), 30.2 (C_s, 1C), 21.6 (C_p, 1C, -(CO)-*C*H$_3$) ppm; **MS** (ESI, positive ion mode, MeCN): m/z = 585 ([M+H]$^+$); **HRMS** (ESI): m/z calcd for [$C_{26}H_{33}Br_2NO_4$]: 581.0776; found: 581.0771.

1-(4,4-Bis(4-hydroxyphenyl)piperidin-1-yl)ethanone (A18):[118] To a solution of phenol (412 mg, 2.06 equiv., 4.38 mmol) in 0.2 mL demin water *N*-acetylpiperidin-4-one (300 mg, 1.00 equiv., 2.13 mmol) was added. Afterwards the solution was cooled to 0°C and 0.43 mL conc. H_2SO_4 was added. The colorless reaction mixture was stirred at rt for 3 d. The formed colorless gel was dissolved in 4.4 mL hot aceton/MeOH 7:3. Then the solution was made neutral by addition of 1 N aq. Na_2CO_3 solution (9 mL) and demin. water was added to a total volume of 17.5 mL. The mixture was cooled to 0°C for 1 h until precipitation was complete. The precipitate was filtered off and washed with demin. water. The solid was recrystallized with EtOH to afford 1-(4,4-bis(4-hydroxyphenyl)piperidin-1-yl)ethanone (**A18**) as a colorless solid (84%).

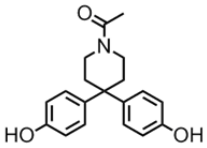

R_f = 0.04 (SiO_2; CH_2Cl_2, 5% MeOH); **m.p.** 298°C; **^{1}H-NMR** (400 MHz, DMSO): δ = 9.20 (s, 2H), 7.07 (d, ^3J(H,H) = 8 Hz, 4H), 6.66 (d, ^3J(H,H) = 8 Hz, 4H), 3.39 (s (broad), 4H), 2.26 (s (broad), 2H), 2.17 (s (broad), 2H), 1.97 (s, 3H) ppm; **^{13}C-NMR** (101 MHz, DMSO): δ = 167.9 (C_q, 1C), 154.9 (C_q, 2C), 137.2 (C_q, 2C), 127.5 (C_t, 4C), 114.9 (C_t, 4C), 42.9 (C_s, 1C), 38.0 (C_s, 1C), 35.9 (C_s, 1C), 35.3 (C_s, 1C), 30.6 (C_q, 1C), 21.2 (C_p, 1C) ppm; **MS** (ESI, positive ion mode, MeCN): m/z (%) = 334 ($[M+Na]^+$).

2-Methyl-4-(4-((trimethylsilyl)ethynyl)phenyl)but-3-yn-2-ol (A26):[136] In an oven-dried Schlenk-tube 1,4-diiodobenzene (8.00 g, 1.00 equiv., 24.2 mmol) was dissolved in 40 mL dry THF. $PdCl_2(PPh_3)_2$ (1.04 g, 6 mol%, 1.48 mmol) and CuI (277 mg, 6 mol%, 1.46 mmol) were added and the solution was degased with argon for 15 min. Afterwards TMS-acetylene (3.36 mL, 1.00 equiv., 24.2 mmol) was added and the now inhomogenous reaction mixture was stirred for 4 h at rt. Then 2-methyl-3-butyn-3-ol (4.74 mL, 2.00 equiv., 48.5 mmol) was added dropwise and the dark-brown reaction mixture was stirred for another 15 h at rt. The solvent was removed by rotary evaporation and the residue was treated with water and extracted with dichloromethane. The combined organic layers were washed with water and brine, dried with sodium sulfate, filtered and evaporated to dryness. The dark-brown residue was purified by flash column chromatography (SiO_2; hexane:CH_2Cl_2 3:7, then CH_2Cl_2) to isolate the product **A26** as a pale yellow solid (45%).

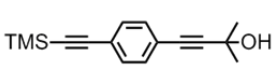

R_f = 0.19 (SiO_2; cyclohexane:CH_2Cl_2 7:3); **m.p.** 108 - 109°C; **^{1}H-NMR** (400 MHz, $CDCl_3$): δ = 7.39 (d, ^3J(H,H) = 8.5 Hz, 2H), 7.33 (d, ^3J(H,H) = 8.5 Hz, 2H), 1.61 (s, 6H), 0.25 (s, 9H) ppm; **^{13}C-NMR** (101 MHz, $CDCl_3$): δ = 131.8 (C_t, 2C), 131.4 (C_t, 2C), 122.9 (C_q, 1C), 122.8

(C_q, 1C), 104.5 (C_q, 1C), 96.1 (C_q, 1C), 95.6 (C_q, 1C), 81.8 (C_q, 1C), 65.6 (C_q, 1C), 31.4 (C_p, 2C), - 0.1 (C_p, 3C) ppm; **MS** (EI +, 70 eV): m/z (%) = 256 (23), 241 (100).

((4-Ethynylphenyl)ethynyl)trimethylsilane (A27):[136]

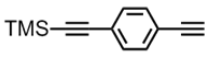

2-Methyl-4-(4-((trimethylsilyl)ethynyl)phenyl)but-3-yn-2-ol (**A26**) (2.63 g, 1.00 equiv., 10.2 mmol) was dissolved in 45 mL dry toluene. To this dark-yellow solution powdered sodium hydroxide (451 mg, 1.10 equiv., 11.2 mmol) was added in one lot and the resulting reaction mixture was heated to reflux for 45 min. After cooling to rt the solvent was removed and the residue was treated with sat. aq. NH_4Cl and extracted with dichloromethane. The combined organic layers were washed with demin. water and brine, dried with sodium sulfate, filtered and the solvent was evaporated *in vacuo*. The solid, brown residue was purified by flash column chromatography (SiO_2; pentane:EtOAc 10:1). According to this procedure product **A27** was isolated as a pale yellow solid (82%).

R_f = 0.69 (SiO_2; cyclohexane:EtOAc 50:1); **m.p.** 124°C; **^{1}H-NMR** (400 MHz, $CDCl_3$): δ = 7.41 (s, 4H), 3.16 (s, 1H), 0.25 (s, 9H) ppm; **^{13}C-NMR** (101 MHz, $CDCl_3$): δ = 131.9 (C_t, 2C), 131.8 (C_t, 2C), 123.6 (C_q, 1C), 122.1 (C_q, 1C), 104.3 (C_q, 1C), 96.5 (C_q, 1C), 83.2 (C_q, 1C), 78.9 (C_q, 1C), - 0.1 (C_p, 3C) ppm; **MS** (EI +, 70 eV): m/z (%) = 198 (26 [M^+]), 184 (18), 183 (100 [M^+-CH_3]).

Trimethyl((4-(phenylethynyl)phenyl)ethynyl)silane (A28):

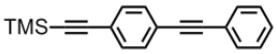

Bis(triphenylphosphine)palladium(II) chloride (25.2 mg, 3 mol%, 35.9 µmol) and CuI (6.84 mg, 3 mol%, 35.9 µmol) were put into an oven-dried 25 mL Schlenk-tube under argon atmosphere. Then a solution of aryl iodide (249 mg, 1.00 equiv., 1.20 mmol) in 2.5 mL THF and a solution of the acetylene **A27** (285 mg, 1.20 equiv., 1.44 mmol) in 2.5 mL THF were added and the mixture was degased for 10 min (argon). Afterwards diisopropylamine (0.592 mL, 424 mg, 3.50 equiv., 4.19 mmol) was added and the reaction mixture was stirred at rt for 4 h. After removing the solvent the crude was taken up in demin. water and dichloromethane. The phases were separated and the aqueous one extracted twice with dichloromethane. The combined org. layers were washed with brine, dried with sodium sulfate, filtered and concentrated. The crude was further purified by column chromatography (SiO_2; dichloromethane:cyclohexane 1:3) (99%).

R_f = 0.25 (SiO_2; cyclohexane:EtOAc 10:1); **m.p.** 120 - 121°C; **^{1}H-NMR** (400 MHz, $CDCl_3$): δ = 7.55 – 7.50 (m, 2H), 7.49 – 7.42 (m, 4H), 7.38 – 7.33 (m, 3H), 0.26 (s, 9H) ppm; **^{13}C-NMR** (101 MHz, $CDCl_3$): δ = 132.0 (C_t, 2C), 131.8 (C_t, 2C), 131.5 (C_t, 2C), 128.6 (C_t,

1C), 128.5 (C_t, 2C), 123.5 (C_q, 2C), 123.1 (C_q, 1C), 123.0 (C_q, 1C), 104.8 (C_q, 1C), 96.4 (C_q, 1C), 91.4 (C_q, 1C), 89.2 (C_q, 1C), 0.1 (C_p, 3C) ppm; **MS** (EI +, 70 eV): m/z (%) = 275 (13), 274 (53 [M^+]), 260 (24), 259 (100 [M^+-CH_3]), 129 (12).

1-Ethynyl-4-(phenylethynyl)benzene (A6): The TMS-protected OPE **A28** (150 mg, 1.00 equiv., 0.547 mmol) was dissolved in 3 mL THF under argon atmosphere in an oven-dried 25 mL Schlenk-tube. Then acetic anhydride (0.103 mL, 112 mg, 2.00 equiv., 1.09 mmol) and acetic acid (62.6 µL, 65.7 mg, 2.00 equiv., 1.09 mmol) were added. The solution was cooled to 0°C and then TBAF (0.662 mL (1 M in THF, 582 mg, 1.21 equiv., 0.662 mmol)) was added dropwise. The reaction mixture was stirred at 0°C for 1 h. Afterwards the reaction mixture was poured into demin. water and extracted three times with dichloromethane. The combined organic layers were washed once with brine, dried with sodium sulfate, filtered and concentrated. The residue was purified by column chromatography (SiO_2; cyclohexane:Et_2O 10:1) to afford OPE **A6** as a white solid after evaporation of the solvent.

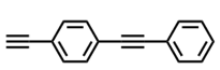

***R**f* = 0.73 (SiO_2; cyclohexane:Et_2O 10:1); **m.p.** 86 - 87°C; **^{1}H-NMR** (400 MHz, $CDCl_3$): δ = 7.56 – 7.51 (m, 2H), 7.50 – 7.45 (m, 4H), 7.38 – 7.33 (m, 3H), 3.18 (s, 1H), ppm; **^{13}C-NMR** (101 MHz, $CDCl_3$): δ = 132.1 (C_t, 2C), 131.8 (C_t, 2C), 131.6 (C_t, 2C), 128.7 (C_t, 1C), 128.5 (C_t, 2C), 123.9 (C_q, 1C), 123.1 (C_q, 1C), 122.0 (C_q, 1C), 91.5 (C_q, 1C), 89.0 (C_q, 1C), 83.4 (C_q, 1C), 79.0 (C_t, 1C) ppm; **MS** (EI +, 70 eV): m/z (%) = 203 (17), 202 (100 [M^+]), 200 (19).

1,1”-Diacteyl-5’-methoxy-dispiro[piperidine-4,2’-[7,11,21,25]-tetraoxacyclopenta[24.2.2.2^{3,6}.2^{12,15}.2^{17,20}]hexatriaconta[3,5,12,14,17,19,26,28,29,31,33,35] dodecaene-16,4”-piperidine] (**A23**) (intermolecular): Cesium carbonate (5.64 g, 10.0 equiv., 17.1 mmol), bisphenol **A18** (534 mg, 1.00 equiv., 1.72 mmol) and dialkyl bromide **A17** (1.00 g, 1.00 equiv., 1.72 mmol) were suspended in 0.6 L MeCN and heated at reflux for 20 h. After cooling to rt the precipitate was filtered off and the filtrate was concentrated. The residue was taken up in dichloromethane and the insoluble white solid was again filtered off. The filtrate was again concentrated and the remaining crude purified by column chromatography (SiO_2; CH_2Cl_2, 5% MeOH). The white solid product was precipitated with EtOH, filtered and washed with EtOH and a small amount of diethyl ether (31%).

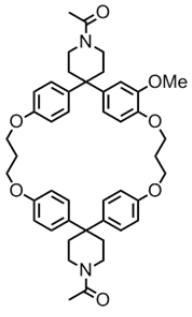

***R**f* = 0.36 (SiO_2; CH_2Cl_2, 5% MeOH); **m.p.** 266°C; **^{1}H-NMR** (400 MHz, $CDCl_3$): δ = 7.16 – 7.07 (m, 6H, Ar-H), 6.76 – 6.67 (m, 8H, Ar-H), 6.63 – 6.59 (m, 1H, Ar-H), 4.08 – 3.98 (m,

8H), 3.85 – 3.74 (m, 1H), 3.68 – 3.58 (m, 5H, including s at 3.62 (-OC*H*$_3$)), 3.58 – 3.40 (m, 5H), 2.46 – 2.27 (m, 8H), 2.24 – 2.11 (m, 4H), 2.07, 2.07 (ds, 6H, -(CO)-C*H*$_3$) ppm; **^{13}C-NMR** (101 MHz, $CDCl_3$): δ = 168.9 (C_q, 2C, *C*=O), 157.3 (C_q, 1C), 157.2 (C_q, 1C), 157.2 (C_q, 1C), 149.4 (C_q, 1C), 147.0 (C_q, 1C), 140.0 (C_q, 1C), 138.9 (C_q, 1C), 138.6 (C_q, 1C), 138.0 (C_q, 1C), 127.2 (C_t, 2C), 126.9 (C_t, 4C), 118.0 (C_t, 1C), 114.8 (C_t, 2C), 114.8 (C_t, 2C), 114.7 (C_t, 2C), 113.1 (C_t, 1C), 110.4 (C_t, 1C), 64.7 (C_s, 1C), 63.6 (C_s, 1C), 63.4 (C_s, 1C), 63.3 (C_s, 1C), 55.9 (C_p, 1C, -O*C*H$_3$), 43.7 (C_q, 1C), 43.6 (C_s, 2C), 43.1 (C_q, 1C), 38.6 (C_s, 1C), 38.6 (C_s, 1C), 36.0 (C_s, 1C), 35.8 (C_s, 1C), 35.1 (C_s, 1C), 34.8 (C_s, 1C), 29.7 (C_s, 1C), 29.6 (C_s, 1C), 21.6 (C_p, 2C, -(CO)-*C*H$_3$) ppm; **MS** (ESI, positive ion mode, MeCN): m/z = 771 ([M+K]$^+$), 755 ([M+Na]$^+$), 733 ([M+H]$^+$; **elemental analysis** calcd (%) for $C_{45}H_{52}N_2O_7$: C 73.75, H 7.15, N 3.82; found: C 73.73, H 6.96, N 3.82.

1,1”-Diacteyl-5’-hydroxy-dispiro[piperidine-4,2’-[7,11,21,25]-tetraoxacyclopenta-[24.2.2.2^{3,6}.2^{12,15}.2^{17,20}]hexatriaconta[3,5,12,14,17,19,26,28,29,31,33,35]dodecaene-16,4”-piperidine] (A11): Cyclophane **A23** (664 mg, 1.00 equiv., 0.906 mmol) and sodium thiomethoxide (317 mg, 5.00 equiv., 4.53 mmol) were dissolved in 70 mL DMF and heated at 160°C under argon atmosphere for 6 h. Then 46 mL 0.1 M aq. HCl was added and the solvents removed under vacuum. The residue was taken up in water and the suspension was filtered. The remaining pale beige solid was washed once with diethyl ether (10 mL). The white powder was recrystallized with methanol (98%).

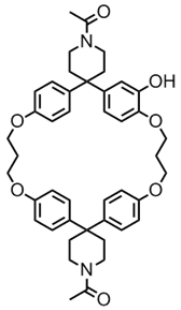

***R*$_f$** = 0.35 (SiO_2; CH_2Cl_2, 5% MeOH); **m.p.** 232°C; **^{1}H-NMR** (400 MHz, $CDCl_3$): δ = 7.16 – 7.05 (m, 6H, Ar-H), 6.79 – 6.60 (m, 9H, Ar-H), 5.64 (broad s, 1H, -O*H*), 4.14 – 4.07 (m, 2H, phenol-O-C*H*$_2$-), 4.06 – 3.98 (m, 6H, Ar-O-C*H*$_2$-), 3.72 – 3.57 (m, 4H), 3.55 – 3.44 (m, 4H), 2.47 – 2.28 (m, 8H), 2.25 – 2.12 (m, 4H), 2.07, 2.06 (ds, 6H, -(CO)-C*H*$_3$) ppm; **^{13}C-NMR** (101 MHz, $CDCl_3$): δ = 168.9 (C_q, 2C, *C*=O), 157.1 (C_q, 1C), 157.1 (C_q, 1C), 156.8 (C_q, 1C), 145.7 (C_q, 1C), 144.2 (C_q, 1C), 140.3 (C_q, 1C), 139.1 (C_q, 1C), 138.5 (C_q, 1C), 138.4 (C_q, 1C), 127.0 (C_t, 4C), 126.9 (C_t, 2C), 116.9 (C_t, 1C), 114.8 (C_t, 2C), 114.7 (C_t, 2C), 114.6 (C_t, 2C), 112.9 (C_t, 1C), 111.6 (C_t, 1C), 65.1 (C_s, 1C), 63.9 (C_s, 1C), 63.3 (C_s, 1C), 63.3 (C_s, 1C), 63.3 (C_s, 1C), 43.6 (C_s, 1C), 43.6 (C_s, 1C), 43.2 (C_q, 1C), 43.1 (C_q, 1C), 38.6 (C_s, 1C), 35.8 (C_s, 1C), 35.8 (C_s, 1C), 34.8 (C_s, 1C), 34.8 (C_s, 1C), 29.6 (C_s, 1C), 29.4 (C_s, 1C), 21.6 (C_p, 2C, -(CO)-*C*H$_3$) ppm; **MS** (ESI, positive ion mode, MeCN): m/z = 757 ([M+K]$^+$), 741 ([M+Na]$^+$), 719 ([M+H]$^+$); **HRMS** (ESI): m/z calcd for [$C_{44}H_{50}N_2O_7$+H]$^+$: 719.3691; found: 719.3691.

1,1”-Diacteyl-5’-(1-iodo-4-phenoxymethylbenzene)-dispiro[piperidine-4,2’-[7,11,21,25]-tetraoxacyclopenta[24.2.2.2^{3,6}.2^{12,15}.2^{17,20}]hexatriaconta[3,5,12,14,17,19,26,28,29,31,33,35]dodecaene-16,4”-piperidine] (A9): The alcohol **A11** (150 mg, 1.00 equiv., 0.209 mmol), 4-iodobenzylbromide (98.0 mg, 1.50 equiv., 0.314 mmol) and cesium carbonate (138 mg, 2.00 equiv., 0.418 mmol) were suspended in 12 mL dry DMF under argon atmosphere. The reaction mixture was heated at 85°C for 20 h. Afterwards, the solvent was evaporated and the residue taken up in dichloromethane and demin. water. The layers were separated and the aqueous one extracted three times with dichloromethane. The combined organic layers were washed with demin. water, brine, dried with sodium sulfate, filtered and concentrated. The crude was purified by column chromatography (SiO_2; CH_2Cl_2 then CH_2Cl_2, 2.5% MeOH). The desired product **A9** was obtained as a white powder (98%).

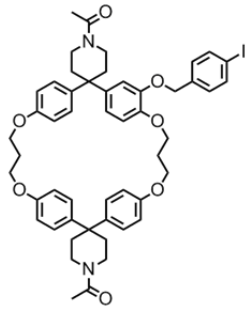

***R*$_f$** = 0.39 (SiO_2; CH_2Cl_2, 5% MeOH); **m.p.** 137°C; **^{1}H-NMR** (400 MHz, $CDCl_3$): δ = 7.64 (d, ^3J(H,H) = 8 Hz, 2H, Iodobenzene-H2), 7.12 – 7.06 (m, 4H, Ar-H), 6.98 (d, ^3J(H,H) = 8 Hz, 2H, Ar-H), 6.94 (d, ^3J(H,H) = 8 Hz, 2H, Ar-H), 6.75 – 6.67 (m, 8H, Ar-H), 6.46 (d, ^4J(H,H) = 2 Hz, 1H, Ar-H), 4.73 (s, 2H, iodobenzene-C*H*$_2$-O-), 4.09 – 3.99 (m, 8H, Ar-O-CH$_2$-), 3.72 – 3.61 (m, 3H), 3.53 – 3.36 (m, 5H), 2.42 – 2.33 (m, 4H), 2.30 – 2.12 (m, 8H), 2.06, 2.06 (ds, 6H, -(CO)-CH$_3$) ppm; **^{13}C-NMR** (101 MHz, $CDCl_3$): δ = 168.4 (C$_q$, 2C, *C*=O), 157.1 (C$_q$, 1C), 157.1 (C$_q$, 1C), 157.0 (C$_q$, 1C), 147.7 (C$_q$, 1C), 147.5 (C$_q$, 1C), 139.8 (C$_q$, 1C), 138.7 (C$_q$, 1C), 138.6 (C$_q$, 1C), 137.7 (C$_q$, 1C), 137.5 (C$_t$, 2C), 137.3 (C$_q$, 1C), 129.4 (C$_t$, 2C), 126.9 (C$_t$, 2C), 126.8 (C$_t$, 4C), 118.7 (C$_t$, 1C), 114.7 (C$_t$, 4C), 114.6 (C$_t$, 2C), 114.3 (C$_t$, 1C), 113.7 (C$_t$, 1C), 93.0 (C$_q$, 1C, *C*-I), 70.4 (C$_s$, 1C, iodobenzene-*C*H$_2$-O-), 64.6 (C$_s$, 1C), 63.3 (C$_s$, 1C), 63.2 (C$_s$, 1C), 63.2 (C$_s$, 1C), 53.5 (C$_s$, 1C), 43.5 (C$_s$, 1C), 43.4 (C$_s$, 1C),43.3 (C$_q$, 1C), 42.9 (C$_q$, 1C), 38.5 (C$_s$, 1C), 35.8 (C$_s$, 1C), 34.8 (C$_s$, 1C), 29.6 (C$_s$, 1C), 29.5 (C$_s$, 1C), 21.5 (C$_p$, 1C, -(CO)-*C*H$_3$), 21.5 (C$_p$, 1C, -(CO)-*C*H$_3$) ppm; **MS** (ESI, positive ion mode, MeCN): m/z = 973 ([M+K]$^+$), 957 ([M+Na]$^+$).

1,1”-Diethyl-5’-(1-iodo-4-phenoxymethylbenzene)-dispiro[piperidine-4,2’-[7,11,21,25]-tetraoxacyclopenta[24.2.2.2^{3,6}.2^{12,15}.2^{17,20}]hexatriaconta[3,5,12,14,17,19,26,28,29,31,33,35]dodecaene-16,4”-piperidine] (A8): In an oven-dried Schlenk-tube amide **A9** (169 mg, 1.00 equiv., 0.181 mmol) was dissolved in 35 mL dichloromethane. After cooling to 0°C (ice bath) DIBAL-*H* (3.62 mL (1 M in hexane), 2.82 g, 20 equiv., 3.62 mmol) was added dropwise over a period of 2.5 h. After stirring for an additional hour at rt the excess of DIBAL-*H* was

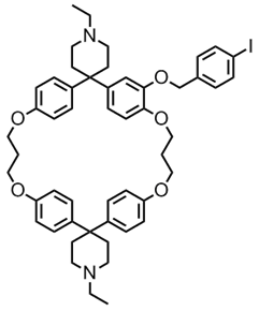

quenched with sat. aq. $NaHCO_3$. The solution was mixed with basic celite and filtered. The phases were separated and the aqueous one extracted with dichloromethane. The combined organic layers were washed once with brine, dried with sodium sulfate, filtered and concentrated. The crude was purified by column chromatography (SiO_2; EtOAc, 5% MeOH, 5% NEt_3) to achieve diamine **A8** as a colorless oil (74%).

$\boldsymbol{R_f}$ = 0.34 (SiO_2; EtOAc, 5% MeOH, 5% NEt_3); **^{1}H-NMR** (400 MHz, $CDCl_3$): δ = 7.63 (d, ^3J(H,H) = 8 Hz, 2H, Iodobenzene-H2), 7.11 – 7.05 (m, 4H, Ar-H), 6.97 (d, ^3J(H,H) = 8 Hz, 2H, Ar-H), 6.94 (d, ^3J(H,H) = 8 Hz, 2H, Ar-H), 6.74 – 6.65 (m, 8H, Ar-H), 6.49 (s, 1H, Ar-H), 4.73 (s, 2H, iodobenzene-CH_2-O-), 4.10 – 4.00 (m, 8H, Ar-O-CH_2-), 2.65 – 2.25 (m, 16H), 2.23 – 2.10 (m, 8H), 1.08 – 0.99 (m, 6H, -CH_2-CH_3) ppm; **^{13}C-NMR** (101 MHz, $CDCl_3$): δ = 156.9 (C_q, 1C), 156.8 (C_q, 1C), 156.6 (C_q, 1C), 145.7 (C_q, 1C), 144.2 (C_q, 1C), 139.8 (C_q, 1C), 138.7 (C_q, 1C), 138.6 (C_q, 1C), 137.7 (C_q, 1C), 137.4 (C_t, 2C), 137.3 (C_q, 1C), 129.1 (C_t, 2C), 127.2 (C_t, 2C), 127.1 (C_t, 4C), 118.7 (C_t, 1C), 114.5 (C_t, 4C), 114.4 (C_t, 2C), 114.3 (C_t, 1C), 113.4 (C_t, 1C), 93.0 (C_q, 1C, *C*-I), 70.4 (C_s, 1C, iodobenzene-*C*H_2-O-), 64.9 (C_s, 1C), 63.7 (C_s, 1C), 63.3 (C_s, 1C), 63.2 (C_s, 1C), 52.3 (C_s, 1C), 49.9 (C_s, 2C), 42.8 (C_s, 1C), 42.7 (C_s, 1C), 42.1 (C_q, 1C), 42.0 (C_q, 1C), 38.5 (C_s, 1C), 29.8 (C_s, 1C), 29.7 (C_s, 1C), 29.6 (C_s, 1C), 29.4 (C_s, 1C), 11.8 (Cp, 2C, -CH_2-*C*H_3) ppm; **MS** (ESI, positive ion mode, MeCN): m/z = 929 ($[M+Na]^+$), 907 ($[M+H]^+$); **HRMS** (ESI): m/z calcd for $[C_{51}H_{59}IN_2O_5+H]^+$: 907.3541; found: 907.3541.

1,1”-Diethyl-5’-[1-(phenoxymethyl)-4-((4-(phenylethynyl)phenyl)ethynyl)benzene]-dispiro[piperidine-4,2’-[7,11,21,25]-tetraoxacyclopenta[24.2.2.2^{3,6}.2^{12,15}.2^{17,20}]-hexatriaconta[3,5,12,14,17,19,26,28,29,31,33,35]dodecaene-16,4”-piperidine] (A2):

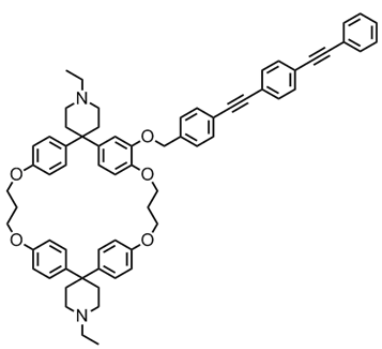

Bis(dibenzylideneacetone)palladium (3.81 mg, 10 mol%, 6.62 mmol), triphenylphosphine (13.0 mg, 0.750 equiv., 49.6 mmol) and CuI (2.52 mg, 20 mol%, 13.2 mmol) were placed in a preheated 25 mL Schlenk-tube. The tube was evacuated and backfilled with argon once. Then a solution of cyclophane **A8** (60.0 mg, 1.00 equiv., 66.2 mmol) in 2 mL THF (crown-cap) and 2 mL diisopropylamine was added. The resulting suspension was degased with argon for 10 min. Afterwards the OPE **A6** (20.1 mg, 1.50 equiv., 99.3 mmol) was added in one lot and the resulting reaction mixture stirred at rt

for 3 h. The reaction mixture was poured into demin. water and extracted three times with EtOAc (30 mL each). The combined organic layers were washed with demin. water and brine, dried with sodium sulfate, filtered and concentrated. The crude was purified by column chromatography (SiO_2; CH_2Cl_2, 5% MeOH, 1% NEt_3) to obtain compound **A2** as a white powder.

$\boldsymbol{R_f}$ = 0.42 (SiO_2; EtOAc, 5% MeOH, 5% NEt_3); **m.p.** 137°C; **^{1}H-NMR** (400 MHz, $CDCl_3$): δ = 7.60 – 7.50 (m, 6H, Ar-H(OPE)), 7.43 (d, ^3J(H,H) = 8 Hz, 2H, Ar-H), 7.38 – 7.33 (m, 3H, Ar-H(OPE)), 7.16 – 7.06 (m, 6H, Ar-H), 6.91 (d, ^3J(H,H) = 8 Hz, 2H, Ar-H), 6.77 – 6.63 (m, 8H, Ar-H), 6.47 (s, 1H, Ar-H), 4.85 (s, 2H, Ar-CH_2-O-Ar), 4.13 – 3.97 (m, 8H, Ar-O-CH_2-), 2.57 – 2.25 (m, 16H), 2.24 – 2.03 (m, 8H), 1.07 – 1.00 (m, 6H, -CH_2-CH_3) ppm; **^{13}C-NMR** (101 MHz, $CDCl_3$): δ = 156.8 (C_q, 1C), 156.7 (C_q, 1C), 156.7 (C_q, 1C), 147.3 (C_q, 1C), 147.1 (C_q, 1C), 138.2 (C_q, 2C), 131.7 (C_t, 1C), 131.6 (C_t, 2C), 131.6 (C_t, 2C), 131.6 (C_t, 2C), 128.5 (C_q, 2C), 128.4 (C_t, 2C), 127.0 (C_t, 4C), 123.2 (C_q, 2C), 123.0 (C_q, 2C), 122.1 (C_q, 1C), 114.4 (C_t, 2C), 114.3 (C_t, 1C), 91.4 (C_q, 1C, -C≡C-), 91.3 (C_q, 1C, -C≡C-), 89.4 (C_q, 1C, -C≡C-), 89.1 (C_q, 1C, -C≡C-), 70.6 (C_s, 1C, Ar-*C*H_2-O-), 63.4 (C_s, 1C), 63.2 (C_s, 1C), 63.0 (C_s, 1C), 53.0 (C_q, 1C), 52.4 (C_s, 2C), 50.0 (C_s, 1C), 50.0 (C_s, 1C), 46.2 (C_s, 4C), 43.0 (C_q, 1C), 42.7 (C_s, 1C), 35.1 (C_s, 1C), 35.0 (C_s, 1C), 29.6 (C_s, 1C), 29.5 (C_s, 1C), 12.1 (C_p, 1C, -CH_2-*C*H_3), 12.0 (C_p, 1C, -CH_2-*C*H_3) ppm; **MS** (ESI, positive ion mode, MeCN): m/z = 1003 ($[M+Na]^+$), 981 ($[M+H]^+$); **elemental analysis** calcd (%) for $C_{67}H_{68}N_2O_5$: C 82.01, H 6.98, N 2.85; found: C 81.58, H 7.34, N 2.87.

1,1,1”1”-Tetraethyl-5’-[1-(phenoxymethyl)-4-((4-(phenylethynyl)phenyl)ethynyl)-benzene]-dispiro[piperidine-4,2’-[7,11,21,25]-tetraoxacyclopenta[24.2.2.2^{3,6}.2^{12,15}.2^{17,20}]-hexatriaconta[3,5,12,14,17,19,26,28,29,31,33,35]dodecaene-16,4”-piperidine] (A1):

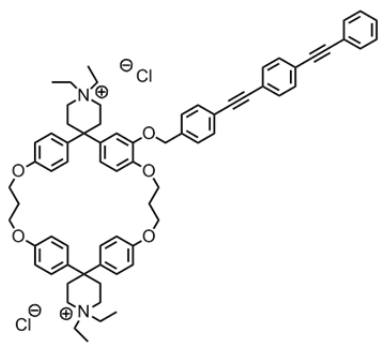

Freshly distilled iodoethane (1.70 mL) was added to diamine **A2** (40.0 mg, 1.00 equiv., 40.8 µmol). To dissolve the whole starting material 1 mL dry dichloromethane was added. The mixture was stirred at rt in the dark for 18 h. Then again 2 mL dichloromethane was added to suspend the precipitate. After 5 d stirring at rt, the solvent was removed and the crude purified by column chromatography (SiO_2 saturated with 12% methanolic NaBr; CH_2Cl_2, 5% MeOH, then CH_2Cl_2, 10% MeOH). The solid was extracted with dichloromethane (Soxhlet). The obtained pale yellow solid was taken up with demin. water and subjected to a ion exchange column (DOWEX 1X8, 200-400 mesh, Cl^-, packed

with water, washed with the eluent) eluting with MeCN:H_2O 1:1. The obtained yellow powder was again taken up with demin. water and the precipitate was filtered off. The pale yellow solid was recrystallized with a MeOH:Et_2O 1:1 mixture to obtain the desired amphiphile **A1** as a grey solid (59%).

$\boldsymbol{R_f}$ = 0.12 (SiO_2; rinsed with 6% (w/v) NaBr in MeOH, CH_2Cl_2, 5% MeOH); **^{1}H-NMR** (400 MHz, methanol-d4): δ = 7.63 – 7.57 (m, 2H, Ar-H), 7.57 – 7.49 (m, 4H, Ar-H), 7.41 – 7.35 (m, 5H, Ar-H), 7.23 – 7.13 (m, 4H, Ar-H), 7.05 – 6.94 (m, 5H, Ar-H), 6.92 – 6.82 (m, 3H, Ar-H), 6.81 – 6.73 (m, 4H, Ar-H), 6.35 (s, 1H, Ar-H), 4.70 (s, 2H, Ar-CH_2-O-Ar), 4.19 – 4.03 (m, 8H, Ar-O-CH_2-), 3.44 – 3.15 (m, 16H), 2.79 – 2.48 (m, 8H), 2.23 – 2.05 (m, 4H), 1.32 – 1.14 (m, 12H, -CH_2-CH_3) ppm; **MS** (ESI, positive ion mode, MeCN): m/z = 519 ($[M\text{-}2Cl^-]^{2+}$), 512 ($[M\text{-}Me\text{-}2Cl^-]^{2+}$), 505 ($[M\text{-}Et\text{-}2Cl^-]^{2+}$).

Appendix

Derivation of equation (2) to determine the aggregation number n and the association constant K_a:

The monomer-aggregate equilibrium in aqueous solution can be expressed as

$$n \text{ Monomer} \overset{K_a}{\rightleftharpoons} \text{Aggregate}$$

where *n* is the aggregation number and K_a the association constant.

C_{mon} is the monomer concentration, C_{agg} the aggregate concentration and C_{tot} the total concentration in solution. The total concentration can be expressed as

$$C_{tot} = C_{mon} + n\, C_{agg}$$

Furthermore the molar fractions are:

$$\frac{C_{mon}}{C_{tot}} + \frac{nC_{agg}}{C_{tot}} = 1 \qquad (7)$$

The observed chemical shift δ_{obs} can be expressed as a weighted average of the corresponding monomer (δ_{mon}) and aggregate (δ_{agg}) shifts.

$$\delta_{obs} = \frac{C_{mon}}{C_{tot}}\,\delta_{mon} + \frac{nC_{agg}}{C_{tot}}\,\delta_{agg} \qquad (8)$$

Subsitution of equation (7) into equation (8) gives:

$$\delta_{obs} = \left(1 - \frac{nC_{agg}}{C_{tot}}\right)\delta_{mon} + \frac{nC_{agg}}{C_{tot}}\,\delta_{agg} \qquad (9)$$

Equation (9) is then transformed to:

$$\delta_{obs} - \delta_{mon} = \frac{nC_{agg}}{C_{tot}}\,(\delta_{agg} - \delta_{mon})$$

$$\Rightarrow\ C_{agg} = \frac{(\delta_{obs}-\delta_{mon})}{(\delta_{agg}-\delta_{mon})} \cdot \frac{C_{tot}}{n} \qquad (10)$$

The association constant K_a is:

$$K_a = \frac{C_{agg}}{(C_{tot} - nC_{agg})^n}$$

$$\Rightarrow \ln K_a = \ln C_{agg} - n \ln(C_{tot} - nC_{agg}) \quad (11)$$

Subsitution of equation (10) in equation (11) gives:

$$\ln K_a = \ln\left(\frac{(\delta_{obs} - \delta_{mon})}{(\delta_{agg} - \delta_{mon})} \cdot \frac{C_{tot}}{n}\right) - n \ln\left(C_{tot} - n \frac{(\delta_{obs} - \delta_{mon})}{(\delta_{agg} - \delta_{mon})} \cdot \frac{C_{tot}}{n}\right)$$

$$\ln K_a = \ln\left(\frac{(\delta_{obs} - \delta_{mon})}{(\delta_{agg} - \delta_{mon})} \cdot \frac{C_{tot}}{n}\right) - n \ln\left(\frac{(\delta_{agg} - \delta_{obs})}{(\delta_{agg} - \delta_{mon})} C_{tot}\right)$$

$$\ln K_a = \ln\left(\frac{(\delta_{obs} - \delta_{mon})}{(\delta_{agg} - \delta_{mon})} \cdot C_{tot}\right) - \ln n - n \ln\left(\frac{(\delta_{agg} - \delta_{obs})}{(\delta_{agg} - \delta_{mon})} C_{tot}\right)$$

$$\ln K_a - \ln n = \ln((\delta_{mon} - \delta_{obs})C_{tot}) - \ln(\delta_{mon} - \delta_{agg}) - n \ln\left((\delta_{obs} - \delta_{agg})C_{tot}\right) + n \ln(\delta_{mon} - \delta_{agg})$$

Transformation gives the final equation (2):

$$\ln((\delta_{mon} - \delta_{obs})C_{tot}) = n \ln\left((\delta_{obs} - \delta_{agg})C_{tot}\right) + \ln K_a + \ln n - (n-1) \ln(\delta_{mon} - \delta_{agg})$$

Literature

[1] V. Balzani, A. Credi, M. Venturi, *Molecular Devices and Machines: Concepts and Perspectives for the Nanoworld*, Wiley-vch, **2008**.

[2] J. Mokyr, *Knowledge, technology, and economic growth during the industrial revolution*, Kluwer/springer, The Hague, **2000**.

[3] L. Han, A. J. Grodzinsky, C. Ortiz, *Annu. Rev. Mater. Res.* **2011**, *41*, 133–168.

[4] S. François, *Cem. Concr. Res.* **2011**, *41*, 616–623.

[5] I. Jerman, M. Koželj, B. Orel, *Sol. Energy Mater. Sol. Cells* **2010**, *94*, 232–245.

[6] J. Irven, *J. Mater. Chem.* **2004**, *14*, 3071–3080.

[7] I. Sinclair, J. Dunton, *Electronic and Electrical Servicing: Consumer and Commercial Electronics*, Routledge, **2007**.

[8] G. Maruccio, R. Cingolani, R. Rinaldi, *J. Mater. Chem.* **2004**, *14*, 542–554.

[9] A. P. H. J. Schenning, E. W. Meijer, *Chem. Commun.* **2005**, 3245–3258.

[10] H. Song, M. A. Reed, T. Lee, *Adv. Mater.* **2011**, *23*, 1583–1608.

[11] T. Verbiest, S. Houbrechts, M. Kauranen, K. Clays, A. Persoons, *J. Mater. Chem.* **1997**, *7*, 2175–2189.

[12] B. H. Kear, P. R. Strutt, *Nanostruct. Mater.* **1995**, *6*, 227–236.

[13] A. Jaroenworaluck, W. Sunsaneeyametha, N. Kosachan, R. Stevens, *Surf. Interface Anal.* **2006**, *38*, 473–477.

[14] H. -J Wernicke, R. W. Fischer, *Chemie Ingenieur Technik* **2006**, *78*, 825–834.

[15] L. Baù, P. Tecilla, F. Mancin, *Nanoscale* **2011**, *3*, 121–133.

[16] J. Kaur, J. H. Lee, M. L. Shofner, *Polymer* **2011**, *52*, 4337–4344.

[17] K. Morris, L. Serpell, *Chem. Soc. Rev.* **2010**, *39*, 3445–3453.

[18] H. W. Gibson, M. C. Bheda, P. T. Engen, *Prog. Polym. Sci.* **1994**, *19*, 843–945.

[19] H.-H. Kausch-Blecken von Schmeling, *Colloid Polm. Sci.* **2011**, *289*, 1407–1427.

[20] J. M. Cowie, *Polymers: Chemistry and Physics of Modern Materials*, **1974**.

[21] G. Wenz, B. H. Han, A. Müller, *Chem. Rev.* **2006**, *106*, 782–817.

[22] F. M. Raymo, J. F. Stoddart, *Chem. Rev.* **1999**, *99*, 1643–1664.

[23] F. Huang, H. W. Gibson, *Prog. Polym. Sci.* **2005**, *30*, 982–1018.

[24] J. F. Stoddart, *Chem. Soc. Rev.* **2009**, *38*, 1802.

[25] L. Fang, M. A. Olson, D. Benítez, E. Tkatchouk, W. A. Goddard III, J. F. Stoddart, *Chem. Soc. Rev.* **2010**, *39*, 17.

[26] J. Watanabe, *Chem. Lett.* **1998**, 1031.

[27] H. Gibson, *Macromolecules* **1997**, *30*, 3711.

[28] C. Gong, *Macromolecules* **1998**, *31*, 5278.

[29] I. Yamaguchi, *Polym. Bull.* **2000**, *44*, 247.

[30] H. Frisch, *J. Am. Chem. Soc.* **1961**, *83*, 3789.

[31] C. Dietrich Buchecker, *Chem. Rev.* **1987**, *87*, 795.

[32] H. Ogino, *J. Am. Chem. Soc.* **1981**, *103*, 1303.

[33] T. Rao, D. D. Lawrence, *J. Am. Chem. Soc.* **1990**, *112*, 3614.

[34] K. Yamanari, *Bull. Chem. Soc. Jpn.* **1983**, *56*, 2283.

[35] B. Allwood, *J. Chem. Soc., Chem. Commun.* **1987**, 1058.

[36] B. Allwood, *J. Chem. Soc., Chem. Commun.* **1987**, 1064.

[37] P. Ashton, *J. Chem. Soc., Chem. Commun.* **1987**, 1066.

[38] M. Reddington, *J. Chem. Soc., Chem. Commun.* **1991**, 630.

[39] D. Philp, *J. Chem. Soc., Chem. Commun.* **1991**, 1584.

[40] A. Benniston, *J. Am. Chem. Soc.* **1993**, *115*, 5298.

[41] A. Bogdan, *Chem. Eur. J.* **2008**, *14*, 8514.

[42] K. Kim, *Chem. Soc. Rev.* **2002**, *31*, 96–107.

[43] V. Balzani, M. Gómez-López, J. F. Stoddart, *Acc. Chem. Res.* **1998**, *31*, 405–414.

[44] H. Tian, Q.-C. Wang, *Chem. Soc. Rev.* **2006**, *35*, 361.

[45] E. R. Kay, D. A. Leigh, F. Zerbetto, *Angew. Chem. Int. Ed.* **2007**, *46*, 72–191.

[46] D. B. Amabilino, P. R. Ashton, V. Balzani, S. E. Boyd, A. Credi, J. Y. Lee, S. Menzer, J. F. Stoddart, M. Venturi, D. J. Williams, *J. Am. Chem. Soc.* **1998**, *120*, 4295–4307.

[47] M. J. Frampton, H. L. Anderson, *Angew. Chem. Int. Ed.* **2007**, *46*, 1028–1064.

[48] A. Harada, J. Li, T. Nakamitsu, M. Kamachi, *J. Org. Chem.* **1993**, *58*, 7524–7528.

[49] C. Gong, H. W. Gibson, *Macromolecules* **1996**, *29*, 7029–7033.

[50] D. Whang, Y.-M. Jeon, J. Heo, K. Kim, *J. Am. Chem. Soc.* **1996**, *118*, 11333–11334.

[51] J. Wu, K. C. F. Leung, J. F. Stoddart, *Proc. Natl. Acad. Sci.* **2007**, *104*, 17266.

[52] L. Meier, *Macromolecules* **1996**, *29*, 718.

[53] W. Herrmann, *Angew. Chem., Int. Ed. Engl.* **1997**, *36*, 2511.

[54] G. Wenz, *Tetrahedron* **1997**, *53*, 15575.

[55] A. Harada, *Macromolecules* **1995**, *28*, 8406.

[56] G. Agam, *J. Am. Chem. Soc.* **1976**, *98*, 5206.

[57] H. Gibson, *J. Am. Chem. Soc.* **1995**, *117*, 852.

[58] C. Gong, *Macromolecules* **1997**, *30*, 8524.

[59] P. Mason, *Angew. Chem., Int. Ed. Engl.* **1996**, *35*, 2238.

[60] J. Reek, *Chem. Commun.* **1998**, 11.

[61] J. Li, X. J. Loh, *Adv. Drug Delivery Rev.* **2008**, *60*, 1000–1017.

[62] S. S. Zhu, P. J. Carroll, T. M. Swager, *J. Am. Chem. Soc.* **1996**, *118*, 8713–8714.

[63] J. J. Li, F. Zhao, J. Li, *Appl. Microbiol. Biotechnol.* **2011**, *90*, 427–443.

[64] S. J. Rowan, J. F. Stoddart, *Polym. Adv. Technol.* **2002**, *13*, 777–787.

[65] P. R. Ashton, I. Baxter, S. J. Cantrill, M. C. T. Fyfe, P. T. Glink, J. F. Stoddart, A. J. P. White, D. J. Williams, *Angew. Chem. Int. Ed.* **1998**, *37*, 1294–1297.

[66] N. H. Evans, P. D. Beer, *Chem. Eur. J.* **2011**, *17*, 10542–10546.

[67] M. C. Jiménez, C. Dietrich-Buchecker, J. Sauvage, *Angew. Chem. Int. Ed.* **2000**, *39*, 3284–3287.

[68] K. Hirotsu, T. Higuchi, K. Fujita, T. Ueda, A. Shinoda, T. Imoto, I. Tabushi, *J. Org. Chem.* **1982**, *47*, 1143–1144.

[69] D. Mentzafos, A. Terzis, A. W. Coleman, C. de Rango, *Carbohydr. Res.* **1996**, *282*, 125–135.

[70] T. Fujimoto, Y. Uejima, H. Imaki, N. Kawarabayashi, J. H. Jung, Y. Sakata, T. Kaneda, *Chem. Lett.* **2000**, *29*, 564–565.

[71] T. Fujimoto, Y. Sakata, T. Kaneda, *Chem. Lett.* **2000**, *29*, 764–765.

[72] T. Fujimoto, Y. Sakata, T. Kaneda, *Chem. Commun.* **2000**, 2143–2144.

[73] T. Fujimoto, A. Nakamura, Y. Inoue, Y. Sakata, T. Kaneda, *Tetrahedron Lett.* **2001**, *42*, 7987–7989.

[74] H. Onagi, C. J. Easton, S. F. Lincoln, *Org. Lett.* **2001**, *3*, 1041–1044.

[75] L.-H. Tong, Z.-J. Hou, Y. Inoue, A. Tai, *J. Chem. Soc., Perkin Trans. 2* **1992**, 1253.

[76] T. Hoshino, M. Miyauchi, Y. Kawaguchi, H. Yamaguchi, A. Harada, *J. Am. Chem. Soc.* **2000**, *122*, 9876–9877.

[77] M. Miyauchi, Y. Kawaguchi, A. Harada, *J. Inclusion Phenom. Macrocyclic Chem.* **2004**, *50*, 57–62.

[78] M. Miyauchi, Y. Takashima, H. Yamaguchi, A. Harada, *J. Am. Chem. Soc.* **2005**, *127*, 2984–2989.

[79] A. Kanaya, Y. Takashima, A. Harada, *J. Org. Chem.* **2010**, *76*, 492–499.

[80] A. Zanotti-Gerosa, E. Solari, L. Giannini, C. Floriani, A. Chiesi-Villa, C. Rizzoli, *Chem. Commun.* **1996**, 119.

[81] J. Bügler, N. A. J. M. Sommerdijk, A. J. W. G. Visser, A. van Hoek, R. J. M. Nolte, J. F. J. Engbersen, D. N. Reinhoudt, *J. Am. Chem. Soc.* **1999**, *121*, 28–33.

[82] P. R. Ashton, I. W. Parsons, F. M. Raymo, J. F. Stoddart, A. J. P. White, D. J. Williams, R. Wolf, *Angew. Chem. Int. Ed.* **1998**, *37*, 1913–1916.

[83] N. Yamaguchi, D. S. Nagvekar, H. W. Gibson, *Angew. Chem. Int. Ed.* **1998**, *37*, 2361–2364.

[84] S. J. Cantrill, G. J. Youn, J. F. Stoddart, D. J. Williams, *J. Org. Chem.* **2001**, *66*, 6857–6872.

[85] S.-H. Chiu, S. J. Rowan, S. J. Cantrill, J. F. Stoddart, A. J. P. White, D. J. Williams, *Chem. Commun.* **2002**, 2948–2949.

[86] S. J. Rowan, S. J. Cantrill, J. F. Stoddart, A. J. P. White, D. J. Williams, *Org. Lett.* **2000**, *2*, 759–762.

[87] M. P. L. Werts, M. van den Boogaard, G. M. Tsivgoulis, G. Hadziioannou, *Macromolecules* **2003**, *36*, 7004–7013.

[88] M. Zhang, S. Li, S. Dong, J. Chen, B. Zheng, F. Huang, *Macromolecules* **2011**.

[89] S.-H. Ueng, S.-Y. Hsueh, C.-C. Lai, Y.-H. Liu, S.-M. Peng, S.-H. Chiu, *Chem. Commun.* **2008**, 817.

[90] J. Wu, K. C.-F. Leung, D. Benítez, J.-Y. Han, S. J. Cantrill, L. Fang, J. F. Stoddart, *Angew. Chem. Int. Ed.* **2008**, *47*, 7470–7474.

[91] L. Fang, M. A. Olson, D. Benítez, E. Tkatchouk, W. A. Goddard III, J. F. Stoddart, *Chem. Soc. Rev.* **2010**, *39*, 17.

[92] L. Fang, M. Hmadeh, J. Wu, M. A. Olson, J. M. Spruell, A. Trabolsi, Y.-W. Yang, M. Elhabiri, A.-M. Albrecht-Gary, J. F. Stoddart, *J. Am. Chem. Soc.* **2009**, *131*, 7126–7134.

[93] S. Tsuda, Y. Aso, T. Kaneda, *Chem. Commun.* **2006**, 3072.

[94] R. E. Dawson, S. F. Lincoln, C. J. Easton, *Chem. Commun.* **2008**, 3980.

[95] D. G. Amirsakis, A. M. Elizarov, M. A. Garcia-Garibay, P. T. Glink, J. F. Stoddart, A. J. P. White, D. J. Williams, *Angew. Chem. Int. Ed.* **2003**, *42*, 1126–1132.

[96] F. J. M. Hoeben, P. Jonkheijm, E. W. Meijer, A. P. H. J. Schenning, *Chem. Rev.* **2005**, *105*, 1491–1546.

[97] X. I. Ambroggio, B. Kuhlman, *Curr. Opin. Struct. Biol.* **2006**, *16*, 525–530.

[98] S. Rimmer, I. Soutar, L. Swanson, *Polymer International* **2009**, *58*, 273–278.

[99] J. Rotzler, D. Vonlanthen, A. Barsella, A. Boeglin, A. Fort, M. Mayor, *Eur. J. Org. Chem.* **2010**, 1096–1110.

[100] D. Vonlanthen, A. Mishchenko, M. Elbing, M. Neuburger, T. Wandlowski, M. Mayor, *Angew. Chem.* **2009**, *48*, 8886–8890.

[101] D. Vonlanthen, J. Rotzler, M. Neuburger, M. Mayor, *Eur. J. Org. Chem.* **2009**, 120–133.

[102] D. Vonlanthen, A. Rudnev, A. Mishchenko, A. Käslin, J. Rotzler, M. Neuburger, T. Wandlowski, M. Mayor, *Chem. Eur. J.* **2011**, *17*, 7236–7250.

[103] G. W. Gokel, W. M. Leevy, M. E. Weber, *Chem. Rev.* **2004**, *104*, 2723–2750.

[104] D. Gust, T. A. Moore, A. L. Moore, *Chem. Commun.* **2005**, 1169–1178.

[105] C. Renner, L. Moroder, *Chem. Bio. Chem.* **2006**, *7*, 868–878.

[106] B. L. Feringa, *J. Org. Chem.* **2007**, *72*, 6635–6652.

[107] M. Fujiki, in *Amplification of Chirality* (Hrsg.: K. Soai), Springer Berlin Heidelberg, **2007**, S. 119–186.

[108] P. M. Mendes, A. H. Flood, J. F. Stoddart, *Appl. Phys. A* **2005**, *80*, 1197–1209.

[109] B. J. Briscoe, S. K. Sinha, *Materialwissenschaft und Werkstofftechnik* **2003**, *34*, 989–1002.

[110] A. G. MacDiarmid, *Angew. Chem. Int. Ed.* **2001**, *40*, 2581–2590.

[111] C. Li, H. Bai, G. Shi, *Chem. Soc. Rev.* **2009**, *38*, 2397–2409.

[112] C. R. Crick, I. P. Parkin, *Chem. Eur. J.* **2010**, *16*, 3568–3588.

[113] L. Fang, M. A. Olson, D. Benítez, E. Tkatchouk, W. A. G. III, J. F. Stoddart, *Chem. Soc. Rev.* **2009**, *39*, 17–29.

[114] S. Cantrill, *J. Org. Chem.* **2001**, *66*, 6857.

[115] L. Fang, *J. Am. Chem. Soc.* **2009**, *131*, 7126.

[116] M. Zhang, S. Li, S. Dong, J. Chen, B. Zheng, F. Huang, *Macromolecules* **2011**, *44*, 9629–9634.

[117] K.-J. Chang, *J. Org. Chem.* **2004**, *69*, 6556.

[118] F. Diederich, *Chem. Ber.* **1985**, *118*, 3588.

[119] F. Diederich, *Angew. Chem., Int. Ed. Engl.* **1988**, *27*, 362–386.

[120] S. Anderson, H. L. Anderson, *Angew. Chem., Int. Ed. Engl.* **1996**, *35*, 1956–1959.

[121] S. Anderson, R. T. Aplin, T. D. W. Claridge, T. Goodson III, A. C. Maciel, G. Rumbles, J. F. Ryan, H. L. Anderson, *J. Chem. Soc., Perkin Trans. 1* **1998**, 2383–2398.

[122] P. N. Taylor, A. J. Hagan, H. L. Anderson, *Org. Biomol. Chem.* **2003**, *1*, 3851.

[123] S. W. Tam-Chang, L. Jimenez, F. Diederich, *Helv. Chim. Acta* **1993**, *76*, 2616–2639.

[124] P. Mattei, F. Diederich, *Helv. Chim. Acta* **1997**, *80*, 1555–1588.

[125] T. Marti, B. R. Peterson, A. Fürer, T. Mordasini-Denti, J. Zarske, B. Jaun, F. Diederich, V. Gramlich, *Helv. Chim. Acta* **1998**, *81*, 109–144.

[126] N. Jenny, *Eur. J. Org. Chem.* **2011**, *2011*, 4965.

[127] L. Testaferri, *Synthesis* **1983**, *1983*, 751.

[128] C. J. Yu, Y. Chong, J. F. Kayyem, M. Gozin, *J. Org. Chem.* **1999**, *64*, 2070–2079.

[129] L. Bluhm, *Tetrahedron Lett.* **1998**, *39*, 3623.

[130] S. McAlpine, *J. Am. Chem. Soc.* **1998**, *120*, 4269.

[131] X. Huang, Y. Han, Y. Wang, Y. Wang, *J. Phys. Chem. B* **2007**, *111*, 12439–12446.

[132] B. O. Persson, T. Drakenberg, B. Lindman, *J. Phys. Chem.* **1976**, *80*, 2124–2125.

[133] T. W. Davey, W. A. Ducker, A. R. Hayman, *Langmuir* **2000**, *16*, 2430–2435.

[134] R. Margalit, N. Shaklai, S. Cohen, *Biochem. J.* **1983**, *209*, 547.

[135] D. Delmarre, N. Hioka, R. Boch, E. Sternberg, D. Dolphin, *Can. J. Chem.* **2001**, *79*, 1068–1074.

[136] S. Goeb, *Org. Lett.* **2007**, *9*, 737.

Part B. Molecular Electronics

Introduction

Maybe the most fascinating assembly of functional materials is the modern computer. It is a marvelous example of using engineered materials so well that a synchronized interplay is possible and powerful machines were produced. If one compares the dimensions of the first computer with todays smartphones or laptops the miniaturization trend in telecommunication techniques gets beyond question. To be able to generate more powerful and smaller electronic devices microchips with more transistors occupying less space are needed. Until now the conducting paths in microchips are produced by lithographic top-down methods with as little as a few nanometer in diameter (32 nm for the new Clarksdale Intel Core i5[1]). Despite this, the physical limits of these fabrication methods will be reached soon with spinning costs for the fabrication. Therefore it is necessary to look for new fabrication methods; one of them can be the bottom-up approach (figure 1).

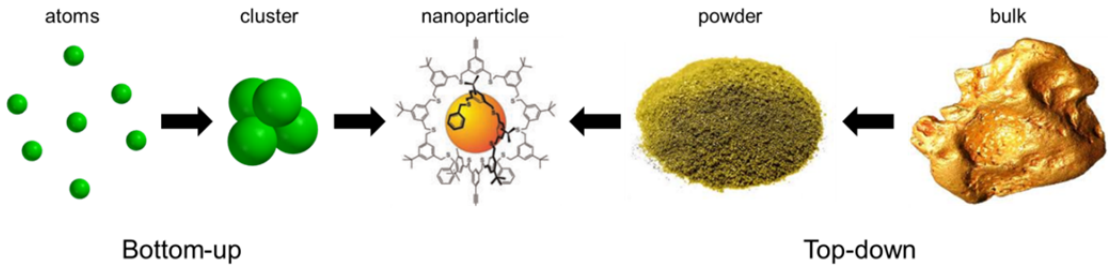

Figure 1. Bottom-up approach starting from atoms and top-down approach starting from bulk materials.

Even though it was shown by physicists that atoms can be placed in an ordered fashion with the STM, the production of processors using this approach will be too complex and too expensive.[2] But in principle conduction pathways with single atom diameters are possible. A resort for this problem without limiting the miniaturization trend can be learning from nature. A vast variety of materials with completely different properties based on only a few structural concepts is available. This structural diversity is mainly based on organic materials. Nearly all electronic processes in nature – from photosynthesis to vision – happen in organic materials and thus demonstrate the capability of organic materials to transport charges.[3] One possibility how to use this feature can be the assembly of organic molecular wires opening up the research area of molecular electronics where until now a variety of silicomimetic molecules where synthesized since the early thoughts of Aviram, Ratner[4] and Woodward[5].

To construct electronic circuits by organic molecules provides several advantages: The use of organic synthetic methods, where for example a selective addition of oxygen to a molecule can be carried out with much higher precision than it is possible with an oxidizing step in microfabrication, allows to precisely equip molecules with specific functionalities.[6] This adds a new dimension of design flexibility because the physical and electronic properties can be specifically tailored by synthetic methods. Additionally large quantities of electronic parts can be produced with the same uniformity but with low costs. A continuous system with a large number of strongly interacting orbitals and a strong interaction between overlapping orbitals are crucial requirements for conducting organic molecules. In other words delocalized π-orbitals across the whole molecule and a perfect alignment with the frontier orbitals of the addressing device are necessary to make an organic molecule into a molecular wire.[7] Because of their extended π-systems and structural rigidity oligophenylene-ethynylenes (OPE) are ideal candidates for applications as molecular wires and are therefore widely used structural motifs in molecular electronics.[8] The use of an oligophenylene-ethynylene molecular thread in water soluble cyclophane **A1** therefore opens up the possibility to use it as a molecular electronic device. Using self-assembly to interconnect electronic circuits will lead to a thermodynamically controlled regime which like in mechanically interlocked macromolecules will eliminate fault structures.[6] Furthermore the expected increase in stability, due to the protective behavior of the cyclophane, makes it possible to overcome one of the major disadvantages of organic conductors – the reduced dimensionality. The twofold-coordination compared to sixfold-coordination in metal-complexes, makes them susceptible to structural distortion. To enable further applicability of the designed molecule **A1** it is therefore necessary to functionalize the OPE rod with suitable anchoring groups to be able to address these molecules by gold-electrodes.

Charge Transport in Molecules

Macroscopic molecular wires obey the Ohm's law meaning electrons travel in a diffusive manner and the conductance is inverse proportional to the length of the conductor. By down-sizing the dimensions of the wire the elastic mean free path becomes larger than the length of the conductor and therefore the electrons move in a ballistic way (figure 2). This transmission process in the quantum regime can be described by the Landauer formula which yields for molecular wires a maximum conductance of $G_0 = 77.4\ \mu S$.

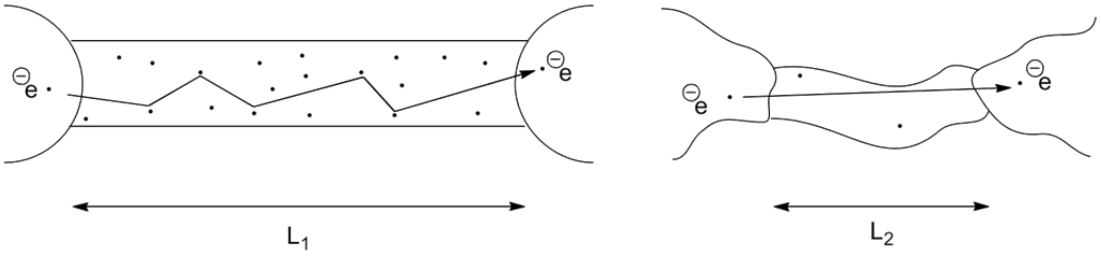

Figure 2. *Left*: diffusive electron transport through a regular sized wire, *right*: ballistic electron transport in molecular wire between two electrodes ($L_1 >> L_2$).

Organic molecules can transport charges by a variety of different processes, depending on the energy of the highest occupied molecular orbital (HOMO) and the lowest unoccupied molecular orbital (LUMO) and their alignment with the Fermi-level of the contacting metal.[9] In the simplest case no free electronic states on the molecule are available for the charge injected from the metal. Therefore the charge will tunnel through the distance between the two electrodes (figure 3). Tunneling is a temperature independent process and strongly depends on the height and width of the tunneling barrier as well as on the rate of the tunneling particle.[3] If a charge can occupy some states on the molecule the whole process gets sensitive to the coupling between the metal contact and the molecule. Thus, a good alignment of the Fermi-level of the electrode and the involved molecular orbital leads to activated hopping and the electronic coupling between the various sites of the molecule will determine the conductivity (figure 3).[10] This is the case when the molecular orbitals of the molecule can hybridize with the metallic orbitals of the electrode. When the coupling between the anchoring group of the molecule and the metal is weaker the charge transport is determined by the hopping of the charges from the metallic contact to the electronic states and to the second contact. Hence two possibilities to induce charges on the molecule arise which are a) thermal activation of activated transport or b) increasing the bias voltage which results in an ideal case in an alignment of the Fermi-level of the metal and the frontier molecular orbitals of the molecule.[9] When the coupling between the molecular linker to the metal is poor, but the charges can find electronic states within the molecular backbone the whole junction acts as a capacitor (one plate metal, one plate molecule) (figure 3).[3] The energy needed to charge a capacitor is inverse proportional to the capacitance which is reduced when the size of the capacitor is reduced. The thermal energy available in such systems is much smaller than the energy needed to charge the molecule by one electron. Therefore the current flow through the molecule is blocked by electrostatic repulsion (Coulomb blockade) and additional energy is necessary to allow charge-transport through the molecular wire.[10] As a result the bias voltage has to be increases until the charging energy is compensated.

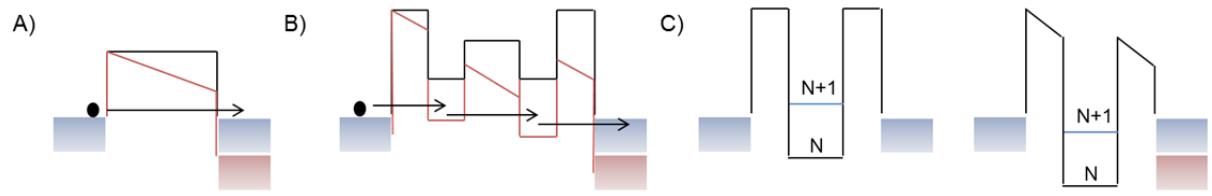

Figure 3. Schematic representation of the different charge transport mechanisms. The Fermi-levels of the metal electrodes are displayed as blue boxes. The black line corresponds to unperturbed electronic energy levels. The red lines show energy levels under an applied field. A) Tunneling; B) activated hopping; C) Coulomb blockade: On the left side the electrode and the molecule act as a capacitor. Upon charging the energy level N, the energy raises to N+1. By applying an electric field the charges can flow (*right*).

As mentioned above the electrode effects strongly influence the conductivity of the organic molecules. Usually thiol anchoring groups are used to address the electrode because of the self-assembling properties of thiols on gold surfaces. Despite advantages like strong covalent binding and efficient electronic coupling thiol-gold bonds have a variety of different binding modes which lead to a partial charging of the molecule to equilibrate the chemical potential and therefore to the formation of so called Schottky-barriers. This effect increases with increasing electronegativity difference between metal and anchoring group. As a result carbon-carbon or carbon-silicon contacts are more reliable than gold-sulfur contacts.[6]

Connecting Molecular Wires to the Macroscopic Scale

Single molecular electronic devices have to be connected to macroscopic setups, which is one of the mayor challenges in molecular electronics. Large progress in this field of research has been made in the last decades by invention of a variety of different test-beds for molecular electronic devices, namely nanopores[11], electromigration[12], mercury drop top contacts[13], vapor deposition techniques[14], wire crossing[15], and 2D-Gold nanoparticle arrays[16]. In all these techniques assemblies of molecules are contacted which allows probing optical properties and is suitable for integration in conventional microelectronic devices.[17] Nevertheless, formation of surface-dipoles (Schottky barriers), domains, defects and interactions of molecules in chemisorbed assemblies as well as distortion of the molecular structure and instable films in physisorbed assemblies makes the investigations of single molecular junctions necessary to understand the molecules electronic signature.[6] Therefore mainly two techniques are used: the mechanically controllable break junction (MCBJ)[18,19] and the scanning tunneling microscope (STM) break junction[20]. In the latter an atomic sharp conducting tip is brought into close proximity to the conducting sample by measuring the tunneling current between the tip and the sample. Vertical adjustment allows to compensate

changes in the tunneling current (imaging) but also to contact with the conducting molecules deposited on the bottom electrode. This can lead to the formation of metal-molecule-metal contacts and thus to single molecule junctions (figure 4). By rapidly moving up and down the STM tip thousands of measurements can be performed in a short time. Hence statistical evaluation of the conductance of single molecules is possible. However the formed molecular bridges do exist only a very short moment (transient junctions) which makes it troublesome to record I/V curves.[21]

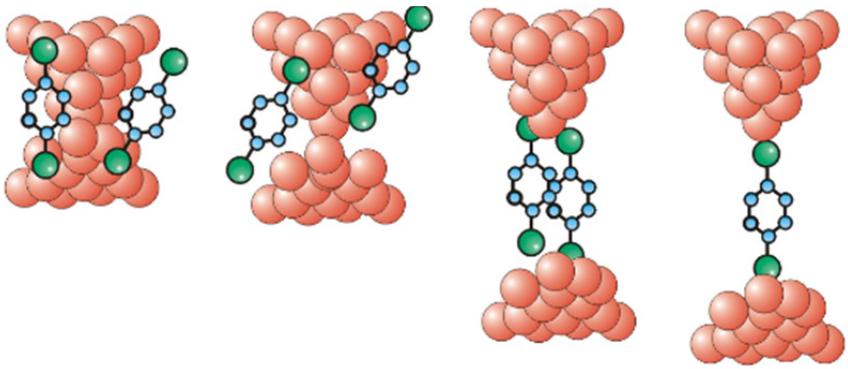

Figure 4. Schematic illustration of a STM break junction. The STM tip is moved into the surface covered with molecules. Because of the binding affinity of the anchor-groups molecular bridges can be formed when the STM tip is moved away from the surface (from *left* to *right*).[22]

The MCBJ is a lithographically fabricated free suspended metal wire where bending of the metal substrate by a central, vertical pushing rod and fixed sides allow horizontal stretching of the wire with a translational factor of 10^{-4} – 10^{-5} (figure 5).[17] By monitoring the resistance of the metal wire the exact breaking point can be determined. The small gap fabricated between metal electrodes can then be bridged with molecules by chemical self-assembly. Therefore molecules can be deposited into the break-junction in solution or by evaporation. This type of device shows a high mechanical stability and therefore allows for recording of I/V curves and for statistical evaluation of the conductance by minute opening and closing of the gap. The applied bias voltage is thus kept constant while the bridge is opened and closed. The current is measured as a function of the distance between the two electrodes.

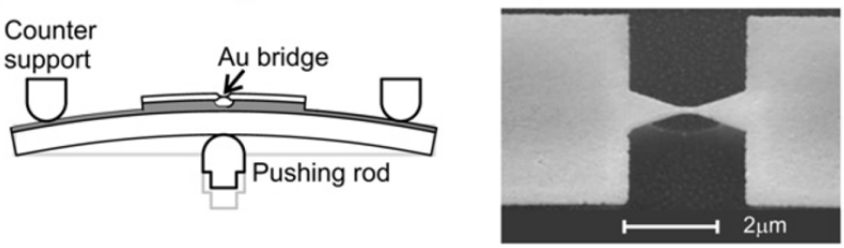

Figure 5. Schematic representation of the mechanically controlled break junction setup. By vertical movement of the pushing rod, the lithographically fabricated free standing gold-bridge gets more and more bend until it breaks. The two electrodes can then be reconnected with molecules.[23]

Molecular Wires

Structures like oligophenylene-ethynylenes (OPE), oligophenylene-vinylenes (OPV), oligophenylenes (OP), oligothiophenes, polyenes, NDI and oligoporphyrins have been used in applications like light-emitting-diodes[24], thin-film field-effect transistors[25], photovoltaic cells[26] or sensors[27]. In principle conjugated oligomers are proconductors where no efficient charge transport is possible unless they get doped with metal-ions, oxidized or reduced to produce localized charges (if a non-degenerate ground state of molecule is present polarons are formed or solitons in the case of a degenerated ground state of molecule) which are located symmetrically within the band gap of the frontier orbitals.[6] Formation of bipolarons or solitons then results in thermally activated hopping between the localized energy states in the polymer backbone. The major drawback of using conjugated polymers as an alternate for conventional semiconductors is that interchain interactions can significantly modify optical and electronic properties. Furthermore the delocalized electronic structure and their small π-π* energy gap makes them highly reactive towards electrophiles, nucleophiles and radicals leading to stable, less conductive intermediates. This environmental reactivity together with the operational instability of organic semiconductors can potentially be overcome by insulating the molecular wires and therefore prevent cross-talk and degrading reactions with the environment.[28] Despite recent advances in so called supramolecular electronics[29,30] where columnar stacks of amphiphilic disc like compounds showed remarkable conductivities and stabilities, polyrotaxanes are ideal candidates for use as insulated molecular wires. As already mentioned the encircling of polymers by macrocycles can lead to a dramatically enhanced stability of the polymeric backbone.[31] Even though encapsulation of conjugated oligomers or polymers principally does not perturb their electronic structure, changes in their photochemical properties can be observed. For example if the insulating macrocycles are able to form a long and straight tube the wire is forced to adopt a linear and planar conformation

which results in a stronger π-overlap of the involved molecular orbitals and thus absorbance at longer wavelengths is observed. Also the opposite case of a more twisted conformation which leads to a blue shift is possible.[28] The restriction of conformational freedom and the reduced flexibility of the excited states lead to enhanced quantum yields for fluorescence. Furthermore no exciton-coupling is possible because of the prevented interchain aggregation and thus low-energy non-emissive states cannot form. By these two effects an enhanced photoluminescence efficiency can be observed in insulated molecular wires making them to ideal candidates for applications in organic light emitting diodes (OLED).[32] However, encircling conjugated polymers can also result in reduced conductivity as the encircling host prevents interchain charge transfer or prevents the movement of charge carriers along the polymer chain by electrostatic repulsion.[33] In contradiction, the forced linear and planar conformation should lead to an enhanced charge mobility.[34] As a result, the system used to create polyrotaxanes also can strongly influence the properties of such, but allows by careful design and knowledge of structure-property relations to tailor these compounds for each individual application.

Single Molecular Switches

Electronic gateways and switches are probably the most important components in electronic devices. Thus it is crucial to develop molecular switches to be able to create electric circuits on a molecular level. Two different conduction levels (On- and Off-state) are necessary in a single molecule towards conductance switches which must be addressable by an external input like light, electricity or a chemical reaction. Therefore a change in the conjugation of the molecule, variation of the distance between both ends of the molecule, formation of altered conduction pathways or different alignment of the energy levels of the frontier molecular orbitals in respect to the Fermi-level of the electrode has to be induced by the external stimulus.[35] Azobenzene-[36,37] and diarylethene-[38,39] based light driven molecular switches were reported so far. Switching of whole crystalline domains with UV-light of a self-assembled monolayer of *mono*-thiobiphenyl azobenzene in a mercury-droplet junction demonstrated that the *cis*-isomer of this thermally reversible (T-type) compound is better conducting as the thermally stable *trans*-isomer because of a decreased tunneling barrier length (figure 6).[36,40]

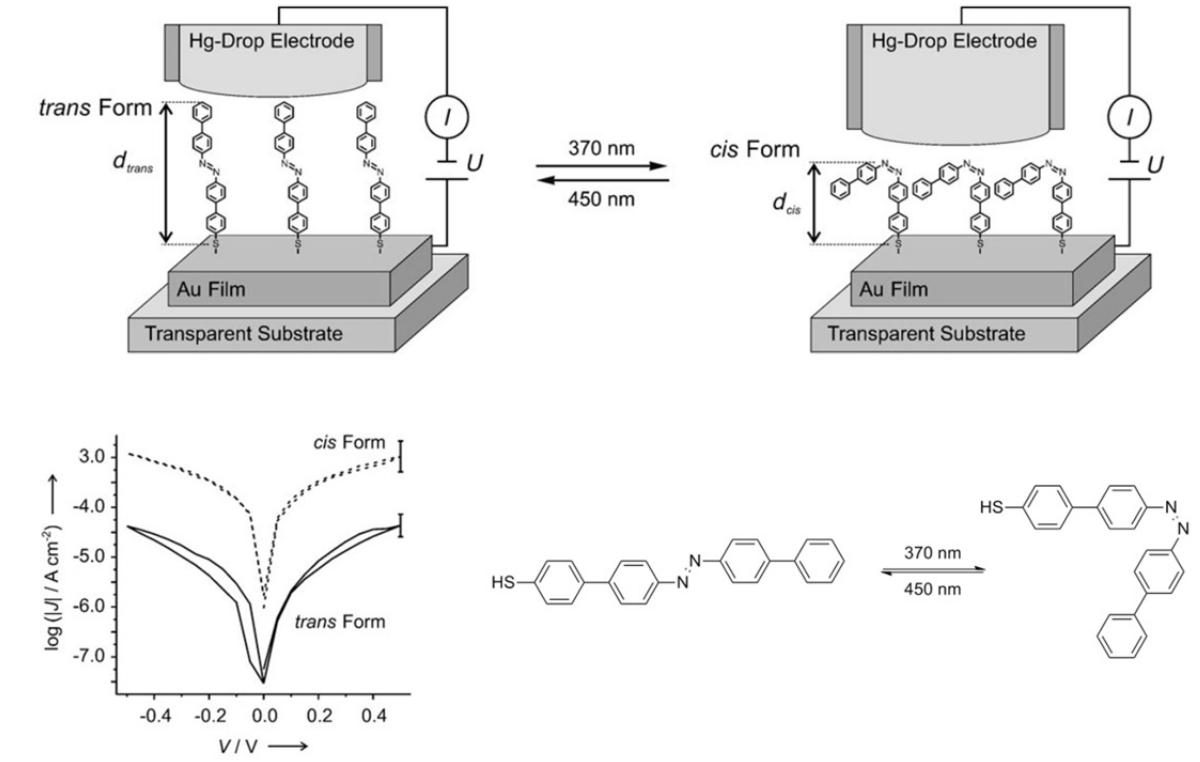

Figure 6. *Top*: Light triggered isomerization of an azoswitch immobilized between a gold-substrate and a mercury-drop electrode. *Bottom left*: I/V curves showing the increased conductance of the *cis*-isomer compared to the *trans*-isomer. *Bottom right*: light driven isomerization of *mono*-thiobiphenyl azobenzene. Reprinted from Ferri *et al*.[40]

A photochemically reversible dithiophene-cyclopentene switch was reported which can be switched back by illumination with visible light (P-type) in contrast to the thermal back-reactions in azobenzene systems. By illumination with UV-light a rearrangement takes place generating a larger conjugated π-system. The enhanced overlap of π-orbitals results in an increased conductance (figure 7). Incorporation of this switch into a MCBJ demonstrated that switching from the On-state to the Off-state results in an increased resistance but unfortunately the back-reaction was hindered probably due to quenching in the Off-state by the Fermi-levels of gold.[39]

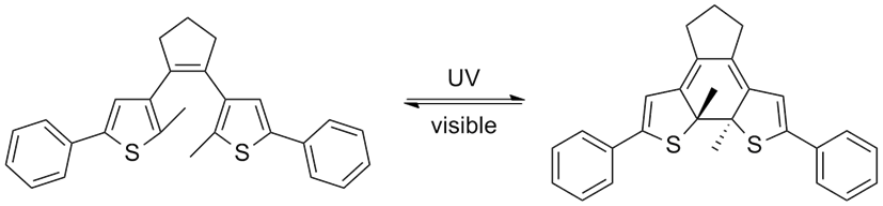

Figure 7. Reversible photoswitching between open- and closed-form of dithienylethene.[38]

As the back and forth switching was possible in solution this example nicely demonstrates that transformation of solution behavior to the setups used in molecular electronics can result in loss of chemical and physical properties. Beside light-driven molecular switches electrically triggered switching can be considered. As already mentioned the conductance in molecules depends on the population and the relative energy of the frontier molecular orbitals. The electrochemical potential of an electrode can be tuned with respect to the molecular energy levels. Charging of the molecule can be achieved by driving the electrochemical potential below or above the energy level of the HOMO and LUMO respectively. To prevent tunneling of the charge out of the molecule some additional mechanism are required for stabilizing the differently charged states and thus allowing permanent charging of the molecules. This involves a reorganization in the molecule and contacts that lowers the energy of the charged state below the Fermi level of the electrodes. Examples for redox-switches are functionalized viologens[41] or quinones[42,43] (figure 8).

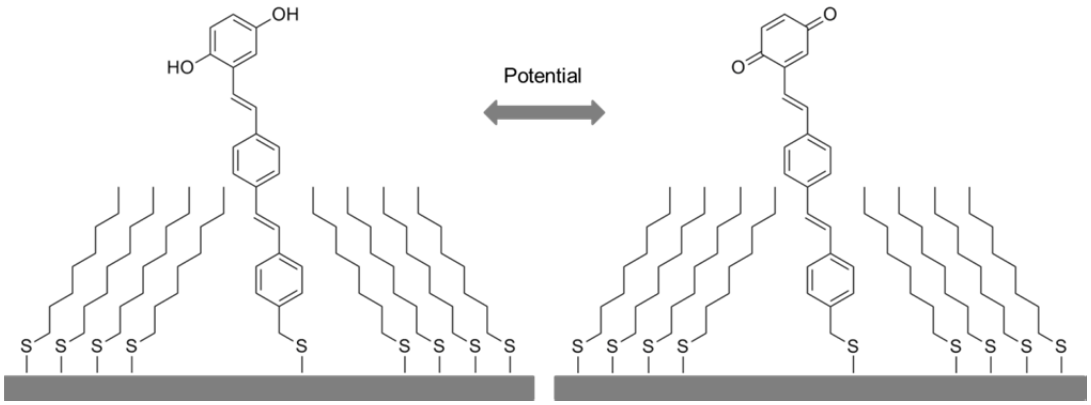

Figure 8. Quinone modified oligo(phenylene-vinylene) (Q-OPV) inserted in an alkanethiol SAM. *Left*: high-conducting reduced hydroquinone-OPV; *right*: low-conducting oxidized quinone-OPV. The full bond conjugation in the hydroquinone form provides an efficient, delocalized tunnel barrier for electron-transport. Reprinted from Tsoi *et al*.[43]

A second type of electrically triggered switches are so called voltage triggered switches. In these systems the On and Off-states have the same oxidation state, but different conductivities. This can be achieved when the electronic properties of a certain moiety are influenced by another structural unit which can be moved towards or away from it. Undoubtly mechanically interlocked molecules are ideal candidates towards such dynamic systems. Similar to molecular muscles an external stimulus can cause a supramolecular rearrangement resulting in delocalization of the host.[44] A molecular thread with two binding sites for the macrocyclic host is necessary while the host is solely located at one preferred recognition site in the ground-state. By functionalization of one stopper with substituents which possess high

affinity towards the employed electrodes the incorporation of such molecular switches into electronic devices gets possible. As an example Stoddart *et al*. used a molecular thread containing a tetrathiafulvalene (TTF) and a 1,5-dihydroxynaphthalene (DNP) binding site (figure 9).[45,46] As a host a cyclobis(paraquat-*p*-phenylene) ($CBQT^{4+}$) cyclophane was used, which is located at the TTF unit as a preferred binding site in the ground state (ground-state co-conformer). By oxidizing the TTF unit, electrostatic repulsion between the two cations causes a shift of the cyclophane to the DNP (meta-stable co-conformer). Current-voltage measurements showed that the meta-stable co-conformer is the On-state of the switch and the ground-state conformer the Off-state. Furthermore hysteretic behavior (delayed response to an applied force) was found in a molecular-switch tunnel junction. Such a loop like behavior allows the use of these switches as molecular memories.

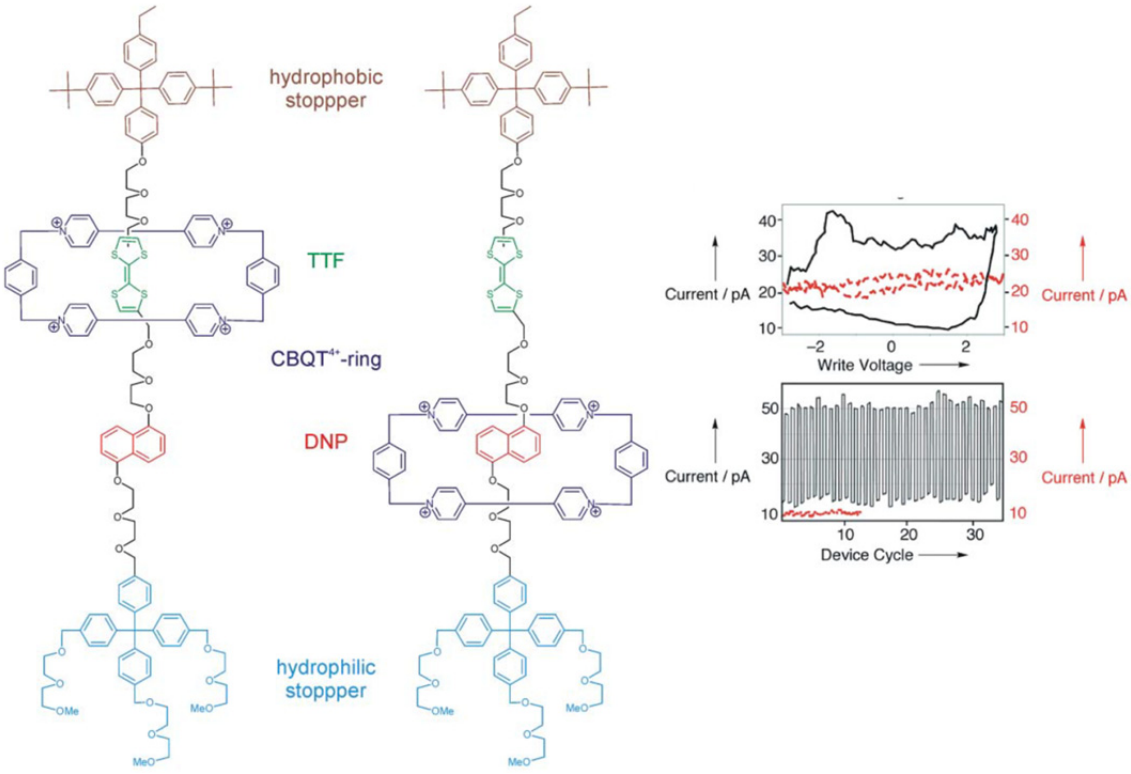

Figure 9. Rotaxane having two recognition sites for the encircling cyclophane. In the ground state the cyclophane is located at the TTF binding site (thermodynamic co-conformer). Upon oxidation the generated electrostatic repulsion results in a non-equilibrium and the cyclophane moves to the DNP moiety to find it new global energy minimum. *Right*: Hysteresis loop and repeated switching of the bistable rotaxane in a MSTJ setup. Reprinted from Luo *et al*.[46] and Weibel *et al*.[47]

Synthesis and Aggregation Studies of a Molecular "Daisy Chain" Formed by Amphiphilic Molecular Rods for Electron Transport Investigations in a Bimolecular Junction – Towards a Molecular Potentiometer

*Jürgen Rotzler, Daniel Häussinger, Marcel Mayor**

Low costs, higher efficiency and lower power dissipation are the requirements for new electronic devices. To fulfill these needs is the aim of molecular electronics where macroscopic electronic devices are mimicked and downscaled to about 1 – 100 nm using organic molecules as functional nanostructures instead of semiconductor based setups.[3] Large progress has been made in understanding the structure-property relations of conducting molecules leading to single molecular rectifiers[4,48–50], switches[36–39,41,42,44,45,51–54], wires[55–60] etc. In order to mimic even more complex electronic devices like potentiometers[61] or memory devices[62–65] the structural requirements of molecules become increasingly more complex. With increasing size and complexity not only higher synthetic efforts and handling-properties have to be concerned, but also structural issues like drop of conductivity by increasing length[6], interruption of the π-systems (effective chain length)[66] and unfavorable conformations have to be attended[21]. All these problems grow with increased complexity, making the search for alternative charge transport pathways and new concepts to interlink and perfectly arrange conducting structural motifs urgently necessary.

Recently, conductance studies of various rod-like molecules (OPE) with only one thiol-anchoring group in a molecular break junction showed surprisingly high conductance.[67] This unexpected outcome was explained by the formation of bimolecular bridges held together by intermolecular π-π stacking, which means charge transport in a molecule hold together by supramolecular interactions.[67–69] Furthermore Nichols and co-workers demonstrated the synthetic tailorability of these bimolecular bridges by substituting the central OPE-core.[70] Interestingly not only the electronic properties of the molecular wire itself were altered but π-π stacking could be prevented by substitution with bulky groups. Conductance measurements on paracyclophanes[71,72] and columnar stacked π-systems[73] confirmed the possibility to use this new charge transport channel in molecular electronics.

Project

To be able to use molecular wires assembled by secondary interactions in new electronic devices it is crucial to investigate in detail the influence of different tunable parameters on the

conductance. Therefore it is necessary to stabilize the bimolecular junctions and construct them by purpose. By formation of stable bimolecular junctions it will then be possible to investigate bimolecular junctions comprising a low degree of π-stacking which is due to their instability not possible in conventional π-stacked molecular wires. In the previous studies of amphiphile **A1** it was shown that water soluble cyclophanes substituted with a molecular rod form [c2]daisy chains at concentrations below 1 mM. The stoichiometric complexing properties of water soluble cyclophanes towards benzene cores and acetylenes are used to design a functionalized version of a [c2]daisy chain, comprising a thiol anchoring group which can be addressed by gold electrodes. This supramolecularly assembled pseudorotaxanes are ideal candidates to further investigate bimolecular junctions (figure 10). Additionally by mechanically contracting and extending of the bimolecular bridge in a molecular break junction it should be possible to vary the extent of π-stacked surface and thus to vary the conductivity mimicking a macroscopic potentiometer (figure 11). In contrast to the conductance switches reported so far the electronic nature of the bimolecular bridge can be varied solely by a horizontal replacement of the molecular wires in respect to each other. This results in a change in the electronic nature of the bimolecular bridge while the individual parts remain unchanged.

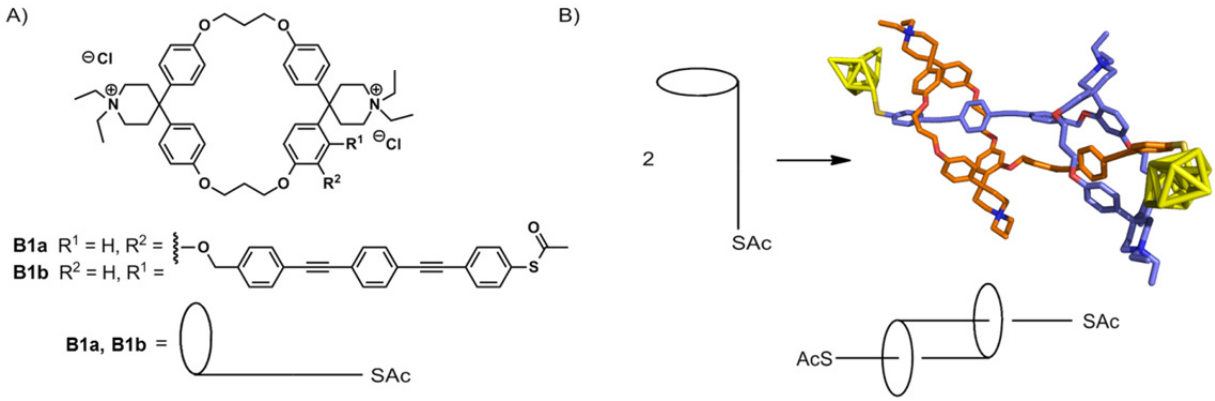

Figure 10. A) Molecular rods **B1a** and **B1b** comprising terminal loops. B) Supramolecular assembly of a mechanically interlinked pseudorotaxane.

Additionally we intended to investigate how aggregation is influenced when the OPE rod is linked to the water soluble cyclophane in closer proximity to the spiro-piperidine part (monomer **B1b**). In this chapter the synthesis and self-aggregation studies of monomer **B1a** and **B1b** are presented to provide the platform for future investigations of bimolecular junctions in single molecular conductance measurements.

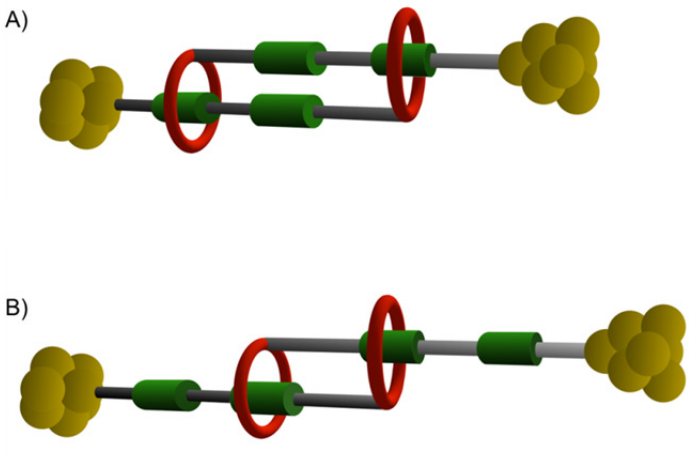

Figure 11. Sketch of dimer **B1** in a molecular break junction acting as a mechanically addressable molecular potentiometer. A) High conductance state, B) low conductance state.

The molecular design of the water soluble cyclophane in **B1a** and **B1b** is in accordance to the unfunctionalized amphiphile **A1** based on the pioneering findings of Diederich *et al*.[74,75] The diphenylmethane units function as rigid cavity walls, whereas the interlinking alkyl chains define the size of the cavity. The water solubility is provided by two doubly ethylated spiro-piperidinyl moieties. Variation of the counterions of these quaternary ammonium centers allow for precisely adjusting the solubility of the amphiphiles in polar solvents. In contrast to amphiphile **A1**, the hydrophobic molecular rod is equipped at the terminus with an acetyl protected thiol anchoring group which makes the amphiphiles addressable by gold electrodes. No excimer formation was observed in emission spectra of **A1** in the concentration range where dimers were present, indicating a non-ideal alignment of the OPEs in the [c2]daisy chain. Therefore the rotation around the benzylic linker and the sideways motion of the OPE has to be restricted to avoid misalignment by limiting the degrees of freedom. This can be achieved by making the rod more rigid, at the expense of increased formation of oligomeric acyclic daisy chains. By considering the spatial arrangement, a shifting of the molecular wire into closer proximity to the spiro-piperidine part (monomer **B1b**) compared to **B1a** is likely to decrease the number of degrees of freedom of the OPE at the interlinking position, potentially causing an improved preorganization of the hydrophobic rods. Thus a more ideal alignment of the molecular wires in the dimeric [c2]daisy chain is caused which is unambiguously necessary to obtain suitable bimolecular junctions. Furthermore an improved preorganization of the amphiphile **B1b** potentially results in an increased stability of the inclusion complex and potentially in the formation of desired [c2]daisy chains at even lower concentrations.

Results and Discussion

Synthesis

In analogy to the unfunctionalized version of **B1a** the assembly of the loop subunit profits to a large extend from the cyclophane chemistry developed by Diederich[74,75] while the rigid molecular rod is based on classical Sonogashira coupling chemistry[76–78]. In our previous studies on the unfunctionalized version of **B1a** the synthesis was designed such that the OPE is coupled to the cyclophane at a late stage of the synthesis to allow alterations of the molecular rod and thus to optimize the extent of intermolecular stacking. From this previous studies we already had cyclophane **A8** bearing the for Sonogashira cross coupling functionalized benzyl linker in hand what allowed coupling of the *S*-acetyl substituted OPE.

The mono-functionalized water soluble cyclophane of monomer **B1b** – featuring a hydrophobic cavity – was synthesized using the same synthetic route as described for **A8**. In short the asymmetric part was synthesized by a Grignard reaction of 4-bromoanisol and *N*-acetylpiperidin-4-one followed by elimination and deprotection with boron tribromide, subsequent introduction of photocleavable protecting group 2-nitrobenzyl and final addition of 3-methoxyphenol to the alkene (scheme 1).

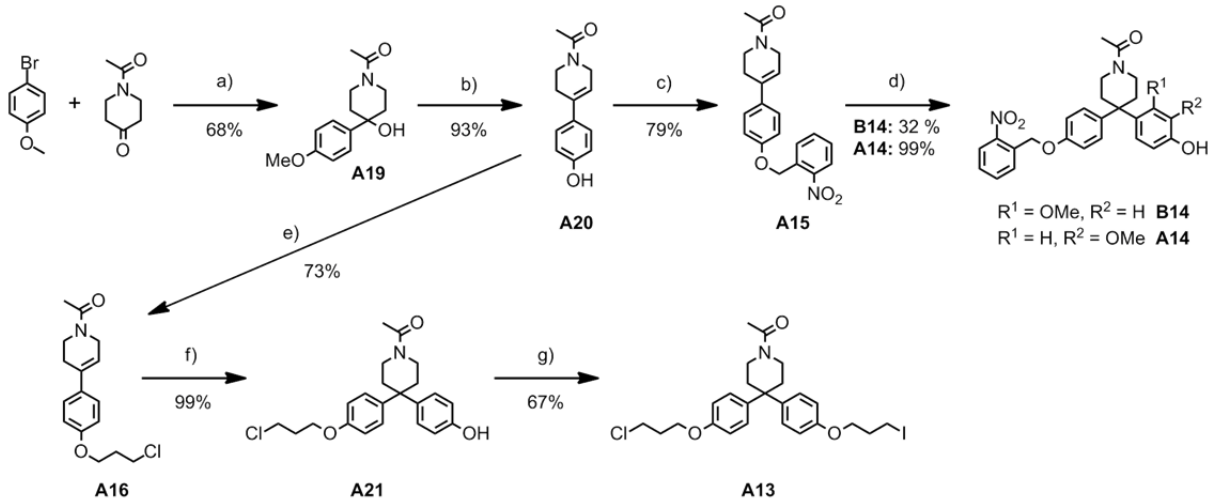

Scheme 1. Synthesis of the two individual cyclophane parts **B14** and **A13**. a) Mg, THF, reflux, 1.5 h, then *N*-acetyl-piperidin-4-one, THF, rt, 4 h; b) BBr_3, CH_2Cl_2, reflux, 3 h; c) 2-nitrobenzyl chloride, K_2CO_3, MeCN, reflux, 6.5 h; d) 3-methoxyphenol, $BF_3{\cdot}OEt_2$, CH_2Cl_2, 28 h, rt; e) 1,3-dichloropropane, K_2CO_3, MeCN, reflux, 26 h; f) phenol, $BF_3{\cdot}OEt_2$, CH_2Cl_2, 23 h, rt; g) 1,3-diiodopropane, BHT, K_2CO_3, acetone, reflux, 5 h.

Unfortunately in the final step after stirring for 72 h at room temperature formation of three isomers was observed, from which the desired asymmetrical diphenylpiperidine unit **B14** was

isolated by column chromatography in 32% yield (scheme 1). One side product could be analyzed by 2D-NMR spectroscopy and was found to be the product where the coupling took place in *para* position of the methoxy group, whereas the second isomer could not be fully characterized. On closer examination of the nucleophilic reaction sites of 3-methoxyphenol it is most probable that the second isomer is the product where the coupling occurred *ortho* to the hydroxyl and methoxy position. A total conversion of 98% was obtained and longer reaction times or different reaction temperatures did not lead to a more favorable product distribution. The symmetrical part **A13** of the cyclophane was synthesized starting from phenol **A20** by introduction of 1,3-dichloropropane in a S_N2-reaction, followed by addition of phenol to the remaining alkene and nucleophilic aliphatic substitution of 1,3-diiodopropane (scheme 1).

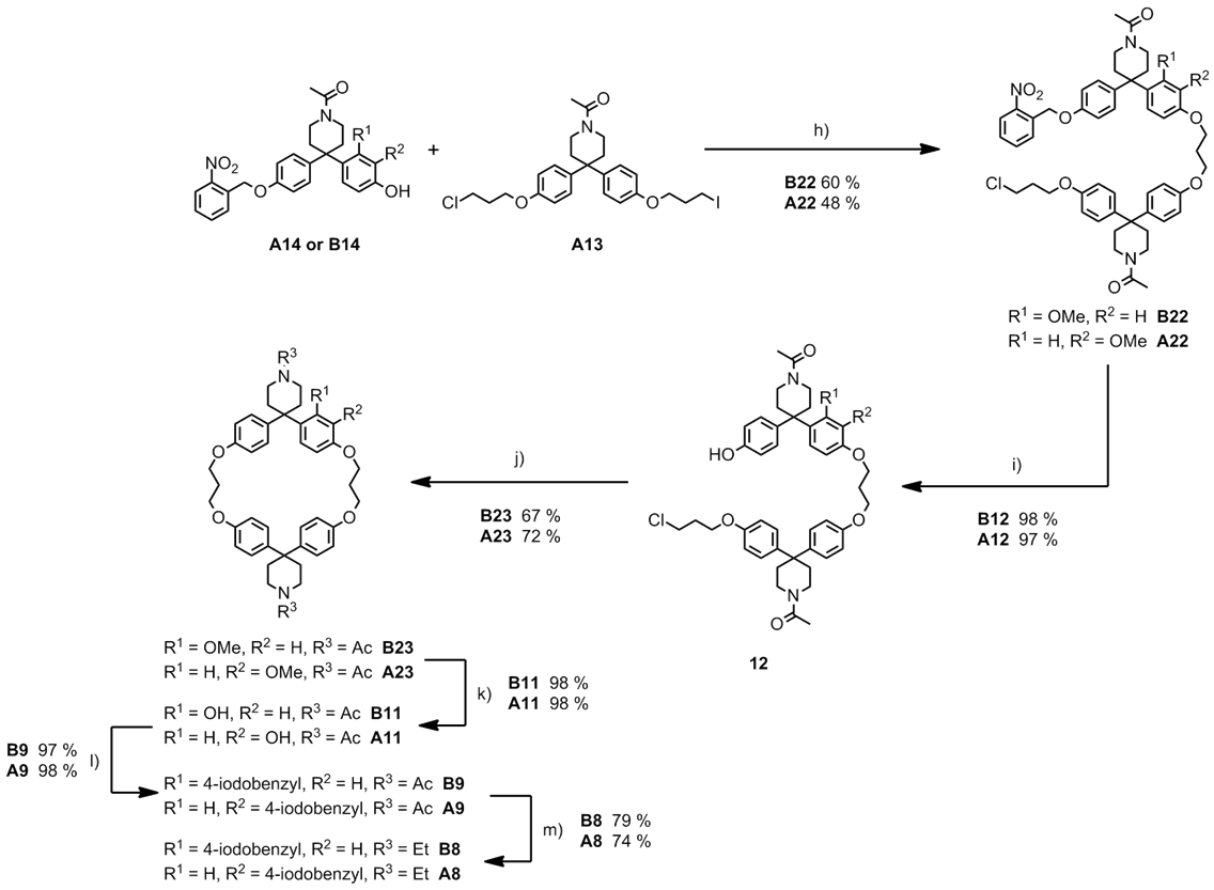

Scheme 2. Stepwise cyclization procedure towards mono-functionalized cyclophanes **8**. h) Cs_2CO_3, acetone, 40°C, 16 h; i) BHT, THF, *hv*, rt, 7 h; j) Cs_2CO_3, MeCN, reflux, 36 h; k) sodium thiomethoxide, DMF, 160°C, 6 h; l) 4-iodobenzyl bromide, Cs_2CO_3, DMF, 85°C, 20 h; m) DIBAL-*H*, CH_2Cl_2, 0°C then rt, 4 h.

Nucleophilic substitution of the two cyclophane parts **B14** and **A14** together with **A13** afforded dimers **A22** and **B22**, which were macrocyclized after photolytic debenzylation (scheme 2). In analogy to the synthesis of **A8** the concentration of **A12** and **B12** were kept

low in solution to prevent oligomerization. Nucleophilic demethylation, coupling of 4-iodobenzyl bromide and subsequent reduction of the diamide **B9** afforded tertiary amine **B8** (scheme 2) which is suitable for subsequent Sonogashira cross-coupling.

The molecular wire **B6** was synthesized starting from literature known ((4-ethynylphenyl)ethynyl)trimethylsilane (**A27**) and *S*-(4-iodophenyl) ethanethioate. The free acetylene was coupled to *S*-(4-iodophenyl) ethanethioate using a classical Sonogashira cross coupling protocol followed by cleavage of the TMS group using TBAF in acidic media to achieve OPE **B6** in 22% yield over five steps (scheme 3).

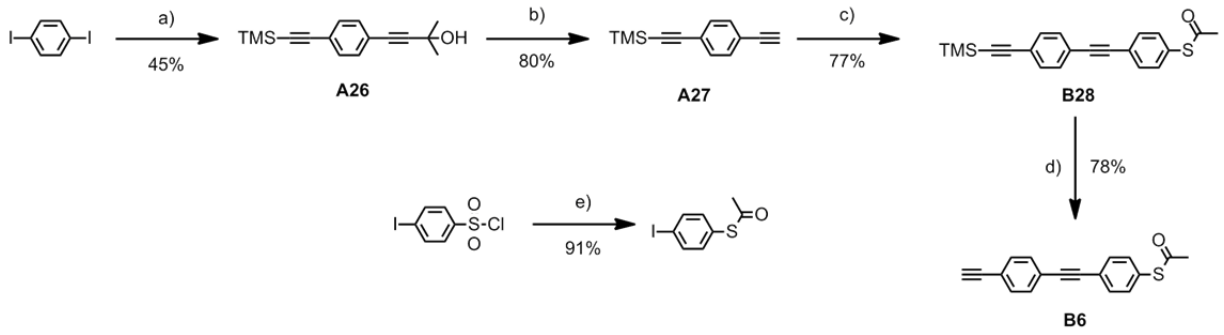

Scheme 3. Synthesis of the oligophenylene-ethynylene building block **B6**. a) $PdCl_2(PPh_3)_2$, CuI, DIPA, THF, 1.) TMS-acetylene, rt, 4 h, 2.) 2-methyl-3-butyn-2-ol, rt, 16 h; b) NaOH, toluene, 80°C, 1 h; c) *S*-(4-iodophenyl) ethanethioate, $PdCl_2(PPh_3)_2$, CuI, DIPA, THF, rt, 4 h; d) TBAF, Ac_2O, AcOH, THF, 0°C; e) 1.) Zn, Me_2SiCl_2, DMA, 1,2-dichloroethane, 75°C, 2 h, 2.) AcCl, 50°C, 15 min.

The OPE-rod **B6** was then cross coupled to the cyclophane **A8** or **B8** with the previously developed method using $Pd(dba)_2$, triphenylphosphine, CuI and diisopropylamine in THF at room temperature in 77% and 59% yield, respectively. Unfortunately the acetyl protection group turned out to be unstable under the reaction conditions as well as on silica. Thus the crude was purified by filtration through a pad of silica to remove any excess of OPE and catalyst followed by washing of the obtained orange solid with methanol. After concentration of the filtrate the desired product was obtained as a yellow solid and was used in the final alkylation without further purification. The previously reported coupling of an unfunctionalized OPE yielded in 92% of desired product what documents the instability of the acetyl protecting group. Using a different protection group for the sulfur anchoring group is not suitable as it would require further steps and transprotection of the already alkylated product is troublesome because of solubility issues. Coupling of OPE **B6** to an already alkylated cyclophane **A3** gave no conversion unfortunately. The ethyl-piperidine units of **B2a** and **B2b** were finally alkylated with freshly distilled iodoethane. The amphiphilic molecules

were isolated by column chromatography using silica as a solid phase and a mixture of acetone:1 M aq. ammonium chloride:acetonitrile 14:2:1, followed by Soxhlet® extraction with dichloromethane to get rid of the ammonium chloride and final ion exchange chromatography (DOWEX 1X8, 200 – 400 mesh, Cl^-). Recrystallization with methanol:diethyl ether 1:1 afforded monomer **B1a** as a pale yellow hygroscopic solid in 20% yield (scheme 4). By applying the same procedure to the final assembly of **B8** and **B6** only traces of the desired product **B1b** were obtained (figure 12). The main difference between in either the 4' or 5' position of the cyclophane functionalized molecules is their solubility. It is therefore hypothesized that alkylation of one of the amines in **B2b** causes the amphiphile to precipitate preventing any further alkylation. This is further documented by the isolation of the monoalkylated product.

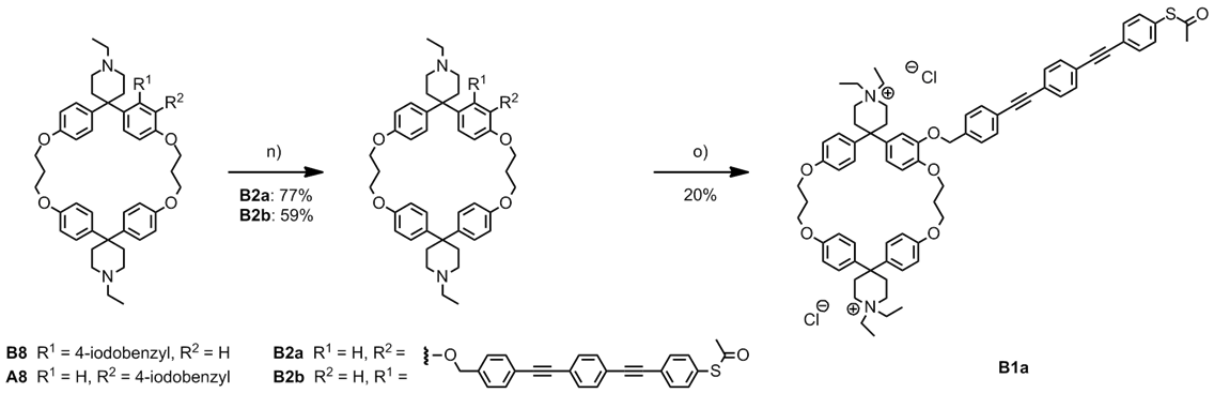

Scheme 4. Final assembly of the amphiphilic monomer **B1a** and **B1b**. n) OPE **B6**, $Pd(dba)_2$, PPh_3, CuI, DIPA, THF, rt, 4 h; o) iodoethane, CH_2Cl_2, rt, 5 d.

Regardless of the poor yields for the final assembly it was found that functionalization of the amphiphilic monomers is possible. This allows for a variety of different target structures potentially making an important contribution to various research areas like polymer science and molecular respectively supramolecular electronics.

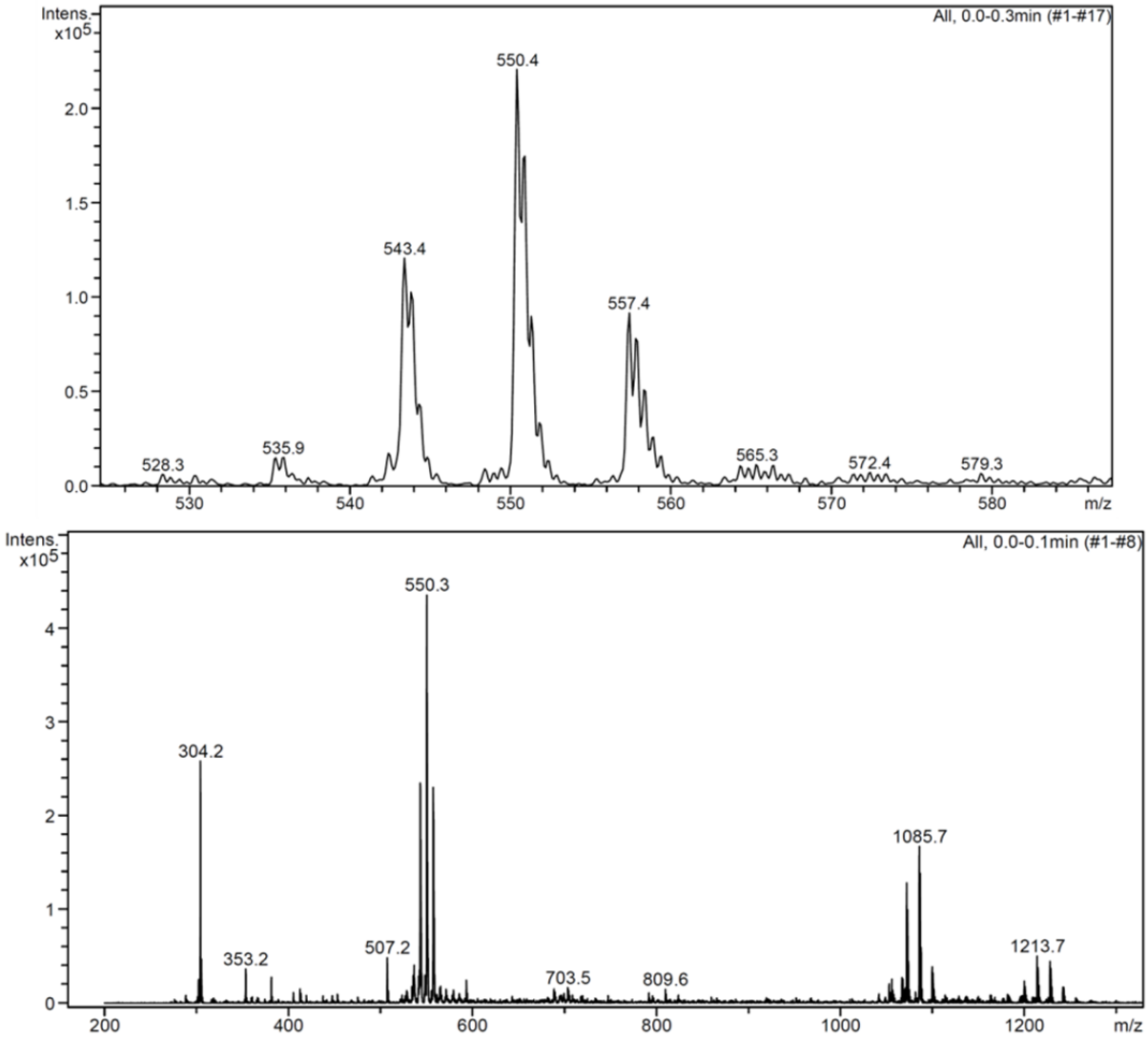

Figure 12. Mass spectrum (ESI-MS) of the amphiphile **B1a** (*top*) showing $[M^{2+}]$, $[M^{2+}\text{-}CH_3]$ and $[M^{2+}\text{-}C_2H_5]$ and mass spectrum of the reaction mixture of **B1b** (*bottom*), where the peak at 1085 m/z corresponds to the monoethylated product.

Aggregation Studies

Such hermaphroditic compounds can potentially form various aggregates in polar solvent since the hydrophobic molecular rod is forced into the hydrophobic cavity of the water soluble hydrophilic cyclophane by the hydrophobic effect (figure 13). As demonstrated in the investigations of amphiphile **A1**, the size of the cavity of **B1a** is large enough to complex neutral compounds in the size of 1,4 substituted benzenes.

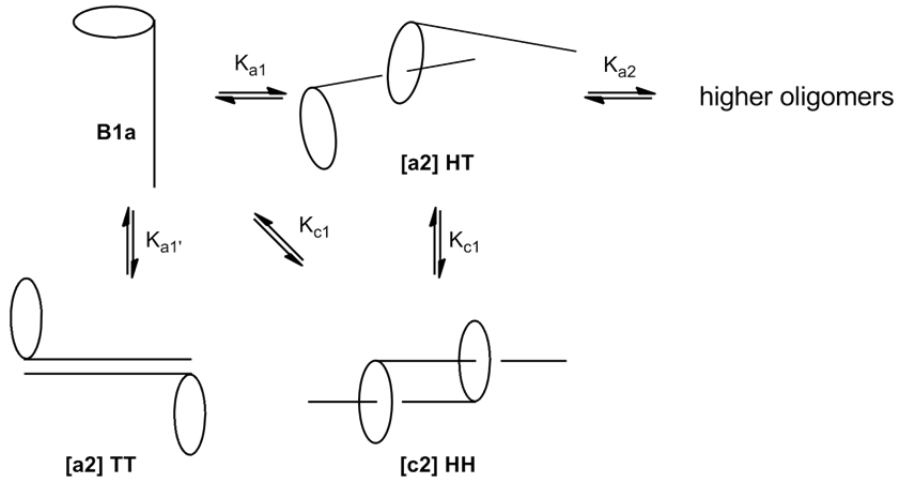

Figure 13. Possible aggregates of hermaphroditic monomer **B1a** in polar solvent.

In the previous studies of the unfunctionalized monomer **A1** it was shown that in a concentration range of approximately 1 mM to 10^{-6} M dimer formation can be observed in a mixture of water:methanol 3:2. Missing excimer formation in the emission spectra excluded aggregates like **[a2]TT**. Together with a reduced intensity of emission, compared to the monomer, a [c2]daisy chain formation seemed very likely. It was now of interest to investigate if functionalization on the OPE rod influences the aggregation behavior of **B1a**. Therefore a ^{1}H-NMR titration was performed (figure 14) to evaluate the critical aggregation concentration (CAC), the aggregation number *n* and the association constant K_a.

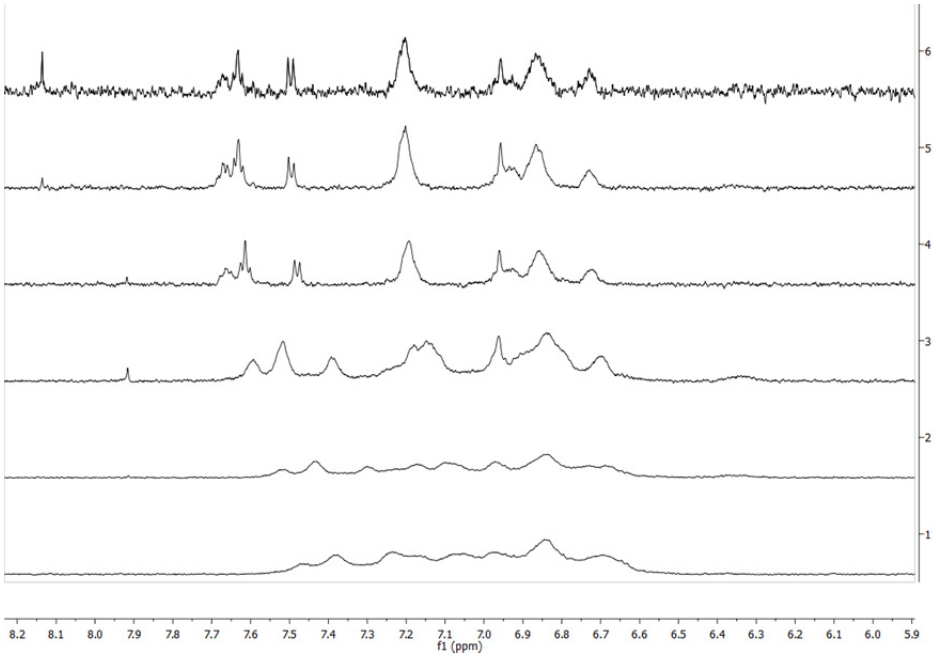

Figure 14. Selection of ^{1}H-NMR spectra of the aromatic region of monomer **B1a** recorded in D_2O:MeOD 3:2 on a 600 MHz spectrometer. 1) 3.59 mM, 2) 1.79 mM, 3) 0.90 mM, 4) 0.22 mM, 5) 0.054 mM, 6) 0.027 mM.

The ^{1}H-NMR spectra of **B1a** and the unfunctionalized version **A1** are very similar at comparable concentrations, showing equal chemical shifts for the aliphatic protons and the aromatic protons of the cyclophane. Due to introduction of a weak electron-accepting *S*-acetyl group the signals of the OPE-domain are slightly shifted downfield. In contrast to the unfunctionalized amphiphile the signals show less fine-splitting and remain broader over the entire concentration range. The protons are in a fast exchange regime and therefore averaged signals for different co-conformations of threaded amphiphiles are observed. Strong association was observed for the unfunctionalized amphiphile whereby the fast exchange regime can be rationalized when the internal flexibility of the inclusion complex is considered. Indicators for an inclusion of the molecular wire into the cavity of the water soluble cyclophane are the strong upfield chemical shifts for the OPE protons with increasing concentrations, likely due to the ring current of the cyclophanes' aromatic systems. Similarly to the unfunctionalized molecule the chemical shifts and the fine structure of the piperidinyl moieties remained unchanged when spectra in methanol-d4 and MeOD:D_2O 3:2 were compared. In contrast, for the aliphatic protons, defining the size of the cavity, a different splitting (alkoxy) and changed chemical shifts (alkyl) were observed, strongly indicating the inclusion of the molecular wire.

Plots of δ_{obs} against the inverse total concentrations resulted in critical aggregation concentrations (CAC) of CAC_1 = 0.37 mM and CAC_2 = 1.16 mM (averaged values of five different protons) (figure 15).

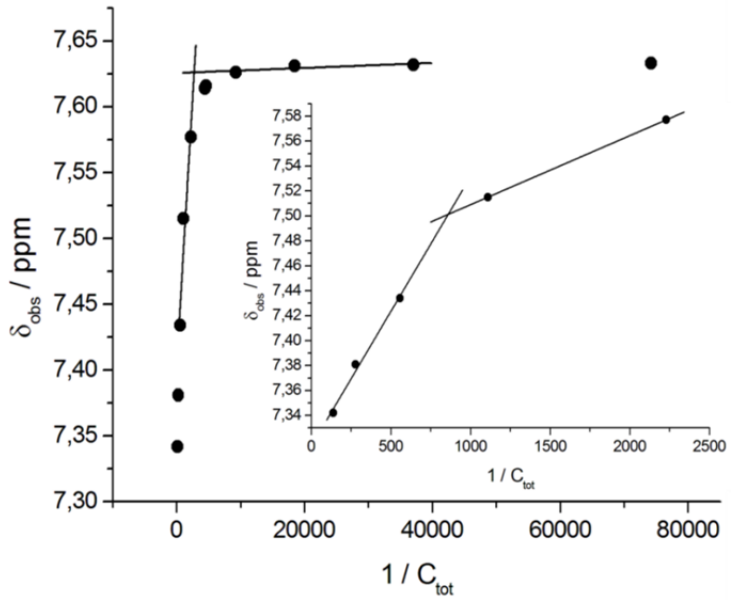

Figure 15. Representative graphical estimation of the critical aggregation concentration of monomer **B1a** by plotting the observed chemical shift δ_{obs} against the inverse total concentration C_{tot}.

These CAC are significantly lower than the values obtained for the unfunctionalized amphiphile pointing at formation of longer oligomers already at lower concentrations. The functionalization of the OPE moiety seems to alter the electronic structure and thus to favor the formation of an inclusion complex.

The aggregation number *n* and the association constant K_a were determined according to equation (2) which is derived from an equilibrium were n monomers form a single aggregate consisting of n units.[79–82]

$$\ln[C_{tot}(|\delta_{obs}-\delta_{mon}|)] = n \ln[C_{tot}(|\delta_{agg}-\delta_{obs}|)] + \ln K_a + \ln n - (n-1)\ln(|\delta_{agg}-\delta_{mon}|) \quad (2)$$

According to this equation plots of $\ln[C_{tot}(|\delta_{obs}-\delta_{mon}|)]$ versus $\ln[C_{tot}(|\delta_{obs}-\delta_{mon}|)]$ gave $n = 2$ for concentrations below 0.4 mM and $n = 4 - 5$ between 0.4 mM and 1.2 mM (figure 16). Above 1.2 mM even higher aggregates were found but the immense broadening of the spectra made a quantitative analysis impossible. On the other hand broadening is a strong indication for the formation of longer aggregates and because an increase in the viscosity of the solution is caused. Extrapolation to the CAC_1 of the plot in figure 14 yielded to chemical shift of the dimer from which a $K_a = 3.5 \cdot 10^6\ M^{-1}$ was calculated (averaged value of five selected protons).

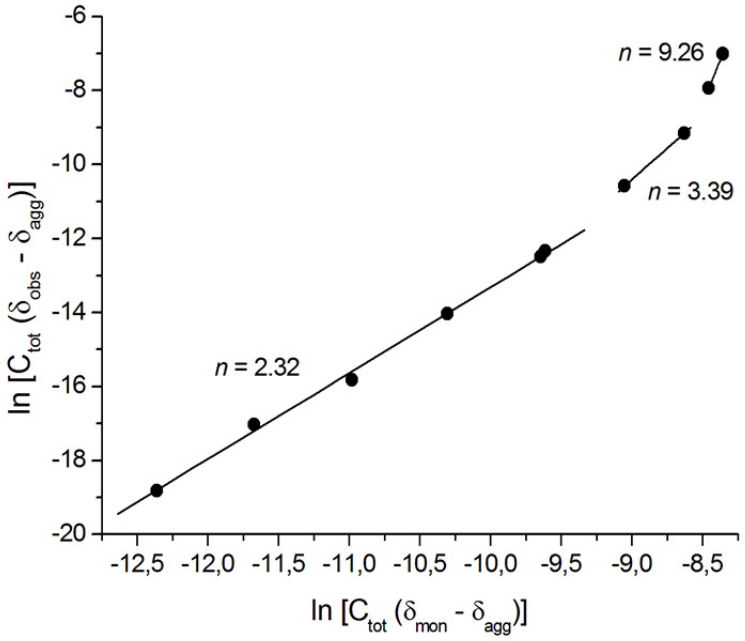

Figure 16. Graphical estimation of the aggregation number *n* from the slope of $\ln[C_{tot}(|\delta_{obs}-\delta_{mon}|)]$ versus $\ln[C_{tot}(|\delta_{obs}-\delta_{mon}|)]$.

The association constant K_a is in the same order of magnitude than the one obtained for the unfunctionalized amphiphile. In contrast to the proceeding example however, the formation of higher oligomers was observed at lower concentrations. Maybe the weak electron-accepting *S*-acetyl is sufficient to make the OPE more electron-deficient and therefore creates a stronger driving force for inclusion in the hydrophobic cavity formed by electron-rich aromatic systems.

Conclusion and Outlook

In summary it was possible to synthesize a water soluble cyclophane mono substituted with an *S*-acetyl functionalized oligophenylene-ethynylene. By ^{1}H-NMR titration it was demonstrated that functionalization did not prevent aggregation. On the contrary at even lower concentrations compared to the unfunctionalized version of **B1a** aggregates consisting of more than two monomer units were observed. An attempt to study the influence of replacing the molecular rod in closer proximity to spiro-piperidine part was not possible however, because alkylation of the tertiary amine **B2b** resulted in mainly monoalkylated product and only in traces in monomer **B1b**. Nevertheless, functionalization of the molecular wire was possible giving access to further investigations especially of the dimer structure by capping the dimer with bulky groups. Furthermore it will be of interest to see how these dimers behave in a molecular break junction setup and if it is possible to achieve different co-conformers with different conductivities by minute opening and closing of the break junction. This would enable detailed analysis of bimolecular bridges, especially of conformers with a low degree of π-stacking surface, as new potential structural motifs in molecular electronics. Additionally it will be of interest to polymerize the functionalized dimers by formation of disulfides which can potentially lead to long daisy chain polymers with unique and novel properties.

Experimental Part

General Remarks: For syntheses dry solvents from *Fluka* were used. With exception of iodoethane, which was distilled before use, all chemicals were directly used without purification. The solvents for chromatography and extractions were distilled before use. For column chromatography *silica gel 60* (40-63 μm) from *Fluka* or *SilicaFlash® P60* (40-63 μm) from *Silicycle* was used. TLC were carried out on *Silica gel 60 F_{254}* glass plates with a thickness of 0.25 mm from *Merck*. Characterizations were performed with the following instruments: ^{1}H-NMR and ^{13}C-NMR spectra were recorded with a *Bruker DPX-NMR* (400

MHz) or a *Bruker DRX-500* (500MHz), the *J* values are given in Hz. Solvents were obtained from *Cambridge Isotope Laboratories*. All spectra were recorded at 298 K. Mass spectra were recorded on a *finnigan MAT 95Q* for Electron Impact (EI) and an *esquire 3000 plus* (Bruker) for Electron Spray Ionisation (ESI); measured in *m/z* (%). Elementary analyses were obtained from a *varioMICROcube* from *elementar*. High resolution mass spectra were recorded by the Schürch group at the University of Bern on a *LTQ Orbitrap XL* from *Thermo Fisher Scientific* using a nanoelectrospray ion source.

NMR-Titrations: The highest concentration recorded was 7.18 mM which was obtained by dissolving 0.51 mg monomer **2** in 60 µL D_2O:methanol-d4 3:2. Dilution of this solution gave the other concentrations. NMR spectra of the corresponding samples were recorded on a *Bruker Avance III* – 600 MHz NMR spectrometer equipped with a TXI probe head at 295 K. For concentrations above 0.2 mM 1.7 mm tubes and for concentration below 0.2 mM 5 mm tubes were used. Solvents were obtained from *Cambridge Isotope Laboratories.* The samples were locked on methanol-d4.

1-(4-(4-Hydroxy-2-methoxyphenyl)-4-(4-(2-nitrobenzyloxy)phenyl)piperidin-1-yl)-ethanone (B14): Alkene **A15** (4.00 g, 1.00 equiv., 2.36 mmol), 2-methoxyphenol (3.74 mL, 4.23 g, 3.00 equiv., 34.0 mmol) and $BF_3{\cdot}OEt_2$ (8.20 mL, 9.43 g, 5.85 equiv., 66.4 mmol) were dissolved in 12 mL dichloromethane and stirred at rt for 3 d under exclusion of light. Then the mixture was quenched with 20 mL MeOH and diluted with dichloromethane. The organic layer was washed with demin. water and brine, dried with sodium sulfate, filtered and concentrated. The crude red oil was purified by column chromatography (SiO_2; CH_2Cl_2, 2.5% MeOH). The resulting colorless oil was washed with MeCN and the white solid precipitate **B14** was filtered off (32%).

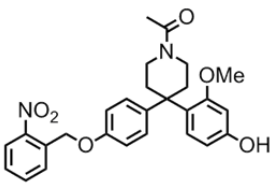

$\boldsymbol{R_f}$ = 0.11 (SiO_2; CH_2Cl_2, 2.5% MeOH); **m.p.** 154°C; **^{1}H-NMR** (400 MHz, $CDCl_3$): δ = 8.14 (dd, ^3J(H,H) = 8 Hz, ^4J(H,H) = 1.2 Hz, 1H, H3(*o*NO_2Ar)), 7.88 (d, ^3J(H,H) = 8 Hz, 1H, H5(*o*NO_2Ar)), 7.66 (dt, ^3J(H,H) = 8 Hz, ^4J(H,H) = 1.2 Hz, 1H), 7.47 (t, ^3J(H,H) = 8 Hz, 1H), 7.16 (d, ^3J(H,H) = 8 Hz, 2H, Ar-H), 7.15 – 7.10 (m, 3H, Ar-H), 6.85 (d, ^3J(H,H) = 8 Hz, 2H, Ar-H), 6.44 – 6.40 (m, 2H, Ar-H), 6.35 (d, ^3J(H,H) = 2.4 Hz, 1H, Ar-H), 5.43 (s, 2H, CH_2(benzyl)), 3.77 – 3.68 (m, 1H), 3.61 – 3.48 (m, 2H), 3.48 – 3.39 (m, 4H, including singlet at 3.44 (s, 3H, -OCH_3)), 2.58 – 2.50 (m, 1H), 2.50 – 2.42 (m, 1H), 2.41 – 2.33 (m, 1H), 2.31 – 2.22 (m, 1H), 2.17 (s, 3H, -(CO)-CH_3) ppm; **^{13}C-NMR** (101 MHz, $CDCl_3$): δ = 169.6 (C_q, 1C,

C=O), 159.6 (C_q, 1C), 156.6 (C_q, 1C), 156.2 (C_q, 1C), 147.3 (C_q, 1C), 140.4 (C_q, 1C), 134.5 (C_q, 1C), 134.3 (C_t, 1C), 129.0 (C_t, 1C), 128.6 (C_t, 1C), 128.6 (C_t, 1C), 128.6 (C_t, 2C), 126.4 (C_q, 1C), 125.3 (C_t, 1C), 114.5 (C_t, 2C), 107.1 (C_t, 1C), 101.6 (C_t, 1C), 67.0 (C_s, 1C, CH_2(benzyl)), 55.3 (C_p, 1C, -OCH_3), 53.6 (C_s, 1C), 44.0 (C_s, 1C), 43.3 (C_s, 1C), 39.1 (C_q, 1C), 35.7 (C_s, 1C), 21.5 (C_p, 1C, -(CO)-CH_3) ppm; **MS** (ESI): m/z (%) = 499 ($[M+Na]^+$); **elemental analysis** calcd (%) for $C_{27}H_{28}N_2O_6$: C 68.05, H 5.92, N 5.88; found: C 67.69, H 6.11, N 5.57.

1-(4-(4-(3-(4-(1-Acetyl-4-(4-((2-nitrobenzyl)oxy)phenyl)piperidin-4-yl)-3-methoxyphenoxy)propoxy)phenyl)-4-(4-(3-chloropropoxy)phenyl)piperidin-1-yl)ethanone (B22): 1-(4-(4-(3-Chloropropoxy)phenyl)-4-(4-(3-iodopropoxy)phenyl)piperidin-1-yl)ethanone

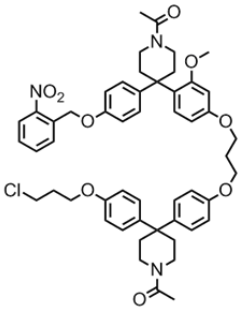

(**A13**) (2.80 g, 1.20 equiv., 5.04 mmol) and 1-(4-(4-hydroxy-2-methoxyphenyl)-4-(4-(2-nitrobenzyloxy)phenyl)piperidin-1-yl)ethanone (**B14**) (2.01 g, 1.00 equiv., 4.20 mmol) were dissolved in 175 mL acetone. Then cesium carbonate (2.77 g, 2.00 equiv., 8.40 mmol) was added and the reaction mixture was stirred at 40°C for 16 h. After cooling to rt the suspension was filtered and washed with acetone. The filtrate was concentrated and purified by flash column chromatography (SiO_2; CH_2Cl_2, 2.5% MeOH) (60%).

R_f = 0.22 (SiO_2; CH_2Cl_2, 2.5% MeOH); **^{1}H-NMR** (400 MHz, $CDCl_3$): δ = 8.14 (d, ^3J(H,H) = 8 Hz, 1H, *nitrobenzyl*), 7.88 (d, ^3J(H,H) = 8 Hz, 1H, *nitrobenzyl*), 7.66 (t, ^3J(H,H) = 8 Hz, 1H, *nitrobenzyl*), 7.47 (t, ^3J(H,H) = 8 Hz, 1H, *nitrobenzyl*), 7.21 (d, ^3J(H,H) = 9 Hz, 1H, *H*5(3-methoxyphenol)), 7.16 – 7.08 (m, 6H), 6.89 – 6.78 (m, 6H), 6.51 – 6.45 (m, 1H, *H*6(3-methoxyphenol)), 6.38 – 6.34 (m, 1H, *H*2(3-methoxyphenol)), 5.43 (s, 2H, CH_2(benzyl)), 4.16 (m, 6H), 3.78 – 3.69 (m, 3H), 3.68 – 3.61 (m, 2H), 3.59 – 3.40 (m, 8H), 2.60 – 2.42 (dm, 2H), 2.40 – 2.27 (m, 6H), 2.28 – 2.18 (m, 4H), 2.08, 2.07 (ds, 6H, -(CO)-CH_3) ppm; **^{13}C-NMR** (101 MHz, $CDCl_3$): δ = 169.0 (C_q, 1C, *C*=O), 169.0 (C_q, 1C, *C*=O), 159.2 (C_q, 1C), 158.9 (C_q, 1C), 157.0 (C_q, 1C), 156.9 (C_q, 1C), 155.9 (C_q, 1C), 147.0 (C_q, 1C), 140.1 (C_q, 1C), 139.0 (C_q, 1C), 138.8 (C_q, 1C), 134.2 (C_q, 1C), 134.0 (C_t, 1C), 128.7 (C_t, 1C), 128.4 (C_t, 1C), 128.3 (C_t, 2C), 128.0 (C_t, 4C), 127.0 (C_q, 1C), 125.0 (C_t, 1C), 114.6 (C_t, 2C), 114.5 (C_t, 2C), 114.2 (C_t, 2C), 104.6 (C_t, 1C, *C*6(3-methoxyphenol)), 101.1 (C_t, 1C, *C*2(3-methoxyphenol)), 66.9 (C_s, 1C), 64.3 (C_s, 1C), 64.2 (C_s, 1C), 55.3 (C_p, 1C, -OCH_3), 43.9 (C_q, 1C), 43.9 (C_s, 1C), 43.7 (C_s, 1C), 43.4 (C_s, 1C), 41.6 (C_s, 1C), 38.9 (C_s, 1C), 38.8 (C_s, 1C), 37.0 (C_s, 1C), 36.1 (C_s, 1C), 35.9 (C_s, 1C), 35.5 (C_s, 1C), 32.3 (C_s, 1C), 29.8 (C_q, 1C), 29.4

(C_s, 1C), 21.6 (C_p, 1C, -(CO)-*C*H$_3$), 21.5 (C_p, 1C, -(CO)-*C*H$_3$) ppm; **MS** (ESI, positive ion mode, MeCN): m/z = 926 ([M+Na]$^+$), 904 ([M+H]$^+$); **HRMS** (ESI): m/z calcd for [$C_{52}H_{58}ClN_3O_9$+H]$^+$: 904.3934; found: 904.3959.

1-(4-(4-(3-(4-(1-Acetyl-4-(4-(3-chloropropoxy)phenyl)piperidin-4-yl)phenoxy)propoxy)-2-methoxyphenyl)-4-(4-hydroxyphenyl)piperidin-1-yl)ethanone (B12): The nitrobenzyl protected alcohol **B22** (1.40 g, 1.00 equiv., 1.55 mmol) was dissolved in 112 mL THF and then radical inhibitor BHT (345 mg, 1.01 equiv., 1.57 mmol) was added. The reaction mixture was irradiated for 7 h at rt in a Rayonet® spectrophotometer equipped with alternating UV-lamps emitting at 300 nm and 366 nm. Afterwards the solvent was evaporated and the residue subjected to column chromatography (SiO_2; CH_2Cl_2:MeOH 20:1) to afford the desired target compound **12a** as a pale brown oil (98%).

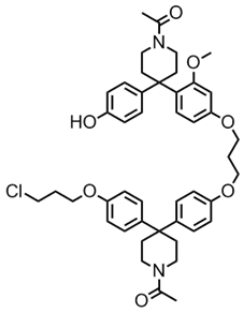

***R*$_f$** = 0.30 (SiO_2; CH_2Cl_2, 5% MeOH); **^{1}H-NMR** (400 MHz, $CDCl_3$): δ = 7.17 (d, ^3J(H,H) = 8.4 Hz, 1H, H5(3-methoxyphenol)), 7.14 – 7.04 (m, 4H), 7.01 (d, ^3J(H,H) = 8.8 Hz, 2H), 6.85 – 6.79 (m, 4H), 6.71 (d, ^3J(H,H) = 8.8 Hz, 2H), 6.46 (dd, ^3J(H,H) = 8.4 Hz, ^4J(H,H) = 2.4 Hz, 1H, H6(3-methoxyphenol)), 6.36 (d, ^4J(H,H) = 2.4 Hz, 1H, H2(3-methoxyphenol)), 4.14 – 4.04 (m, 6H), 3.75 – 3.67 (m, 3H), 3.66 – 3.60 (m, 2H), 3.59 – 3.04 (m, 8H, including s at 3.43 (-OC*H*$_3$)), 2.59 – 2.40 (dm, 2H), 2.38 – 2.25 (m, 6H), 2.25 – 2.16 (m, 4H), 2.08, 2.07 (ds, 6H, -(CO)-C*H*$_3$) ppm; **^{13}C-NMR** (101 MHz, $CDCl_3$): δ = 169.3 (C_q, 1C, *C*=O), 169.3 (C_q, 1C, *C*=O), 159.3 (C_q, 1C), 158.9 (C_q, 1C), 157.1 (C_q, 1C), 156.9 (C_q, 1C), 154.3 (C_q, 1C), 139.0 (C_q, 1C), 138.7 (C_q, 1C), 138.1 (C_q, 1C), 128.3 (C_t, 1C), 128.1 (C_t, 2C), 128.0 (C_t, 4C), 127.4 (C_q, 1C), 114.8 (C_t, 2C), 114.6 (C_t, 4C), 104.6 (C_t, 1C, *C*6(3-methoxyphenol)), 101.2 (C_t, 1C, *C*2(3-methoxyphenol)), 64.4 (C_s, 1C), 64.3 (C_s, 1C), 55.4 (C_p, 1C, -O*C*H$_3$), 44.0 (C_q, 1C), 43.9 (C_s, 1C), 43.8 (C_s, 1C), 43.3 (C_s, 1C), 41.7 (C_s, 1C), 39.1 (C_s, 1C), 38.9 (C_s, 1C), 37.0 (C_s, 1C), 36.1 (C_s, 1C), 35.9 (C_s, 1C), 35.5 (C_s, 1C), 32.4 (C_s, 1C), 29.5 (C_q, 1C), 29.4 (C_s, 1C), 21.5 (C_p, 1C, -(CO)-*C*H$_3$), 21.5 (C_p, 1C, -(CO)-*C*H$_3$) ppm; **MS** (ESI, positive ion mode, MeCN): m/z = 791 ([M+Na]$^+$); **HRMS** (ESI): m/z calcd for [$C_{45}H_{53}ClN_2O_7$+H]$^+$: 769.3614; found: 769.3614.

1,1”-Diacteyl-4’-methoxy-dispiro[piperidine-4,2’-[7,11,21,25]-tetraoxacyclopenta[24.2.2.2^{3,6}.2^{12,15}.2^{17,20}]hexatriaconta[3,5,12,14,17,19,26,28,29,31,33,35] dodecaene-16,4”-piperidine] (B23): Cesium carbonate (430 mg, 6.00 equiv., 1.31 mmol) was suspended in 7 mL MeCN and heated to reflux. To this suspension a solution of phenol

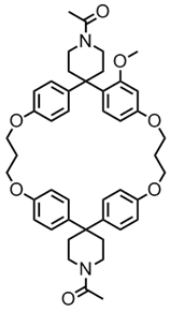

B12 (168 mg, 1.00 equiv., 0.218 mmol) in 14 mL MeCN was added dropwise over a period of 30 h. After further heating for additional 6 h the solvent was evaporated and the crude purified by column chromatography (SiO_2; dichloromethane, 5% MeOH). A yellow oil was obtained from which the product was precipitated with EtOH. The white solid was filtered off and washed once with EtOH and once with diethyl ether (67%).

$\boldsymbol{R_f}$ = 0.41 (SiO_2; CH_2Cl_2, 5% MeOH); **m.p.** 271°C; **^{1}H-NMR** (400 MHz, $CDCl_3$): δ = 7.16 – 7.07 (m, 7H), 6.74 (d, ^3J(H,H) = 8.8 Hz, 2H), 6.72 (d, ^3J(H,H) = 8.8 Hz, 2H), 6.67 (d, ^3J(H,H) = 8.8 Hz, 2H), 6.36 (dd, ^3J(H,H) = 8.4 Hz, ^4J(H,H) = 2.4 Hz, 1H, H6(3-methoxyphenol)), 6.24 (d, ^4J(H,H) = 2.4 Hz, 1H, H2(3-methoxyphenol)), 4.08 – 4.00 (m, 8H), 3.67 – 3.59 (m, 4H), 3.51 – 3.44 (m, 4H), 3.42 (s, 3H, -OCH_3)), 2.60 – 2.32 (m, 8H), 2.18 – 2.10 (m, 4H), 2.06, 2.06 (ds, 6H, -(CO)-CH_3) ppm; **^{13}C-NMR** (101 MHz, $CDCl_3$): δ = 168.9 (C_q, 1C, *C*=O), 168.9 (C_q, 1C, *C*=O), 159.1 (C_q, 1C), 159.0 (C_q, 1C), 157.3 (C_q, 1C), 157.2 (C_q, 1C), 156.9 (C_q, 1C), 138.8 (C_q, 1C), 138.7 (C_q, 1C), 138.1 (C_q, 1C), 127.9 (C_t, 2C), 127.4 (C_q, 1C), 127.1 (C_t, 1C), 127.0 (C_t, 2C), 126.9 (C_t, 2C), 114.9 (C_t, 2C), 114.9 (C_t, 2C), 114.2 (C_t, 2C), 106.1 (C_t, 1C, *C*6(3-methoxyphenol)), 101.6 (C_t, 1C, *C*2(3-methoxyphenol)), 63.9 (C_s, 1C), 63.8 (C_s, 1C), 63.7 (C_s, 1C), 63.3 (C_s, 1C), 55.1 (C_p, 1C, -O*C*H$_3$), 43.8 (C_q, 1C), 43.6 (C_s, 1C), 43.2 (C_s, 1C), 43.1 (C_s, 1C), 38.8 (C_s, 1C), 38.1 (C_s, 1C), 35.9 (C_s, 1C), 35.9 (C_s, 1C), 35.6 (C_s, 1C), 35.5 (C_s, 1C), 35.0 (C_s, 1C), 34.9 (C_s, 1C), 29.7 (C_q, 1C), 29.6 (C_s, 1C), 21.5 (C_p, 2C, -(CO)-*C*H$_3$) ppm; **MS** (ESI, positive ion mode, MeCN): m/z = 771 ([M+K]$^+$), 755 ([M+Na]$^+$); **elemental analysis** calcd (%) for $C_{45}H_{52}N_2O_7$: C 73.75, H 7.15, N 3.82; found: C 73.57, H 6.90, N 3.76.

1,1”-Diacteyl-4’-hydroxy-dispiro[piperidine-4,2’-[7,11,21,25]-tetraoxacyclopenta-[24.2.2.2^{3,6}.2^{12,15}.2^{17,20}]hexatriaconta[3,5,12,14,17,19,26,28,29,31,33,35]dodecaene-16,4”-piperidine] (B11): Cyclophane **B23** (372 mg, 1.00 equiv., 0.508 mmol) and sodium thiomethoxide (198 mg, 5.00 equiv., 2.54 mmol) were dissolved in 40 mL DMF and heated at 160°C under argon atmosphere for 5 h. Then 26 mL 0.1 M aq. HCl was added and the solvents removed under vacuum. The residue was taken up in demin. water and the suspension was filtered. The remaining pale beige solid was washed once with diethyl ether (10 mL). The white powder was recrystallized with methanol (98%).

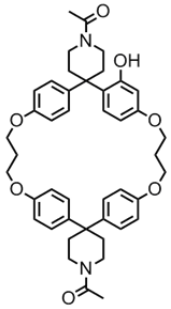

R_f = 0.35 (SiO_2; CH_2Cl_2, 5% MeOH); **m.p.** 212 - 213°C; **^{1}H-NMR** (400 MHz, MeOD): δ = 7.17 – 7.11 (m, 7H, Ar-H), 6.78 – 6.74 (m, 4H, Ar-H), 6.69 (d, ^3J(H,H) = 8.5 Hz, 2H, Ar-H), 6.35 (dd, ^3J(H,H) = 8.5 Hz, ^4J(H,H) = 2.5 Hz, 1H, H35'), 6.14 (d, ^4J(H,H) = 2.5 Hz, 1H, H5'), 4.60 (broad s, 1H, -O*H*), 4.11 – 4.02 (m, 8H, Ar-O-CH_2-), 3.77 – 3.70 (m, 1H), 3.63 – 3.52 (m, 6H), 2.76 – 2.69 (m, 1H), 2.67 – 2.60 (m, 1H), 2.45 – 2.31 (m, 6H), 2.29 – 2.22 (m, 1H), 2.15 – 2.10 (m, 4H), 2.08, 2.07 (ds, 6H, -(CO)-CH_3) ppm; **^{13}C-NMR** (101 MHz, $CDCl_3$): δ = 168.9 (C_q, 2C, *C*=O), 157.1 (C_q, 1C), 157.1 (C_q, 1C), 156.8 (C_q, 1C), 145.7 (C_q, 1C), 144.2 (C_q, 1C), 140.3 (C_q, 1C), 139.1 (C_q, 1C), 138.5 (C_q, 1C), 138.4 (C_q, 1C), 127.0 (C_t, 4C), 126.9 (C_t, 2C), 116.9 (C_t, 1C), 114.8 (C_t, 2C), 114.7 (C_t, 2C), 114.6 (C_t, 2C), 112.9 (C_t, 1C), 111.6 (C_t, 1C), 65.1 (C_s, 1C), 63.9 (C_s, 1C), 63.3 (C_s, 1C), 63.3 (C_s, 1C), 63.3 (C_s, 1C), 43.6 (C_s, 1C), 43.6 (C_s, 1C), 43.2 (C_q, 1C), 43.1 (C_q, 1C), 38.6 (C_s, 1C), 35.8 (C_s, 1C), 35.8 (C_s, 1C), 34.8 (C_s, 1C), 34.8 (C_s, 1C), 29.6 (C_s, 1C), 29.4 (C_s, 1C), 21.6 (C_p, 2C, -(CO)-*C*H_3) ppm; **MS** (ESI, positive ion mode, MeCN): m/z = 741 ([M+Na]$^+$); **HRMS** (ESI): m/z calcd for [$C_{44}H_{50}N_2O_7$+H]$^+$: 719.3691; found: 719.3691.

1,1"-Diacteyl-4'-(1-iodo-4-phenoxymethylbenzene)-dispiro[piperidine-4,2'-[7,11,21,25]-tetraoxacyclopenta[24.2.2.2^{3,6}.2^{12,15}.2^{17,20}]hexatriaconta[3,5,12,14,17,19,26,28,29,31,33,35] dodecaene-16,4"-piperidine] (B9): The alcohol **B11** (250 mg, 1.00 equiv., 0.384 mmol), 4-iodobenzylbromide (163 mg, 1.50 equiv., 0.522 mmol) and cesium carbonate (229 mg, 2.00 equiv., 0.696 mmol) were suspended in 14 mL dry DMF under argon atmosphere. The reaction mixture was heated at 85°C for 20 h. Afterwards the solvent was evaporated and the residue taken up with dichloromethane and water. The layers were separated and the aqueous one extracted three times with dichloromethane. The combined organic layers were washed with demin. Water and brine, dried with sodium sulfate, filtered and concentrated. The crude was purified by column chromatography (SiO_2; dichloromethane then dichloromethane, 2.5% MeOH). The desired product **B9** was obtained as a colorless oil (97%).

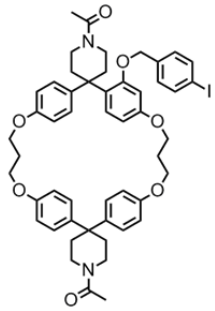

R_f = 0.41 (SiO_2; CH_2Cl_2, 5% MeOH); **^{1}H-NMR** (400 MHz, $CDCl_3$): δ = 7.68 (d, ^3J(H,H) = 8 Hz, 2H, Iodobenzene-H2), 7.20 (d, ^3J(H,H) = 8 Hz, 1H, H34'), 7.12 – 7.06 (m, 4H, Ar-H), 6.92 (d, ^3J(H,H) = 8 Hz, 2H, Ar-H), 6.82 (d, ^3J(H,H) = 8 Hz, 2H, Ar-H), 6.78 – 6.71 (m, 4H, Ar-H), 6.58 (d, ^3J(H,H) = 8 Hz, 2H, Ar-H), 6.42 (dd, ^3J(H,H) = 8.5 Hz, ^4J(H,H) = 2.5 Hz, 1H, H35'), 6.31 (d, ^4J(H,H) = 2.5 Hz, 1H, H5'), 4.54 – 4.43 (s, 2H, iodobenzene-CH_2-O-), 4.13 – 3.99 (m, 8H, Ar-O-CH_2-), 3.68 – 3.53 (m, 4H), 3.51 – 3.37 (m, 4H), 2.54 – 2.24 (m, 8H), 2.22

– 2.10 (m, 4H), 2.06, (s, 3H, -(CO)-CH_3), 2.03 (s, 3H, -(CO)-CH_3) ppm; **^{13}C-NMR** (101 MHz, $CDCl_3$): δ = 168.8 (C_q, 1C, *C*=O), 168.7 (C_q, 1C, *C*=O), 159.0 (C_q, 1C), 157.7 (C_q, 1C), 157.2 (C_q, 1C), 157.0 (C_q, 1C), 156.8 (C_q, 1C), 138.7 (C_q, 1C), 138.1 (C_q, 1C), 137.5 (C_t, 2C), 136.2 (C_q, 1C), 129.9 (C_t, 2C), 128.0 (C_t, 1C), 127.7 (C_q, 1C), 127.0 (C_q, 1C), 126.9 (C_t, 4C), 114.7 (C_t, 2C), 114.6 (C_t, 2C), 114.1 (C_t, 2C), 106.6 (C_t, 1C), 102.1 (C_t, 1C), 93.6 (C_q, 1C, *C*-I), 69.7 (C_s, 1C, iodobenzene-*C*H_2-O-), 64.1 (C_s, 1C), 63.9 (C_s, 1C), 63.6 (C_s, 1C), 63.2 (C_s, 1C), 43.7 (C_s, 1C), 43.5 (C_s, 1C),43.1 (C_q, 1C), 43.0 (C_q, 1C), 38.7 (C_s, 1C), 38.5 (C_s, 1C), 35.8 (C_s, 1C), 35.8 (C_s, 1C), 35.4 (C_s, 1C), 35.2 (C_s, 1C), 29.6 (C_s, 1C), 29.5 (C_s, 1C), 21.5 (C_p, 1C, -(CO)-*C*H_3), 21.4 (C_p, 1C, -(CO)-*C*H_3) ppm; **MS** (ESI, positive ion mode, MeCN): m/z = 957 ([M+Na]$^+$); **HRMS** (ESI): m/z calcd for [$C_{51}H_{55}IN_2O_7$+H]$^+$: 935.3127; found: 935.3127.

1,1”-Diethyl-4’-(1-iodo-4-phenoxymethylbenzene)-dispiro[piperidine-4,2’-[7,11,21,25]-tetraoxacyclopenta[24.2.2.2^{3,6}.2^{12,15}.2^{17,20}]hexatriaconta[3,5,12,14,17,19,26,28,29,31,33,35] dodecaene-16,4”-piperidine] (B8): In an oven-dried Schlenk-tube amide **B9** (150 mg, 1.00 equiv., 0.160 mmol) was dissolved in 35 mL dichloromethane. After cooling to 0°C (ice bath) DIBAL-*H* (3.20 mL (1 M in hexane), 2.50 g, 20 equiv., 3.20 mmol) was added dropwise over a period of 3 h. After stirring for an additional hour at rt the excess of DIBAL-*H* was quenched with 0.5 mL methanol. The solution was mixed with basic celite and filtered. The phases were separated and the aqueous one extracted with dichloromethane. The combined organic layers were washed once with brine, dried with sodium sulfate, filtered and concentrated. The crude was purified by column chromatography (SiO_2; EtOAc, 5% MeOH, 5% NEt_3) to achieve diamine **B8** as a colorless oil (79%).

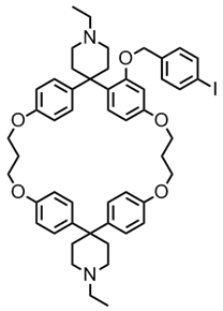

***R*$_f$** = 0.31 (SiO_2; EtOAc, 5% MeOH, 5% NEt_3); **^{1}H-NMR** (400 MHz, $CDCl_3$): δ = 7.67 (d, ^3J(H,H) = 8 Hz, 2H, Iodobenzene-H2), 7.26 (d, ^3J(H,H) = 8 Hz, 2H, H34’), 7.11 – 7.07 (m, 4H, Ar-H), 6.92 (d, ^3J(H,H) = 8 Hz, 2H, Ar-H), 6.81 (d, ^3J(H,H) = 8 Hz, 2H, Ar-H), 6.74 – 6.68 (m, 4H, Ar-H), 6.55 (d, ^3J(H,H) = 8 Hz, 2H, Ar-H), 6.42 (dd, ^3J(H,H) = 8 Hz, ^4J(H,H) = 2.5 Hz, 1H, H35’), 6.29 (d, ^4J(H,H) = 2.5 Hz, 1H, H5’), 4.44 (s, 2H, iodobenzene-CH_2-O-), 4.07 (t, ^3J(H,H) = 5 Hz, 4H, Ar-O-CH_2-), 4.03 (t, ^3J(H,H) = 5 Hz, 4H, Ar-O-CH_2-), 2.65 – 2.35 (m, 16H), 2.32 (quart, ^3J(H,H) = 7 Hz, 4H, -N-CH_2-CH_3), 2.17 – 2.10 (m, 4H, -CH_2-CH_2-CH_2-), 1.04 (t, ^3J(H,H) = 7 Hz, 3H, -CH_2-CH_3), 1.03 (t, ^3J(H,H) = 7 Hz, 3H, -CH_2-CH_3) ppm; **^{13}C-NMR** (101 MHz, $CDCl_3$): δ = 158.7 (C_q, 1C), 157.8 (C_q, 1C), 156.8 (C_q, 1C), 156.7 (C_q, 1C), 156.5 (C_q, 1C), 137.4 (C_t, 4C), 136.5 (C_t, 1C), 129.9 (C_t, 4C), 128.3

(C_q, 1C), 128.2 (C_q, 1C), 127.2 (C_q, 1C), 127.2 (C_q, 1C), 126.9 (C_q, 1C), 114.4 (C_t, 4C), 114.4 (C_t, 4C), 113.9 (C_t, 4C), 106.5 (C_t, 1C), 102.0 (C_t, 1C), 93.4 (C_q, 1C, *C*-I), 70.4 (C_s, 1C, iodobenzene-*C*H_2-O-), 69.7 (C_s, 1C, benzyl), 64.0 (C_s, 1C), 63.9 (C_s, 1C), 63.5 (C_s, 1C), 63.1 (C_s, 1C), 52.4 (C_s, 2C), 50.3 (C_s, 1C), 50.0 (C_s, 2C), 42.8 (C_s, 2C), 42.7 (C_q, 1C), 42.7 (C_q, 1C), 35.3 (C_s, 2C), 29.6 (C_s, 1C), 29.5 (C_s, 1C), 12.1 (Cp, 1C, -CH_2-*C*H_3), 12.0 (Cp, 1C, -CH_2-*C*H_3) ppm; **MS** (EI +, 70 eV): m/z (%) = 906 (15, [M^+]), 691 (42), 690 (94, [M^+-C_7H_6I]), 689 (23), 662 (24), 661 (17), 607 (14), 606 (36), 604 (12), 202 (12), 85 (48), 84 (100); **HRMS** (ESI): m/z calcd for [$C_{51}H_{59}IN_2O_5$+H]$^+$: 907.3541; found: 907.3541.

***S*-(4-Iodophenyl) ethanethioate:**[83] To a suspension of zinc powder (741 mg, 3.53 equiv., 11.3 mmol) and dichlorodimethylsilane (1.34 mL, 1.42 g, 3.42 equiv., 11.0 mmol) in 4 mL 1,2-dichloroethane was added pipsyl chloride (1.00 g, 1.00 equiv., 3.21 mmol) in one lot. Then the suspension was diluted with additional 4 mL dichloroethane and finally *N*,*N*-dimethylacetamide (0.88 mL, 825 g, 2.95 equiv., 9.47 mmol) was added. The reaction mixture was heated for 2 h at 75°C until the zinc completely vanished. Then the mixture was cooled to 50°C and AcCl (0.29 mL; 320 mg, 1.27 equiv., 4.08 mmol) was added. After 15 min at 50°C the reaction mixture was poured into water and extracted three times with dichloromethane. The combined organic layers were dried with sodium sulfate, filtered and concentrated. The crude was purified by flash column chromatography (SiO_2; cyclohexane:CH_2Cl_2 4:1). The product was obtained as a colorless liquid (91%).

***R*$_f$** = 0.38 (SiO_2; CH_2Cl_2:cyclohexane 1:4); **^{1}H-NMR** (400 MHz, $CDCl_3$): δ = 7.74 (d, ^3J(H,H) = 8.4 Hz, 2H, H3), 7.13 (d, ^3J(H,H) = 8.4 Hz, 2H, H2), 2.42 (s, 3H, SCOCH_3) ppm; **^{13}C-NMR** (101 MHz, $CDCl_3$): δ = 193.3 (C_q, 1C, S*C*OCH$_3$), 138.5 (C_t, 2C, C3), 136.1 (C_t, 2C, C2), 127.9 (C_q, 1C, C1), 96.1 (C_q, 1C, C4), 30.4 (C_p, 1C, -S(CO)*C*H$_3$), ppm. The analytic data were according to literature.[83]

***S*-(4-((4-((Trimethylsilyl)ethynyl)phenyl)ethynyl)phenyl) ethanethioate (B28):** The palladium catalyst $Pd(PPh_3)_2Cl_2$ (57.8 mg, 3 mol%, 82.2 µmol) and CuI (15.7 mg, 3 mol%, 82.2 µmol) were put into an oven-dried 25 mL Schlenk-tube. A solution of the aryl iodide (762 mg, 1.00 equiv., 2.74 mmol) in 4.5 mL THF and a solution of acetylene **A27** (652 mg, 1.20 equiv., 3.29 mmol) in 4.5 mL THF were added and the mixture was degased for 10 min (argon). Afterwards diisopropylamine (1.36 mL, 970 mg, 3.50 equiv., 9.59 mmol) was added and the reaction

mixture was stirred at rt for 4 h. After removing the solvent the crude was taken up in demin. water and dichloromethane. The phases were separated and the aqueous one extracted twice with dichloromethane. The combined organic layers were washed with brine, dried with sodium sulfate, filtered and concentrated. The crude was further purified by column chromatography (SiO_2; CH_2Cl_2:cyclohexane 1:3).

$\boldsymbol{R_f}$ = 0.15 (SiO_2; CH_2Cl_2:cyclohexane 1:3); **^{1}H-NMR** (400 MHz, $CDCl_3$): δ = 7.54 (d, ^3J(H,H) = 8.4 Hz, 2H), 7.48 – 7.42 (m, 4H), 7.40 (d, ^3J(H,H) = 8.4 Hz, 2H), 2.44 (s, 3H, $SCOCH_3$), 0.26 (s, 9H, Si-$(CH_3)_3$) ppm; **^{13}C-NMR** (101 MHz, $CDCl_3$): δ = 193.5 (C_q, 1C, S*C*OCH_3), 134.4 (C_t, 2C), 132.3 (C_t, 2C), 132.1 (C_t, 2C), 131.6 (C_t, 1C), 128.5 (C_q, 1C), 124.4 (C_q, 1C), 123.4 (C_q, 1C), 123.1 (C_q, 1C), 104.7 (C_q, 1C), 96.6 (C_q, 1C), 90.8 (C_q, 1C), 90.6 (C_q, 1C), 30.4 (C_p, 1C, SCO*C*H_3), 0.1 (C_p, 3C, Si-(*C*$H_3)_3$) ppm. The analytic data were according to literature.[84]

***S*-(4-((4-Ethynylphenyl)ethynyl)phenyl) ethanethioate (B6):** The TMS-protected OPE **B28**

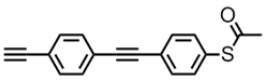

(715 mg, 1.00 equiv., 2.05 mmol) was dissolved in 11 mL THF in an oven-dried Schlenk-tube under argon atmosphere. Then acetic anhydride (0.385 mL, 419 mg, 2.00 equiv., 4.10 mmol), acetic acid (0.235 mL; 246 mg, 2.00 equiv., 4.10 mmol) and TBAF (2.48 mL, 2.18 g, 1.21 equiv., 2.48 mmol) were added and the reaction mixture was stirred for 1 h at rt. The mixture was poured into demin. water and extracted with dichloromethane (3 times). The combined organic layers were washed once with brine, dried with sodium sulfate, filtered and concentrated. The crude was taken up in a mixture of cyclohexane:*t*BME 10:1 and the insoluble orange oil was filtered off. The *t*BME was removed by evaporation and the remaining filtrate kept in the fridge for 3 h. The precipitate was filtered off and washed with cold cyclohexane (77%).

$\boldsymbol{R_f}$ = 0.44 (SiO_2; cyclohexane, 10% *t*BME); **^{1}H-NMR** (250 MHz, $CDCl_3$): δ = 7.56 (d, ^3J(H,H) = 8.3 Hz, 2H), 7.51 – 7.45 (m, 4H), 7.41 (d, ^3J(H,H) = 8.3 Hz, 2H), 3.19 (s, 1H, C≡C-*H*), 2.44 (s, 3H, SCOC*H*$_3$) ppm; **^{13}C-NMR** (101 MHz, $CDCl_3$): δ = 193.5 (C_q, 1C, S*C*OCH_3), 134.4 (C_t, 2C), 132.3 (C_t, 2C), 132.2 (C_t, 2C), 131.7 (C_t, 1C), 128.5 (C_q, 1C), 124.4 (C_q, 1C), 123.5 (C_q, 1C), 122.3 (C_q, 1C), 90.7 (C_q, 1C), 90.6 (C_q, 1C), 83.3 (C_q, 1C), 79.2 (C_t, 1C, -C≡*C*-H), 30.4 (C_p, 1C, SCO*C*H_3) ppm. The analytic data were according to literature.[84]

1,1,1"1"-Tetraethyl-4'-[1-(phenoxymethyl)-4-((4-(phenylethynyl)phenyl)ethynyl)benzene]-dispiro[piperidine-4,2'-[7,11,21,25]-tetraoxacyclopenta[24.2.2.2^{3,6}.2^{12,15}.2^{17,20}]hexatriaconta[3,5,12,14,17,19,26,28,29,31,33,35]dodecaene-16,4"-piperidine] (B1b): Bis(dibenzylideneacetone)palladium (4.85 mg, 10 mol%, 8.43 µmol), triphenylphosphine (16.6 mg, 0.75 equiv., 63.2 µmol) and CuI (3.21 mg, 20 mol%, 16.9 µmol) were placed in a preheated 50 mL Schlenk-tube. The tube was evacuated and backfilled with argon once. Then a solution of cyclophane **B8** (76.5 mg, 1.00 equiv., 84.3 µmol) in 2 mL THF (crown-cap) and 2 mL diisopropylamine was added. The resulting suspension was degased with argon for 10 min. Afterwards the OPE **B6** (41.9 mg, 1.80 equiv., 152 µmol) was added in one lot and the resulting reaction mixture was stirred at rt for 4.5 h. The solvent and the base were removed and the residue taken up in dichloromethane and water. The two phases were separated and the aqueous one extracted twice with dichloromethane. The combined organic layers were washed with brine, dried with sodium sulfate, filtered and concentrated. The crude was purified by column chromatography (SiO_2; dichloromethane, 5% MeOH, 1% NEt_3). The obtained brown oil was taken up in MeOH and the solid was filtered off and rinsed with plenty of methanol. The filtrate was concentrated to obtain the desired product **B2b** as a pale yellow solid.

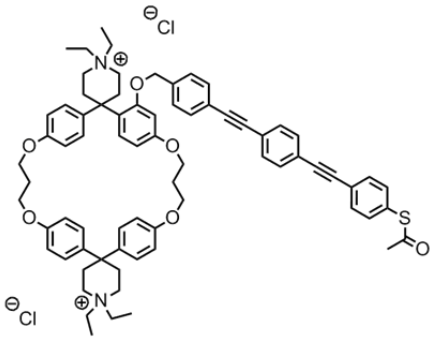

For ethylation the diamine **B2b** (46.0 mg, 1.00 equiv., 43.6 µmol) was dissolved in 2 mL dichloromethane. Then freshly distilled 2-iodoethane (2.00 mL, 3.90 g, 562 equiv., 24.5 mmol) was added and the reaction mixture was stirred at rt under exclusion of light for 3 d. Then again 2 mL dichloromethane was added and the mixture was stirred for another 5 d. The solvent was removed and the crude was purified by column chromatography (SiO_2; acetone:1 M NH_4Cl:acetonitrile 14:2:1). After pooling of the desired fractions the solvent was removed and the obtained solid was extracted by Soxhlet extraction with dichloromethane for 24 h. The solvent was evaporated and the residue was subjected to an ion exchange column (DOWEX 1X8, 200-400 mesh, Cl^-, packed with water, washed with the eluent) eluting with MeCN:H_2O 1:1. The product **B1b** was obtained in traces (> 0.2 mg).

B2b: $\boldsymbol{R_f}$ = 0.56 (SiO_2; CH_2Cl_2, 5% MeOH, 1% NEt_3); **^{1}H-NMR** (400 MHz, $CDCl_3$): δ = 7.59 – 7.45 (m, 9H, Ar-H), 7.29 (d, ^3J(H,H) = 8.8 Hz, 2H, Ar-H), 7.11 – 7.01 (m, 6H, Ar-H), 6.92 (d, ^3J(H,H) = 8.8 Hz, 2H, Ar-H), 6.76 (d, ^3J(H,H) = 8.8 Hz, 2H, Ar-H), 6.72 – 6.65 (m, 2H,

Ar-H), 6.60 (d, ^3J(H,H) = 8.8 Hz, 2H, Ar-H), 6.40 (d (broad), ^3J(H,H) = 8.4 Hz, 1H, Ar-H), 6.29 (s (broad), 1H, Ar-H), 4.63 (s (broad), 2H, Ar-CH_2-O-Ar), 4.11 – 3.97 (m, 8H, Ar-O-CH_2-), 3.15 – 2.45 (m, 22H), 2.22 – 2.10 (m, 5H), 1.33 – 1.23 (m, 6H, -CH_2-CH_3) ppm; **MS** (ESI, positive ion mode, MeCN): m/z = 1055 ([M+H]$^+$), 639.

B1b: R_f = 0.24 (SiO_2; acetone:1 M NH_4Cl:acetonitrile 14:2:1); **MS** (ESI, positive ion mode, MeCN): m/z = 557 ([M-2Cl$^-$]$^{2+}$), 550 ([M-Me-2Cl$^-$]$^{2+}$), 543 ([M-Et-2Cl$^-$]$^{2+}$).

1,1,1"1"-Tetraethyl-5'-[1-(phenoxymethyl)-4-((4-(phenylethynyl)phenyl)ethynyl)-benzene]-dispiro[piperidine-4,2'-[7,11,21,25]-tetraoxacyclopenta[24.2.2.2^{3,6}.2^{12,15}.2^{17,20}]-hexatriaconta[3,5,12,14,17,19,26,28,29,31,33,35]dodecaene-16,4"-piperidine] (B1a): By

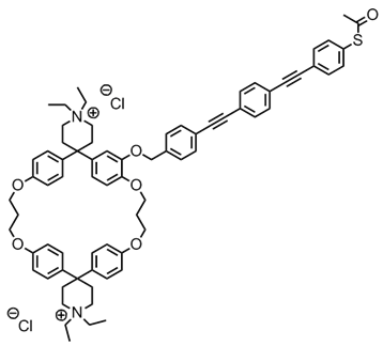

applying the same Sonogashira cross-coupling protocol as described for **B2b** using cyclophane **A8** (167 mg, 1.00 equiv., 184 mmol), diamine **B2a** was obtained as a pale yellow solid which was immediately ethylated using 2-iodoethane (2 mL). The mixture was stirred in the dark for 5 d. Then the formed solid was filtered off and the filtrate was concentrated. The crude was purified by column chromatography (SiO_2; acetone:1 M NH_4Cl:acetonitrile 14:2:1). The white solid was extracted with dichloromethane (Soxhlet, 18 h). After evaporation, the obtained pale yellow solid was subjected to ion-exchange chromatography (DOWEX 1X8, 200-400 mesh, Cl^-). The column was packed with water and the product dissolved in MeOH, the column was performed with a 7:2 mixture of acetonitrile/water. The obtained oil was solidified by treatment with THF. The pale yellow product was again purified by prep. TLC (SiO_2; acetone:1 M NH_4Cl:acetonitrile 14:2:1). Finally the product was further purified by recrystallization (MeOH:Et_2O 1:1).

B2a: R_f = 0.61 (SiO_2; CH_2Cl_2, 5% MeOH, 1% NEt_3); **^{1}H-NMR** (400 MHz, $CDCl_3$): δ = 7.60 – 7.49 (m, 5H, Ar-H), 7.48 – 7.38 (m, 4H, Ar-H), 7.15 – 7.05 (m, 6H, Ar-H), 6.90 (d, ^3J(H,H) = 8.5 Hz, 2H, Ar-H), 6.78 – 6.61 (m, 9H, Ar-H), 6.46 (s (broad), 1H, Ar-H), 4.85 (s (broad), 2H, Ar-CH_2-O-Ar), 4.12 – 3.97 (m, 8H, Ar-O-CH_2-), 2.65 – 2.29 (m, 22H), 2.23 – 2.14 (m, 5H), 1.09 – 1.02 (m, 6H, -CH_2-CH_3) ppm; **MS** (ESI, positive ion mode, MeCN): m/z = 1057 ([M+H]$^+$).

B1a: R_f = 0.26 (SiO_2; acetone:1 M NH_4Cl:acetonitrile 14:2:1); **^{1}H-NMR** (400 MHz, methanol-d4): δ = 7.64 – 7.52 (m, 5H, Ar-H), 7.45 (d, ^3J(H,H) = 8.4 Hz, 2H, Ar-H), 7.35 (d, ^3J(H,H) = 8.0 Hz, 2H, Ar-H), 7.23 – 7.12 (m, 4H, Ar-H), 7.03 – 6.94 (m, 4H, Ar-H), 6.93 –

6.83 (m, 4H, Ar-H), 6.83 – 6.72 (m, 4H, Ar-H), 6.28 (s, 2H, Ar-H), 4.60 (s, 2H, Ar-CH_2-O-Ar), 4.22 – 4.05 (m, 8H, Ar-O-CH_2-), 3.45 – 3.15 (m, 14H), 3.09 – 2.98 (m, 4H), 2.86 – 2.45 (m, 8H), 2.25 – 2.06 (m, 5H), 1.39 – 1.15 (m, 12H, -CH_2-CH_3) ppm; **MS** (ESI, positive ion mode, MeCN): m/z = 557 ($[M\text{-}2Cl^-]^{2+}$), 550 ($[M\text{-}Me\text{-}2Cl^-]^{2+}$), 543 ($[M\text{-}Et\text{-}2Cl^-]^{2+}$).

Literature

[1] „2nd Gen Intel® Core™ Processor, LGA1155 Socket: Thermal Guide“, can be found under http://www.intel.com/content/www/de/de/processors/core/2nd-gen-core-lga1155-socket-guide.html.

[2] G. Maruccio, R. Cingolani, R. Rinaldi, *J. Mater. Chem.* **2004**, *14*, 542.

[3] J. R. Heath, M. A. Ratner, *Physics Today* **2003**, *56*, 43.

[4] A. Aviram, M. A. Ratner, *Chem. Phys. Lett.* **1974**, *29*, 277–283.

[5] M. P. Cava, M. V. Lakshmikantham, R. Hoffmann, R. M. Williams, *Tetrahedron* **2011**, *67*, 6771–6797.

[6] M. A. Reed, T. Lee, *Molecular Nanoelectronics*, American Scientific Publishers, **2003**.

[7] R. L. Carroll, C. B. Gorman, *Angew. Chem. Int. Ed.* **2002**, *41*, 4378–4400.

[8] D. K. James, J. M. Tour, in *Molecular Wires and Electronics*, Springer Berlin Heidelberg, Berlin, Heidelberg, **2005**, S. 33–62.

[9] F. Chen, N. J. Tao, *Acc. Chem. Res.* **2009**, *42*, 429–438.

[10] A. Erbe, S. Verleger, *Acta Phys. Polon. A* **2009**, *115*, 455–61.

[11] J. Chen, M. A. Reed, A. M. Rawlett, J. M. Tour, *Science* **1999**, *286*, 1550–1552.

[12] H. Park, A. K. L. Lim, A. P. Alivisatos, J. Park, P. L. McEuen, *Appl. Phys. Lett.* **1999**, *75*, 301–303.

[13] R. E. Holmlin, R. Haag, M. L. Chabinyc, R. F. Ismagilov, A. E. Cohen, A. Terfort, M. A. Rampi, G. M. Whitesides, *J. Am. Chem.Soc.* **2001**, *123*, 5075–5085.

[14] *J. Mater. Res.* **2004**, *19*, 1889–1916.

[15] J. G. Kushmerick, A. S. Blum, D. P. Long, *Anal. Chim. Acta* **2006**, *568*, 20–27.

[16] L. Bernard, Y. Kamdzhilov, M. Calame, S. J. van der Molen, J. Liao, C. Schönenberger, *J. Phys. Chem. C* **2007**, *111*, 18445–18450.

[17] Q. Shen, X. Guo, M. L. Steigerwald, C. Nuckolls, *Chem.-Asian J.* **2010**, *5*, 1040–1057.

[18] L. Grüter, M. T. González, R. Huber, M. Calame, C. Schönenberger, *Small* **2005**, *1*,

1067–1070.

[19] R. H. M. Smit, Y. Noat, C. Untiedt, N. D. Lang, M. C. van Hemert, J. M. van Ruitenbeek, *Nature* **2002**, *419*, 906–909.

[20] B. Xu, N. J. Tao, *Science* **2003**, *301*, 1221–1223.

[21] H. Song, M. A. Reed, T. Lee, *Adv. Mater.* **2011**, *23*, 1583–1608.

[22] S. Nakashima, Y. Takahashi, M. Kiguchi, *Beilstein J. Nanotechnol.* **2011**, *2*, 755–759.

[23] S. Jan van der Molen, P. Liljeroth, *Journal of Physics: Condensed Matter* **2010**, *22*, 133001.

[24] G. Gustafsson, Y. Cao, G. M. Treacy, F. Klavetter, N. Colaneri, A. J. Heeger, *Nature* **1992**, *357*, 477–479.

[25] H. Sirringhaus, N. Tessler, R. H. Friend, *Science* **1998**, *280*, 1741–1744.

[26] M. Granstrom, K. Petritsch, A. C. Arias, A. Lux, M. R. Andersson, R. H. Friend, *Nature* **1998**, *395*, 257–260.

[27] S. W. Thomas, G. D. Joly, T. M. Swager, *Chem. Rev.* **2007**, *107*, 1339–1386.

[28] M. J. Frampton, H. L. Anderson, *Angew. Chem. Int. Ed.* **2007**, *46*, 1028–1064.

[29] A. P. H. J. Schenning, E. W. Meijer, *Chem. Commun.* **2005**, 3245.

[30] F. J. M. Hoeben, P. Jonkheijm, E. W. Meijer, A. P. H. J. Schenning, *Chem. Rev.* **2005**, *105*, 1491–1546.

[31] F. Huang, H. W. Gibson, *Prog. Polym. Sci.* **2005**, *30*, 982–1018.

[32] J. J. Michels, M. J. O'Connell, P. N. Taylor, J. S. Wilson, F. Cacialli, H. L. Anderson, *Chem. Eur. J.* **2003**, *9*, 6167–6176.

[33] D. J. Cardin, *Adv. Mater.* **2002**, *14*, 553–563.

[34] R. J. O. M. Hoofman, M. P. de Haas, L. D. A. Siebbeles, J. M. Warman, *Nature* **1998**, *392*, 54–56.

[35] N. Fuentes, A. Martín-Lasanta, L. Á. de Cienfuegos, M. Ribagorda, A. Parra, J. M. Cuerva, *Nanoscale* **2011**, *3*, 4003–4014.

[36] G. Pace, V. Ferri, C. Grave, M. Elbing, C. von Hänisch, M. Zharnikov, M. Mayor, M. A. Rampi, P. Samorì, *PNAS* **2007**, *104*, 9937–9942.

[37] P. Ahonen, T. Laaksonen, D. J. Schiffrin, K. Kontturi, *Phys. Chem. Chem. Phys.* **2007**, *9*, 4898–4901.

[38] M. Irie, *Chem. Rev.* **2000**, *100*, 1685–1716.

[39] D. Dulić, S. J. van der Molen, T. Kudernac, H. T. Jonkman, J. J. D. de Jong, T. N. Bowden, J. van Esch, B. L. Feringa, B. J. van Wees, *Phys. Rev. Lett.* **2003**, *91*,

207402.

[40] V. Ferri, M. Elbing, G. Pace, M. D. Dickey, M. Zharnikov, P. Samorì, M. Mayor, M. A. Rampi, *Angew. Chem. Int. Ed.* **2008**, *47*, 3407–3409.

[41] W. Haiss, H. van Zalinge, S. J. Higgins, D. Bethell, H. Höbenreich, D. J. Schiffrin, R. J. Nichols, *J. Am. Chem. Soc.* **2003**, *125*, 15294–15295.

[42] E. H. van Dijk, D. J. T. Myles, M. H. van der Veen, J. C. Hummelen, *Org. Lett.* **2006**, *8*, 2333–2336.

[43] S. Tsoi, I. Griva, S. A. Trammell, A. S. Blum, J. M. Schnur, N. Lebedev, *ACS nano* **2008**, *2*, 1289–1295.

[44] A. R. Pease, J. O. Jeppesen, J. F. Stoddart, Y. Luo, C. P. Collier, J. R. Heath, *Acc. Chem. Res.* **2001**, *34*, 433–444.

[45] J. O. Jeppesen, K. A. Nielsen, J. Perkins, S. A. Vignon, A. Di Fabio, R. Ballardini, M. T. Gandolfi, M. Venturi, V. Balzani, J. Becher, u. a., *Chem. Eur. J.* **2003**, *9*, 2982–3007.

[46] Y. Luo, C. P. Collier, J. O. Jeppesen, K. A. Nielsen, E. DeIonno, G. Ho, J. Perkins, H. Tseng, T. Yamamoto, J. F. Stoddart, u. a., *Chem. Phys. Chem.* **2002**, *3*, 519–525.

[47] N. Weibel, S. Grunder, M. Mayor, *Org. Biomol. Chem.* **2007**, *5*, 2343–2353.

[48] M. Pomerantz, A. Aviram, R. A. Mccorkle, L. Li, A. G. Schrott, *Science* **1992**, *255*, 1115–1118.

[49] R. M. Metzger, B. Chen, U. Höpfner, M. V. Lakshmikantham, D. Vuillaume, T. Kawai, X. Wu, H. Tachibana, T. V. Hughes, H. Sakurai, u. a., *J. Am. Chem.Soc.* **1997**, *119*, 10455–10466.

[50] M. Elbing, R. Ochs, M. Koentopp, M. Fischer, C. von Hänisch, F. Weigend, F. Evers, H. B. Weber, M. Mayor, *PNAS* **2005**, *102*, 8815–8820.

[51] S. J. Tans, A. R. M. Verschueren, C. Dekker, *Nature* **1998**, *393*, 49–52.

[52] T. Sato, H. Ahmed, D. Brown, B. F. G. Johnson, *J. Appl. Phys.* **1997**, *82*, 696–701.

[53] Y. Wada, *Pure Appl. Chem.* **1999**, *71*, 2055.

[54] C. P. Collier, G. Mattersteig, E. W. Wong, Y. Luo, K. Beverly, J. Sampaio, F. M. Raymo, J. F. Stoddart, J. R. Heath, *Science* **2000**, *289*, 1172–1175.

[55] A. Aviram, *J. Am. Chem. Soc.* **1988**, *110*, 5687–5692.

[56] M. J. Crossley, P. L. Burn, *J. Chem. Soc., Chem. Commun.* **1991**, 1569–1571.

[57] D. L. Pearson, J. M. Tour, *J. Org. Chem.* **1997**, *62*, 1376–1387.

[58] M. T. Cygan, T. D. Dunbar, J. J. Arnold, L. A. Bumm, N. F. Shedlock, T. P. Burgin, L. Jones, D. L. Allara, J. M. Tour, P. S. Weiss, *J. Am. Chem. Soc.* **1998**, *120*, 2721–2732.

[59] L. A. Bumm, J. J. Arnold, M. T. Cygan, T. D. Dunbar, T. P. Burgin, L. Jones, D. L. Allara, J. M. Tour, P. S. Weiss, *Science* **1996**, *271*, 1705–1707.

[60] K. Slowinski, R. V. Chamberlain, C. J. Miller, M. Majda, *J. Am. Chem. Soc.* **1997**, *119*, 11910–11919.

[61] J. S. Meisner, M. Kamenetska, M. Krikorian, M. L. Steigerwald, L. Venkataraman, C. Nuckolls, *Nano Lett.* **2011**.

[62] T. Rueckes, K. Kim, E. Joselevich, G. Y. Tseng, C.-L. Cheung, C. M. Lieber, *Science* **2000**, *289*, 94–97.

[63] Y.-K. Kwon, D. Tománek, S. Iijima, *Phys. Rev. Lett.* **1999**, *82*, 1470–1473.

[64] G. Binnig, M. Despont, U. Drechsler, W. Häberle, M. Lutwyche, P. Vettiger, H. J. Mamin, B. W. Chui, T. W. Kenny, *Appl. Phys. Lett.* **1999**, *74*, 1329–1331.

[65] K. Roth, *J. Vac. Sci. Technol. B* **2000**, *18*, 2359.

[66] A. Tsuda, *Science* **2001**, *293*, 79–82.

[67] S. Wu, M. T. González, R. Huber, S. Grunder, M. Mayor, C. Schönenberger, M. Calame, *Nature Nanotechnol.* **2008**, *3*, 569–574.

[68] L.-L. Lin, J.-C. Leng, X.-N. Song, Z.-L. Li, Y. Luo, C.-K. Wang, *J. Phys. Chem. C* **2009**, *113*, 14474–14477.

[69] L. L. Lin, X. N. Song, Y. Luo, C. K. Wang, *J. Phys. Condens. Matter* **2010**, *22*, 325102.

[70] S. Martín, I. Grace, M. R. Bryce, C. Wang, R. Jitchati, A. S. Batsanov, S. J. Higgins, C. J. Lambert, R. J. Nichols, *J. Am. Chem. Soc.* **2010**, *132*, 9157–9164.

[71] D. S. Seferos, S. A. Trammell, G. C. Bazan, J. G. Kushmerick, *PNAS* **2005**, *102*, 8821.

[72] S. T. Schneebeli, M. Kamenetska, Z. Cheng, R. Skouta, R. A. Friesner, L. Venkataraman, R. Breslow, *J. Am. Chem. Soc.* **2011**.

[73] M. Kiguchi, T. Takahashi, Y. Takahashi, Y. Yamauchi, T. Murase, M. Fujita, T. Tada, S. Watanabe, *Angew. Chem. Int. Ed.* **2011**, *50*, 5708–5711.

[74] P. Mattei, F. Diederich, *Helv. Chim. Acta* **1997**, *80*, 1555–1588.

[75] T. Marti, B. R. Peterson, A. Fürer, T. Mordasini-Denti, J. Zarske, B. Jaun, F. Diederich, V. Gramlich, *Helv. Chim. Acta* **1998**, *81*, 109–144.

[76] M. Nielsen, K. V. Gothelf, *J. Chem. Soc., Perk. Trans. 1* **2001**, 2440–2444.

[77] K. Onitsuka, M. Fujimoto, H. Kitajima, N. Ohshiro, F. Takei, S. Takahashi, *Chem. Eur. J.* **2004**, *10*, 6433–6446.

[78] S. Percec, R. Getty, W. Marshall, G. Skidd, R. French, *J. Polym. Sci A;* **2004**, *42*, 541–550.

[79] S. McAlpine, *J. Am. Chem. Soc.* **1998**, *120*, 4269.

[80] X. Huang, Y. Han, Y. Wang, Y. Wang, *J. Phys. Chem. B* **2007**, *111*, 12439–12446.

[81] B. O. Persson, T. Drakenberg, B. Lindman, *J. Phys. Chem.* **1976**, *80*, 2124–2125.

[82] T. W. Davey, W. A. Ducker, A. R. Hayman, *Langmuir* **2000**, *16*, 2430–2435.

[83] M. Delalande, S. Clavaguera, M. Toure, A. Carella, S. Lenfant, D. Deresmes, D. Vuillaume, J.-P. Simonato, *Chem. Commun.*, *47*, 6048–6050.

[84] A. K. Flatt, Y. Yao, F. Maya, J. M. Tour, *J. Org. Chem.* **2004**, *69*, 1752–1755.

Part C. From Electronics to Photonics: Nonlinear Optic Materials

Introduction

The increasing need for more powerful and smaller technical devices, which is the major platform for research in molecular electronics, is accompanied with the demand for faster transmission and processing of ever growing data packets. Even though the conventional lithographic methods to produce smaller transistors will some day reach their limits, data transfer, processing and storage will be troublesome before.[1] Therefore the real speed limitation of our communication tools is the interconnection of them. A resort of this problem can be the use of optical interconnects which are able to transfer digital data more than 1000 times faster than conventional metal wires. In these so called photonic devices photons are used instead of electrons to acquire, store, process and transmit information.[2] Photons (light quantum) have a much faster mobility than electrons (10^8 m/s compared to 10^5 m/s) and are not susceptible to electrical and magnetic interference. Furthermore photons possess no mass or charge and can therefore be transferred without influencing each other. Additionally photonic circuits are fully compatible with existing fiber optic networks. The major disadvantage is however, that until now optical cables are also 1000 times larger than their electronic counterparts preventing an efficient combination of both.[3] Especially carrying the digital information within the microprocessor from one end to the other will be laborious because of this size mismatch. An ideal solution can be the use of circuits with nanoscale features that carry optical signals and electric currents. Surface plasmons – electromagnetic waves that propagate along the surface of conductors – are ideal candidates for this purpose.[4] Despite these outlined disadvantages, photonic communication is used to transfer data at high rates and over long distances creating higher bandwidths for internet traffic.[5] To be able to do so rapid optical switching, electro-optic modulation, data transfer without loss and a high light stability are important. The maybe most promising materials for this purpose are nonlinear optic materials because of their ultra-fast optical response which potentially allows switching and modulation of electric signals into optic signals at the speed of light.[2]

Nonlinear Optics (NLO)

Optics describes the phenomena and characteristics of light. The interactions of light with matter are particular interesting for new applications in material science and are therefore an

everlasting topic in research. The blue sky, rainbows and shadows are phenomena resulting from interactions of matter with light of weak field intensities of about 600 V/m (e.g. sunlight). Tailor made devices like lenses, concentrating reflectors and mirrors are the outcome of investigations in linear optics.[6] Light can be described as an oscillating electromagnetic field. If this propagating wave interacts with matter a charge displacement is caused within the molecules of the material which results in induced dipoles.[7] By applying weak light intensities this polarization (P) is proportional to the applied field intensity (E),

$$P = \alpha E \qquad \text{or} \qquad P = \chi E \tag{1}$$

where α is the proportionality factor for microscopic objects and χ the proportionality factor for macroscopic objects, also called electric susceptibility.[8] Two fundamental principles result from these relations: the superposition principle – two propagating waves do not interfere with each other and superimpose without disturbing each other – and the frequency of the wave is maintained by the interaction of light with matter. Thus the displacement of an electron in a molecule is proportional to the applied force, causing the potential energy of the electron to be of parabolic nature. This is only valid for small values of the potential energy. If light with strong field intensities interacts with the polarizable matter (e.g. laser light; $> 10^6$ V/m) a distortion of the interatomic forces ($10^7 - 10^{10}$ V/m) takes place and causes a change in the potential energy of the electrons (Morse potential) (figure 1). Therefore the rules of linear optics are no longer valid and the now nonlinear polarization can be described by a Taylor-series.[9]

$$P = P_0 + \alpha E + \beta E^2 + \gamma E^3 + \ldots \tag{2}$$

P_0 is the molecular static polarization resulting from permanent dipoles of the molecule, α is the linear polarization and the coefficients β and γ are the first and second hyperpolarizability, respectively. The values of β and γ are compared to the linear polarizability about 10 to 17 dimensions smaller and therefore only relevant above applied field strengths of 10^3 to 10^4 V/m.[7] Thus there was hardly any application of this effect prior to the availability of strong electromagnetic fields by the invention of the Laser in 1960.[10] With the ability to produce electromagnetic fields of sufficient strength, the non-linear optical effect of second harmonic generation (SHG) was observed in quartz in 1961.[11]

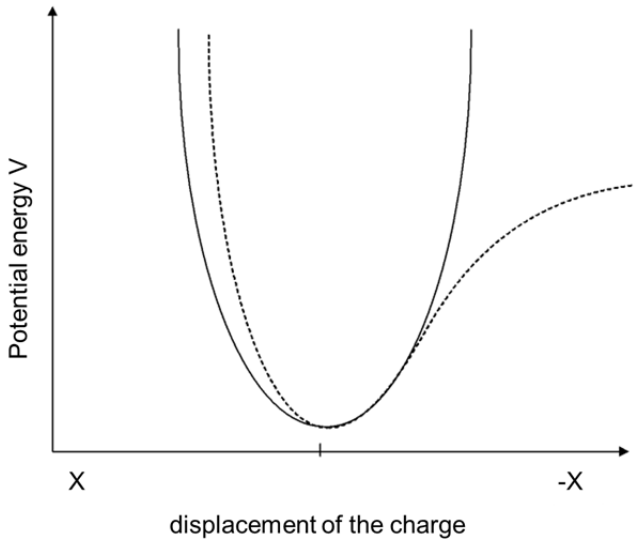

Figure 1. Potential energy of electrons influenced by light of weak intensities (straight line) and Morse potential of electrons influenced by light of strong intensities (dotted line).

In molecules featuring an inversion center (centrosymmetric molecules) the displacement of the charge is of symmetrical nature and therefore the polarization at positive field intensities equals the negative polarization at negative field intensities (P(+E) = -P(-E)) (figure 2).[7,8] This is only possible if the even terms of equation (2) are equal to zero. Thus the first nonlinear contribution to the polarization is the second order hyperpolarizability γ. In turn contributions of even order nonlinear effects can only be observed in molecules without a center of inversion (noncentrosymmetric) (figure 2). The same holds true for an assembly of molecules. While on a molecular level structures can be easily designed in a noncentrosymmetric fashion (e.g. benzene with two different substituents in 1 and 4 position), by transformation to the macroscopic scale this molecular property has to be preserved.[12] Therefore noncentrosymmetric crystals have to be grown which is laborious. A strategy to overcome this problem, which is crucial for the use of nonlinear optic materials in applications, densely packed self-assembled monolayers (e.g. Langmuir-Blodgett-films) can be an ideal solution.[13,14] Furthermore poled polymer films were produced to achieve the transformation of molecular nonlinearity to the macroscopic scale.[15] There, molecular dipoles were imbedded into a polymer by mixing the polymer with the NLO material and melting them. In the solution phase an external electric field was applied to orient the dipoles in a noncentrosymmetric fashion. The solution was then cooled while the external electric field was still applied preserving the orientation of the dipoles in the solid state yielding NLO active polymers.

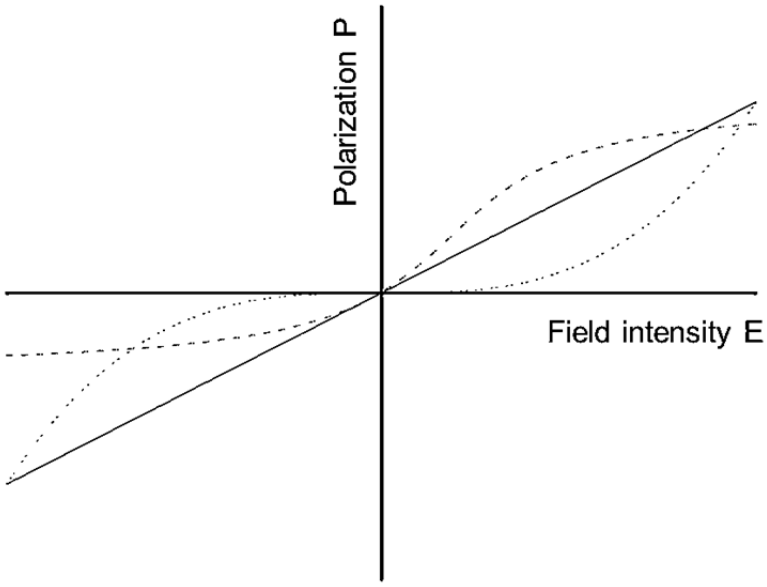

Figure 2. Polarization of different types of molecules in relation to the field intensity E. *straight line*: linear polarization, *dotted line*: nonlinear polarization of a centrosymmetric molecule, *dash-dotted line*: nonlinear polarization of a noncentrosymmetric molecule.[7]

In a noncentrosymmetric molecule an asymmetric polarization response to a symmetric electric field is exhibited. Thus the harmonic components of the polarization will produce a photonic electric field of harmonic frequencies (E(2ω)). What results is frequency doubling, known as the second harmonic generation (SHG), which means the conversion of coherent light of the frequency ω into light with the frequency 2ω and optical rectification in the direction of the frequency doubling (figure 3).[7] Furthermore the superposition principle is no longer valid. The phenomenological outcome is a superimposed light wave of a constant light, a basic wave and a wave with doubled frequency (figure 4).[16]

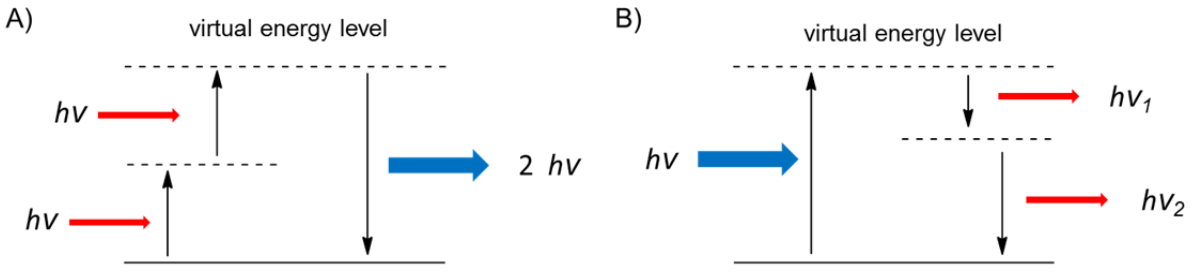

Figure 3. Schematic representation of A) second harmonic generation (SHG) and B) sum frequency generation.

Apart from SHG three other second order effects were found experimentally,[8] the linear electro-optic effect also known as Pockel's effect (1883), sum-frequency generation (figure 3) and optical rectification. The Pockel effect also arises through the second-order response, but the polarization has a contribution of E(0)E(ω) and not of $E^2(\omega)$ like in the SHG. The change

in polarization – induced by the two interacting field components – effectively alters the refractive index of the medium. As a result, the refractive index becomes field dependent.[17] The sum-frequency generation is like the SHG a three-photonic process where one photon with energy $h\nu$ is absorbed and two photons with energy $h\nu_1$ and $h\nu_2$ are emitted.[18] Optical rectification is the conversion of an applied electromagnetic field (sinusoidal wave) to an average DC polarization. Therefore the symmetry properties of the nonlinear medium are important. The polarization will not reverse its sign at the same time as the driving field in the presence of a preferred internal direction. This process can lead to significant carrier acceleration.[7]

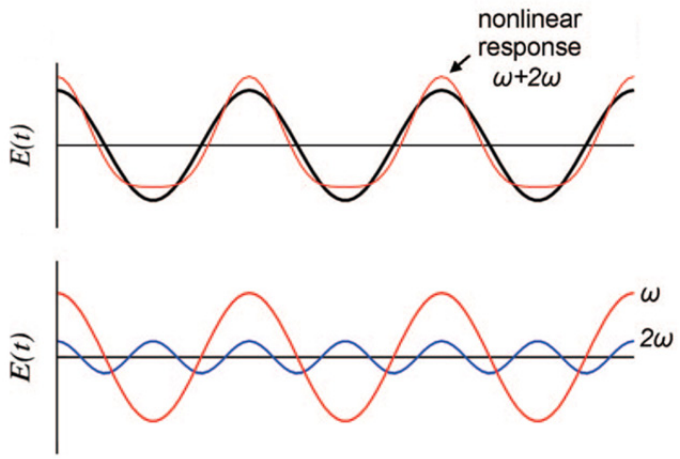

Figure 4. Polarization response P to an electromagnetic wave of field strength E(t) in a noncentrosymmetric medium described by a classical harmonic oscillator model. The plot below show the Fourier components of P at frequencies ω and 2ω.[6] The nonsinusoidal periodic response (*top*) can be described by the sum of a series of sinusoidal functions with appropriate coefficients of harmonics of the fundamental frequency ω (*bottom*).[18]

Molecular Design for Frequency Doubling Compounds

To obtain high hyperpolarizabilities β easily polarizable materials have to be used. Inorganic materials are used in applications like laser light modulation (green laser pointer) because of their high bulk susceptibility and their tendency to grow in noncentrosymmetric fashion (e.g. $LiNbO_3$).[19] Organic polyenes and aromatic systems are considered to replace them because of their ultra-fast response time due to weakly bound π-electrons.[20] In inorganic materials the response is significantly slower due to the contribution of heavy atoms. Ideal organic compounds are donor-acceptor substituted chromophores (push-pull systems) because they can be easily polarized. In addition the donor and acceptor already introduce partially dislocated and polarized mesomeric structures which contribute to the static polarization. Furthermore these dipoles can be arranged by external stimuli in a noncentrosymmetric

fashion and thus allows together with other advantages of organic materials a facilitated processability. Visible light absorption and thermal degradation by laser light have to be mentioned as disadvantages.[1]

To be able to design organic molecules that show a large NLO response, the hyperpolarizability β must be optimized for each individual type of NLO active chromophore. This calls for a deeper understanding of the contributions to β. It has to be taken into account that the induced polarization in a molecule has characteristics of a vector, related with the electric field vectors.[7] The hyperpolarizability β can therefore be written as

$$\beta = \beta_{zxx} + \beta_{zyy} + \beta_{zzz} \qquad (3)$$

Two different design concepts are possible: 1.) In molecules with a dipole moment (1D-NLO-chromophore) like donor-chromophore-acceptor systems only the tensor parallel to the dipole axis has a significant contribution to the overall hyperpolarizability. As a result the hyperpolarizability β of these chromophores is dependent on the polarity of the solvent. 2.) The second design possibility are 2D-NLO-chromophores (e.g. alternating donor-acceptor hexa substituted benzenes) where also non-diagonal elements of the β-tensor contribute to the hyperpolarizability. 2D-chromophores show NLO-effects which are less susceptible to the polarity of the solvent and are often apolar molecules without dipole moments.[21]

Optimization of the hyperpolarizability of donor-π-chromophore-acceptor systems can be achieved by variation of the nature of the donor, the acceptor and the interlinking π-system. While various studies about the influence of different donors and acceptors were reported, only a few are available systematically investigating the influence of changes in the chromophore.[20–23] These studies mainly focus on the length of the chromophore and on well known dyes. However, Marder *et al*. realized that the bond length alternation (BLA) of the π-bridge in the ground state of the molecule strongly depends on the donor and acceptor strength.[24–27] In push-pull systems the bonding properties can be expressed by mesomeric structures. The BLA is a measure of the difference of neighboring single and double bond lengths in conjugated systems. If donor and acceptor are in communication with each other – mediated by the π-system of the chromophore – a compensation of the bond lengths take place depending on the polarizability of the π-system. Marder *et al*. could show that upon increasing of the donor and acceptor strength the hyperpolarizability β changes sinusoidal (figure 5).[26,27] By knowing the initial hyperpolarizability of the parent push-pull system this sinusoidal curve allows predictions how β will change not only when the donor and/or

acceptor strength is changed but also when the π-chromophore is altered. Therefore the bond length alternation is a suitable tool for optimizing the hyperpolarizability β. The BLA can be divided into several parts. For compounds with β-values in the region A (figure 5) a change to easier polarizable chromophores or changing to substituents which enhance the charge-transfer will result in increased hyperpolarizabilities. Chromophores which have a large proportion of charge separated mesomeric structures belong to region B. Cyanine like structures show zero hyperpolarizabilities (cyanine limit).

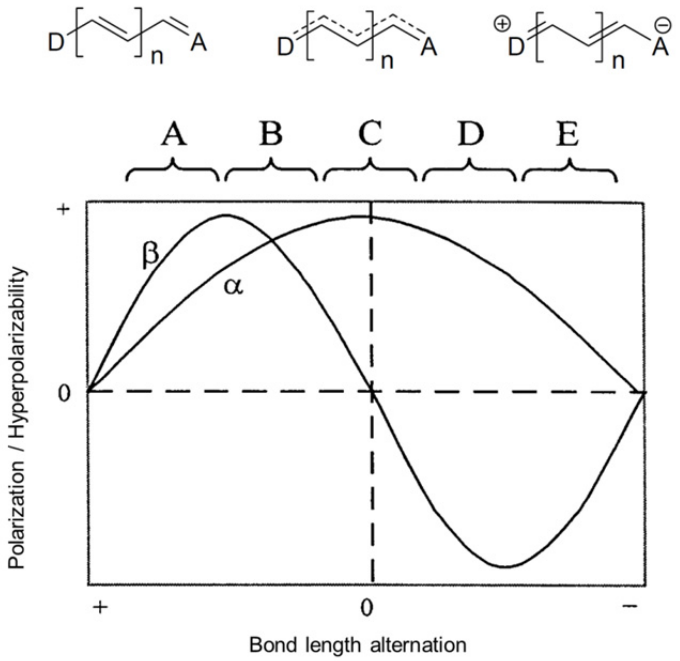

Figure 5. Sinusoidal shape of the first hyperpolarizability β with the bond length alternation of donor-acceptor substituted polyenes.[26] α corresponds to the linear polarization. The three polyene structures shown above the plot corresponds to region A – B (*left*), C (*middle*) and D – E (*right*).

Region D and E represent hyperpolarizabilities of compounds having a more polar ground state than the first excited charge-transfer state, like for example zwitterionic compounds. Even though for such compounds high β-values are possible other issues like lower solubility in organic solvents and the increased tendency to orient antiparallel in bulk have to be considered. The BLA was developed for polyene structures and unfortunately no explicit BLA values are available for aromatic compounds. It was demonstrated however that the BLA correlation can be used as a good approximation for the development of aromatic push-pull systems. The maybe most important outcome of this study was that increasing the donor and acceptor strength not necessarily increases the hyperpolarizability. Hence detailed investigations for each individual π-chromophore are crucial towards the optimization of the

β-values. In contrast to polyene structures, benzene based NLO active compounds have a higher stability but in contradiction the energy needed to form chinoid structures is higher. Thus heteroaromatic based systems like thiophenes[28] or furans[29] are maybe better suited to form stable and high performing NLO compounds. Furthermore it was demonstrated that conjugated polymers – because of their high degree of weakly bound delocalized electrons – showed high nonlinear polarizabilities.[20]

Models for the Understanding of β

Several models for a quantitative analysis of the hyperpolarizability β have been developed so far. Emanating from the EIF-model (Equivalent Internal Field)[30,31] and the additivity model[32–34] Oudar and Chemla developed the two-state model based on the dictation of NLO response by excited states.[35,36] They assumed that the large responses in donor/acceptor chromophores were due to an intramolecular charge-transfer interaction between the acceptor and donor. Therefore β is a sum of two variables β_{add} and $\beta_{CT.}$ β_{add} accounts for the interaction between the individual substituents and the π-network, whereas β_{CT} accounts for the charge-transfer term, arising from the interaction of donor and acceptor moieties (Eq. 4).

$$\beta = \beta_{add} + \beta_{CT} \qquad (4)$$

β_{CT} is a two-level interaction between the ground state and the first excited state. Thus, β_{CT} is dependent on the energy of the absorbed Laser photon, the energy difference between the ground state and the first excited state (HOMO/LUMO-gap), the oscillator strength of a ground state - first excited state transition and the difference between the dipole moments in the ground state and the first excited state.[8] β_{CT} can be obtained by quantum mechanical calculations based on the two-level model.

Other studies have shown that many organic donor-acceptor molecules undergo structural changes in the excited state,[37] significantly changing the π-electron delocalization compared to the ground state. This leads to deviations from the by the two-level model predicted values. Therefore detailed studies of the influence of backbone twists on the charge-transfer term β_{CT} and with it on the hyperpolarizability β can provide a platform towards new chromophore design possibilities in nonlinear optics.

Experimental Methods for the Determination of β

Several methods are known for the estimation of the hyperpolarizability β, namely the Kurtz-powder technique[38], the Hyper-Rayleigh-scattering[39], the electric field induced second harmonic generation measurements (EFISH)[7,40], the ellipsometric reflection[41], and the electro-optic absorption measurement (EOAM)[28]. In this contribution to the research in nonlinear optics the electric field induced second harmonic generation measurements were used to determine β and will be outlined in greater detail in the following section.

EFISH measurements can be performed in solution and are therefore a widely used method for investigation of SHG on a molecular basis. Typical EFISH measurements are performed in an optical cell holding the dissolved nonlinear optic active molecules (figure 6).

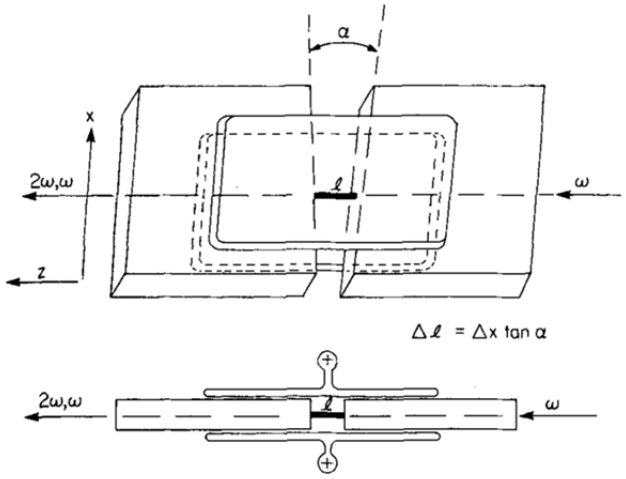

Figure 6. Top view (*top*) of a cell used for EFISH measurements. The gap l between the glass is about 1 – 2 mm. The electrodes are about five times longer than the gap to avoid nonuniform electric fields at the interface (edge view, *bottom*). Reprinted from Williams.[7]

To break the macroscopic centrosymmetry of the solution, the molecular dipoles are oriented in an applied high voltage DC-field. By illuminating the optical cell with a Laser beam at frequency ω, the second harmonic response of the solution at frequency 2ω can be observed, due to interaction of the optical field of the Laser with the molecules. To correct the fluctuations in intensity in the Laser beam, the Laser beam is splitted and also directed into a quartz crystal with known second-order response. The scalar product of the molecular dipole moment and the hyperpolarizability tensor β_{zzz} is obtained from the ratio of the signals of the sample cell and the reference material. By measuring the molecular dipole moment μ the hyperpolarizability β of the compound can be calculated.

Project Outline

In the following publication a novel universal synthetic route towards biphenyls based push-pull-systems (**C1a** – **C1g**) is reported, which are molecules suitable for investigations in this ongoing research area of NLO. These biphenyl based push-pull systems bearing a terminal electron-rich piperidinyl moiety (donor) and an electron-deficient nitro group (acceptor) at the opposite end, are bridged between 2 and 2' position by a variable number of methylene groups, giving them a defined and restricted torsion angle between the two phenyl rings. Thus these biphenyls are ideal model compounds to investigate the influence of π-conjugation dictated by the torsion angle in the backbone on the nonlinear optical properties. The target molecules were synthesized starting by converting dibromobiphenyl or ditriflate substituted biphenyl derivatives into their diamine analoga. The development of the synthetic routes towards the starting materials were part of the thesis of *David Vonlanthen* and published in "*Synthesis of Rotationally Restricted and Modular Biphenyl Building Blocks",* David Vonlanthen, Jürgen Rotzler, Markus Neuburger, and Marcel Mayor, *Eur. J. Org. Chem.* **2010**, 120 – 133 and in "*Conformationally Controlled Electron Delocalization in n-Type Rods: Synthesis, Structure, and Optical, Electrochemical, and Spectroelectrochemical Properties of Dicyanocyclophanes*", David Vonlanthen, Alexander Rudnev, Artem Mishchenko, Alexander Käslin, Jürgen Rotzler, Markus Neuburger, Thomas Wandlowski, and Marcel Mayor, *Chem. Eur. J.* **2011**, *17*, 7236 – 7250. My contribution was the synthesis of 3,9-bis(trifluoromethylsulfonyloxy)-6,7-dihydro-5*H*-dibenzo[*a*,*c*]cycloheptene (**C2e**) and 3,10-dibromo-5,6,7,8-tetrahydrodibenzo-[*a*,*c*]cyclooctene (**C2f**) which were then used for the synthesis of their diamine analoga. 3,11-Bis(trifluoromethylsulfonyloxy)-6,7,8,9-tetrahydro-5*H*-dibenzo-[*a*,*c*]cyclononene (**C2g**) was resynthesized to provide sufficient starting material for assembly of the corresponding push-pull system. To show the complete synthetic route of the torsion angle restricted push-pull systems the synthesis of the precursors was included in the following section extracted from the corresponding publications.

Furthermore the racemization dynamics of these axial chiral push-pull systems were investigated with the aim to modify the structures such that separation of the individual enantiomers gets possible. Subsequent crystal growing would lead to noncentrosymmetric crystals with a high potential for future applications. In this project *Heiko Gsellinger* and *Daniel Häussinger* carried out the ^{1}H-NMR coalescence measurements. Analysis of the results and the studies by dynamic HPLC were performed by myself.

Variation of the Backbone Conjugation in NLO Model Compounds: Torsion Angle Restricted Biphenyl-Based Push-Pull Systems

Jürgen Rotzler, David Vonlanthen, Alberto Barsella, Alex Boeglin,
Alain Fort and Marcel Mayor,

Eur. J. Org. Chem. **2010**, *6*, 1096 – 1110.

Introduction

While the discovery of the Kerr effect,[42] which is the quadratic electric field induced change in the refraction index of a medium, is the earliest nonlinear response reported in the study of optics, it is the availability of strong electromagnetic fields, after the invention of the laser in 1960,[43] that made it possible to systematically investigate such effects. Given the ability to produce optical fields of sufficient strength, the observation of the phenomenon of second harmonic generation (SHG) in quartz in 1961[44] marks the advent of nonlinear optical (NLO) studies. Since then, the search for NLO active media has been extended to organic compounds where it has developed into an amazingly broad field because of numerous potential applications in photonic technologies, including all-optical switching, data processing,[45–48] or even scanning electron microscopy.[49]

To design molecules for quadratic NLO responses, the first hyperpolarizability β must be optimized. Several models were developed for a quantitative analysis of the nonlinear optical response.[50–54] Oudar and Chemla established that the main contribution to β may be attributed to the lowest intramolecular charge-transfer (ICT) band characterized by a transition energy, an oscillator strength and a change in permanent dipole moment, thus defining their well known two-level model.[55] ICT is dependent on the backbone chromophore as well as on the substituents.[56] Therefore, the design of efficient organic materials for quadratic nonlinear optics is based on units containing highly delocalized π-electron moieties and additional electron donor and electron acceptor groups on opposite ends of the chromophore.

Donor-acceptor substituted biphenyl derivatives are particularly interesting model compounds exhibiting intramolecular charge-transfer since the extent of "backbone"-conjugation and thus the extent of charge-transfer between both substituents depends on a controllable structural feature, namely the torsion angle between the two phenyl rings.[57–60] Correlations between intramolecular torsion angles and resulting NLO properties were already reported for

quinopyrans by Ratner and co-workers.[61] Using numerical simulations for NLO properties and UV/Vis absorption spectra, the tuning of transition frequency and NLO amplitudes was achieved by effecting charge separation and by stabilizing the charge.[61] Also biphenyl based chromophores have already been considered in theoretical studies. *Ab initio* calculations of fluorenyl based push-pull systems suggested that the value of β corresponds to the energy difference between HOMO and LUMO.[62] By comparing the NLO properties of comparable substituted (-NH_2 and -NO_2) biphenyl and fluorene derivatives a considerably increased response was observed for the planar fluorene compound, pointing at the importance of the π-conjugation in the central chromophore. Furthermore, correlations between backbone torsion angle and NLO properties have already been reported for zwitterionic compounds.[57]

The complexity of the non-linear optical responses makes the design of new NLO materials very challenging. Especially on the molecular level, numerous publications document the very basic comprehension of structure-property relationships, despite the fact that great progress has been made in the last few years.[57,62–69] Indeed, large π-conjugated systems with donor and acceptor groups have been synthesized with a high potential for large nonlinear optical effects. Despite the advances in chromophore design, a deeper comprehension of structural features governing the NLO properties is required to enable reliable theoretical predictions and thus, allowing an improved design of tailor-made NLO materials. Improved theoretical models on the other hand can only be developed with suitable experimental data obtained from model compounds in which a particular structural feature is varied systematically.

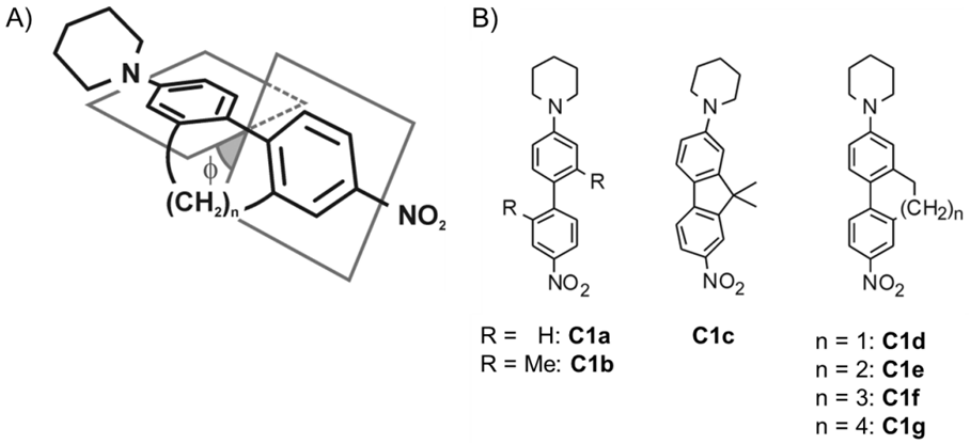

Figure 7. A) Illustration of the concept to fix the torsion angle *Φ* between the two phenyl rings by an additional interphenyl alkyl-bridge of various length. B) Target push-pull systems with increasing torsion angle from **C1c** to **C1g**. **C1a** and **C1b** were used as preliminary model compounds.

Following this systematic approach, the synthesis of the entire series of neutral biphenylic push-pull systems with restricted torsion angles **C1a – C1g** as NLO model compounds varying mainly in the extent of backbone π-conjugation is reported (figure 7). Furthermore, first optical studies like UV/Vis and EFISH (electric field induced second harmonic generation) experiments were performed to investigate the consequences of the alteration in torsion angle on their optical properties. The observed correlations are further accompanied by semi-empirical simulations based on the AM1 Hamiltonian.

Results and Discussion

Molecular Design and Synthetic Strategy

For sizeable quadratic optical responses in linear push-pull systems a permanent dipole moment induced by electron acceptor and donor substituents and an intense intramolecular charge-transfer absorption band are required. While effects arising from the donor and acceptor substituents have been investigated extensively,[62,70–75] hardly any systematic study of the influence of the backbone's π-conjugation has been reported so far.[56,57] We recently developed a series of biphenyl building blocks – terminally functionalized with leaving groups – comprising alkyl chains of various lengths interlinking both phenyl rings to restrict the torsion angle of their biphenyl backbone.[76] These functional building blocks are ideally suited as starting materials of the here reported series of biphenyl based push-pull systems as NLO model compounds with varying backbone conjugation. Nitrogen substituents in varied oxidation states have been chosen as push-pull substituents. While a terminal nitro group acts as electron acceptor, a piperidinyl substituent acts as electron donor on the opposed side. These substituents on a parent biphenyl core should provide a donor-acceptor system exhibiting a moderate hyperpolarizability, leaving investigation space for both, systems with stronger and weaker hyperpolarizabilities. To keep the model compounds as comparable as possible the terminal substituents were maintained throughout the series.

To preliminarily investigate the suitability of the push-pull system the parent 4-nitro-4'-piperidinyl-biphenyl was straight forwardly synthesized by assembling the biphenyl backbone applying a *Suzuki* coupling protocol. However, the synthetic aim of this project was to develop a universal synthetic strategy for 4-nitro-4'-piperidinyl substituted biphenyl systems based on available building blocks comprising terminal leaving groups such as bromides and triflates. The synthetic strategies considered are displayed in scheme 1.

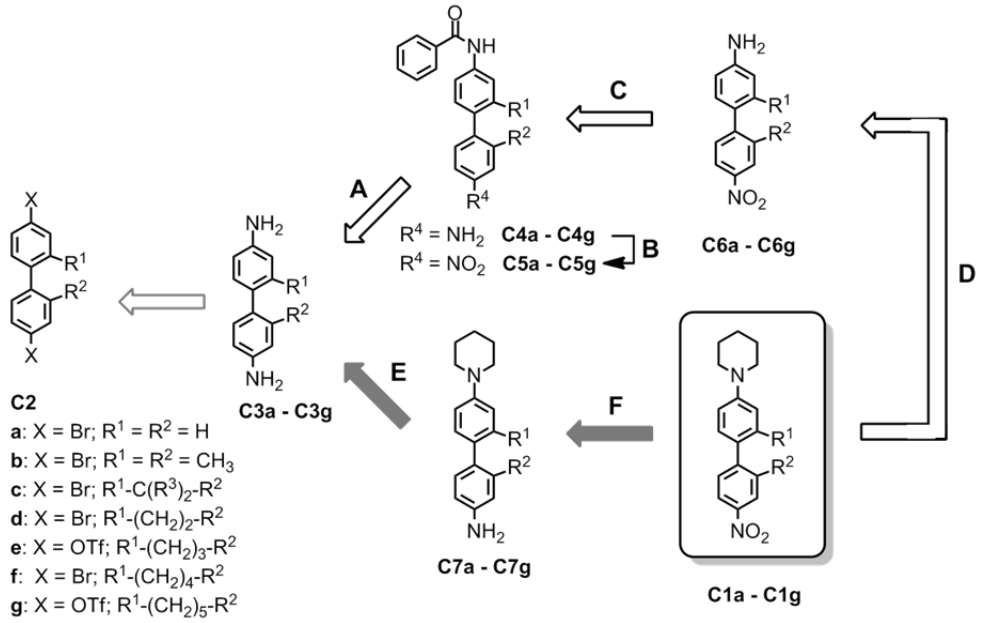

Scheme 1. Synthetic routes considered towards the desired biphenyl based push-pull systems (R^3=H for **C2**, **C3** and **C7**; $R^3 = CH_3$ for **C1**).

In the target compounds the oxidation state of both terminal nitrogen atoms differs by six units. Starting from symmetric diamino derivatives, which should be obtained either by palladium catalyzed *Hartwig-Buchwald*-type chemistry[77,78] or by copper catalyzed *Ullmann*-type reactions,[79,80] the synthetic challenge will be to oxidize exclusively one of the two nitrogen atoms. Furthermore, a suitable assembly sequence of the electron-donating piperidinyl unit and the electron-withdrawing nitro group had to be found. Two synthetic approaches were considered and are displayed as **A** – **D** and **E** – **F** in scheme 1.

If the piperidinyl donor-group is introduced first (**E**), oxidation of the remaining amino-group (**F**) will be challenging, as tertiary amines are prone to the formation of *N*-oxides. However, a careful choice of the oxidation conditions might overcome this drawback of the **E** – **F** strategy. Alternatively, the oxidation step providing the electron-withdrawing nitro group could be considered prior to the assembly of the piperidinyl group (strategy **A** – **D**). Monoprotection of the diamine with a benzoyl group (**A**) should provide selectivity[81] and should reduce the electron density of the remaining amine providing an increased control over its oxidation (**B**), as electron-rich anilines are prone to side reactions during oxidations due to their large reduction potentials. After deprotection (**C**), the assembly of the piperidinyl group was envisaged by an azacycloalkylation. However, the nucleophilicity of the remaining amino group is decreased due to the electron-withdrawing nitro group. Interestingly, the extent of this effect is expected to correlate with the backbone conjugation of the biphenyl core.

Synthesis

Synthesis of the Starting Materials

The starting materials **C2a** – **C2d** were commercially available or were easily synthesized according to literature known protocols in a single reaction. The propyl-bridged ditriflate biphenyl derivative **C2e** was synthesized starting from the bulk chemical 4-bromo-3-methylanisole **C8** (scheme 2). An oxidative iron-catalyzed homo-coupling reaction,[83] using stoichiometric amounts of 1,2-dichloroethane as the re-oxidation agent, afforded the building block **C9** in 92% yield. Subsequent double benzylic bromination with *N*-bromosuccinimide (NBS) afforded the key intermediate **C10** in 68% yield.

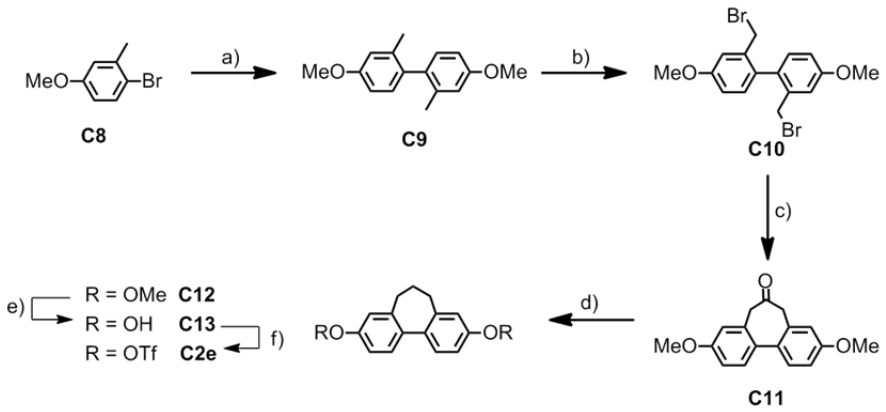

Scheme 2. Synthesis of the ditriflate biphenyl cyclophane **C2e**. a) Mg^0, methyl-THF, $FeCl_3$, 1,2-dichloroethane, reflux, 92%; b) NBS, benzoyl peroxide, CCl_4, reflux, 68%; c) TosMic, CH_2Cl_2, NaOH, tetrabutylammonium bromide (TBAB) (6.3 mol%), then HCl, *t*BME/H_2O, 83%; d) KOH, hydrazine monohydrate, diethylene glycol, 195°C, 86%; e) BBr_3, CH_2Cl_2, 0°C to rt; f) Tf_2O, pyridine, rt, 84% over two steps.

To achieve the oxo-functionalized propyl-bridge in **C11**, an additional carbon atom was introduced through an intramolecular cyclization reaction of the dibromide **C10**, using the masked formaldehyde equivalent (tolylsulfonyl)methyl isocyanide (TosMic)[84] to provide the dimethoxy ketone **C11** as a white solid in a yield of 83%. Reduction using a Wolff‑Kishner protocol,[85] affording **C12** in 86% yield. Subsequent functional-group transformations allowed **C12** to be transformed into ditriflate derivative **C2e**.[86] The unfunctionalized propyl-bridge in **C12** allowed electrophilic cleavage of the two methyl groups of the biaryl diether with boron tribromide at room temperature. Subsequent esterification of the diol **C13** with triflic anhydride in pyridine gave the triflate building block **C2e** in a yield of 84% over two steps. An overall yield of 38% was obtained for this six-step reaction sequence.

The key intermediate dibenzyl dibromide **C14** (Scheme 3) towards the synthesis of the butyl-bridged dibromobiphenyl derivative **C2f** was synthesized on a large scale: 4,4'-dibromodiphenic acid (**C15**) was synthesized from the bulk chemical 5-bromoanthranilic acid according to the procedure of Helms *et al*.[87] by formation of the diazonium salt followed by copper mediated homo-coupling in 70% yield. The crude diphenic acid **C15** was reduced to the diol **C16** by using sodium borohydride and $BF_3 \cdot Et_2O$ as the activating Lewis acid.[88] The crude diol **C16** was subsequently transformed into the dibenzyl dibromide by an S_N2 reaction to obtain the key intermediate **C14** in a yield of 63% (over two steps).[89] Immediate purification of the crude diol by flash chromatography improved the yields considerably. Interestingly, attempts to repeat an already reported synthesis of **C14** based on radical bromination[90] was not successful in our laboratory, and instead of the desired compound a tarry inseparable mixture was obtained. The key intermediate **C14** (scheme 3) was transformed by a copper-mediated alkylation, with the Normant reagent generated *in situ*, to the diallylbiphenyl **C17**. Despite of reported challenges faced during the formation of eight-membered rings[91] by ring-closing metathesis (RCM), the cyclization proceeded smoothly in the case of **C17**, probably due to the conformationally predisposed allyl chains.[92,93] The metathesis reaction, first- and second-generation Grubbs' catalyst were found to be equally effective, afforded **C18** in good yield of 79% as a white solid. Subsequent hydrogenation with palladium on charcoal at atmospheric pressure yielded the doubly halogenated building block **C2f** almost quantitatively.

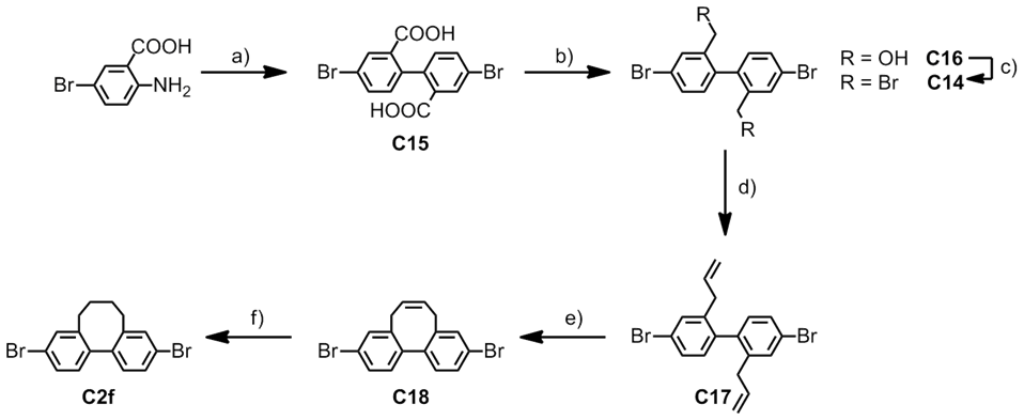

Scheme 3. Synthesis of dibromobiphenyl **C2f**. a) $NaNO_2$, HCl, 0°C, then $CuSO_4$, $HONH_2$, NH_4OH, H_2O, 0°C-70°C, 70%; b) $NaBH_4$, $BF_3 \cdot Et_2O$, THF, 67%; c) PBr_3, CH_2Cl_2, 0°C, 63% (over two steps); d) $CH_2CHMgBr$, CuI, CH_2Cl_2, -40°C to rt, 79%; e) Grubb's catalyst, CH_2Cl_2, reflux, 94%; f) H_2, 10% Pd/C, rt, EtOAc, 98%.

An alternative strategy was used to assemble the cyclononane structure in **C2g**. As shown in scheme 4, the interring pentyl chain was established prior to the formation of the biphenyl

backbone. The symmetric 1,5-bis(3-methoxyphenyl) pentane (**C19**) was synthesized according to a literature known procedure.[94–96] Thus, *meta*-anisaldehyde underwent a double aldol condensation with acetone[94,95] followed by a hydrogenation reaction[96] to afford **C20** in 46% yield over two steps. The reduction to **C19** was achieved by a classic Wolf–Kishner reaction in 72% yield.[96] Subsequent bromination afforded regioselectively the dibromo key intermediate **C21** in 42% yield as precursor of the cyclization reaction.[97] Repeated recrystallization turned out to be crucial to remove the regioisomeric side products formed in this step. The readily synthesized key substrate **C21** underwent a copper-mediated C–C biaryl bond-forming reaction. Whitesides[98] and more recently Lipshutz and co-workers[99–102] applied oxidants to aryl cuprates to form biaryls intermolecularly. By adapting the experimental procedure of Schreiber and co-workers,[103] which allows the synthesis of a series of asymmetric biaryl-containing macrocyclic rings, the cyclononane structure **C22** was synthesized successfully.

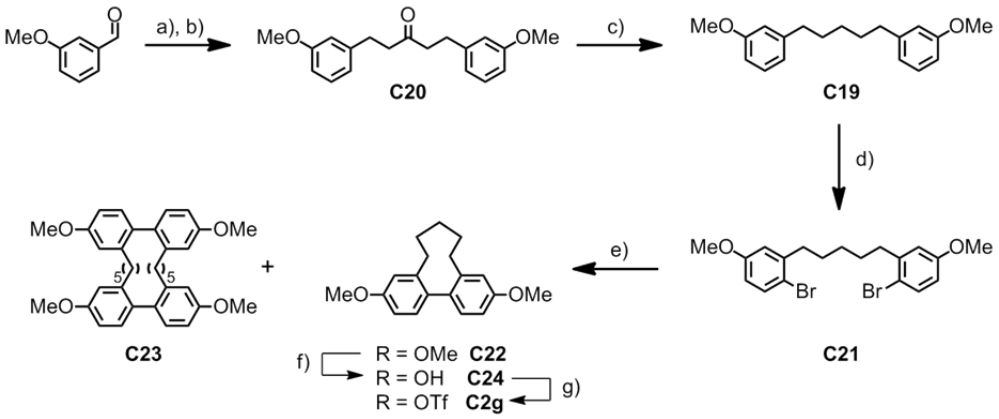

Scheme 4. Synthesis of cyclononane **C2g**. a) acetone, NaOH, EtOH;[94,95] b) 1 atm H_2, 10% Pd/C, EtOAc, 46% (over two steps);[96] c) hydrazine (85%), KOH, triethyleneglycol, 190–200°C, 72%;[96] d) Br_2, pyridine, -10°C to rt, 42%;[97] e) *t*BuLi, CuCN, LiBr, MeTHF, -60°C, then 1,3-dinitrobenzene, 23% for **C22**, 27% for **C23**; f) BBr_3, CH_2Cl_2, rt; g) Tf_2O, pyridine, 0°C to rt, quant.

Treatment of the dibromide **C21** with *tert*-butyllithium followed by CuCN led to the formation of a cyclic biaryl cuprate as the intermediate. Upon exposure to 1,3-dinitrobenzene as the oxidant, two major products were isolated in about equal amounts after purification by flash chromatography. Intermolecular dimerization of two molecules of **C21** gave the undesired dimer **C23**, which was formed in a yield of 27%, whereas the intramolecular reaction provided the desired macrocycle **C22** in a yield of 23%. Attempts to favor the intramolecular reaction by applying high-dilution conditions did not improve the isolated yield of the monomeric product **C22**. Subsequent functional-group transformations allowed

C22 with terminal methoxy groups to be transformed into the building block **C2g** bearing triflate groups. The unfunctionalized pentyl-bridge in **C22** allowed electrophilic cleavage[104] of the two methyl groups of the biaryl diether with boron tribromide at room temperature. The crude biaryldiol **C24** was obtained as a fluffy material that was pure enough to be used directly in the next step. Subsequent esterification of the diol **C24** with triflic anhydride in pyridine, acting as the base, gave the key building block **C2g** as a colorless oil.

*Synthesis of the Push-Pull Biphenyls (**C1a** – **C1g**)*

To investigate the suitability of these new types of biphenyl based push-pull systems for EFISH experiments a straight forward assembly of the parent 4-nitro-4'-piperidinyl-biphenyl **C1a** was considered. Particularly appealing is the synthesis of the biphenyl core by a *Suzuki-Miyaura*-coupling as suitably functionalized phenyl precursors were already available.[82] As displayed in scheme 5, 1-(4-iodophenyl)piperidine and 4,4,5,5-tetramethyl-2-(4-nitrophenyl)-1,3,2-dioxaborolane were treated with a palladium catalyst and a base in a refluxing toluene/methanol mixture to provide the desired NLO model compound **C1a** in 26% yield after column chromatography (CC). Promising preliminary optical investigations of **C1a** motivated the development of a general synthetic route to make the entire series of NLO model compounds available.

Both considered strategies (**A** – **D** and **E** – **F**) have the 4,4'-diaminobiphenyl synthon as a common precursor. Numerous catalyst-ligand systems for *Hartwig-Buchwald* cross-coupling reactions to substituted aryl-halides, including 4-bromobiphenyl and 1,4-dibromobenzene[105] have been reported.[106] However, to the best of our knowledge, typical *Hartwig-Buchwald* conditions were neither applied to ditriflate- nor dibromobiphenyl systems. While 4,4'-dibromobiphenyl systems (**C2a** – **C2d**, **C2f**) as precursors allowed rather harsh reaction conditions, this was less the case for 4,4'-ditriflatebiphenyl systems (**C2e** and **C2g**) which are prone to hydrolysis. To investigate the suitability of the synthetic strategy, the commercially available 4,4'-dibromobiphenyl (**C2a**) was treated with benzophenone imine as an ammonia synthon[107] and sodium *tert*-butanolate as base in the presence of catalytic amounts of $Pd_2(dba)_3$ as Pd(0) source and BINAP as ligand in 80°C hot toluene (condition b in scheme 5).

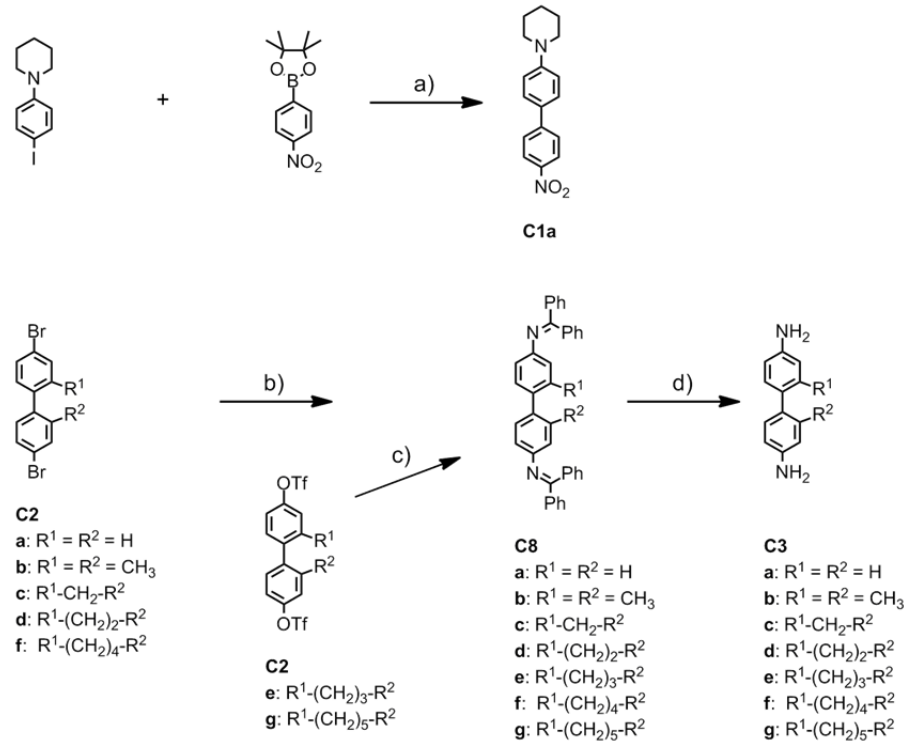

Scheme 5. Assembly of **C1a** by *Suzuki-Miyaura*-coupling (*top*). Synthesis of the 4,4'-diamino derivatives **C3a-g** applying a *Hartwig-Buchwald* protocol (*bottom*). Reagents and conditions: a) $Pd(PPh_3)_4$, Cs_2CO_3, toluene:MeOH 3:1, reflux, 18 h, 26%; b) benzophenone imine, $Pd_2(dba)_3 \cdot CHCl_3$, BINAP, NaO*t*Bu, toluene, 80°C, 4 h, 85%-quant.; c) benzophenone imine, $Pd(OAc)_2$, BINAP, Cs_2CO_3, THF, 65°C, 17 h, 98% for **C8e**, 60% for **C8g**; d) 3% aq. HCl, THF, rt, 2 h, 80%-quant.

To protect the intermediate air sensitive catalyst-ligand-complex, the reaction was carried out under inert gas atmosphere and dry conditions. After 4 hours the starting material was consumed as observed by thin layer chromatography (TLC). The diimine-biphenyl derivative **C8a** was isolated by precipitation of the catalyst and recrystallization from methanol. In a first attempt, the diimine **C8a** was cleaved using ammonium formate and catalytic amounts of palladium on charcoal.[107] As only 35% yield of the desired 4,4'-diaminobiphenyl (**C3a**) was isolated, acidic hydrolysis was considered. Thus, **C8a** was dissolved in tetrahydrofurane (THF) and hydrochloric acid was added. The desired diamine **C3a** was isolated by column chromatography (CC) in 80% yield over both steps. Starting from the ditriflates **C2e** and **C2g**, the strong base sodium *tert*-butanolate was no longer considered. Instead cesium carbonate was used as base in THF together with a $Pd(OAc)_2$/BINAP catalysator system (conditions c) in scheme 5).[107] With these conditions, comparable yields were obtained for the ditriflates as for the dibromides providing good access to the 4,4'-diaminobiphenyl systems required for both strategies. It is noteworthy that all these biphenyl diamine derivatives **C3a** – **C3g** displayed limited stability due to immediate partial oxidation when exposed to air. Thus,

elemental analyses were obtained for the corresponding bis(trifluoroacetic acid) salts which displayed considerably improved stabilities.

With the series of diamines **C3a** – **C3g** in hand, the strategy **A** – **D** was investigated first, again using the parent 4,4'-diaminobiphenyl **C3a** as model compound to explore the potential of the envisaged synthetic route (scheme 6). To distinguish between both terminal amines protection with a benzoyl protection group was considered, which was reported to provide selectively only the monoprotected derivative of 1,4-diaminobenzene.[81] In analogy to the reported procedure, the diamine **C3a** was dispersed in water by adding sodium dodecyl sulfate (SDS) and benzoic anhydride dissolved in acetonitrile was added at once. After work-up and recrystallization from hot toluene a yield of only 50% of the desired monoprotected diamine **C4a** was obtained, pointing at its almost statistical formation. As the selectivity in the case of 1,4-diaminobenzene probably arises from the different solubilities of the unprotected and the monoprotected form, which precipitates the desired monoprotected product out of the reaction mixture, the fact that **C3a** in water with SDS was a dispersion rather than a solution already raised questions whether this strategy towards monoprotected diamines will be generally applicable to the series of diamines **C3a** – **C3g**, for which differences in their solubility features had been expected.

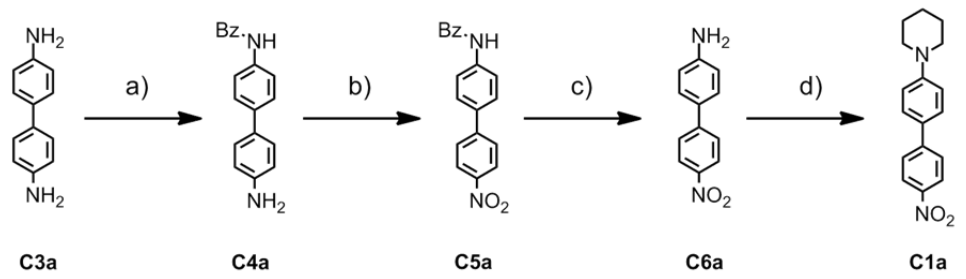

Scheme 6. Synthetic steps along the strategy **A-D**. Reagents and conditions: a) benzoic anhydride, MeCN, H_2O, SDS, rt, 10 min, 50%; b) $NaBO_3 \cdot 4H_2O$, AcOH, 55-60°C, 16 h, quant.; c) 10 M aq. KOH, DMSO, 80°C, 60 h, 25%; d) 1,5-dibromopentane, K_2CO_3, toluene:EtOH 1:1, MW, 150°C, 40 min, 40%.

However, with reasonable quantities of **C4a** in hand we further investigated the proposed strategy. Interestingly, the benzoyl protection group should also support the control over the oxidation of the remaining amine, as deactivated anilines containing electron-withdrawing groups are smoothly oxidized to the corresponding nitroarenes upon treatment with sodium perborate, whereas activated anilines containing electron-donating groups notoriously tend to overoxidation.[108] And indeed, treating the monoprotected **C4a** with an excess of sodium perborate tetrahydrate in acetic acid at 60°C provided the protected nitro derivative **C5a** quantitatively without overoxidation. Strong basic conditions were considered to cleave the

benzamide protection group of **C5a**. By treatment with 10 M aqueous potassium hydroxide in dimethyl sulfoxide (DMSO)[109] the amine **C6a** was obtained in poor yields of 25% after column chromatography as a red solid. As there was only a final step remaining the synthetic strategy **A**-**D** was accomplished in spite of the poor yield of this intermediate step. An azacycloalkylation was suggested to transform the remaining amine group of **C6a** into a piperidinyl substituent. While piperidine subunits are usually introduced as nucleophiles substituting a halide in an *Ullmann*-type coupling reaction,[110–112] double alkylation of arylamines and hydrazines with alkyldihalides based on a microwave-assisted approach was reported recently.[113,114] Thus, the amino biphenyl **C6a** was treated with 1,5-dibromopentane and potassium carbonate as a base in a toluene/ethanol (1:1) mixture at 150°C for 40 minutes in the microwave set-up. The desired 4-nitro-4'-piperidinyl-biphenyl **C1a** was isolated in 40% yield as an orange solid by column chromatography.

With the formation of the model compound **C1a** the entire strategy **A** – **D** was accomplished, but several steps with moderate to poor yields considerably disfavor this approach. Initial attempts to apply the same strategy to the fluorene diamine starting compound **C3c** provided even lower yields of the monoprotected intermediate **C4c** than observed in the case of **C4a**, further disqualifying the synthetic strategy.

The major drawback of the alternative strategy **E** – **F** was the statistical introduction of the piperidinyl substituent, even though the resulting mixture was expected to be easily separable into its components by column chromatography. Furthermore, selective oxidation of primary amines in the presence of tertiary ones is synthetically challenging. However, as the yield of monoprotection of the strategy **A** – **D** did not exceed statistical values, the approach **E** – **F** with a reduced number of synthetic steps moved again into the focus of interest. The two synthetic steps are displayed in scheme 7. To transform one of the two terminal amino groups of the model compound **C3a** into a piperidinyl substituent, a microwave assisted double alkylation with 1,5-dibromopentane[113] was considered,[114] mainly due to its reported superior yields compared with thermally activated heterocyclization reactions of aniline derivatives. Following a reported protocol,[114] commercially available 4,4'-diaminobiphenyl (**C3a**) was treated in the microwave reactor with 1,5-dibromopentane in water with potassium carbonate (K_2CO_3) as a base. The desired mono-piperidinyl derivative **C7a** was isolated in a poor yield of only 10% and the formation of a black tar at the bottom of the reaction vessel, probably arising from the large amount of undissolved starting material was observed. In a second attempt toluene was added to increase the solubility of **C3a**. The two phase mixture

was exposed for 20 minutes to microwave irradiation at 120°C. To our surprise only the formation of the mono-piperidinyl derivative **C7a** was observed by TLC with comparable low yields as obtained in pure water. Inspired by this unexpected chemoselectivity different solvent mixtures were screened, as summarized in table 1. The yields of the reactions were determined by reverse phase HPLC (RP18) using acetonitrile as eluent. In water almost equal quantities of mono- and di-piperidinyl (45:55) functionalized biphenyl were observed and large amounts of starting material was lost to side reactions (entries 1 and 2). By addition of toluene both starting materials, the benzidine **C3a** and the 1,5-dibromopentane, were dissolved in the organic phase while the microwave energy was absorbed by the aqueous phase. While the promising chemoselectivity of the system was corroborated (entries 3 and 4), low yields disfavored these reaction conditions. To bring the microwave absorbing species into the organic phase, ethanol (EtOH) was considered instead of water. In a 1:1 mixture of toluene and ethanol a conversion of 50% of the starting benzidine **C3a** was observed with a chemoselectivity of 84:16 in favor of the desired mono-piperidinyl substituted biphenyl system **C7a** (entry 5). A further increase of the dibromopentane concentration decreased the chemoselectivity by a comparable conversion (entry 6), while an increase of the EtOH fraction (entry 7) or the use of acetone as neat solvent (entry 8) increased the chemoselectivity by drastically reducing the conversion.

Table 1. Screening results for the reaction of **C3a** to **C7a**.

	solvent	eq. dihalide	temperature	reaction time	obtained ratio (mono:di)	conversion[a] (mono+di)
1	water	1.10	120°C	20 min	50 : 50[b]	20%
2	water	1.10	150°C	40 min	45 : 55	47%
3	toluene/water 1:1	1.10	120°C	40 min	100 : 0	14%
4	toluene/water 1:1	1.10	120°C to 150°C	40 min	mono > di[b]	40%
5	toluene/EtOH 1:1	1.10	150°C	40 min	84 : 16	50%

Table 1. continued

	solvent	eq. dihalide	temperature	reaction time	obtained ratio (mono:di)	conversion[a] (mono+di)
6	toluene/EtOH 1:1	1.50	145°C	40 min	77 : 23	53%
7	toluene/EtOH 10:1	1.10	80°C	40 min	100 : 0	2%
8	acetone	1.10	75°C	40 min	100 : 0	14%

[a] Conversion is related to the reisolated starting material. [b] Ratios determined qualitatively by TLC.

We suggest that the activated secondary amine of the formed mono-piperidinyl functionalized biphenyl system might be partially protonated during the reaction to explain its surprising stability towards a second cycloalkylation reaction. This hypothesis is further corroborated by the fact that K_2CO_3 is not dissolved in the most promising solvent mixture (toluene:EtOH 1:1) suggesting the deprotonation at the phase boundary as the rate determining and reaction controlling step. The best compromise between chemoselectivity and conversion was found empirically for entry 5 and similar reaction conditions were thus applied for the transformations of the diamines **C3b – C3g** to the piperidine derivatives **C7b – C7g**. The obtained yields and observed chemoselectivities are summarized in table 2.

Table 2. Azacycloalkylation of amines **C3a – C3g**.

product	yield[a]	selectivity (mono : di)
C7a	41%	42 : 8
C7b	40%	n. d.
C7c	43%	43 : 15
C7d	44%	44 : 7
C7e	32%	32 : 3
C7f	41%	41 : 5
C7g	34%	34 : 8

[a] Yields of the desired monoazacycloalkylated products **C7** isolated by CC.

For all diamines yields between 30% and 45% of the corresponding mono-piperidinyl functionalized biphenyl system were obtained, pointing at the general applicability of the transformation procedure. With the exception of the fluorene derivative **C7c**, very comparable chemoselectivities were observed. The slightly increased formation of the doubly piperidinyl functionalized fluorene may point at an increased activation of the second amine by the first piperidinyl substituent due to the pronounced electronic coupling of both phenyl rings in the flat fluorene core.

Finally, to accomplish the synthesis of the target structures **C1a** – **C1g**, the remaining amino group had to be oxidized to a nitro group. Unfortunately, most oxidants that are routinely used for the oxidation of primary amines to nitro groups are also able to oxidize tertiary amines. And indeed, immediate overoxidation to 1-(4'-nitrobiphenyl-4-yl) piperidine 1-oxide (isolated and characterized by ^{1}H-NMR- and IR-spectroscopy) was observed by applying standard oxidation conditions such as *in situ* generated peracetic acid as an oxidizing agent and sulfuric acid as a catalyst, or sodium perborate in acetic acid.[108,115] Smooth oxidation conditions for the conversion of anilines to nitrobenzene derivatives profiting from water soluble tungsto-phosphoric acid ($H_3PW_{12}O_{40}\cdot n\ H_2O$) as catalyst and phasetransfer oxidant and sodium per-borate as an oxidant in micellular media have been reported.[116] According to the hypothesized mechanism, oxidation occurs in micelles of organic molecules where the concentration of the sterically demanding active species is low, providing very mild oxidation conditions.[117,118] By applying the described conditions to compound **C7a** (scheme 7), the target push-pull system **C1a** was isolated in 55% yield after column chromatography as a red solid without detectable formation of the *N*-oxide. Similar reaction conditions applied to the diamines **C3a** – **C3g** provided the desired target structures **C1b** and **C1d** – **C1g** in reasonable yields between 45% and 64%. However, in the case of the fluorene derivative **C7c** the formation of the desired nitro derivative was not observed, probably different solubility properties of **C7c** arising from the acidity of the hydrogen-atoms in C9 position avoided its oxidation. Nevertheless, besides the moderate yields it is noteworthy that, to the best of our knowledge, it is the first time that suitable oxidation conditions for oxidation of primary amines to nitro groups in the presence of alkylated amino groups were found. As displayed at the bottom of scheme 7, the terminally nitro and piperidinyl substituted fluorene derivate **C1c** comprising two methyl groups at the C9 position was synthesized based on previously reported synthetic steps.[110,119]

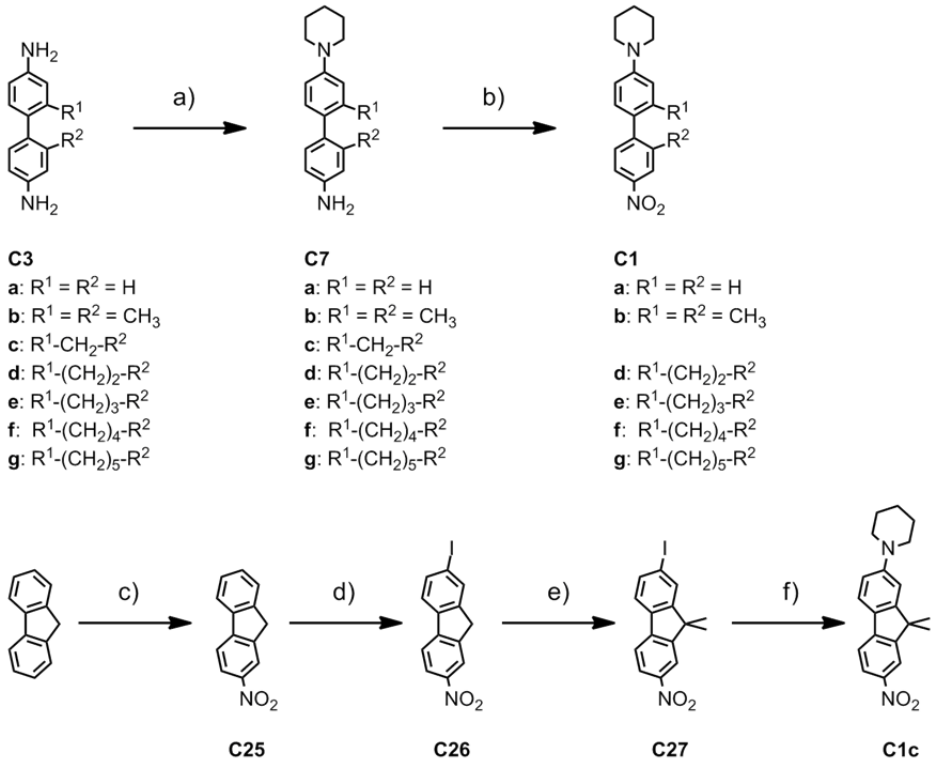

Scheme 7. *Top*: Synthesis of the target structures **C1a-b** and **C1d-g** following the strategy **E – F**. *Bottom*: Synthesis of the target structure **C1c** based on an individual strategy. Reagents and conditions: a) 1,5-dibromopentane, K_2CO_3, toluene:EtOH 1:1, MW, 150°C, 40 min, 34-44%; b) $NaBO_3 \cdot 4H_2O$, $H_3PW_{12}O_{40}$, CTAB (hexadecyltrimethylammonium bromide) (10 cmc in water), 55-60°C, 16 h, 45-64%; c) HNO_3/AcOH, -43°C, 6 h, 15%; d) I_2, AcOH, rt, 10 min, then conc. H_2SO_4, $NaNO_2$, reflux, 30 min, 76%; e) MeI, KI, KOH, DMSO, rt, 2 h, 95%; f) piperidine, CsOAc, CuI, DMSO, 90°C, 24 h, 15%.

In short, nitration and iodination of fluorene provided the terminally nitro and iodo functionalized fluorene **C26**, which was methylated to remove the acidic hydrogen-atoms in the 9 position. Finally, the piperidine group was introduced by substituting the iodine atom in an *Ullmann* coupling-reaction to provide **C1c** as a red solid in poor yields of about 2% over the four steps (scheme 7). However, the focus was set on the completion of the series of model compound and thus this already reported procedure was not further optimized for the system under investigation.

All new compounds were fully characterized by ^{1}H- and ^{13}C-NMR spectroscopy, mass spectrometry and refraction index or melting points. The purity of the target structures is further documented by elemental analysis.

Summarizing the synthetic section, with the strategy **E – F** almost the entire series of push-pull model compounds was obtained in reasonable quantities enabling NLO investigations.

Despite only moderate yields for both steps (**E**: 30-45%; **F**: 45-64%), the shortness and the general applicability clearly favors this strategy over the initially privileged approach **A** – **D**.

Optical Properties

The π-conjugation in the bridged target compounds **C1c** – **C1g** was investigated by UV/Vis measurements. The in 2 and 2' position unsubstituted push-pull system **C1a** showed absorption maxima at 268 nm (ε = 19840 $Lmol^{-1}cm^{-1}$) and 398 nm (ε = 19646 $Lmol^{-1}cm^{-1}$). The shorter wavelength absorption band can be assigned to a subfragment band of the biphenyl unit. The observed bathochromic shift compared to biphenyl (247 nm) probably arises from enlargement of the conjugated π-system due to substitution with lonepair containing nitrogen units.[120] The long wavelength absorption λ_{max} at 398 nm which levels off around 560 nm is assigned to a charge-transfer band.[121,122] Since a strong donor and a strong acceptor was used in the target push-pull systems **C1c** – **C1g**, the participation of the HOMO-LUMO-transition decreases considerably for the long-wavelength absorption and the ICT-affected correction term reaches zero. Thus λ_{max}-values of this charge-transfer band were used as indicator of the π-conjugation instead of its onset which reflects the HOMO-LUMO-transition.[121] The subfragment absorption (λ_{max} ca. 268 nm) remains the same throughout the whole series, whereas a hypsochromic as well as a hypochromic shift was observed for the charge-transfer absorption with increasing torsion angle Φ (figure 8). Values for Φ were obtained by semi-empirical calculations (MOPAC 2002 program[123] using the AM1 semi-empirical Hamiltonian[124]). The absorption data for the bridged compounds **C1c** – **C1g** are summarized in table 3.

Table 3. λ_{max} of the CT-bands and the corresponding extinction coefficients ε of **C1c** – **C1g**.

	λ_{max}(CT)	ε / $Lmol^{-1}cm^{-1}$
C1c	418 nm	21703
C1d	416 nm	20782
C1e	388 nm	12074
C1f	371 nm	7551
C1g	351 nm	3019

The hypochromic shift can be explained by an increase of the transition energy due to larger torsion angles when going from **C1c** to **C1g**. By increasing torsion angle Φ the conjugation is

less pronounced leading to higher excitation energies and therefore to absorption at lower wavelengths. According to studies of similar compounds the hypsochromic shift can be related to $\cos^2(\Phi)$ (figure 9).[121,122]

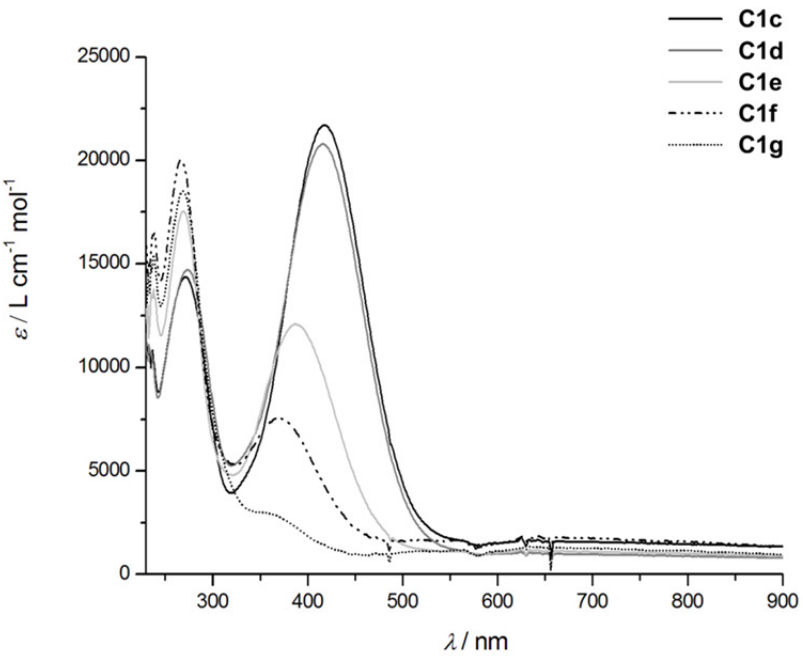

Figure 8. Cumulated absorption spectra of the push-pull systems **C1c – C1g**.

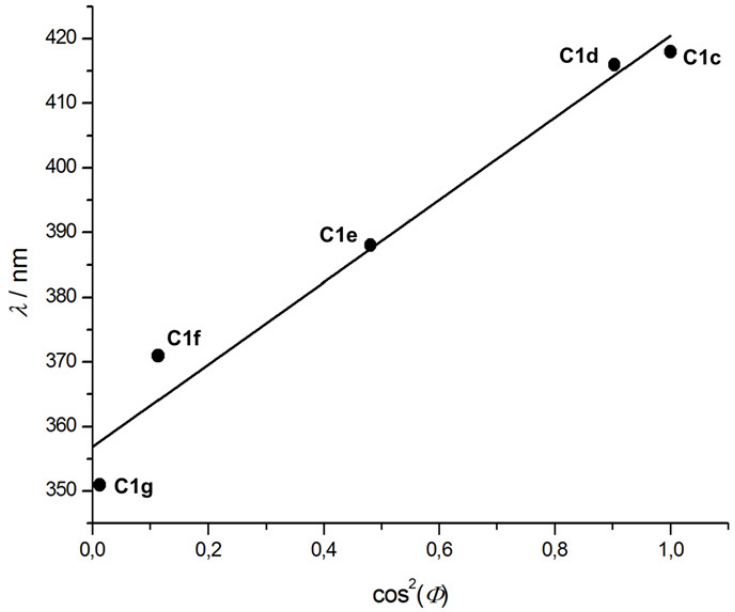

Figure 9. Correlation of λ_{max} to the calculated $\cos^2(\Phi)$.

This correlation beautifully illustrates the dependence of the conjugation to the torsion angle Φ in such biphenyl systems.

Quadratic Response

The molecular μβ values were measured using an EFISH setup.[125] Multiple measurements were performed for each molecule with different concentrations. The experimental results are shown in table 4. The experimental uncertainties vary from 5% to 15% as the signal level intensities decrease except for **C1b** for which the spread in repeated measurements was unusually large. The numerical simulations were performed with the MOPAC 2002 program[123] using the AM1 semi-empirical Hamiltonian.[124] The permanent ground state dipole moments and the zero frequency hyperpolarizability tensor components obtained for the resulting equilibrium geometry have been combined to yield the theoretical μβ values listed in table 4, together with the optimized inter-aryl torsion angle. The predicted response is consistently 30% below the experimental values extrapolated to zero frequency with the dispersion relation of the two-level model[55] using the CT-band frequencies deduced from the UV/Vis absorption spectra.

Table 4. Experimental EFISH results, Two-Level-System extrapolated zero frequency values, and MOPAC 2002 predictions with the AM1 Hamiltonian expressed in 10^{-48} esu.

compound	$\mu\beta$(1.907μm)	$\mu\beta$(0) from TLS	$\mu\beta$(0) by AM1	torsion angle[a]
C1a	245±15	190	136	38.4°
C1b	70±35	55	83	58.4°
C1c	410±40	300	192	0.1°
C1d	400±20	295	163	18.1°
C1e	230±10	180	132	46.1°
C1f	130±20	105	76	70.3°
C1g	75±10	60	62	83.5°

[a] Equilibrium position torsion angle.

This trend is not followed by the open dimethyl compound (**C1b**) nor by the one containing the longest bridge (**C1g**): the dynamical variations in torsion angles driven by solvent motion are the most likely explanations for these exceptions. Indeed, especially for compound **C1b**, the equilibrium geometry corresponds to the lowest torsion angle, i.e. the best conjugation, compatible with the steric constrains. In this situation, the calculations will overestimate the

actual response because less favorable geometries are not taken into account. It is noteworthy that the 2,2'-dimethyl biphenyl building block has already been integrated in molecular devices to tailor electronic transport properties.[76,126] In these compounds the interring torsion angle of the 2,2'-dimethyl biphenyl subunit was found to be close to 90°, at least in the solid state. Assuming a comparable torsion angle Φ for **C1b**, the measured and calculated values would be shifted horizontally to $\cos^2\Phi = 0$ and would fit nicely with the linear regression calculated for the remaining members of the series.

The quadratic NLO responses have been plotted as a function of the $\cos^2\Phi$ of the equilibrium torsion angle in figure 10. The finite frequency, zero frequency, and finite field results give rise to nearly linear progressions, if we overlook the values for compound **C1b** as argued above.

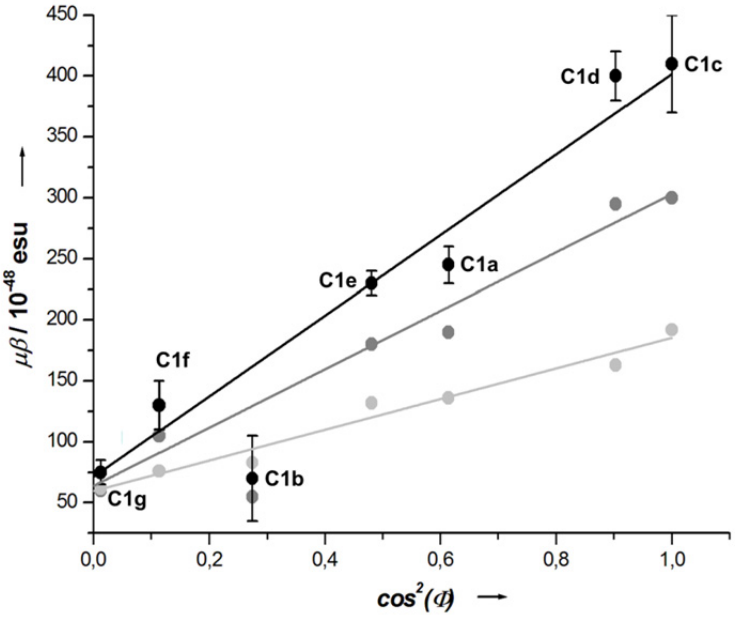

Figure 10. Quadratic nonlinear response as a function of the calculated equilibrium torsion angle Φ. *black*: EFISH results. *gray*: scaled results. *Light gray*: MOPAC 2002 predictions with the AM1 Hamiltonian. The values of compound **C1b** were not considered for the least squares fits displayed by the solid lines.

The finite frequency measurements include the dispersion effect resulting from the shifts in transition energies of the absorption bands, but, because of the excitation wavelength used, it is hardly discernable in the plot. In any case, the fact that the dispersion corrected results follow the $\cos^2\Phi$ law almost as well as the calculated values is an indication that it is the overlap between the π_z orbitals of the central carbon atoms which is the relevant parameter. Since the absorption bands at short wavelengths show much less dependence on torsion angle

than the CT bands, we may assume that the two-level model should be able to account for the observed trend. In this model, the quadratic response is proportional to the product of the oscillator strength, the change in dipole moment upon excitation, and the ground state dipole moment. We are thus led to the conclusion that the dominant effect of increasing torsion angles lies in the resulting loss of oscillator strength while the permanent dipoles of the ground and the CT states are affected to a lesser degree.

Conclusions

To provide a series of push-pull systems which vary in the extend of π-conjugation of their central chromophores, a universal synthetic route towards terminal piperidinyl and nitro functionalized biphenyls comprising a restricted interring torsion angle due to an interlinking chain of various length between the 2 and 2' position was developed. By following the most straightforward synthetic pathway **E** – **F**, target molecules **C1a** – **C1g** were synthesized, starting from the corresponding dibromo or ditriflate derivatives **C2a** – **C2g** in only three steps (scheme 7). Conditions for a *Hartwig-Buchwald* hetero-cross-coupling reaction to exchange the bromide and triflate substituents to amino groups were developed with the biphenyl model compound **C2a**, using benzophenone imine as an ammonia synthon. Similar reaction conditions were subsequently successfully applied to all biphenyl dihalides **C2b** – **C2e** and ditriflates **C2f** and **C2g**, providing the corresponding diamines **C3a** – **C3g** in good yields. Furthermore, a microwave-assisted azacycloalkylation allowed the rather selective and inexpensive assembly of a piperidine ring at only one terminal amine group of the diaminobiphenyls **C3a** – **C3g**. By systematic solvent-screening encouraging selectivities and moderate conversions were reached with all diamines to provide the amino-piperidinyl derivatives **C7a** – **C7g**. Finally, a mild and selective oxidation of aminobiphenyls bearing a piperidinyl donor-group was developed and applied successfully to the synthesis of the model compounds **C1a**, **C1b** and **C1d** – **C1g**. The series was complemented by the dimethylfluorene derivative **C1c** which was assembled by an alternative route. The NLO properties of this series of torsion angle restricted biphenyl based push-pull systems have been successfully investigated by EFISH measurements. The results agree qualitatively with semi-empirical simulations based on the AM1 Hamiltonian. In particular, the linear dependence of the quadratic response on the $\cos^2\Phi$ of the inter-aryl dihedral angle points to oscillator strength loss as the dominant effect of increasing backbone twist, which would indicate that the change in permanent dipole moment upon CT transition is much less affected. To probe this aspect will require to conduct experiments where the chromophores are excited at resonance such as

two-photon absorption cross-section measurements. It will then be of interest to see how more sophisticated electronic structure calculations will fare in describing the effect of the gradual twist of the conjugation path.

Racemization Dynamics of Torsion Angle Restricted Biphenyl Push-Pull Cyclophanes

Jürgen Rotzler, Heiko Gsellinger, Markus Neuburger, David Vonlanthen, Daniel Häussinger and Marcel Mayor

Org. Biomol. Chem. **2011**, *9*, 86 – 91.

Introduction

Despite the fact that great progress in understanding the influence of different structural parts of such push-pull systems on the nonlinear optical activity has been made and molecules with large hyperpolarizabilities have been published,[127–129] the transformation of this on the microscopic scale NLO active molecules to the macroscopic level still causes serious problems towards their application.[130] Two main physical properties are crucial for a strong nonlinear optic response, which are a large hyperpolarizability of the chromophore and a noncentrosymmetric centre. This molecular noncentrosymmetry, which can be obtained by rational design of nonlinear optic active compounds, can be transferred to the macroscopic scale by an external physical input. Examples include the application of an electric field to cause a noncentrosymmetric arrangement of dissolved dipoles[131,132] (EFISH: electric-field-induced second-harmonic generation measurements) or the incorporation of the push-pull systems into noncentrosymmetric structures such as poled polymer films, self-assembled films[133] or crystals.[134–136] It is also known that crystal packing or supramolecular assembly of such materials can enhance the physical output dramatically.[137,138]

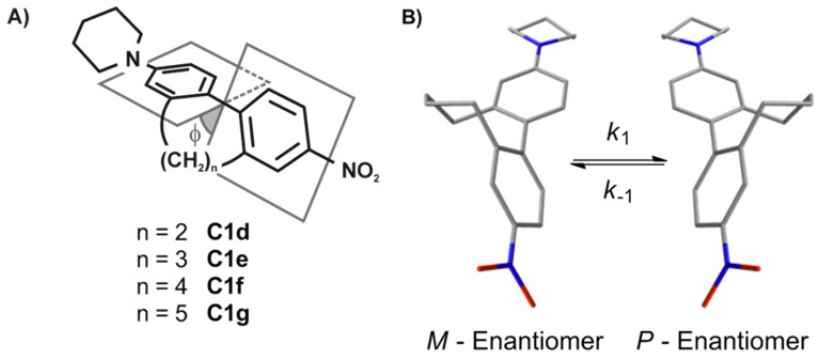

Figure 11. A) Sketch of the concept to restrict the interphenyl torsion angle by an additional interlinking alkyl chain of various length; B) The two atropisomers of **C1f** (structures calculated with a MM2 basic set) and the rotation around the central C-C bond showing the atropisomerization reaction.

The investigated in 2 and 2' position alkyl-bridged biphenyl-based cyclophanes **C1d – C1g** are axial chiral and therefore consist of a racemic mixture of two atropisomers (figure 11). In crystallography it is well known that optical pure enantiomers tend to crystallize in noncentrosymmetric point groups, whereas racemic mixtures especially of donor-π-acceptor molecules crystallize in a centrosymmetric fashion since their dipoles force such an arrangement (figure 12). Therefore the described push-pull systems **C1d – C1g** are potential candidates to realize such a transformation of the noncentrosymmetry from a molecular level to the macroscopic scale by enantiomeric resolution and subsequent crystal growth.

To gain further insight into the conformational stability of the nonlinear active cyclophanes **C1d – C1g** and to check if it is possible to separate the two atropisomers, the rotation barrier around the central C-C bond moved into the focus of interest.

For such thermodynamic studies mainly three different experimental methods are applicable. Coalescence measurements by ^{1}H-NMR,[139] dynamic chromatography[140–144] and monitoring the change in the optical rotation of a chiral non-racemic mixture. For the latter, separated enantiomers are required, whereas the first two methods can easily be performed using racemic mixtures of the molecules under investigation. Fast dynamic molecular processes can be investigated by NMR spectroscopy, whereas dynamic chromatography is more suitable for isomerization studies of more conformationally stable compounds. Herein the enantiomerization dynamics of torsion angle restricted biphenyl push-pull cyclophanes **C1d – C1g** are reported to obtain further insight about their dynamic behavior and the interaction of the two phenyls under these conditions.

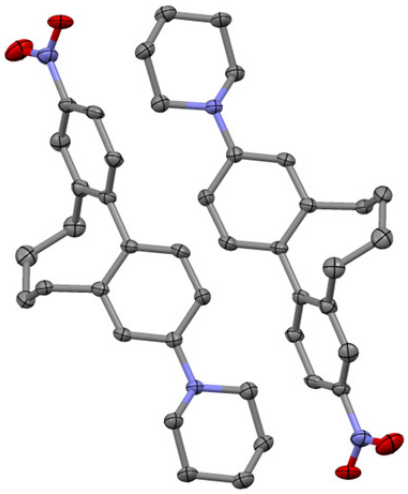

Figure 12. Centrosymmetric pairwise arrangement of the *P* (right) and *M* (left) atropisomers of the push-pull derivative **C1f** in the solid state.

Materials and Methods

Solid State Structure

Single crystals of cyclophane **C1f** suitable for X-ray analysis were obtained upon slow evaporation of a solution of **C1f** in a mixture of *i*PrOH and hexane. The racemic mixture of **C1f** crystallized in the monoclinic, centrosymmetric space group C 2/c. One unit cell consists of 8 molecules with alternating *M* and *P* enantiomers of **C1f** (figure 12). In figure 13 an ORTEP presentation of the *P* enantiomer of **C1f** is displayed. (Detailed information about the crystal structure are given in the experimental section.)

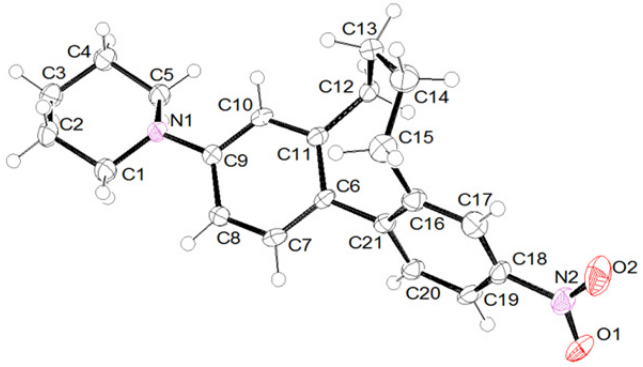

Figure 13. Solid state structure of the *P* enantiomer of **C1f**. Thermal ellipsoids are set at the 50% probability level.

NMR-Studies

Samples of **C1e** (10 mM) were prepared in deuterated solvents (>99.8% D, Cambridge Isotope Laboratories, Burgdorf, CH). All NMR experiments were performed on a Bruker DRX-600 NMR spectrometer, equipped with a self-shielded *z*-axis pulsed field gradient dual broadband inverse probe-head. Chemical shifts were referenced to residual solvent peaks and the temperature was calibrated using a methanol sample.[145] To ensure thermal equilibrium at the various temperatures, at least 15 min of equilibration time was allowed for each temperature step. Unambiguous resonance assignment was obtained by two-dimensional COSY, NOESY and HMQC experiments. The acquisition in the direct dimension was performed using 2048 points (170 ms) in all cases. For the indirect dimension 512 increments were measured, corresponding to 85 ms, 85 ms and 40 ms, respectively. The NOE mixing time was set to 1 s. The total experiment times were 60 min, 93 min and 20 min, respectively. For each solvent, several experiments with 10 K temperature steps were performed in order to estimate the

coalescence temperature. The activation energy was calculated from the following form of the *Eyring* equation (5):

$$\Delta G^{\ddagger} = 0.0191 \cdot T_c \cdot (9.97 + \log(T_c/\Delta v) \qquad (5)$$

Dynamic HPLC

For the determination of the free energy of rotation $\Delta G^{\ddagger}$ around the central C-C bond of the biphenyl-based push-pull system **C1f** temperature dependent dynamic HPLC was performed. An approximately 1 mg/mL solution of compound **C1f** in *i*PrOH was prepared. 1 µL of this solution was injected into a chiral Chiralpak AD-H column (0.46 x 25 cm; Daicel Chemical Industries Ltd.) at the defined temperature (CTO-10AS VP oven from Shimadzu). The atropisomers were eluted with a mixture of 97:3 of *n*-hexane and *i*PrOH (SCL-10A VP HPLC from Shimadzu) at a flow rate of 0.5 mL/min. To guarantee an efficient mixing of both solvents the eluent was prepared as a 94:6 mixture of *n*-hexane and *i*PrOH/*n*-hexane 1:1. This premixing procedure turned out to be required due to the poor solubilty of **C1f** at low concentrations of *i*PrOH in *n*-hexane. For detection of the chromatogram an UV/Vis detector (SPD-M10A VP from Shimadzu) operating at the absorption maxima of the compound under investigation was used (λ_{max} = 270 nm and 371 nm). The column was preconditioned for 10 h under the conditions used for dynamic HPLC experiments before a set of temperature dependent measurements was performed. The studies were performed at temperatures between 10°C and 25°C in 5°C steps. Three different samples of **C1f** were measured twice in a row. The forward reaction rate constants k_1 were evaluated with the unified equation[146] valid for such first order processes by direct integration of the elution profiles to the software program DCXplorer[147] developed by Trapp. The Gibbs free activation energy $\Delta G^{\ddagger}(T)$ was calculated by estimation of the activation enthalpy $\Delta H^{\ddagger}$ of the enantiomerization process from the slope of the *Eyring* plot (ln (k_1/T) vs. $1/T$) and the activation entropy $\Delta S^{\ddagger}$ from the intercept.

Results and Discussion

The interconversion of the two atropisomers of cyclophanes **C1d – C1g** can be monitored by NMR coalescence experiments if the half lifes of the enantiomers are in the range of microseconds to seconds. In this case, at temperatures below the coalescence temperature, the exchange between the two enantiomeric forms is slow compared to the NMR time scale ("slow exchange") and the diastereotopic protons on a CH_2-group in the alkyl-bridge have

different chemical environment and, hence, give rise to two separate signals. In contrast, at temperatures higher than the coalescence ("fast exchange"), an averaged signal is observed for the two methylene protons. Determination of the coalescence temperature and the difference in chemical shift of the diastereotopic methylene protons allows calculation of the Gibbs free activation energy for the racemization at the coalescence temperature, $\Delta G^{\ddagger}(T_c)$ using a modified form of the *Eyring* equation (equation (5)). In order to compare the appropriate chemical shifts, it is necessary to have an unambiguous assignment for all protons of the cyclophanes in the slow exchange regime. This was accomplished by two-dimensional proton-proton and proton-carbon correlation experiments (COSY, NOESY, HMQC).

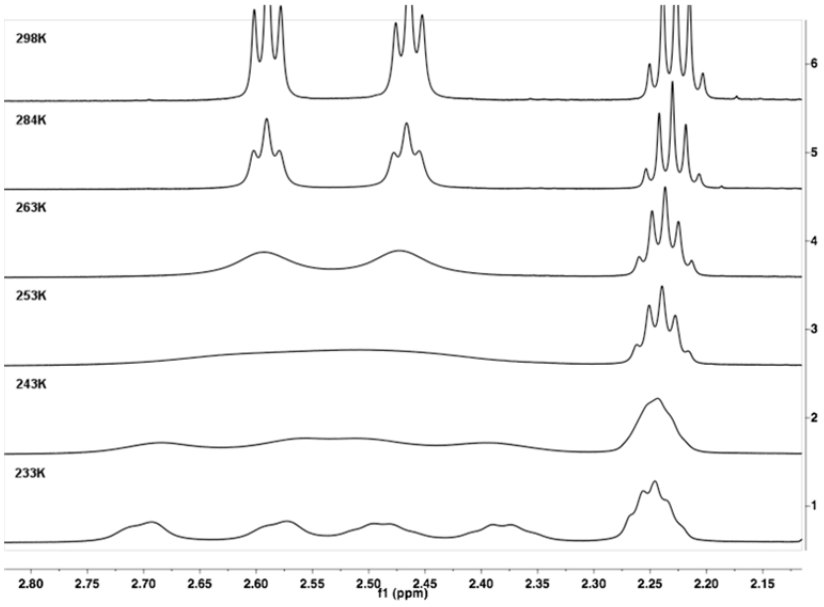

Figure 14. Stacked plot of the low temperature NMR spectra of **C1e** measured in $CDCl_3$. Starting from fast exchange at 298 K reaching the coalescence temperature at 252 K ending in the slow exchange at 233 K where the signals for the four protons are separated.

The coalescence temperature (T_c) of the push-pull system shown in figure 14 (**C1e**) was measured in different solvents to obtain changes in the activation energy due to solvent effects. As the chemical shifts for **C1e** can be solvent dependent, the coalescence temperature must also show a variation with the solvent, even in the case of unchanged activation parameters. It is, however, possible that differences in the solvation of the sterically demanding transition state of the racemization lead to differences in the activation energy. The results of the measurements of **C1e** in different solvents are shown in table 1.

It was possible to record NMR spectra below and above as well as exactly at the coalescence temperature for most solvents used. Only the melting point of benzene was too high so that

further cooling was not feasible. For toluene, two T_c for two different sets of resonances were observed. The two different data sets led to the very same activation energy, as expected. As seen in table 1, the influence of different solvents on the activation energy is not very pronounced.

Table 1. Coalescence temperatures of the push-pull system **C1e** (figure 1) in different solvents with their characteristic separation $\Delta\nu$ and the resulting Gibbs activation energy.

Solvent	T_c / K	$\Delta\nu$ / Hz	$\Delta G^{\ddagger}$ / kJ/mol	$\Delta\Delta G^{\ddagger}$
DMF d7	249	144	48.5	±0.5
Toluene d8	248	102	49.0	±0.5
Toluene d8	242	60	48.9	±0.5
Benzene d6	--	--	--	--
TFA d1	278	180	53.9	±0.5
MeOD d4	257	174	49.8	±0.5
$CDCl_3$	252	120	49.6	±0.5
$C_2D_2Cl_4$	250	108	49.3	±0.5

The polarity of the solvent does not seem to significantly influence the activation energy for the interconversion of the enantiomers. Only in the case of strongly protic conditions (trifluoroacetic acid), a significantly higher activation energy was obtained. This is most likely due to the protonation of the amino group, leading to a pull-pull, rather than a push-pull substitution pattern. In a pull-pull system the tendency to form a conjugated and, therefore, nearly planar arrangement will be less pronounced compared to the push-pull case, where this resonance stabilization factor determinates the racemization energy.[148] Additionally two electron-withdrawing groups reduce the π-electron density at the 1 and 1' positions which makes an out-of-plane bending of the axis bond more difficult and therefore becomes the dominating contribution to the energy barrier.[149,150] In turn, a higher activation is necessary to force the cyclophane to racemization.

In the case of the ethyl-bridged biphenyl **C1d**, it was not possible to lower the temperature far enough (<230 K) to reach the coalescence in any solvent. In marked contrast, for compounds **C1f** and **C1g** there was no fast exchange regime obtained, even when heating was continued to 353 K in deuterated tetrachloroethane, what is consistent with findings of earlier studies on unsubstituted biphenyl cyclophanes.[151,152] In addition 2D-EXSY experiments at the elevated temperature indicated, that the rate constant of the atropisomerization had to be below 10^{-2} s^{-1}.[153]

As mentioned above it was not possible to determine the rotation barrier of the C-C bond of the butyl- and pentyl- bridged biphenyl derivative **C1f** and **C1g** by coalescence measurements using ^{1}H-NMR spectroscopy. Careful analysis of the ^{1}H-NMR spectra clearly showed a fixed torsion angle for both push-pull systems. Another useful method to estimate isomerization energies in cases where NMR spectroscopy fails is dynamic chromatography.[140–144] As previously described for such investigations only minute sample amounts are required and stereoisomers do not have to be isolated prior to the analysis. A chromatogram with two separated peaks is expected in the case of a fixed torsion angle of the compounds under investigation when they are separated on a chiral stationary phase. When racemization occurs on the chromatographic time scale a temperature dependent plateau formation between the two peaks is expected. A third case that can occur in dynamic HPLC is peak coalescence. This occurs when the enantioconversion is significantly faster than the chromatographic separation process.[154] Hence it was tried to separate the two atropisomers of **C1f** and **C1g** by chiral HPLC. Screening of several cellulose- and amylose-derived HPLC columns revealed that the enantiomers of **C1f** showed a tendency to separate on Chiralpak AD-H. At 20°C the two peaks could be separated by approximately 2 min when the compound was eluted with a mixture of *n*-hexane:*i*PrOH 97:3 at a flow rate of 0.5 mL/min. Furthermore, plateau formation between the two peaks was observed pointing at the expected interconversion process of atropisomers (figure 16). The UV/Vis spectra of the two distinctive peaks in the chromatogram and the plateau were the same (figure 15), indicating the presence of only one compound and therefore verifying the presence of two atropisomers. The rate constant of enantioconversions can be directly calculated from these typical chromatograms by iterative comparison of experimental and simulated chromatograms.

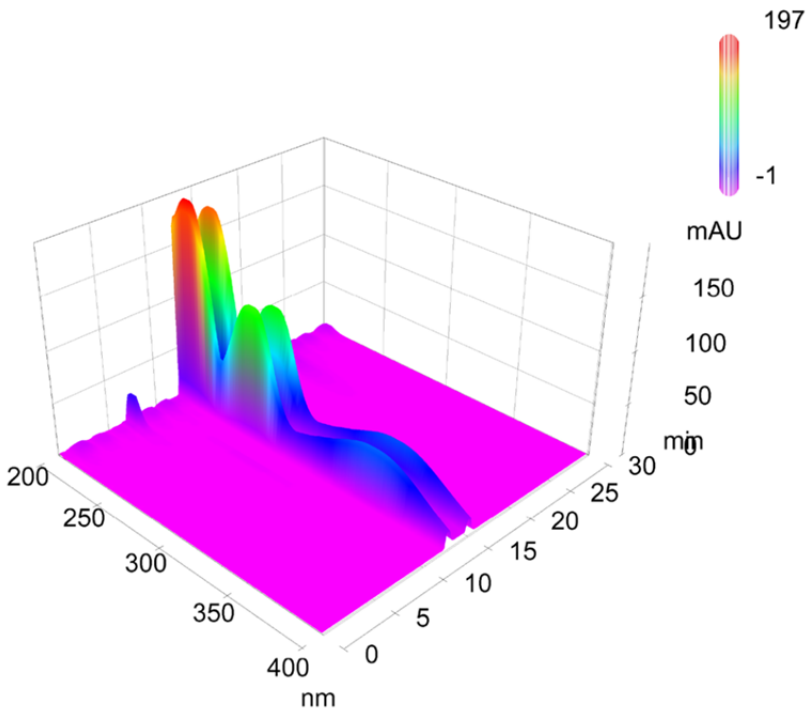

Figure 15. Representative chromatogram of push-pull cyclophane **C1f**, separated by a Chiralpak AD-H column eluting with a mixture of *n*-hexane:*i*PrOH 97:3 and a flow rate of 0.5 mL/min at 25°C. In the third dimension the UV/Vis spectra of the separated parts are shown.

Thanks to the remarkable work of Schurig[142] and Trapp[147,155] powerful computer simulation tools are now available. The simulation programs profit from the so called theoretical plate model,[141] its statistical description namely the stochastic model[155] or more recently the unified equation[146] to determine the rate constants of enantiomerization. Temperature dependent dynamic chromatography gives access to thermodynamic data by applying the *Eyring* equation (6).

$$k_1 = (k_B T)/h \cdot \exp(-\Delta G^{\ddagger}/RT) \qquad (6)$$

Thus temperature dependent dynamic HPLC experiments were performed for compound **C1f**. Repeated series of measurements were performed between 10°C and 25°C in 5°C steps. To overcome reproducibility problems the column was preconditioned for 10 h operating at the desired conditions. After two series the conditioning was repeated and the measurements were then performed again with a different sample of the same compound. A statistical evaluation was then performed. Peak coalescence or baseline separation were not observed in this temperature range. By computer simulations, using the DCXplorer software,[147] of the experimentally obtained elution profiles (figure 16) the enantiomerization rate constants at

different temperatures were obtained (table 2). Since enantiomerizations are degenerate processes k_1 and k_{-1} were assumed to be equal.

Table 2. Kinetic data of **C1f** obtained from the elution profiles by comparison of simulated and experimental elution profiles.

T / K	298.2	293.2	288.2	283.2
k_1[a] / s^{-1}	$9.25 \cdot 10^{-4}$	$6.44 \cdot 10^{-4}$	$4.21 \cdot 10^{-4}$	$2.75 \cdot 10^{-4}$

[a] average values of five repeated measurements.

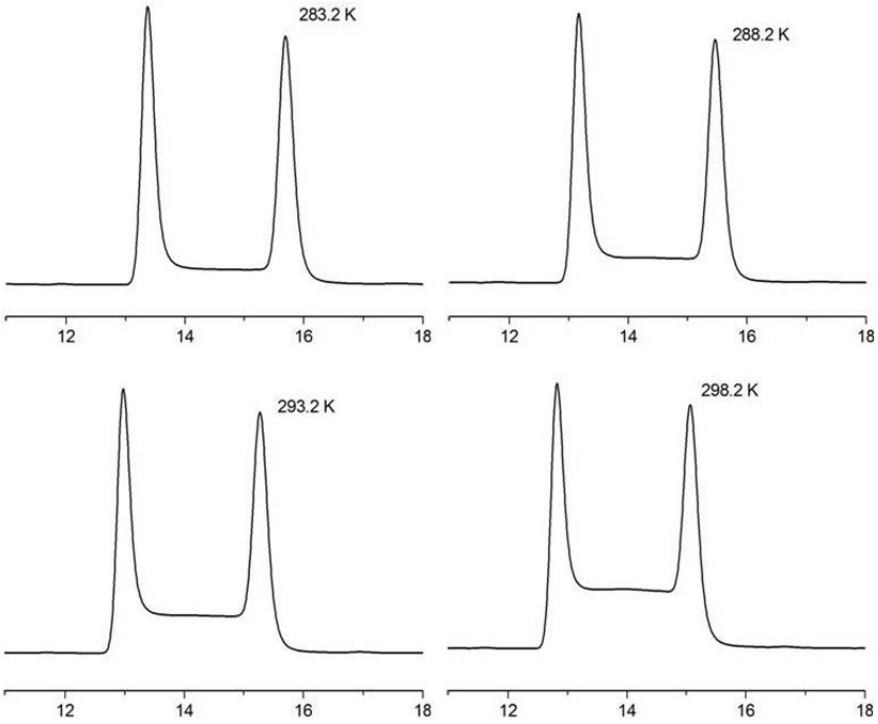

Figure 16. Selected experimental enantiomerization profiles of push-pull cyclophane **C1f** at different temperatures on Chiralpak AD-H using a mixture of *n*-hexane:*i*PrOH 97:3 as eluent.

The with the unified equation obtained enantiomerization rate constants of **C1f** were plotted according to the *Eyring* equation ($\ln(k_1/T)$ versus $1/T$). By linear regression analysis (figure 17), $\Delta H^{\ddagger}$ was found to be $\Delta H^{\ddagger} = 54.5 \pm 3.9$ kJ/mol and $\Delta S^{\ddagger} = -120 \pm 14$ J/(K mol). From this $\Delta G^{\ddagger}$ was calculated to be $\Delta G_{298K}{}^{\ddagger} = 90.3 \pm 0.2$ kJ/mol which is in the region of 2-phenyl-2'-isopropylbiphenyl and 2-cyclohexyl-2'-phenylbiphenyl (both approx. 91 kJ/mol) but above the rotational energy barrier of 2,2'-dimethylbiphenyl (approx. 78 kJ/mol) and below that of of 2,2'-diisopropylbiphenyl (approx. 110 kJ/mol) reported by Wolf.[156]

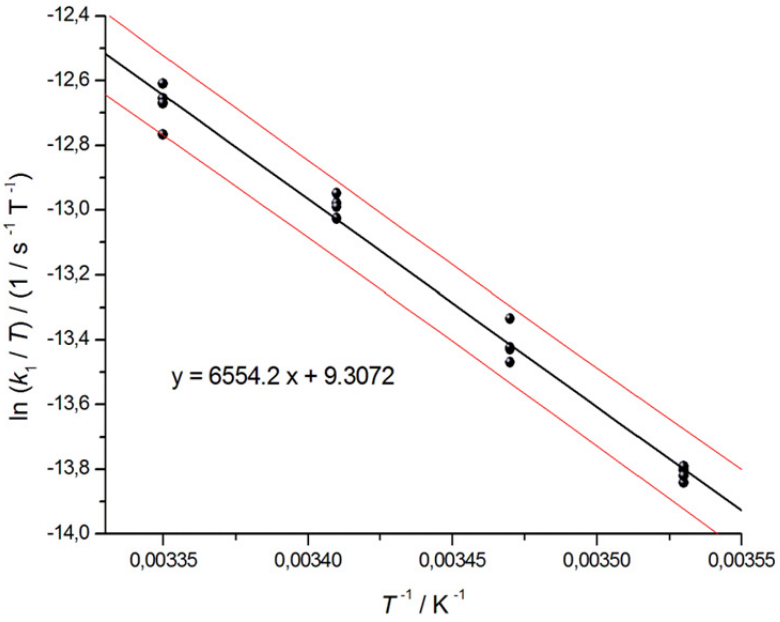

Figure 17. *Eyring* plot for the atropisomerization of **C1f**: temperature dependent dynamic HPLC measurements analysed by linear regression. The upper and lower curves represent the error bands of the linear regression with a level of confidence of 95%. For the linear regression, four measurements for each temperature were considered.

Unfortunately such an investigation for the pentyl-bridged biphenyl-based push-pull system **C1g** was not possible by dynamic chromatography as coalescence was observed even at low temperatures. Thus an enantioconversion faster than the chromatographic separation process can be assumed. Since ^{1}H-NMR coalescence measurements showed a fixed conformation of the two phenyls of compound **C1g** it is obvious that the free energy of rotation is between 50 kJ/mol obtained for the 7-membered ring derivative **C1e** and 90 kJ/mol obtained for the 8-membered cyclophane **C1f**.

By comparison of the rotational energy barriers of the torsion angle restricted biphenyl-based push-pull cyclophanes **C1d** – **C1g** it is obvious that the butyl-bridged system **C1f** is the conformational most stable compound of the series followed by the pentyl-bridged derivative **C1g**. Compound **C1f** atropisomerizes with a half life time $\tau_{1/2}$ of 12.5 min which means that this compound can be assumed to have a fixed torsion angle in most physical investigations such as EFISH measurements. For the propyl-bridged push-pull system **C1e** this is not the case since the energy barrier for atropisomerization is relatively low and therefore, depending on the time frame of the experiment, isomerization can take place during measurements which would lead to a distribution of different torsion angles and therefore to an averaged torsion

angle over the course of the experiment. The same is true for the ethyl-bridged derivative **C1d** which is even more flexible than **C1e**.

To explain this rather unexpected grading in enantiomerization energies, we hypothesize a sterically more crowded transition through a planar, linear conformation in the isomerization process. Linearity of the biphenyl core can be assumed since partial double-bond character of the central C-C bond was observed in the crystal structure of the in 2 and 2' position unsubstituted push-pull system. This means that the longer the alkyl-bridge, the closer the methylene groups have to pass by each other in the planar conformation. The pentyl-bridge in system **C1d** seems to have too many degrees of freedom and hence it can arrange in a sterically more favorable fashion to allow isomerization in an energetically more convenient way.

Conclusion

In summary, the rotational energy barrier of **C1e** (3-nitro-9-(piperidin-1-yl)-6,7-dihydro-5*H*-dibenzo[*a*,*c*]cycloheptene) was estimated to be $\Delta G_{298K}^{\ddagger} = 50$ kJ/mol by ^{1}H-NMR coalescence measurements. Using computer simulation of experimentally obtained temperature dependent dynamic HPLC elution profiles the barrier of rotation of **C1f** (3-nitro-10-(piperidin-1-yl)-5,6,7,8-tetrahydrodibenzo[*a*,*c*]cyclooctene) was determined to be $\Delta G_{298K}^{\ddagger} = 90$ kJ/mol. The rotational energy barrier of **C1d** (1-(7-nitro-9,10-dihydrophenanthren-2-yl)piperidine) and **C1g** (3-nitro-11-(piperidin-1-yl)-6,7,8,9-tetrahydro-5*H*-dibenzo[*a*,*c*]cyclo-nonene) could only be evaluated qualitatively by comparison of them with the two quantitatively analysed derivatives **C1e** and **C1f**.

Unfortunately the separation of the two atropisomers failed for all nonlinear optic active compounds **C1d** – **C1g** and thus it was not possible to grow noncentrosymmetric crystals. Nevertheless, we obtained insight in the conformational stability of our systems **C1d** – **C1g**. For compound **C1d** the rotation around the central C-C bond is rather fast and so the system has to be considered to be flexible. Also the rotation around the central axis of the propyl-bridged push-pull cyclophane **C1e** is quite fast at room temperature. Depending on the physical experiment compound **C1f** and **C1g** can be assumed as torsion angle fixed systems when the experimental timescale is in the region of seconds. Nevertheless the maximal possible torsion angle was defined by bridging the biphenyl core with alkyl chains. Motivated by this results it will now be of interest to determine the rotational energy barrier of 2,2'-alkyl-bridged and in 4 and 4' position donor substituted biphenyl systems and 4,4'-diacceptor

substituted biphenyl systems which are available in our group and have already been investigated in single molecule conductance measurements.[157,158,159]

Experimental Section

General Remarks: All chemicals were directly used for the syntheses without purification if not stated otherwise. Dry solvents were purchased from Fluka. The solvents for chromatography and extractions were distilled before use. When Schlenk-technique was used the solvents were degased with argon for several minutes. Characterizations were performed with the following instruments: ^{1}H-NMR and ^{13}C-NMR spectra were recorded with a Bruker DPX-NMR (400 MHz) or a Bruker BZH-NMR (250 MHz), the J values are given in Hz (J ± 0.1 Hz). Mass spectra were recorded on an esquire 3000 plus (Bruker) for Electron Spray Ionization (ESI), a finnigan MAT 95Q for Electron Impact (EI) or a Voyger-DeTM Pro for MALDI-ToF; measured in m/z (%).The elementary analyses were measured on an Analysator 240 from Perkin-Elmer. The absorption spectra were recorded on an Agilent 8453 Diode Array Spectrophotometer using 1 cm cuvettes (10^{-5} M solutions in chloroform). The measurements were performed at room temperature. λ_{max} (relative intensity, %) was measured in nm. For column chromatography silica gel 60 (40-63 μm) from Fluka was used. TLC were carried out on Silica gel 60 F254 glass plates with a thickness of 0.25 mm from Merck. Elementary analyses of the diamines **C3f** – **C3g** were obtained from the TFA salts of these compounds. This was not possible for the amines **C7a** – **C7g** due to the air sensitivity of these compounds.

EFISH-Measurements: The excitation source was a Nd: YAG laser, actively Q-switched at 10 Hz, emitting 7 ns pulses at 1.064 μm wavelength. In order to avoid absorption of the fundamental and second harmonic beams, the pulses were Raman-shifted to 1.907 μm through a high pressure hydrogen cell, bringing the second harmonic signal to 953 nm, beyond the absorption band of the studied molecules. The nonlinear signal was selected using an appropriate interferential filter placed before a photomultiplier.

In order to determine the absolute value of the second harmonic generation, a quartz wedge as a reference was used,[55] taking its quadratic susceptibility $d_{11} = 1.2 \cdot 10^{-9}$ esu at 1.064 μm and extrapolating it to $1.1 \cdot 10^{-9}$ esu at 1.907 μm. The molecules in chloroform were oriented by an electrical pulse of 2 kV/mm amplitude and of 5 μs duration synchronized to the laser excitation.

Solid State Structure: Crystal data and structure refinement for cyclophane **C1f**: The crystal was measured on a Bruker Kappa Apex2 diffractometer at 123 K using graphite-monochromated Mo K_α-radiation with λ = 0.71073 Å, Θ_{max} = 27.655°. Minimal/maximal transmission 0.99/0.99, μ = 0.08 mm^{-1}. 1c formula $C_{21}H_{24}N_2O_2$, M = 336.43 g/mol, F(000) = 1440, yellow block, size 0.070 · 0.130 · 0.290 mm^3, monoclinic, space group C 2/c, Z = 8, a = 25.437(6) Å, b = 10.510(2) Å, c = 17.615(5) Å, α = 90°, β = 132.55(2)°, γ = 90°, V = 3469.1(18) $Å^3$, $D_{calc.}$ = 1.288 $Mg \cdot m^{-3}$. The Apex2 suite has been used for data collection and integration. From a total of 21978 reflections, 4017 were independent (merging r = 0.111). From these, 2392 were considered as observed ($I>2.0\sigma(I)$) and were used to refine 226 parameters. The structure was solved by direct methods using the program SIR92. Least-squares refinement against F was carried out on all non-hydrogen atoms using the program CRYSTALS. R = 0.0533 (observed data), wR = 0.1511 (all data), GOF = 1.0519. Minimal/maximal residual electron density = -0.31/0.33 e $Å^{-3}$. Chebychev polynomial weights were used to complete the refinement. Plots were produced using CAMERON.

Representative Procedure A (*Syntheses of the Diamino-derivatives* (C3)):[107] Toluene was degased in an oven-dried Schlenk-tube. In a Schlenk-tube $Pd_2(dba)_3 \cdot CHCl_3$ (4 mol%) and BINAP (12 mol%) were dissolved in degased toluene (0.16 M with respect to the dibromobiphenyl). The black solution was stirred for 15 min at rt, while dibromobiphenyl (**C2**) (1.00 equiv.) and NaO*t*Bu (2.80 equiv.) were added. To this dark-red solution benzophenone imine (2.40 equiv.) was added dropwise. The red reaction mixture was stirred at 80°C until the starting material was consumed as monitored by TLC. Afterwards, the mixture was cooled to rt and diluted with ether (4 × volume of toluene). The suspension was filtered over celite and concentrated under reduced pressure. The crude was purified by recrystallization from methanol to afford *N*,*N*-bis(diphenylmethylene)biphenyl-diamine (**C8**) as a yellow solid. Diimine **C8** (1.00 equiv.) was dissolved in THF (0.15 M) and 3 M aq. HCl (30% by volume of THF) was added. The pale yellow reaction mixture was stirred at rt until the starting material was consumed as monitored by TLC. Afterwards the solution was partitioned between 0.5 M aq. HCl and hexane:EtOAc (2:1). The organic layer was washed three times with 0.5 M aq. HCl and the combined aqueous layers were made alkaline with 1 M aq. NaOH. The brown liquid was extracted with dichloromethane, dried with sodium sulfate, filtered and concentrated *in vacuo*. The crude was purified by column chromatography (SiO_2; hexane:EtOAc 1:1, 5% NEt_3) to afford diamine **C3**.

Benzidine (C3a): From 4,4'-Dibromobiphenyl (200 mg, 1.00 equiv., 0.641 mmol) (**C2a**), 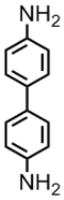 $N^4,N^{4'}$-bis(diphenylmethylene)biphenyl-4,4'-diamine (**C8a**) (177.5 mg, 54%) was obtained as a yellow solid after purification by column chromatography (SiO_2; hexane:EtOAc 5:1, 5% NEt_3) and recrystallization from methanol. Diimine **C8a** (73.0 mg, 1.00 equiv., 0.142 mmol) was cleaved following general procedure A to achieve benzidine (**C3a**) (21.5 mg, 82%).

C8a: $\boldsymbol{R_f}$ = 0.24 (SiO_2; hexane:EtOAc 5:1, 5% NEt_3); **m.p.** 237 – 239°C; **^{1}H-NMR** (400 MHz, $CDCl_3$): δ = 7.75 (d, ^3J(H,H) = 7.0 Hz, 4H), 7.47 (t, ^3J(H,H) = 7.3 Hz, 2H), 7.41 (m, 4H), 7.34 (d, ^3J(H,H) = 8.5 Hz, 4H), 7.30 – 7.24 (m, 6H), 7.18 – 7.12 (m, 4H), 6.75 (d, ^3J(H,H) = 8.5 Hz, 4H) ppm; **^{13}C-NMR** (101 MHz, $CDCl_3$): δ = 168.6 (C_q, 2C), 150.5 (C_q, 2C), 140.2 (C_q, 2C), 136.7 (C_q, 2C), 135.9 (C_q, 2C), 131.1 (C_t, 2C), 130.0 (C_t, 4C), 129.8 (C_t, 4C), 129.1 (C_t, 2C), 128.6 (C_t, 4C), 128.5 (C_t, 4C), 127.0 (C_t, 4C), 121.9 (C_t, 4C) ppm; **MS** (MALDI-ToF): m/z (%) = 514 (25), 513 (53), 512 (100); **elemental analysis** calcd (%) for $C_{38}H_{28}N_2$: C 89.03, H 5.50, N 5.46; found: C 88.81, H 5.67, N 5.23.

C3a: $\boldsymbol{R_f}$ = 0.26 (SiO_2; hexane:EtOAc 1:1, 5% NEt_3); **m.p.** 118°C; **^{1}H-NMR** (400 MHz, $CDCl_3$): δ = 7.34 (d, ^3J(H,H) = 8.6 Hz, 4H), 6.72 (d, ^3J(H,H) = 8.6 Hz, 4H), 3.65 (s (broad), 4H) ppm; **^{13}C-NMR** (101 MHz, $CDCl_3$): δ = 145.4 (C_q, 2C), 132.2 (C_q, 2C), 127.7 (C_t, 4C), 115.9 (C_t, 4C) ppm; **IR**: ν/cm^{-1} = 3402 (w), 3319 (w), 3171 (w), 3019 (w), 1602 (m), 1496 (s), 1263 (s), 1175 (m), 848 (s); **MS** (EI +, 70 eV): m/z (%) = 185 (13), 184 (100), 183 (10), 156 (5), 92 (7).

9*H*-Fluorene-2,7-diamine (C3c): General procedure A was followed using 1.00 g 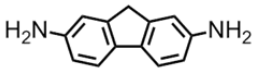 (1.00 equiv., 3.09 mmol) 2,7-dibromo-fluorene (**C2c**) to afford 440 mg (81%) 2,7-diamino-9*H*-fluorene (**C3c**) after purification by column chromatography (SiO_2; hexane:EtOAc 1:3, 5% NEt_3).

C8c: $\boldsymbol{R_f}$ = 0.27 (SiO_2; hexane:EtOAc 1:3, 5% NEt_3); **m.p.** 219 – 220°C; **^{1}H-NMR** (400 MHz, $CDCl_3$): δ = 7.75 (d, ^3J(H,H) = 7.0 Hz, 4H), 7.46 (t, ^3J(H,H) = 7.3 Hz, 2H), 7.42 – 7.38 (m, 6H), 7.28 – 7.23 (m, 6H), 7.17 – 7.13 (m, 4H), 6.89 – 6.86 (m, 2H), 6.66 (dd, ^3J(H,H) = 8.0 Hz, ^4J(H,H) = 1.9 Hz, 2H), 3.62 (s, 2H) ppm; **^{13}C-NMR** (101 MHz, $CDCl_3$): δ = 167.8 (C_q, 2C), 149.7 (C_q, 2C), 143.7 (C_q, 2C), 139.9 (C_q, 2C), 137.1 (C_q, 2C), 136.4 (C_q, 2C), 130.6 (C_t, 2C), 129.6 (C_t, 4C), 129.3 (C_t, 4C), 128.5 (C_t, 2C), 128.2 (C_t, 4C), 128.0 (C_t, 4C), 119.9 (C_t, 2C), 119.2 (C_t, 2C), 118.0 (C_t, 2C), 36.8 (C_s, 1C) ppm; **MS** (MALDI-ToF): m/z (%) = 526 (6), 525 (11), 524 (100).

C3c: R_f = 0.12 (SiO_2; hexane:EtOAc 1:1, 5% NEt_3); **m.p.** 168 – 169°C; **^{1}H-NMR** (400 MHz, $CDCl_3$): δ = 7.42 (d, ^3J(H,H) = 8.0 Hz, 2H), 6.85 – 6.82 (m, 2H), 6.67 (dd, ^3J(H,H) = 8.0 Hz, ^4J(H,H) = 2.2 Hz, 2H), 3.72 (s, 2H), 3.65 (s (broad), 4H) ppm; **^{13}C-NMR** (101 MHz, $CDCl_3$): δ = 144.3 (C_q, 2C), 144.1 (C_q, 2C), 133.5 (C_q, 2C), 119.2 (C_t, 2C), 113.8 (C_t, 2C), 112.0 (C_t, 2C), 36.7 (C_s, 1C) ppm; **MS** (MALDI-ToF): m/z (%) = 197 (38), 196 (100).

9,10-Dihydrophenanthrene-2,7-diamine (C3d): General procedure A was followed using

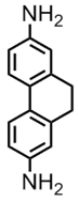

400 mg (1.00 equiv., 1.18 mmol) 2,7-dibromo-9,10-dihydrophenanthrene (**C2d**) to afford 584 mg (92%) N^2,N^7-bis(diphenylmethylene)-9,10-dihydrophenanthrene-2,7-diamine (**C8d**) as a pale yellow powder. The diimine **C8d** (570 mg, 1.00 equiv., 1.08 mmol) was used without further purification to achieve diamine **C3d** (185 mg, 83%) after purification by column chromatography (SiO_2; hexane:EtOAc 1:5, 5% NEt_3) as a white solid.

C8d: R_f = 0.47 (SiO_2; hexane:EtOAc 5:1); **m.p.** 230°C; **^{1}H-NMR** (400 MHz, $CDCl_3$): δ = 7.74 (d, ^3J(H,H) = 7.0 Hz, 4H), 7.46 (t, ^3J(H,H) = 7.2 Hz, 2H), 7.42 – 7.37 (m, 6H), 7.29 – 7.23 (m, 6H), 7.17 – 7.13 (m, 4H), 6.62 (d, ^4J(H,H) = 2.1 Hz, 2H), 6.55 (dd, ^3J(H,H) = 8.2 Hz, ^4J(H,H) = 2.2 Hz, 2H), 2.64 (s, 4H) ppm; **^{13}C-NMR** (101 MHz, $CDCl_3$): δ = 167.8 (C_q, 2C), 149.8 (C_q, 2C), 139.8 (C_q, 2C), 137.2 (C_q, 2C), 136.4 (C_q, 2C), 130.6 (C_t, 2C), 129.7 (C_q, 2C), 129.5 (C_t, 4C), 129.3 (C_t, 4C), 128.6 (C_t, 2C), 128.2 (C_t, 4C), 128.0 (C_t, 4C), 123.3 (C_t, 2C), 121.0 (C_t, 2C), 119.5 (C_t, 2C), 29.0 (C_s, 2C) ppm; **MS** (MALDI-ToF): m/z (%) = 197 (38), 196 (100), 540 (98), 539 (100).

C3d: R_f = 0.43 (SiO_2; hexane:EtOAc 1:5, 5% NEt_3); **m.p.** 157 – 159°C; **^{1}H-NMR** (400 MHz, $CDCl_3$): δ = 7.44 (d, ^3J(H,H) = 8.2 Hz, 2H), 6.59 (dd, ^3J(H,H) = 8.2 Hz, ^4J(H,H) = 2.4 Hz, 2H), 6.53 (d, ^4J(H,H) = 2.4 Hz, 2H), 3.61 (s (broad), 4H), 2.74 (s, 4H) ppm; **^{13}C-NMR** (101 MHz, $CDCl_3$): δ = 144.6 (C_q, 2C), 137.6 (C_q, 2C), 125.9 (C_q, 2C), 123.7 (C_t, 2C), 114.7 (C_t, 2C), 113.7 (C_t, 2C), 29.4 (C_s, 2C) ppm; **MS** (EI +, 70 eV): m/z (%) = 211 (16), 210 (100), 209 (27).

3,10-Diamino-5,6,7,8-tetrahydrodibenzo[*a*,*c*]-cyclooctene (C3f): From dibromide **C2f**

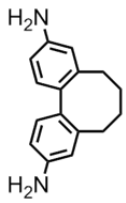

(1.20 g, 1.00 equiv., 3.28 mmol), diimine **C8f** (1.57 g, 85%) was obtained as a yellow powder. Diimine **C8f** (1.56 g, 1.00 equiv., 2.76 mmol) was cleaved following general procedure A yielding in 605 mg (71%) of the diamine **C3f** as a white solid after purification by column chromatography (SiO_2; hexane:EtOAc 1:1, 5% NEt_3). For analytical purpose a small amount of **C3f** was dissolved in 2-propanol.

While stirring at rt, conc. TFA (1 mL) was added in one lot. The solution was stirred at rt for 15 min. Afterwards the TFA salt of **C3f** was precipitated with ice cold diethyl ether, filtered, washed with plenty of diethyl ether and dried.

C8f: $\boldsymbol{R_f}$ = 0.34 (SiO_2; hexane:EtOAc 5:1); **m.p.** 121 – 122°C; **^{1}H-NMR** (400 MHz, $CDCl_3$): δ = 7.77 (d, ^3J(H,H) = 7.0 Hz, 4H), 7.47 (t, ^3J(H,H) = 7.2 Hz, 2H), 7.44 – 7.38 (m, 4H), 7.30 – 7.21 (m, 6H), 7.16 – 7.10 (m, 4H), 6.97 (d, ^3J(H,H) = 8.0 Hz, 2H), 6.61 (dd, ^3J(H,H) = 8.0 Hz, ^4J(H,H) = 2.1 Hz, 2H), 6.53 (d, ^4J(H,H) = 2.1 Hz, 2H), 2.41 (dd, ^2J(H,H) = 13.1 Hz, ^3J(H,H) = 8.3 Hz, 2H), 1.89 – 1.76 (m, 4H), 1.15 – 1.05 (m, 2H) ppm; **^{13}C-NMR** (101 MHz, $CDCl_3$): δ = 168.3 (C_q, 2C), 150.6 (C_q, 2C), 142.8 (C_q, 2C), 139.7 (C_q, 2C), 136.4 (C_q, 2C), 135.5 (C_t, 2C), 130.6 (C_t, 2C), 129.6 (C_q, 2C), 129.3 (C_t, 4C), 129.0 (C_t, 4C), 128.4 (C_t, 2C), 128.2 (C_t, 4C), 127.8 (C_t, 4C), 121.7 (C_t, 2C), 118.5 (C_t, 2C), 32.5 (C_s, 2C), 29.5 (C_s, 2C) ppm; **MS** (MALDI-ToF): m/z (%) = 568 (48), 567 (73), 566 (100).

C3f: $\boldsymbol{R_f}$ = 0.22 (SiO_2; hexane:EtOAc 1:1, 5% NEt_3); **^{1}H-NMR** (400 MHz, $CDCl_3$): δ = 7.02 (d, ^3J(H,H) = 7.9 Hz, 2H), 6.61 – 6.54 (m, 4H), 3.62 (s (broad), 4H), 2.57 (dd, ^2J(H,H) = 13.2 Hz, ^3J(H,H) = 8.5 Hz, 2H), 2.16 – 2.06 (m, 2H), 2.06 – 1.97 (m, 2H), 1.51 – 1.42 (m, 2H) ppm; **^{13}C-NMR** (101 MHz, $CDCl_3$): δ = 145.5 (C_q, 2C), 143.8 (C_q, 2C), 131.5 (C_q, 2C), 130.1 (C_t, 2C), 115.7 (C_t, 2C), 112.7 (C_t, 2C), 32.9 (C_s, 2C), 29.7 (C_s, 2C) ppm; **MS** (EI +, 70 eV): m/z (%) = 239 (18), 238 (100), 237 (5), 209 (21), 208 (9), 196 (6), 195 (20), 104 (6); **elemental analysis** calcd for $C_{16}H_{18}N_2$ (TFA-salt): C 51.51, H 4.32, N 6.01; found: C 51.55, H 4.33, N 5.97.

Representative Procedure B (*Syntheses of the Diamino-derivatives* (C3) *starting from the triflate substituted tricyclic-biphenyl-derivatives*):[107] THF (abs.) was degased by three freeze and thaw cycles. $Pd(OAc)_2$ (10 mol%), BINAP (15 mol%), ditriflate (1.00 equiv.) and cesium carbonate (2.80 equiv.) were given in a Schlenk-tube and dissolved in degased THF (0.07 M with respect to the ditriflate). To this yellow/orange suspension benzophenone imine (2.40 equiv.) was added dropwise and the resulting reaction mixture was stirred at 65°C until the starting material was consumed as monitored by TLC (overnight). Afterwards, the mixture was cooled to rt and diluted with *t*BME (4 × volume of toluene). The suspension was filtered over celite and concentrated under reduced pressure. The crude was purified by recrystallization from methanol to afford *N*,*N*-bis(diphenylmethylene)biphenyl-diamine (**C8**) as a yellow solid. Cleavage of the diimine **C8** was performed according to procedure A.

3,9-Diamino-6,7-dihydro-5*H*-dibenzo[*a*,*c*]-cycloheptene (C3e): According to representative procedure B, ditriflate **C2e** (1.40 g, 1.00 equiv., 2.85 mmol) was reacted to diimine **C8e** (1.54 g, 98%) which was isolated as a yellow powder. The diimine **C8e** was cleaved without further purification. Diimine **C8e** (1.51 g, 1.00 equiv., 2.73 mmol) was dissolved in THF (30 mL), adding 3 M aq. HCl (10 mL). Purification of the crude was performed by column chromatography (SiO_2; hexane:EtOAc 1:1, 5% NEt_3). Diamine **C3e** (496 mg, 81%) was isolated as a colorless oil. The TFA salt of **C3e** was obtained in the same manner as the TFA salt of **C3f**.

C8e: R_f = 0.41 (SiO_2; hexane:EtOAc 5:1); **m.p.** 212 – 213°C; **^{1}H-NMR** (400 MHz, $CDCl_3$): δ = 7.76 (d, ^3J(H,H) = 7.2 Hz, 4H), 7.46 (t, ^3J(H,H) = 7.2 Hz, 2H), 7.44 – 7.38 (m, 4H), 7.32 – 7.21 (m, 6H), 7.18 – 7.11 (m, 4H), 7.07 (d, ^3J(H,H) = 8.0 Hz, 2H), 6.63 (dd, ^3J(H,H) = 8.0 Hz, ^4J(H,H) = 2.1 Hz, 2H), 6.58 (d, ^4J(H,H) = 2.0 Hz, 2H), 2.23 (t, ^3J(H,H) = 6.9 Hz, 4H), 1.91 (quint, ^3J(H,H) = 6.9 Hz, 2H) ppm; **^{13}C-NMR** (101 MHz, $CDCl_3$): δ = 168.1 (C_q, 2C), 150.0 (C_q, 2C), 139.8 (C_q, 2C), 139.7 (C_q, 2C), 136.4 (C_q, 2C), 135.9 (C_t, 2C), 130.6 (C_t, 2C), 129.6 (C_q, 2C), 129.6 (C_t, 4C), 129.3 (C_t, 4C), 128.5 (C_t, 2C), 128.2 (C_t, 4C), 127.8 (C_t, 4C), 121.3 (C_t, 2C), 119.0 (C_t, 2C), 33.1 (C_s, 1C), 31.3 (C_s, 2C) ppm; **MS** (EI +, 70 eV): m/z (%) = 554 (9), 553 (42), 552 (100), 475 (6), 276 (8), 237 (5), 199 (13).

C3e: R_f = 0.34 (SiO_2; hexane:EtOAc 1:1, 5% NEt_3); **^{1}H-NMR** (400 MHz, $CDCl_3$): δ = 7.13 (d, ^3J(H,H) = 8.0 Hz, 2H), 6.64 (dd, ^3J(H,H) = 8.0 Hz, ^4J(H,H) = 2.4 Hz, 2H), 6.58 (d, ^4J(H,H) = 2.4 Hz, 2H), 3.62 (s (broad), 4H), 2.43 (t, ^3J(H,H) = 7.0 Hz, 4H), 2.12 (quint, ^3J(H,H) = 7.0 Hz, 2H) ppm; **^{13}C-NMR** (101 MHz, $CDCl_3$): δ = 145.1 (C_q, 2C), 140.5 (C_q, 2C), 131.8 (C_q, 2C), 128.8 (C_t, 2C), 115.3 (C_t, 2C), 113.2 (C_t, 2C), 32.8 (C_s, 1C), 31.7 (C_s, 2C) ppm; **MS** (MALDI-ToF): m/z (%) = 225 (36), 224 (100); **elemental analysis** calcd (%) for $C_{15}H_{16}N_2$ (TFA salt)**:** C 50.45, H 4.01, N 6.19; found: C 49.68, H 4.09, N 6.28.

3,11-Diamino-6,7,8,9-tetrahydro-5*H*-dibenzo[*a*,*c*]-cyclononene (C3g): By applying representative procedure B, ditriflate **C2g** (1.40 g, 1.00 equiv., 2.70 mmol) was converted to diimine **C8g** (930 mg, 60%), which was isolated as a yellow powder. The diimine **C8g** was cleaved without further purification, to achieve diamine **C3g** (391 mg, quant.) as a colorless oil. The TFA salt of **C3g** was obtained in the same manner as the TFA salt of **C3f**.

C8g: R_f = 0.73 (SiO_2; hexane:EtOAc 1:1, 5% NEt_3); **m.p.** 146 – 147°C; **^{1}H-NMR** (400 MHz, $CDCl_3$): δ = 7.77 (d, ^3J(H,H) = 7.1 Hz, 4H), 7.47 (t, ^3J(H,H) = 7.2 Hz, 2H), 7.45 – 7.38 (m,

4H), 7.31 – 7.21 (m, 6H), 7.18 – 7.11 (m, 4H), 6.88 (d, ^3J(H,H) = 8.0 Hz, 2H), 6.63 (dd, ^3J(H,H) = 7.9 Hz, ^4J(H,H) = 2.1 Hz, 2H), 6.47 (d, ^4J(H,H) = 2.0 Hz, 2H), 2.40 – 2.29 (m, 2H), 1.85 – 1.74 (m, 2H), 1.55 – 1.43 (m, 2H), 1.17 – 0.97 (m, 4H) ppm; **^{13}C-NMR** (101 MHz, $CDCl_3$): δ = 168.4 (C_q, 2C), 150.4 (C_q, 2C), 142.1 (C_q, 2C), 139.7 (C_q, 2C), 136.8 (C_q, 2C), 136.5 (C_t, 2C), 130.7 (C_t, 2C), 129.6 (C_t, 4C), 129.3 (C_t, 4C), 128.9 (C_t, 2C), 128.4 (C_t, 2C), 128.2 (C_t, 4C), 127.8 (C_t, 4C), 121.1 (C_t, 2C), 118.4 (C_t, 2C), 32.9 (C_s, 2C), 29.0 (C_s, 2C), 28.0 (C_s, 1C) ppm; **MS** (EI+, 70 eV): m/z (%) = 582 (10), 581 (45), 580 (100), 213 (9).

C3g: R_f = 0.42 (SiO_2; hexane:EtOAc 1:1, 5% NEt_3); **^{1}H-NMR** (400 MHz, $CDCl_3$): δ = 6.91 (d, ^3J(H,H) = 7.7 Hz, 2H), 6.59 – 6.53 (m, 4H), 3.62 (s (broad), 4H), 2.57 – 2.48 (m, 2H), 2.14 – 2.10 (m, 2H), 1.79 – 1.68 (m, 2H), 1.55 – 1.35 (m, 4H) ppm; **^{13}C-NMR** (101 MHz, $CDCl_3$): δ = 145.2 (C_q, 2C), 143.3 (C_q, 2C), 132.7 (C_q, 2C), 130.1 (C_t, 2C), 115.3 (C_t, 2C), 112.5 (C_t, 2C), 33.2 (C_s, 2C), 29.0 (C_s, 2C), 28.2 (C_s, 1C) ppm; **MS** (MALDI-ToF): m/z (%) = 253 (28), 252 (100); **elemental analysis** calcd (%) for $C_{17}H_{20}N_2$ (TFA salt): C 52.50, H 4.62, N 5.83; found: C 52.53, H 4.61, N 5.88.

***N*-(4'-Aminobiphenyl-4-yl)benzamide (C4a):**[81] To a stirred heterogeneous suspension of diamine **C3a** (461 mg, 1.00 equiv., 2.50 mmol) in water (15 mL) sodium dodecyl sulfate (SDS) (120 mg) was added. Then benzoic anhydride (566 mg, 1.00 equiv., 2.50 mmol) dissolved in acetonitrile (2.5 mL) was added at once to the still heterogeneous brown suspension. After stirring for 10 min at room temperature the gray suspension was diluted with acetonitrile (10 mL). After evaporation of the organic solvent, solid sodium hydrogen carbonate was added in portions to adjust pH 7. The remaining aqueous layer containing gray precipitate was filtered and the solid washed with water (100 mL). The solid gray product **C8a** was azeotroped with toluene and dried on high vacuum. The product was dissolved in toluene and the precipitated byproduct was filtered off. The remaining liquid was concentrated to afford product **C4a** (363 mg, 50%).

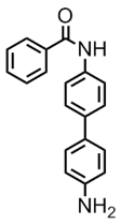

R_f = 0.12 (SiO_2; hexane:EtOAc 3:1); **m.p.** 228°C; **^{1}H-NMR** (400 MHz, DMSO-d6): δ = 10.25 (s, 1H), 7.96 (d, ^3J(H,H) = 7.2 Hz, 2H), 7.79 (d, ^3J(H,H) = 8.7 Hz, 2H), 7.64 – 7.50 (m, 3H), 7.53 (d, ^3J(H,H) = 8.6 Hz, 2H), 7.36 (d, ^3J(H,H) = 8.5 Hz, 2H), 6.63 (d, ^3J(H,H) = 8.5 Hz, 2H), 5.20 (s (broad), 2H) ppm; **^{13}C-NMR** (101 MHz, [D_6]DMSO): δ = 165.3 (C_q, 1C), 147.9 (C_q, 1C), 137.0 (C_q, 1C), 136.0 (C_q, 1C,), 135.0 (C_q, 1C,), 131.4 (C_q, 1C,), 128.3 (C_t, 2C), 127.5 (C_t, 2C), 127.1 (C_t, 1C), 126.7 (C_t, 2C), 125.2 (C_t, 2C), 120.6 (C_t, 2C), 114.2

(C_t, 2C) ppm; **IR**: ν/cm^{-1} = 3340 (m), 3039 (w), 1650 (s), 1604 (m), 1512 (s), 1404 (w), 1319 (w), 1265 (w), 903 (w), 810 (s), 710 (m), 648(s); **MS** (MALDI-ToF): m/z (%) = 288 (100).

***N*-(4'-Nitrobiphenyl-4-yl)benzamide (C5a):**[108] Sodium perborate tetrahydrate (544 mg, 5.00 equiv., 3.54 mmol) was dissolved in conc. acetic acid (9 mL) and heated to 60°C. To this colorless solution a pale brown suspension of *N*-(4'-aminobiphenyl-4-yl)benzamide (**C4a**) (204 mg, 1.00 equiv., 0.707 mmol) in conc. acetic acid (14 mL) was added dropwise over a period of 35 min. Afterwards the scarlet red suspension was stirred for 15 h at 60°C. The pale red suspension containing sodiumborate was cooled down to rt and then the solvent was removed under reduced pressure. The brown residue was dissolved in H_2O and EtOAc. The red organic layer was separated, the aqueous layer reextracted with EtOAc (2 × 30 mL). Then the combined organic layers were washed with H_2O (1 × 20 mL) and brine (1 × 20 mL), dried with sodium sulfate, filtered and evaporated to dryness. Column chromatography (SiO_2; hexane:EtOAc 1:1) afforded *N*-(4'-nitrobiphenyl-4-yl)benzamide (**C5a**) as a red-brown solid. The crude was recrystallized from methanol and dried at high vacuum for 5 h to afford product **C5a** (226 mg, quantitative) as a yellow solid.

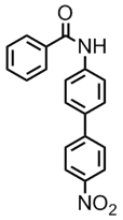

***R*$_f$** = 0.25 (SiO_2; hexane:EtOAc 3:1); **m.p.** 257 – 258°C; **^{1}H-NMR** (400 MHz, [D_6]DMSO): δ = 10.46 (s, 1H), 8.30 (d, ^3J(H,H) = 8.8 Hz, 2H), 8.00 – 7.95 (m, 6H), 7.84 (d, ^3J(H,H) = 8.8 Hz, 2H), 7.62 (t, ^3J(H,H) = 7.2 Hz, 1H), 7.56 (t, ^3J(H,H) = 7.2 Hz, 2H) ppm; **^{13}C-NMR** (101 MHz, DMSO-d6): δ = 165.6 (C_q, 1C), 146.1 (C_q, 1C), 146.0 (C_q, 1C), 140.1 (C_q, 1C), 134.6 (C_q, 1C), 132.4 (C_q, 1C), 131.6 (C_t, 1C), 128.3 (C_t, 2C), 127.6 (C_t, 2C), 127.5 (C_t, 2C), 127.1 (C_t, 2C), 124.0 (C_t, 2C), 120.4 (C_t, 2C) ppm; **IR**: ν/cm^{-1} = 3364 (w), 1659 (s), 1589 (m), 1504 (s), 1420 (w), 1350 (s), 1249 (w), 833 (s); **MS** (MALDI-ToF): m/z (%) = 319 (100).

4'-Nitrobiphenyl-4-amine (C6a):[109] *N*-(4'-Nitrobiphenyl-4-yl)benzamide (**C5a**) (260 mg, 1.00 equiv., 0.817 mmol) was dissolved in dimethyl sulfoxide (5 mL). To this yellow solution 10 M aq. KOH (10 mL) and EtOH (1 mL) was added. The reaction mixture was heated to 80°C for 60 h, then neutralized with 1 M aq. HCl (until solution is pale yellow) and extracted with *tert*-butylmethyl ether (3 × 70 ml), dried with sodium sulfate, filtered and concentrated *in vacuo*. The resulting oil was purified by column chromatography (SiO_2; toluene:EtOAc, 1:1) to afford 4'-nitrobiphenyl-4-amine (**C6a**) (43.3 mg, 25%) as a dark red solid.

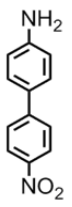

R_f = 0.53 (SiO_2; toluene:EtOAc 1:1); **m.p.** 202 – 203°C; **^{1}H-NMR** (400 MHz, $CDCl_3$): δ = 8.24 (d, ^3J(H,H) = 8.9 Hz, 2H), 7.66 (d, ^3J(H,H) = 8.9 Hz, 2H), 7.47 (d, ^3J(H,H) = 8.7 Hz, 2H), 6.78 (d, ^3J(H,H) = 8.7 Hz, 2H), 3.90 (s (broad), 2H) ppm; **^{13}C-NMR** (101 MHz, $CDCl_3$): δ = 147.5 (C_q, 2C), 147.5 (C_q, 1C), 128.5 (C_q, 1C), 128.4 (C_t, 2C), 126.4 (C_t, 2C), 124.1 (C_t, 2C), 115.3 (C_t, 2C) ppm; **MS** (MALDI-ToF): m/z (%) = 216 (17), 215 (64), 214 (60), 198 (100).

1-(4'-Nitrobiphenyl-4-yl)piperidine (C1a):[113] 4'-Nitrobiphenyl-4-amine (**C6a**) (20.0 mg, 1.00 equiv., 93.4 µmol) was dissolved in toluene (3.5 mL) and ethanol (3.5 mL). The orange solution was transferred to a pressure tube and potassium carbonate (15.5 mg, 1.20 equiv., 0.112 mmol) was added as well as 1,5-dibromopentane (14.0 µL, 1.10 equiv., 0.103 mmol, 23.9 mg). The reaction mixture was placed in a microwave-synthesis-system operating at 140°C for 1 h (3 min ramp-time). Afterwards the mixture was quenched with water (10 mL) and extracted with dichloromethane (3 × 15 mL). The extract was dried with sodium sulfate, filtered and concentrated under reduced pressure. Purification was performed by column chromatography (SiO_2; CH_2Cl_2). According to this procedure 1-(4'-nitrobiphenyl-4-yl)piperidine (**C1a**) (10.5 mg, 40%) was obtained as an orange solid.

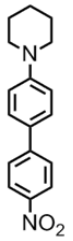

R_f = 0.69 (SiO_2; CH_2Cl_2); **m.p.** 220°C; **^{1}H-NMR** (400 MHz, $CDCl_3$): δ = 8.24 (d, ^3J(H,H) = 9.0 Hz, 2H), 7.69 (d, ^3J(H,H) = 9.0 Hz, 2H), 7.55 (d, ^3J(H,H) = 8.9 Hz, 2H), 7.00 (d, ^3J(H,H) = 8.8 Hz, 2H), 3.28 (t, ^3J(H,H) = 5.8 Hz, 4H), 1.76 – 1.67 (m, 4H), 1.67 – 1.59 (m, 2H) ppm; **^{13}C-NMR** (101 MHz, $CDCl_3$): δ = 152.3 (C_q, 1C), 147.4 (C_q, 1C), 146.0 (C_q, 1C), 128.1 (C_t, 2C), 127.9 (C_q, 1C), 126.4 (C_t, 2C), 124.1 (C_t, 2C), 115.8 (C_t, 2C), 49.6 (C_s, 2C), 25.5 (C_s, 2C), 24.3 (C_s, 1C) ppm; **IR**: $\tilde{\nu}$/cm^{-1} = 2949 (w), 2844 (w), 1589 (m), 1506 (s), 1337 (s), 1242 (s), 1224 (s), 1111 (m), 852 (s), 756 (s); **MS** (MALDI-ToF): m/z (%) = 283 (55), 282 (100); **elemental analysis** calcd (%) for $C_{17}H_{18}N_2O_2$: C 72.32, H 6.43, N 9.92; found: C 72.02, H 6.51, N 9.93; **UV/Vis** (chloroform): λ_{max} (ε) = 268 nm (19840 Lmol^{-1}cm^{-1}), λ_{max} (ε) = 398 nm (19646 Lmol^{-1}cm^{-1}).

Representative procedure C (*syntheses of the 4'-(piperidin-1-yl)biphenyl-4-amine derivatives* (C7)):[113] Diamine **C3** (1.00 equiv.) and K_2CO_3 (1.20 equiv.) were weighed into a pressure tube. 1,5-Dibromopentane (1.10 equiv.) was added and the mixture was dissolved in the according solvent system (see table 1) (0.1 M with respect to the diamine). The reaction tube was placed in a microwave-synthesis-system, operated at 150°C for 40 min. Afterwards

1 M aq. HCl was added and the mixture stirred for another 30 min at rt. EtOAc was added and the aqueous layer was separated. The organic layer was reextracted twice with 1 M aq. HCl. The combined aqueous layers were made alkaline by 1 M aq. NaOH and extracted with dichloromethane. The pale yellow organic layer was dried with sodium sulfate, filtered and the solvent removed under reduced pressure. The pale brown solid was purified by column chromatography (SiO_2; hexane:EtOAc 3:1, 5% NEt_3) to afford the product **C7**.

4'-(Piperidin-1-yl)biphenyl-4-amine (C7a): From benzidine **C3a** (50.0 mg, 1.00 equiv., 0.271 mmol) colorless, solid product **C7a** (29.5 mg, 43%) and 4,4'-di(piperidin-1-yl)biphenyl (6.3 mg) were obtained by purification with column chromatography (SiO_2; hexane:EtOAc 3:1, 5% NEt_3). A second column chromatography (SiO_2; CH_2Cl_2, 3% MeOH) provided pure, colorless, solid product **C7a** (29.0 mg, 42%).

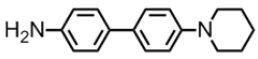

***R*f** = 0.86 (SiO_2; hexane:EtOAc 1:1, 5% NEt_3); **m.p.** 101 – 102°C; **^{1}H-NMR** (400 MHz, $CDCl_3$): δ = 7.45 (d, ^3J(H,H) = 8.9 Hz, 2H), 7.38 (d, ^3J(H,H) = 8.6 Hz, 2H), 6.99 (d, ^3J(H,H) = 8.8 Hz, 2H), 6.74 (d, ^3J(H,H) = 8.6 Hz, 4H), 3.67 (s, 2H), 3.19 (t, ^3J(H,H) = 5.5 Hz, 4H), 1.74 (quint, ^3J(H,H) = 5.6 Hz, 4H), 1.60 (quint, ^3J(H,H) = 5.6 Hz, 2H) ppm; **^{13}C-NMR** (101 MHz, $CDCl_3$): δ = 150.7 (C_q, 1C), 145.0 (C_q, 1C), 132.1 (C_q, 1C), 131.6 (C_q, 1C), 127.3 (C_t, 2C), 126.9 (C_t, 2C), 116.7 (C_t, 2C), 115.4 (C_t, 2C), 50.7 (C_s, 2C), 25.8 (C_s, 2C), 24.3 (C_s, 1C) ppm; **IR**: ν/cm^{-1} = 3391 (w), 3316 (w), 3208 (w), 3019 (w), 2930 (w), 2809 (w), 1604 (m), 1499 (s), 1447 (m), 1385 (m), 1333 (m), 1264 (s), 1234 (s), 1124 (s), 1023 (m), 918 (m), 803 (s), 578 (s); **MS** (MALDI-ToF): m/z (%) = 253 (26), 252 (100).

Side product: ^{1}H-NMR (400 MHz, $CDCl_3$): δ = 7.48 (d, ^3J(H,H) = 8.8 Hz, 4H), 7.00 (d, ^3J(H,H) = 8.8 Hz, 4H), 3.20 (t, ^3J(H,H) = 5.5 Hz, 8H), 1.75 (quint, ^3J(H,H) = 5.6 Hz, 8H), 1.60 (quint, ^3J(H,H) = 5.6 Hz, 4H) ppm; **^{13}C-NMR** (101 MHz, $CDCl_3$): δ = 150.8 (C_q, 2C), 131.8 (C_q, 2C), 126.9 (C_t, 4C), 116.7 (C_t, 4C), 50.6 (C_s, 4C), 25.8 (C_s, 4C), 24.3 (C_s, 2C) ppm; **MS** (MALDI-ToF): m/z (%) = 321 (17), 320 (100).

2,2'-Dimethyl-4'-(piperidin-1-yl)biphenyl-4-amine (C7b): In accordance to general procedure C, 2,2'-dimethylbiphenyl-4,4'-diamine (**C3b**) (150 mg, 1.00 equiv., 0.707 mmol), was converted into product **C7b** (79.7 mg, 40%), which was isolated as a pale purple powder.

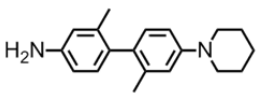

***R*f** = 0.60 (SiO_2; hexane:EtOAc 3:1, 5% NEt_3); **m.p.** 135 – 136°C; **^{1}H-NMR** (400 MHz, $CDCl_3$): δ = 6.99 (d, ^3J(H,H) = 8.3 Hz, 1H), 6.91 (d, ^3J(H,H) = 8.0 Hz, 1H), 6.85 (d, ^4J(H,H)

= 2.6 Hz, 1H), 6.80 (dd, ^3J(H,H) = 8.3 Hz, ^4J(H,H) = 2.6 Hz, 1H), 6.61 (d, ^4J(H,H) = 2.5 Hz, 1H), 6.55 (dd, ^3J(H,H) = 8.0 Hz, ^4J(H,H) = 2.5 Hz, 1H), 3.61 (s (broad), 2H), 3.19 (t, ^3J(H,H) = 5.6 Hz, 4H), 2.05 (s, 3H), 2.00 (s, 3H), 1.75 (quint, ^3J(H,H) = 5.6 Hz, 4H), 1.64 – 1.55 (m, 2H) ppm; **^{13}C-NMR** (101 MHz, $CDCl_3$): δ = 145.0 (C_q, 1C), 137.3 (C_q, 1C), 136.9 (C_q, 2C), 132.2 (C_q, 2C), 130.7 (C_t, 1C), 130.5 (C_t, 1C), 117.7 (C_q, 1C), 116.3 (C_t, 1C), 113.6 (C_t, 1C), 112.3 (C_t, 1C), 50.8 (C_s, 2C), 26.0 (C_s, 2C), 24.3 (C_s, 1C), 20.3 (C_p, 1C), 20.0 (C_s, 1C) ppm; **MS** (MALDI-ToF): m/z (%) = 282 (4), 281 (36), 280 (100).

7-(Piperidin-1-yl)-9*H*-fluorene-2-amine (C7c): By following the synthetic procedure C, from 2,7-diaminofluorene (**C3c**) (250 mg, 1.00 equiv., 1.27 mmol) 7-(piperidin-1-yl)-9*H*-fluorene-2-amine (**C7c**) (145 mg, 43%) was obtained. Purification was performed by column chromatography (SiO_2; hexane:EtOAc 1:1, 5% NEt_3).

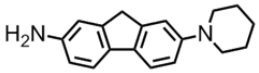

***R*$_f$** = 0.36 (SiO_2; hexane:EtOAc 1:1, 5% NEt_3); **m.p.** 186 – 187°C; **^{1}H-NMR** (400 MHz, $CDCl_3$): δ = 7.49 (d, ^3J(H,H) = 8.3 Hz, 1H), 7.44 (d, ^3J(H,H) = 8.0 Hz, 1H), 7.10 (d, ^4J(H,H) = 2.1 Hz, 1H), 6.93 (dd, ^3J(H,H) = 8.3 Hz, ^4J(H,H) = 2.1 Hz, 1H), 6.84 (d, ^4J(H,H) = 2.1 Hz, 1H), 6.67 (dd, ^3J(H,H) = 8.0 Hz, ^4J(H,H) = 2.1 Hz, 1H), 3.75 (s, 2H), 3.65 (s (broad), 2H), 3.16 (t, ^3J(H,H) = 5.4 Hz, 4H), 1.74 (quint, ^3J(H,H) = 5.5 Hz, 4H), 1.62 – 1.54 (m, 2H) ppm; **^{13}C-NMR** (101 MHz, $CDCl_3$): δ = 150.8 (C_q, 1C), 144.5 (C_q, 1C), 144.5 (C_q, 1C), 143.5 (C_q, 1C), 134.3 (C_q, 1C), 133.4 (C_q, 1C), 119.6 (C_t, 1C), 118.9 (C_t, 1C), 115.8 (C_t, 1C), 113.8 (C_t, 2C), 112.0 (C_t, 1C), 51.7 (C_s, 2C), 36.9 (C_s, 1C), 26.0 (C_s, 2C), 24.3 (C_s, 1C) ppm; **MS** (MALDI-ToF): m/z (%) = 266 (25), 265 (98), 264 (100); **elemental analysis** calcd (%) for $C_{18}H_{20}N_2$: C 81.78, H 7.62, N 10.60; found: C 81.72, H 7.66, N 10.37.

7-(Piperidin-1-yl)-9,10-dihydrophenanthren-2-amine (C7d): The general procedure C was followed using 9,10-dihydrophenanthren-2,7-diamine (**C3d**) (174 mg, 1.00 equiv., 0.829 mmol). Column chromatography (SiO_2; hexane:EtOAc 1:1, 5% NEt_3) was performed to isolate product **C7d** (101 mg, 44%) as a red oil.

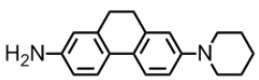

***R*$_f$** = 0.43 (SiO_2; hexane:EtOAc 1:1, 5% NEt_3); **^{1}H-NMR** (400 MHz, $CDCl_3$): δ = 7.52 (d, ^3J(H,H) = 8.5 Hz, 1H), 7.47 (d, ^3J(H,H) = 8.2 Hz, 1H), 6.85 (dd, ^3J(H,H) = 8.5 Hz, ^4J(H,H) = 2.6 Hz, 1H), 6.78 (d, ^4J(H,H) = 2.5 Hz, 1H), 6.61 (dd, ^3J(H,H) = 8.2 Hz, ^4J(H,H) = 2.4 Hz, 1H), 6.54 (d, ^4J(H,H) = 2.3 Hz, 1H), 3.59 (s (broad), 2H), 3.17 (t, ^3J(H,H) = 5.5 Hz, 4H), 2.83 – 2.73 (m, 4H), 1.72 (quint, ^3J(H,H) = 5.5 Hz, 4H), 1.58 (quint, ^3J(H,H) = 5.5 Hz, 2H) ppm;

^{13}C-NMR (101 MHz, $CDCl_3$): δ = 144.8 (C_q, 1C), 137.8 (C_q, 1C), 137.0 (C_q, 1C), 123.9 (C_q, 1C), 123.3 (C_t, 2C), 116.1 (C_q, 1C), 115.0 (C_q, 1C), 114.7 (C_t, 2C), 113.7 (C_t, 2C), 50.8 (C_s, 2C), 29.8 (C_s, 1C), 29.5 (C_s, 1C), 25.8 (C_s, 2C), 24.3 (C_s, 1C) ppm; **MS** (MALDI-ToF): m/z (%) = 279 (100), 278 (95).

3-Amino-9-(piperidin-1-yl)-6,7-dihydro-5*H*-dibenzo[*a*,*c*]cycloheptene (C7e): By following the synthetic procedure C, using diamine **C3e** (439 mg, 1.00 equiv., 1.96 mmol) product **C7e** (224 mg, 39%) was isolated as a colorless oil. Purification was performed by column chromatography (SiO_2; hexane:EtOAc 1:1, 5% NEt_3).

***R*$_f$** = 0.46 (SiO_2; hexane:EtOAc 1:1, 5% NEt_3); **^{1}H-NMR** (400 MHz, $CDCl_3$): δ = 7.21 (d, ^3J(H,H) = 8.3 Hz, 1H), 7.14 (d, ^3J(H,H) = 8.0 Hz, 1H), 6.87 (dd, ^3J(H,H) = 8.4 Hz, ^3J(H,H) = 2.6 Hz, 1H), 6.82 (d, ^4J(H,H) = 2.6 Hz, 1H), 6.64 (dd, ^3J(H,H) = 8.1 Hz, ^4J(H,H) = 2.5 Hz, 1H), 6.58 (d, ^4J(H,H) = 2.4 Hz, 1H), 3.64 (s (broad), 2H), 3.19 (t, ^3J(H,H) = 5.5 Hz, 4H), 2.47 (t, ^3J(H,H) = 7.0 Hz, 2H), 2.42 (t, ^3J(H,H) = 7.0 Hz, 2H), 2.13 (quint, ^3J(H,H) = 7.0 Hz, 2H), 1.77 – 1.69 (m, 4H), 1.62 – 1.54 (m, 2H) ppm; **^{13}C-NMR** (101 MHz, $CDCl_3$): δ = 145.1 (C_q, 1C), 140.6 (C_q, 1C), 140.1 (C_q, 2C), 131.7 (C_q, 1C), 128.8 (C_q, 1C), 128.4 (C_q, 2C), 116.7 (C_t, 1C), 115.2 (C_t, 1C), 114.3 (C_t, 1C), 113.1 (C_t, 1C), 50.9 (C_s, 2C), 32.9 (C_s, 1C), 32.1 (C_s, 1C), 31.7 (C_s, 1C), 25.9 (C_s, 2C), 24.2 (C_s, 1C) ppm; **MS** (MALDI-ToF): m/z (%) = 293 (62), 292 (100).

3-Amino-10-(piperidin-1yl)-5,6,7,8-tetrahydrodibenzo[*a*,*c*]cyclooctene (C7f): By applying general procedure C, diamine **C3f** (581 mg, 1.00 equiv., 2.44 mmol) was converted into product **C7f** (308 mg, 41%), which was isolated as a colorless oil. Purification was performed by column chromatography (SiO_2; hexane:EtOAc 1:1, 5% NEt_3).

***R*$_f$** = 0.31 (SiO_2; hexane:EtOAc 3:1, 5% NEt_3); **^{1}H-NMR** (400 MHz, $CDCl_3$): δ = 7.10 (d, ^3J(H,H) = 8.2 Hz, 1H), 7.03 (d, ^3J(H,H) = 7.9 Hz, 1H), 6.86 – 6.79 (m, 2H), 6.60 (d, ^4J(H,H) = 2.3 Hz, 1H), 6.58 (dd, ^3J(H,H) = 7.9 Hz, ^4J(H,H) = 2.4 Hz, 1H), 3.62 (s (broad), 2H), 3.19 (t, ^3J(H,H) = 5.5 Hz, 4H), 2.68 – 2.52 (m, 2H), 2.22 – 1.96 (m, 4H), 1.73 (quint, ^3J(H,H) = 5.5 Hz, 2H), 1.63 – 1.54 (m, 2H), 1.54 – 1.44 (m, 2H) ppm; **^{13}C-NMR** (101 MHz, $CDCl_3$): δ = 151.5 (C_q, 1C), 145.5 (C_q, 1C), 143.8 (C_q, 1C), 143.3 (C_q, 1C), 132.0 (C_q, 1C), 131.5 (C_q, 1C), 130.0 (C_t, 1C), 129.7 (C_t, 1C), 117.0 (C_t, 1C), 115.7 (C_t, 1C), 113.8 (C_t, 1C), 112.7 (C_t,

1C), 50.7 (C_s, 2C), 33.4 (C_s, 1C), 32.9 (C_s, 1C), 29.8 (C_s, 1C), 29.7 (C_s, 1C), 26.0 (C_s, 2C), 24.3 (C_s, 1C) ppm; **MS** (MALDI-ToF): m/z (%) = 308 (13), 307 (26), 306 (100).

3-Amino-11-(piperidin-1-yl)-6,7,8,9-tetrahydro-5*H*-dibenzo[*a*,*c*]cyclononene (C7g): The

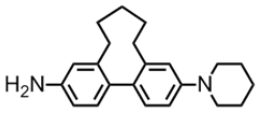

general procedure C was followed using 363 mg (1.00 equiv., 1.44 mmol) diamine **C3g**. Column chromatography (SiO_2; hexane:EtOAc 3:1, 5% NEt_3) was performed to isolate product **C7g** (154 mg, 34%) and diazacycloalkylated side product (43.2 mg, 8%).

R_f = 0.30 (SiO_2; hexane:EtOAc 3:1, 5% NEt_3); **^{1}H-NMR** (400 MHz, $CDCl_3$): δ = 6.99 (d, ^3J(H,H) = 8.9 Hz, 1H), 6.92 (d, ^3J(H,H) = 7.8 Hz, 1H), 6.83 – 6.77 (m, 2H), 6.59 – 6.53 (m, 2H), 3.48 (s (broad), 2H), 3.17 (t, ^3J(H,H) = 5.5 Hz, 4H), 2.62 – 2.54 (m, 1H), 2.54 – 2.46 (m, 1H), 2.16 – 2.04 (m, 2H), 1.81 – 1.64 (m, 6H), 1.62 – 1.54 (m, 2H), 1.54 – 1.43 (m, 2H), 1.43 – 1.34 (m, 2H) ppm; **^{13}C-NMR** (101 MHz, $CDCl_3$): δ = 151.4 (C_q, 1C), 145.3 (C_q, 1C), 143.2 (C_q, 1C), 142.9 (C_q, 1C), 133.3 (C_q, 1C), 132.9 (C_q, 1C), 130.0 (C_t, 1C), 129.8 (C_t, 1C), 116.8 (C_t, 1C), 115.3 (C_t, 1C), 113.6 (C_t, 1C), 112.5 (C_t, 1C), 50.8 (C_s, 2C), 33.8 (C_s, 1C), 33.1 (C_s, 1C), 29.1 (C_s, 2C), 28.3 (C_s, 1C), 26.0 (C_s, 2C), 24.3 (C_s, 1C) ppm; **MS** (MALDI-ToF): m/z (%) = 322 (2), 321 (25), 320 (100).

Representative Procedure D (*mild oxidation of the amines* (C7)):[116] Phosphotungstic acid hydrate (0.45 mol%) was dissolved in CTAB (10 cmc, 0.02 M in water) and stirred for 5 min at rt. Afterwards, sodium perborate tetrahydrate (7.00 equiv.) was added and the resulting milky, colorless solution was heated to 60°C. Then a warm solution of amine **C7** (1.00 equiv.) in CTAB was added dropwise to the mixture. The cloudy, red-brown reaction mixture was stirred for 15 h at 60°C and then cooled to rt. The orange, organic layer was extracted with *t*BME, washed with H_2O, dried with anhydrous sodium sulfate, filtered and concentrated under reduced pressure. Purification was performed by column chromatography (SiO_2; CH_2Cl_2:hexane 2:1).

1-(4'-Nitrobiphenyl-4-yl)piperidine (C1a): The general procedure D was followed using

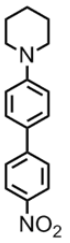

2.62 mg (0.45 mol%, 0.91 µmol) phosphotungstic acid hydrate in CTAB (0.6 mL, 10 cmc, 0.02 M) and 320 mg (10.0 equiv., 2.08 mmol) sodium perborate tetrahydrate. Amine **C7a** (52.0 mg, 1.00 equiv., 0.206 mmol) in CTAB (10 mL) was added dropwise to the mixture. The cloudy, brown reaction mixture was stirred for 15 h at 60°C. Purification was performed by column chromatography (SiO_2; CH_2Cl_2). According to this procedure the red, solid target compound **C1a** (32.0 mg, 55%) was isolated.

R_f = 0.71 (SiO_2; CH_2Cl_2); **m.p.** 220°C; **^{1}H-NMR** (400 MHz, $CDCl_3$): δ = 8.24 (d, ^3J(H,H) = 9.0 Hz, 2H), 7.68 (d, ^3J(H,H) = 9.0 Hz, 2H), 7.55 (d, ^3J(H,H) = 8.9 Hz, 2H), 7.00 (d, ^3J(H,H) = 8.9 Hz, 2H), 3.28 (t, ^3J(H,H) = 5.5 Hz, 4H), 1.77 – 1.68 (m, 4H), 1.67 – 1.60 (m, 2H) ppm; **^{13}C-NMR** (101 MHz, $CDCl_3$): δ = 152.3 (C_q, 1C), 147.4 (C_q, 1C), 146.0 (C_q, 1C), 128.1 (C_t, 2C), 127.9 (C_q, 1C), 126.4 (C_t, 2C), 124.1 (C_t, 2C), 115.8 (C_t, 2C), 49.6 (C_s, 2C), 25.5 (C_s, 2C), 24.3 (C_s, 1C) ppm; **IR**: ν/cm^{-1} = 2949 (w), 2844 (w), 1589 (m), 1506 (s), 1337 (s), 1242 (s), 1224 (s), 1111 (m), 852 (s), 756 (s); **MS** (MALDI-ToF): m/z (%) = 283 (55), 282 (100); **elemental analysis** calcd (%) for $C_{17}H_{18}N_2O_2$: C 72.32, H 6.43, N 9.92; found: C 72.02, H 6.51, N 9.93.

1-(2,2'-Dimethyl-4'-nitrobiphenyl-4-yl)piperidine (C1b): By following the general procedure D, 2,2'-dimethyl-4'-(piperidin-1-yl)biphenyl-4-amine (**C7b**) (50.0 mg, 1.00 equiv., 0.178 mmol) in CTAB (15 mL) was added dropwise to a warmed mixture of phosphotungstic acid hydrate (1.57 mg, 0.45 mol%, 0.545 µmol) in CTAB (0.4 mL, 10 cmc, 0.02 M) and sodium perborate tetrahydrate (192 mg, 7.00 equiv., 1.25 mmol). The pale yellow reaction mixture was stirred for 15 h at 60°C. Column chromatography (SiO_2; CH_2Cl_2) provided the solid, yellow target compound **C1b** (35.6 mg, 64%).

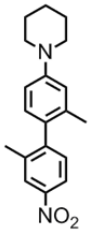

R_f = 0.69 (SiO_2; CH_2Cl_2); **m.p.** 116 – 117°C; **^{1}H-NMR** (400 MHz, $CDCl_3$): δ = 8.13 (d, ^4J(H,H) = 2.4 Hz, 1H), 8.05 (dd, ^3J(H,H) = 8.4 Hz, ^4J(H,H) = 2.4 Hz, 1H), 7.26 (d, ^3J(H,H) = 8.3 Hz, 1H), 6.93 (d, ^3J(H,H) = 8.3 Hz, 1H), 6.87 – 6.85 (m, 1H), 6.85 – 6.80 (m, 1H), 3.21 (t, ^3J(H,H) = 5.6 Hz, 4H), 2.17 (s, 3H), 2.01 (s, 3H), 1.78 – 1.69 (m, 4H), 1.64 – 1.58 (m, 2H) ppm; **^{13}C-NMR** (101 MHz, $CDCl_3$C): δ = 151.7 (C_q, 1C), 149.0 (C_q, 1C), 146.8 (C_q, 1C), 138.5 (C_q, 2C), 135.7 (C_q, 1C), 130.8 (C_t, 1C), 129.2 (C_t, 1C), 124.5 (C_t, 1C), 120.6 (C_t, 1C), 117.5 (C_t, 1C), 113.5 (C_t, 1C), 50.3 (C_s, 2C), 25.8 (C_s, 2C), 24.3 (C_s, 1C), 20.1 (C_p, 1C), 20.0 (C_p, 1C) ppm; **MS** (MALDI-ToF): m/z (%) = 310 (100); **elemental analysis** calcd (%) for $C_{19}H_{22}N_2O_2$: C 73.52, H 7.14, N 9.03; found: C 73.41, H 7.20, N 8.77; **UV/Vis** (chloroform): λ_{max} (ε) = 270 nm (17598 Lmol^{-1}cm^{-1}), λ_{max} (ε) = 354 nm (3003 Lmol^{-1}cm^{-1}).

1-(7-Nitro-9,10-dihydrophenanthren-2-yl)piperidine (C1d): Following the general procedure D using 2.94 mg (0.45 mol%, 1.02 µmol) phosphotungstic acid hydrate in CTAB (0.7 mL, 10 cmc, 0.02 M). After adding sodium perborate tetrahydrate (360 mg, 7.00 equiv., 2.34 mmol) the temperature was raised to 60°C. Amine **C7d** (93.0 mg, 1.00 equiv., 0.334 mmol) in CTAB (20 mL) was added dropwise to the mixture. The red reaction mixture was stirred for 17 h at 60°C. Column chromatography (SiO_2; CH_2Cl_2) was used for purification. According to this procedure the solid, red target compound **C1d** (57.4 mg, 56%) was isolated.

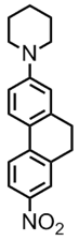

***R*$_f$** = 0.61 (SiO_2; CH_2Cl_2); **m.p.** 114 – 115°C; **^{1}H-NMR** (400 MHz, $CDCl_3$): δ = 8.08 (dd, ^3J(H,H) = 8.6 Hz, ^4J(H,H) = 2.4 Hz, 1H), 8.04 (d, ^4J(H,H) = 2.3 Hz, 1H), 7.69 (d, ^3J(H,H) = 8.6 Hz, 1H), 7.64 (d, ^3J(H,H) = 8.7 Hz, 1H), 6.86 (dd, ^3J(H,H) = 8.7 Hz, ^4J(H,H) = 2.4 Hz, 1H), 6.77 (d, ^4J(H,H) = 2.4 Hz, 1H), 3.29 (t, ^3J(H,H) = 5.7 Hz, 4H), 2.96 – 2.82 (m, 4H), 1.75 – 1.66 (m, 4H), 1.66 – 1.59 (m, 2H) ppm; **^{13}C-NMR** (101 MHz, $CDCl_3$): δ = 152.4 (C_q, 1C), 145.2 (C_q, 1C), 141.6 (C_q, 1C), 139.3 (C_q, 2C), 136.9 (C_q, 1C), 125.9 (C_t, 1C), 123.1 (C_t, 1C), 122.7 (C_t, 1C), 122.4 (C_t, 1C), 114.5 (C_t, 1C), 114.1 (C_t, 1C), 49.4 (C_s, 2C), 29.2 (C_s, 1C), 29.0 (C_s, 1C), 25.5 (C_s, 2C), 24.3 (C_s, 1C) ppm; **MS** (MALDI-ToF): m/z (%) = 309 (11), 308 (43), 307 (100); **elemental analysis** calcd (%) for $C_{19}H_{20}N_2O_2$: C 74.00, H 6.54, N 9.08; found: C 73.63, H 6.61, N 9.03; **UV/Vis** (chloroform): λ_{max} (ε) = 274 nm (14713 $Lmol^{-1}cm^{-1}$), λ_{max} (ε) = 416 nm (20782 $Lmol^{-1}cm^{-1}$).

3-Nitro-9-(piperidin-1-yl)-6,7-dihydro-5*H*-dibenzo[*a*,*c*]cycloheptene (C1e): In accordance to the general procedure D, 6.20 mg (0.45 mol%, 7.15 µmol) phosphotungstic acid hydrate in CTAB (0.2 mL, 10 cmc, 0.02 M) and 771 mg (7.00 equiv., 5.01 mmol) sodium perborate tetrahydrate were used. Amine **C7e** (209 mg, 1.00 equiv., 0.715 mmol) in CTAB (14 mL) was added dropwise to the mixture at 60°C. The red reaction mixture was stirred for 15 h at 60°C. By column chromatography (SiO_2; CH_2Cl_2) the crude was purified to achieve the push-pull system **C1e** (135 mg, 59%) as a dark red solid.

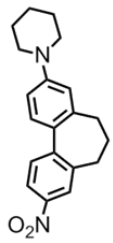

***R*$_f$** = 0.58 (SiO_2; CH_2Cl_2); **m.p.** 109 – 110°C; **^{1}H-NMR** (400 MHz, $CDCl_3$): δ = 8.16 (dd, ^3J(H,H) = 8.4 Hz, ^4J(H,H) = 2.4 Hz, 1H), 8.09 (d, ^4J(H,H) = 2.4 Hz, 1H), 7.45 (d, ^3J(H,H) = 8.4 Hz, 1H), 7.27 (d, ^3J(H,H) = 8.6 Hz, 1H), 6.92 (dd, ^3J(H,H) = 8.5 Hz, ^4J(H,H) = 2.5 Hz, 1H), 6.84 (d, ^4J(H,H) = 2.4 Hz, 1H), 3.27 (t, ^3J(H,H) = 5.5 Hz, 4H), 2.59 (t, ^3J(H,H) = 7.0 Hz, 2H), 2.46 (t, ^3J(H,H) = 7.0 Hz, 2H), 2.23 (quint, ^3J(H,H) = 7.0 Hz, 2H), 1.77 – 1.69 (m, 4H),

1.66 – 1.58 (m, 2H) ppm; **^{13}C-NMR** (101 MHz, $CDCl_3$): δ = 152.4 (C_q, 1C), 148.6 (C_q, 1C), 146.2 (C_q, 1C), 140.8 (C_q, 1C), 140.5 (C_q, 1C), 129.3 (C_t, 1C), 129.1 (C_q, 1C), 128.4 (C_t, 1C), 123.5 (C_t, 1C), 121.8 (C_t, 1C), 115.9 (C_t, 1C), 113.8 (C_t, 1C), 49.9 (C_s, 2C), 32.9 (C_s, 1C), 31.8 (C_s, 1C), 31.7 (C_s, 1C), 25.7 (C_s, 2C), 24.3 (C_s, 1C) ppm; **MS** (EI+, 70 eV): m/z (%) = 323 (24), 322 (100), 321 (51), 275 (6), 191 (7); **elemental analysis** calcd (%) for $C_{20}H_{22}N_2O_2$: C 74.51, H 6.88, N 8.69; found: C 74.41, H 6.90, N 8.43; **UV/Vis** (chloroform): λ_{max} (ε) = 269 nm (17538 Lmol^{-1}cm^{-1}), λ_{max} (ε) = 388 nm (12074 Lmol^{-1}cm^{-1}).

3-Nitro-10-(piperidin-1-yl)-5,6,7,8-tetrahydrodibenzo[*a*,*c*]cyclooctene (C1f): In

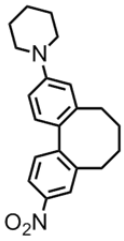

accordance to the general procedure D, 8.71 mg (0.45 mol%, 9.89 µmol) phosphotungstic acid hydrate in CTAB (2.3 mL, 10 cmc, 0.02 M) and 1.07 g (7.00 equiv., 6.93 mmol) sodium perborate tetrahydrate were used. Amine **C7f** (303 mg, 1.00 equiv., 0.989 mmol) in CTAB (80 mL) was added dropwise to the mixture at 60°C. The orange reaction mixture was stirred for 15 h at 60°C. By column chromatography (SiO_2; CH_2Cl_2:hexane 2:1) the crude was purified to achieve the push-pull system **C1f** (149 mg, 45%) as an orange solid.

***R*$_f$** = 0.34 (SiO_2; CH_2Cl_2:hexane 2:1); **m.p.** 124 – 125°C; **^{1}H-NMR** (400 MHz, $CDCl_3$): δ = 8.14 (d, ^4J(H,H) = 2.4 Hz, 1H), 8.06 (dd, ^3J(H,H) = 8.4 Hz, ^4J(H,H) = 2.4 Hz, 1H), 7.37 (d, ^3J(H,H) = 8.4 Hz, 1H), 7.10 (d, ^3J(H,H) = 9.2 Hz, 1H), 6.86 – 6.83 (m, 2H), 3.24 (t, ^3J(H,H) = 5.5 Hz, 4H), 2.81 (dd, ^3J(H,H) = 8.2 Hz, ^2J(H,H) = 13.3 Hz, 1H), 2.69 (dd, ^3J(H,H) = 8.2 Hz, ^2J(H,H) = 13.4 Hz, 1H), 2.30 – 2.20 (m, 1H), 2.19 – 1.94 (m, 3H), 1.79 – 1.70 (m, 4H), 1.66 – 1.49 (m, 4H) ppm; **^{13}C-NMR** (101 MHz, $CDCl_3$): δ = 152.5 (C_q, 1C), 147.8 (C_q, 1C), 147.1 (C_q, 1C), 144.3 (C_q, 1C), 143.0 (C_q, 1C), 130.0 (C_t, 1C), 129.4 (C_t, 1C), 129.2 (C_q, 1C), 124.2 (C_t, 1C), 120.7 (C_t, 1C), 116.7 (C_t, 1C), 113.6 (C_t, 1C), 50.1 (C_s, 2C), 33.1 (C_s, 1C), 32.8 (C_s, 1C), 29.5 (C_s, 1C), 29.0 (C_s, 1C), 25.8 (C_s, 2C), 24.3 (C_s, 1C) ppm; **MS** (EI+, 70 eV): m/z (%) = 337 (24), 336 (100), 335 (42), 289 (5); **elemental analysis** calcd (%) for $C_{21}H_{24}N_2O_2$: C 74.97, H 7.19, N 8.33; found: C 74.55, H 7.13, N 8.23; **UV/Vis** (chloroform): λ_{max} (ε) = 271 nm (20019 Lmol^{-1}cm^{-1}), λ_{max} (ε) = 370 nm (7551 Lmol^{-1}cm^{-1}).

3-Nitro-11-(piperidin-1-yl)-6,7,8,9-tetrahydro-5*H*-dibenzo[*a*,*c*]cyclononene (C1g): In

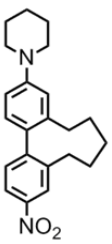

accordance to the general procedure D, 3.76 mg (0.45 mol%, 4.27 µmol) phosphotungstic acid hydrate in CTAB (1 mL, 10 cmc, 0.02 M) and 460 mg (7.00 equiv., 2.99 mmol) sodium perborate tetrahydrate were used. Amine **C7g** (137 mg, 1.00 equiv., 0.427 mmol) in CTAB (33 mL) was added dropwise to the

mixture at 60°C. The orange-yellow reaction mixture was stirred for 15 h at 60°C. By column chromatography (SiO_2; CH_2Cl_2:hexane 2:1) the crude was purified to achieve the push-pull system **C1g** (75 mg, 50%) as a yellow solid.

R_f = 0.44 (SiO_2; CH_2Cl_2:hexane 2:1); **m.p.** 125 – 126°C; **^{1}H-NMR** (400 MHz, $CDCl_3$): δ = 8.10 (d, ^4J(H,H) = 1.9 Hz, 1H), 8.05 (dd, ^3J(H,H) = 8.3 Hz, ^4J(H,H) = 1.9 Hz, 1H), 7.30 (d, ^3J(H,H) = 8.3 Hz, 1H), 6.96 (d, ^3J(H,H) = 7.9 Hz, 1H), 6.88 – 6.80 (m, 2H), 3.22 (t, ^3J(H,H) = 5.3 Hz, 4H), 2.76 – 2.59 (m, 2H), 2.30 – 2.20 (m, 1H), 1.97 – 1.70 (m, 7H), 1.66 – 1.28 (m, 6H) ppm; **^{13}C-NMR** (101 MHz, $CDCl_3$): δ = 152.2 (C_q, 1C), 149.6 (C_q, 1C), 147.2 (C_q, 1C), 144.3 (C_q, 1C), 141.8 (C_q, 1C), 130.7 (C_q, 1C), 130.3 (C_t, 1C), 128.8 (C_t, 1C), 123.6 (C_t, 1C), 120.6 (C_t, 1C), 116.6 (C_t, 1C), 113.7 (C_t, 1C), 50.4 (C_s, 2C), 33.7 (C_s, 1C), 33.2 (C_s, 1C), 28.9 (C_s, 1C), 28.8 (C_s, 1C), 28.2 (C_s, 1C), 25.9 (C_s, 2C), 24.3 (C_s, 1C) ppm; **MS** (MALDI-ToF): m/z (%) = 351 (10), 350 (18), 336 (26), 235 (43), 321 (86), 320 (45), 319 (100); **elemental analysis** calcd (%) for $C_{22}H_{25}N_2O_2$: C 75.40, H 7.48, N 7.99; found: C 75.12, H 7.42, N 7.79; **UV/Vis** (chloroform): λ_{max} (ε) = 269 nm (18523 $Lmol^{-1}cm^{-1}$), λ_{max} (ε) = 347 nm (3019 $Lmol^{-1}cm^{-1}$).

2-Nitro-9*H*-fluorene (C25): Compound **C25** was synthesized according to a literature known procedure (colorless solid, 15%).[159]

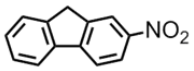

R_f = 0.39 (SiO_2; hexane:ethyl acetate (5:1); **m.p.** 162°C; **^{1}H-NMR** (400 MHz, $CDCl_3$): δ = 8.40 (d, ^4J(H,H) = 2.0 Hz, 1H), 8.30 (dd, ^3J(H,H) = 8.4 Hz, ^4J(H,H) = 2.0 Hz, 1H), 7.89 – 7.86 (m, 2H), 7.63 – 7.61 (m, 1H), 7.48 – 7.41 (m, 2H), 4.01 (s, 2H) ppm; **^{13}C-NMR** (101 MHz, $CDCl_3$): δ = 148.0 (C_q, 2C), 144.8 (C_q, 1C), 143.9 (C_q, 1C), 139.4 (C_q, 1C), 128.8 (C_t, 1C), 127.4 (C_t, 1C), 125.4 (C_t, 1C), 123.1(C_t, 1C), 121.3 (C_t, 1C), 120.5 (C_t, 1C), 119.8 (C_t, 1C), 37.0 (C_s, 1C) ppm; **MS** (EI+, 70 eV): m/z (%) = 212 (10); 211 (68); 194 (26); 166 (13); 165 (100); 164 (41); 163 (30).

7-Iodo-2-Nitro-9*H*-fluorene (C26): Compound **C26** was synthesized according to a literature known procedure (yellow powder, 76%).[160]

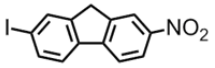

R_f = 0.56 (SiO_2; hexane:EtOAc 3:1); **^{1}H-NMR** (400 MHz, $CDCl_3$): δ = 8.40 (s, 1H), 8.31 (d, ^3J(H,H) = 8.4 Hz, 1H), 7.99 (s, 1H), 7.85 (d, ^3J(H,H) = 8.4 Hz, 1H), 7.79 (d, ^3J(H,H) = 8.3 Hz, 1H), 7.61 (d, ^3J(H,H) = 8.1 Hz, 1H), 3.99 (s, 2H) ppm; **^{13}C-NMR** (101 MHz, $CDCl_3$): δ = 147.1 (C_q, 2C), 146.7 (C_q, 1C), 143.4 (C_q, 1C), 139.0 (C_q, 1C), 136.5 (C_t, 1C), 134.7 (C_t,

1C), 123.3 (C_t, 1C), 122.7 (C_t, 1C), 120.5 (C_t, 1C), 120.1 (C_t, 1C), 94.8 (C_q, 1C), 36.6 (C_s, 1C) ppm; **MS** (MALDI-ToF): m/z (%) = 338 (11), 337 (100).

7-Iodo-9,9-dimethyl-2-nitro-9*H*-fluorene (C27):[119] 7-Iodo-2-nitrofluorene (**C26**) (200 mg, 1.00 equiv., 0.593 mmol), iodomethane (80.0 µL, 2.05 equiv., 1.22 mmol, 173 mg) and potassium iodide (10.8 mg, 0.110 equiv., 653 µmol) were dissolved in dimethyl sulfoxide (2 mL) under argon atmosphere. Powdered potassium hydroxide (141 mg, 4.25 equiv., 2.52 mmol) was added in 15 portions to the solution. The green reaction mixture was stirred at rt for 1 h and quenched with water. After extraction with dichloromethane (3 × 50 ml), the combined organic layers were dried with sodium sulfate, filtered and concentrated. The resulting solid was purified by column chromatography (SiO_2; hexane:EtOAc 5:1) to afford 7-iodo-9,9-dimethyl-2-nitrofluorene (**C27**) (205 mg, 95%) as a yellow solid.

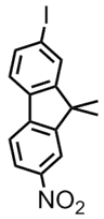

***R*$_f$** = 0.62 (SiO_2; hexane:EtOAc 3:1); **m.p.** 215 – 216°C; **^{1}H-NMR** (400 MHz, $CDCl_3$): δ = 8.29 – 8.24 (m, 2H), 7.84 (d, ^4J(H,H) = 1.2 Hz, 1H), 7.79 (d, ^3J(H,H) = 8.1 Hz, 1H), 7.75 (dd, ^3J(H,H) = 8.0 Hz, ^4J(H,H) = 1.5 Hz, 1H), 7.54 (d, ^3J(H,H) = 8.0 Hz, 1H), 1.53 (s, 6H) ppm; **^{13}C-NMR** (101 MHz, $CDCl_3$): δ = 157.0 (C_q, 1C), 154.0 (C_q, 1C), 147.6 (C_q, 1C), 144.7 (C_q, 1C), 136.7 (C_t, 1C), 136.4 (C_q, 1C), 132.5 (C_t, 1C), 123.5 (C_t, 1C), 122.9 (C_t, 1C), 120.3 (C_t, 1C), 118.3 (C_t, 1C), 95.5 (C_q, 1C), 47.5 (C_q, 1C), 26.6 (C_p, 2C) ppm; **MS** (EI+, 70 eV): m/z (%) = 366 (16), 265 (100), 350 (64), 304 (15), 177 (18), 176 (25).

1-(9,9-Dimethyl-7-nitro-9*H*-fluorene-2-yl)piperidine (C1c):[110] To a pale yellow solution of 7-iodo-(9,9-dimethyl)-2-nitro-9*H*-fluorene (**C27**) (140 mg, 1.00 equiv., 0.383 mmol) in dimethyl sulfoxide (2 mL), piperidine (0.170 mL, 4.40 equiv., 1.69 mmol, 144 mg), cesium acetate (174 mg, 2.37 equiv., 0.909 mmol) and copper iodide (3.65 mg, 5 mol%, 19.2 µmol) were added. The red-brown reaction mixture was stirred for 23 h at 90°C. After cooling to rt the crude was quenched with water (20 ml), extracted with EtOAc (3 × 30 mL) and washed with brine (2 × 20 mL). The organic layers were dried with sodium sulfate, filtered and concentrated *in vacuo*. The reddish residue was purified by column chromatography (SiO_2; hexane:EtOAc 5:1, 5% NEt_3) and by a second column (SiO_2; CH_2Cl_2). According to this procedure the desired product **C1c** (18.5 mg, 15%) was isolated as a red solid.

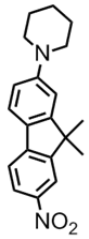

***R*$_f$** = 0.55 (SiO_2; hexane:EtOAc 3:1); **m.p.** 163 – 164°C; **^{1}H-NMR** (400 MHz, $CDCl_3$): δ = 8.22 – 8.19 (m, 2H), 7.66 – 7.60 (m, 2H), 6.98 (d, ^4J(H,H) = 2.1 Hz, 1H), 6.94 (dd, ^3J(H,H) =

8.5 Hz, ^4J(H,H) = 2.2 Hz, 1H), 3.31 (t, ^3J(H,H) = 5.6 Hz, 4H), 1.75 (quint, ^3J(H,H) = 5.5 Hz, 4H), 1.67 – 1.60 (m, 2H), 1.50 (s, 6H) ppm; **^{13}C-NMR** (101 MHz, $CDCl_3$): δ = 156.9 (C_q, 1C), 153.8 (C_q, 1C), 153.4 (C_q, 1C), 146.5 (C_q, 1C), 145.7 (C_q, 1C), 127.4 (C_q, 1C), 123.6 (C_t, 1C), 122.3 (C_t, 1C), 118.4 (C_t, 1C), 118.0 (C_t, 1C), 115.2 (C_t, 1C), 109.6 (C_t, 1C), 50.2 (C_s, 1C), 47.1 (C_q, 1C), 27.0 (C_p, 2C), 25.7 (C_s, 1C), 24.3 (C_s, 1C) ppm; **MS** (MALDI-ToF): m/z (%) = 323 (10), 322 (14), 321 (21), 307 (12), 293 (57), 292 (100); **elemental analysis** calcd (%) for $C_{20}H_{22}N_2O_2$: C 74.51, H 6.88, N 8.69; found: C 74.25, H 6.78, N 8.52; **UV/Vis** (chloroform): λ_{max} (ε) = 271 nm (14362 Lmol^{-1}cm^{-1}), λ_{max} (ε) = 418 nm (21703 Lmol^{-1}cm^{-1}).

1-(4'-Nitrobiphenyl-4-yl)piperidine (C1a) ***(by Suzuki-Miyaura coupling)*****:** A solution of 1-(4-iodophenyl)piperidine (500 mg, 1.50 equiv., 1.74 mmol) in toluene (9 mL) and methanol (3 mL) was purged with argon for 15 min. Afterwards cesium carbonate (757 mg, 2.00 equiv., 2.32 mmol), 4,4,5,5-tetramethyl-2-(4-nitrophenyl)-1,3,2-dioxaborolane (289 mg, 1.00 equiv., 1.16 mmol) and tetrakis-(triphenylphosphine)palladium (134 mg, 10 mol%, 0.116 mmol) were added to the stirred reaction at rt. The dark-brown reaction mixture was heated at reflux for 18 h. After cooling to rt the mixture was filtered over celite and concentrated under reduced pressure. The resulting residue was purified by column chromatography (SiO_2; CH_2Cl_2) to achieve push-pull system **C1a** as an orange solid (26%).

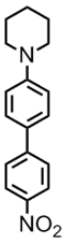

R_f = 0.73 (SiO_2; CH_2Cl_2); **m.p.** 220°C; **^{1}H-NMR** (400 MHz, $CDCl_3$): δ = 8.24 (d, ^3J(H,H) = 9.0 Hz, 2H), 7.68 (d, ^3J(H,H) = 9.0 Hz, 2H), 7.55 (d, ^3J(H,H) = 8.9 Hz, 2H), 7.00 (d, ^3J(H,H) = 8.9 Hz, 2H), 3.28 (t, ^3J(H,H) = 5.5 Hz, 4H), 1.77 – 1.68 (m, 4H), 1.67 – 1.60 (m, 2H) ppm; **^{13}C-NMR** (101 MHz, $CDCl_3$): δ = 152.3 (C_q, 1C), 147.4 (C_q, 1C), 146.0 (C_q, 1C), 128.1 (C_t, 2C), 127.9 (C_q, 1C), 126.4 (C_t, 2C), 124.1 (C_t, 2C), 115.8 (C_t, 2C), 49.6 (C_s, 2C), 25.5 (C_s, 2C), 24.3 (C_s, 1C) ppm; **MS** (MALDI-ToF): m/z (%) = 283 (55), 282 (100).

4,4'-Dimethoxy-2,2-dimethylbiphenyl (C9): Under an inert atmosphere, 1-bromo-4-methoxy-2-methylbenzene (34.90 g, 0.174 mol, 1.00 equiv.) was added dropwise into a suspension of magnesium (6.10 g, 0.251 mol, 1.40 equiv.) in dry methyltetrahydrofuran (MeTHF, 150 mL) at such a rate that the moderate conversion of the halogenide was maintained. Then the reaction mixture was heated at reflux for 30 min and cooled to room temperature. The Grignard reagent was slowly transferred to a refluxing solution of 1,2-dichloroethane (23.0 mL, 0.292 mol, 1.70 equiv.) and anhydrous $FeCl_3$ (2.00 g, 12.3 mmol, 7.1 mol%) in dry diethyl ether (250 mL). The reaction mixture was

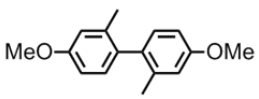

heated at reflux for 70 min, cooled to room temperature, and poured onto ice. Then, conc. aq. HCl (20 mL) was added, the organic layer was separated, and the aqueous phase was extracted with methyl *tert*-butyl ether (3 × 50 mL). The combined extracts were washed with NaOH (2 × 50 mL, 1.0 M) and filtered through a silica pad. The colorless oil was dried *in vacuo* to afford **C9** (19.40 g, 80.06 mmol, 92%) which was pure enough to be used in the next step without further purification. For analytical purposes flash chromatography was performed (SiO_2; CH_2Cl_2 in hexane, 20-100%).

^{1}H-NMR (400 MHz, $CDCl_3$): δ = 2.06 (s, 6 H), 3.85 (s, 6H), 6.78 (dd, ^3J(H,H) = 8.3 Hz, ^4J(H,H) = 2.5 Hz, 2 H), 6.84 (d, ^4J(H,H) = 2.5 Hz, 2H), 7.03 (d, ^3J(H,H) = 8.3 Hz, 2H) ppm; **^{13}C-NMR** (100 MHz, $CDCl_3$): δ = 20.6, 55.6, 111.2, 115.6, 131.1, 134.2, 138.1, 159.0 ppm; **MS** (EI+, 70 eV): m/z (%) = 242.1 (100) [M^+]; **elemental analysis** calcd (%) for $C_{16}H_{18}O_2$: C 79.31, H 7.49; found: C 78.14, H 7.26.

2,2'-Bis(bromomethyl)-4,4'-dimethoxybiphenyl (C10): NBS (3.10 g, 17.4 mmol, 2.10 equiv.) and benzoyl peroxide (0.20 g, 0.62 mmol, 7.5 mol%, 75%) were added to a solution of **C9** (2.00 g, 8.25 mmol, 1.00 equiv.) in CCl_4 (60 mL). The reaction was kept at reflux until all starting material was converted (GC-MS, 2 h). The cooled reaction mixture was filtered through a silica pad and the solvent was evaporated. Flash chromatography was performed (SiO_2; CH_2Cl_2 in hexane, 30–90%) to afford pure 2,2'-bis(bromomethyl)-4,4'-dimethoxy-biphenyl (**C10**) (68%) as a thick colorless oil that solidified upon standing.

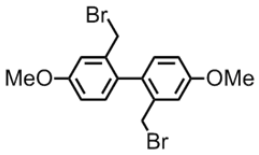

M.p. 75°C; **^{1}H-NMR** (250 MHz, $CDCl_3$): δ = 3.87 (s, 6 H), 4.17 (d, ^2J(H,H) = 9.9 Hz, 2H), 4.31 (d, ^2J(H,H) = 9.9 Hz, 2H), 6.91 (dd, ^3J(H,H) = 8.4 Hz, ^4J(H,H) = 2.7 Hz, 2H), 7.06 (d, ^4J(H,H) = 2.7 Hz, 2H), 7.18 (d, ^3J(H,H) = 8.4 Hz, 2H) ppm; **^{13}C-NMR** (100 MHz, $CDCl_3$): δ = 32.6, 55.8, 114.7, 115.8, 131.9, 132.1, 137.9, 159.8 ppm; **MS** (EI+, 70 eV): m/z (%) = 398.0 (50), 400.0 (100), 402.0 (49) [M^+]; **HRMS** (ESI): m/z calcd for $C_{16}H_{16}O_2Br_2$ [M+Na]$^+$: 420.9416; found: 420.9414; **elemental analysis** calcd (%) for $C_{16}H_{16}Br_2O_2$: C 48.03, H 4.03; found: C 47.94, H 3.91.

3,9-Dimethoxy-5,7-dihydrodibenzo[*a*,*c*]cyclohepten-6-one (C11): Under ice cooling, NaOH (294 mg, 7.35 mmol, 5.00 equiv.) was dissolved in H_2O (4 mL) and added to a suspension of **C10** (589 mg, 1.47 mmol, 1.00 equiv.), toluenesulfonylmethyl isocyanide (287 mg, 1.47 mmol, 1.00 equiv.), and tetrabutylammonium bromide (TBAB, 30.0 mg, 93.0 mmol, 6.3 mol%) in CH_2Cl_2

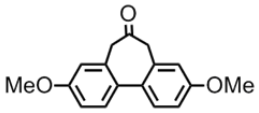

(10 mL). The two-phase mixture was stirred vigorously at room temperature overnight. *t*BME (16 mL) and conc. aq. HCl (8 mL) were added, and the mixture was stirred for 3 h. The phases were separated and the organic layer was washed with saturated $NaHCO_3$, dried with $MgSO_4$, and the solvent was evaporated. The crude product was purified by flash chromatography (SiO_2; CH_2Cl_2) to afford **C11** as a white solid (326 mg, 1.22 mmol, 83%).

M.p. 126°C; **^{1}H-NMR** (250 MHz, $CDCl_3$): δ = 3.45 (d, ^2J(H,H) = 13.0, 2 H), 3.59 (d, ^2J(H,H) = 13.0 Hz, 2 H), 6.79 (d, ^4J(H,H) = 2.6 Hz, 2H), 6.94 (dd, ^3J(H,H) = 8.5 Hz, ^4J(H,H) = 2.6 Hz, 2H), 7.44 (d, ^3J(H,H) = 8.5 Hz, 2H) ppm; **^{13}C-NMR** (100 MHz, $CDCl_3$): δ = 50.0, 55.8, 113.7, 114.9, 130.6, 132.1, 134.3, 159.4, 210.5 ppm; **MS** (EI+, 70 eV): m/z (%) = 268.1 (100) [M^+], 225.1 (67), 165.1 (15), 153.1 (11); **HRMS** (ESI): m/z calcd for $C_{17}H_{16}O_3$ $[M+Na]^+$: 291.0997; found: 291.0993.

3,9-Dimethoxy-6,7-dihydro-5H-dibenzo[*a*,*c*]cycloheptene (C12): Hydrazine monohydrate

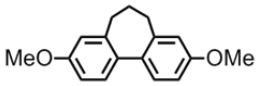

(0.35 mL, 7.21 mmol, 2.3 equiv.) was added to a suspension of **C11** (854 mg, 3.18 mmol, 1.00 equiv.) and powdered KOH (750 mg, 13.4 mmol, 4.20 equiv.) in diethylene glycol (10 mL) under ice cooling. The mixture was heated at reflux for 2 h. The water and excess of hydrazine was distilled off at an oil-bath temperature of 190°C. After a total reaction time of 3 h and a maximum oil-bath temperature of 195°C, the reaction was stopped. Water (40 mL) was added to the cooled reaction mixture, followed by extraction with *t*BME (4 × 20 mL). The combined organic layers were washed with HCl (1 × 20 mL, 1.0 M), water (3 × 10 mL), and brine (1 × 30 mL), dried with $MgSO_4$, and filtered through a short silica pad. After evaporation of the solvent, **C12** was obtained as a white oil that solidified upon standing (86%).

M.p. 110°C; **^{1}H-NMR** (250 MHz, $CDCl_3$): δ = 2.16 (m, 2H), 2.47 (m, 4 H), 7.19 (d, ^4J(H,H) = 2.4 Hz, 2 H), 7.27 (dd, ^3J(H,H) = 8.4 Hz, ^4J(H,H) = 2.6 Hz, 2H), 7.41 (d, ^3J(H,H) = 8.4 Hz, 2H) ppm; **^{13}C-NMR** (101 MHz, $CDCl_3$): δ = 32.2, 33.3, 55.7, 111.9, 114.6, 129.5, 133.9, 141.3, 159.1 ppm; **HRMS** (ESI): m/z calcd for $C_{17}H_{19}O_2$ $[M+Na]^+$: 255.1385; found: 255.1385.

3,9-Dihydroxy-6,7-dihydro-5H-dibenzo[*a*,*c*]cycloheptene (C13): BBr_3 (2.90 mL,

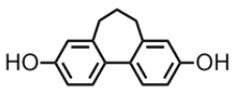

30.6 mmol, 5.50 equiv.) was slowly dropped into a solution of **C12** (1.50 g, 5.59 mmol, 1.00 equiv.) in dry CH_2Cl_2 (80 mL) at 0°C. Stirring was continued at room temperature until TLC showed full conversion of the starting material (1.5 h). The reaction was quenched with MeOH under ice cooling. The reaction mixture was

washed with water (50 mL) and dried with $MgSO_4$ and the solvent was evaporated. The crude **C16** (1.67 g) was obtained as a white powder which was pure enough to be used for the next step. Flash chromatography was performed (SiO_2; hexane:*t*BME, 2:1) to obtain a sample for analytical purposes.

^{1}H-NMR (250 MHz, $CDCl_3$): δ = 2.14 (m, 2H), 2.44 (m, 4 H), 4.66 (br s, 2H), 6.72 (d, ^4J(H,H) = 2.4 Hz, 2 H), 6.78 (dd, ^3J(H,H) = 8.0 Hz, ^4J(H,H) = 2.4 Hz, 2H), 7.19 (d, ^3J(H,H) = 2.6 Hz =8.0 Hz, 2H) ppm; **^{13}C-NMR** (100 MHz, $CDCl_3$): δ = 31.5, 32.7, 113.0, 115.2, 128.9, 132.6, 140.7, 155.4 ppm; **MS** (MALDI-TOF): m/z (%) = 226.4 [M^+].

3,9-Bis-(trifluoromethanesulfonyloxy)-6,7-dihydro-5H-dibenzo[*a*,*c*]cycloheptene (C2e):

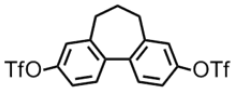

The crude diol **C13** was esterified with triflic anhydride and pyridine as the base, according to a known protocol.[42] The ditriflate **C2e** was obtained as a colorless oil. The yield over two steps was 84%.

^{1}H-NMR (250 MHz, $CDCl_3$): δ = 2.24 (m, 2 H), 2.52 (m, 4H), 7.19 (d, ^4J(H,H) = 2.5 Hz, 2H), 7.27 (dd, ^3J(H,H) = 8.4 Hz, ^4J(H,H) = 2.5 Hz, 2H), 7.41 (d, ^3J(H,H) = 8.4 Hz, 2H) ppm; **^{13}C-NMR** (101 MHz, $CDCl_3$): δ = 31.2, 32.6, 119.6, 121.4, 130.0, 139.6, 142.1, 149.0 ppm; ^{19}F-NMR: δ = 74.0 ppm; **MS** (EI+, 70 eV): m/z (%) = 490.0 (37) [M+]; **elemental analysis** calcd (%) for $C_{17}H_{12}F_6O_6S_2$: C 41.64, H 2.47; found: C 41.72, H 2.48.

4,4'-Dibromobiphenyl-2,2'-dicarboxylic acid (C15): 2-Amino-5-bromobenzoic acid

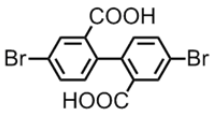

(23.9 g, 0.140 mmol, 1.00 equiv.) was suspended in conc. aq. HCl (49.6 mL, 0.600 mol) and water (110 mL). At 0°C the amine was diazotized by adding slowly a solution of $NaNO_2$ (11.5 g, 0.169 mol, 1.20 equiv.) in water (40 mL). After stirring 1 h at 0°C the solution was carefully induced via canula into a freshly prepared solution of $CuSO_4$ pentahydrate (69.3 g, 0.278 mol, 2.00 equiv.), NH_4OH (148 mL, 0.960 mmol, 6.90 equiv., 25%), water (250 mL) and hydroxylamine·HCl (20.7 g, 0.300 mmol, 2.10 equiv.) dissolved in a NaOH solution (49.5 mL, 0.300 mol, 2.10 equiv.). Then stirring was continued by increasing the temperature from 25°C to 70°C for 1 h. The mixture was cooled to room temperature and acidified with conc. aq. HCl. After filtering, washing with water and drying in the oven (70°C) 4,4'-dibromobiphenyl-2,2'-dicarboxylic acid (**C15**) was obtained as a beige powder (70%).

R_f = 0.06 (SiO_2; ethyl acetate); **m.p.** 246-250°C; **^{1}H-NMR** (400 MHz, DMSO-d6): δ = 7.05-7.20 (m, 2H), 7.67-7.50 (m, 2H), 7.94 (br s, 2H), 13.1 (br s, 2H); **^{13}C-NMR** (101 MHz, CD_3OD): δ = 121.4, 133.5, 134.7; **MS** (EI+, 70 eV): m/z (%) = 397.9, 399.9, 401.9 [M^+].

4,4'-Dibromo-2,2'-biphenyldimethanol (C16): Under inert atmosphere 4,4'-dibromobiphenyl-2,2'-dicarboxylic acid (**C15**) (17.1 g, 55.0 mmol, 1.00 equiv.) was dissolved in dry THF (200 mL). $NaBH_4$ (6.24 g, 0.165 mol, 3.00 equiv.) was added in portions keeping the temperature below 30°C. After stirring at room temperature for 1 h $BF_3{\cdot}Et_2O$ (31.1 mL, 0.253 mol, 4.60 equiv.) was added dropwise to the reaction mixture keeping the temperature between 10°C to 25°C. The mixture was stirred overnight and quenched with HCl (aq., 5%), diluted with ethyl acetate (450 mL) and filtered through a celite pad. The brown solution was washed with sat. Na_2CO_3, brine and dried with $MgSO_4$. After evaporation of the solvents 4,4'-dibromo-2,2'-biphenyldimethanol (**C16**) was obtained as a brown oily solid (16.4 g), which was used without further purification for the next step. For analytical purposes a sample was purified by flash chromatography (SiO_2; hexane:ethyl acetate, 7:3).

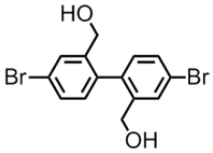

R_f = 0.40 (SiO_2; hexane/ethyl acetate, 1:1); **m.p.** 133-134°C; **^{1}H-NMR** (400 MHz, DMSO-d6): δ = 4.05 (dd, ^2J(H,H) = 14.1 Hz, ^3J(H,H) = 5.5 Hz, 4H), 4.15 (dd, ^2J(H,H) = 14.1 Hz, ^3J(H,H) = 5.4 Hz, 2H), 5.23 (dd, ^3J(H,H) = 5.5 Hz, ^3J(H,H) = 5.5 Hz, 2H), 7.01 (d, ^3J(H,H) = 8.1 Hz, 2H), 7.47 (dd, ^3J(H,H) = 8.0 Hz, ^4J(H,H) = 1.9 Hz, 2H), 7.69 (d, ^4J(H,H) = 1.9 Hz, 2H); **^{13}C-NMR** (101 MHz, DMSO-d6): δ = 61.0, 122.0, 130.1, 130.4, 131.9, 136.8, 143.4. **MS** (FAB): m/z (%) = 372.9 ([M+H]$^+$); **elemental analysis** calcd for $C_{14}H_{12}Br_2O_2$: C 45.20, H 3.25; found: C 44.63, H 3.43.

4,4'-Dibromo-2,2'-bis(bromomethyl)biphenyl (C14):

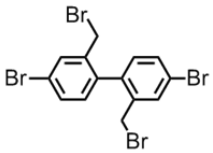

4,4'-Dibromo-2,2'-biphenyldimethanol **C16** (16.4 g, assuming 55.0 mmol, 1.00 equiv.) was dissolved in dry dichloromethane (100 mL). The brown solution was cooled to 5°C and PBr_3 (12.9 mL, 0.136 mol, 2.50 equiv.) was slowly added dropwise to the reaction mixture. After stirring at 0°C – 25°C for 30 h, water (40 mL) was carefully added to quench the reaction. The aqueous phase was separated and extracted with dichloromethane (40 mL) and the combined organic phases were filtered through a silica pad. After evaporation of the solvents and purification by flash chromatography (SiO_2; CH_2Cl_2 in hexane, 10-80%), 4,4'-dibromo-2,2'-bis(bromomethyl)biphenyl (**C14**) was obtained as yellow crystals (63% over two steps).

R_f = 0.27 (SiO_2; hexane:*t*-BME, 1:1); **m.p.** 147°C; **^{1}H-NMR** (400 MHz, $CDCl_3$): δ = 4.09 (d, ^2J(H,H) = 10.3 Hz, 2H), 4.26 (d, ^2J(H,H) = 10.3 Hz, 2H), 7.12 (d, ^3J(H,H) = 8.2 Hz, 2H), 7.50 (dd, ^3J(H,H) = 8.2 Hz, ^4J(H,H) = 2.0 Hz, 2H), 7.69 (d, ^4J(H,H) = 2.0 Hz, 2H); **^{13}C-NMR** (101 MHz, $CDCl_3$): δ = 30.7, 123.1, 131.98, 132.00, 134.0, 137.5, 138.4; **MS** (EI+, 70 eV): m/z (%) = 493.7, 495.7, 497.7, 499.7, [M^+]; **elemental analysis** calcd for $C_{14}H_{10}Br_4$: C 33.78, H 2.02; found: C 33.67, H 2.01.

2,2'-Diallyl-4,4'-dibromobiphenyl (C17): Under argon atmosphere 4,4'-dibromo-2,2'-bis(bromomethyl)biphenyl **C14** (673 mg, 1.65 mmol, 1.00 equiv.) was dissolved in dichloromethane (15 mL). CuI (313 mg, 1.64 mmol, 1.00 equiv.) was added at once and the reaction mixture was cooled to -70°C. In absence of light vinyl magnesium bromide (9.40 mL, 6.58 mmol, 4.00 equiv., 0.7 M) in dry THF was slowly added to the reaction mixture and stirring was continued at -70°C for 1 h. After stirring overnight (0°C – 25°C), the reaction was quenched with sat. NH_4Cl (50 mL) and brine (50 mL). The mixture was extracted with *t*BME (3 x 50 mL), separated and the combined organic phases were dried with magnesium sulfate. The crude product was purified by flash chromatography (SiO_2; hexane:CH_2Cl_2, 95:5) to afford 2,2'-diallyl-4,4'-dibromobiphenyl (**C17**) as a smelly and colorless oil (79%).

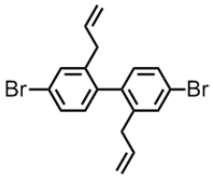

R_f = 0.46 (SiO_2; hexane:CH_2Cl_2, 95:5); **^{1}H-NMR** (400 MHz, $CDCl_3$): δ = 3.13- 2.97 (m, 4H), 4.87 (dd, ^2J(H,H) = 1.6 Hz, ^3J(H,H) = 17.0 Hz, 2H), 5.01 (dd, ^2J(H,H) = 1.6 Hz, ^3J(H,H) = 10.1 Hz, 2H), 5.80-5.67 (m, 2H), 6.95 (d, ^3J(H,H) = 8.1 Hz, 2H), 7.37 (dd, ^3J(H,H) = 8.4 Hz, ^4J(H,H) = 2.1 Hz, 2H), 7.43 (d, ^4J(H,H) = 2.4 Hz, 2H) ppm; **^{13}C-NMR** (101 MHz, $CDCl_3$): δ = 37.3, 116.8, 121.8, 129.1, 131.3, 132.2, 135.9, 138.4, 140.1; **MS** (EI+, 70 eV): m/z (%) = 390.0, 392.0, 394.0 [M^+]; **elemental analysis** calcd for $C_{18}H_{16}Br_2$: C 55.13, H 4.11; found: C 55.24, H 4.19.

3,10-Dibromo-5,8-dihydrodibenzo[*a*,*c*]cyclooctene (C18): 2,2'-Diallyl-4,4'-dibromo-biphenyl **C17** (121 mg, 0.400 mmol, 1.00 equiv.) and Grubbs catalyst (2nd generation, 20.4 mg, 24.0 µmol, 6.0 mol%) was refluxed in dichloromethane (30 mL). After 3 h the solvent was evaporated and the crude product was purified by flash chromatography (SiO_2; hexane, 0 – 5% CH_2Cl_2) to yield 3,10-dichloro-5,8-dihydrodibenzo[*a*,*c*]cyclooctene (**C18**) as an off-white solid (94%).

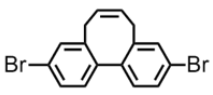

R_f = 0.61 (SiO_2; hexane:CH_2Cl_2, 95:5); **m.p.** 147°C; **^{1}H-NMR** (400 MHz, $CDCl_3$): δ = 2.91 (d, ^2J(H,H) = 14.7 Hz, 2H), 3.02-3.13 (m, 2H), 5.79-5.87 (m, 2H), 7.11 (d, ^3J(H,H) = 8.1 Hz,

2H), 7.37 (d, ^4J(H,H) = 2.0 Hz, 2H), 7.42 (dd, ^3J(H,H) = 8.1 Hz, ^4J(H,H) = 2.0 Hz, 2H) ppm; **^{13}C-NMR** (101 MHz, $CDCl_3$): δ = 32.9, 122.3, 128.7, 129.2, 129.3, 132.1, 138.8, 139.7. **MS** (EI+, 70 eV): m/z (%) = 361.9, 363.9, 365.9 [M^+]; **elemental analysis** calcd for $C_{16}H_{12}Br_2$ (364.07): C 52.78, H 3.32; found: C 52.66, H 3.35.

3,10-Dibromo-5,6,7,8-tetrahydrodibenzo[*a*,*c*]cyclooctene (C2f): 3,10-dibromo-5,8-

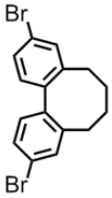

dihydrodibenzo[*a*,*c*]cyclooctene (**C18**) (102 mg, 0.370 mmol, 1.00 equiv.) was dissolved in ethyl acetate (6 mL) and Pd/C (10% Pd, 10.0 mg, 2.5 mol%) was added. The mixture war stirred under a hydrogen atmosphere (1 atm) for 3 h. Then the suspension was filtered through a silica pad, washed with ethyl acetate and the solvent was evaporated. 3,10-Dibromo-5,6,7,8-tetrahydrodibenzo[*a*,*c*]cyclooctene (**C2f**) was collected as a white solid (98%).

***R*$_f$** = 0.75 (SiO_2; hexane:CH_2Cl_2, 95:5); **m.p.** 168-170°C; **^{1}H-NMR** (400 MHz, $CDCl_3$): δ = 1.45-1.53 (m, 2H), 2.03-2.14 (m, 4H), 2.69 (dd, ^2J(H,H) = 13.4 Hz, ^3J(H,H) = 8.4 Hz, 2H), 7.07 (d, ^3J(H,H) = 8.1 Hz, 2H), 7.37 (dd, ^3J(H,H) = 8.1 Hz, ^4J(H,H) = 2.0 Hz, 2H), 7.43 (d, ^4J(H,H) = 2.0 Hz, 2H); **^{13}C-NMR** (101 MHz, $CDCl_3$): δ = 29.3, 32.6, 122.1, 129.0, 130.6, 132.4, 138.5, 144.9; **MS** (EI+, 70 eV): m/z (%) = 363.9, 365.9, 367.9 [M^+]; **elemental analysis** calcd for $C_{16}H_{14}Br_2$: C 52.49, H 3.85; found: C 52.45, H 3.81.

1,5-Bis(3-methoxyphenyl)-1,4-pentadien-3-one: To a solution of NaOH (15.0 g, 0.375 mol,

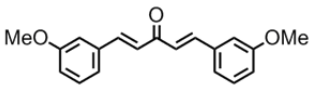

5.10 equiv.) in EtOH (125 mL) and water (125 mL) was added dropwise a solution of *m*-anisaldehyde (20.0 g, 0.147 mol, 2.00 equiv.), acetone (5.40 mL, 73.0 mmol, 1.00 equiv) in EtOH (30 mL) while maintaining the reaction temperature at 20°C with a water bath. After stirring the mixture at room temperature for 2 h dichloromethane (100 mL) was added and the phases were separated. The organic layer was washed with brine:water (80 mL, 1:1) and dried with magnesium sulfate. After evaporation of the solvent, a yellow high viscous oil (22.5 g) was obtained which was used without further purification for the next step. For analytical purposes a sample was recrystallized from EtOH/water.

***R*$_f$** = 0.55 (SiO_2; hexane:ethyl acetate, 2:1); **m.p.** 109°C; **^{1}H-NMR** (400 MHz, $CDCl_3$): δ = 3.85 (s, 6H), 6.93-6.98 (m, 2H), 7.06 (d, ^3J(H,H) = 15.9 Hz, 2H), 7.12-7.14 (m, 2H), 7.19-7.23 (m, 2H), 7.33 (m, 2H), 7.70 (m, 2H); **^{13}C-NMR** (101 MHz, $CDCl_3$): δ = 55.8, 113.7, 116.8, 121.1, 126.1, 130.4, 136.6, 143.6, 160.4, 189.3; **MS** (EI+, 70 eV): m/z (%) = 294.1

(100) [M^+], 263.1 (32) [M^+ - CH_3O], 161.1 (23), 121.1 (23); **elemental analysis** calcd for $C_{19}H_{18}O_3$: C 77.53, H 6.16; found: C 77.39, H 6.27.

1,5-Bis(3-methoxyphenyl)-3-pentanone (C20): The crude 1,5-bis(3-methoxyphenyl)-1,4-pentadien-3-one (assuming 73.5 mmol) was dissolved in ethyl acetate (200 mL) and Pd/C (500 mg, 10% Pd) was added under an inert atmosphere. The suspension was saturated with hydrogen gas and then vigorously stirred until the required volume of hydrogen (3.3 L, 147 mmol, 2.00 equiv.) was consumed. The suspension was degased and filtered through a short silica pad. After evaporation of the solvent a flash chromatography (SiO_2; hexane, 30 – 60% ethyl acetate) was performed to obtain 1,5-bis(3-methoxyphenyl)-3-pentanone (**C20**) (46% over 2 steps) as an oil.

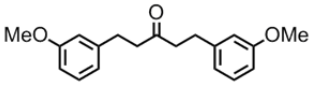

$\boldsymbol{R_f}$ = 0.43 (SiO_2; CH_2Cl_2); **^{1}H-NMR** (400 MHz, $CDCl_3$): δ = 2.71 (t, ^3J(H,H) = 8.0 Hz, 4H), 2.85 (t, ^3J(H,H) = 8.0 Hz, 4H), 3.79 (s, 6H), 6.73 (m, 6H), 7.16-7.22 (m, 2H); **^{13}C-NMR** (101 MHz, $CDCl_3$, 25 °C): δ = 30.2, 44.8, 55.6, 111.8, 114.5, 121.1, 129.9, 143.1, 160.1, 209.4; **MS** (EI+, 70 eV): m/z (%) = 298.2 (34) [M^+], 163.1 (22), 135.1 (100), 121.1 (40), 91.1 (14); **elemental analysis** calcd for $C_{19}H_{22}O_3$: C 76.48, H 7.43; found: C 75.55, H 7.43.

1,5-Bis(3-methoxyphenyl)pentane (C19): To a suspension of 1,5-bis(3-methoxyphenyl)-3-pentanone (**C20**) (3.83 g, 12.8 mmol, 1.00 equiv.) and powdered KOH (2.88 g, 51.3 mmol, 4.00 equiv.) in triethylenglycole (13 mL) was added hydrazine hydrate (2.30 mL, 39.0 mmol, 3.00 equiv, 85%) under cooling. The mixture was heated at reflux for 2 h. The water and excess of hydrazine was distilled off at an oil bath temperature of 190°C. After 4 h at this reaction temperature the reaction mixture was cooled to 0°C, water was added and the mixture was extracted with hexane:ethyl acetate 4:1 (3 x 60 mL). The combined organic layers were washed with water (3 x 15 mL) and brine (50 mL) and dried with $MgSO_4$. After evaporation of the solvent and purification by flash chromatography (SiO_2; hexane:ethyl acetate, 6:1) 1,5-bis(3-methoxyphenyl)pentane (**C19**) was obtained as a colorless oil (72%).

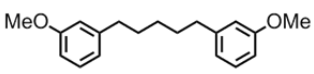

$\boldsymbol{R_f}$ = 0.53 (SiO_2; hexane:ethyl acetate, 5:1); **^{1}H-NMR** (400 MHz, $CDCl_3$): δ = 1.41 (m, 2H), 1.65 (m, 4H), 2.59 (t, ^3J(H,H) = 8.0 Hz, 4H), 3.82 (s, 6H), 6.72-6.78 (m, 6H), 7.18-7.22 (m, 2H); **^{13}C-NMR** (101 MHz, $CDCl_3$): δ = 29.4, 31.7, 36.4, 55.5, 111.3, 114.6, 121.3, 129.6, 144.9, 159.9; **MS** (EI+, 70 eV): m/z (%) = 284.2 (54) [M^+], 163.1 (8), 135.1(23), 122.1 (100), 91.1 (15); **elemental analysis** calcd for $C_{19}H_{24}O_2$: C 80.24, H 8.51; found: C 80.36, H 8.62.

1,5-Bis(2-bromo-5-methoxyphenyl)pentane (C21): To a solution of 1,5-bis(3-methoxyphenyl)pentane (**C19**) (4.10 g, 14.4 mmol, 1.00 equiv.) and dry pyridine (4.00 mL, 49.7 mmol, 3.50 equiv.) in dichloromethane (40 mL) a solution of bromine (5.30 g, 33.2 mmol, 2.30 equiv.) in dichloromethane (20 mL) was added dropwise at -10°C over 30 min. After stirring another 2 h at room temperature, the reaction mixture was washed with sat. $NaHCO_3$ and dried with $MgSO_4$. After evaporation of the solvent, a short flash chromatography (SiO_2; CH_2Cl_2:hexane, 1:1) was performed to obtain the crude product. The chromatographically inseparable impurities could be removed by recrystallization with pentane (60 mL) at 4°C. The pure 1,5-bis(2-bromo-5-methoxyphenyl)pentane (**C21**) was collected as fine white crystals (42%).

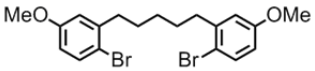

***R*$_f$** = 0.53 (SiO_2; hexane:ethyl acetate, 5:1); **m.p.** 44-45°C; **^{1}H-NMR** (400 MHz, $CDCl_3$): δ = 1.43-1.51 (m, 2H), 1.62-1.72 (m, 4H), 2.70 (t, ^3J(H,H) = 8.0 Hz, 4H), 3.78 (s, 6H), 6.62 (dd, ^4J(H,H) = 3.0 Hz, ^3J(H,H) = 8.7 Hz, 2H), 6.78 (d, ^4J(H,H) = 3.0 Hz, 2H), 7.41 (d, ^3J(H,H) = 8.7 Hz, 2H); **^{13}C-NMR** (101 MHz, $CDCl_3$): δ = 29.5, 30.1, 36.7, 55.8, 113.4, 115.3, 116.4, 133.6, 143.4, 159.3; **MS** (EI+, 70 eV): m/z (%) = 440.0, 442.0, 444.0 [M^+]; **elemental analysis** calcd for $C_{19}H_{22}Br_2O_2$: C 51.61, H 5.01; found: C 51.63, H 5.03.

3,11-Dimethoxy-6,7,8,9-tetrahydro-5*H*-dibenzo[*a*,*c*]cyclononene (C22): Under inert atmosphere 1,5-bis(2-bromo-5-methoxyphenyl)-pentane (**C21**) (2.00 g, 4.50 mmol, 1.00 equiv.) was dissolved in dry *Me*THF (170 mL). The solution was cooled to -50°C in a dry ice/acetone bath and *t*BuLi (11.1 mL, 18.0 mmol, 4.00 equiv.) was added dropwise. After the addition was completed the yellow solution was stirred at this temperature for another 15 min. A fresh solution of anhydrous LiBr (825 mg, 9.50 mmol, 2.10 equiv.) and CuCN (425 mg, 4.75 mmol, 1.10 equiv) in *Me*THF (10 mL) was prepared. This almost clear green copper solution was transferred to the reaction mixture over 10 min while keeping the reaction temperature below -50°C. The cloudy reaction mixture was then stirred for another hour at -20°C and afterwards cooled again to -40°C. 1,3-Dinitrobenzene (3.00 g, 18.0 mmol, 4.00 equiv.) was added at once and the cooling was removed. After stirring at room temperature overnight, the black reaction mixture was quenched with a mixture of NH_4Cl (40 mL, 10%) and NH_4OH (40 mL, 25%). The layers were separated and the aqueous phase was extracted with *t*BME (2 x 80 mL). The combined organic layers were washed with brine and dried with magnesium sulfate. After evaporation of the solvent a flash chromatography (SiO_2; hexane, 0 – 20% *t*BME) was

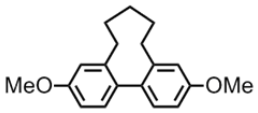

performed to obtain the monomer-fraction **C22** and a fraction containing the dimer **C23** according to the MS (27%). A recrystallization of the monomer-fraction from hexane (10 mL) afforded the pure monomer **C22** (23%) as colorless crystals.

R_f = 0.53 (SiO_2; hexane:*t*BME, 5:1); **m.p.** 112-113°C; **^{1}H-NMR** (400 MHz, $CDCl_3$): δ = 1.37-1.43 (m, 2H), 1.48-1.56 (m, 2H), 1.71-1.77 (m, 2H), 2.06-2.13 (m, 2H), 2.57-2.64 (m, 2H), 3.80 (s, 6H), 6.76-6.78 (m, 4H), 7.03-7.06 (m, 2H); **^{13}C-NMR** (101 MHz, $CDCl_3$): δ = 28.6, 29.5, 33.9, 55.6, 111.2, 114.5, 130.5, 134.7, 144.1, 159.3; **MS** (EI+, 70 eV): m/z (%) = 282.2 (100) [M^+], 267.2 (6) [M^+ - CH_3], 239.1 (10), 225.1 (9), 211.1 (7), 165.1 (6), 122.1 (6); **elemental analysis** calcd for $C_{19}H_{22}O_2$: C 80.82, H 7.85; found: C 80.47, H 7.93.

3,11-Dihydroxy-6,7,8,9-tetrahydro-5*H*-dibenzo[*a*,*c*]cyclononene (C24): To a solution of

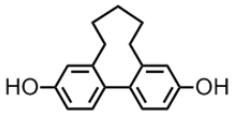

3,11-dimethoxy-6,7,8,9-tetrahydro-5*H*-dibenzo-[*a*,*c*]cyclononene (**C22**) (288 mg, 1.02 mmol, 1.00 equiv.) in dry dichloromethane (20 mL) was slowly added a solution of BBr_3 (4.10 mL, 4.10 mmol, 4.00 equiv, 1.0 M in dichloromethane) at 0°C. Stirring was continued at room temperature until TLC showed full conversion of the starting material (1.5 h). The reaction was quenched with MeOH under ice cooling. The reaction mixture was then washed with water (10 mL), dried with magnesium sulfate and the solvents were evaporated. The crude 3,11-dihydroxy-6,7,8,9-tetrahydro-5*H*-dibenzo[*a*,*c*]cyclononene (**C24**) as a white powder was obtained which was pure enough to use for the next step.

R_f = 0.40 (SiO_2; hexane:*t*BME, 1:2); **^{1}H-NMR** (400 MHz, $CDCl_3$): δ = 1.31-1.37 (m, 2H), 1.41-1.52 (m, 2H), 1.65-1.76 (m, 2H), 2.00-2.09 (m, 2H), 2.47-2.56 (m, 2H), 6.64-6.70 (m, 4H), 6.93 (d, ^3J(H,H) = 8.0 Hz, 2H); **^{13}C-NMR** (101 MHz, $CDCl_3$): δ = 28.1, 29.0, 33.2, 112.4, 115.3, 130.1, 133.8, 143.7, 155.4; **MS** (EI+, 70 eV): m/z (%) = 254.1 (100) [M^+], 211.1 (25), 198.1 (15), 108.1 (16).

3,11-Bis(trifluoromethanesulfonyloxy)-6,7,8,9-tetrahydro-5*H*-dibenzo[*a*,*c*]cyclononene

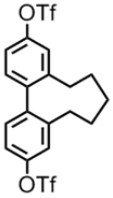

(C2g): The crude 3,11-dihydroxy-6,7,8,9-tetrahydro-5*H*-dibenzo[*a*,*c*]cyclononene (**C24**) (assuming 1.02 mmol, 1.00 equiv.) from the previous step was dissolved in dry pyridine (8 mL). Then triflic anhydride (677 µL, 4.02 mmol, 4.00 equiv.) was added slowly to the solution. Stirring was continued at rt (30 min) and the beige solution was quenched with a cold $NaHCO_3$ solution. The product was extracted with dichloromethane (3 x 30 mL) and the combined organic phases were dried with $MgSO_4$. After evaporation of the solvent a flash chromatography (SiO_2; hexane:CH_2Cl_2, 7:3) was performed

to afford 3,11-bis(trifluoromethanesulfonyloxy)-6,7,8,9-tetrahydro-5*H*-dibenzo[*a*,*c*]-cyclononene (**C2g**) as a colorless oil. Upon standing at room temperature a sample of the triflate solidified after a few weeks (quant.).

R_f = 0.73 (SiO_2; hexane:*t*BME, 1:2); **^{1}H-NMR** (400 MHz, $CDCl_3$): δ = 1.34-1.39 (m, 2H), 1.47-1.56 (m, 2H), 1.76-1.87 (m, 2H), 1.99-2.06 (m, 2H), 2.67-2.73 (m, 2H), 7.15-7.22 (m, 6H); **^{13}C-NMR** (101 MHz, $CDCl_3$): δ = 28.3, 29.1, 33.7, 119.1, 119.2 (q, J(C,F) = 321Hz), 122.1, 130.9, 140.8, 145.2, 149.7; **MS** (EI+, 70 eV): m/z (%) = 518.0 [M^+], 385.1 (17) [M^+ - $SOCF_3$], 252.1 (34) [M^+ - 2 $SOCF_3$], 235.1 (44), 107 (23); **elemental analysis** calcd for $C_{19}H_{16}F_6O_6S_2$: C 44.02, H 3.11; found: C 44.15, H 3.04.

Literature

[1] V. Degiorgio, C. Flytzanis, S. italiana di fisica, *Nonlinear Optical Materials: Principles and Applications : Varenna on Lake Como, Villa Monastero, 20-30 July 1993*, Ios Press, **1995**.

[2] P. N. Prasad, B. A. Reinhardt, *Chem. Mater.* **1990**, *2*, 660–669.

[3] R. Menzel, *Photonics: linear and nonlinear interactions of laser light and matter*, Springer Verlag, **2001**.

[4] E. Ozbay, *Science* **2006**, *311*, 189–193.

[5] A. F. . Levi, *Proceedings of the IEEE* **2000**, *88*, 750–757.

[6] P. A. Tipler, *Physik*, Spektrum Verlag**.**

[7] D. J. Williams, *Angew.Chem. Int. Ed. Engl.* **1984**, *23*, 690–703.

[8] D. Kanis, *Chem. Rev.* **1994**, *94*, 195.

[9] A. Buckingham, *Advances in Chemical Physics*, Wiley, New York, **1967**.

[10] T. H. Maiman, *Nature* **1960**, *187*, 493.

[11] P. A. Franken, A. E. Hill, C. W. Peters, G. Weinreich, *Phys. Rev. Lett.* **1961**, *7*, 118.

[12] P. N. Prasad, D. J. Williams, *Introduction to Nonlinear Optical Effects in Molecules and Polymers*, Wiley-interscience, **1991**.

[13] K. Clays, N. J. Armstrong, M. C. Ezenyilimba, T. L. Penner, *Chem. Mater.* **1993**, *5*, 1032–1036.

[14] F. Embs, *Adv. Mater.* **1991**, *3*, 25.

[15] J. A. Delaire, K. Nakatani, *Chem. Rev.* **2000**, *100*, 1817–1846.

[16] J. F. Nye, *Physical Properties of Crystals: Their Representation by Tensors and Matrices*, Oxford University Press, **1985**.

[17] K. D. Singer, M. G. Kuzyk, J. E. Sohn, *J. Opt. Soc. Am. B* **1987**, *4*, 968–976.

[18] R. D. Wampler, A. J. Moad, C. W. Moad, R. Heiland, G. J. Simpson, *Acc. Chem. Res.* **2007**, *40*, 953–960.

[19] A. Ashkin, G. D. Boyd, J. M. Dziedzic, R. G. Smith, A. A. Ballman, J. J. Levinstein, K. Nassau, *Appl. Phys. Lett.* **1966**, *9*, 72–74.

[20] H. Meier, *Angew. Chem. Int. Ed.* **2005**, *44*, 2482–2506.

[21] T. Verbiest, S. Houbrechts, M. Kauranen, K. Clays, A. Persoons, *J. Mater. Chem.* **1997**, *7*, 2175–2189.

[22] A. Dulcic, C. Sauteret, *J. Chem. Phys.* **1978**, *69*, 3453–3457.

[23] A. Dulcic, C. Flytzanis, C. L. Tang, D. Pépin, M. Fétizon, Y. Hoppilliard, *J. Chem. Phys.* **1981**, *74*, 1559–1563.

[24] C. B. Gorman, S. R. Marder, *Chem. Mater.* **1995**, *7*, 215–220.

[25] S. R. Marder, C. B. Gorman, B. G. Tiemann, L. T. Cheng, *J. Am. Chem. Soc.* **1993**, *115*, 3006–3007.

[26] S. M. Risser, D. N. Beratan, S. R. Marder, *J. Am. Chem. Soc.* **1993**, *115*, 7719–7728.

[27] G. Bourhill, J.-L. Bredas, L.-T. Cheng, S. R. Marder, F. Meyers, J. W. Perry, B. G. Tiemann, *J. Am. Chem. Soc.* **1994**, *116*, 2619–2620.

[28] F. Würthner, F. Effenberger, R. Wortmann, P. Krämer, *Chem. Phys.* **1993**, *173*, 305–314.

[29] L. Groenendaal, M. J. Bruining, E. H. J. Hendrickx, A. Persoons, J. A. J. M. Vekemans, E. E. Havinga, E. W. Meijer, *Chem. Mater.* **1998**, *10*, 226–234.

[30] J. L. Oudar, D. S. Chemla, *Opt. Commun.* **1975**, *13*, 164–168.

[31] D. S. Chemla, J. L. Oudar, J. Jerphagnon, *Phys. Rev. B* **1975**, *12*, 4534–4546.

[32] C. K. Miller, J. F. Ward, *Phys. Rev. A* **1977**, *16*, 1179–1185.

[33] A. D. Buckingham, B. J. Orr, *Q. Rev. Chem. Soc.* **1967**, *21*, 195–212.

[34] J. Zyss, *J. Chem. Phys.* **1979**, *71*, 909–916.

[35] J. L. Oudar, D. S. Chemla, *J. Chem. Phys.* **1977**, *66*, 2664–2668.

[36] J. L. Oudar, *J. Chem. Phys.* **1977**, *67*, 446–457.

[37] E. Lippert, W. Rettig, *Advances in Chemical Physics*, Wiley, New York, **1987**.

[38] S. K. Kurtz, T. T. Perry, *J. Appl. Phys.* **1968**, *39*, 3798–3813.

[39] K. Clays, A. Persoons, *Phys. Rev. Lett.* **1991**, *66*, 2980–2983.

[40] B. F. Levine, C. G. Bethea, *J. Chem. Phys.* **1975**, *63*, 2666–2682.

[41] C. C. Teng, H. T. Man, *Appl. Phys. Lett.* **1990**, *56*, 1734–1736.

[42] B. Culshaw, *Optical Fibre Sensing and Signal Processing*, IET, London, **1984**.

[43] T. H. Maiman, *Nature* **1960**, *189*, 493.

[44] P. A. Franken, C. W. Peters, G. Weinreich, *Phys. Rev. Lett.* **1961**, *7*, 118.

[45] S. R. Marder, B. Kippelen, A. K. Y. Jen, N. Peyghammbarian, *Nature* **1997**, *388*, 845.

[46] S. R. Marder, J. W. Perry, *Adv. Mater.* **1993**, *5*, 804.

[47] W. H. Steier, A. Chen, S.-S. Lee, S. Garner, H. Zhang, V. Chuyanov, L. R. Dalton, F. Wang, A. S. Ren, C. Zhang, G. Todorova, A. Harper, H. R. Fetterman, D. Chen, A. Udupa, D. Bhattacharya, B. Tsap, *Chem. Phys.* **1999**, *245*, 487.

[48] D. R. Kanis, M. A. Ratner, T. J. Marks, *Chem. Rev.* **1994**, *94*, 195.

[49] Y. Nakayama, P. J. Pauzauskie, A. Radenovic, R. M. Onorato, R. J. Saykally, J. Liphardt, P. Yang, *Nature* **2007**, *447*, 1098.

[50] J. L. Oudar, H. Le Person, *Opt. Commun.* **1975**, *15*, 258.

[51] D. S. Chemla, J. L. Oudar, J. Jerphagnon, *Phys. Rev. B* **1975**, *12*, 4534.

[52] F. Kajzar, J. Messier, *Phys. Rev. A: Gen. Phys.* **1985**, *32*, 2352.

[53] J. Zyss, *J. Chem. Phys.* **1979**, *70*, 3341.

[54] J. Zyss, *J. Chem. Phys.* **1979**, *71*, 909.

[55] J. L. Oudar, D. S. Chemla, *J. Chem. Phys.* **1977**, *66*, 2664.

[56] J. Y. Lee, K. S. Kim, B. J. Mhin, *J. Chem. Phys.* **2001**, *115*, 9484.

[57] A. Fort, A. Boeglin, L. Mager, C. Amyot, C. Combellas, A. Thiebault, V. Rodriguez, *Synth. M.* **2001**, *124*, 209.

[58] L. Venkataraman, J. E. Klare, C. Nuckolls, M. S. Hybertsen, M. L. Steigerwald, *Nature* **2006**, *442*, 904.

[59] Y. S. Park, J. R. Widawsky, M. Kamenetska, M. L. Steigerwald, M. S. Hybertsen, C. Nuckolls, L. Venkataraman, *J. Am. Chem. Soc.* **2009**, *131*, 10820.

[60] J. A. Malen, P. Doak, K. Baheti, T. D. Tilley, A. Majumdar, R. A. Segalman, *Nano Lett.* **2009**, *9*, 3406.

[61] I. D. L. Albert, T. J. Marks, M. A. Ratner, *J. Am. Chem. Soc.* **1998**, *120*, 11174.

[62] K. S. Thanthiriwatte, K. M. Nalin de Silva, *Theochem* **2002**, *617*, 169.

[63] P. Hrobarik, I. Sigmundova, P. Zahradnik, *Synthesis* **2005**, 600.

[64] E. M. Breitung, C.-F. Shu, R. J. McMahon, *J. Am. Chem. Soc.* **2000**, *122*, 1154.

[65] C. R. Moylan, S. Ermer, S. M. Lovejoy, I. H. McComb, D. S. Leung, R. Wortmann, P. Krdmer, R. J. Twieg, *J. Am. Chem. Soc.* **1996**, *118*, 12950.

[66] J. W. Perry, G. Bourhill, S. R. Marder, D. Lu, G. Chen, W. A. Goddard, III, *Polym. Prepr. (Am. Chem. Soc., Div. Polym. Chem.)* **1994**, *35*, 148.

[67] S. M. Risser, D. N. Beratan, S. R. Marder, *J. Am. Chem. Soc.* **1993**, *115*, 7719.

[68] C. Dehu, F. Meyers, J. L. Bredas, *J. Am. Chem. Soc.* **1993**, *115*, 6198.

[69] C. G. Claessens, D. Gonzalez-Rodriguez, T. Torres, G. Martin, F. Agullo-Lopez, I. Ledoux, J. Zyss, V. R. Ferro, J. M. Garcia de la Vega, *J. Phys. Chem. B* **2005**, *109*, 3800.

[70] A. K. Y. Jen, V. P. Rao, K. Y. Wong, K. J. Drost, *J. Chem. Soc., Chem. Commun.* **1993**, 90.

[71] V. P. Rao, A. K. Y. Jen, K. Y. Wong, K. J. Drost, *Tetrahedron Lett.* **1993**, *34*, 1747.

[72] L. T. Cheng, W. Tam, S. H. Stevenson, G. R. Meredith, G. Rikken, S. R. Marder, *J. Phys. Chem.* **1991**, *95*, 10631.

[73] S. R. Marder, D. N. Beratan, L. T. Cheng, *Science* **1991**, *252*, 103.

[74] J. L. Oudar, D. S. Chemla, *J. Chem. Phys.* **1977**, *66*, 2664.

[75] J. L. Oudar, *J. Chem. Phys.* **1977**, *67*, 446.

[76] D. Vonlanthen, J. Rotzler, M. Neuburger, M. Mayor, *Eur. J. Org. Chem.* **2010**, 120–133.

[77] A. S. Guram, R. A. Rennels, S. L. Buchwald, *Angew. Chem. Int. Ed. Engl.* **1995**, *34*, 1348.

[78] J. Louie, J. F. Hartwig, *Tetrahedron Lett.* **1995**, *36*, 3609.

[79] A. Klapars, J. C. Antilla, X. Huang, S. L. Buchwald, *J. Am. Chem. Soc.* **2001**, *123*, 7727.

[80] C.-Z. Tao, J. Li, Y. Fu, L. Liu, Q.-X. Guo, *Tetrahedron Lett.* **2007**, *49*, 70.

[81] S. Naik, G. Bhattacharjya, B. Talukdar, B. K. Patel, *Eur. J. Org. Chem.* **2004**, 1254.

[82] D. J. Sinclair, M. S. Sherburn, *J. Org. Chem.* **2005**, *70*, 3730.

[83] a) T. Nagano, T. Hayashi, *Org. Lett.* **2005**, *7*, 491–493; b) G. Cahiez, C. Chaboche, F. Mahuteau-Betzer, M. Ahr, *Org. Lett.* **2005**, *7*, 1943–1946.

[84] O. Possel, A. M. van Leusen, *Tetrahedron Lett.* **1977**, *18*, 4229–4231.

[85] R. W. McDonald, W. Bunjobpon, T. Liu, S. Fessler, O. E. Pardo, I. K. Freer, M. Glaser, M. J. Seckl, D. J. Robins, *Anti-Cancer Drug Des.* **2001**, *16*, 261–270.

[86] J. Rotzler, D. Vonlanthen, A. Barsella, A. Boeglin, A. Fort, M. Mayor, *Eur. J. Org. Chem.* 2010, 1096–1110.

[87] A. Helms, D. Heiler, G. McLendon, *J. Am. Chem. Soc.* **1992**, *114*, 6227–6238.

[88] J. W. Ciszek, J. M. Tour, *Tetrahedron Lett.* **2004**, *45*, 2801–2803.

[89] L. M. Tolbert, M. Z. Ali, *J. Org. Chem.* **1982**, *47*, 4793–4795.

[90] W. Wenner, *J. Org. Chem.* **1952**, *17*, 523–528.

[91] T. A. Kirkland, R. H. Grubbs, *J. Org. Chem.* **1997**, *62*, 7310–7318.

[92] A. Michaut, J. Rodriguez, *Angew. Chem. Int. Ed.* **2006**, *45*, 5740–5750.

[93] A. Iuliano, P. Piccioli, D. Fabbri, *Org. Lett.* **2004**, *6*, 3711–3714.

[94] W. M. Weber, L. A. Hunsaker, S. F. Abcouwer, L. M. Deck, D. L. Vander Jagt, *Bioorg. Med. Chem.* **2005**, *13*, 3811–3820.

[95] W. M. Weber, L. A. Hunsaker, C. N. Roybal, E. V. Bobrovnikova-Marjon, S. F. Abcouwer, R. E. Royer, L. M. Deck, D. L. Vander Jagt, *Bioorg. Med. Chem.* **2006**, *14*, 2450–2461.

[96] R.W. McDonald, W. Bunjobpon, T. Liu, S. Fessler, O. E. Pardo, I. Freer, M. Glaser, M. J. Seckl, J. Robins, *Anti-Canc. Drug Des.* **2001**, *16*, 261–270.

[97] V. B. Birman, A. L. Rheingold, K.-C. Lam, *Tetrahedron: Asymmetry* **1999**, *10*, 125–131.

[98] G. M. Whitesides, E. R. Stedronsky, C. P. Casey, J. San Filippo, *J. Am. Chem. Soc.* **1970**, *92*, 1426–1427.

[99] B. H. Lipshutz, K. Siegmann, E. Garcia, F. Kayser, *J. Am. Chem. Soc.* **1993**, *115*, 9276–9282.

[100] B. H. Lipshutz, F. Kayser, Z.-P. Liu, *Angew. Chem. Int. Ed. Engl.* **1994**, *33*, 1842–1844.

[101] B. H. Lipshutz, Z.-P. Liu, F. Kayser, *Tetrahedron Lett.* **1994**, *35*, 5567–5570.

[102] B. H. Lipshutz, F. Kayser, N. Maullin, *Tetrahedron Lett.* **1994**, *35*, 815–818.

[103] D. R. Spring, S. Krishnan, S. L. Schreiber, *J. Am. Chem. Soc.* **2000**, *122*, 5656–5657.

[104] J. F. W. McOmie, M. L. Watts, D. E. West, *Tetrahedron* **1968**, *24*, 2289–2292.

[105] S. Lee, M. Jorgensen, J. F. Hartwig, *Org. Lett.* **2001**, *3*, 2729.

[106] J. F. Hartwig, *Angew. Chem. Int. Ed. Engl.* **1998**, *37*, 2046.

[107] J. P. Wolfe, J. Ahman, J. P. Sadighi, R. A. Singer, S. L. Buchwald, *Tetrahedron Lett.* **1997**, *38*, 6367.

[108] A. McKillop, J. A. Tarbin, *Tetrahedron* **1987**, *43*, 1753.

[109] J. Clayden, N. Greeves, S. Warren, P. Wothers, *Organic Chemistry*, Oxford University Press, Oxford, **2001**.

[110] M. Sarkar, A. Samanta, *Synth.* **2006**, 3425.

[111] B. de Lange, M. H. Lambers-Verstappen, L. Schmieder-van de Vondervoort, N. Sereinig, R. de Rijk, A. H. M. de Vries, J. G. de Vries, *Synlett* **2006**, 3105.

[112] A. S. Gajare, K. Toyota, M. Yoshifuji, F. Ozawa, *Chem. Commun.* **2004**, 1994.

[113] Y. Ju, S. Varma Rajender, *Org. Lett.* **2005**, *7*, 2409.

[114] Y. Ju, R. S. Varma, *J. Org. Chem.* **2006**, *71*, 135.

[115] W. D. Emmons, *J. Am. Chem. Soc.* **1957**, *79*, 5528.

[116] H. Firouzabadi, N. Iranpoor, K. Amani, *Green Chemistry* **2001**, *3*, 131.

[117] I. V. Kozhevnikov, *Chem. Rev.* **1998**, *98*, 171.

[118] S. Sakaue, T. Tsubakino, Y. Nishiyama, Y. Ishii, *J. Org. Chem.* **1993**, *58*, 3633.

[119] K. D. Belfield, K. J. Schafer, W. Mourad, B. A. Reinhardt, *J. Org. Chem.* **2000**, *65*, 4475.

[120] A. Shaporenko, M. Elbing, A. Blaszczyk, C. Von Haenisch, M. Mayor, M. Zharnikov, *J. Phys. Chem. B* **2006**, *110*, 4307.

[121] H. Meier, *Angew. Chem., Int. Ed.* **2005**, *44*, 2482.

[122] L. T. Cheng, W. Tam, S. R. Marder, A. E. Stiegman, G. Rikken, C. W. Spangler, *J. Phys. Chem.* **1991**, *95*, 10643.

[123] J. J. P. Stewart*, Vol. Tokyo*, MOPAC 2002 Version 2.3.0 ed., Fujitsu Limited, Tokyo, **2002**.

[124] M. J. S. Dewar, E. G. Zoebisch, E. F. Healy, J. J. P. Stewart, *J. Am. Chem. Soc.* **1985**, *107*, 3902.

[125] T. Thami, P. Bassoul, M. A. Petit, J. Simon, A. Fort, M. Barzoukas, A. Villaeys, *J. Am. Chem. Soc.* **1992**, *114*, 915.

[126] M. Elbing, R. Ochs, M. Koentopp, M. Fischer, C. von Haenisch, F. Weigend, F. Evers, H. B. Weber, M. Mayor, *Proc. Natl. Acad. Sci. U. S. A.* **2005**, *102*, 8815.

[127] H. Kang, A. Facchetti, H. Jiang, E. Cariati, S. Righetto, R. Ugo, C. Zuccaccia, A. Macchioni, C. L. Stern, Z. Liu, S.-T. Ho, E. C. Brown, M. A. Ratner, T. J. Marks, *J. Am. Chem. Soc.* **2007**, *129*, 3267–3286.

[128] N. J. Long, *Angew. Chem., Int. Ed. Engl.* **1995**, *34*, 21–38.

[129] M. Barzoukas, M. Blanchard-Desce, D. Josse, J. M. Lehn, J. Zyss, *Chem. Phys.* **1989**, *133*, 323–329.

[130] T. Verbiest, S. Houbrechts, M. Kauranen, K. Clays, A. Persoons, *J. Mater. Chem.* **1997**, *7*, 2175–2189.

[131] C. Bosshard, G. Knoepfle, P. Pretre, P. Guenter, *J. Appl. Phys.* **1992**, *71*, 1594–1605.

[132] R. Spreiter, C. Bosshard, G. Knopfle, P. Gunter, R. R. Tykwinski, M. Schreiber, F. Diederich, *J. Phys. Chem. B* **1998**, *102*, 29–32.

[133] A. Facchetti, A. Abbotto, L. Beverina, M. E. van der Boom, P. Dutta, G. Evmenenko, T. J. Marks, G. A. Pagani, *Chem. Mater.* **2002**, *14*, 4996–5005.

[134] T. J. Marks, M. A. Ratner, *Angew. Chem., Int. Ed. Engl.* **1995**, *34*, 155–173.

[135] J. Zyss, J. F. Nicoud, M. *J.* Coquillay, *Chem. Phys.* **1984**, *81*, 4160–4167.

[136] J. L. Oudar, R. Hierle, *J. Appl. Phys.* **1977**, *48*, 2699–2704.

[137] T. Verbiest, S. Van Elshocht, M. Karuanen, L. Heliemans, J. Snauwaert, C. Nuckolls, T. J. Katz, A. Persoons, *Science* **1998**, *282*, 913–915.

[138] G. Iftime, G. G. A. Balavoine, J.-C. Daran, P. G. Lacroix, E. Manoury, *C. R. Acad. Sci., Ser. IIc: Chim.* **2000**, *3*, 139–146.

[139] G. Binsch, H. Kessler, *Angew. Chem.* **1980**, *92*, 445–463.

[140] V. Schurig, W. Buerkle, A. Zlatkis, C. F. Poole, *Naturwissenschaften* **1979**, *66*, 423–424.

[141] W. Buerkle, H. Karfunkel, V. Schurig, *J. Chromatogr.* **1984**, *288*, 1–14.

[142] M. Jung, V. Schurig, *J. Am. Chem. Soc.* **1992**, *114*, 529–534.

[143] O. Trapp, G. Schoetz, V. Schurig, *Chirality* **2001**, *13*, 403–414.

[144] C. Wolf, *Chem. Soc. Rev.* **2005**, *34*, 595–608.

[145] A. L. Van Geet, *Anal. Chem.* **1968**, *40*, 2227–2229.

[146] O. Trapp, *Anal. Chem.* **2006**, *78*, 189–198.

[147] O. Trapp, *J. Chromatogr., B: Anal. Technol. Biomed. Life Sci.* **2008**, *875*, 42–47.

[148] M. Oki, H. Iwamura, G. Yamamoto, *Bull. Chem. Soc. Jpn.* **1971**, 44, 262–265.

[149] M. Oki, G. Yamamoto, *Bull. Chem. Soc. Jap.* **1971**, *44*, 266–270.

[150] M. Oki, *Methods in Stereochemical Analysis, Vol. 4: Applications of Dynamic NMR Spectroscopy to Organic Chemistry*, **1985**.

[151] K. Ohkata, R. L. Paquette, L. A. Paquette, *J. Am. Chem. Soc.* **1979**, *101*, 6687–6693.

[152] R. B. Bates, F. A. Camou, V. V. Kane, P. K. Mishra, K. Suvannachut, J. J. White, *J. Org. Chem.* **1989**, *54*, 311–317.

[153] C. L. Perrin, T. J. Dwyer, *Chem. Rev.* **1990**, *90*, 935–967.

[154] V. Schurig, *Chirality* **1998**, *10*, 140–146.

[155] O. Trapp, V. Schurig, *Comput. Chem.* **2001**, *25*, 187–195.

[156] C. Wolf, H. Xu, *Tetrahedron Lett.* **2007**, *48*, 6886–6889.

[157] D. Vonlanthen, A. Mishchenko, M. Elbing, M. Neuburger, T. Wandlowski, M. Mayor, *Angew. Chem., Int. Ed.* **2009**, *48*, 8886–8890.

[158] A. Mishchenko, D. Vonlanthen, V. Meded, M. Burkle, C. Li, I. V. Pobelov, A. Bagrets, J. K. Viljas, F. Pauly, F. Evers, M. Mayor, T. Wandlowski, *Nano Lett.* **2010**, *10*, 156–163.

[159] T. Ohwada, *J. Am. Chem. Soc.* **1992**, *114*, 8818.

[160] V. C. Marhevka, N. A. Ebner, R. D. Sehon, P. E. Hanna, *J. Med. Chem.* **1985**, *28*, 18.

Part D. Thermodynamic Studies of 4 and 4' Substituted Torsion Angle Restricted 2,2' Alkyl-Bridged Biphenyl Cyclophanes

In the following section the influence on the atropisomerization process of electron-donors and electron-acceptors of variable strength in 4 and 4' position of in 2 and 2' alkyl-bridged axial chiral biphenyl cyclophanes was studied. In the case of the propyl-bridged biphenyl derivatives the free energies $\Delta G(T)$ of the rotation around the central biphenyl bond were estimated by ^{1}H-NMR coalescence measurements. By line shape analysis the rate constants were calculated and by the use of the Eyring equation the enthalpic and entropic contributions were evaluated. The NMR studies were carried out by *Heiko Gsellinger* and *Daniel Häussinger*. Theoretical calculations were performed by *Angela Bihlmeier* and *Willem Klopper* to evaluate an isomerization mechanism by comparison of the measured and calculated thermodynamic data. The compounds were synthesized by *Markus Gantenbein*, *David Vonlanthen* and myself. Evaluation and interpretation of the obtained data as well as project planning and the dynamic HPLC studies of the butyl-bridged derivatives were carried out by myself. The results of the investigations on the propyl-bridged biphenyl cyclophanes were summarized in the following publication. Again the supporting information was incorporated into the running text. Preliminary results of the butyl-bridged derivatives are attached at the end of the document, but are not part of the publication itself.

Thermodynamic Studies of 4 and 4' Substituted Torsion Angle Restricted 2,2' Propyl-Bridged Biphenyl Cyclophanes

Jürgen Rotzler, Heiko Gsellinger, Angela Bihlmeier, Markus Gantenbein, David Vonlanthen, Daniel Häussinger, Willem M. Klopper, Marcel Mayor

Introduction

The well-defined spacing of the terminal units in biaryls caused by their rigidity and the ability to provide detectable signals even in poorly communicating conformations because of their compactness, make biaryls maybe to the simplest compounds to study the communication between two individual π-systems.[1,2] The possibility to adjust this communication by variation of the surrounding of biphenyls[3,4] and bipyridines[5] leads to unique physical and chemical properties. The success of such structural motifs can be documented in the use of biphenyl and bipyridine structural elements in an amazing amount of compounds in material science like polymers[6], OLEDS[7], nonlinear optics[8], molecular motors[9], molecular electronics[1,3,4], light harvesting metal complexes[10,11], dyes[12], artificial photosynthesis[13] and catalysis[14–17] to name just a few possible applications (figure 1).

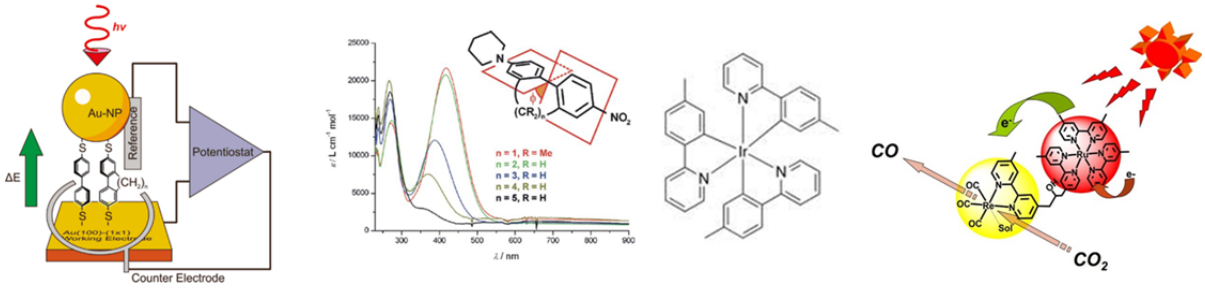

Figure 1. Selected applications of biphenyls. *Left*: molecular electronics[18], *middle left*: nonlinear optics[8], *middle right*: light-harvesting iridium-complex[19], *right*: component of a photosensitive solar cell[20].

By variation of the torsion angle *Φ* between the planes of the two phenyl rings, the degree of π-overlap in the two phenyl rings and the resulting extent of delocalization over both π-systems can be fine-tuned. In most cases known in literature, this tuning was performed by substituting biaryls in 2 and 2' position with different sterically demanding groups[21] or by interlinking the two positions with chains of different lengths[3,4,8,22]. By substituting biaryls in 2,2' position differently from the 6,6' position not only the torsion angle is adjusted but also axial chirality is introduced which opens up a variety of new potential applications like POLED (based on circular polarized luminescence),[23] or new powerful ligands for enantioselective catalytic processes. Although enantioselective syntheses of axial chiral

biphenyls are known, the preparation is up to date synthetically challenging, time consuming and mostly limited to in 2,2',6,6' crowded biphenyl compounds.[24–29] Much easier still is the separation of the two atropisomers which can be separated by chiral HPLC or GC when the rotation barrier between the two phenyl rings is higher than 93.5 kJ/mol at 300 K.[26] One of the major problems towards applications using axial chiral 2,2' substituted biaryls is, among others, their relatively low atropisomerization energies. Low barriers essentially lead to fast racemization when these compounds are incorporated into more complex structures or when used as ligands for metal complexes in catalysis or light-harvesting molecules. The configurational stability of axial chiral biaryls is determined by the steric demand of substituents, existence, rigidity and length of bridges and involvement of atropisomerization mechanisms different from a physical rotation, for example by chemically or photochemically induced processes.[26] One possibility to enhance the isomerization energies of axial chiral biaryls is therefore to introduce sterically demanding groups in 6,6' position different from the ones in 2,2' position. Major drawbacks include that coordination sites will be blocked, the torsion angle will be close to 90° lowering the communication between the two aryl-rings significantly, or even worse an overall change in the electronic nature of the biaryl.

To design molecules with rotation energies high enough to separate the two enantiomers and to be able to perform chemical reactions with the enantiomerically pure atropisomers it is necessary to study the inversion mechanism and the influence of substituents on the 2,2' substituted biaryls in detail. By understanding the inversion mechanism it will then be possible to substitute biaryls in positions where for example the electronic structure is not influenced and/or important binding sites are not blocked. Up to date several investigations on the atropisomerization of biaryls were carried out leading to conflicting outcomes.[30–40] From most available studies on the physical rotation of biaryls to date, it was concluded that only the push-pull cases show a linear and planar transition state whereas in all other cases an out-of-plane bending is the dominating factor which significantly influences the energy barrier (figure 2).

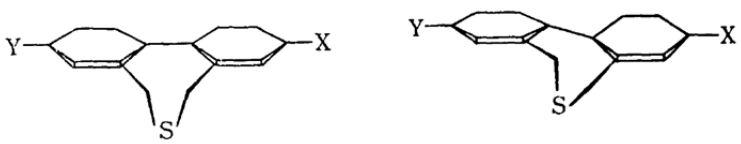

Figure 2. Proposed transition states for the atropisomerization of 2,2' bridged biphenyls. *Left*: push-pull case, *right*: donor-donor or acceptor-acceptor substituted biphenyls. Reprinted from Oki *et al*.[32]

Furthermore Müllen and co-workers estimated the energy barriers of an amazing collection of 2,2',6,6' substituted biphenyls by NMR coalescence studies and derived an inversion mechanism where the interlinking 1 and 1' carbons stay in plane, whereas the individual phenyls are distorted (figure 3).[34]

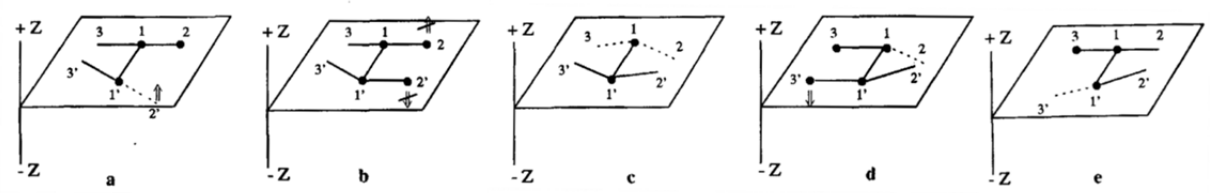

Figure 3. Enantiomeric transition states of the atropisomerization mechanism of biphenyls including a distortion of the individual phenyl rings proposed by Müllen *et al*. 1,1' is the central C-C bond. 2,2' and 3,3' the *ortho* carbon atoms of the phenyls. Reprinted from Müllen *et al*.[34]

In our studies of biphenyl based push-pull cyclophanes it was shown that the racemization barrier reflects the crowdedness of the transition state.[35] Encouraged by these somehow contradicting hypotheses of out-of-plane bending, distortion of the phenyl and planar transition as rotation barrier determining factors it was decided to investigate the thermodynamic behavior of 4,4'-disubstituted torsion angle restricted biphenyl cyclophanes **D1a** – **D1l** synthesized in our group that were already investigated in single molecular conductance measurements (figure 1).[3,4] By correlation of the obtained data with the Hammett-parameter we wanted to gain further insight into the influence of substituents in *para* position to the central biphenyl bond. By comparison of the measured inversion energy with quantum chemical calculations we also intended to clarify the influence of the propyl-bridge on the atropisomerization mechanism in order to see if substitution on the bridge possibly allows restriction of the rotation around the central C1-C1' bond without distortion of the electronic nature and the torsion angle of the biphenyl system.

Methods and Materials

The previous studies of 2,2' alkyl-bridged push-pull biphenyls showed that the ethyl-bridged derivative isomerized too fast to record the coalescence temperature by ^{1}H-NMR measurements, whereas for the propyl-bridged derivative **D1i** the interconversion of the two enantiomers was slow enough to be monitored. The butyl- and the pentyl-bridged push-pull cyclophanes atropisomerized even slower so that only separated diastereotopic protons were observed in the ^{1}H-NMR.[35] Since it was of interest to study the inversion process it was decided to perform the above mentioned studies on the influence of different substituents in

4,4’ position with a series of propyl-bridged biphenyls **D1a** – **D1l** (figure 4) to exclude already conformational stable atropisomers which potentially can occur in the butyl- or pentyl-bridged derivatives.

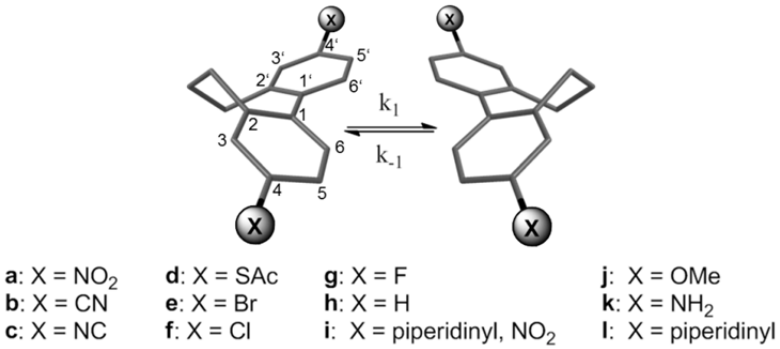

Figure 4. Studied torsion angle restricted biphenyl cyclophanes **D1a** – **D1l**.

Synthesis

Compound **D1a** was synthesized starting from the already available diamino derivative **D1k**[8] by oxidation using a potassium iodide – *tert*-butyl hydroperoxide catalytic system (scheme 1).[41] The dipiperidinyl substituted biphenyl cyclophane **D1l** was obtained by an azacycloalkylation of the diamino biphenyl precursor with 1,5-dibromopentane in an aqueous sodiumdodecylsulfate solution and sodium hydrogen carbonate as a base.[8] The difluoro biphenyl derivative **D1g** was obtained from 4,4’-diaminobiphenyl **D1k** by a Schiemann-type-reaction using tetrafluoroboric acid.[42] Dibromobiphenyl derivative **D1e** was treated with *t*BuLi and afterwards quenched with saturated aqueous ammonium chloride solution to obtain the defunctionalized derivative **D1h** (scheme 1).[43] All other compounds were previously synthesized in our laboratory.[3,4,8,44]

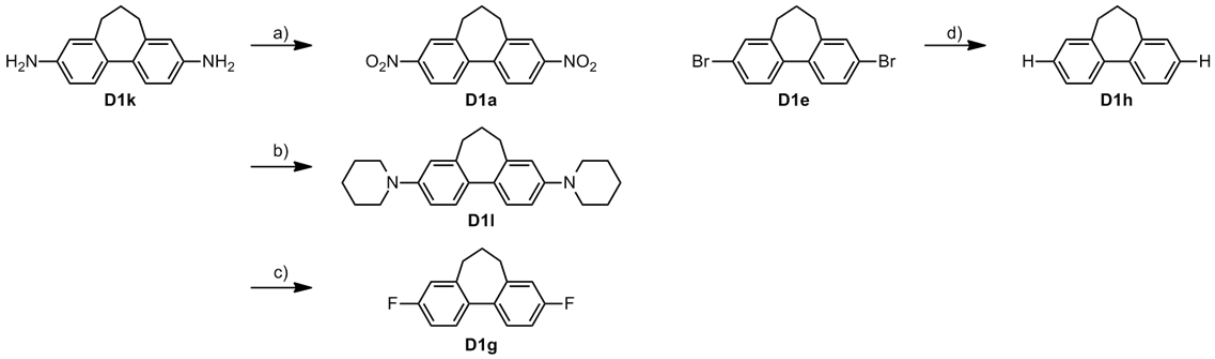

Scheme 1. Synthesis of the biphenyl derivatives **D1a**, **D1l**, **D1g** and **D1h**. a) KI (5 mol%), *tert*-butyl hydroperoxide, MeCN, 80°C, 18 h, 32%; b) 1,5-dibromopentane, SDS, $NaHCO_3$, water, 80°C, 2 h, 52%; c) $NaNO_2$, tetrafluoroboric acid, water, 0°C, 18 h, 88%; d) 1.) *t*BuLi, -78°C, 1.5 h, 2.) sat. aq. ammonium chloride, rt, 30 min, 95%.

NMR-Studies

All samples were prepared in deuterated solvents (>99.8% D, Cambridge Isotope Laboratories, Burgdorf, CH). The NMR experiments were performed on a Bruker Avance III – 600 MHz NMR spectrometer, equipped with a self-shielded z-axis pulsed field gradient dual channel broadband inverse probe-head. Chemical shifts were referenced to residual solvent peaks and the temperature was calibrated using a 4% methanol in 96% methanol-d4 sample.[45] The temperature calibration was performed using equation (1) for temperatures between 200 – 265 K and equation (2) for temperatures between 265 – 300 K.[45] Temperature calibration is crucial for variable temperature NMR spectroscopy as the temperature unit in the spectrometer is placed below the sample and therefore only a hint to the stability and absolute value of the temperature can be obtained. Each temperature was measured three times to prove the stability of the system. The temperature variation during the experiment was less than 0.05 K (three measurements were recorded for each temperature) and therefore much smaller than the estimated calibration error of 1 K. In figure 5 the calibration curve with the statistical errors is depicted. All temperatures for calculations of thermodynamic data were normalized to the calibrated temperature data.

$$T = (3.92 - \Delta\delta) / 0.008 \qquad (1)$$

$$T = (4.109 - \Delta\delta) / 0.008708 \qquad (2)$$

T = absolute temperature [K], $\Delta\delta$ = chemical shift difference between CH_3 and OH resonance in MeOH.

To ensure thermal equilibrium, at least 15 min of equilibration time was allowed for each temperature step.

The activation energy was calculated from the following form of the Eyring equation (3).[46]

$$\Delta G = 0.0191\ T_c\,(9.97 + \lg\,(T_c/(\Delta\nu))) \qquad (3)$$

ΔG = Gibbs free activation energy, T_c = coalescence temperature, $\Delta\nu$ = chemical shift difference in slow exchange.

Kinetic data were obtained from line shape analysis of the propyl-bridged spin system as it is involved in the rotation process. Line shape analysis was performed with the commercially available software d-NMR (Bruker Bio Spin AG®). The confidence interval between simulated and measured spectra was set to 95%. Impurities within the fitted region were not fitted. The resulting rate constants were further analyzed by Eyring plots and the

thermodynamic data calculated using equation (4) and (5).[47,48] The coalescence temperatures were determined by line width analysis for each temperature followed by a Lorentzian fitting.

$$\Delta H = -m\,R \qquad (4)$$

$$y(x=0) = \ln (k_B/h) + (\Delta S/R) \qquad (5)$$

ΔH = activation enthalpy, m = slope of the Eyring plot, R = universal Gas constant = 8.3144 [kJ/(mol K)], y(x=0) = intercept of the Eyring plot, k_B = Boltzmann constant = $1.38 \cdot 10^{-23}$ [J/K], h = Plank constant = $6.626 \cdot 10^{-34}$ [J s].

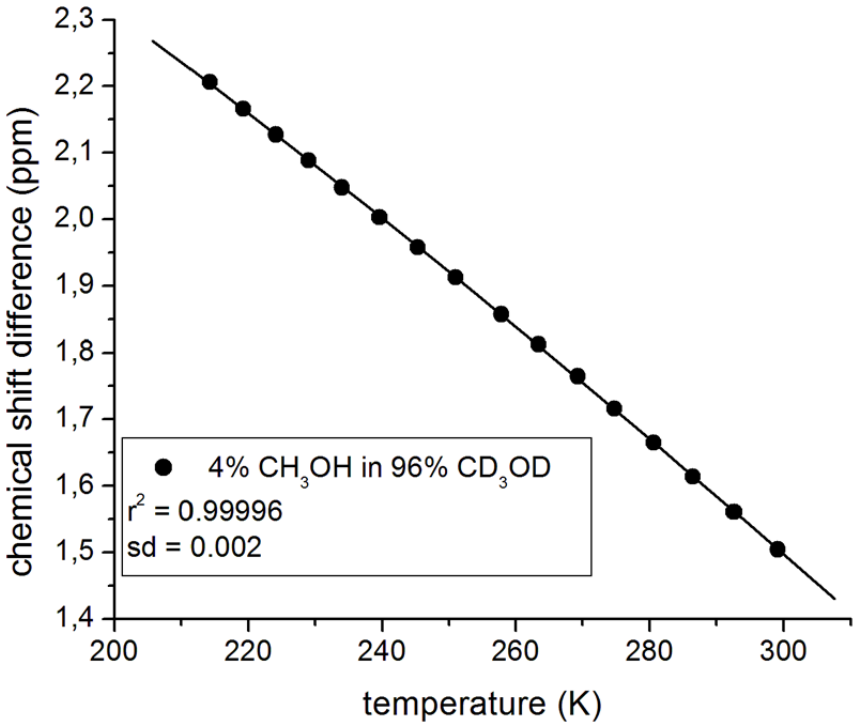

Figure 5. Temperature calibration for low temperature NMR-experiments with a CH_3OH (4%) in CD_3OD (96%)

Computational Studies

All calculations in this work were performed with the TURBOMOLE program package.[49] Equilibrium and transition state structures involved in the atropisomerization process of symmetrically substituted biphenyl cyclophanes were optimized within the framework of density functional theory (DFT). In order to assess the performance of different types of density functionals, we chose the generalized gradient approximation (GGA) functional BP86[50–52], the meta-GGA functional TPSS[53], and the hybrid functional B3LYP[54]. Each functional was used in combination with a def2-TZVP basis set[55], tight convergence criteria (SCF energy: 10^{-8} E_h, energy gradient: 10^{-4} E_h/a_0 or less, inclusion of derivatives of quadrature weights), and fine quadrature grids (m5).[56] For non-hybrid functionals, the efficient

resolution of the identity (RI) approximation for two-electron Coulomb integrals was employed. The nature of the obtained stationary points (minimum or first order saddle point) was confirmed through analysis of the force constants and vibrational frequencies.

Gibbs free activation energies were computed for a standard pressure of 0.1 MPa and for the coalescence temperatures T_c as determined in the NMR experiment. For the calculation of the partition functions, the vibrational frequencies were scaled by a factor of 0.9914 (BP86 and TPSS) or 0.9614 (B3LYP).[57]

In case of X = NH_2, OMe, SAc and piperidinyl, the rotation about the C–X bond as well as rotations within the substituent allowed for several conformational isomers. Here, we considered all energetically low lying equilibrium structures with C_2 symmetry together with their corresponding transition states. The reported values for these substituents were obtained by taking the Boltzmann average of the respective conformers.

Results

The interconversion of the two atropisomers of cyclophanes **D1a** – **D1l** can be monitored by NMR coalescence experiments if the half lifes of the enantiomers are in the range of microseconds to seconds. For thermodynamic investigations three different states have to be accessible. The slow exchange where the signals of the two protons are obtained as well separated resonances. The coalescence where the signal reaches a plateau and the line width is extremely broadened and finally the fast exchange where the signals are obtained as an averaged signal (figure 6). Determination of the coalescence temperature and the chemical shift differences in the slow exchange regime yield the Gibbs free activation energy $\Delta G^{\ddagger}(T)$ using the modified form of the Eyring equation (3). Coalescence temperatures were estimated from the measured spectra with an accuracy of 1 K. As shown in table 1 different $\Delta G^{\ddagger}(T)$ were obtained for the push-push, push-pull and pull-pull systems depending on different substituents. The activation energy is in the range of 44 to 55 kJ/mol for all compounds **D1a** – **D1l**.

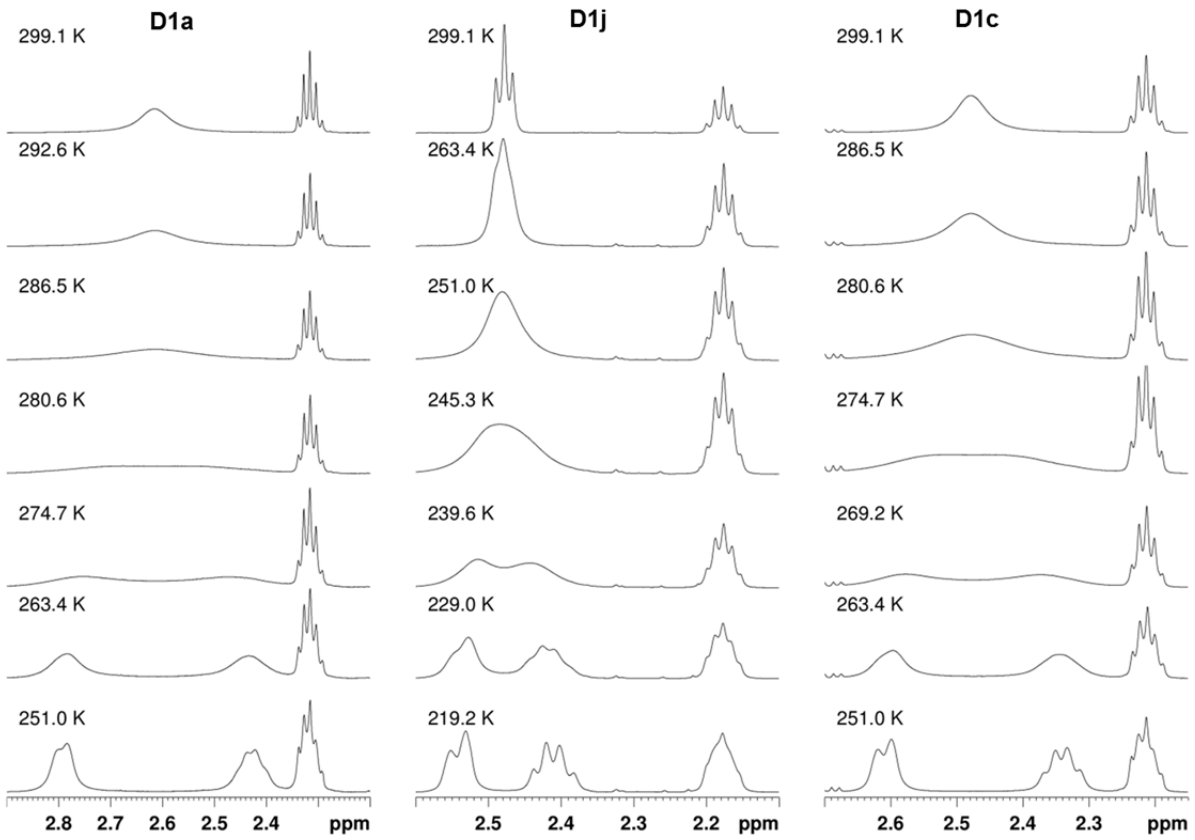

Figure 6. Stacked plots of the low temperature NMR spectra of **D1a** (*left*), **D1j** (*middle*) and **D1c** (*right*) measured in $CDCl_3$. Starting from fast exchange at 299.1 K reaching the coalescence temperature at 281.4 K, 242.1 K and 275.1 K, respectively, ending in the slow exchange at 251 K, 219.2 K and 251 K where the signals for the four protons are separated.

The line shape analysis delivered insight into the kinetics of the rotation.[48,58,59] Rate constants for each temperature and substituent were determined and analyzed using Eyring plots. According to this enthalpy and entropy parameters were obtained using equation (4) and (5). A representative comparison of experimental and calculated spectra is shown in figure 7 and the corresponding Eyring plot in figure 8.

Table 1. Coalescence temperatures of the biphenyl cyclophanes **D1a** – **D1l** (figure 1) in chloroform with their characteristic separation $\Delta\nu$ and the resulting Gibbs activation energy $\Delta G^{\ddagger}$(T) with standard deviation ($\Delta\Delta G^{\ddagger}$(T)).

Compound	T_c / K	$\Delta\nu$ / Hz	$\Delta G^{\ddagger}$ / kJ/mol
D1a	281.4 ± 1	218.0	54.2 ± 0.5
D1b	275.1 ± 1	181.0	53.3 ± 0.5
D1c	270.1 ± 1	161.0	52.6 ± 0.5
D1d	259.6 ± 1	111.0	51.3 ± 0.5

Table 1. continued

Compound	T_c / K	Δv / Hz	$\Delta G^{\ddagger}$ / kJ/mol
D1e	260.2 ± 1	113.0	51.3 ± 0.5
D1f	260.7 ± 1	118.0	51.4 ± 0.5
D1g	265.0 ± 1	109.0	52.4 ± 0.5
D1h	263.3 ± 1	95.0	52.4 ± 0.5
D1i	245.0 ± 1	132.0	47.9 ± 0.5
D1j	242.1 ± 1	79.0	48.4 ± 0.5
D1k	224.2 ± 1	31.0	46.4 ± 0.5
D1l	218.9 ± 1	44.0	44.6 ± 0.5

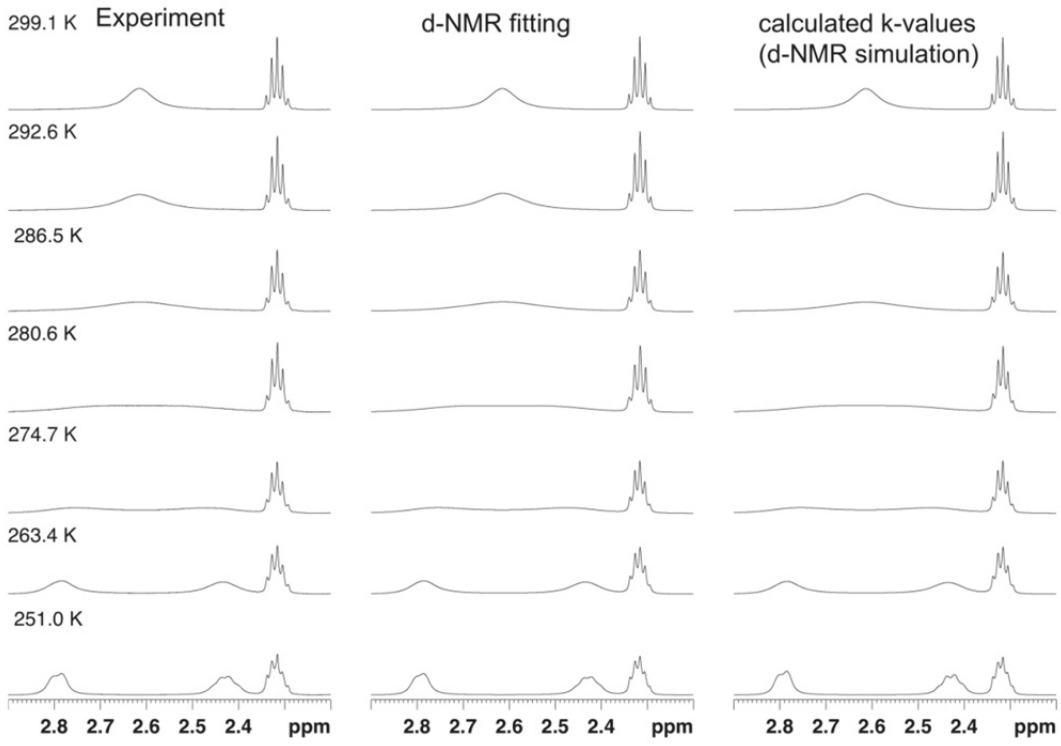

Figure 7. Comparison of experimental and simulated NMR spectra for the dinitro substituted biphenyl **D1a** at variable temperatures. Line shape analysis was performed for the whole propyl-bridged spin system involved in the rotation process. The simulated spectra have an accuracy of >95%.

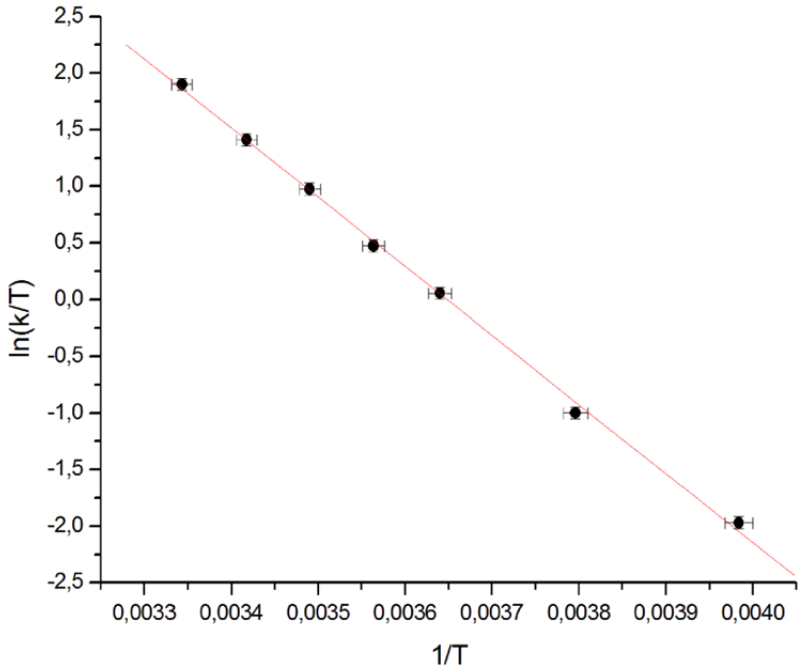

Figure 8. Eyring plot for the dinitro substituted biphenyl **D1a** correlating the rate of rotation with temperature. Linear regression delivers directly the thermodynamic data.

Activation enthalpy $\Delta H_{\text{Eyring}}^{\ddagger}$, activation entropy $\Delta S_{\text{Eyring}}^{\ddagger}$ and the free energy $\Delta G_{\text{Eyring}}^{\ddagger}(\text{T})$ are shown in table 2. The coalescence temperatures T_c were estimated from the recorded spectra whereas the calculated coalescence temperatures $T_{\text{c-lineshape}}$ were obtained after Lorentzian fitting of the line width. The coalescence temperatures were calculated from the line width of the coalescent peak. The line width was therefore plotted against the temperature and the resulted points were fitted with a Lorentzian shaped curve. A high analogy with the experimental coalescence temperatures was obtained except for the dipiperidinyl substituted biphenyl **D1l**, where the limiting factor was the freezing point of $CDCl_3$. An example for the determination of the coalescence temperature is shown in figure 9. The maximum of the calculated curve delivers directly the coalescence temperature.

In order to validate the two site model used for the interpretation of the experimental data and the determination of the free energy, the results for $\Delta G^{\ddagger}(\text{T})$ obtained from experimental and simulated NMR data (table 1 and 2) were compared. The error on the Gibbs free activation energy depends on the coalescence temperature estimated from measured NMR spectra. The accuracy of calculated coalescence temperatures is mainly influenced by the number of points measured in fast exchange and slow exchange. Therefore the calculated data for compounds with a low coalescence temperature is less precise compared to the ones with higher coalescence temperatures.

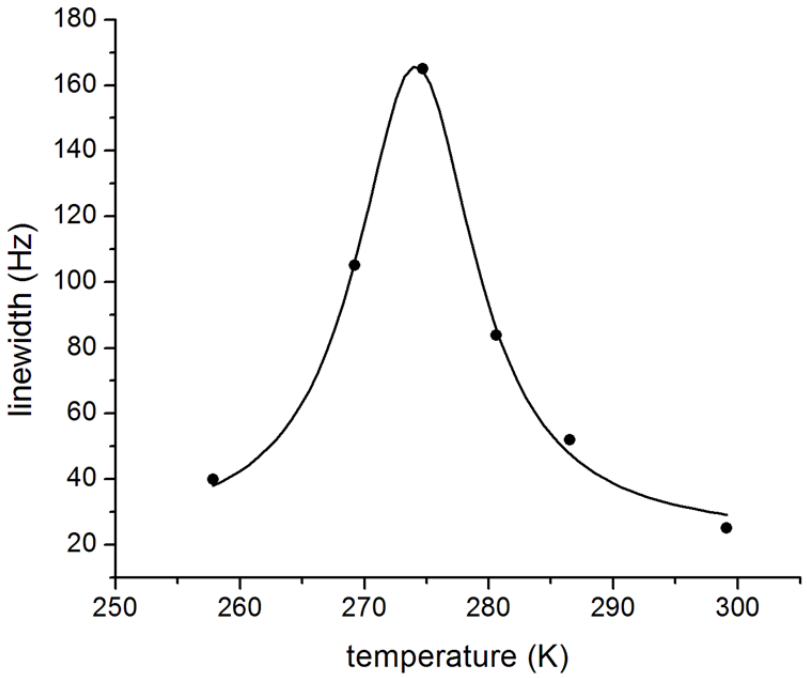

Figure 9. Calculation of the coalescence temperature for **D1b** from the line width of the experimentally obtained peaks.

Simulation of spectra of **D1j** and **D1l** was quite difficult because of the low coalescence temperature. Only two spectra could be measured below T_c because the freezing point of $CDCl_3$ was reached. The increased viscosity of $CDCl_3$ at low temperatures resulted in broader NMR signals which led to rate constants, that are larger than they are in reality. Therefore a correction factor for slow exchange rate constants was estimated by measuring a reference sample. Error calculations were performed with temperature errors (T ± 1 K) and rate constant errors (k ± 5% except **D1l** where an error of 20% was used). In addition, the errors from Eyring analysis were included in the error of the simulated $\Delta G_{Eyring}^{\ddagger}(T)$. The differences between experimental and simulated $\Delta G^{\ddagger}(T)$ values are quite small (0.0 to 0.8 kJ/mol) and for all cases within the experimental error except **D1l**. It has been shown, therefore, that the two state model approach is valid and that differences in the determined $\Delta G^{\ddagger}(T)$ values of more than 1 kJ/mol are statistically significant.

Table 2. Overview over thermodynamic data calculated from line shape analysis with d-NMR. The coalescence temperatures were calculated by Lorentzian fitting of the line width. Thermodynamic data were obtained from Eyring plots.

Compound	$T_{\text{c-lineshape}}$ / K	$\Delta G_{\text{Eyring}}^{\ddagger}$ / kJ/mol	$\Delta H_{\text{Eyring}}^{\ddagger}$ / kJ/mol	$\Delta S_{\text{Eyring}}^{\ddagger}$ / J/molK
D1a	280.4 ± 1.1	54.2 ± 0.1	50.7 ± 1.6	-12.6 ± 5.6
D1b	274.1 ± 1.3	53.2 ± 0.1	52.7 ± 2.0	-1.9 ± 7.3
D1c	269.1 ± 1.1	52.6 ± 0.1	49.9± 1.3	-10.0 ± 4.6
D1d	261.6 ± 1.7	51.6 ± 0.1	45.9 ± 1.0	-21.8 ± 3.6
D1e	263.2 ± 1.3	51.7 ± 0.1	50.0 ± 2.7	-6.4 ± 10.4
D1f	259.7 ± 1.3	51.5 ± 0.1	46.0 ± 1.0	-21.0 ± 3.7
D1g	263.0 ± 1.6	52.6 ± 0.1	47.8± 1.3	-18.4 ± 4.7
D1h	262.3 ± 1.4	52.4 ± 0.1	47.4 ± 1.2	-19.1 ± 4.6
D1i	244.0 ± 1.2	47.8 ± 0.1	37.4 ± 0.8	-42.6 ± 3.0
D1j	241.1 ± 1.3	48.8 ± 0.1	43.4 ± 1.5	-22.5 ± 6.2
D1k	221.6 ± 2.1	46.8 ± 0.1	39.3 ± 1.5	-33.8 ± 6.6
D1l	217.9 ± 1.4	45.4 ± 0.2	28.3 ± 1.7	-78.4 ± 7.3

Density functional theory calculations were performed in order to gain further insight into the atropisomerization mechanism of the propyl-bridged biphenyls. In this context it was also of interest to have a closer look at the influence of the different substituents in *para* position on the structural parameters as well as on the thermodynamic properties. All aforementioned synthesized compounds except of the unsymmetrically substituted push-pull system **D1i** were considered.

All optimized equilibrium structures exhibit (or in case of conformational freedom were chosen to exhibit) C_2 symmetry and the torsion angle between the phenyl rings amounts to about 47° (figure 10). The careful inspection of the rotation about the central phenyl-phenyl bond revealed that the two atropisomers are connected via a single transition state. The relevant structures are shown in figure 11 for the unfunctionalized compound **D1h**. It can be seen that the transition state is accessible from the equilibrium structure via rotation of an *ortho* methylene group, which results in a geometry with a torsion angle of 0°. The phenyl rings are coplanar but, as slightly bent towards the unbridged side, not perfectly linear.

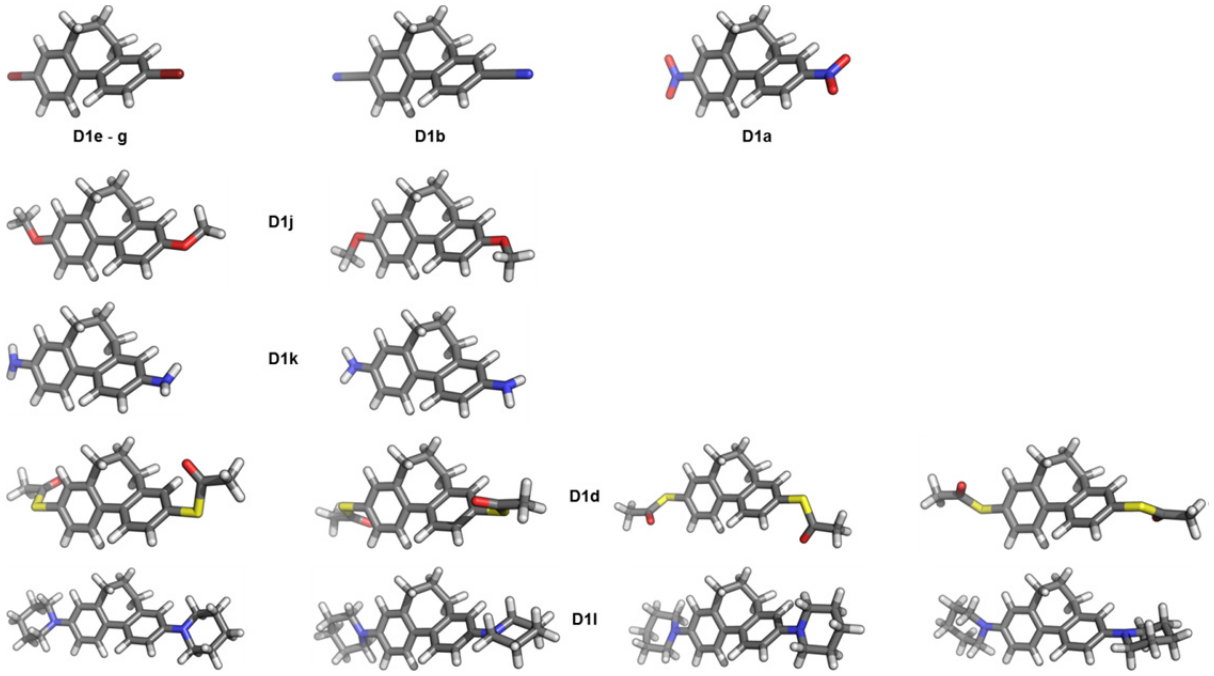

Figure 10. Different ground state conformers of **D1a** – **D1l**, where for **D1a**, **D1b**, **D1e** – **D1g** only one, for **D1j** and **D1k** two and for **D1d** and **D1l** four ground state conformer in respect to the substituents are possible. For simplification only one atropisomer is shown.

On the basis of the determined species in the reaction pathway, the Gibbs free energy of activation ($\Delta G_{theo}^{\ddagger}$) was computed. The results for the various density functionals and substituents are summarized in table 3. Similar trends for the dependence on the substituents are observed, but the absolute values are systematically shifted (BP86 < TPSS < B3LYP). The contributions of the enthalpy of activation ($\Delta H_{theo}^{\ddagger}$) and the entropy of activation ($\Delta S_{theo}^{\ddagger}$) are given in table 4. It was found that all obtained absolute values for $\Delta S_{theo}^{\ddagger}$ are smaller than 4 J/(mol K), and thus of about the size of the error we expect for the underlying method.

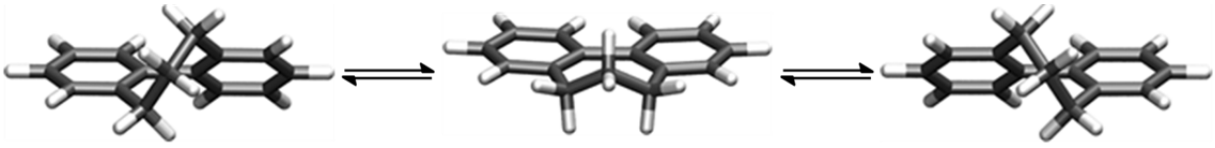

Figure 11. Calculated atropisomerization mechanism: equilibrium structure before the rotation of the phenyl rings (*left*), transition state structure (*middle*), and equilibrium structure after the rotation (*right*).

Table 3. Calculated Gibbs free activation energies $\Delta G_{theo}^{\ddagger}$ using different types of density functionals. All values are given in kJ/mol.

Compound	$\Delta G_{BP86}^{\ddagger}$	$\Delta G_{TPSS}^{\ddagger}$	$\Delta G_{B3LYP}^{\ddagger}$
D1a	48.4	49.7	52.0
D1b	47.6	48.7	51.2
D1c	47.2	48.2	50.6
D1d	48.0	48.9	52.4
D1e	47.0	48.0	50.4
D1f	47.0	48.0	50.3
D1g	48.4	49.4	51.6
D1h	48.4	49.3	51.7
D1j	45.7	46.5	48.9
D1k	44.0	44.8	47.3
D1l	42.5	43.3	46.2

Table 4. Enthalpy ($\Delta H_{theo}^{\ddagger}$) and entropy ($\Delta S_{theo}^{\ddagger}$) contributions to the Gibbs free activation energy as calculated with different types of density functionals. Values for $\Delta H_{theo}^{\ddagger}$ are given in kJ/mol, values for $\Delta S_{theo}^{\ddagger}$ are given in J/(mol K).

Compound	$\Delta H_{BP86}^{\ddagger}$	$\Delta S_{BP86}^{\ddagger}$	$\Delta H_{TPSS}^{\ddagger}$	$\Delta S_{TPSS}^{\ddagger}$	$\Delta H_{B3LYP}^{\ddagger}$	$\Delta S_{B3LYP}^{\ddagger}$
D1a	49.1	2.5	50.1	1.4	52.5	1.8
D1b	48.1	1.9	48.8	0.6	51.7	1.6
D1c	47.6	1.5	48.3	0.5	50.9	1.2
D1d	47.8	-0.9	48.5	-1.5	51.5	-3.7
D1e	47.3	0.9	48.0	-0.1	50.6	0.8
D1f	47.2	0.8	47.9	-0.2	50.5	0.7
D1g	48.6	0.6	49.3	-0.3	51.8	0.5
D1h	48.8	1.2	49.4	0.3	52.0	1.2
D1j	45.9	0.9	46.5	0.0	49.0	0.8
D1k	44.2	0.7	44.8	-0.1	47.5	0.5
D1l	43.1	2.8	43.7	1.9	46.7	2.3

Discussion

The atropisomerization energies $\Delta G^{\ddagger}(T)$ obtained by the modified form of the Eyring equation (1) were calculated for all compounds **D1a** – **D1l** to be between 45 kJ/mol for the strongest π-donor piperidinyl **D1l** and 55 kJ/mol for the nitro substituted derivative **D1a** as the strongest π-acceptor. These results demonstrate that the influence of the substituents in 4,4' position on the racemization is less pronounced than variation of the length of the alkyl-bridge as shown in the investigation of the push-pull cyclophanes.[35] For the diacceptor substituted propyl-bridged biphenyl derivatives **D1a** – **D1c** significantly higher rotation barriers $\Delta G^{\ddagger}(T)$ were measured as for the compounds substituted with two donors. The free energy of dimethoxy cyclophane **D1j** is slightly higher than the one of the push-pull system **D1i**, which is consistent with the values obtained by Oki.[33] As demonstrated there, acceptors increase the rotation energy of such systems whereas donors decrease the free energy. For the only weak π-donating halogen substituted cyclophane derivatives **D1e** – **D1g** and the unfunctionalized derivative **D1h** similar atropisomerization energies $\Delta G^{\ddagger}(T)$ around 52 kJ/mol were measured.

Since it was of interest to investigate the influence of donors and acceptors of variable strength, the measured free energies $\Delta G^{\ddagger}(T)$ were plotted against the Hammett-parameters σ_p (figure 12).[60,61] The σ-parameters can be used in this case as a collective measure of the total electronic effects (resonance and inductive effect) and reflects the ability to withdraw or donate electrons from the reaction site in this particular case the central C-C bond of the biphenyl. To obtain adequate parameters for the two substituents in 4 and 4' position the Hammett-parameters for each individual substituent were summed up as demonstrated by Hart[62] and Wirz[63]. The influence of the propyl chain was disregarded because its influence was constant throughout the whole series. The free energy $\Delta G^{\ddagger}(T)$ is dependent on the logarithm of the rate constant and therefore these Hammett-parameters can be directly correlated to $\Delta G^{\ddagger}(T)$.[61] By performing such a correlation the effect of the substituents on the transition state compared to the initial state can be visualized. Since the reference system, namely the unfunctionalized derivative **D1h** is included in the correlation, a normalization was not performed.

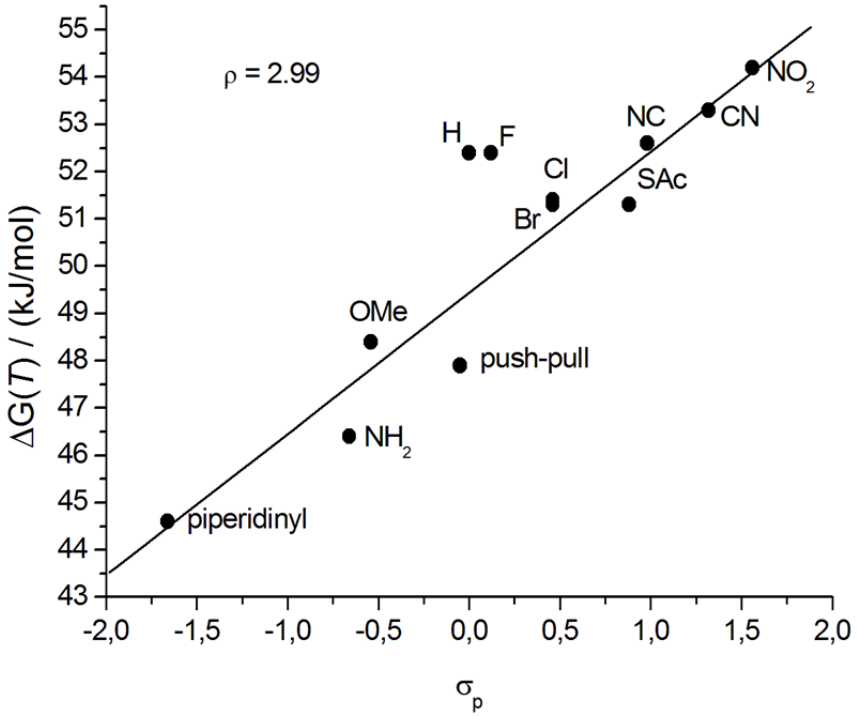

Figure 12. Hammett-correlation of the propyl-bridged biphenyl systems **D1a** – **D1l**.

Inspection of the obtained Hammett-plot clearly shows a linear free energy relation, which implies that the atropisomerization process is strongly dependent on the electron density at the central C1-C1'-bond. According to this observation the rotation barrier is increased when the electron density is reduced at the reaction site and decreased when the electron density is increased. Furthermore the slope of the linear free energy relationship ρ of 2.99 indicates the sensitivity of the atropisomerization process on electronic perturbation. Additionally, the fact that there are only minor deviations from linearity indicates that all derivatives **D1a** – **D1l** follow the same atropisomerization mechanism. To gain further insight into the effect of the substituents, the Hammett-parameters σ_p were splitted in accordance to Swain and Lupton into their field effect (F) parts and their resonance (R) parts.[64] Correlation of the obtained free energy values to the modified parameters F and R clearly demonstrate that the substituents in 4 and 4' position influence the atropisomerization process by disturbing the π-system of the biphenyl system (figure 13). No linear free energy relationship for the inductive effect, a measure for the polarization of the σ-skeleton of the reaction site, was observed which is in stark contrast to the in earlier publications postulated partial rehybridization of the central carbon atoms.[32]

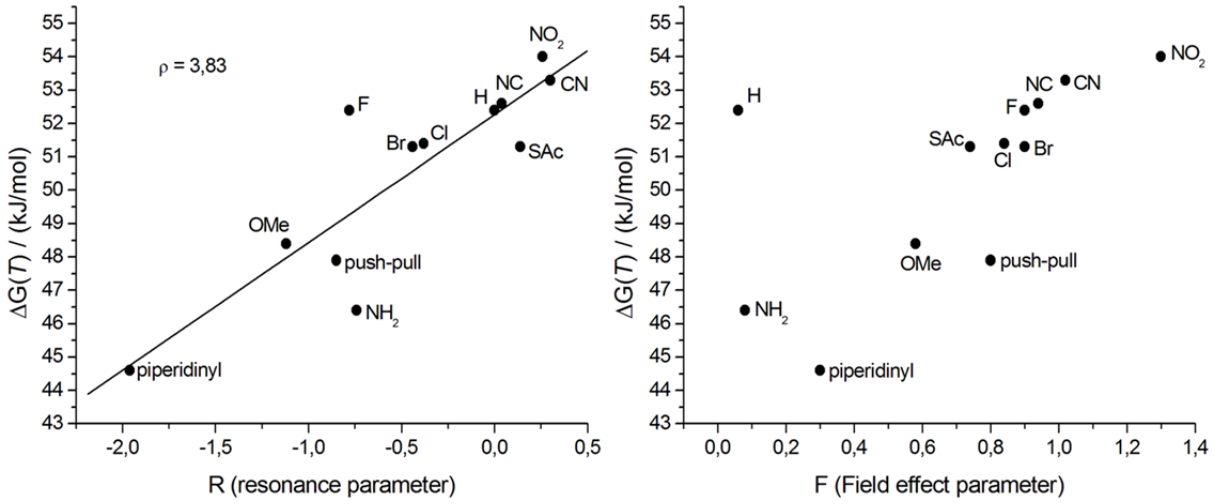

Figure 13. *left*: correlation of $\Delta G^{\ddagger}$(T) with the resonance parameter R, *right*: correlation of $\Delta G^{\ddagger}$(T) with the field effect parameter F.

By the above described line shape analyses of the ^{1}H-NMR coalescence spectra the rate constants for the interconversion process were estimated at different temperatures and by using the Eyring equation the free energies of rotation $\Delta G^{\ddagger}$(T) were divided into their enthalpic and entropic parts (table 2). Thereby it gets evident that the main contribution to the rotation barrier of the central biphenyl bond is dominated by the enthalpic contribution. Interestingly the influence of entropy is increased the stronger electron-donating the substituents in 4,4' positions get (push-push case). The enthalpy $\Delta H^{\ddagger}$ of the bridged biphenyl cyclophanes **D1a** – **D1l** is the energy one atropisomer has to overcome to access the transition state. By again plotting the enthalpy values obtained by line shape analysis for each individual cyclophane against the Hammett-parameter σ_p the same trend as for the free energy $\Delta G^{\ddagger}$(T) is observed, but with a more significant deviation from linearity (figure 14). Splitting of the Hammett-parameter σ_p in the resonance and field effect part gave no further evidence about the inversion mechanism. (figure 14).

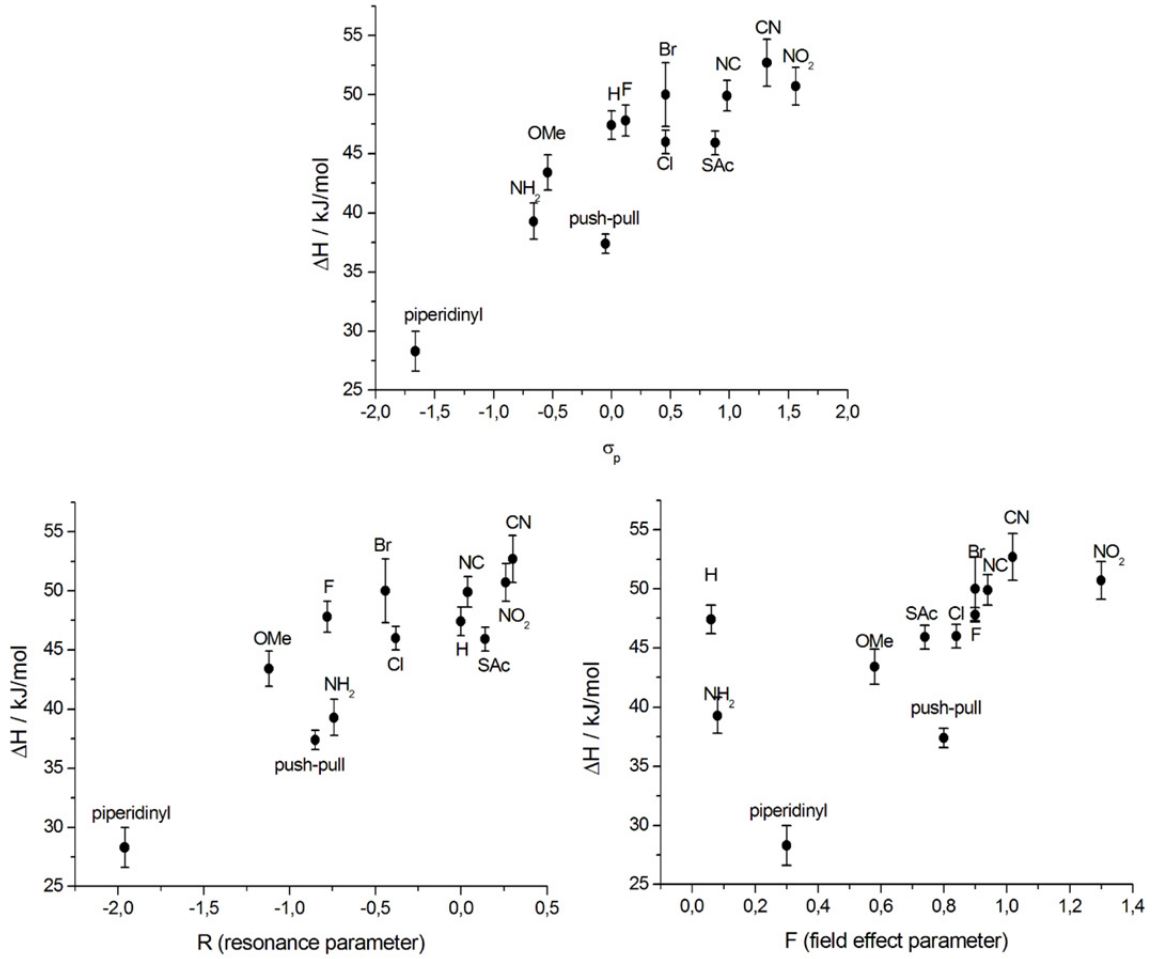

Figure 14. *top:* Hammett-correlation of the enthalpy values $\Delta H_{Eyring}^{\ddagger}$ of the isomerization process, *bottom left:* correlation of $\Delta H_{Eyring}^{\ddagger}$ with the resonance parameter R, *bottom right:* correlation of $\Delta H_{Eyring}^{\ddagger}$ with the field effect parameter F.

The same holds true when analyzing the entropy $\Delta S_{Eyring}^{\ddagger}$, where unfortunately the linear correlation is even less pronounced (figure 15). A fact that is not surprising as the entropy reflects the number of possibilities of populating the microscopic configurations of the microcanonical ensemble (e.g. rotational states, vibrational states etc.) and should therefore be more or less independent of the substituents. These correlations of the free energy $\Delta G^{\ddagger}(T)$, the enthalpy $\Delta H^{\ddagger}$ and the entropy $\Delta S^{\ddagger}$ of the atropisomerization process to the Hammett-parameters of 2,2' propyl-bridged biphenyl derivatives **D1a** – **D1l** (figure 12 – 15) allow for a number of conclusions about the inversion mechanism. The much more pronounced linear relationships of $\Delta G^{\ddagger}(T)$ to the resonance parameter R, a measure for the influence of different end-groups on the conjugation in the biphenyl system, indicate that the different substituents in 4 and 4' position dictate the energy needed for the isomerization process by distortion of the π-system of the biphenyl core. Thus a planar transition state for the atropisomerization can be postulated. Furthermore the linear free energy relationship points out that the electron

density at the central C1-C1'-biphenyl bond is the dominating factor for increasing or decreasing the rotation barrier within a series of biphenyls bearing the same 2,2' substitution pattern.

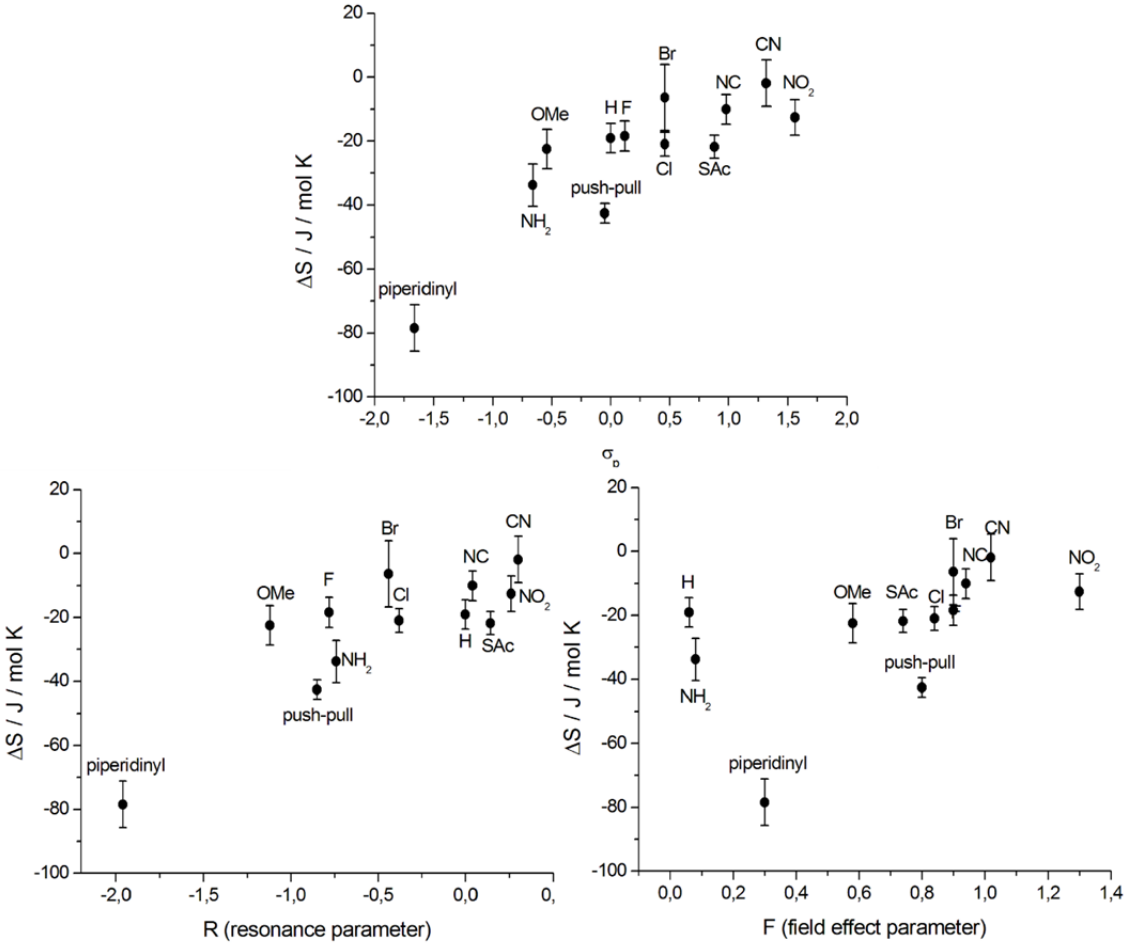

Figure 15. Correlation of the entropies $\Delta S_{Eyring}^{\ddagger}$ of compounds **D1a** – **D1l** against: *top*: Hammett-parameter σ_p, *bottom left*: resonance parameter R, *bottom right*: filed effect parameter F.

For strong donors the rotation is facile compared to the unfunctionalized reference system and the enthalpic contribution to the free energy $\Delta G^{\ddagger}(T)$ is minor, whereas for strong acceptors the rotation is much more hindered and the free energy $\Delta G^{\ddagger}(T)$ is dominated by the enthalpic contribution. Considering a planar transition state and taking into account that the substituents donate or withdraw electrons from the central biphenyl bond via the π-system as indicated by the Hammett-correlation, it can be hypothesized that strong donors rise the π-electron density at the C1-C1' bond and therefore generate a partial negative charge at the C1 atoms. In the case of the strong acceptors the electron density at the C1 atoms is decreased causing a partial positive charge.

Comparison of the experimentally determined free energies $\Delta G^{\ddagger}(T)$ with the calculated values using DFT methods (table 3) shows a good agreement (figure 16). For the donor substituted

cyclophanes **D1j** and **D1k** the by use of the density function BP86/SV(P) calculated free energies $\Delta G_{theo}^{\ddagger}(T)$ are consistent with measured energies. However, for the strongly electron-accepting substituents **D1a** – **D1c** the hybrid function B3LYP/SV(P) gives the best fit. These correlations of calculated and measured free energy values that deviate as a function of electron density indicates that the underlying calculated inversion mechanism (figure 11) reflects the atropisomerization process. In the calculated mechanism only one transition state is present and the molecule showing a C_2 symmetry equilibrium state, rotates into a planar and nearly linear transition state with a C_s or C_1-symmetry depending on the substituents (figure 11). Therefore the two *ortho* CH_2-groups of the bridge have two pass by each other which feasibility seems to be the crucial factor dictating the inversion energy.

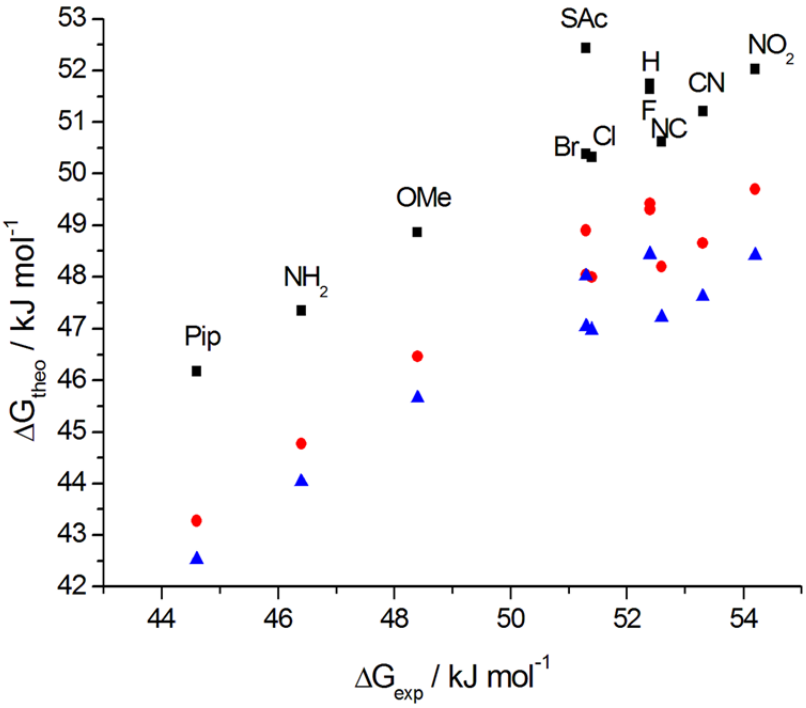

Figure 16. Plot of the calculated free energies $\Delta G_{theo}^{\ddagger}(T)$ against measured free energies $\Delta G^{\ddagger}(T)$. *blue*: BP86/SV(P); *red*: TPSS/TZVP, *black*: B3LYP.

Furthermore the change in distance from the ground state (ca. 148 pm) to the transition state (151 – 152 pm) between the two individual phenyl rings varies as a function of the free energy $\Delta G^{\ddagger}(T)$ and with it as a function of the donor and acceptor strength of the substituents (figure 17). For lower free energy values the change in bond length is less pronounced than for higher values which corresponds to the fact that in the donor substituted biphenyls the elongation of the C1-C1' bond is minor compared to the elongation in the acceptor substituted ones. The length of a chemical bond is strongly related to its electron density and therefore this observed change is in excellent agreement with the conclusions drawn from the Hammett-

correlations, where strong donors enhance the electron density at the central bond and strong acceptors decrease it. This further supports that the electron density at the central bond is the dominant factor which influences the energy of rotation. Because of the rigidity of the phenyl rings an elongation of the C1-C1' bond seems to be necessary to create enough space for the *ortho* methylene groups to pass by each other. In contradiction the degree of elongation which is dictated by the substituents in *para* position is closely related to the rotation barrier of the biphenyl cyclophanes **D1a** – **D1l**. As a result it seems that a stronger elongation causes a deviation from linearity and therefore reduces the space between the methylene groups. Hence, in the acceptor substituted biphenyls the half space containing the bridge is more crowded, causing a more hindered rotation. Furthermore this explains the unexpected low rotation barrier of the push-pull system **D1i**, where a contraction of the central bond due to a double bond character is expected.

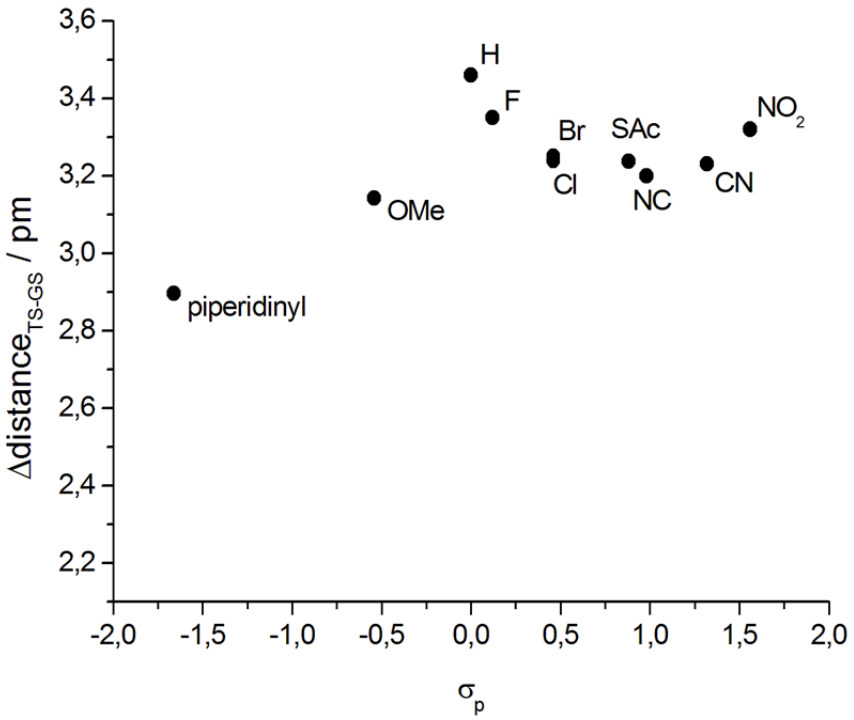

Figure 17. Correlation of the difference of the calculated phenyl-phenyl distance in the transition state and the ground state with the Hammett-parameter σ_p.

Comparison of the calculated enthalpies (table 4) with the experimentally obtained ones (table 2) show that the deviation in the case of donating substituents is more pronounced whereas in the case of accepting and neutral substituents again a nice agreement is obtained (figure 18). The calculated entropies which are constant and near zero for all compounds **D1a** – **D1l** on the contrary deviate significantly from the measured ones where values between -1 and -23 J/mol K were estimated by line shape analyses, except of the push-pull **D1i**, the amine

substituted biphenyl **D1k** and the piperidine substituted one **D1l**, where strong negative changes in entropy were measured.

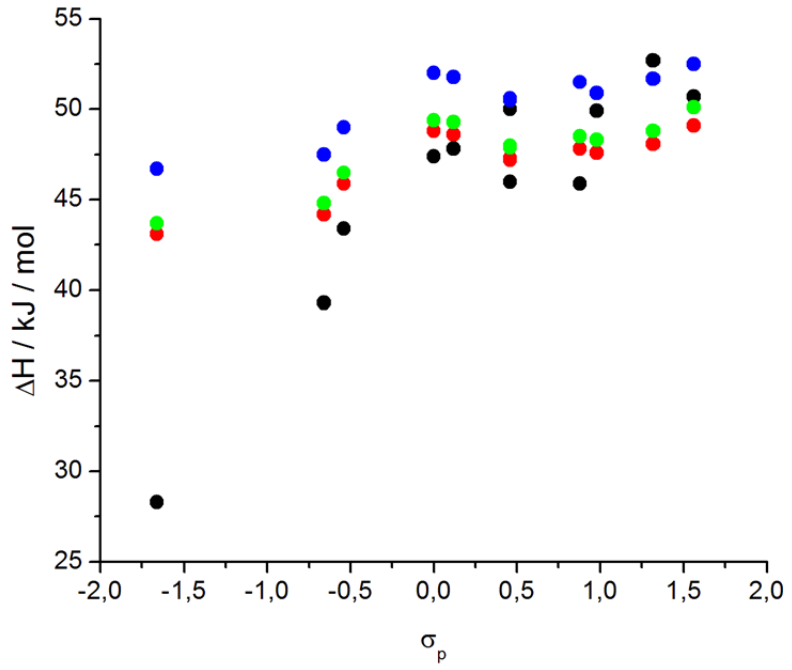

Figure 18. Plot of the enthalpy $\Delta H^{\ddagger}$ against the Hammett-parameter σ_p. *black*: measured values; *red*: BP86; *yellow*: TPSS; *blue*: B3LYP.

In DFT calculations single molecules in gas phase were investigated whereas in NMR measurements an ensemble of molecules was investigated. A large difference in entropy is obtained for these two different methods. Reasons for this difference could be intermolecular interactions either with a neighbouring biphenyl (π-π-stacking) or with the surrounding solvent in the experiment. Formation of aggregates was excluded by ^{1}H-NMR titration with a limited series of concentrations. Hence solvent dependent ^{1}H-NMR coalescence measurements were performed to evaluate if the thermodynamic parameters which are more susceptible to the experiment, namely the enthalpy $\Delta H^{\ddagger}$ and the entropy $\Delta S^{\ddagger}$, change with solvent. Methanol as a polar protic solvent and toluene as a π-donating solvent were chosen to gain insight into the stabilizing effect on the transition state. Therefore a donor substituted (**D1j**), a neutral (**D1e**) and an acceptor substituted biphenyl (**D1b**) were measured in both solvents and then compared to the thermodynamic data obtained in chloroform (table 5). In all cases the free energy $\Delta G^{\ddagger}$(T) remained similar in all solvents as expected as it is independent of the experiment in the same aggregation state, whereas the enthalpies $\Delta H^{\ddagger}$ and the entropies $\Delta S^{\ddagger}$ significantly changed when measured in different solvents.

Table 5. Solvent effect on the thermodynamic data obtained by line shape analyses of ^{1}H-NMR coalescence measurements in different solvents.

	D1e ($CDCl_3$)	**D1e** (MeOD)	**D1e** (toluene)
$\Delta S_{Eyring}^{\ddagger}$ / J/molK	-6.4 ± 10.4	-8.0 ± 4.6	-18.0 ± 5.5
$\Delta H_{Eyring}^{\ddagger}$ / kJ/mol	50.0 ± 2.7	49.0 ± 1.3	45.9 ± 1.4
$\Delta G_{Eyring}^{\ddagger}$ / kJ/mol	51.7 ± 0.1	51.1 ± 0.1	50.4 ± 0.1
$\Delta G_{exp}^{\ddagger}$ / kJ/mol	51.3 ± 0.5	51.0 ± 0.5	50.5 ± 0.5
	D1b ($CDCl_3$)	**D1b** (MeOD)	**D1b** (toluene)
$\Delta S_{Eyring}^{\ddagger}$ / J/molK	-10.3 ± 7.3	-8.3 ± 4.2	-39.9 ± 3.5
$\Delta H_{Eyring}^{\ddagger}$ / kJ/mol	50.4 ± 2.0	50.1 ± 1.2	41.7 ± 0.9
$\Delta G_{Eyring}^{\ddagger}$ / kJ/mol	53.2 ± 0.1	52.3 ± 0.1	51.9 ± 0.1
$\Delta G_{exp}^{\ddagger}$ / kJ/mol	53.3 ± 0.5	52.4 ± 0.5	52.0 ± 0.5
	D1j ($CDCl_3$)	**D1j** (MeOD)	**D1j** (toluene)
$\Delta S_{Eyring}^{\ddagger}$ / J/molK	-22.5 ± 6.2	-12.8 ± 4.0	-5.0 ± 4.9
$\Delta H_{Eyring}^{\ddagger}$ / kJ/mol	43.4 ± 1.5	45.6 ± 1.0	47.9 ± 1.3
$\Delta G_{Eyring}^{\ddagger}$ / kJ/mol	48.8 ± 0.1	48.7 ± 0.1	49.1 ± 0.1
$\Delta G_{exp}^{\ddagger}$ / kJ/mol	48.4 ± 0.5	48.5 ± 0.5	48.9 ± 0.5

The enthalpy of the methoxy substituted biphenyl **D1j** was increased when going from chloroform to methanol to toluene. A contrary trend was observed for the acceptor substituted cyclophane **D1b** and neutral **D1e** where the lowest enthalpic contribution was measured in toluene. Since the free energy remained the same throughout this limited series it is self-evident that the entropy follows the opposed trend compared to the enthalpy. The only chemical property which similarly follows the obtained trend for donor substituted **D1j** is the acidity of the solvents where chloroform is the most acidic and toluene the less acidic one. The above mentioned Hammett-correlations show induction of a partial negative charge at the central C1 atoms with donor substituted biphenyls, thus it is hypothesized that protic solvents can stabilize the transition state of the atropisomerization process and therefore lower enthalpies are obtained. Furthermore when a partial positive charge is induced as with

electron-poor systems π-electron-rich toluene can stabilize the transition state and therefore lower rotation barriers are obtained. Interestingly toluene also seems to stabilize the transition state by π-π stacking of the π-donating but inductively accepting bromide **D1e**. According to these observations it can be concluded that the absence of solvent molecules and therefore the missing stabilization of solvents on the transition state leads to the large discrepancy in measured and calculated enthalpy and entropy values when measured in chloroform, especially in the case of donor substituted biphenyls **D1j** and **D1l**.

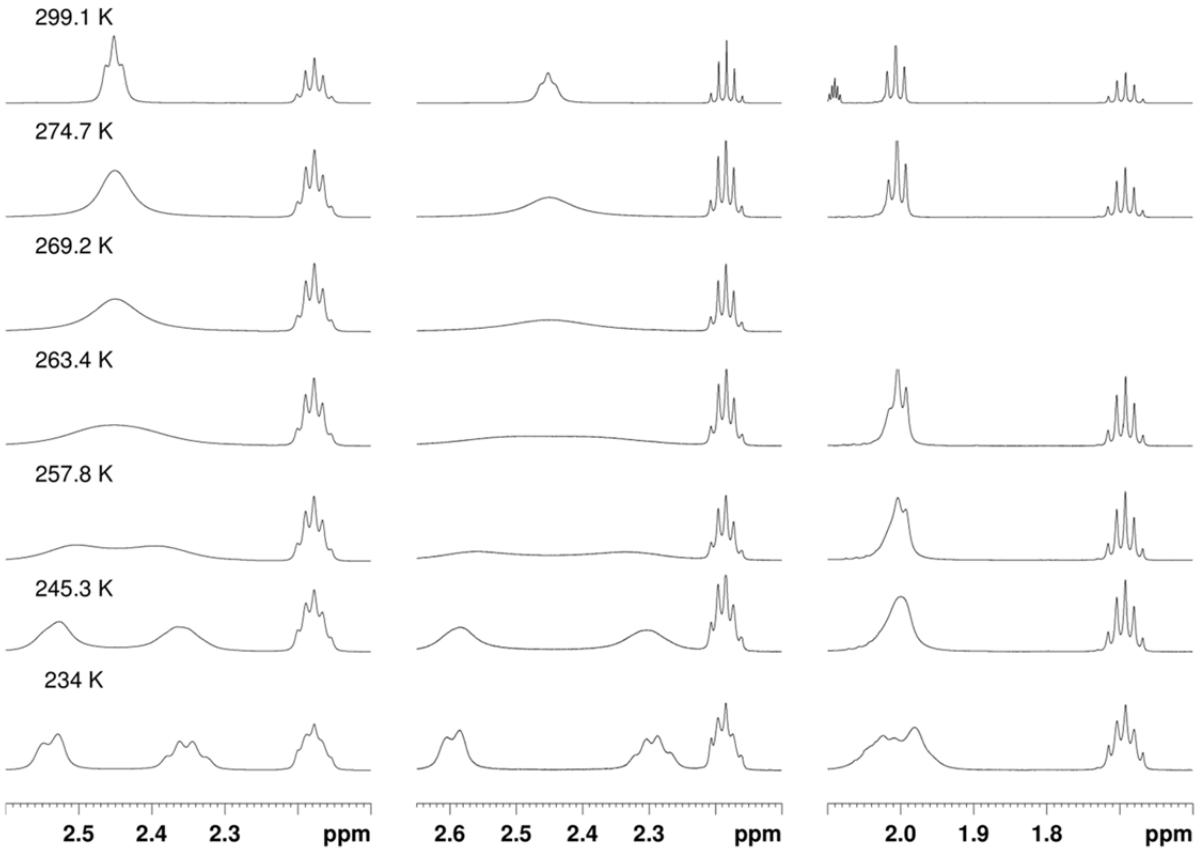

Figure 19. Solvent dependent NMR spectra of **D1e** at variable temperatures. *left*: $CDCl_3$; *middle*: MeOD-d4; *right*: toluene-d6. The coalescence of the signals is reached at completely different temperatures. The Gibbs free activation energy $\Delta G^{\ddagger}(T)$ remains constant because the changes in chemical shift differences compensates the changed coalescence temperature equation (3).[46]

Conclusion and Outlook

In conclusion it was possible to show that the rotation barriers of in 2,2' position propyl-bridged biphenyls are strongly dependent on the nature of the phenyl-phenyl bond and with it on the nature of substituents in *para* position to this bond. Atropisomerization processes were quantified by ^{1}H-NMR coalescence measurements and by correlation of the obtained free energies $\Delta G^{\ddagger}(T)$ to the Hammett-parameter σ_p, the resonance parameter R and the field effect

parameter F, allowed for identifying the π-electron density as the predominant factor which dictates the rotation barrier. This was further confirmed by DFT calculations, from which also a planar and almost linear single transition state was obtained. Solvent dependent ^{1}H-NMR coalescence measurements further documented the importance of the nature of the central C1-C1' bond to the atropisomerization process. Furthermore the calculated transition state showed that the length of the central phenyl-phenyl bond not only influences the energy needed for inversion but also dictates the distance between the *ortho* methylene groups of the propyl-bridge. It will now be of interest to substitute the biphenyl cyclophanes **D1a** – **D1l** in these positions to further hinder the atropisomerization without changing the electronic nature of the system or without changing the torsion angle. In addition it will be interesting to investigate the influence of the bridge length for which already preliminary results showed higher rotation barriers when elongated compared to the propyl-bridged systems.[35]

Thermodynamic Studies of 4 and 4' Substituted Torsion Angle Restricted 2,2' Butyl-Bridged Biphenyl Cyclophanes

Introduction

The investigations of **D1a** – **D1g** demonstrated that the energy needed for atropisomerization of diacceptor substituted biphenyl derivatives is higher compared to donor substituted derivatives. Nevertheless, the changes of the free energy are in the range of 10 kJ/mol and therefore rather small compared to the influence of modifications at the 6,6' position (approximately doubling of the inversion barrier).[34] In contrast previous studies on 2,2' alkyl-bridged push-pull systems have shown that the elongation of the bridge causes a significant change in the atropisomerization energy of about 40 kJ/mol (about 50 kJ/mol for the propyl-bridged derivative and about 90 kJ/mol for the butyl-bridged derivative).[35] Furthermore preliminary ^{1}H-NMR coalescence measurements of an in the benzylic positions tetramethylated dibenzo[*c*,*e*]oxepine derivative (figure 20) showed a rise of the free energy of the isomerization by approximately 20 kJ/mol.

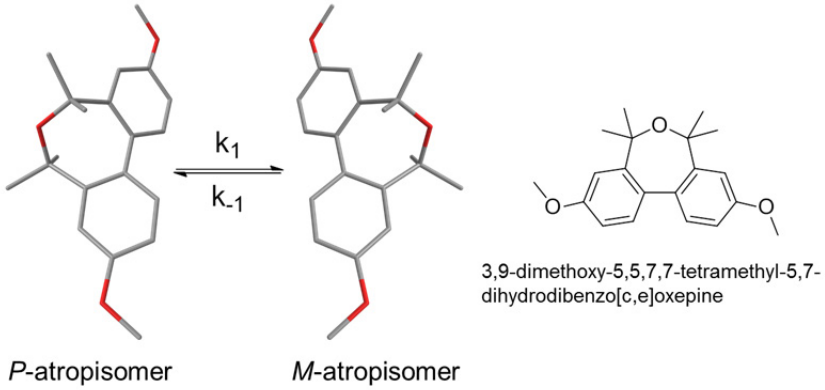

Figure 20. Schematic representation of the two atropisomers of dihydrodibenzo[*c*,*e*]oxepine.

To be able to separate two atropisomers, a rotation barrier around the central C-C bond of about 93 kJ/mol at 300 K is necessary.[65] As previously noted it is most promising to modify 2,2' butyl-bridged biphenyls to be able to achieve entirely conformationally fixed biphenyl derivatives. Such conformationally stable axial chiral biphenyl derivatives can then be further functionalized on the aromatic core to allow oligomerization or even polymerization in analogy to Vögtles Geländeroligomers (figure 21) but without formation of *meso* structures which are for optical applications inactive.[23] A successful synthesis of solely one conformationally stable, oligomeric atropisomer can be a significant contribution towards

molecules which can convert common light into circular polarized light en route to applications like POLEDs (polarized organic light emitting diodes).[66]

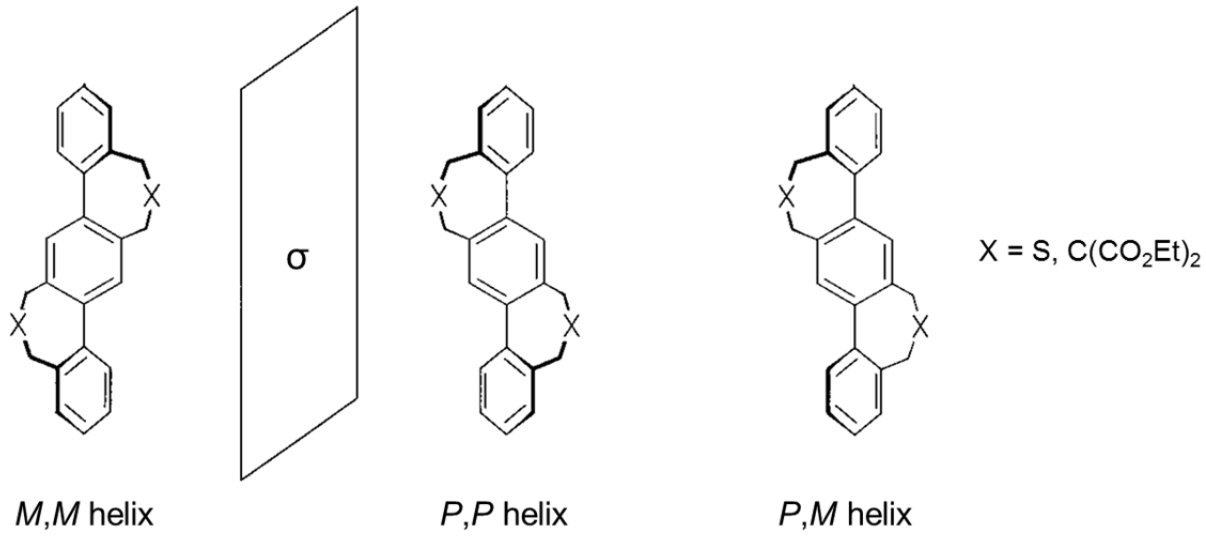

Figure 21. Geländeroligomers reported by Vögtle *et al*. The twisted terphenylophanes form three different conformers. (*M*,*M*) and (*P*,*P*) are atropisomers and (*P*,*M*) is the *meso* form. Reprinted from Kiupel *et al*.[23]

It was of interest to investigate the change of the rotation barrier in a series of in 4,4' donor or acceptor substituted 2,2' butyl-bridged biphenyl derivatives **D2a** – **D2f** (figure 22) in analogy to the studies on the propyl-bridged derivatives **D1a** – **D1l**. By comparison of the experimentally obtained free energies with theoretically calculated ones, an inversion mechanism can be calculated, which potentially allows conclusions about suitable positions for modifications on the alkyl-bridge. Furthermore it was of interest to see whether the elongation of the bridge significantly influences the structure of the transition state.

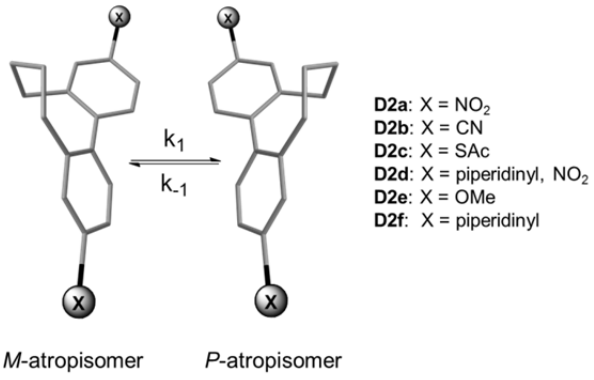

Figure 22. Series of studied 4,4' substituted torsion angle restricted, 2,2' butyl-bridged biphenyl cyclophanes **D2a** – **D2f**.

Materials and Methods

Synthesis

Compound **D2a** and **D2f** were synthesized according to the procedures used for the propyl-bridged derivatives **D1a** and **D1l** starting from the already available diamino derivative **D2g**.[8] The protocols feature an oxidation using a potassium iodide – *tert*-butyl hydroperoxide catalytic system[41] (scheme 2) and an azacycloalkylation with 1,5-dibromopentane in an aqueous sodiumdodecylsulfate solution and sodium hydrogen carbonate as a base, respectively.[8] Dicyano substituted derivative **D2b**,[4] *S*-acetyl substituted derivative **D2c**[3] and dimethoxy substituted biphenyl **D2d**[4] were available in our group from molecular electronic investigations. Compound **D2b** was synthesized by hetero cross-coupling of potassium cyanide and ditriflate derivative **D2h** using a Pd^0 catalyst ($Pd_2(dba)_3$) and Xanthphos as a ligand. Compound **D2c** was obtained by nucleophilic aromatic substitution of dibromobiphenyl **D2i** with sodium thiomethanolate to afford the free thiol which was *in situ* transprotected with acetyl chloride. The push-pull cyclophane **D2d** was available from nonlinear optic investigations (see Part C).[8]

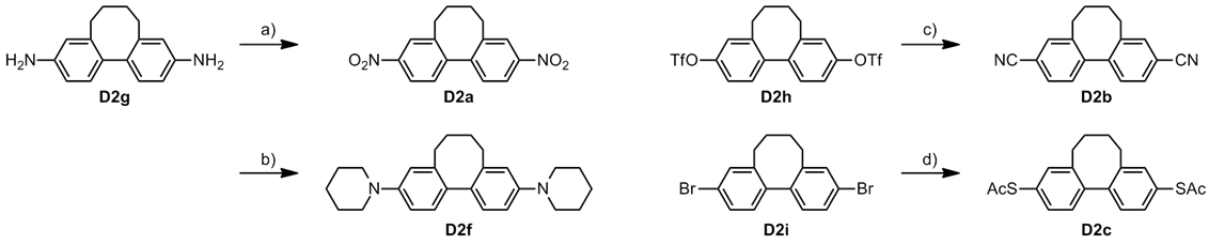

Scheme 2. Synthesis of the 2,2' butyl-bridged biphenyl cyclophanes **D2a** – **D2c** and **D2f**. a) KI (5 mol%), *tert*-butyl hydroperoxide, MeCN, 80°C, 18 h, 32%; b) 1,5-dibromopentane, SDS, $NaHCO_3$, water, 80°C, 2 h, 52%; c) $[Pd_2(dba)_3]\cdot CHCl_3$ (10.0 mol%), Xanthphos (10.0 mol%), tributyltin chloride (3.6 mol%), KCN, acetonitrile, reflux, 16 h, 86%; d) $NaSCH_3$, DMI, 110°C, 18 h, then AcCl, rt, 18 h, 32%.)

Dynamic HPLC

The free energies $\Delta G^{\ddagger}(T)$ of the atropisomerization processes of **D2a** – **D2f** were determined by temperature dependent dynamic HPLC measurements. Solutions of compound **D2a** – **D2f** of approximately 1 mg/mL in *i*PrOH were prepared. 3 µL of these solutions were injected into a chiral Chiralpak AD-H column (0.46 x 25 cm; Daicel Chemical Industries Ltd.) at the defined temperature (CTO-10AS VP oven from Shimadzu). The atropisomers were eluted with a mixture of 97:3 of *n*-hexane and *i*PrOH for **D2a**, **D2b** and **D2d** – **D2f** and *n*-hexane/*i*PrOH 95:5 for **D2c** (SCL-10A VP HPLC from Shimadzu) at a flow rate of

0.5 mL/min. To guarantee an efficient mixing of both solvents the eluent was prepared as a 94:6 or 90:10 mixture of *n*-hexane and *i*PrOH/*n*-hexane 1:1. For detection of the chromatogram an UV/Vis detector (SPD-M10A VP from Shimadzu) operating at the absorption maxima of the compound under investigation was used (λ_{max} = 254 nm). The column was preconditioned for 2 h under the conditions used for dynamic HPLC experiments before a set of temperature dependent measurements was performed. After each run the column was equilibrated for half an hour. The studies were performed at temperatures between 15°C and 35°C in 5°C steps. Two different samples of each compound were measured twice in the whole temperature range. The forward reaction rate constants k_1 were evaluated with the unified equation[67] valid for such first order processes by direct integration of the elution profiles to the software program DCXplorer[68]. The Gibbs free activation energy $\Delta G^{\ddagger}(T)$ was calculated by estimation of the activation enthalpy $\Delta H^{\ddagger}$ of the enantiomerization process from the slope of the *Eyring* plot (ln (k_1/T) vs. $1/T$) and the activation entropy $\Delta S^{\ddagger}$ from the intercept.

Theoretical Calculations

Geometries of equilibrium and transition states were optimized with density functional theory (DFT) using different functionals (BP86, TPSS, B3LYP) and basis sets (SV(P)=small basis, TZVP=large basis). The nature of the located stationary points was verified by calculations of force constants and vibrational frequencies (equilibrium state: all frequencies > 0, transition state: one imaginary frequency corresponding to the inversion of the phenyl rings).

Results

Several techniques to investigate conformational or constitutional molecular changes are known, which are ^{1}H-NMR coalescence measurements[69], dynamic HPLC[65,70], measurement of the H/D exchange rates by high resolution mass spectroscopy[71] or stopped flow chromatography[72]. ^{1}H-NMR coalescence measurement is a suitable tool to investigate structural interconversions in the lower kJ range, but has limitations like experimental temperature and exchange time scale. Thus dynamic HPLC turned out to be a powerful method to study slow interconversion processes.[73,74] Thanks to the pioneering work of Trapp and Schurig a computer based quantification of such isomerization processes is possible.[68,75] Typical peak profiles like peak broadening, plateau formation or peak coalescence are indicators for “on column” isomerization in dynamic chromatography.[76] These prerequisites allow for determination of the rate constants of the isomerization and therefore for the

determination of the interconversion energy barriers $\Delta G^{\ddagger}(T)$. In our studies on the racemization dynamics of torsion angle restricted biphenyl based push-pull cyclophanes no coalescence was observed for the butyl-bridged derivative **D2d** by ^{1}H-NMR within the instrumental temperature range.[35] Careful analysis of the ^{1}H-NMR spectra of compound **D2a** – **D2f** revealed that for all compounds of interest a slow exchange on the NMR time scale can be expected, because for each individual proton of the butyl-bridge an individual set of NMR signals was observed (figure 23).

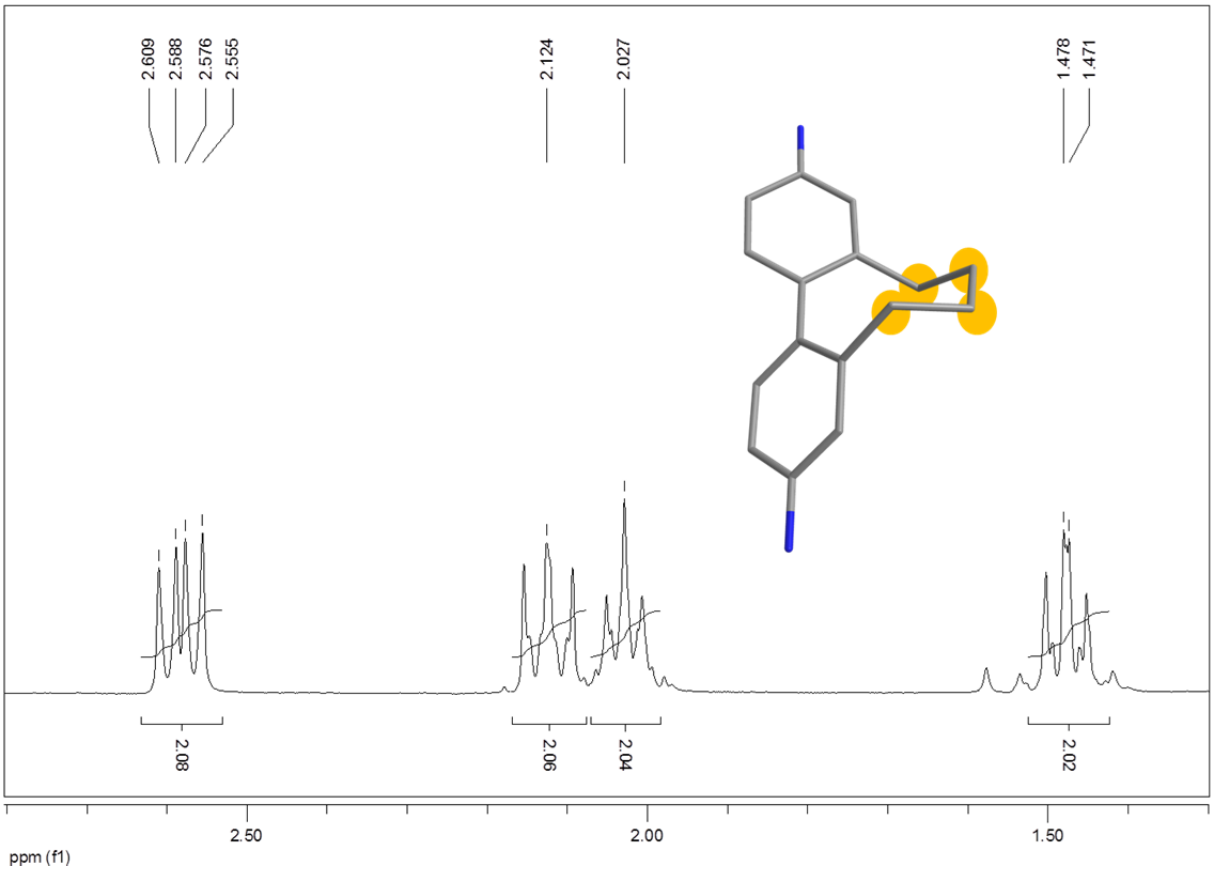

Figure 23. Proton signals of the butyl-bridge in the slow exchange regime.

Dynamic HPLC has proven to be an ideal method to estimate the rotation barrier around the central C-C bond of push-pull cyclophane **D2d**.[35] Hence, temperature dependent dynamic HPLC measurements were performed to evaluate the racemization process of these rotationally more hindered compounds **D2a** – **D2f**. The chromatography was performed on a coated chiral amylose derived Chiralpak AD-H column eluting with *i*PrOH/*n*-hexane mixtures of 97:3 for **D2a**, **D2b**, **D2d** – **D2f** and 95:5 for **D2c**. For all compounds temperature dependent plateau formation was observed ranging from nearly separated peaks (**D2b** and **D2c** at 15°C) and peak profiles close to coalescence (**D2f** at 35°C) (figure 24). Separation of less polar

derivatives like halogen substituted butyl-bridged biphenyls was not possible on a variety of differently coated columns.

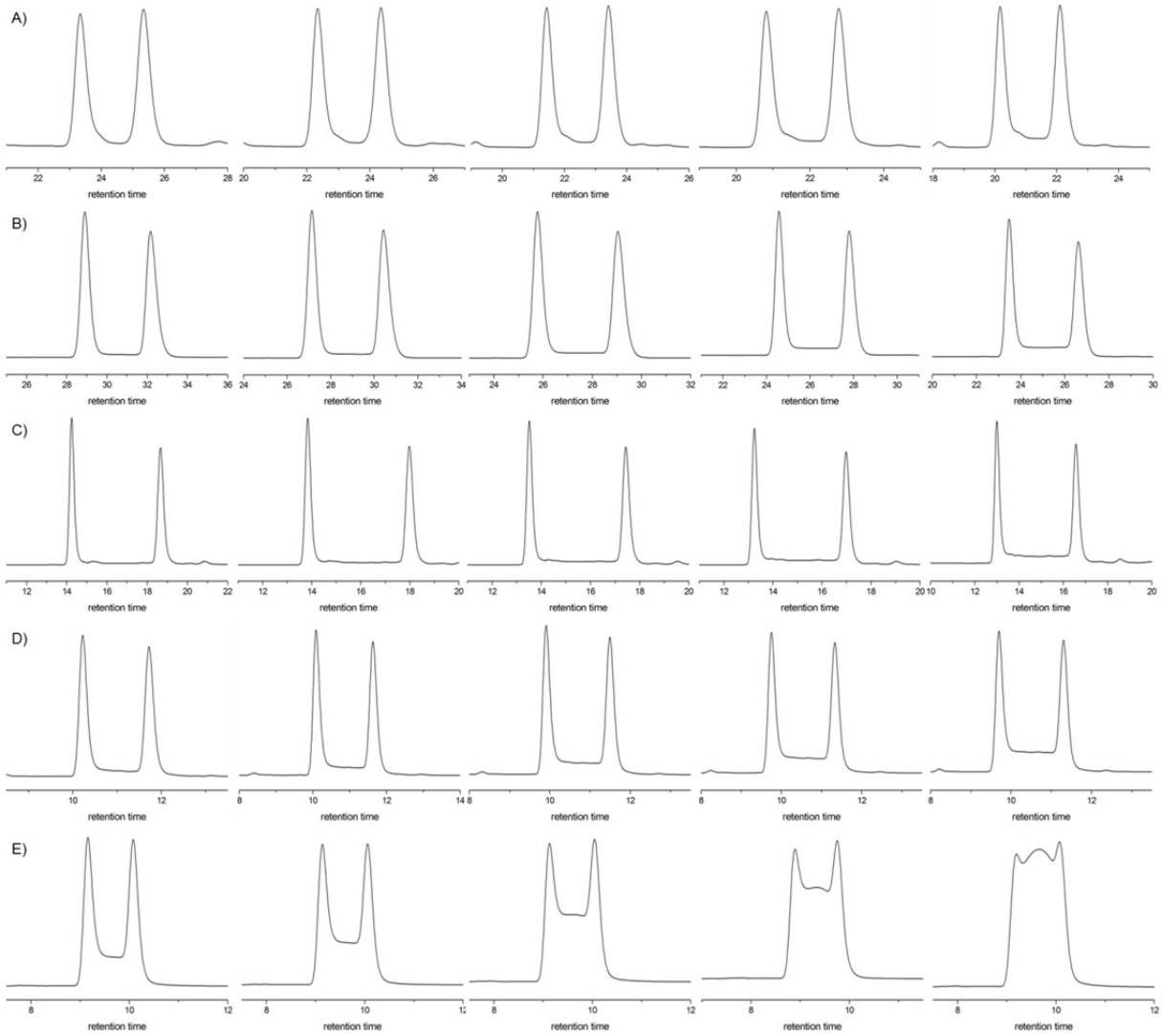

Figure 24. Elution profiles of compounds **D2a** – **D2f** on an amylose derived Chiralpak AD-H column between 15°C and 35°C in 5°C steps (left to the right). A) **D2a**, B) **D2b**, C) **D2c**, D) **D2e**, E) **D2f**.

The rate constants of atropisomerization were directly calculated by using the software DCXplorer (table 6). The software is based on the unified equation which was derived by Trapp from the theoretical plate model.[67,70] In the theoretical plate model the column is minicompartmentalized into small plates where each plate is considered as a chemical reactor.[73] Three consecutive processes occur during separation in each plate: 1.) establishment of the distribution equilibrium of the two stereoisomers between the mobile and the stationary phases in presence of the resolving sorbent, 2.) reversible first-order enantiomerization in the stationary phase, and 3.) shifting of the mobile phase to the next plate

(figure 25). The rate constant can therefore be directly related to the height of the formed plateau.[75]

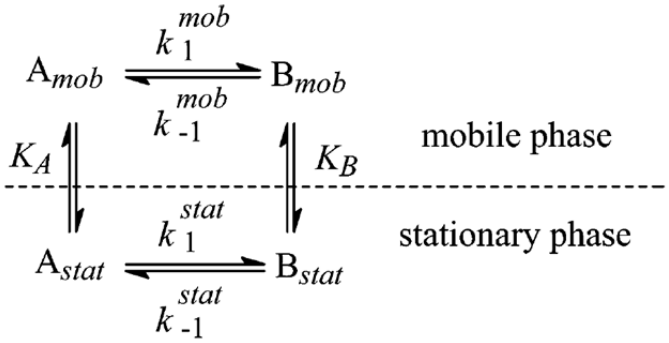

Figure 25. Equilibrium in a chromatographic theoretical plate model. A is the first eluted compound, B the second eluted one. k_1 and k_{-1} are the rate constants in the mobile and stationary phase of the forward and backward reaction, respectively. K denotes the distribution constant. Reprinted from Trapp.[67]

Table 6. Rate constants of the enantiomerization process between 15°C and 35°C in 5°C steps calculated with the DCXplorer software.

T / K	308	303	298	293	288
D2a k_1[a] / s^{-1}	$1.448 \cdot 10^{-4}$	$9.85 \cdot 10^{-5}$	$8.27 \cdot 10^{-5}$	$6.06 \cdot 10^{-5}$	$2.61 \cdot 10^{-5}$
D2b k_1[a] / s^{-1}	$1.658 \cdot 10^{-4}$	$1.194 \cdot 10^{-4}$	$9.00 \cdot 10^{-5}$	$5.74 \cdot 10^{-5}$	$3.86 \cdot 10^{-5}$
D2c k_1[a] / s^{-1}	$3.621 \cdot 10^{-4}$	$2.677 \cdot 10^{-4}$	$1.898 \cdot 10^{-4}$	$1.326 \cdot 10^{-4}$	$8.93 \cdot 10^{-5}$
D2d k_1[a] / s^{-1}			$9.25 \cdot 10^{-4}$	$6.44 \cdot 10^{-4}$	$4.21 \cdot 10^{-4}$
D2e k_1[a] / s^{-1}	$8.038 \cdot 10^{-4}$	$6.041 \cdot 10^{-4}$	$4{,}417 \cdot 10^{-4}$	$3.083 \cdot 10^{-4}$	$2.217 \cdot 10^{-4}$
D2f k_1[a] / s^{-1}	$2.254 \cdot 10^{-3}$	$1.810 \cdot 10^{-3}$	$1.297 \cdot 10^{-3}$	$9.090 \cdot 10^{-4}$	$6.887 \cdot 10^{-4}$

[a] averaged value of four repeated measurements

The theoretical plate model was improved to include the time-dependent probability density function and the division of the elution profile into Gaussian distribution functions of the non-interconverted species (stochastic model).[77] These two models led to the establishment of iterative methods to calculate the rate constants by comparison of experimentally obtained chromatograms with simulated ones.[75,78] By considering that the mass balance has to be fulfilled in these on-column processes it can be concluded that the distribution of enantiomer B, converted from enantiomer A, is proportional to a linear function where the starting amount A_0-A(t) decreases to 0 and vice versa. The division of the interconverted amount by the difference of the retention times results in the time dependent amount of interconverted enantiomer at the running time *t*. Therefore a unified equation can be derived where the rate constant is directly accessible from the retention times of the two enantiomers, the height of the plateau, the width of the enantiomer peaks at half height and the number of theoretical plates.[67] Furthermore the equation is independent on the initial amount of compound and thus less susceptible to errors.

The free energy of the atropisomerization process $\Delta G^{\ddagger}$(T) was calculated using the Eyring equation (1) by plotting ln(k_1/T) against the inverse temperature. The enthalpy $\Delta H^{\ddagger}$ is obtained from the slope and the entropy $\Delta S^{\ddagger}$ from the intercept of a linear regression analysis.

$$k_1 = (k_B T)/h \cdot \exp(-\Delta G^{\ddagger}/RT) \qquad (1)$$

The thermodynamic data is summarized in table 7.

Table 7. Thermodynamic data of the biphenyl systems **D2a** – **D2f** calculated from the kinetic data obtained by temperature dependent dynamic HPLC measurements.

	$\Delta G^{\ddagger}(T)$[a] / kJ·mol^{-1}	$\Delta H^{\ddagger}$[a] / kJ·mol^{-1}	$\Delta S^{\ddagger}$[a] / J·mol^{-1}·K^{-1}
D2a	96.75 ± 0.12	47.11 ± 6.2	-166 ± 21
D2b	96.29 ± 0.04	51.42 ± 0.8	-150 ± 3
D2c	94.31 ± 0.05	49.30 ± 1.2	-151 ± 4
D2d	90.3 ± 0.2	54.50 ± 4	-120 ± 14
D2e	92.22 ± 0.04	45.50 ± 0.4	-157 ± 2
D2f	89.52 ± 0.03	42.48 ± 0.4	-158 ± 2

[a] averaged value of four repeated measurements with absolute error.

To calculate the thermodynamic parameters of the atropisomerization process by density functional theory the ground state conformation was evaluated resulting in the same ground state geometries as obtained for the propyl-bridged derivatives **D1a** – **D1l** (figure 10). For the strong electron acceptor substituted biphenyls **D2a** and **D2b** only one ground state conformation was found where the substituents are placed linearly, essentially planar to the biphenyl. For the dimethoxy derivative **D2e** two ground state conformers are possible, depending on the spatial arrangement of the methyl in respect to the bridge. For **D2c** and **D2f** six conformers were found from which four are energetically favored namely when the carbonyl-oxygen points towards the biphenyl for **D2c** and when the piperidinyl is in a chair like conformation for **D2f**. According to these starting terms preliminary results about the height of the rotation barrier and the spatial arrangement of the relevant species in the reaction path were obtained based on DFT functionals BP86 and B3LYP using basis set SV(P). Two different energy barriers were found for all derivatives **D2a** – **D2f**. The first transition corresponds to the formation of a second biphenyl conformer, the second transition to the inversion process. The obtained rotation barriers are displayed in table 8.

Table 8. Atropisomerization energies of **D2a** – **D2f** calculated with DFT functionals BP86 and B3LYP. E_{TS1} corresponds to the preorganization of the butyl-bridge, E_{C2} to the energy of the second conformer resulting from the first transition and E_{TS2} corresponds to the rotation barrier of the inversion process.

	BP86/SV(P)			**B3LYP/SV(P)**		
X	E_{TS1} / kJmol^{-1}	E_{C2} / kJmol^{-1}	E_{TS2} / kJmol^{-1}	E_{TS1} / kJmol^{-1}	E_{C2} / kJmol^{-1}	E_{TS2} / kJmol^{-1}
D2a	32.41	14.42	97.75	33.62	16.26	104.15
D2b	32.40	14.44	96.11	33.60	16.27	102.71
D2c	32.32	14.31	95.04	33.50	16.13	101.77
D2e	32.56	14.42	92.83	33.76	16.12	99.24
D2f	32.72	13.80	88.28	33.83	15.62	96.03

Discussion

Already by comparing the rate constants it can be seen that the donor substituted biphenyl cyclophanes **D2e** and **D2f** rotate significantly faster than their diacceptor substituted analoga

D2a – **D2c**. Furthermore the push-pull case **D2d** seems to be an exception as the rate constants are higher than the rate constants of the dimethoxy substituted derivative **D2e**.

The measured free energies of the atropisomerization $\Delta G^{\ddagger}(T)$ range from 89 kJ/mol for the strongest donor substituted compound **D2f** to 97 kJ/mol for **D2a** comprising the strongest acceptor. The rotation barriers follow the same trend as in the propyl-bridged biphenyl series, where diacceptor substituted biphenyls displayed higher values than the donor substituted ones. In analogy to the propyl-bridged derivatives **D1a** – **D1l** the influence of varying the substituents is small compared to the influence of the bridge length. However, to get insight into the inversion process $\Delta G^{\ddagger}(T)$ was correlated to the strength of the donors and acceptors by plotting the free energy against the Hammett-parameters σ_p (figure 26). Thereby the influence of the alkyl-bridge was neglected as it remains constant throughout the entire series. The individual Hammett-parameters of each substituents in 4,4' position were summed up to include the contribution of both substituents.

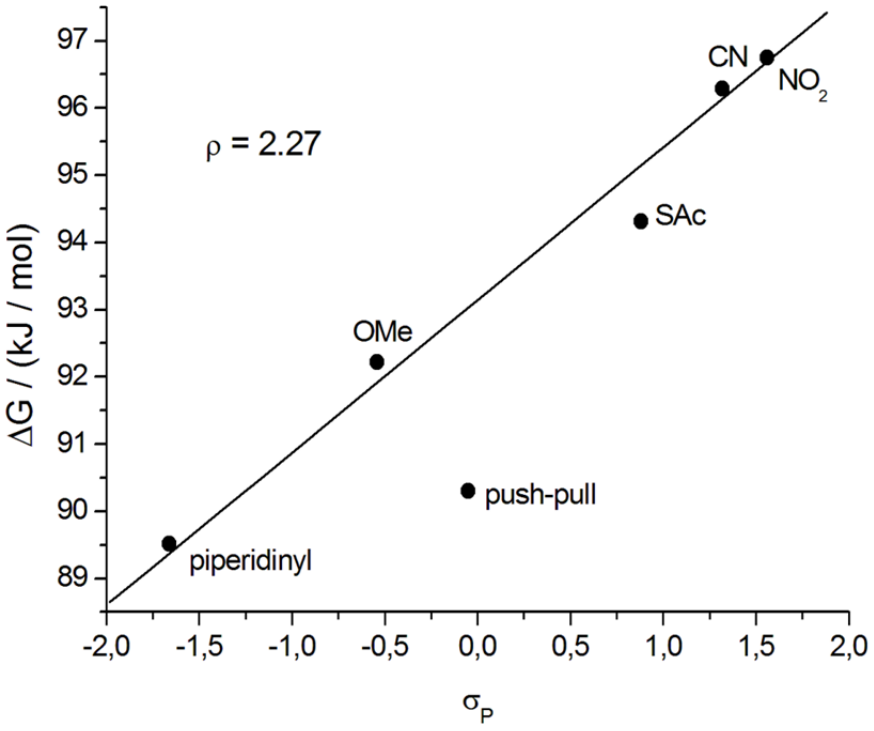

Figure 26. Hammett-correlation of the atropisomerization energies of butyl-bridged biphenyl cyclophanes **D2a** – **D2f**.

Similar to the propyl-bridged derivatives **D1a** – **D1l** a linear free energy relationship was obtained for **D2a** – **D2f** indicating the susceptibility of the whole inversion process to the electronic nature of the central C-C biphenyl bond. Furthermore, except of the push-pull cyclophane **D2d**, all values show no significant deviation from linearity again suggesting an

interconversion mechanism which is valid for the whole series. About the low $\Delta G^{\ddagger}(T)$ value of the push-pull system **D2d** it can only be speculated. Either a different inversion mechanism is present, the summation of the Hammett-parameters does not correctly represent the electronic influence of the different substituents in the push-pull case or the partial double bond character of the central C-C bond leads to a less crowded transition state. However, the sensitivity to electronic perturbations is less pronounced for **D2a** – **D2f** than in the shorter alkyl-bridged series **D1a** – **D1l** (ρ = 2.27 for **D2a** – **D2f** compared to ρ = 2.99) but still significant. Splitting of the Hammett-parameters σ_p into their fractions for influences on the π- and σ-systems (resonance and field effect) furthermore demonstrates the analogy of the inversion process to the propyl-bridged analoga (figure 27).

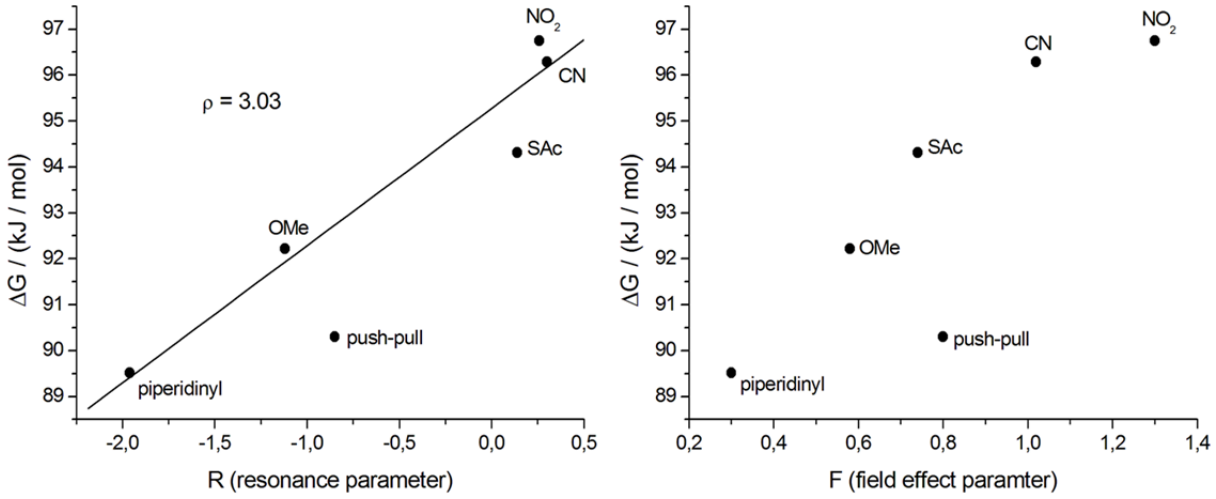

Figure 27. *left*: correlation of $\Delta G^{\ddagger}(T)$ with the resonance parameter R, *right*: correlation of $\Delta G^{\ddagger}(T)$ with the field effect parameter F. Compound **D2d** was excluded from linear regression.

Inspection of the correlation of $\Delta G^{\ddagger}(T)$ against the resonance parameter R according to Swain and Lupton[64] shows that in the case of **D2a** – **D2f** a good correlation (R^2 = 0.96) for the resonance part is obtained pointing to the influence of the substituents on the π-systems and therefore towards an electronically dominated inversion mechanism. Additionally the correlation against the field effect parameter F reveals a more pronounced correlation compared to **D1a** – **D1l** (R^2 = 0.84 compared to R^2 = 0.68), indicating a stronger distortion of the σ-skeleton in the transition state of the inversion process.

Analysis of the enthalpic ($\Delta H^{\ddagger}$) and entropic ($\Delta S^{\ddagger}$) contribution to the free energy $\Delta G^{\ddagger}(T)$ clearly demonstrates that the energy needed to access the transition state ($\Delta H^{\ddagger}$) is less distinct for **D2a** – **D2f** (table 6) than in the case of **D1a** – **D1l** where the entire process is dominated by this event. The significant contribution of vibrational, rotation and reorganization degrees

of freedom ($\Delta S^{\ddagger}$) to the free energy $\Delta G^{\ddagger}(T)$ reflects that either the molecular structure of the biphenyl has to be reorganized to access the transition state or that the binding to the stationary phase of the column during the separation process highly organizes the microcanonical ensemble. The latter is further supported by the strong negative $\Delta S^{\ddagger}$ values compared to the values of **D1a** – **D1l** and by the fact that the entropy is nearly constant for all compounds **D2a** – **D2f** and therefore independent on the electronic nature of the biphenyl system. In figure 28 the correlation of the enthalpy $\Delta H^{\ddagger}$ and the entropy $\Delta S^{\ddagger}$ to the Hammett-parameter σ_p is shown.

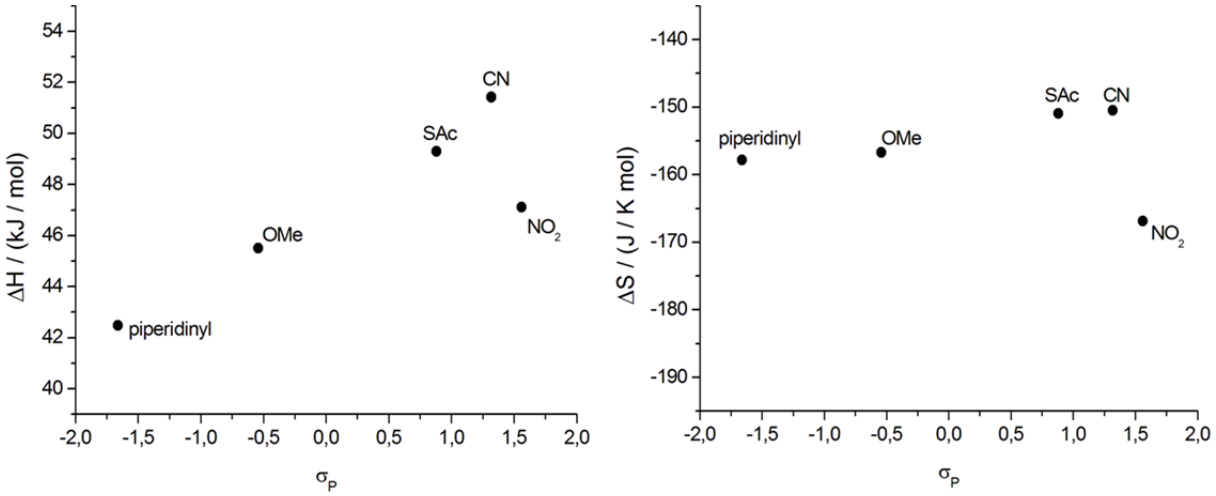

Figure 28. Hammett-correlations of $\Delta H^{\ddagger}$ (*left*) and $\Delta S^{\ddagger}$ (*right*).

The enthalpy correlation increases linearly from the strong donor piperidinyl **D2f** to the strong acceptor cyano **D2b** in contrast to the entropy which remains constant. Thus it can be concluded that the variations in the free energy $\Delta G^{\ddagger}(T)$ seem to arise solely from the activation energy. Similar to the propyl-bridged derivatives the rotation barrier is dictated exclusively by the electron density and the length of the central C-C bond. Due to the observed impurities in the case of **D2a** the deviating value is not representative.

Even though calculated free energies $\Delta G^{\ddagger}(T)$, enthalpies $\Delta H^{\ddagger}$ and entropies $\Delta S^{\ddagger}$ are not accessible, yet, the calculated activation energies of the individual transitions further support the conclusions obtained from the dynamic HPLC measurements. For all derivatives **D2a** – **D2f** a preorganization by spatial distortion of the butyl-bridge was found, leading to an energetically more unfavored conformer (**B** and **D**) which then can undergo atropisomerization (figure 29). This preorganization seems to be necessary to allow energetically reasonable rotation around the central biphenyl bond. A planar transition state (**C**) was calculated based on the experimentally obtained data. In contrast to the transition

state of the propyl-bridged derivatives **D1a** – **D1l** a larger deviation from linearity was observed, which is in good agreement with the observation that the influence of the substituents on the σ-skeleton is more pronounced for **D2a** – **D2f** (figure 29). The energies needed for the interconversion into the second conformer (**B** and **D**) remain more or less constant throughout the entire series **D2a** – **D2f**. Furthermore the energies of the second conformers deviate only marginally for the acceptor and donor substituted compounds **D2a** – **D2f** (figure 30). In contrast the energy of the rotation of the phenyls around the central biphenyl bond – the process with which one atropisomer is converted into the other – is strongly dependent on the electronic nature of the central bond and with that on the substituents (table 8) (figure 30). In accordance to the obtained correlations of $\Delta G^{\ddagger}$(T) and $\Delta H^{\ddagger}$ the rotation barrier is lower for the biphenyl cyclophanes substituted with strong donor (**D2e** and **D2f**) compared to the values for the acceptor substituted biphenyls **D2a** – **D2c**.

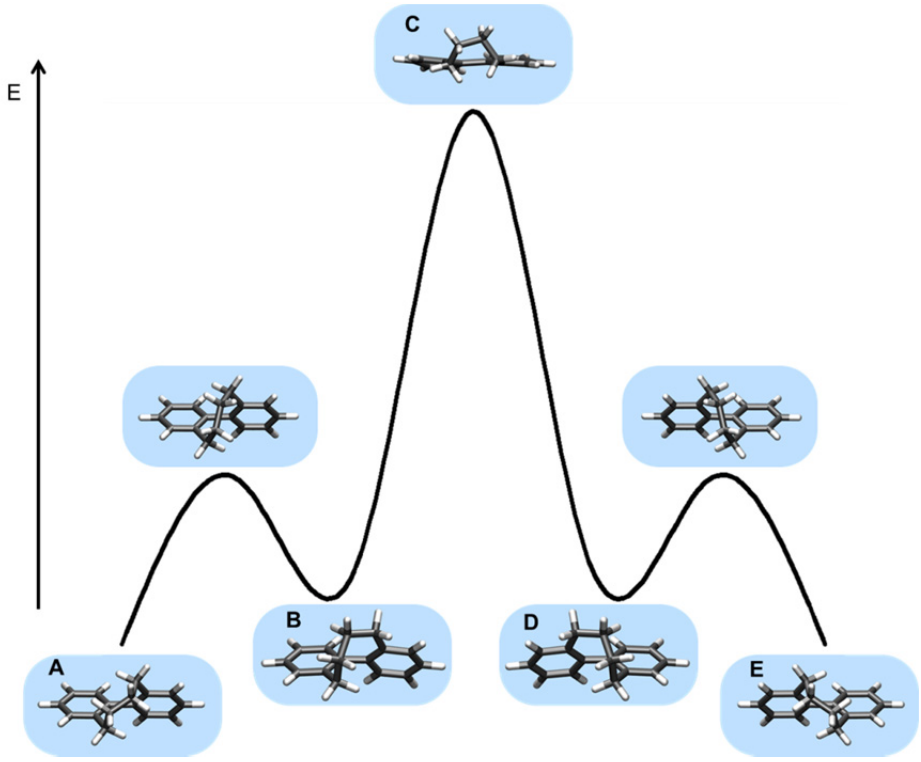

Figure 29. Schematic energy profile of the atropisomerization process of butyl-bridged biphenyl derivatives. The *M*-enantiomer (**A**) is interconverted into its second conformer (**B**) which is able to undergo isomerization by rotation of one phenyl. The *P*-enantiomer (**E**) is reached via the planar transition state (**C**).

The rotation barrier seems to be strongly dependent on the electronic nature of the central C-C bond, especially since the steric hindrance of the bridge is equal in the whole series. This finding is therefore in excellent agreement with the hypothetical conclusions drawn from the Hammett-correlations.

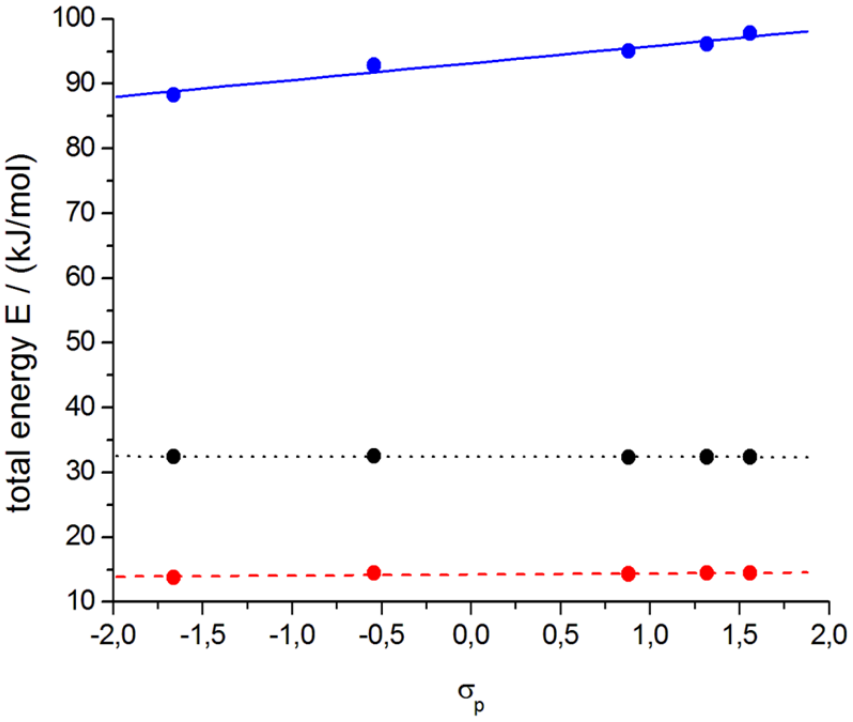

Figure 30. Correlation of the calculated energies against the donor and acceptor strength of the substituents in 4,4' position of the butyl-bridged biphenyl cyclophanes **D2a** – **D2f**. *black*: energies of the preorganization of the butyl-bridge; *red*: energies of the second conformer; *blue*: energies of the transition state of the atropisomerization process.

The calculated activation energies are in remarkable accordance, especially the ones calculated by the general gradient approximation functional BP86, to the measured free energy values $\Delta G^{\ddagger}$(T) (table 7 and 8). The energy values calculated by the hybrid functional B3LYP overestimate the measured ones, but display like the values calculated by the BP86 functional and the measured free energies the same trend with the lowest value for the strongest donor and the highest value for the strongest acceptor. This further supports the validity of the calculated underlying reaction mechanism (figure 29) which shows in contrast to the earlier postulated inversion mechanisms of out-of-plane bending and distortion of the individual phenyls itself a planar transition state. Furthermore, the fact that only the rotation process around the central C-C bond is susceptible to the electronic nature of the substituents is confirmed by the observed linear correlation of the measured free energy $\Delta G^{\ddagger}$(T) to the Hammett-parameters, since they are a measure for the ability of the substituents to withdraw or donate electrons from the reaction site. Interestingly, it seems like the calculated preorganization process is reflected in the improved correlation, compared to the propyl-bridged system, of the measured free energy to the field effect parameter and the significant larger contribution of the entropy to $\Delta G^{\ddagger}$(T). However, it has to be mentioned that the

influence of the chemical environment on the HPLC column cannot be disregarded. Therefore it will be of interest if the calculated entropic contribution to the inversion process is, similar to the propyl-bridged cyclophanes, constant and close to zero or according to the measured values strongly negative.

Conclusion

In summary, the atropisomerization energies $\Delta G^{\ddagger}(T)$ were estimated for a series of 4,4' donor and acceptor substituted 2,2' butyl-bridged biphenyl cyclophanes **D2a** – **D2f**. By a linear free energy relation the sensitivity of the racemization process to the electronic nature of the central biphenyl bond was shown. Furthermore splitting of the Hammett-parameters σ_p into their resonance R and field effect F part gave evidence that the substituents influence the electron density of the phenyl-phenyl bond via the π-system, indicating a planar transition state for racemization. These findings were further supported by preliminary theoretical calculations based on density functional theory leading to an atropisomerization mechanism valid for the entire series **D2a** – **D2f**. In contrast to the propyl-bridged derivatives **D1a** – **D1l** the inversion of the larger cyclophanes **D2a** – **D2f** proceeds via a preorganization of the butyl-bridge resulting in a second conformer which is able to undergo enantiomerization through a planar transition state. In addition, this transition state is in contrast to the propyl-bridged one stronger bent, which is in good agreement with the more pronounced correlation of $\Delta G^{\ddagger}(T)$ to the field effect parameter F. Furthermore only the rotation around the central C-C bond is susceptible to the donor or acceptor strength of the substituents, revealing that the enantiomerization process is dominated by the electronic nature of the central biphenyl bond and therefore by the distance between the two phenyl rings. The increased free energy values $\Delta G^{\ddagger}(T)$ compared to the propyl-bridged derivatives can be explained by a more crowded transition state in accordance to the conclusions drawn from our studies of the racemization dynamics of biphenyl based push-pull systems.[35] The calculated mechanism is in contradiction to the previously reported biphenyl atropisomerization mechanisms where an out-of-plane bending of the two phenyls or a distortion of the phenyls itself were postulated.[32–34] It will now be of interest to functionalize the alkyl-bridge by alkyl substituents to further increase the crowdedness of a possible transition state and therefore completely prevent rotation around the central C-C bond.

Experimental Part

3,9-Dinitro-6,7-dihydro-5H-dibenzo[*a*,*c*][7]annulene (D1a): Diamine **D1k** (133 mg, 0.590 mmol, 1.00 equiv.) and KI (4.97 mg, 30.0 µmol, 5 mol%) were dissolved in 2 ml acetonitrile. To this solution 70% aq. TBHP (0.620 ml, 4.50 mmol, 7.60 equiv.) was added dropwise at 0°C. The black solution was stirred at 80°C overnight. After cooling the reaction mixture to rt, it was quenched with $Na_2S_2O_3$, washed with brine, extracted with ethyl acetate (3 x 20 ml) and dried with $MgSO_4$. The solvent was removed *in vacuo* and the residual crude was purified by column chromatography (SiO_2; cylohexane:CH_2Cl_2; 5:1, 1% MeOH) yielding **D1a** as a white solid (31.5%)

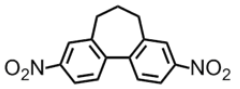

***R*$_f$** = 0. 0.71 (SiO_2; cyclohexane:CH_2Cl_2 5:1, 1% MeOH); **^{1}H-NMR** (400 MHz, $CDCl_3$): δ = 8.25 (dd, ^3J(H,H) = 8.4 Hz, ^4J(H,H) = 2.3 Hz, 2H, Ar-H), 8.18 (d, ^4J(H,H) = 2.3 Hz, 2H, Ar-H), 7.57 (d, ^3J(H,H) = 8.4 Hz, 2H, Ar-H), 2.62 (br. s, 4H), 2.32 (q, ^3J(H,H) = 7.0 Hz, 2H) ppm; **^{13}C-NMR** (400 MHz, $CDCl_3$): δ = 148.1 (C_q, 2C), 145.6 (C_q, 2C), 141.3 (C_q, 2C), 129.5 (C_t, 2C), 123.9 (C_t, 2C), 122.3 (C_t, 2C), 32.7 (C_s, 2C), 31.2 (C_s, 1C); **MS** (EI +, 70 eV): m/z (%) = 284 (100), 267 (3), 237 (9), 191 (32), 165 (16), 152 (8); **elemental analysis** calcd (%) for $C_{15}H_{12}N_2O_4$: C 63.38, H 4.25, N 9.85; found: C 63.94, H 4.64, N 9.76.

3,9-Di(piperidin-1-yl)-6,7-dihydro-5H-dibenzo[a,c][7]annulene (D1l): Diamine **D1k** (177 mg, 0.789 mmol, 1.00 equiv.) was suspended in 3 ml water. To this suspension was added SDS (4.55 mg, 20.0 µmol, 2 mol%), $NaHCO_3$ (292 mg, 3.47 mmol, 4.40 equiv.) and 1,5-dibromopentane (798 mg, 3.47 mmol, 4.40 equiv.). The reaction mixture was then heated at 80°C for 2 h. After cooling to room temperature, 1 M NaOH was added to the mixture and extracted with 3 x 50 ml dichloromethane. The combined organic layers were dried with $MgSO_4$ and filtered. The solvent was removed under reduced pressure. Purification by column chromatography (SiO_2; cyclohexane:EtOAc; 3:1, 5% NEt_3) yielded **D1l** as white solid (52%). For further analysis the product was recrystallized from pure ethyl acetate.

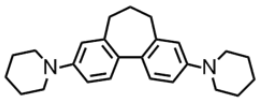

***R*$_f$** = 0.89 (SiO_2; cyclohexane:ethyl acetate 3:1, 5% NEt_3); **^{1}H-NMR** (400 MHz, $CDCl_3$): δ = 7.22 (d, ^3J(H,H) = 8.3 Hz, 2H, Ar-H), 6.87 (dd, ^3J(H,H) = 8.3 Hz, ^4J(H,H) = 2.5 Hz, 2H, Ar-H), 6.82 (d, ^4J(H,H) = 2.4 Hz, 2H, Ar-H), 3.20-3.18 (m, 8H), 2.46 (t, ^3J(H,H) = 7.0 Hz, 4H), 2.14 (q, ^3J(H,H) = 7.0 Hz, 2H), 1.76-1.70 (m, 8H), 1.61-1.56 (m, 4H); **^{13}C-NMR** (101 MHz, $CDCl_3$): δ = 151.1 (C_q, 2C), 140.2 (C_q, 2C), 132.3 (C_q, 2C), 128.5 (C_t, 2C), 116.7 (C_t, 2C), 114.24 (C_t, 2C), 50.8 (C_s, 2C), 33.1 (C_s, 2C), 32.2 (C_s, 1C), 26.0 (C_s, 2C), 24.4 (C_s,

2C); **MS** (ESI, positive ion mode, MeCN): m/z = 360 ([M^+]), 303, 180; **elemental analysis** calcd (%) for C25H32N2: C 83.28, H 8.95, N 7.77; found: C 83.37, H 9.24, N 7.71.

3,9-Difluoro-6,7-dihydro-5H-dibenzo[*a*,*c*][7]annulene (D1g):[42] To a suspension of

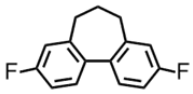

diamine **D1k** (110 mg, 1.00 equiv., 0.490 mmol) in 20 mL 48% tetrafluoroboric acid sodium nitrite (71.0 mg, 2.10 equiv., 1.03 mmol) dissolved in 4 mL H_2O was added dropwise at 0°C. 20 mL dichloromethane was added to completely dissolve the starting materials. After stirring at 0°C for 10 min the brown reaction mixture was irradiated with a mercury vapor lamp at 0°C overnight. Then 40% aqueous NaOH was added at 0°C for neutralization. The mixture was extracted three times with ethyl acetate. The combined organic layers where washed once with brine and dried with $MgSO_4$. After evaporation of the solvent, the crude was purified by column chromatography (SiO_2; cyclohexane) to achieve 100 mg (88%) of **D1g** as a white solid. For further analysis difluoride **D1g** was recrystallized from a mixture of methanol and water (25:1).

$\boldsymbol{R_f}$ = 0.49 (SiO_2; cyclohexane); **^{1}H-NMR** (400 MHz, $CDCl_3$): δ = 7.28 (dd, ^3J(H,H) = 8.4 Hz, ^4J(H,F) = 5.7 Hz, 2H, Ar-H), 7.01 (td, ^3J(H,H) = 8.5 Hz, ^3J(H,F) = 2.7 Hz, 2H, Ar-H), 6.95 (dd, ^3J(H,H) = 9.3 Hz, ^3J(H,F) = 2.7 Hz, 2H, Ar-H), 2.46 (t, ^3J(H,H) = 7.1 Hz, 4H), 2.17 (q, ^3J(H,H) = 7.1 Hz, 2H) ppm; **^{13}C-NMR** (101 MHz, $CDCl_3$): δ = 162.3 (d, ^1J(C,F) = 245.9 Hz, C_q, 2C), 141.7 (d, ^3J(C,F) = 7.4 Hz, C_q, 2C), 136.2 (d, ^4J(C,F) = 3.1 Hz, C_q, 2C), 129.8 (d, ^3J(C,F) = 8.3 Hz, C_t, 2C), 115.4 (d, ^2J(C,F) = 21.1 Hz, C_t, 2C), 113.4 (d, ^2J(C,F) = 21.2 Hz, C_t, 2C), 32.9 (C_s, 2C), 31.5 (C_s, 1C) ppm; **MS** (EI +, 70 eV): m/z (%) = 230.1 (100), 215.1 (41), 201.0 (24), 195.1 (12), 183.1 (6); **elemental analysis** calcd (%) for $C_{15}H_{12}F_2$: C 78.24, H 5.25; found: C 77.86, H 5.57.

6,7-Dihydro-5H-dibenzo[*a*,*c*][7]annulene (D1h): The dibromide **D1e** (50.0 mg, 1.00 equiv.,

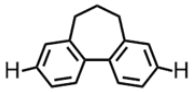

0.142 mmol) was dissolved in 2 mL THF (abs., crown-cap) under argon atmosphere and cooled to -78°C. Then *t*BuLi (0.373 mL, 246 mg, 4.20 equiv., 0.596 mmol) was added dropwise. The reaction mixture (green) was stirred at the elevated temperature for 1.5 h. Then 2 mL sat. aq. ammonium chloride solution was added and after stirring for 30 min at rt the phases were separated. The aqueous one was extracted twice with cyclohexane. The combined organic layers were washed with brine, dried with sodium sulfate, filtered and concentrated. The crude was purified by column chromatography (SiO_2; cyclohexane). According to the described procedure the desired target compound was obtained as a colorless liquid.

R_f = 0.41 (SiO_2; cyclohexane); **^{1}H-NMR** (400 MHz, $CDCl_3$): δ = 7.39 (dd, ^3J(H,H) = 7.2 Hz, ^4J(H,H) = 1.6 Hz, 2H, Ar-H), 7.35 (dt, ^3J(H,H) = 7.2 Hz, ^4J(H,H) = 1.6 Hz, 2H, Ar-H), 7.30 (dt, ^3J(H,H) = 7.2 Hz, ^4J(H,H) = 1.6 Hz, 2H, Ar-H), 7.25 (dd, ^3J(H,H) = 7.2 Hz, ^4J(H,H) = 1.6 Hz, 2H, Ar-H), 2.51 (t, ^3J(H,H) = 6.8 Hz, 4H), 2.20 (quint, ^3J(H,H) = 7.2 Hz, 2H) ppm. The analytic data is according to literature.[34]

3,10-Dinitro-5,6,7,8-tetrahydrodibenzo[*a*,*c*][8]annulene (D2a): The 4,4' dinitro substituted butyl-bridged biphenyl derivative **D2a** was synthesized according to the procedure used to synthesize the propyl-bridged derivative **D1a** (32%).

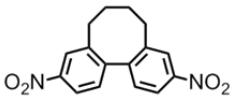

R_f = 0.75 (SiO_2; cylohexane:CH_2Cl_2 5:1, 1% MeOH); **^{1}H-NMR** (400 MHz, $CDCl_3$): δ = 8.20 (d, ^4J(H,H) = 2.4 Hz, 2H, Ar-H), 8.14 (dd, ^3J(H,H) = 8.4 Hz, ^4J(H,H) = 2.4 Hz, 2H, Ar-H), 7.41 (d, ^3J(H,H) = 8.4 Hz, 2H, Ar-H), 2.94 – 2.85 (m, 2H), 2.24 – 2.10 (m, 4H), 1.65 – 1.51 (m, 2H) ppm; **^{13}C-NMR** (400 MHz, $CDCl_3$): δ = 151.7 (C_q, 2C), 143.5 (C_q, 2C), 132.1 (C_q, 2C), 129.8 (C_t, 2C), 117.1 (C_t, 2C), 113.9 (C_t, 2C), 33.5 (C_s, 2C), 29.8 (C_s, 2C) ppm.

3,10-di(piperidin-1-yl)-5,6,7,8-tetrahydrodibenzo[*a*,*c*][8]annulene (D2f): The 4,4' dipiperidinyl substituted butyl-bridged biphenyl derivative **D2f** was synthesized according to the procedure used to synthesize the propyl-bridged derivative **D1l** (48%).

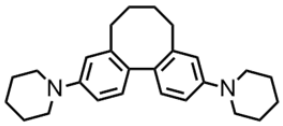

R_f = 0.89 (SiO_2; c;clohexane:EtOAc 3:1, 5% NEt_3); **^{1}H-NMR** (400 MHz, $CDCl_3$): δ = 7.12 (d, ^3J(H,H) = 8.0 Hz, 2H, Ar-H), 6.92 – 6.79 (m, 4H, Ar-H), 3.20 (t, ^3J(H,H) = 5.6 Hz, 8H), 2.66 (d, ^3J(H,H) = 8.4 Hz, 1H), 2.62 (d, ^3J(H,H) = 8.4 Hz, 1H), 2.19 – 2.10 (m, 2H), 2.08 – 1.99 (m, 2H), 1.84 – 1.70 (m, 8H), 1.64 – 1.55 (m, 4H), 1.55 – 1.47 (m, 2H) ppm.

Literature

[1] L. Venkataraman, J. E. Klare, C. Nuckolls, M. S. Hybertsen, M. L. Steigerwald, *Nature* **2006**, *442*, 904–907.

[2] J. Wang, G. Cooper, D. Tulumello, A. P. Hitchcock, *J. Phys. Chem. A* **2005**, *109*, 10886–10896.

[3] D. Vonlanthen, A. Mishchenko, M. Elbing, M. Neuburger, T. Wandlowski, M. Mayor, *Angew. Chem.* **2009**, *48*, 8886–8890.

[4] D. Vonlanthen, A. Rudnev, A. Mishchenko, A. Käslin, J. Rotzler, M. Neuburger, T. Wandlowski, M. Mayor, *Chem. Eur. J.* **2011**, *17*, 7236–7250.

[5] R. P. Thummel, F. Lefoulon, R. Mahadevan, *J. Org. Chem.* **1985**, *50*, 3824–3828.

[6] N. Berton, F. Lemasson, J. Tittmann, N. Stürzl, F. Hennrich, M. M. Kappes, M. Mayor, *Chem. Mater.* **2011**, *23*, 2237–2249.

[7] W.-Y. Wong, C.-L. Ho, *J. Mater. Chem.* **2009**, *19*, 4457.

[8] J. Rotzler, D. Vonlanthen, A. Barsella, A. Boeglin, A. Fort, M. Mayor, *Eur. J. Org. Chem.* **2010**, *6*, 1096–1110.

[9] C. Tepper, G. Haberhauer, *Chem. Eur. J.* **2011**, *17*, 8060–8065.

[10] D. Kuang, S. Ito, B. Wenger, C. Klein, J.-E. Moser, R. Humphry-Baker, S. M. Zakeeruddin, M. Grätzel, *J. Am. Chem. Soc.* **2006**, *128*, 4146–4154.

[11] C. Giansante, P. Ceroni, V. Balzani, F. Vögtle, *Angew. Chem.* **2008**, *47*, 5422–5425.

[12] H. Langhals, A. Hofer, S. Bernhard, J. S. Siegel, P. Mayer, *J. Am. Chem. Soc.* **2011**, *76*, 990–992.

[13] N. Sakai, R. Bhosale, D. Emery, J. Mareda, S. Matile, *J. Am. Chem. Soc.* **2010**, *132*, 6923–6925.

[14] E. R. Strieter, D. G. Blackmond, S. L. Buchwald, *J. Am. Chem. Soc.* **2003**, *125*, 13978–13980.

[15] S. Lee, M. Jørgensen, J. F. Hartwig, *Org. Lett.* **2001**, *3*, 2729–2732.

[16] J. J. Becker, P. S. White, M. R. Gagné, *J. Am. Chem. Soc.* **2001**, *123*, 9478–9479.

[17] K. Mikami, T. Korenaga, M. Terada, T. Ohkuma, T. Pham, R. Noyori, *Angew. Chem. Int. Ed.* **1999**, *38*, 495–497.

[18] L. Cui, B. Liu, D. Vonlanthen, M. Mayor, Y. Fu, J.-F. Li, T. Wandlowski, *J. Am. Chem. Soc.* **2011**, *133*, 7332–7335.

[19] X. Wang, M. R. Andersson, M. E. Thompson, O. Inganäs, *Thin Solid Films* **2004**, *468*, 226–233.

[20] Y. Tamaki, K. Watanabe, K. Koike, H. Inoue, T. Morimoto, O. Ishitani, *Faraday Discuss.* **2012**, *155*, 115–127.

[21] K. Mislow, M. A. W. Glass, R. E. O'Brien, P. Rutkin, D. H. Steinberg, J. Weiss, C. Djerassi, *J. Am. Chem.Soc.* **1962**, *84*, 1455–1478.

[22] A. Boeglin, A. Barsella, H. Chaumeil, E. Ay, J. Rotzler, M. Mayor, A. Fort, San Diego, California, USA, **2010**, S. 777408–777410.

[23] B. Kiupel, C. Niederalt, M. Nieger, S. Grimme, F. Vögtle, *Angew. Chem.* **1998**, *110*, 3206–3209.

[24] J. L. Gustafson, D. Lim, S. J. Miller, *Science* **2010**, *328*, 1251 –1255.

[25] J. Hassan, M. Sévignon, C. Gozzi, E. Schulz, M. Lemaire, *Chem. Rev.* **2002**, *102*, 1359–1470.

[26] G. Bringmann, A. J. Price Mortimer, P. A. Keller, M. J. Gresser, J. Garner, M. Breuning, *Angew. Chem. Int. Ed.* **2005**, *44*, 5384–5427.

[27] G. Bringmann, M. Breuning, R.-M. Pfeifer, W. A. Schenk, K. Kamikawa, M. Uemura, *J. Organomet. Chem.* **2002**, *661*, 31–47.

[28] K. Kamikawa, M. Uemura, *Synlett* **2000**, 938–949.

[29] P. Lloyd-Williams, E. Giralt, *Chem. Soc. Rev.* **2001**, *30*, 145–157.

[30] K. Ohkata, R. L. Paquette, L. A. Paquette, *J. Am. Chem. Soc.* **1979**, *101*, 6687–6693.

[31] R. B. Bates, F. A. Camou, V. Kane, P. K. Mishra, K. Suvannachut, J. J. White, *J. Org. Chem.* **1989**, *54*, 311–317.

[32] M. Oki, H. Iwamura, G. Yamamoto, *Bull. Chem. Soc. Jpn.* **1971**, *44*, 262–265.

[33] M. Oki, G. Yamamoto, *Bull. Chem. Soc. Jpn.* **1971**, *44*, 266–270.

[34] K. Müllen, W. Heinz, F. Klärner, W. R. Roth, I. Kindermann, O. Adamczak, M. Wette, J. Lex, *Chem. Ber.* **1990**, *123*, 2349–2371.

[35] J. Rotzler, H. Gsellinger, M. Neuburger, D. Vonlanthen, D. Häussinger, M. Mayor, *Org. Biomol. Chem.* **2011**, *9*, 86.

[36] L. Meca, D. Řeha, Z. Havlas, *J. Org. Chem.* **2003**, *68*, 5677–5680.

[37] C. C. K. Ling, M. M. Harris, *J. Chem. Soc.* **1964**, 1825–1835.

[38] A. C. T. Van Duin, B. Hollanders, R. A. Smits, J. M. A. Baas, B. Van de Graaf, M. P. Koopmans, J. S. S. Damste, J. W. De Leeuw, *Org. Geochem.* **1996**, *24*, 587–591.

[39] G. Bringmann, H. Busse, U. Dauer, S. Güssregen, M. Stahl, *Tetrahedron* **1995**, *51*, 3149–3158.

[40] M. Irie, K. Yoshida, K. Hayashi, *J. Phys.Chem.* **1977**, *81*, 969–972.

[41] K. R. Reddy, C. U. Maheswari, M. Venkateshwar, M. L. Kantam, *Adv. Synth. Catal.* **2009**, *351*, 93–96.

[42] B. Dolensky, *J. Fluorine Chem.* **2001**, *107*, 147.

[43] X.-Z. Shu, Y.-F. Yang, X.-F. Xia, K.-G. Ji, X.-Y. Liu, Y.-M. Liang, *Org. Biomol. Chem.* **2010**, *8*, 4077.

[44] D. Vonlanthen, J. Rotzler, M. Neuburger, M. Mayor, *Eur. J. Org. Chem.* **2009**, 120–133.

[45] S. Berger, S. Braun, *200 and More NMR Experiments: A Practical Course*, Wiley-vch Verlag Gmbh & Co. Kgaa, **2004**.

[46] M. Hesse, H. Meier, B. Zeeh, *Spektroskopische Methoden in der organischen Chemie*, Thieme, Stuttgart, **2005**.

[47] H. Friebolin, *Ein- und zweidimensionale NMR-Spektroskopie*, Wiley-vch, **1999**.

[48] M. Oki, *Applications of Dynamic Nmr Spectroscopy to Organic Chemistry*, Vch Pub, **1985**.

[49] *Program Package for ab initio Electronic Structure Calculations. TURBOMOLE, Version 6.3; a development of University of Karlsruhe and Forschungszentrum Karlsruhe GmbH 1989−2007, Turbomole GmbH since 2007, http://www.turbomole.com.*

[50] S. H. Vosko, L. Wilk, M. Nusair, *Can. J. Phys.* **1980**, *58*, 1200–1211.

[51] J. P. Perdew, *Phys. Rev. B* **1986**, *33*, 8822–8824.

[52] A. Becke, *Phys. Rev. A* **1988**, *38*, 3098.

[53] J. Tao, J. P. Perdew, V. N. Staroverov, G. E. Scuseria, *Phys. Rev. Lett.* **2003**, *91*, 146401.

[54] A. D. Becke, *J. Chem. Phys.* **1993**, *98*, 5648–5652.

[55] F. Weigend, R. Ahlrichs, *Phys. Chem. Chem. Phys.*, *7*, 3297–3305.

[56] O. Treutler, R. Ahlrichs, *J. Chem. Phys.* **1995**, *102*, 346–354.

[57] A. P. Scott, L. Radom, *J. Phys. Chem.* **1996**, *100*, 16502–16513.

[58] K. Marjani, *Spectrochim. Acta A* **2011**, *79*, 1798.

[59] S. Toyota, *Bull. Chem. Soc. Jpn.* **2000**, *73*, 2591.

[60] H. H. Jaffé, *Chem. Rev.* **1953**, *53*, 191–261.

[61] C. Hansch, A. Leo, R. W. Taft, *Chem. Rev.* **1991**, *91*, 165–195.

[62] H. Hart, E. A. Sedor, *J. Am. Chem. Soc.* **1967**, *89*, 2342–2347.

[63] F. Kita, W. Adam, P. Jordan, W. M. Nau, J. Wirz, *J. Am. Chem. Soc.* **1999**, *121*, 9265–9275.

[64] C. G. Swain, E. C. Lupton, *J. Am. Chem. Soc.* **1968**, *90*, 4328–4337.

[65] C. Wolf, *Chem. Soc. Rev.* **2005**, *34*, 595.

[66] S. M. Jeong, Y. Ohtsuka, N. Y. Ha, Y. Takanishi, K. Ishikawa, H. Takezoe, S. Nishimura, G. Suzaki, *Appl. Phys. Lett.* **2007**, *90*, 211106–211113.

[67] O. Trapp, *Anal. Chem.* **2006**, *78*, 189–198.

[68] O. Trapp, *J. Chromatogr. B* **2008**, *875*, 42–47.

[69] G. Binsch, H. Kessler, *Angew. Chem., Int. Ed. Engl.* **1980**, *19*, 411–428.

[70] O. Trapp, *Chirality* **2006**, *18*, 489–497.

[71] L. S. Busenlehner, R. N. Armstrong, *Arch. Biochem. Biophys.* **2005**, *433*, 34–46.

[72] G. Weseloh, C. Wolf, W. A. König, *Angew. Chem., Int. Ed. Engl.* **1995**, *34*, 1635–1636.

[73] W. Burkle, H. Karfunkel, V. Schurig, *J. Chromatogr. B* **1984**, *288*, 1–14.

[74] O. Trapp, L. Sahraoui, W. Hofstadt, W. Könen, *Chirality* **2010**, *22*, 284–291.

[75] O. Trapp, V. Schurig, *Computers & Chemistry* **2001**, *25*, 187–195.

[76] V. Schurig, *Chirality* **1998**, *10*, 140–146.

[77] J. Veciana, M. I. Crespo, *Angew. Chem., Int. Ed. Engl.* **1991**, *30*, 74–76.

[78] M. Jung, V. Schurig, *J. Am. Chem. Soc.* **1992**, *114*, 529–534.

Part E. Tuning the Charge Injection of P3HT-Based Organic Thin-Film Transistors Through Electrode Functionalization with Oligo-Phenylene SAMs[1]

Introduction

Since the early studies of Hiroshi Suzuki in 1959 demonstrating that the bathochromic shift in electronic absorption spectra is related to the spatial configuration of 2,2' alkylated biphenyl chromophores,[2,3] biphenyl systems emerged as popular model compounds for investigations in electron transfer and transport systems.[4–17] A further benchmark in using biphenyls with different torsion angles in electron transfer investigations is the work of Benniston *et al*.[18] Two terpyridine metal complexes were bridged with various torsion angle restricted biphenyls where the conjugation of the individual π-systems was adjusted by bridging the 2,2' position with a variable number of ethylene glycol units (figure 1).[19] Therefore a range of different torsion angles between 0° and 90° became accessible proportional to the number of ether units in the bridge.

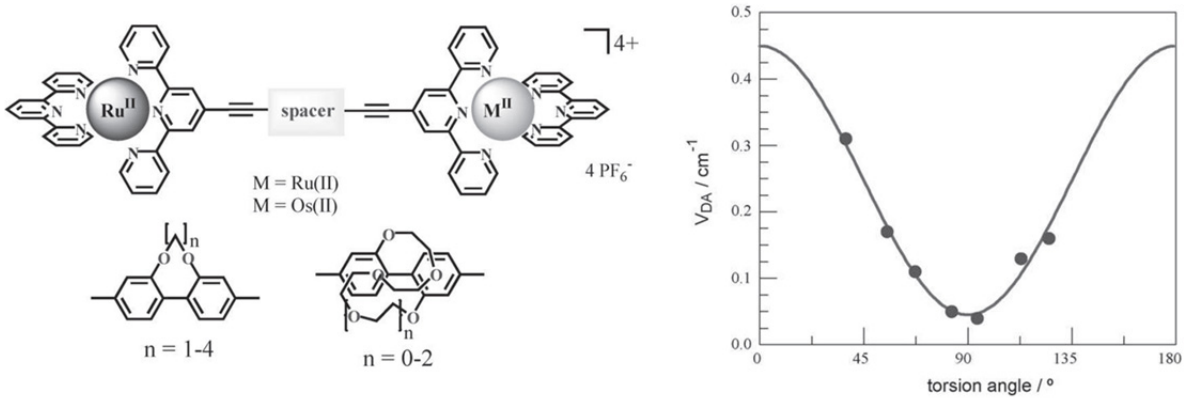

Figure 1. Model systems used by Benniston *et al.* to measure the effect of the torsion angle on the electron exchange (*left*). The length of the interlinking bridge dictates the degree of the aryl-aryl angle. Variation in the electronic coupling with changes in the torsion angle for mixed-metal complexes (M = Os). Reprinted from Benniston *et al*.[19]

Venkataraman *et al*. introduced the concept of changing the conjugation in biphenyls by alteration of the torsion angle between the phenyls to the research in molecular electronics.[20] The conductance of 4,4'-diaminobiphenyls with a variety of different torsion angles were measured in a STM break junction, demonstrating the interdependence between the single molecular conductance and the molecular conformation (figure 2).

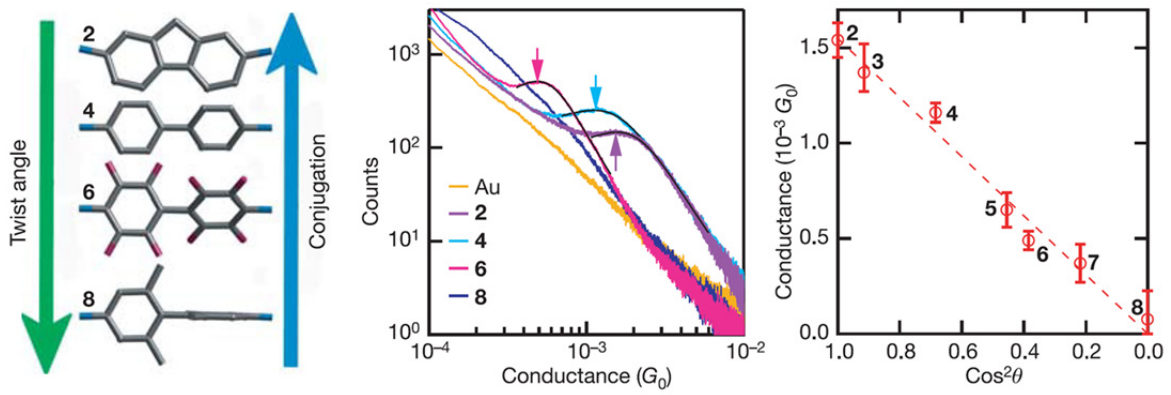

Figure 2. *left*: Model compounds studied by Venkataraman *et al*. showing the antidromic trend between torsion angle and conjugation. *middle*: Conductance histograms of the model compounds. *right*: Conductance plotted against $\cos^2\Phi$. Reprinted from Venkataraman *et al*.[20]

But not only the possibility to precisely adjust the conjugation across the π-system of biphenyls by changing the substituents in 2 and 2' position makes them to ideal model compounds in all research areas where the nature of chromophores play an important role. The on the chromophore dependent physical parameters like conductance, hyperpolarizability or absorption show a unique cosine square relationship to the torsion angle.[21,22] This makes torsion angle Φ restricted biphenyls to ideal compounds for investigations on a single molecular level as the observation of a $\cos^2\Phi$ relation is a direct proof for the involvement of the chromophore in the physical process. The $\cos^2\Phi$ relation arises from the π-orbital-overlap-integral A_{RS} – a measure for the extend of interactions between two adjacent π-orbitals – which is proportional to the resonance integral β_{RS}.[23] R and S are decoupled chromophores. Therefore the resonance energy E_{RS} relative to the isolated chromophores R and S is a measure for the interactions across the bond, interlinking R and S. Theoretical calculations demonstrated that this energy varies approximately with $\cos^2\Phi$.[23]

These two features of torsion angle restricted biphenyls allow to precisely alter the injection of charges in an electrode-biphenyl-conducting medium setup, where the presence of a $\cos^2\Phi$ relation gives further evidence about the injection mechanism. Such a device is an integral part of organic thin film transistors (OTFT). Their inorganic counterparts (silicon-based metal-oxide-semiconductor field effect transistors (MOSFET)) are devices used in every computer processor and in LCD displays. Until now no OTFT are available in commercial applications because of their minor performance compared to conventional MOSFET.[24] Nevertheless, OTFTs are attracting an increasing interest as promising candidates for printable, flexible and large area electronics.[25–27] In particular, the use of solution-

processable polymers having semiconducting properties pave the way towards commercialization of OTFTs as they can be developed for example using roll-to-roll techniques which are suitable for the mass production of low-cost electronics. Thin film transistors consist of three basic elements: 1.) a thin semiconducting film, 2.) an insulating layer, 3.) three electrodes (figure 3).[24] Two electrodes, the source and the drain electrode, are in contact with the semiconducting film. The gate electrode is separated by an insulating layer from the conducting layer. In OTFT the semiconducting film consists of semiconducting polymers like oligothiophenes or oligoacenes.[28] By applying a gate voltage at the gate electrode, charges with opposite sign are induced at the source electrode. Depending on the relative energies of the HOMO and LUMO to the Fermi level of the electrode charges can be injected to the semiconducting layer. If the HOMO of the semiconducting layer is perfectly aligned with the Fermi level of a gold electrode, a negative gate voltage will charge the source electrode positively and holes can be injected from the source to the semiconductor, leading to so called *p*-type transistors.[24]

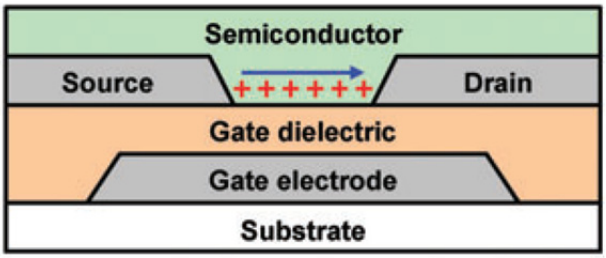

Figure 3. Schematic cross section of an organic thin film transistor (bottom-gate, bottom-contact geometry).

When applying a positive gate voltage on the other hand, no charge injection from the source to the semiconductor is possible and the transistor is blocked. The hole injection to the semiconductor layer results in the formation of an conducting channel at the semiconductor-insulating layer interface. The thickness of this channel strongly depends on the applied gate voltage. Thus, the charge flow from the source electrode to the drain electrode – arising when a voltage is applied between the drain and the source – can be adjusted by the gate voltage. Important parameters for the performance of OTFT are a) the charge carrier mobility which is dependent on the semiconducting conjugated polymer and b) the contact resistance which is related to the difference between the ionization energy of the organic material and the work function of the metal electrode.[24] At the early beginnings of OTFT the charge carrier mobility was the crucial factor determining the performance. But since conducting properties of conjugated polymers where enhanced in course of the development of organic light

emitting diodes (OLEDs), the charge injection got the new bottle neck of performance.[29] Therefore investigations on the adjustment of the work function of the metal and the HOMO or LUMO of the semiconducting organic medium are crucial. It is well known that the work function of metal electrodes can be tailored by covering it with self-assembled monolayers (SAM).[30–32] Previous studies using alkanethiols to adjust the alignment between the Fermi level of gold and the HOMO of the semiconducting polymer demonstrated that also the interfacial morphology and the tunneling resistance of the thiol SAM influences the charge injection.[33] To gain further insight into the crucial parameters of charge injection torsion angle restricted mono-thiolated biphenyl cyclophanes are ideal candidates, as biphenyls are known as molecular wires with a decreased tunneling resistance compared to alkanethiols. The possibility to vary the tunneling resistance by altering the length of the interlinking alkyl-bridge in 2,2' position allows to fine tune the work function of the gold electrode. Furthermore, a potential cosine square relation on the torsion angle would demonstrate the involvement of the electrode covering SAM in the charge injection process.

Results and Discussion

To investigate the influence of biphenyl-4-thiol SAMs on the work function and the charge injection in OTFTs model compounds **E1** – **E5** were synthesized. The terphenyl **E2** was used together with commercially available thiophenol for preliminary investigations on the influence of the length of the oligophenylene SAM on the field-effect mobility and threshold voltage of a bottom gate OTFT setup.[1]

Several different strategies can be envisaged to introduce a thiol moiety on aromatic systems. The maybe most straight forward ones are displayed in scheme 1. Nucleophilic aromatic substitution of aryl halides with a strong nucleophilic thiol is a valuable method if the resulting thiophenol has to be obtained in a protected form (method A). Furthermore this method allows to use fluoride as a leaving group which is more or less inert in cross-coupling reactions. Additionally fluorides can activate the oxidative addition of the aryl halide because of their strong electron-withdrawing nature. As a major disadvantage a further deprotection step is required towards free thiols. A second strategy can be the introduction of the thiol by reacting a lithiated aryl with sulfur, forming the sulfide, followed by trapping with a protection group or protonation (method B). Method C can be an alternative strategy if the syntheses of aryl halide precursors are troublesome, for example because of low selectivity. The precursor for the final Newman-Kwart rearrangement is a phenol for which a variety of different synthetic routes are known. Furthermore the polarity of the phenol often improves

the purification and isolation procedures. As a major disadvantage of strategy C the increased number of synthetic transformations has to be mentioned. For the successful introduction of the pentyl-bridge in torsion angle restricted biphenyl cyclophanes the presence of substituents in 4 and 4' position of the biphenyl are crucial to provide selectivity in the assembly strategy.[5] Even though such larger cyclophane systems were not envisaged for the investigations of the charge injection in OTFT method D followed by method C is proposed to achieve mono-thiolated biphenyls starting from dimethoxy precursors. It was shown in our laboratory that a nucleophilic cleavage of the methoxy groups always yielded the mono-deprotected phenol. To drive the reaction to completion a vast excess of thiomethoxide was necessary. Therefore this deprotection procedure seems to be ideally suited towards mono-functionalized biphenyl compounds. The free phenol functionality can be removed by forming the triflate, followed by conversion to the corresponding Grignard reagent and final quenching with a proton source. The obtained mono-methoxy biphenyl can then be converted to the thiol by using method C or by C-S hetero cross coupling protocols (method E).

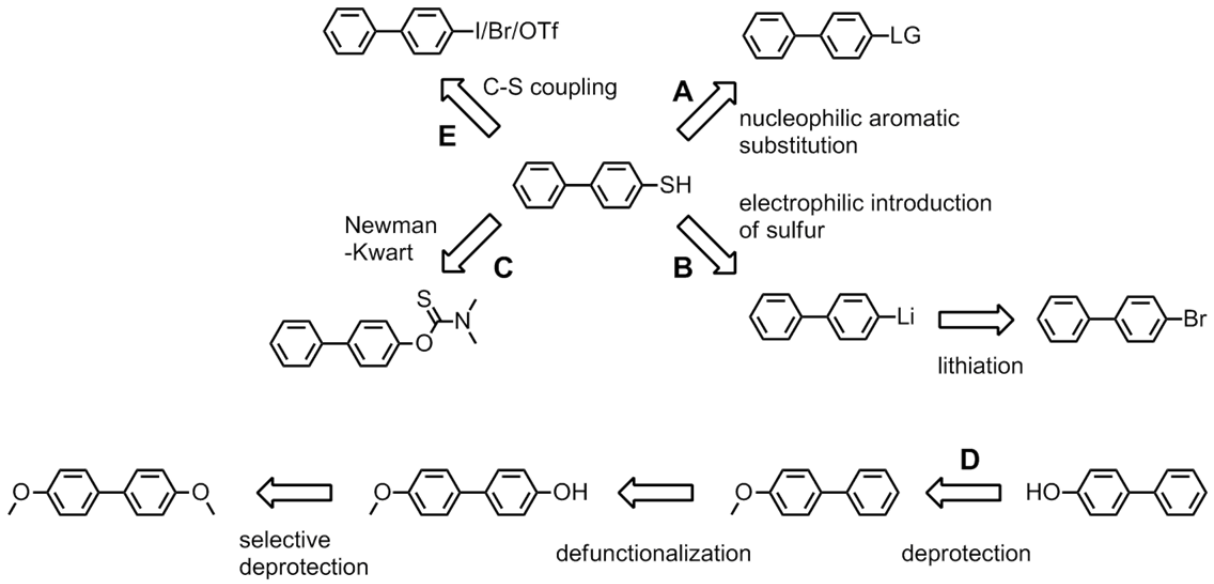

Scheme 1. Retrosynthetic strategies to introduce the sulfur moiety to a biphenyl core.

Compounds **E1** and **E2** were synthesized according to synthetic strategy B. The commercially available 4-bromobiphenyl **E6** and 4-bromo-1,1':4',1''-terphenyl **E7** were treated with *tert*-butyl lithium at -78°C for 1 h. Then pestled elemental sulfur was added to the lithiated oligophenylenes in small portions. The final target compounds **E1** and **E2** were obtained after quenching of the sulfides with hydrochloric acid and purification by basic extraction followed by sublimation in 52% and 36% yield, respectively (scheme 2).

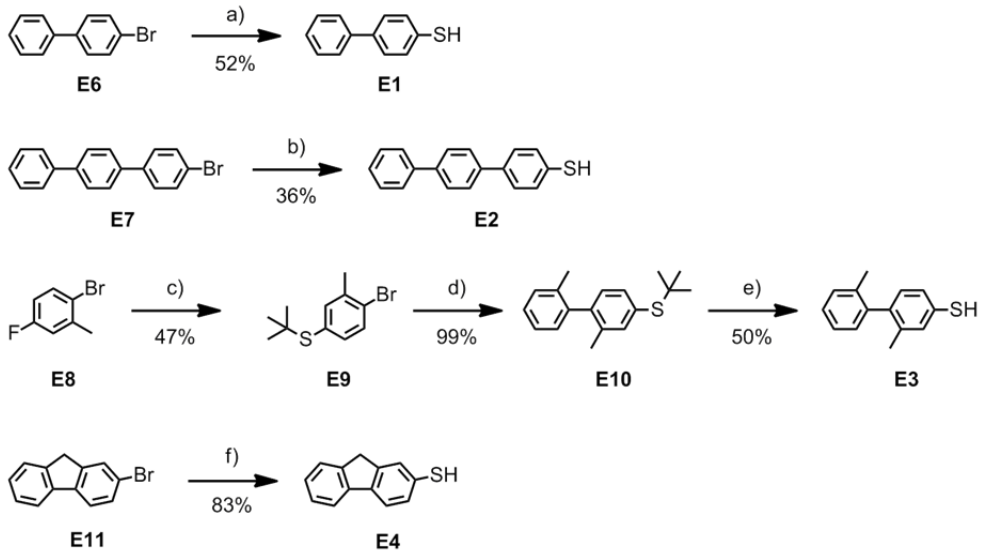

Scheme 2. Synthesis of 4-thiobiphenyls with varying torsion angles **E1**, **E3**, and **E4** as well as terphenyl **E2**. a), b) 1.) *t*BuLi, THF, -78°C, 1 h, then rt, 2.) S_8, rt, 3 h, 3.) aq. HCl, rt, 30 min; c) sodium 2-methylpropane-2-thiolate, DMF, reflux 2 h; d) *o*-tolylboronic acid, $Pd(PPh_3)_4$, Cs_2CO_3, toluene:EtOH 2:1, 95°C, 24 h; e) BBr_3 (1 M in dichloromethane), 0°C, 2.5 h, then MeOH; f) sodium thiomethoxide, DMI, 120°C, 18 h, then aq. HCl.

2,2'-Dimethyl-4-thiobiphenyl (**E3**) was synthesized in a three step sequence starting from 1-bromo-4-fluoro-2-methylbenzene (**E8**) (scheme 2). The thiol moiety was introduced at the first step of the synthesis since nucleophilic substitution of 2,2'-dimethyl-4-fluorobiphenyl with sodium *tert*-butyl thiolate was not successful. Compound **E8** was transferred to (4-bromo-3-methylphenyl)-(*tert*-butyl)sulfane (**E9**) with a nucleophilic aromatic substitution using sodium *tert*-butylthiolate as a nucleophile. Subsequent Suzuki cross-coupling with *o*-tolylboronic acid using tetrakis(triphenylphosphine)palladium as a catalyst and cesium carbonate as a base in a solvent mixture of toluene:EtOH 2:1 afforded the *tert*-butyl protected biphenylthiol **E10**. Deprotection by boron tribromide yielded after quenching with methanol the desired target compound **E3** in 23% yield over three steps. For the synthesis of the fluorene derivative **E4** synthetic route A was used (scheme 2). In contrast to the synthesis of compounds **E1** and **E2** the presence of a strong base readily leads to deprotonation of the bridging methylene protons, due to the increased acidity of this doubly stabilized benzylic position. To prevent side products commercially available 2-bromo-9*H*-fluorene **E11** was reacted with sodium thiomethoxide in DMI at 120°C. Nucleophilic aromatic substitution yields the methyl protected thiophenol which is *in situ* deprotected by the excess of sodium thiomethoxide. After quenching with hydrochloric acid, basic extraction afforded target compound **E4** in high purity (83%). The 2-thio-9,10-dihydrophenanthrene **E5** was synthesized by use of a Newman-Kwart rearrangement of literature known 9,10-

dihydrophenanthren-2-ol (**E12**).[34] Attempts to mono-brominate 9,10-dihydrophenanthrene in 4 position were not successful. Even though the formation of the desired starting material was observed by ^{1}H-NMR it was impossible to isolate 2-bromo-9,10-dihydrophenanthrene from the crude, due to the lack of polarity of all formed compounds. To avoid the difficulties in regioselectivity and isolation in a first step 9,10-dihydrophenanthrene was acetylated in 2 position using a Friedel-Crafts acylation protocol.[34] Therefore the dihydrophenanthrene **E13** was reacted with acetyl chloride in the presence of aluminium chloride as a Lewis acid. Several regioisomers formed during the reaction, but doubly acetylated products were prevented due to the deactivating nature of the introduced acetyl. The desired product **E14** was isolated by column chromatography in 37% yield. A sequence of Baeyer-Villiger-oxidation followed by ester cleavage afforded 9,10-dihydrophenanthren-2-ol (**E12**) in 77% over both steps (scheme 3). The *O*-thiocarbamate necessary for the envisaged Newman-Kwart rearrangement was then synthesized by reacting the dihydrophenthrene-2-ol **E12** with dimethylcarbamoylchloride using sodium hydride as a base. The thermally activated Newman-Kwart rearrangement, where an *O*-thiocarbamate rearranges to a *S*-thiocarbamate, was carried out at 260°C in diphenylether. The rearrangement was chosen because a possible hetero cross-coupling reaction of the corresponding triflate to introduce the thiol moiety was not successful. After successful rearrangement the solvent was removed by column chromatography and the obtained *S*-thiocarbamate **E15** cleaved in strong basic medium to yield the free thiol **E5** in 98%. The free thiol **E5** was not stable towards formation of disulfides even when stored at -18°C under argon atmosphere. The biphenyl compounds were synthesized to cover the source and drain electrode of OTFTs with aryl thiol SAMs which can also be achieved with disulfides.

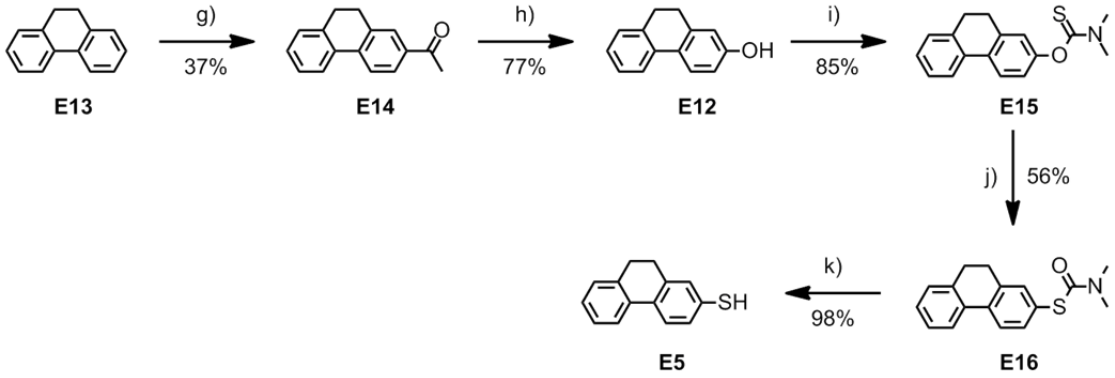

Scheme 3. Synthesis of 2-thio-9,10-dihydrophenanthrene (**E5**). g) acetyl chloride, $AlCl_3$, dichloromethane, 0°C, 1 h, then rt, 2 h; h) 1.) *m*-CPBA, dichloromethane, 0°C, 3 h, then rt, 95 h, 2.) conc. aq. HCl, MeOH, rt, 18 h; i) dimethylcarbamoyl chloride, NaH, DMF, 80°C, 2 h, then rt, 15 h; j) Ph_2O, 260°C, 2 h; k) KOH, MeOH, 80°C, 3 h.

In summary the five desired 4-thiobiphenyl derivatives **E1** – **E5** comprising different torsion angles were successfully synthesized by the use of three different synthetic strategies to introduce the sulfur functionality.

Investigations of the charge injection of organic thin film transistors by functionalization of the electrodes with oligophenylene SAMs were carried out in the group of Samori.[1] Preliminary results of the influence of oligophenylene thiols with variable length (phenyl, biphenyl and terphenyl) were already obtained. The setup used in these investigations was a bottom-contact bottom-gate transistor where the semiconducting thin film was a poly(3-hexylthiophene) (P3HT). The source and drain gold electrodes were covered with an oligophenylene SAM using the spin coating technique. The insulating layer was a silicon oxide layer which separated the semiconductor from the n^{++}-silicium gate electrode. The experiments were performed under inert gas atmosphere. A schematic sketch of the setup is shown in figure 4.

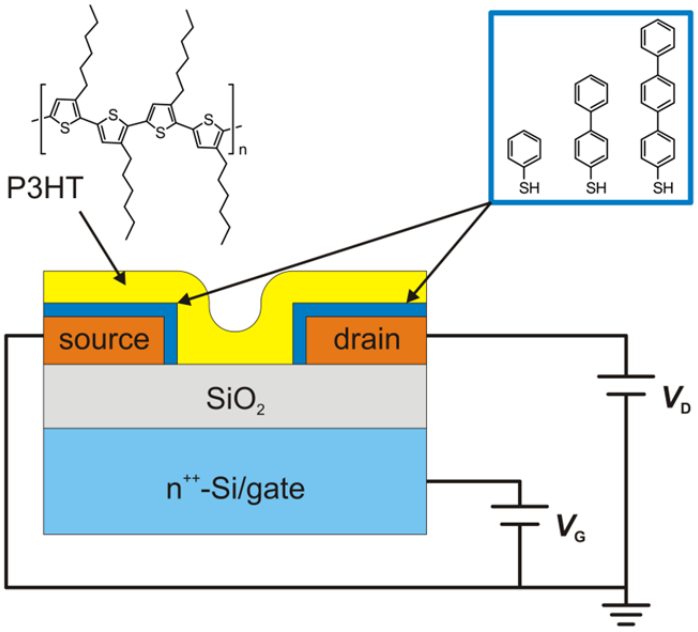

Figure 4. Bottom-contact bottom-gate transistor with different types of SAMs functionalized gold electrodes. P3HT was used as the semiconducting layer.

Output curves of the P3HT-based transistors with different electrode functionalizations are shown in figure 5. All devices revealed an excellent *p*-type behavior confirmed from the almost ideal spacing between the curves recorded at different gate voltage (V_G). Cyclic voltammetry measurements demonstrated that the work function Φ_M of the bare gold electrode and the thiophenol functionalized one should theoretically result in an Ohmic

contact between the electrode and the HOMO of P3HT (-4.96 eV). Furthermore a small injection barrier was found for the longer oligophenylenes **E1** and **E2**.

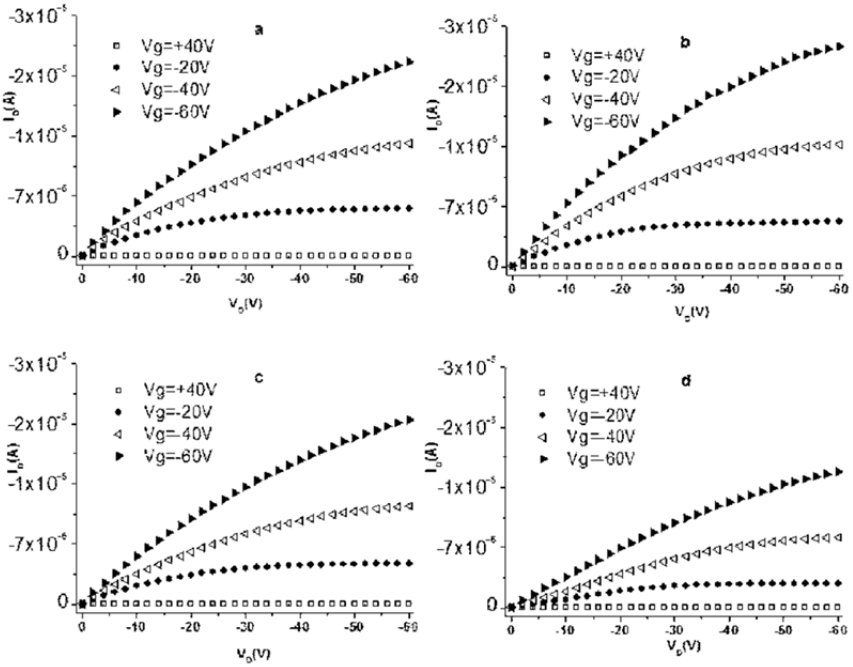

Figure 5. Output curves (I_D/V_D) of P3HT-based transistors (W=10000 µm, L = 20 µm) with (a) bare Au source and drain electrodes (b) gold source and drain electrodes functionalized with thiophenol (c) gold source and drain electrodes functionalized with 4-thiobiphenyl (d) gold source and drain electrodes functionalized with 4-thioterphenyl.

Surprisingly no S-shape curves at low gate voltages were observed for all setups (figure 5) which would be indicative for a difficult charge injection. The measured drain current was higher for the thiophenol covered electrode compared to the bare Au electrode. Even though the work function in the terphenylthiol setup is lowest (table 1), the 4-thiobiphenyl setup showed a higher drain current.

Table 1. Overview of the electrical/surface properties of the bottom-contact bottom-gate P3HT-based transistors (L=20 µm, W=10000 µm) with gold source and drain electrodes functionalized with thiophenol, **E1** and **E2**.

	Φ_M / eV	Contact Angle (Water)	R_C / kΩ
Bare Au	5.12	65.4 ± 1.6°	70 ± 17
Thiophenol	5.05	84.5 ± 5.4°	23 ± 5
E1	4.90	78.7 ± 1.8°	75 ± 5
E2	4.87	82.1 ± 1.4°	98 ± 17

To cast light onto this phenomenon the contact resistance was measured for each individual setup (table 1). The values obtained confirmed the observed trend in drain current which decreases with increasing contact resistance. Surprisingly, the contact resistance of the thiophenol devices was found to be lower compared to the non-functionalized electrodes. One would expect the presence of SAMs to give room for an additional resistive contribution, since it is known from conductance measurements that the resistance increases with increasing number of phenyl units. The decreased contact resistance in the thiophenol setup can be explained by the more hydrophobic surface compared to the bare gold (table 1) (investigated with contact angle measurements) and therefore with a better packing of the P3HT in the thiophenol case. The increased contact resistance of **E1** and **E2** can be attributed to either an induced misalignment of the work function of the whole electrode system (including the SAM) to the HOMO of the semiconducting layer or by a higher tunneling resistance.

The measured charge mobility followed the observed trend of the contact resistance, revealing that the best mobility values were extracted on devices with thiophenol functionalized electrodes. Additionally it was found that by covering the electrodes with self-assembled monolayers the morphology is improved which prevents interfacial defects at the semiconductor/electrode interface and thus leads to a decreased threshold voltage (figure 7).

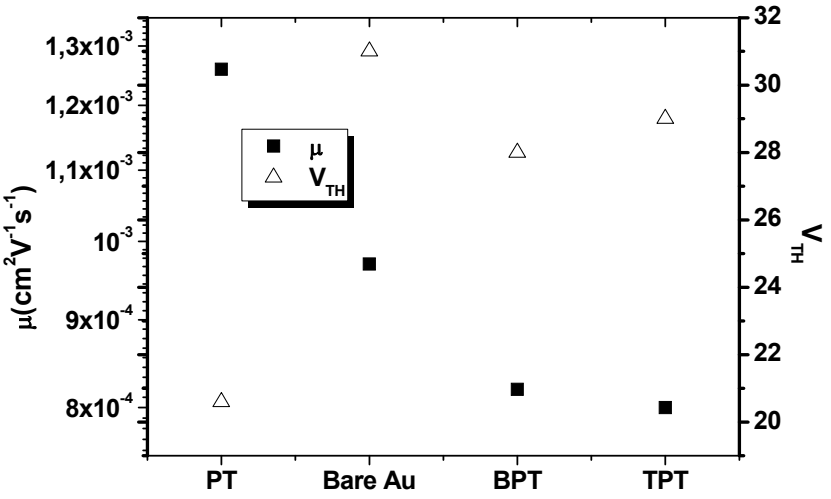

Figure 7. Field-effect mobility and threshold voltage values extracted from P3HT-based transistors (W = 10000 μm, L = 10 μm) with different source and drain functionalization.

A more precise fine tuning to evaluate the influence of the source and drain covering SAM to the overall system is expected for the four mono-thiolated biphenyl cyclophanes **E1**, **E3** – **E5**. In multicomponent systems like OTFT the precise alignment of the frontier molecular orbitals of each individual component to the next one is crucial. For the synthesized torsion angle restricted biphenyls it is expected that the HOMO-LUMO gap increases with increasing torsion angle which results in an order **E4**≤**E5**<**E1**<**E3**. Aryl thiols and P3HT are known as p-type conductors leading to p-type OTFT. Therefore the extent of the HOMO overlap between the interfaces dominates the charge injection and mobility. Preliminary measurements of 2,2'-dimethyl-4-thiobiphenyl **E3** showed a difficult charge injection which was not the case for the parent biphenyl **E1**. To evaluate whether this phenomenon was caused by the nature of the molecule itself or by a reduced quality of the electrodes morphology cyclovoltammetry experiments were performed. Therefore gold electrodes covered with the mono-thiobiphenyl derivatives as working electrodes were used in presence of a redox active compound. If the SAM has a low quality (not well packed, disorder, etc.) redox peaks will arise, if the SAM is well formed, the molecules cannot reach the gold electrode and the redox active compounds will not be reduced or oxidized. It was shown that the SAMs composed out of biphenyls with larger torsion angles are of poorer quality compared to a SAM formed by conventional biphenyls. Surprisingly, in contrast to this expected grading, the fluorene derivative **E4** formed the SAM with the poorest quality. The reason for this finding is yet uncertain, especially since well ordered SAMs composed out of fluorene derivatives are already reported in literature.[35] The purity of the mono-thiolated fluorene was confirmed by elemental analysis, GC-MS and NMR. Thus critical parameters for the difficult charge injection can be the quality of the gold electrode itself or other setup relevant parameters. To further investigate the influence of torsion angle restricted biphenyl SAMs on the performance of OTFT careful and detailed studies on the morphology of the gold electrode, as well as on the packing properties of the corresponding biphenyls are required and part of our ongoing research.

Conclusion

In summary, a series of mono-functionalized 4-thiobiphenyls **E1** – **E5** were successfully synthesized by use of nucleophilic aromatic substitution (compounds **E3** and **E4**), lithiation followed by electrophilic substitution (compounds **E1** and **E2**) and a Newman-Kwart rearrangement (**E5**). In most cases a basic extraction procedure was good enough to obtain the desired target compounds in high purity. Preliminary investigations on the influence of

covering the source and the drain electrode of OTFT devices with SAMs of oligophenylenes with an increasing number of phenyls demonstrated that a fine tuning of both the field-effect mobility and the threshold voltage can be achieved. These investigations also suggests that the macroresistive contribution can be explained by taking into account a concomitant effect of energetic levels alignment, tunneling resistance of the SAMs and interfacial morphology between the semiconducting layer and the electrode. These findings are of importance to optimize OTFT in view of their technological applications in logic circuits as they provide tools for a better control over the charge injection mechanism. It will now be of further interest to perform experiments with biphenylthiol with varying torsion angles (**E1**, **E3** – **E5**) to evaluate if the alignment to the HOMO of P3HT or the increased tunneling barrier is the dominant factor leading to high contact resistance. Furthermore it will be interesting to see if the fine tuning of the torsion angles in the biphenyl compounds can lead to an increased charge injection.

Experimental Part

All chemicals were directly used for the syntheses without purification, dry solvents were purchased from *Fluka*. The solvents for extractions were distilled before use. Characterizations were performed with the following instruments: ^{1}H-NMR and ^{13}C-NMR spectra were recorded with a *Bruker DPX-NMR* (400 MHz), the *J* values are given in Hz. Mass spectra were recorded on a *finnigan MAT 95Q* for Electron Impact (EI) measured in *m/z* (%). The elementary analyses were measured on an *Analysator 240* from Perkin-Elmer.

[1,1'-Biphenyl]-4-thiol (E1): 4-Bromobiphenyl (200 mg, 0.858 mmol, 1.00 equiv.) was weighed into a preheated 25 mL Schlenk-tube under argon atmosphere. The tube was evacuated and backfilled with argon three times. Then the solid was dissolved in 5 mL THF (crown-cap) and cooled to -78°C. Afterwards *t*BuLi (1.13 mL (1.6 M in pentane), 1.80 mmol, 2.10 equiv.) was added dropwise and the resulting pale brown suspension was stirred at -78°C for 1 h. Afterwards the suspension was allowed to warm to rt and then finely grounded sulfur (30.3 mg, 0.944 mmol, 1.10 equiv.) was added in 5 portions over a period of half an hour. The brown reaction mixture was stirred for 3 h at rt and then quenched with 1 M aq. HCl (2 mL). The mixture was diluted with demin. water (10 mL) and the phases were separated. The aqueous one was extracted twice with EtOAc (25 mL each). Afterwards the combined organic layers were made alkaline with 1 M aq. NaOH (5 mL) and extracted three times with demin. water (50 mL each). The pH of the collected aqueous phases was then adjusted to pH 6 with 1 M aq. HCl (12 mL). After extraction with EtOAc (3 × 75 mL), the

combined organic layers were washed with brine and demin. water, dried with sodium sulfate, filtered and concentrated. The obtained yellow solid was further purified by vacuum sublimation (52 %).

R_f = 0.62 (SiO_2; cyclohexane:EtOAc 10:1); **m.p.** 110 − 111°C; **^{1}H-NMR** (400 MHz, DMSO-d6): δ = 7.63 (d, ^3J(H,H) = 7 Hz, 2H, Ar-H), 7.55 (d, ^3J(H,H) = 8 Hz, 2H, Ar-H), 7.43 (t, ^3J(H,H) = 7 Hz, 2H, Ar-H), 7.38 (d, ^3J(H,H) = 8 Hz, 2H, Ar-H), 7.34 (t, ^3J(H,H) = 7 Hz, 1H, Ar-H), 5.53 (s, 1H; -SH) ppm; **^{13}C-NMR** (126 MHz, DMSO-d6): δ = 139.4 (C_q), 136.6 (C_q), 131.7 (C_q), 128.8 (C_t), 128.7 (C_t), 127.2 (C_q), 127.2 (C_t), 126.2 (C_t) ppm; **MS** (EI +, 70 eV): m/z (%) = 187 (16), 186 (100) [M^+], 185 (69) [M^+ − H], 153 (8) [$C_{12}H_9^+$], 152 (21); **elemental analysis** calcd (%) for $C_{12}H_{10}S$: C 77.38, H 5.41; found: C 77.15, H 5.65.

[1,1':4',1"-Terphenyl]-4-thiol (E2): The terphenylthiol was synthesized according to procedure described for **E1** using 4-bromo-*p*-terphenyl (200 mg, 0.647 mmol, 1.00 equiv.). After quenching with 1 M aq. HCl the precipitate formed was filtered off and washed with EtOAc (100 mL). The workup was continued with the filtrate as described above to afford **E2** as a white solid (35 %).

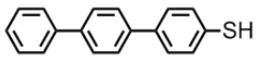

M.p. 217 − 218°C; **^{1}H-NMR** (400 MHz, DMSO-d6): δ = 7.75 (s, 4H, Ar-H), 7.72 (d, ^3J(H,H) = 7 Hz, 2H, Ar-H), 7.62 (d, ^3J(H,H) = 8 Hz, 2H, Ar-H), 7.48 (t, ^3J(H,H) = 7 Hz, 2H, Ar-H), 7.40 (d, ^3J(H,H) = 8 Hz, 2H, Ar-H), 7.38 (t, ^3J(H,H) = 7 Hz, 1H, Ar-H), 5.56 (s, 1H; -SH) ppm; **^{13}C NMR** (101 MHz, DMSO-d6): δ = 138.3 (C_q), 136.0 (C_q), 132.9 (C_q), 131.5 (C_q), 130.6 (C_q), 128.9 (C_t), 128.8 (C_t), 128.6 (C_t), 127.1 (C_t), 127.0 (C_t), 126.7 (C_t), 126.4 (C_t) ppm; **MS** (EI +, 70 eV): m/z (%) = 263 (20), 262 (100) [M^+], 261 (25) [M^+ − H], 282 (10).

(4-Bromo-3-methylphenyl)(*tert*-butyl)sulfane (E9): In a dry 250 ml Schlenk-tube sodium-2-methylpropanethiolate (882 mg, 7.86 mmol, 1.50 equiv.) and 2-bromo-5-fluorotoluene (**E8**) (0.67 mL, 1.00 g, 5.24 mmol, 1.00 equiv.) were added and dissolved in 40 ml DMF. The reaction mixture was stirred at reflux for 2 h. After cooling to rt, demin. water was added to the mixture and extracted twice with diethyl ether. The combined organic layers were dried with Na_2SO_4 and filtered. The solvent was removed *in vacuo* and the residue was purified by column chromatography (SiO_2; cyclohexane) which resulted in a colorless oil (47%).

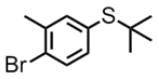

R_f = 0.70 (SiO_2; cyclohexane); **^{1}H-NMR** (400 MHz, $CDCl_3$): δ = 7.48 (d, ^3J(H,H) = 8.2 Hz, 1H, Ar-H), 7.39 (d, ^4J(H,H) = 1.5 Hz, 1H, Ar-H), 7.19 (dm, ^3J(H,H) = 8.2 Hz, 1H, Ar-H),

2.39 (s, 3H, -CAr-CH_3), 1.28 (s, 9H, -C-(CH_3)$_3$) ppm; **^{13}C-NMR** (100 MHz, $CDCl_3$): δ = 139.5 (C_t), 138.0 (C_q), 136.1 (C_t), 132.3 (C_t), 131.8 (C_q), 125.9 (C_q), 46.0 (C_q, -*C*-(CH_3)$_3$), 30.9 (C_p, -C-(*C*H$_3$)$_3$), 22.8 (C_p, -CAr-*C*H$_3$) ppm; **MS** (EI +, 70 eV): m/z (%) = 260 (38), 258 (37, [M^+]), 203 (100), 201 (99, [M^+-*t*Bu]), 123 (30, [M^+-*t*Bu-Br]), 122 (12), 121 (14), 57 (31, [*t*Bu$^•$]).

***tert*-Butyl(2,2'-dimethyl-[1,1'-biphenyl]-4-yl)sulfane (E10):** In a dry 25 ml Schlenk-tube 3-

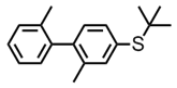

(4-bromo-3-methylphenyl)(tert-butyl)sulfane (**E9**) (200 mg, 0.772 mmol, 1.00 equiv.), 2-tolylboronic acid (133 mg, 0.926 mmol, 1.20 equiv.), $Pd(PPh_3)_4$ (18.0 mg, 15.4 µmol, 2 mol%) and Cs_2CO_3 (762 mg, 2.32 mmol, 3.00 equiv.) were added consecutively and suspended in 5 mL toluene and 2.5 mL EtOH. The suspension was then heated at reflux for 24 h. The reaction mixture was allowed to cool to rt, diluted with tBME and filtered through a pad of celite. The solvent was removed under reduced pressure and the residue was purified by column chromatography (SiO_2; cyclohexane:EtOAc 10:1) which resulted in a pale red oil (99.6 %).

***R*$_f$** = 0.39 (SiO_2; cyclohexane); **^{1}H-NMR** (400 MHz, $CDCl_3$): δ = 7.44 (s, 1H, Ar-H), 7.39 (dd, ^4J(H,H) = 1.6 Hz, ^3J(H,H) = 7.7 Hz, 1H, Ar-H), 7.24 – 7.29 (m, 2H, Ar-H), 7.19 – 7.24 (m, 1H, Ar-H), 7.10 (d, ^3J(H,H) = 7.1 Hz, 1H, Ar-H), 7.06 (d, ^3J(H,H) = 7.7 Hz, 1H, Ar-H), 2.05 (s, 3H, -CAr-C*H*$_3$), 1.34 (s, 9H, -C-(C*H*$_3$)$_3$) ppm; **^{13}C-NMR** (100 MHz, $CDCl_3$): δ = 142.1 (C_q), 140.9 (C_q), 138.7 (C_t), 136.1 (C_q), 135.7 (C_q), 134.5 (C_t), 131.1 (C_q), 129.1 (C_t), 129.3 (C_t), 129.1 (C_t), 127.3 (C_t), 125.6 (C_t), 45.8 (C_q, -C-(*C*H$_3$)$_3$), 31.0 (C_p, -C-(*C*H$_3$)$_3$), 19.8 (C_p, -CAr-*C*H$_3$), 19.7 (C_p, -CAr-*C*H$_3$) ppm; **MS** (MALDI-ToF): m/z (%) = 271 (20), 270 (100, [M^+]).

2,2'-Dimethyl-[1,1'-biphenyl]-4-thiol (E3): In an oven-dried Schlenk-tube the tert-butyl

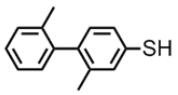

protected biphenylthiol **E10** (60.0 mg, 0.222 mmol, 1.00 equiv.) was dissolved in 2 mL dichloromethane and degased for 10 min by bubbling argon through the solution. After cooling the solution to 0°C, BBr_3 (1.55 mL (1 M in dichloromethane), 2.28 g, 1.55 mmol, 7.00 equiv.) was added dropwise. The reaction mixture was stirred at rt for 2.5 h and was afterwards quenched with MeOH. The solution was extracted three times with 1 M aq. NaOH. The combined aqueous phases were acidified with conc. aq. HCl and extracted with dichloromethane. The combined organic layers were dried with sodium sulfate, filtered and concentrated. The crude was purified by flash column chromatography (SiO_2; cyclohexane, 0.5% EtOAc) to isolate the desired thiol **E3** as a colorless liquid (50%).

R_f = 0.37 (SiO_2; cyclohexane, 1% EtOAc); **^{1}H-NMR** (500 MHz, $CDCl_3$): δ = 7.27 – 7.25 (m, 2H, Ar-H), 7.24 – 7.19 (m, 2H, Ar-H), 7.14 (dd, ^4J(H,H) = 1.5 Hz, ^3J(H,H) = 7.5 Hz, 1H, Ar-H), 7.06 (d, ^3J(H,H) = 7.5 Hz, 1H, Ar-H), 6.98 (d, ^3J(H,H) = 8.0 Hz, 1H, Ar-H), 3.45 (s, 1H, -SH), 2.05 (s, 3H, -CAr-CH_3), 2.00 (s, 9H, -C-(CH_3)$_3$) ppm; **^{13}C-NMR** (126 MHz, $CDCl_3$): δ = 140.9 (C_q), 139.4 (C_q), 137.1 (C_q), 136.0 (C_q), 130.9 (C_t), 130.2 (C_t), 130.0 (C_t), 129.5 (C_t), 129.1 (C_q), 127.5 (C_t), 126.9 (C_t), 125.7 (C_t), 20.0 (C_p, -CAr-*C*H$_3$), 19.9 (C_p, -CAr-*C*H$_3$) ppm; **MS** (EI +, 70 eV): m/z (%) = 215 (14), 214 (100, [M^+]), 199 (14), 181 (29, [M^+-SH]), 166 (52), 165 (36); **elemental analysis** calcd (%) for $C_{14}H_{14}S$: C 78.46, H 6.58; found: C 78.56, H 6.69.

9*H*-Fluorene-2-thiol (E4): 2-Bromofluorene (**E11**) (250 mg, 1.02 mmol, 1.00 equiv.) was

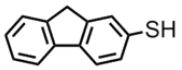

dissolved in 10 mL DMI and degased for 10 min with argon. Afterwards the solution was heated to 120°C and sodium thiomethoxide (357 mg, 5.10 mmol, 5.00 equiv.) was added at once. The dark red reaction mixture was stirred at 120°C for 18 h. Then 10 mL 1 M aq. hydrochloric acid and 10 mL Et_2O were added. The mixture was stirred until the aqueous phase turned clear. The layers were separated and the aqueous one extracted twice with diethyl ether. The combined organic layers were extracted three times with 1 M aq. NaOH and the collected aqueous phases acidified (pH 6). The aqueous layers were extracted again three times with diethyl ether and the combined organic layers washed once with demin. water and once with brine. The etheric solution was dried with sodium sulfate, filtered and concentrated.

R_f = 0.45 (SiO_2; cyclohexane:EtOAc 20:1); **^{1}H-NMR** (400 MHz, $CDCl_3$): δ = 7.74 (d, ^3J(H,H) = 7.6 Hz, 1H, Ar-H), 7.65 (d, ^3J(H,H) = 8.0 Hz, 1, Ar-H), 7.53 (d, ^3J(H,H) = 7.6 Hz, 1H, Ar-H), 7.47 (s, 1H, Ar-H), 7.37 (t, ^3J(H,H) = 7.6 Hz, 1H, Ar-H), 7.33 – 7.27 (m, 2H, Ar-H), 3.86 (s, 2H, Ar-CH_2-Ar), 3.54 (s, 1H, -SH) ppm; **MS** (EI +, 70 eV): m/z (%) = 198 (56, [M^+]), 197 (13), 166 (14), 165 (100, [M^+-SH]); **elemental analysis** calcd (%) for $C_{13}H_{10}S$: C 78.75, H 5.08; found: C 78.35, H 5.17.

2-Acetyl-9,10-dihydrophenanthrene (E14):[34] 9,10-Dihydrophenenthrene (**E13**) (550 mg,

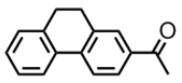

2.87 mmol, 1.00 equiv.) was dissolved in 5.5 mL dry dichloromethane in a preheated 50 mL Schlenk-tube. The solution was cooled to 0°C, then anhydrous $AlCl_3$ (574 mg, 4.30 mmol, 1.50 equiv.) was added in one lot. After stirring for 10 min at 0°C a solution of acetyl chloride (0.25 mL, 270 mg, 3.44 mmol, 1.2 equiv.) in 1.5 mL dichloromethane was added dropwise to the brown reaction mixture. The suspension was stirred for another 30 min at 0°C and then 2 h at rt. Afterwards the mixture was poured

onto ice and 0.9 mL conc. aq. HCl was added. The mixture was stirred for 20 min at rt. The layers were separated and the organic one washed with sat. aq. $NaHCO_3$, dried with sodium sulfate, filtered and concentrated. The resulting yellow oil was purified by Kugelrohr-distillation (3 x 10^{-1} mbar, 200°C) and column chromatography (SiO_2; cyclohexane:EtOAc 10:1) (37%).

$\boldsymbol{R_f}$ = 0.33 (SiO_2; cyclohexane:EtOAc 10:1); **^{1}H-NMR** (400 MHz, $CDCl_3$): δ = 7.89 (dd, ^4J(H,H) = 2.0 Hz, ^3J(H,H) = 8.0 Hz, 1H, Ar-H), 7.86 – 7.77 (m, 3H, Ar-H), 7.47 – 7.31 (m, 1H, Ar-H), 7.31 – 7.22 (m, 2H, Ar-H), 3.00 – 2.85 (m, 4H, Ar-CH_2-CH_2-Ar), 2.62 (s, 3H, -(CO)-CH_3) ppm; **^{13}C-NMR** (101 MHz, $CDCl_3$): 197.8 (C_q, -(*C*O)-CH_3), 139.1 (C_q), 138.0 (C_q), 137.5 (C_q), 135.7 (C_q), 133.4 (C_q), 128.6 (C_t), 128.3 (C_t), 128.0 (C_t), 127.2 (C_t), 127.1 (C_t), 124.4 (C_t), 123.7 (C_t), 28.9 (C_s, Ar-*C*H_2-CH_2-Ar), 28.8 (C_s, Ar-*C*H_2-CH_2-Ar), 26.6 (C_p, -(CO)-*C*H_3) ppm. All analytic data are according to literature.

2-Hydroxy-9,10-dihydrophenanthrene (E12):[34] 2-Acetyl-9,10-dihydrophenanthrene (**E14**)

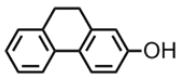

(225 mg, 1.01 mmol, 1.00 equiv.) was dissolved in 5 mL dichloromethane (dry) and then *m*CPBA (498 mg, 2.02 mmol, 2.00 equiv.) was added in one lot. After stirring for 3 h at rt the solution was let stand for 95 h. Afterwards the reaction mixture was further diluted with dichloromethane and washed once with 50 mL 5% aq. KOH and once with brine. After that the organic layer was dried with sodium sulfate, filtered and concentrated. The obtained yellow oil **E15** was pure enough to be used for further reaction without purification. 2-Acetoxy-9,10-dihydrophenanthrene was dissolved in 10 mL MeOH and while stirring at rt 0.3 mL conc. HCl were added. The reaction mixture (red) was stirred at rt for 18 h and then solid NaOAc (550 mg) was added. The resulting NaCl was filtered off and the filtrate was concentrated. The residue was taken up in EtOAc and water and the layers were separated. The organic layer was washed with sat. $NaHCO_3$, dried with sodium sulfate, filtered and concentrated. The crude was purified by column chromatography (SiO_2; cyclohexane:EtOAc 5:1) (77% over two steps).

$\boldsymbol{R_f}$ = 0.32 (SiO_2; cyclohexane:EtOAc 5:1); **^{1}H-NMR** (400 MHz, $CDCl_3$): δ = 7.67 (d, ^3J(H,H) = 7.6 Hz, 1H, Ar-H), 7.64 (d, ^3J(H,H) = 8.4 Hz, 1H, Ar-H), 7.29 (dt, ^4J(H,H) = 2.0 Hz, ^3J(H,H) = 7.6 Hz, 1H, Ar-H), 7.24 – 7.16 (m, 2H, Ar-H), 6.78 (dd, ^4J(H,H) = 2.8 Hz, ^3J(H,H) = 8.4 Hz, 1H, Ar-H), 6.72 (d, ^4J(H,H) = 2.4 Hz, 1H, Ar-H), 4.87 (s, 1H, -O*H*), 2.90 – 2.78 (m, 4H, Ar-CH_2-CH_2-Ar) ppm; **^{13}C-NMR** (101 MHz, $CDCl_3$): 155.0 (C_q), 139.5 (C_q), 136.6 (C_q), 134.5 (C_q), 128.2 (C_t), 127.8 (C_q), 127.1 (C_t), 126.7 (C_t), 125.3 (C_t), 123.1 (C_t), 115.0 (C_t),

113.9 (C_t), 29.4 (C_s, Ar-*C*H_2-CH_2-Ar), 29.1 (C_s, Ar-CH_2-*C*H_2-Ar) ppm. All analytic data are according to literature.

***O*-(9,10-dihydrophenanthren-2-yl) dimethylcarbamothioate (E15):** A solution of 2-hydroxy-9,10-dihydrophenanthrene (**E12**) (140 mg, 0.713 mmol, 1.00 equiv.) in 3 mL DMF was added to a suspension of NaH (55% in oil) (93.4 mg, 2.14 mmol, 3.00 equiv.) in 2.5 mL DMF at 0°C. The mixture was stirred for 30 min at rt. The dimethylcarbamoyl chloride (265 mg, 2.14 mmol, 3.00 equiv.) was added and the reaction mixture was stirred at 80°C for 2 h. The reaction mixture was partitionated between 1 M aq. NaOH and *t*BME. The layers were separated and the aqueous one extracted twice with *t*BME. The combined organic layers were washed once with 5% aq. HCl and once with brine, dried with sodium sulfate, filtered and concentrated. The crude was purified by column chromatography (SiO_2; dichloromethane:cyclohexane 5:1) to give the thiocarbamate as white solid (85%).

***R*$_f$** = 0.54 (SiO_2; cyclohexane:EtOAc 3:1); **^{1}H-NMR** (400 MHz, $CDCl_3$): δ = 7.76 (d, ^3J(H,H) = 8.4 Hz, 1H, Ar-H), 7.72 (d, ^3J(H,H) = 7.6 Hz, 1H, Ar-H), 7.32 – 7.26 (m, 1H, Ar-H), 7.25 – 7.22 (m, 2H, Ar-H), 7.02 (dd, ^4J(H,H) = 2.8 Hz, ^3J(H,H) = 8.4 Hz, 1H, Ar-H), 6.96 (d, ^4J(H,H) = 2.4 Hz, 1H, Ar-H), 3.48 (s, 3H, -(CS)-N(C*H*$_3$)$_2$), 3.36 (s, 3H, -(CS)-N(C*H*$_3$)$_2$), 2.89 (s, 4H, Ar-C*H*$_2$-C*H*$_2$-Ar) ppm; **^{13}C-NMR** (101 MHz, $CDCl_3$): 187.7 (C_q, -(*C*S)-N(CH_3)$_2$), 153.1 (C_q), 138.6 (C_q), 137.0 (C_q), 133.9 (C_q), 132.4 (C_q), 128.1 (C_t), 127.3 (C_t), 127.0 (C_t), 124.5 (C_t), 123.7 (C_t), 122.1 (C_t), 121.1 (C_t), 43.2 (C_p, -(CS)-N(*C*H$_3$)$_2$), 38.7 (C_p, -(CS)-N(*C*H$_3$)$_2$), 29.1 (C_s, Ar-*C*H_2-CH_2-Ar), 28.8 (C_s, Ar-CH_2-*C*H_2-Ar) ppm; **MS** (EI +, 70 eV): m/z (%) = 284 (12), 283 (69, [M$^+$]), 165 (11), 88 (100), 72 (99); **elemental analysis** calcd (%) for $C_{17}H_{17}NOS$: C 72.05, H 6.05, N 4.94; found: C 72.04, H 6.22, N 4.85.

***S*-(9,10-dihydrophenanthren-2-yl) dimethylcarbamothioate (E16):** The *O*-thiocarbamate **E15** (172 mg, 0.608 mmol, 1.00 equiv.) and diphenylether (0.750 mL, 800 mg, 4.70 mmol, 7.70 equiv.) were placed in a preheated 2-neckflask equipped with a condenser under argon atmosphere. The reaction mixture was heated at reflux (260°C) for 2 h. the reaction mixture was cooled to rt and subjected directly to column chromatography (SiO_2; cyclohexane:EtOAc 5:1, then cyclohexane:EtOAc 3:1) to isolated the *S*-thiocarbamate **E16** as a colorless oil (56%).

***R*$_f$** = 0.41 (SiO_2; cyclohexane:EtOAc 3:1); **^{1}H-NMR** (500 MHz, $CDCl_3$): δ = 7.75 (d, ^3J(H,H) = 8.0 Hz, 1H, Ar-H), 7.74 (d, ^3J(H,H) = 7.5 Hz, 1H, Ar-H), 7.42 (dd, ^4J(H,H) = 1.5 Hz,

^3J(H,H) = 8.0 Hz, 1H, Ar-H), 7.39 – 7.37 (m, 1H, Ar-H), 7.33 – 7.28 (m, 1H, Ar-H), 7.26 – 7.22 (m, 2H, Ar-H), 3.11 (s, 3H, -(CO)-N(CH_3)$_2$), 3.05 (s, 3H, -(CO)-N(CH_3)$_2$), 2.88 (s, 4H, Ar-CH_2-CH_2-Ar) ppm; **^{13}C-NMR** (126 MHz, $CDCl_3$): 163.8 (C_q, -(*C*O)-N(CH_3)$_2$), 138.0 (C_q), 137.6 (C_q), 135.5 (C_q), 135.2 (C_t), 134.2 (C_t), 133.9 (C_q), 128.2 (C_t), 127.8 (C_t), 127.1 (C_q), 127.0 (C_t), 124.3 (C_t), 124.0 (C_t), 36.9 ($2C_p$, -(CS)-N(*C*H_3)$_2$), 28.9 (C_s, Ar-*C*H_2-CH_2-Ar), 28.8 (C_s, Ar-CH_2-*C*H_2-Ar) ppm; **MS** (EI +, 70 eV): m/z (%) = 284 (12), 283 (69, [M^+]), 165 (11), 88 (100), 72 (99); **elemental analysis** calcd (%) for $C_{17}H_{17}NOS$: C 72.05, H 6.05, N 4.94; found: C 71.97, H 6.12, N 4.81.

9,10-Dihydrophenanthrene-2-thiol (E5): A solution of *S*-thiocarbamate **E16** (85.0 mg, 0.300 mmol, 1.00 equiv.) in 6.5 mL MeOH was degased with argon. Then pestle, solid KOH (135 mg, 2.40 mmol, 8.00 equiv.) was added and the resulting reaction mixture was heated at 80°C for 3 h. The reaction mixture was then quenched with 1 M aq. HCl at 0°C. After extraction with dichloromethane, the combined organic layers were washed with brine, dried with sodium sulfate and concentrated.

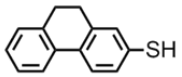

$\boldsymbol{R_f}$ = 0.78 (SiO_2; cyclohexane:EtOAc 5:1); **^{1}H-NMR** (400 MHz, $CDCl_3$): δ = 7.72 (d, ^3J(H,H) = 7.6 Hz, 1H, Ar-H), 7.71 (d, ^3J(H,H) = 8.0 Hz, 1H, Ar-H), 7.53 (d, ^3J(H,H) = 7.6 Hz, 1H, Ar-H), 7.47 (s, 1H, Ar-H), 7.37 (t, ^3J(H,H) = 7.6 Hz, 1H, Ar-H), 7.33 – 7.27 (m, 2H, Ar-H), 3.86 (s, 4H, Ar-CH_2-CH_2-Ar), 3.54 (s, 1H, -S*H*) ppm; **^{13}C-NMR** (101 MHz, $CDCl_3$): 138.3 (C_q), 137.2 (C_q), 135.8 (C_q), 133.8 (C_q), 133.7 (C_q), 128.1 (C_t), 127.6 (C_t), 127.3 (C_t), 127.0 (C_t), 126.3 (C_t), 124.4 (C_t), 123.6 (C_t), 29.0 (C_s, Ar-*C*H_2-CH_2-Ar), 28.8 (C_s, Ar-CH_2-*C*H_2-Ar) ppm; **MS** (MALDI-ToF): m/z (%) = 423 (37), 422 (100, [M^+]), 211 (26) (disulfide).

Literature

[1] E. Orgiu, N. Crivillers, J. Rotzler, M. Mayor, P. Samorì, *J. Mater. Chem.* **2010**, *20*, 10798.

[2] H. Suzuki, *Bull. Chem. Soc. Jpn.* **1959**, *32*, 1340.

[3] H. Suzuki, *Bull. Chem. Soc. Jpn.* **1959**, *32*, 1350.

[4] D. Vonlanthen, A. Mishchenko, M. Elbing, M. Neuburger, T. Wandlowski, M. Mayor, *Angew. Chem.* **2009**, *48*, 8886–8890.

[5] D. Vonlanthen, A. Rudnev, A. Mishchenko, A. Käslin, J. Rotzler, M. Neuburger, T. Wandlowski, M. Mayor, *Chem. Eur. J.* **2011**, *17*, 7236–7250.

[6] N. Berton, F. Lemasson, J. Tittmann, N. Stürzl, F. Hennrich, M. M. Kappes, M. Mayor, *Chem. Mater.* **2011**, *23*, 2237–2249.

[7] W.-Y. Wong, C.-L. Ho, *J. Mater. Chem.* **2009**, *19*, 4457.

[8] J. Rotzler, D. Vonlanthen, A. Barsella, A. Boeglin, A. Fort, M. Mayor, *Eur. J. Org. Chem.* **2010**, *6*, 1096–1110.

[9] C. Tepper, G. Haberhauer, *Chem. Eur. J.* **2011**, *17*, 8060–8065.

[10] D. Kuang, S. Ito, B. Wenger, C. Klein, J.-E. Moser, R. Humphry-Baker, S. M. Zakeeruddin, M. Grätzel, *J. Am. Chem. Soc.* **2006**, *128*, 4146–4154.

[11] C. Giansante, P. Ceroni, V. Balzani, F. Vögtle, *Angew. Chem.* **2008**, *47*, 5422–5425.

[12] H. Langhals, A. Hofer, S. Bernhard, J. S. Siegel, P. Mayer, *J. Am. Chem. Soc.* **2011**, *76*, 990–992.

[13] N. Sakai, R. Bhosale, D. Emery, J. Mareda, S. Matile, *J. Am. Chem. Soc.* **2010**, *132*, 6923–6925.

[14] E. R. Strieter, D. G. Blackmond, S. L. Buchwald, *J. Am. Chem. Soc.* **2003**, *125*, 13978–13980.

[15] S. Lee, M. Jørgensen, J. F. Hartwig, *Org. Lett.* **2001**, *3*, 2729–2732.

[16] J. J. Becker, P. S. White, M. R. Gagné, *J. Am. Chem. Soc.* **2001**, *123*, 9478–9479.

[17] K. Mikami, T. Korenaga, M. Terada, T. Ohkuma, T. Pham, R. Noyori, *Angew. Chem. Int. Ed.* **1999**, *38*, 495–497.

[18] A. C. Benniston, A. Harriman, P. V. Patel, C. A. Sams, *Eur. J. Org. Chem.* **2005**, 4680–4686.

[19] A. C. Benniston, A. Harriman, *Coord. Chem. Rev.* **2008**, *252*, 2528–2539.

[20] L. Venkataraman, J. E. Klare, C. Nuckolls, M. S. Hybertsen, M. L. Steigerwald, *Nature* **2006**, *442*, 904–907.

[21] E. A. Braude, W. F. Forbes, *J. Chem. Soc.* **1955**, 3776–3782.

[22] L. T. Cheng, W. Tam, S. R. Marder, A. E. Stiegman, G. Rikken, C. W. Spangler, *J. Phys. Chem.* **1991**, *95*, 10643–10652.

[23] H. H. Jaffé, M. Orchin, *Theory and Applications of Ultraviolet Spectroscopy*, Wiley, **1962**.

[24] G. Horowitz, *J. Mater. Res.* **2011**, *19*, 1946–1962.

[25] C. D. Dimitrakopoulos, P. R. . Malenfant, *Adv. Mater.* **2002**, *14*, 99–117.

[26] G. Gelinck, P. Heremans, K. Nomoto, T. D. Anthopoulos, *Adv. Mater.* **2010**, *22*, 3778–3798.

[27] E. C. P. Smits, S. G. J. Mathijssen, P. A. van Hal, S. Setayesh, T. C. T. Geuns, K. A. H. A. Mutsaers, E. Cantatore, H. J. Wondergem, O. Werzer, R. Resel, u. a., *Nature* **2008**, *455*, 956–959.

[28] H. Klauk, *Chem. Soc. Rev.* **2010**, *39*, 2643.

[29] H. E. Katz, *J. Mater. Chem.* **1997**, *7*, 369–376.

[30] I. H. Campbell, S. Rubin, T. A. Zawodzinski, J. D. Kress, R. L. Martin, D. L. Smith, N. N. Barashkov, J. P. Ferraris, *Phys. Rev. B* **1996**, *54*, R14321–R14324.

[31] B. de Boer, A. Hadipour, M. M. Mandoc, T. van Woudenbergh, P. W. M. Blom, *Adv. Mater.* **2005**, *17*, 621–625.

[32] D. Cornil, Y. Olivier, V. Geskin, J. Cornil, *Adv. Funct. Mater.* **2007**, *17*, 1143–1148.

[33] P. Stoliar, R. Kshirsagar, M. Massi, P. Annibale, C. Albonetti, D. M. de Leeuw, F. Biscarini, *J. Am. Chem. Soc.* **2007**, *129*, 6477–6484.

[34] S. Liao, R. Harvey, J. Pataki, *EP0363128 (A2) — 1990-04-11*.

[35] A. Shaporenko *et al*., *J. Phys. Chem. B* **2006**, *110*, 4307–4317.

Part F. Summary and Outlook

This work was purposive to the development of new functional materials in the research areas of material science, namely polymer chemistry, molecular electronics and nonlinear optics. Fundamental physical chemical investigations on twisted chromophores provided basical aspects towards future applications in photonics, catalysis, device fabrication in communication technologies or even separation techniques for carbon nanotubes. It was demonstrated that manipulations on the molecular dimension in the chemical structure of the compounds, in the intermolecular aggregation, the spatial arrangements or the intramolecular conformations can cause a dramatic change in physical properties. It is unambiguously necessary to investigate the fundamental aspects of intra- and intermolecular interactions on the molecular scale to be then able to transfer these nanoscale properties to the macroscopic dimension towards altered and tailored materials. Hence the cooperation of experts in physics, analytical chemistry, theoretical chemistry and synthetic chemistry was essential in this work to understand these complex intra- and intermolecular interplays. However, the focus of this thesis was on the design and synthesis, as well as on preliminary physical chemical investigation of tailor made compounds.

In the first part, the synthesis of an oligophenylene-ethynylene molecular rod comprising a terminal cyclophane loop was described. The design of the water soluble cyclophane, having a hydrophobic cavity, allowed for the formation of inclusion complexes with the molecular rod. Interlinking the cyclophane (host) and rod (guest) provided an amphiphilic molecule which is able to form intermolecular self-aggregating supermolecules, so called daisy chains. The synthesis was performed in a 21 step reaction sequence (if intramolecular macrocyclization was used to assemble the cyclophane) or a 17 step sequence (if intermolecular macrocyclization was used). The synthesis of the cyclophane moiety, starting from cheap, commercially available compounds, was straight forward and was scaled up to 2 g target cyclophane. For the assembly of the two subunits (cyclophane and OPE) a five step sequence was developed, where the first three steps were used to provide a suitable station for Sonogashira cross-coupling. In short, chemoselective demethylation, introduction of a benzylic linker, reduction, Sonogashira cross-coupling and final ethylation provided the desired target compound **A1** (scheme 1). The introduction of the OPE at this late stage of the synthetic route provides a modular way towards a variety of altered compounds, which then allows to investigate the aggregation behavior in detail.

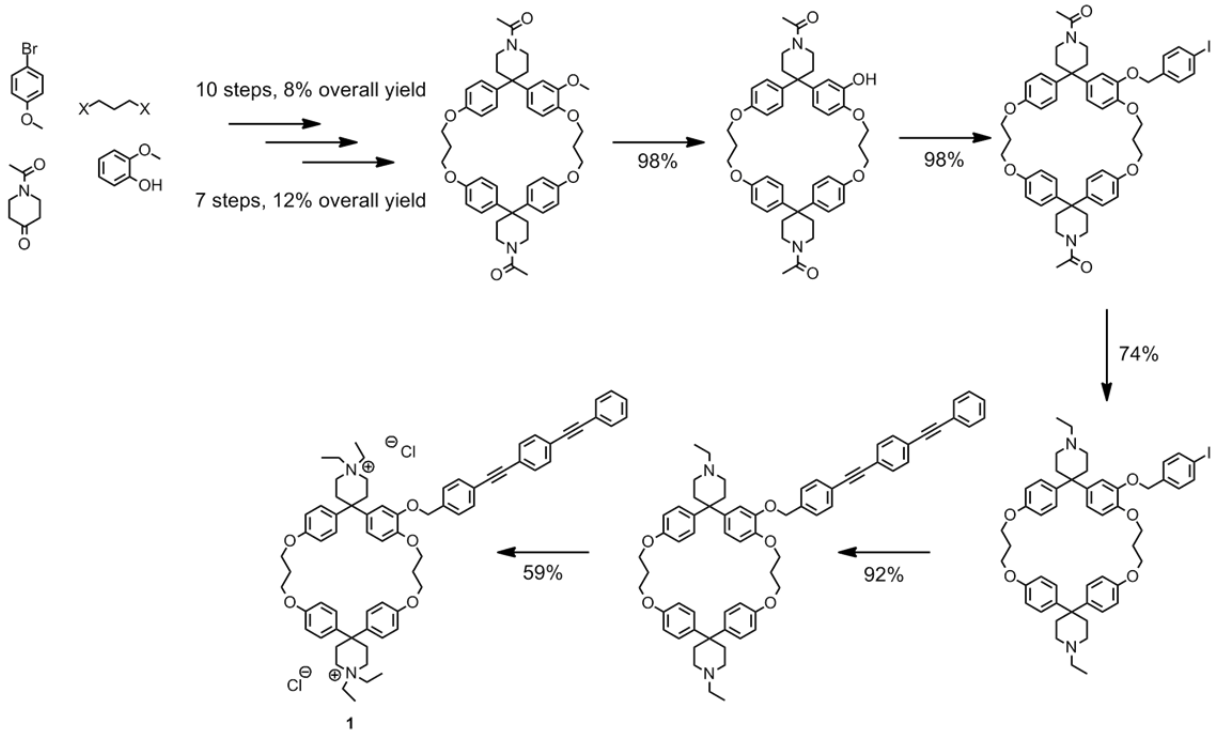

Scheme 1. Overview of the synthesis of the hermaphroditic molecular rod comprising a water soluble terminal loop **A1**. X = halide.

The intermolecular aggregation behavior of amphiphile **A1** was investigated using ^{1}H-NMR titration and fluorescence titration. Analysis of the obtained data demonstrated the formation of cyclic dimeric daisy chains ([c2]daisy chain) in a concentration range between $1.83 \cdot 10^{-6}$ M and $0.94 \cdot 10^{-3}$ M (figure 1). The high association constant of the supermolecule (K_a = $1.33 \cdot 10^{6}\,M^{-1}$) was attributed to the long guest molecule whose length prevent rapid dissociation. Unfortunately, no direct evidence for the formation of the inclusion complex was found by NOESY and ROESY-NMR, which can be explained by the internal rapid movement of the macrocycle along the rod, resulting in a fast exchange regime on the NMR time scale. Nevertheless, the high association constant, the prominent upfield chemical shift with increasing concentration, the observation of dimers over a broad concentration range and at very low concentrations, as well as the changing chemical equivalence of the protons of the interlinking propyl chains strongly point towards the formation of dimeric daisy chains rather than preformation of micelles. Furthermore, the strongly decreased emission in water/methanol mixtures compared to emission in dichloromethane suggest the inclusion of both OPE rods into the cavity of the cyclophane – driven by a strong hydrophobic effect – resulting in [c2]daisy chains. Direct evidence for the formation of aggregates was obtained in the gas phase by high resolution ESI-MS, where masses of dimers to pentamers were observed already at low concentrations (10^{-5} M). Between concentrations of 1 mM and 3 mM

in a water:methanol 3:2 mixture, graphical estimation of the aggregation number gave evidence for the formation of aggregates composed out of four to six repeat units (figure 1). Above 3 mM, hints for the formation of even longer oligomers were obtained, but the strong broadening of the NMR signals prevented an accurate estimation of the aggregation number.

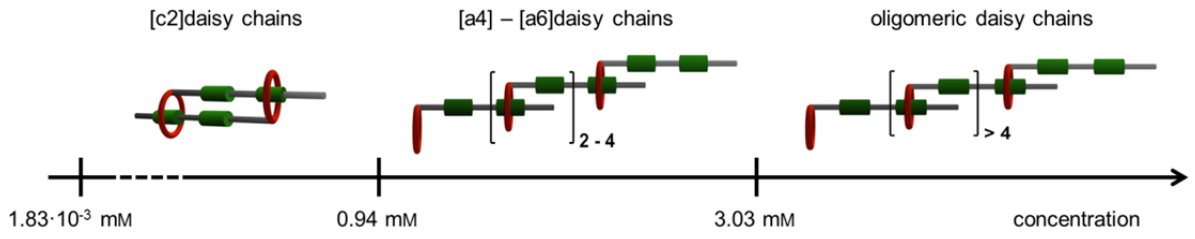

Figure 1. Aggregates formed by amphiphile **A1** in aqueous solution depending on the concentration.

To be able to further investigate the aggregation behavior of hermaphroditic monomer **A1** it is proposed to functionalize the molecular rod such that an incorporation into the cavity gets impossible. From a synthetic point of view it is maybe more reliable to terminally functionalize the OPE rod with a hydroxyl group which potentially leads to several advantages. Due to the increased electron density of the OPE it is expected that the critical aggregation concentrations are shifted to higher concentrations and therefore facilitates the ^{1}H-NMR investigations since resolution is increased and less measurement time is needed. The presence of such a functionality at the terminus allows for capping with bulky triphenylmethane (figure 2). By prevention of aggregate formation the monomer chemical shifts in the ^{1}H-NMR can be estimated and therefore a more precise analysis of both the aggregation number and the association constant by ^{1}H-NMR gets possible. Furthermore this proposed compound can act as a reference compound for investigations of higher oligomers by vapor pressure osmometry or DOSY-NMR.

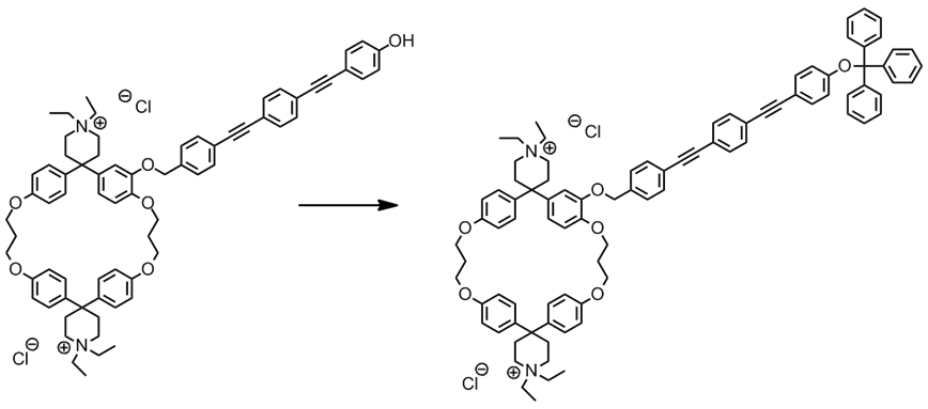

Figure 2. Capping of a hydroxyl functionalized amphiphilic monomer to prevent aggregation.

Additionally aggregates like the dimers can be fixed accordingly preventing the fast exchange on the NMR time scale. Addition of suitable cross linkers to the proposed hydroxylated amphiphile allows for controlled conventional polymerization leading to mechanically contractable linear chains or even flexible polymer networks (figure 3).

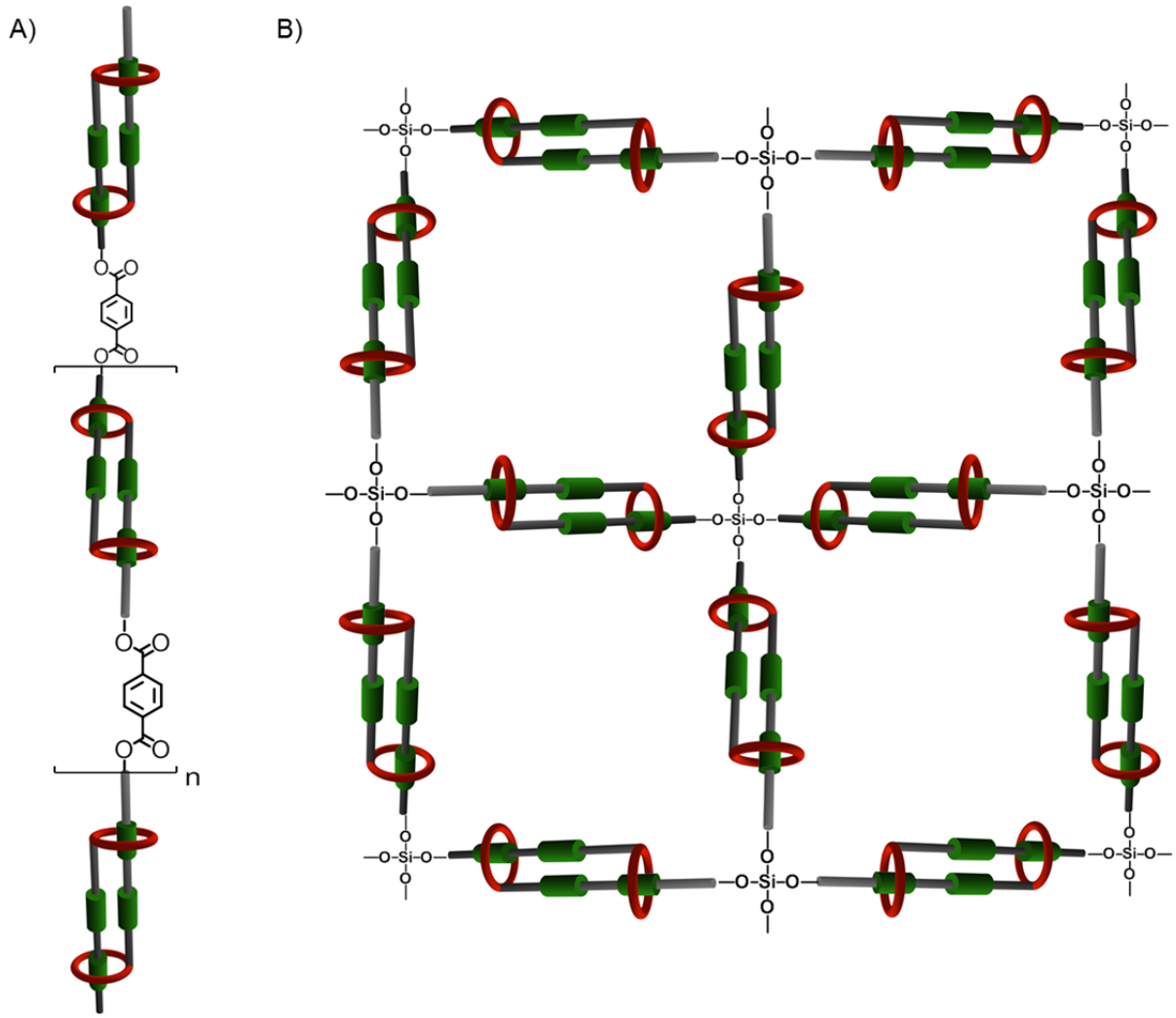

Figure 3. Schematic representation of polymers having a mechanical bond as an integral part. A) linear polymer chain with a terephthalate linking unit; B) polymer network composed of hydroxylated amphiphile **A1** and orthosilicate.

The possibility for functionalization was demonstrated by introduction of a terminally *S*-acetyl substituted OPE rod in the target amphiphile. Sonogashira cross-coupling and subsequent ethylation gave the desired target compound **B1a** (scheme 2). A critical issue in the synthesis was the instability of the *S*-acetyl moiety, leading to low yields at the late stages of the synthetic route. Aggregation studies by ^{1}H-NMR demonstrated the formation of dimers and higher oligomers in aqueous solutions. Due to the decreased electron density at the OPE, higher oligomers were observed at lower concentrations compared to the unfunctionalized

version **A1**. The desired dimeric aggregates were observed between 0.0135 mM and 0.37 mM. Again the same hints for the formation of inclusion complexes as for **A1** were observed in the ^{1}H-NMR. It will now be of interest to perform conductance studies of these [c2]daisy chains in a mechanical controlled break junction setup, to see if by mechanical contraction and elongation differences in the conductivity can be observed. This would lead to the first mechanically controlled single molecular potentiometer. Furthermore detailed investigations of the electronic properties of bimolecular bridges could be performed, which opens up the possibility to establish a new charge transport mechanism. This new concept of using supramolecular interactions as interconnection possibility of electronically active species will hopefully find its way in single molecular electronics.

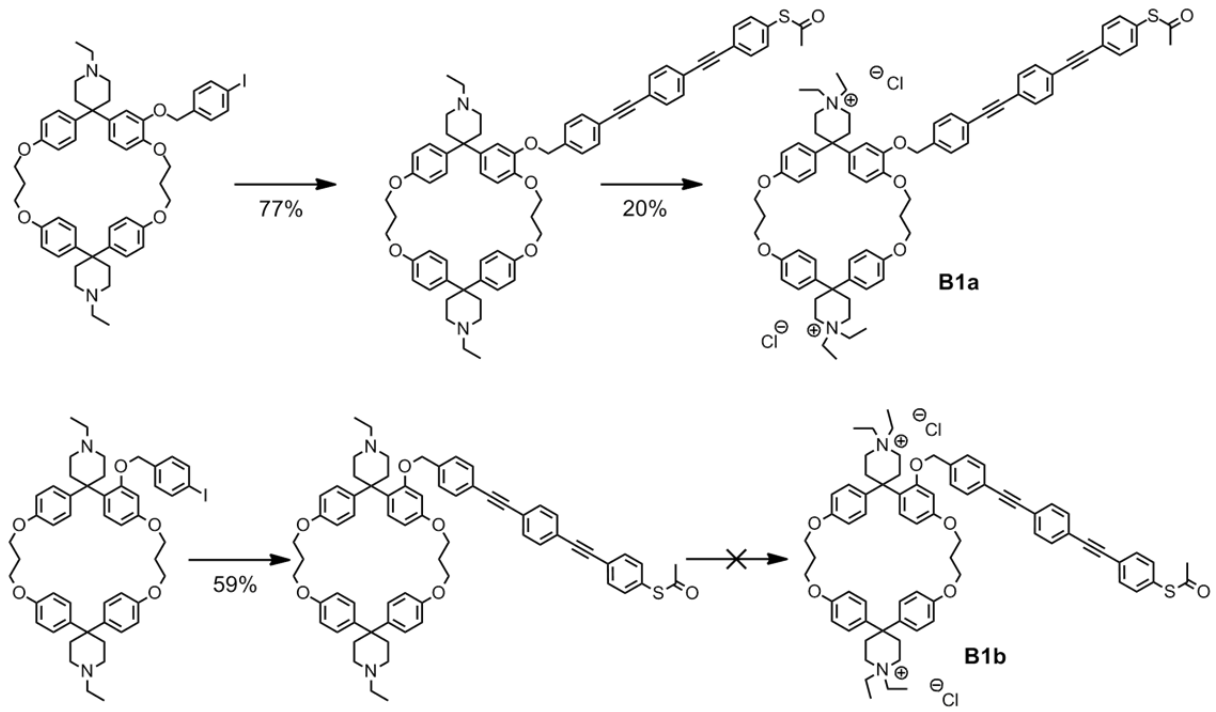

Scheme 2. Synthesis of *S*-acetyl functionalized amphiphile **B1a** and unsuccessful synthesis of amphiphile **B1b**.

Unfortunately the synthesis of a second derivative of amphiphile **B1b** where the OPE is interlinked to the cyclophane in 4' position rather than 5' position was not successful (scheme 2). In the final ethylation step only traces of desired target compound were obtained. To further investigate this final step the precursors of amphiphile **B1b** have to be provided in larger amounts, which was not yet possible due to the low yielding introduction of the mono-functionality. To improve the efficiency of the synthetic protocol a new pathway towards asymmetrical functionalized diphenylmethane units is proposed (scheme 3). Already preliminary test reactions showed that an introduction of 3-methoxyphenol is possible prior to the unfunctionalized phenol. However, in the proposed sequence the availability of the

starting material is the bottle-neck. Therefore an efficient and short way for the synthesis of 4-bromo-3-methoxyphenol has to be developed to provide sufficient amounts starting material.

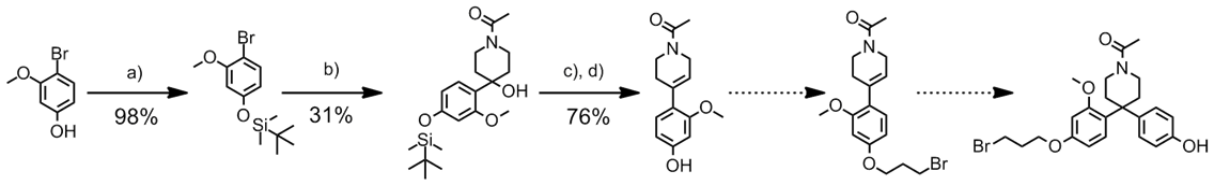

Scheme 3. Proposed synthesis of the asymmetric diphenylmethane unit to avoid the low yielding addition of 3-methoxyphenol to the styrene moiety. a) TBDMS-Cl, imidazole, DMF, rt, 20 h; b) 1.) Mg, THF, reflux, 4 h, 2.) *N*-acetyl-4-piperidone, THF, rt, 3 h; c) *p*-TsOH, toluene, reflux, 1.5 h; d) TBAF, THF, 0°C, 2 h.

In summary in the first two projects a synthetic strategy was developed towards new amphiphilic monomers. The aggregation studies revealed the high potential of using the hydrophobic effect as driving force for the formation of molecular daisy chains. Furthermore it was shown that terminal functionalization of the molecular rod does not disturb the formation of strong inclusion complexes. Therefore these projects can have a great impact on research in polymer science and single molecular electronics.

In the second part of this thesis biphenyl compounds with restricted torsion angles were synthesized for investigations in nonlinear optics and organic thin film transistors. In addition the racemization dynamics of propyl- and butyl-bridged biphenyl structures were studied to be able to separate the atropisomers which can lead to new model structures to investigate circular polarized luminescence, new ligands for enantioselective catalysis or even new polymers with which separation of nanotubes can be possible.

Nonlinear optics materials attracted attention among physical chemists and physicists during the last decades, because of the potential to integrate such materials in devices for a variety of applications. Until today, not all calculated nonlinear optic responses, based on several models, were consistent with measured hyperpolarizabilities. For further progress in this complex research field, a better understanding of the structure-property relationship is necessary. Therefore a series of molecules with moderate second-order nonlinear responses were synthesized during this thesis. Two main physical phenomena contribute to the hyperpolarizability, which are charge-transfer and the contribution of the substituents. While the contributions of the substituents are well understood, comprehension of the interplay between charge-transfer and the contributions of the substituents is still lacking. The within this thesis synthesized push-pull systems having torsion angles between 0° and 90° are ideal

model compounds enabling a detailed investigation of the correlation between NLO properties and π-conjugation, respectively torsion angle, in the backbone of the molecule. The 4-piperidinyl-4'-nitro substituted biphenyl target compounds **C1a** – **C1g** were synthesized starting from dibromo or ditriflate biphenyls by a Hartwig-Buchwald C-N hetero cross-coupling reaction, followed by selective azacycloalkylation of one aniline moiety and final mild, chemoselective oxidation of the remaining primary amine (scheme 4). The developed synthetic route was generally implementable to all desired derivatives **C1a** – **C1g**. Furthermore the final oxidation step is according to our knowledge the first example where a primary amine was oxidized to a nitro functionality in presence of a tertiary amine.

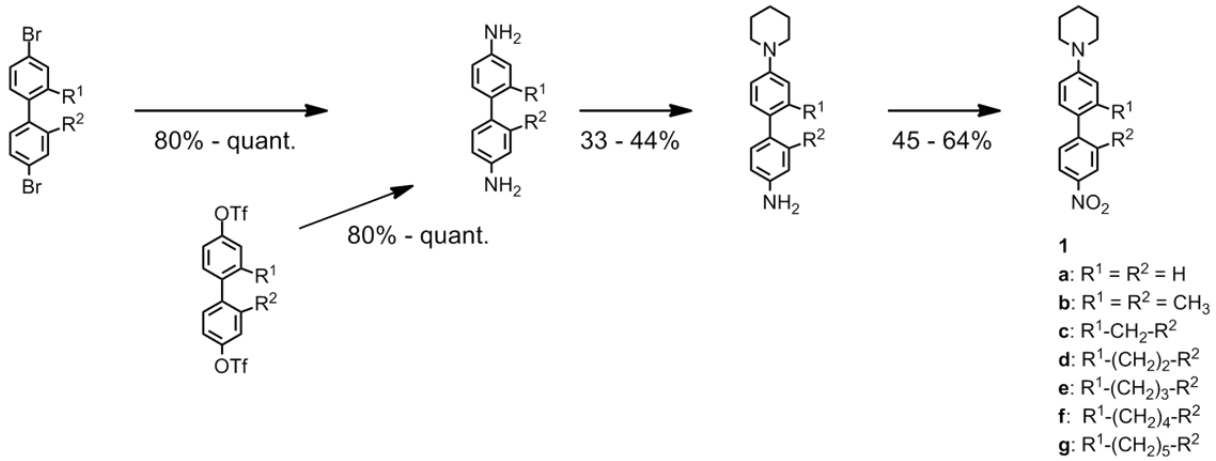

Scheme 4. General implementable synthetic route towards biphenyl based push-pull cyclophanes **C1a** – **C1g**.

The NLO properties of this series of torsion angle restricted biphenyl based push-pull systems have been successfully investigated by EFISH measurements. The results agree qualitatively with semi-empirical simulations based on the AM1 Hamiltonian. In particular, the linear dependence of the quadratic response on the $\cos^2\Phi$ of the inter-aryl dihedral angle points to oscillator strength loss as the dominant effect of increasing backbone twist, which would indicate that the change in permanent dipole moment upon CT transition is much less affected. To probe this aspect will require to conduct experiments where the chromophores are excited at resonance such as two-photon absorption cross-section measurements. It will then be of interest to see how more sophisticated electronic structure calculations will fare in describing the effect of the gradual twist of the conjugation path.

Towards possible applications of organic materials in nonlinear optics the transformation of the microscopic noncentrosymmetry to the macroscopic scale is unambiguous. One possibility to achieve this goal is the growth of noncentrosymmetric crystals wherefore enantiomerically pure compounds seems to be ideal candidates. The axial chiral push-pull systems **C1d** – **C1g**

were synthesized as racemic mixtures. Therefore separation of the atropisomers using chiral HPLC was envisaged. To select potential candidates for this purpose the inversion barriers of these axial chiral compounds were measured by ^{1}H-NMR coalescence measurements and dynamic HPLC. The rotational energy barrier of the propyl-bridged push-pull cyclophane **C1e** was estimated to be $\Delta G_{298K}^{\ddagger}$ = 50 kJ/mol and the rotational barrier of the butyl-bridged derivative **C1f** to be $\Delta G_{298K}^{\ddagger}$ = 90 kJ/mol. The rotational energy barrier of **C1d** and **C1g** could only be evaluated qualitatively by comparison of them with the two quantitatively analysed derivatives **C1e** and **C1f**. Unfortunately the separation of the two atropisomers was not successful for all nonlinear optic active compounds **C1d** – **C1g** and thus it was not possible to grow noncentrosymmetric crystals.

Encouraged by this outcome the inversion dynamics of 4,4'-donor and 4,4'-acceptor substituted 2,2' propyl- and butyl-bridged biphenyl cyclophanes were investigated (figure 4). By ^{1}H-NMR coalescence measurements, it was possible to show that the rotation barriers of in 2,2' position propyl-bridged biphenyls **D1a** – **D1l** are strongly dependent on the nature of the phenyl-phenyl bond and with it on the nature of substituents in *para* position to this bond. The free energies $\Delta G^{\ddagger}$(T) were calculated to be for all compounds between 45 kJ/mol for the strongest π-donor piperidinyl **D1l** and 55 kJ/mol for the nitro substituted derivative **D1a** as the strongest π-acceptor. These energies were correlated to the Hammett-parameter σ_p, the resonance parameter R and the field effect parameter F, what allowed for identifying the π-electron density as the predominant factor which dictates the rotation barrier.

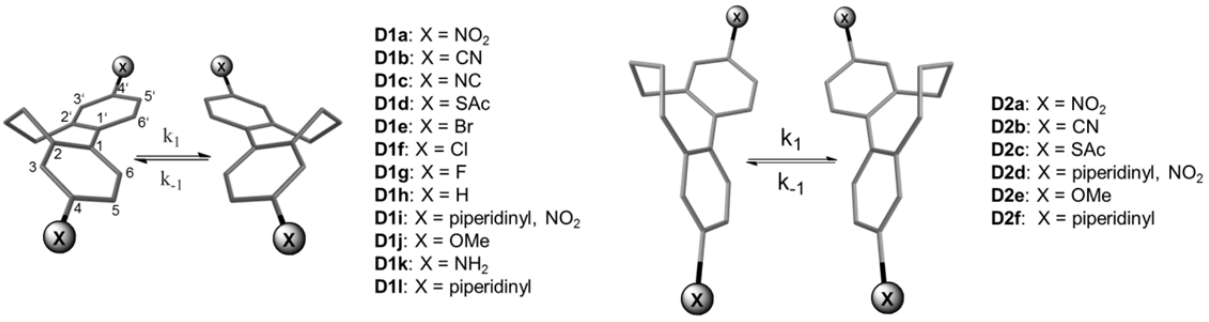

Figure 4. Propyl and butyl-bridged torsion angle restricted, axial chiral biphenyl cyclophanes studied by ^{1}H-NMR coalescence measurements and dynamic HPLC.

This was further confirmed by DFT calculations, from which also a planar and nearly linear single transition state was obtained. Solvent dependent ^{1}H-NMR coalescence measurements further documented the importance of the nature of the central C1-C1' bond to the atropisomerization process. Furthermore the calculated transition state showed that the length

of the central phenyl-phenyl bond not only influences the energy needed for inversion but also dictates the distance between the *ortho* methylene groups of the propyl-bridge. Analysis of the butyl-bridged analoga **D2a** – **D2f** (figure 4) by temperature dependent dynamic HPLC yielded atropisomerization energies $\Delta G^{\ddagger}(T)$ of 89 kJ/mol for the strongest donor substituted compound **D2f** to 97 kJ/mol for the strongest acceptor **D2a**. In contrast to the propyl-bridged derivatives the inversion of the larger cyclophanes proceeds via a preorganization of the butyl-bridge resulting in a second conformer which is able to undergo enantiomerization through a planar transition state. In addition, this transition state showed in contrast to the propyl-bridged one a stronger deviation from linearity. Furthermore, again only the rotation around the central C-C bond is susceptible to the donor or acceptor strength of the substituents, revealing that the enantiomerization process is dominated by the electronic nature of the central biphenyl bond and therefore by the distance between the two phenyl rings. The increased free energy values $\Delta G^{\ddagger}(T)$ of **D2a** – **D2f** compared to the propyl-bridged derivatives **D1a** – **D1l** can be explained by a more crowded transition state in accordance to the conclusions drawn from our studies of the racemization dynamics of biphenyl based push-pull systems. The calculated mechanism is in contradiction to the previously reported biphenyl atropisomerization mechanisms where an out-of-plane bending of the two phenyls or a distortion of the phenyls itself were postulated. Even though the discrepancy in measured enthalpy and entropy values to the calculated ones is not fully understood, it was possible to demonstrate that the rotation barrier can be affected by the length of the bridge, the electronic nature of the substituents in *para* position to the central phenyl-phenyl bond and the solvent, where the latter two have only a small influence on $\Delta G^{\ddagger}(T)$ compared to the bridge length. Atropisomers can be theoretically separated when the rotational energy is about 93 kJ/mol at 300 K, but which was not conceivable in the temperature range applicable for chiral HPLC. Comparison of the two calculated inversion mechanisms as well as the increased free energies $\Delta G^{\ddagger}(T)$ for all butyl-bridged derivatives **D2a** – **D2f** point towards the possibility to enhance the rotation barrier by introduction of bulky substituents on the interlinking alkyl-bridge. Therefore it is proposed to synthesize model compounds comprising octamethylated butyl-bridges to hinder the enantioconversion allowing the separation of the two atropisomers by chiral HPLC (scheme 5). Enantiomerically pure and kinetically stable 2,2’ alkyl-bridged biphenyls can then be used not only for the growth of noncentrosymmetric crystals towards applications in nonlinear optics but also for the synthesis of circular polarizable luminescent oligomers or even polymers. Therefore it will be of interest to synthesize biphenyls which are stable to atropisomerization at and above room temperature to enable chemical modifications.

Functionalization of separated enantiomers and subsequent coupling of an aromatic compound can potentially lead to doubly bridged terphenyls without formation of chiroptically mute *meso* forms (scheme 5).

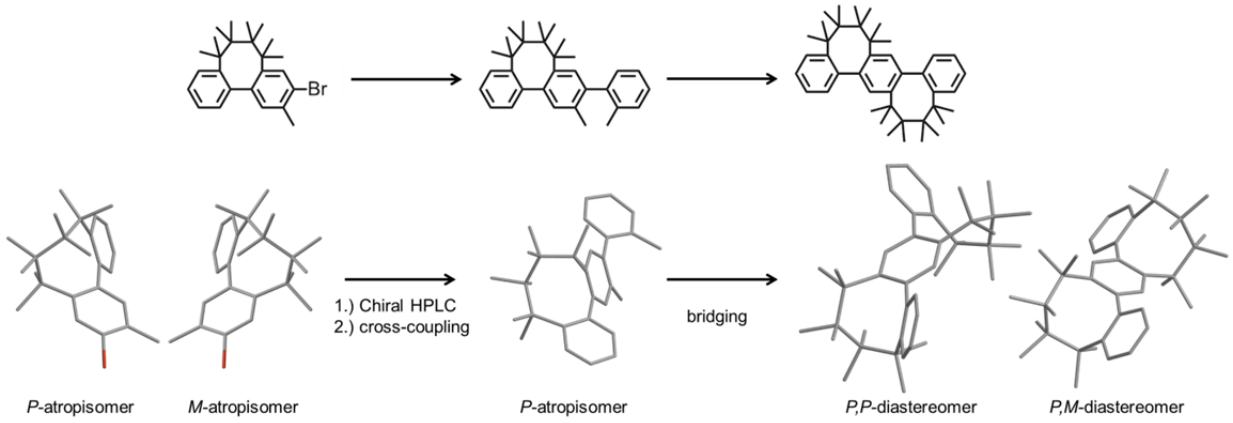

Scheme 5. Sketch of a possible synthesis towards a Geländeroligomer starting from enantiomerically pure octamethylated butyl-bridged biphenyl by efficiently hindering the racemization.

Finally, a series of mono-functionalized torsion angle restricted 4-thiobiphenyls was successfully synthesized (figure 5) to tune the charge injection barrier by immobilizing the electrodes of organic thin film transistors with a thiol monolayer. Preliminary investigations using oligophenylenes with an increasing number of phenyls demonstrated that a fine tuning of both the field-effect mobility and the threshold voltage can be achieved. These investigations also suggests that the macro-resistive contribution can be explained by taking into account a concomitant effect of energetic levels alignment, tunneling resistance of the SAMs and interfacial morphology between the semiconducting layer and the electrode. These findings are of importance to optimize OTFTs in view of their technological applications in logic circuits as they provide tools for a better control over the charge injection mechanism. It will now be of further interest to perform experiments with biphenylthiol with varying torsion angles to evaluate if the alignment to the HOMO of P3HT or the increased tunneling barrier is the dominant factor leading to high contact resistance. Furthermore it will be interesting to see if the fine tuning of the torsion angles in the biphenyl compounds can lead to an increased charge injection.

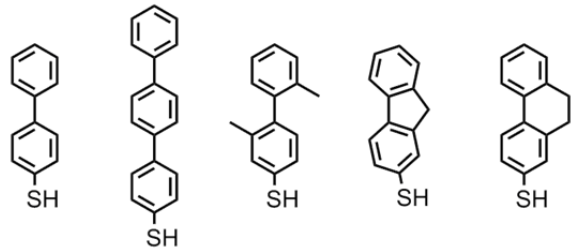

Figure 5. Mono-thiolated biphenyl compounds with either variable length or different torsion angle.

Curriculum Vitae

Personal Data: Name: Jürgen Stefan Rotzler

Date/Place of Birth: December 30th, 1982, Lörrach, Germany

Nationality: German

Education:

5/2008 – 5/2012 Dissertation in Nanotechnology and Organic Chemistry;
Advisor: Prof. Dr. Marcel Mayor; University of Basel
Referees: Prof. Dr. Karl Gademann; University of Basel
Prof. Dr. Jean-Pierre Sauvage; Université de Strasbourg (F) and Northwestern University (USA)

"Tailoring Intra- and Intermolecular Properties: From Cyclophanes to Daisy Chains"

3/2008 Master degree in Chemistry

8/2007 – 2/2008 Master thesis; advisor: Prof. Dr. Marcel Mayor; University of Basel: "*A universal synthetic route towards torsion angle restricted biphenyl based push-pull-systems"*

10/2006 – 8/2007 Master studies at the University of Basel

Practical courses:

"*Synthesis of chiral ferrocene-based ligands for asymmetric hydrogenation*", advisor: Prof. Dr. Andreas Pfaltz

"*A chemoselective, microwave assisted azacycloalkylation of benzidine*", advisor: Prof. Dr. Marcel Mayor

10/2003 – 10/2006 Bachelor study at the University of Basel

1993 – 2002 German Abitur, Theodor-Heuss-Gymnasium, Schopfheim, Germany

Oral Presentations:

9/2011 *"A molecular "Daisy chain" formed by amphiphilic molecular rods – The influence of aromatic coupling on electronic transport in bimolecular junctions"* J. Rotzler, Summer School 2011 "Challenges in Organic Synthesis", Villar-sur-Ollon, Switzerland.

Poster Presentations:

8/2008	"*A universal synthetic route towards torsion angle restricted biphenyl based push-pull systems*" J. Rotzler, M. Mayor, Summer School "Quo vadis electron - from radicals to ET", Villar-sur-Ollon, Switzerland.
1/2010	"*Non-linear optical properties of torsion angle restricted biphenyl-based push-pull-systems*" J. Rotzler, D. Vonlanthen, A. Barsella, A. Boeglin, A. Fort, M. Mayor, International Conference on Molecular Electronics, Emmetten, Switzerland.
4/2010	"*A microscopic potentiometer – The influence of aromatic coupling on electronic transport in bimolecular junctions*" J. Rotzler, M. Mayor, NCCR-meeting, Basel, Switzerland.
9/2010	"*Variation of the backbone conjugation in NLO model compounds: torsion angle restricted biphenyl-based push-pull-systems*" J. Rotzler, D. Vonlanthen, A. Barsella, A. Boeglin, A. Fort, H. Gsellinger, D. Häussinger, M. Mayor, 3rd EuCheMS Chemistry Congress: Chemistry - the Creative Force, Nürnberg, Germany.
9/2011	*"A non-linear optic and dynamic study of torsion angle restricted biphenyl push-pull cyclophanes"* J. Rotzler, D. Vonlanthen, A. Barsella, A. Boeglin, A. Fort, H. Gsellinger, D. Häussinger, M. Mayor, 31st Regio-Symposium, Sornetan, Switzerland.

Relevant Experiences:

9/2008 – 1/2010	Teaching assistant: introductory organic chemistry course (2 semester), advanced organic chemistry course (1 semester)
2005 – 2007	Member of the executive board of the Verband-Basler-Chemiestudenten (association of chemistry students in Basel)
9/2002 – 4/2003	Civilian Service: University Hospital Freiburg
4/2003 – 10/2003	Expansion works on private residential building (parents) and preparations of the studies in chemistry.

Current Funding: Swiss National Science Foundation

Languages: German: native speaker; English: fluent spoken and written

Affiliation: Swiss Chemical Society (SCS)

During the eductation lectures were attended given by: W. P. Meier, H. Wennemers, B. Giese, M. Oehme, U. Sequin, K. Fromm, H.-J. Wirz, A. Pfaltz, E. Constable, P. Hauser, J. P. Maier, W. Woggon, C. Housecroft, M. Meuwly, M. Mayor, H. Wegner, K. Gademann